EFFECT OF CHLORIDE ION, SULFATE ION AND CONJOINT CHLORIDE-SULFATE IONS ON CORROSION BEHAVIOUR OF STEEL REINFORCEMENT AND PERFORMANCE OF CONCRETE

A thesis submitted in partial fulfilment of the requirements for the award of

DOCTOR OF PHILOSOPHY

In

Civil Engineering

By

Fouzia Shaheen

(10610424)

Under the supervision of

Dr. Bulu Pradhan

Associate Professor

DEPARTMENT OF CIVIL ENGINEERING
INDIAN INSTITUTE OF TECHNOLOGY GUWAHATI
GUWAHATI-781039, ASSAM, INDIA

NOVEMBER 2017

CERTIFICATE

This is to certify that the thesis entitled "**Effect of Chloride Ion, Sulfate Ion and Conjoint Chloride-Sulfate Ions on Corrosion Behaviour of Steel Reinforcement and Performance of Concrete**", being submitted by **Ms. Fouzia Shaheen** (Roll. No. 10610424) to the Indian Institute of Technology Guwahati, India, for the award of the degree of "**DOCTOR OF PHILOSOPHY** in Civil Engineering", is a record of original bonafide research work carried out by her under my guidance and supervision. To the best of my knowledge, the thesis has reached the requisite standard. The material contained in this thesis has not been submitted, in part or full to any other University or Institute for the award of any degree or diploma.

Dr. Bulu Pradhan
Associate Professor
Department of Civil Engineering
Indian Institute of Technology Guwahati
Guwahati-781039, Assam, India

Dedicated to

MY FATHER

A humble tribute for the sacrifices he made to educate me

ACKNOWLEDGEMENTS

First and foremost, I deeply express my countless thanks and gratitude to God for granting me the ability to proceed successfully.

I would like to express my deep gratitude and heartfelt thanks to my supervisor Dr. Bulu Pradhan, Associate Professor, Department of Civil Engineering, Indian Institute of Technology Guwahati, Assam, India, for his consistent supervision, guidance, encouragement and gracious support throughout my research work. His valuable suggestions, effusive co-operation and encouraging interactions were great driving force for me to carry out this research work. Conducting the research and writing this dissertation would not have been possible without his patience, guidance and tireless devotion to this work.

I deeply express my sincere thanks to the chairman of doctoral committee Prof. Anjan Dutta and the committee members Prof. Subashisa Dutta and Dr Chandan Das for their sincere advice and suggestions to improve the quality of work. I would also like to extend my sincere gratitude to the Head, Department of Civil Engineering, IIT Guwahati, for all the support and encouragement extended to me directly or indirectly to carry out my research. I am also thankful to Prof. S. K. Deb, Dr. C. Mallikarjuna, Dr. Kaustubh Dasgupta, and the other faculty members for their support and encouragement extended to me at various stages of work. I also express my sincere thanks to all the staff for their help and support in various aspects.

I would like to convey my thanks to my fellow research scholars Ms. Swapnali Barman, Mr. Subrat Kumar Mallick, Mr. Randeep Singh, Mr. Srikanth Vadlamudi, Mr. Julaganti Ashok, Mr. Sudheer Kumar and others for their inspiration, encouragement and unconditional support.

I would also like to take this opportunity to thanks all the other faculty members, staff and students of IIT Guwahati, who has supported and encouraged me directly or indirectly in various aspects. I wish to express my appreciation to Om Prakash Prasad, who assisted me during my concrete laboratory works.

I am grateful to my Parents for being pillars of my strength, motivation and inspiration. I have no words to express my heartfelt gratitude for their unwavering faith in me, for their words of wisdom, unconditional love and countless blessing they have always showered

on me. I also express my gratitude to my in-laws, siblings and all other family members for their immense love, support and encouragement. I express my special thanks to my brother-in-law, Mr. Syed Younus for his support at all difficult times.

I wish to express my indebted love and gratitude to my husband, Dr. Syed Omar, who supported me through his enlightened heart and sacrifice during our stay at IIT Guwahati. I have no words to express my deep love and feelings to my son Syed Muntasir Yusuf and my daughter Ayesha Mafaz, their innocent faces and charming smiles also gave me constant inspiration to make this research work possible. Last but not the least, I would like to express my deepest gratitude to all those who have contributed directly or indirectly in the course of my research work and throughout my passage of life. I am thankful to them for inspiring me through their enlightened hearts, for touching me through their acts of kindness and honesty, and illuminating me through their wisdom and knowledge. I may not be able to recall all their names, but I am grateful to them in helping me to learn, to rise and to achieve in life.

"Thank You" Almighty for blessing me with this wonderful life, amazing family, loving friends, countless well-wishers and ample opportunities, without which this work would not have been possible.

Fouzia Shaheen

ABSTRACT

Reinforced concrete structures are affected by various durability problems during their service life. Deterioration due to corrosion of steel reinforcement and degradation of concrete due to sulfate attack are the most significant durability problems encountered in reinforced concrete structures and have major financial implications around the world. Concrete durability problems are the major cause of concern all over the world especially in the coastal areas where the structures are subjected to both chloride induced reinforcement corrosion and sulfate attack, and mechanism of deterioration may become more complex because of ingress of both chloride and sulfate ions. Chloride and sulfate ions can either be present in the concrete ingredients (internal) and/or penetrate into the hardened concrete from outside environment (external). The corrosion behaviour of steel reinforcement and the performance of concrete may vary significantly in the conjoint presence of chloride-sulfate ions as compared to that in the presence of only chloride and sulfate ions. In this research work, a comprehensive experimental investigation has been carried out to study the effect of conjoint presence of chloride ions and sulfate ions along with the associated cation type on corrosion behaviour of steel reinforcement in electrolytic concrete powder solution (ECPS) and in concrete by incorporating different types of cement, steel and water-cement (w/c) ratio. In addition, to analyze the effect of chemical composition of the electrolytic concrete powder solution on corrosion behaviour of steel reinforcement, the ionic concentration, pH and conductivity of the concrete powder solutions were determined. Further, the performance of concrete by incorporating different types of binder and water-binder ratios (w/b ratio) under different exposure conditions in sulfate and conjoint chloride-sulfate environment was assessed. To evaluate the changes in phase composition of hardened concrete in the presence of chloride and sulfate ions, various microstructural techniques such as X-ray diffraction (XRD), Field emission scanning electron microscopy (FESEM), and Fourier transform infrared (FTIR) spectroscopy analyses were also carried out.

In the present research work, the entire experimental program was divided into three series. In series I, the effect of chloride and conjoint chloride-sulfate contamination on 28 day compressive strength of concrete; microstructural changes occurred in concrete due to the presence of chloride and conjoint chloride-sulfate ions; ionic concentration, pH and conductivity of electrolytic concrete powder solution; and corrosion behaviour of steel in

electrolytic concrete powder solution (ECPS) have been investigated. For this purpose, two types of cement namely: ordinary Portland cement (OPC) and Portland pozzolana cement (PPC), and two types of thermo-mechanically treated (TMT) steel bars of diameter 12 mm namely Tempcore TMT and Thermex TMT steel bars were used as the steel reinforcement. The concrete mixes were prepared with two w/c ratios of 0.45 and 0.5. Chloride and sulfate salts were admixed at the time of preparation of concrete in the mixing water as percentage by mass of cement content. Sodium chloride (NaCl) was used as the source of chloride ions, whereas sodium sulfate (Na_2SO_4) and magnesium sulfate ($MgSO_4$) were used as the sources of sulfate ions. The concentrations of NaCl used were 3%, 5% and 7% and those of Na_2SO_4 and $MgSO_4$ used were 3%, 6% and 12% each by mass of cement content. A total of 1056 cube specimens of size 150 mm were prepared from 88 concrete mixes (i.e. from control mix and mixes contaminated with varying concentrations of chloride and composite chloride-sulfate salts) with twelve replicate specimens from each mix. The cube specimens were subjected to moist curing till the age of 28 days from the day of preparation. After that, three replicate specimens from a given concrete mix were tested to determine the 28 day compressive strength and remaining nine replicate specimens were kept in laboratory exposure condition till the period of 56 days for obtaining the concrete powder. From the obtained concrete powder, electrolytic concrete powder solutions (ECPS) was prepared. The obtained electrolytic concrete powder solution was chemically analyzed to determine its ionic concentration, pH and conductivity. The electrochemical tests such as potentiodynamic polarization test and linear polarization resistance (LPR) test on bare steel specimens were conducted in electrolytic concrete powder solution. A total of 704 bare steel specimens were prepared and tested. From the potentiodynamic polarization test on bare steel specimens in ECPS, anodic polarization curves were obtained and these were used to identify different zones of corrosion namely active zone, passive zone and pitting zone. From these zones of corrosion, corrosion potential (E_{corr}), act/pass boundary potential and pass/pitt boundary potential were determined. From LPR test, the variations in corrosion potential and corrosion current density of steel reinforcement in electrolytic concrete powder solution were evaluated. The results of 28 day compressive strength of cube specimens prepared from OPC and PPC concrete admixed with chloride and chloride-sulfate ions at w/c ratios of 0.45 and 0.5 indicated that the varying concentrations of chloride and chloride-sulfate ions have significant effect on compressive strength of concrete. The results of microstructural changes occurred in concrete due to chloride and chloride-sulfate

contamination (studied through XRD, FTIR and FESEM analyses) showed the formation of various compounds and also indicated the variations in the formations of these compounds due to the effect of cement type, concentrations of chloride salts and sulfate salts along with the associated cation type. The results obtained from the measurement of ionic concentration, pH, and conductivity of electrolytic concrete powder solution indicated that the change in cement type, w/c ratio, concentrations of admixed NaCl, Na_2SO_4 and $MgSO_4$ and cation type associated with sulfate ions i.e. Na^+ and Mg^{++} affect the electrolytic concrete powder solution chemistry. From the results of potentiodynamic polarization test on bare steel specimens in ECPS, it is found that the presence of sodium sulfate in chloride environment has mitigated the effect of chloride ions on reducing the passivity of both types of steel reinforcement. On the other hand, the presence of magnesium sulfate in chloride environment has stimulated the effect of chloride ions on reducing the passivity of steel reinforcement for Tempcore TMT steel whereas Thermex TMT steel performed better in the conjoint presence of NaCl and $MgSO_4$ in maintaining the passivity as compared to that in the presence of only NaCl. From the effect of cation type i.e. Na^+ and Mg^{++} associated with sulfate ions, it is inferred that the range of passive zone of both Tempcore TMT and Thermex TMT steel is more in NaCl plus Na_2SO_4 environment as compared to that in NaCl plus $MgSO_4$ environment for both types of cement and w/c ratio. This implies that Mg-oriented sulfate attack is more aggressive in the presence of chloride ions in reducing the passivity of steel reinforcement as compared to Na-oriented sulfate attack. From the results of LPR test on bare steel specimens in electrolytic concrete powder solution, it is observed that Tempcore TMT steel, OPC and w/c ratio of 0.5 showed lower corrosion current density in NaCl and NaCl plus $MgSO_4$ environment, thereby likely to exhibit longer corrosion propagation period. Similarly in NaCl plus Na_2SO_4 environment, Tempcore TMT steel, PPC and w/c ratio of 0.5 are likely to exhibit longer corrosion propagation period. Further, there exists a good correlation between passivity range and corrosion parameters (corrosion potential and corrosion current density) of steel reinforcement in NaCl, NaCl plus Na_2SO_4 and NaCl plus $MgSO_4$ contaminated electrolytic concrete powder solutions.

In series II, the corrosion behaviour of steel reinforcement embedded in chloride-sulfate contaminated concrete and subsequently exposed to chloride-sulfate environment was investigated by measuring corrosion potential and corrosion current density at the age of 90, 180 and 270 days from the day of preparation of the specimens by using linear

polarization resistance (LPR) technique. For this purpose prismatic reinforced concrete specimens of size 72 mm × 72 mm × 300 mm with a steel bar of 12 mm diameter placed centrally with a concrete cover of 30 mm on all the sides and at the bottom were prepared using ordinary Portland cement (OPC), Portland pozzolana cement (PPC), OPC plus 20% fly ash (OPC+20FA) and OPC plus 30% fly ash (OPC+30FA) at a w/b ratio of 0.5. Tempcore TMT and Thermex TMT steels were used as the steel reinforcement. Chloride and sulfate salts were admixed at the time of preparation of concrete in the mixing water as percentage by mass of binder content. The admixed concentrations of NaCl were 3%, 5% and 7% and those of Na_2SO_4 and $MgSO_4$ were 3% and 6% each. A total of 312 prismatic reinforced concrete specimens were prepared from 52 concrete mixes (i.e. from control mix and mixes contaminated with varying concentrations of composite chloride-sulfate salts) with three replicate specimens from each mix and for each type of steel. After 28 days of moist curing, the prismatic reinforced concrete specimens were removed from the curing tank and were kept in the laboratory exposure condition for a period of 90 days from the day of preparation. After that, the specimens were exposed to normal water and composite chloride-sulfate solutions (concentration of salts in the solution same as that admixed at the time of preparation of concrete specimens) with alternate wetting-drying cycles (each cycle comprising of 7 days of partial immersion in the test solution followed by 14 days of drying in the laboratory condition). From the results it is observed that the probability of occurrence of steel reinforcement corrosion in concrete increased in the presence of chloride and sulfate ions for all types of binder and steel reinforcement. From the variations in corrosion current density, it is observed that the corrosion current density of both types of steel in blended cement concrete specimens were lower than those in OPC concrete specimens in the conjoint presence of NaCl plus Na_2SO_4, whereas the opposite variation was observed in the conjoint presence of NaCl plus $MgSO_4$ i.e. the corrosion current density values in OPC concrete were lower than those in blended cement concrete specimens. Further Tempcore TMT steel exhibited lower corrosion density as compared to Thermex TMT steel in the composite chloride-sulfate environment.

In series III, the effect of sulfate ions and that of composite chloride-sulfate ions on deterioration of concrete have been investigated through the measurement of change in weight and compressive strength of cube specimens after 360 days of exposure to these aggressive ions. Further to examine the effect of sulfate ions and conjoint sulfate-chloride

ions on the microstructure of hardened concrete. XRD and FESEM analyses were also conducted. Cube specimens of size 150 mm were prepared with different types of binder such as OPC, PPC and OPC plus fly ash at different replacement levels (20% and 30% by mass of binder content) and w/b ratios of 0.45 and 0.5. A total of 912 cube specimens were prepared from different concrete mixes. The specimens were subjected to moist curing in curing tank till the age of 28 days from the day of preparation and were then kept in the laboratory condition for a period of 7 days. After that, the specimens were exposed to normal water, sulfate solutions and composite chloride-sulfate solutions. The concentrations of NaCl used in the preparation of exposure solutions were 3% and 5% and those of Na_2SO_4 and $MgSO_4$ used were 3%, 6% and 12% each. The exposure solutions were prepared by dissolving the required quantities of Na_2SO_4, $MgSO_4$, NaCl plus Na_2SO_4 and NaCl plus $MgSO_4$ in water. From each concrete mix, three replicate cubes were subjected to a given exposure solution with alternate wetting and drying cycles comprising of 7 days of full immersion in the exposure solution followed by 14 days of drying in the laboratory condition and another set of three replicate cubes were continuously immersed in the exposure solution till the end of exposure period. The results indicated that the effect of sulfate attack in terms of weight loss of concrete was more prominent in sulfate and composite chloride-sulfate exposure solutions when the sulfate ion is associated with Mg^{++} cation as compared to that associated with Na^{+} cation. While comparing the effect of exposure solutions on compressive strength of concrete, it is observed that the reduction in compressive strength of concrete decreased in the order: $MgSO_4$ > Na_2SO_4 > NaCl plus $MgSO_4$ > NaCl plus Na_2SO_4. This implies that chloride ions mitigate the sulfate attack on concrete when concomitantly present with sulfate ions.

TABLE OF CONTENTS

LIST OF FIGURES

LIST OF TABLES

LIST OF SYMBOLS AND ABBREVIATIONS

Cl^-	Chloride ion
e^-	Electron
Fe^{++}	Ferrous ion
OH^-	Hydroxyl ion
SO_4^{2-}	Sulfate ion
θ	Diffraction angle of X-rays
λ	Wave length of X-ray
η	Overpotential
I_{corr}	Corrosion current density
APHA	American Public Health Association
AE	Auxiliary electrode
Al_2O_3	Aluminium oxide
$AgNO_3$	Silver nitrate
$BaCl_2$	Barium chloride
CH	Calcium hydroxide or Portlandite
CC	Calcium carbonate
CCA	Calcium chloroaluminate or Friedel's salt
C-S-H	Calcium silicate hydrate
C_3A	Tricalcium aluminate
C_2S	Dicalcium silicate
C_3S	Tricalcium silicate
C_4AF	Tetracalcium aluminoferrite
CaO	Calcium oxide
ECPS	Electrolytic concrete powder solution

E	Ettringite
EDX	Energy-dispersive X-ray
FA	Fly ash
FTIR	Fourier Transform Infrared
FESEM	Field Emission Scanning Electron Microscopy
Fe_2O_3	Ferric oxide
G	Gypsum
KOH	Potassium hydroxide
K_2O	Potassium oxide
KBr	Potassium bromide
NaOH	Sodium hydroxide
LPR	Linear polarization resistance
MH	Magnesium hydroxide or Brucite
MS	Magnesium sulfate
M-S-H	Magnesium silicate hydrate
MSA	Maximum size aggregate
MgO	Magnesium oxide
N	Normality of $AgNO_3$
NC	Sodium chloride
NS	Sodium sulfate
Na_2O	Sodium oxide
OPC	Ordinary Portland cement
PPC	Portland pozzolana cement
P_2O_5	Phosphorus pentoxide
Q	Quartz
RE	Reference electrode
SCE	Saturated calomel electrode
SEM	Scanning electron microscopy
SiO_2	Silicon dioxide
SO_3	Sulphur trioxide

T	Thaumasite
TMT	Thermomechanically treated
TiO_2	Titanium dioxide
WE	Working electrode
XRD	X-ray diffraction
XRF	X-ray fluorescence

CHAPTER 1

INTRODUCTION

1.1 GENERAL

Concrete is of increasing importance for all types of construction around the world, due to its versatility, low maintenance cost during service life and energy efficiency [1]. In addition to general construction, construction activity has also been extending to coastal areas because of the increasing number of oil and seabed mining operations. A large portion of these installations has been made from Portland cement concrete and there are greater demands of it for increased safety and long-term durability [2]. Performance of concrete is generally judged by its strength and durability properties [3]. ACI Committee 201 defined concrete durability as: its resistance to deteriorating influences, which may through inadvertence or ignorance reside in the concrete itself, or which are inherent in the environment to which the concrete is exposed [1]. Concrete is a complex composite material, whose internal structure and properties can change over time. It is generally recognized that the environmental degradation of concrete infrastructure is a major concern to the construction industry around the world [4]. Specifying concrete merely on strength considerations while ignoring number of other factors essentially related to durability will cause a gross mismatch between the specifications for concrete and the characteristics of the environment and would result in a number of problems of varying severity [5].

Concrete is a composite material comprising of cement, aggregates, chemical admixtures, mineral admixtures and water [2]. It is a versatile material with its own special properties. Cement paste is the active constituent of concrete and the performance of concrete is mainly determined by the characteristics of cement paste. The major constituents of unhydrated cement are tricalcium silicate (C_3S: $3CaO.SiO_2$), dicalcium silicate (C_2S: $2CaO.SiO_2$), tricalcium aluminate (C_3A: $3CaO.Al_2O_3$) and tetracalcium aluminoferrite (C_4AF: $4CaO.Al_2O_3.Fe_2O_3$). When the required amount of water is added to the concrete mix, hydration of cement takes place through chemical reactions that result in formation of hydration products. The hydration of cement is exothermic in nature and results in the hardening of concrete as it progresses. Normally, gypsum is added to the cement clinker

to control the early setting and hardening behaviour of cement [6, 7]. The hydration of major compounds i.e. calcium silicates such as C_3S and C_2S forms calcium silicate hydrate (C-S-H), which occurs as fine fibrous growths and calcium hydroxide ($Ca(OH)_2$), which occurs as platy hexagonal crystals [8]. These hydration products bridge the individual particles, fill up the capillary pores, bind the aggregates together, and promote the formation of rigid microstructure and strength development of concrete [9]. The minor compounds such as C_3A and C_4AF react with gypsum ($CaSO_4.2H_2O$), which is interground with Portland cement clinker as setting time regulator, to form first a trisulfoaluminate ($3CaO.Al_2O_3.3CaSO_4.32H_2O$) also called as primary ettringite, which appears in thin needles and then a monosulfoaluminate ($3CaO.3CaSO_4.12H_2O$), which appears in platy crystals [10]. The hydrated cement paste exhibits capillary porosity with the pores partially filled with the pore solution. The pore solution of concrete is highly alkaline with a pH value between 12-14, which is due to the presence of calcium hydroxide along with small amounts of Na_2O and K_2O [9].

Reinforced concrete structures are affected by various durability problems during their service life. Corrosion of steel in concrete is a serious durability problem encountered in reinforced concrete structures around the world [3]. Corrosion of steel reinforcement initiates due to its exposure to aggressive agents that may be found in nature such as in some groundwater, soil, seawater; and also exposure to industrial effluents. The most aggressive ions that affect the long term durability of reinforced concrete structures are the chloride and sulfate ions [11]. Corrosion deterioration in bridge decks, parking structures, coastal structures etc. are some of the significant durability problems encountered in civil infrastructure. The repair and maintenance of the corroded reinforced concrete structures incurs huge cost. For instance in United States of America, it was estimated in the year 1989 that more than $20 billion are needed for repair of corroded steel-reinforced concrete bridges [12]. According to a Federal Highway Administration (FHWA) corrosion cost study in the year 2002, the estimated total cost of corrosion is $276 billion per year, which makes 3.1% of the national Gross Domestic Product (GDP) in U.S.A. [13]. In UK, the Department of Transport estimated a total repair cost of £616.5 million due to the damage caused by corrosion in motorway bridges [14].

Keeping in view the detrimental effect of degradation processes, it should be realized that a basic understanding of these processes is needed by all involved in the design and construction of reinforced concrete structures [10]. Careful consideration of all potential

deterioration mechanisms at the design stage can permanently protect the steel reinforcement embedded in concrete against corrosion during normal service life of reinforced concrete structures, even under aggressive environmental conditions [15].

1.2 PASSIVATION OF STEEL IN CONCRETE

The highly alkaline environment in concrete results in the formation of a tightly adhering thin protective film of iron oxide of few nanometers thick on the surface of reinforcing steel, which passivates the steel and protects it from corrosion [16, 17, 18]. This passive layer is composed of more or less hydrated iron oxides with varying ratios between Fe^{2+} and Fe^{3+} [18]. The passive layer is dynamic in nature i.e. it will breakdown and reform and lasts long under favorable conditions [17]. This protective layer on the surface of reinforcing steel prevents iron cations (Fe^{++}) from entering into the solution in the electrolyte and acts as a barrier to prevent oxygen anions (O^{2-}) from contacting the steel surface [19].

1.3 CORROSION OF STEEL REINFORCEMENT IN CONCRETE

Corrosion is the destructive attack of a metal by chemical or electrochemical reactions with its environment [20]. Steel is thermodynamically unstable on earth's atmosphere and always has the tendency to revert to the lower energy state such as oxide and hydroxide by reactions with oxygen and water [21]. Corrosion of steel in concrete can occur, if the concrete is not of adequate quality, the structure is not properly designed for the service environment, or the environment was not as anticipated or changed during the service life of the concrete structure [16]. As already stated, corrosion of steel reinforcement is one of the most significant degradation problems encountered in reinforced concrete structures and has major financial implications around the world. Corrosion initiation of steel reinforcement takes place, if the passivity of steel gets disrupted. The depassivation of steel reinforcement occurs, if the concrete is permeable to the extent that carbonation front reaches the concrete in contact with steel and lowers the pH to about 9 or soluble chlorides can penetrate up to the steel reinforcement level, and water and oxygen are present [6, 22]. The corrosion of steel reinforcement proceeds only when oxygen and moisture are available in the vicinity of the steel reinforcement. Hence, there is no corrosion in dry or totally submerged concrete even in the presence of large quantities of

chloride ions [6]. Once corrosion is initiated, it is the electrical conductance of the concrete that controls the rate of corrosion.

Corrosion is often indicated by rust spots, which appear on the external surface of the concrete, or by cracks in the concrete cover developed by the expansion of the corrosion products. The corrosion products occupy a much larger volume than the original steel. Depending on the composition and degree of hydration, the volume of the corrosion products can be 2 to 6 times greater than that of the original steel [18]. The products of corrosion is a mixtures of iron oxides such as Fe_3O_4, $Fe(OH)_2$, $Fe(OH)_3$, $Fe(OH)_3.3H_2O$, whose volumes are 2, 3, 4, and 6 times respectively greater than the parent steel [18]. As the corrosion progresses, the corrosion products continue to accumulate and produce tensile stresses, which generate cracks in the concrete cover and results in spalling in the localized area or complete delamination of concrete.

1.4 ELECTROCHEMICAL MECHANISM OF STEEL REINFORCEMENT CORROSION

Corrosion of reinforcing steel is an electrochemical process involving a galvanic cell, wherein chemical energy is converted to electrical energy [20]. Once corrosion is initiated, it progresses almost at a steady rate and shortens the service life of the reinforced concrete structure, by causing surface cracking and subsequently spalling of the concrete cover [23]. The rate of corrosion directly affects the extent of remaining service life of a corroding reinforced concrete structure. The corrosion occurs because of the difference in the electrochemical potential on the steel surface, which forms anodic and cathodic regions, connected by an electrolyte in the form of concrete pore solution [23]. The electrode at which the oxidation occurs (or +ve electricity leaves the electrode and enters the electrolyte) is called as anode, and that at which the chemical reduction occurs is called as cathode [20]. The reactions at anodes and cathodes are referred as half-cell reactions [16].

The overall process of corrosion is complex. In the corrosion process, due to the difference in the potential between anodic and cathodic regions, positively charged metal ions at the anode pass into the solution as Fe^{++} and the free electrons (e^-) pass along the steel into the cathode. These electrons are absorbed by the constituents of the electrolyte and combine with water and oxygen to form hydroxyl ions. The hydroxyl ions complete

the electric circuit by moving back to the anodic site, where they combine with the ferrous ions (Fe^{++}) to form ferric hydroxide i.e. the rust product [6, 9, 20]. The schematic diagram of electrochemical mechanism of corrosion of steel in concrete is shown in Fig. 1.1 [24] and the electrochemical reactions are described as follows [6]:

$$Fe \rightarrow Fe^{++} + 2e^{-} \quad (1.1)$$

$$4e^{-} + O_2 + 2H_2O \rightarrow 4(OH)^{-} \quad (1.2)$$

$$Fe^{++} + 2(OH)^{-} \rightarrow Fe(OH)_2 \quad (1.3)$$

$$4Fe(OH)_2 + 2H_2O + O_2 \rightarrow 4Fe(OH)_3 \quad (1.4)$$

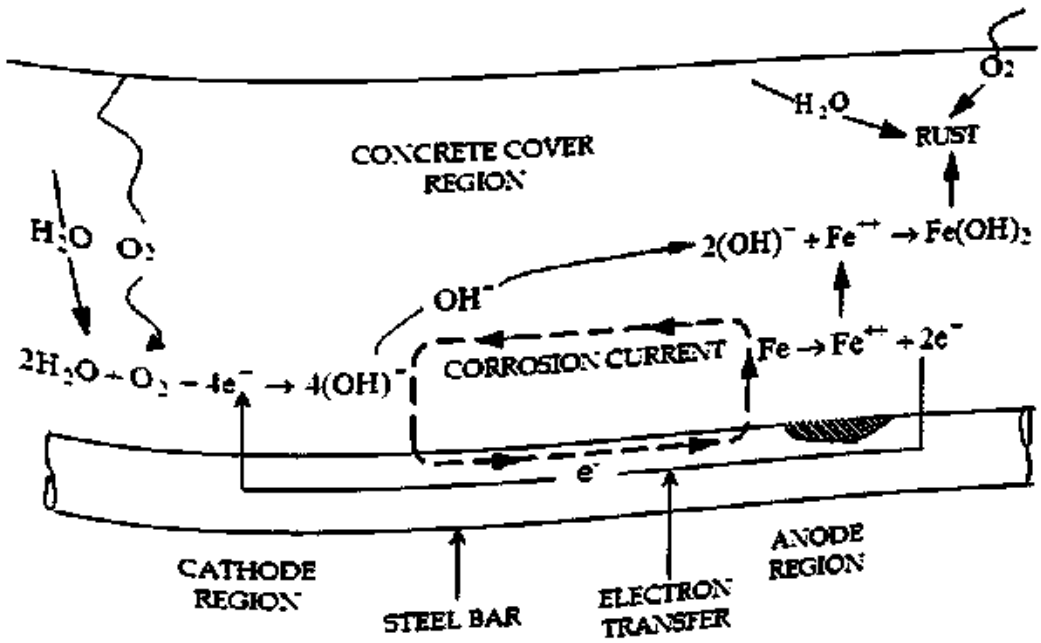

Fig.1.1 Basic corrosion process of steel reinforcement in concrete [24]

The corroding steel has an open circuit potential also called as rest potential; which is related to the standard redox potentials of the reactions shown in Eq. 1.1 and Eq. 1.2. composition of the aqueous medium, temperature, and polarization of these half-cells [16]. The rates at which the anodic and cathodic processes take place depend on the electrochemical potential.

1.5 CORROSION TENDENCY

The tendency of a metal to corrode in an environment depends on the thermodynamics, which provides information about the energy changes involved in the electrochemical reactions of corrosion [25]. The energy changes provide the driving force and control the spontaneous direction for the chemical reaction. Therefore, the information on the

conditions to make corrosion impossible can be obtained from thermodynamics. M. Pourbaix developed a summary of thermodynamic data in the form of equilibrium potential-pH diagrams that relate to the electrochemical and corrosion behavior of metals in aqueous environment [25, 26]. The Pourbaix diagram of iron in water at 25 °C is illustrated in Fig. 1.2. The Pourbaix diagram is useful in identifying potential-pH domains i.e. domains of immunity, passivity and corrosion as shown in Fig. 1.2.

In potential-pH diagram (Fig. 1.2), the domains of stability of various substances considered are bounded by lines that represent conditions of equilibrium for the different reactions involved. In the Pourbaix diagram (Fig. 1.2), the vertical lines represent the chemical reactions involving H^+ and OH^- ions, sloping lines denote electrochemical reactions involving H^+ and OH^- ions and horizontal lines represent the electrochemical reactions without participation of H^+ and OH^- ions. In the equilibrium potential-pH diagram for the Fe – H_2O system at 25 °C shown in Fig. 1.2, the concentrations of dissolved ions other than H^+ and OH^- are taken as 1 μmol/l and the solid phases are assumed to be pure [26];.

In the corrosion domain, the soluble ions are stable and are likely to be associated with corrosion, since the anodic reactions leading to the formation of Fe^{2+} or $FeO.OH^-$ are thermodynamically favoured and the reactions are as follows [26];

$$Fe = Fe^{2+} + 2e^- \quad (1.5)$$

$$Fe + 3OH^- = FeO.OH^- + H_2O + 2e^- \quad (1.6)$$

In the passive domain, the oxides, Fe_3O_4 and Fe_2O_3 are stable and are likely to exhibit a condition of passivity, since significant corrosion may be stifled due to the anodic formation of a protective oxide layer on the metal surface and the reactions are as follows [26];

$$3Fe + 4H_2O = Fe_3O_4 + 8H^+ + 8e^- \quad (1.7)$$

$$2Fe + 3H_2O = Fe_2O_3 + 6H^+ + 6e^- \quad (1.8)$$

In the immune domain, Fe is stable and immune from corrosion, since the metal is thermodynamically unable to undergo anodic reactions [26].

The equilibrium potential-pH diagrams provide useful information for predicting the conditions under which the particular reactions are likely to influence the corrosion behaviour of the metals. However, these diagrams do not convey any information on the kinetics of the possible reactions [26].

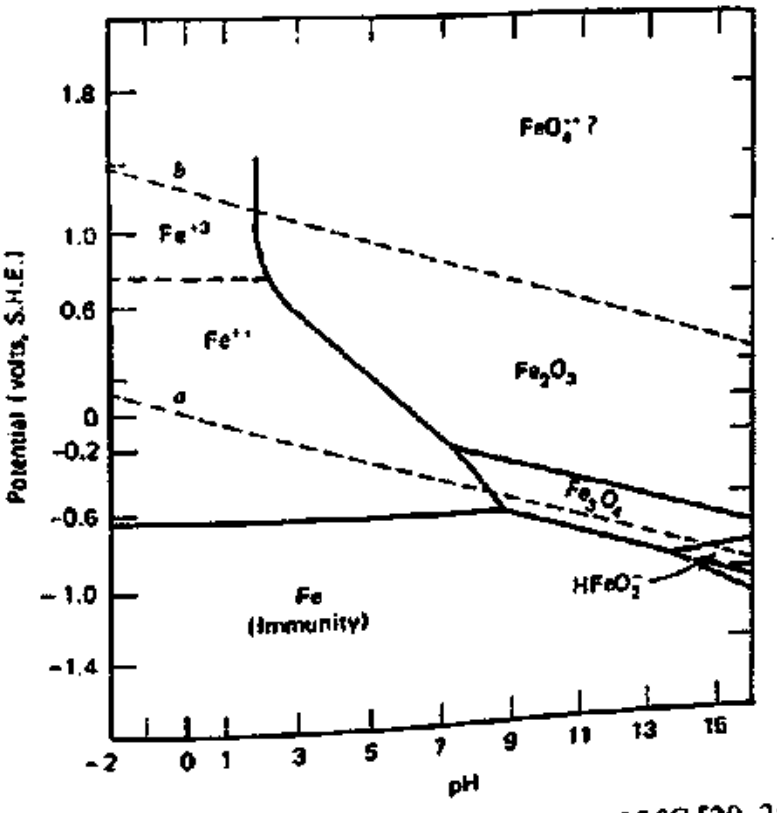

Fig. 1.2 Pourbaix diagram for Fe – H_2O system at 25 °C [20, 25, 26]

1.6 ELECTROCHEMICAL POLARIZATION

The electrochemical polarization also known as polarization, is the change in electrode potential caused by net current flow [20]. The measured potential of the electrode is altered to an extent that depends on the magnitude of the external current and its direction. The corrosion behaviour of the reinforcing steel can be described by means of polarization curves that relate the potential with anodic or cathodic current density [27, 18]. The degree of polarization is defined as overpotential and is given by the following relationship [26, 27];

$$\eta = E - E_o \qquad (1.9)$$

Where, η is the overpotential, E is the electrode potential for some condition of current flow and E_o is the electrode potential for zero current flow, also known as corrosion potential, open-circuit potential or rest potential. Anodic polarization is the displacement of the electrode potential in the positive direction ($E > E_o$), so that the electrode acts more anodic. In other words, for anodic polarization, electrons are removed from the metal and the deficiency of electrons results in a positive potential change due to slow liberation of electrons by the surface reaction. Cathodic polarization is the displacement of the electrode potential in the negative direction ($E < E_o$), so that the electrode acts more

cathodic. For cathodic polarization, electrons are supplied to the metal surface and the buildup of the electrons due to slow reaction rate results in a negative potential change [25].

The potential of the working electrode is measured with respect to a reference electrode and the current is applied through an auxiliary electrode. The polarization curves are determined by the corrosion monitoring instrument i.e. potentiostat [15]. The polarization curves provide quantitative information about instantaneous corrosion rate of working electrode through Tafel extrapolation method. Further from the linear polarization resistance technique, the polarization curve for a few millivolts around the corrosion potential provides quantitative information about instantaneous corrosion rate through the measurement of polarization resistance [15].

The polarization curves may also provide information about the morphology of attack (generalized corrosion or passivation and pitting) and the effects of different depassivating substances may also be compared through the determination of pitting or breakdown potential. The polarization curves also provide information about the protection potential (thermodynamic information) and protection current density (kinetic information) for the steel reinforcement. To obtain the polarization curves, polarization may be applied by any one of three methods viz. potentiodynamic, potentiostatic or galvasnostatic. The potentiodynamic and potentiostatic polarization methods are based on measurement of current at controlled potential, whereas galvanostatic polarization method is based on measurement of change in potential at fixed current [15].

The concrete is a complex composite material. The characteristics of concrete and its electrolyte dominantly affect the corrosion process. In addition to the moisture content that affects conductivity and imperviousness of concrete that affects polarization, the characteristics of non-uniformity of concrete from place to place also affect the corrosion process to a greater extent [28]. Due to this variability in the electrolytic environment of concrete and its high resistivity, it is complicated to conduct polarization study on steel embedded in concrete [29]. However, the polarization curves can be determined indirectly by conducting polarization study on steel reinforcement in simulated concrete pore solutions.

1.7 CAUSES OF STEEL REINFORCEMENT CORROSION IN CONCRETE

As already stated earlier, the most significant causes of corrosion of reinforcing steel in concrete are carbonation and presence of chloride ions at the steel reinforcement level in concrete.

1.7.1 Carbonation Induced Steel Reinforcement Corrosion in Concrete

Carbonation is the reaction of carbon dioxide with the hydrated cement [6]. The atmospheric carbon dioxide enters the pores of concrete and dissolves in the pore water to form carbonic acid, which in turn reacts with calcium hydroxide ($Ca(OH)_2$) to form insoluble calcium carbonate ($CaCO_3$) as shown in Eq. 1.10 and Eq. 1.11 [17].

$$CO_2 + H_2O \rightarrow H_2CO_3 \quad (1.10)$$

$$Ca(OH)_2 + H_2CO_3 \rightarrow CaCO_3 + 2H_2O \quad (1.11)$$

The reaction in Eq. 1.11 results in a significant reduction in the alkalinity of concrete pore solution due to removal of hydroxyl ions from the pore water. At low pH value, the passive film is depassivated and corrosion can occur [30]. The rate of carbonation depends on the permeability of concrete, its moisture content; and on CO_2 content and relative humidity of the ambient medium [6].

1.7.2 Chloride Induced Steel Reinforcement Corrosion in Concrete

The chloride induced steel reinforcement corrosion is a serious durability problem in reinforced concrete structures. Chloride ions are considered to be the primary cause of corrosion and play a dominant role in initiating the corrosion in concrete by depassivating the protective layer of steel reinforcement [31]. Chloride ions may enter into the concrete through two routes namely; (i) incorporated in concrete during mixing and/or (ii) penetration into hardened concrete from the external environment [16, 32, 33].

During mixing, the chloride ions enter into the concrete through chloride contaminated aggregates, chloride containing admixtures, or mixing water. In the hardened concrete, chloride ions may enter through deicing salts, seawater, soil, and groundwater, which contain chloride salts [32, 33]. In case of incorporation of chloride ions during mixing of concrete, the chlorides readily react with the aluminate and ferrite phases in cement to form the incongruently soluble chloride compounds. In case of penetration of chloride ions into the hardened concrete, the rate of formation of the chloride compounds is

reduced as the hydration proceeds [34]. Not all the chloride ions that are in or penetrate into concrete remain free in the pore solution. Some of the chloride ions are bound with the cement hydrates through a chemical reaction to form calcium chloroaluminate (Friedel's salts) [35 - 37], while others get adsorbed on various hydrates of cement [18]. Thus, only a portion of the chloride ions remains free. Equilibrium conditions tend to establish between free chloride ions and bound chlorides, depending on the composition of the cement and its binding capacity [18]. The binding of chloride ions is affected by the associated cations of the chloride sources for instance, in case of calcium chloride ($CaCl_2$), the binding of chloride ions is higher than that in case of sodium chloride (NaCl) [38]. It is the free chloride ions in the pore solution that are mainly responsible for causing damage to the concrete structures by disrupting passive layer of reinforcing steel.

The disruption of the passive layer takes place when the concentration of chloride ions in the vicinity of the reinforcing steel exceeds the threshold value [39, 40] and it depends on various factors such as cement type, concrete mix proportion, water/cement (w/c) ratio, C_3A content of the cement, blended materials, chloride binding, steel type/steel surface condition, concentration of hydroxyl ions, temperature, relative humidity and source of chloride ions etc.

There are three theories regarding the effect of chloride ions on corrosion of reinforcing steel: (a) Oxide Film Theory- according to this theory, chloride ions penetrate the oxide film (passive film) on steel through pores or defects in the film easily than other ions (e.g., SO_4^{2-}). Alternatively, the chloride ions may colloidally disperse on the oxide film thereby making it easier to penetrate; (b) Adsorption Theory- according to this theory, chloride ions are adsorbed on the rebar surface in competition with dissolved oxygen or hydroxyl ions. Thus, chloride ions promote the hydration of the iron ions and facilitate the corrosion of reinforcing steel; and (c) Transitory Complex Theory- according to this theory, the chloride ions compete with hydroxyl ions for the ferrous ions produced by corrosion and forms a complex of iron chloride. This complex can diffuse away from the anode, destroy the passive layer of $Fe(OH)_2$ and permit corrosion to continue. The complex of iron chloride breaks down at some distance from electrode leading to precipitation of iron hydroxide and the chloride ions are free to transport more ferrous ions from the anode [9, 16]. The reactions are presented in Eq. 1.12 and Eq. 1.13.

$$Fe(OH)_x + xCl^- \rightarrow FeCl_x + xOH^- \quad (1.12)$$

$$FeCl_x + xOH^- \rightarrow Fe(OH)_x + xCl^- \quad (1.13)$$

Where 'x' can be 2 or 3, depending on the oxidation state of iron. The non-homogeneous distribution of chloride ions over the steel surface and the imperfections of the passive iron oxide film allow easy incorporation of the chloride ions and breakdown of the passive film locally. The local active areas act as anodes where the iron will easily dissolve at a relatively low potential and the remaining passive area acts as cathode where, oxygen reduction takes place at a higher potential [9].

1.8 SERVICE LIFE OF REINFORCED CONCRETE STRUCTURES

The functional service life of reinforced concrete structures affected by the ingress of aggressive species like carbon dioxide and/or chloride ions is divided into two distinct phases [18]. The first phase is corrosion initiation and the second phase is corrosion propagation. Tuutti's model [18] shown in Fig. 1.3 indicates the initiation and propagation periods for corrosion in the reinforced concrete structures. The corrosion initiation period is represented by the time needed for CO_2 or chloride ions to transport from the external environment through the concrete cover and reach the steel reinforcement in sufficient concentration such that the protective passive layer on steel reinforcement may be locally destroyed. Once the corrosion is initiated, its propagation is controlled primarily by the supply of oxygen and moisture on the surface of steel reinforcement. The length of the corrosion propagation period is the time period from the end of corrosion initiation period till the time it takes to reach any one of the critical conditions in the life of structure such as, a severe loss of cross-section of the steel reinforcement, cracking of the concrete cover, spalling and delamination of the concrete cover and eventually collapse, as shown in Fig. 1.3 [18].

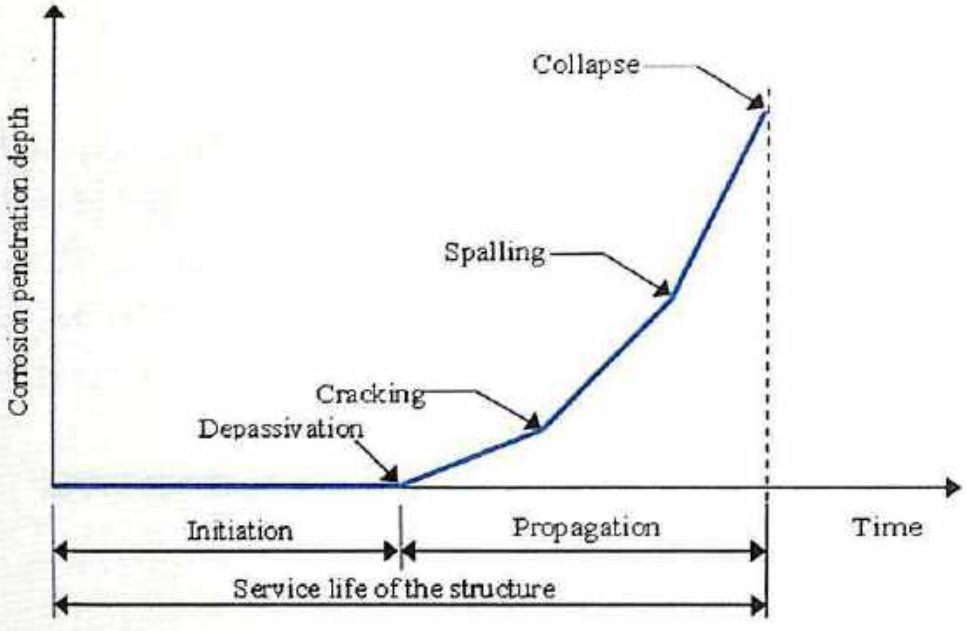

Fig. 1.3 Initiation and propagation periods for corrosion in a reinforced concrete structure (Tuutti's model) [18]

1.9 SULFATE ATTACK

Sulfate attack is one of the major threats to the durability of concrete. When concrete is in contact with the salts containing sulfate, interactions between solid phase and sulfate solution occur in the concrete, leading to chemical reactions and subsequently to the deterioration of concrete [41]. The severity of attack depends mainly on the concentration of the sulfates in the soil or in the water in contact with concrete; and also on the cation type associated with sulfate ions [18]. Vicat, as early as in the year 1818, reported a chemical attack on concrete due to the presence of sulfate ions in sea water, while in the year 1890, Candolt established the formation of an expansive hydration product by the interaction of aqueous solutions of calcium aluminates and calcium sulfate [42]. Michaelis in the year 1892, attributed the disruption of concrete when attacked by sulfate waters, to the reaction between C_3A in Portland cement and sulfate ions leading to the formation of ettringite [42].

Sulfate attack is initiated mainly due to the contribution of sulfate ions by the external exposure conditions. In addition, the sulfate ions are also sometimes originated in the concrete mix internally through contaminated aggregates, mixing and curing water, and admixtures [43]. The different sulfate salts, which are present in the soils and groundwater are sodium sulfate, magnesium sulfate and calcium sulfate. Since the solubility of calcium sulfate is very low, sulfate attack is predominantly attributed to the

reaction of cement hydrates with sodium sulfate and magnesium sulfate [44]. Sulfate ions attack some or all of the three main hydrate compounds of hardened concrete i.e. calcium hydroxide, calcium aluminate hydrate and calcium silicate hydrate, depending on the type of sulfate in the solution involved [42].

Action of sulfate ions on calcium hydroxide:

Sodium sulfate and magnesium sulfate can react with the calcium hydroxide formed in the hydration of calcium silicates to form gypsum ($CaSO_4.2H_2O$), sodium hydroxide (NaOH) and magnesium hydroxide ($Mg(OH)_2$) according to the following reactions [17, 42, 45, 46].

$$Ca(OH)_2 + Na_2SO_4 + 2H_2O \rightarrow CaSO_4.2H_2O + 2NaOH \quad (1.14)$$

$$Ca(OH)_2 + MgSO_4 + 2H_2O \rightarrow CaSO_4.2H_2O + 2Mg(OH)_2 \quad (1.15)$$

The formation of gypsum is destructive due to increase in volume that leads to expansion of the concrete and results a reduction in stiffness and strength of concrete [17, 45].

Action of sulfate ions on calcium aluminate hydrates:

The gypsum formed in reactions shown in Eq. 1.14 and Eq. 1.15 can react with hydrated calcium aluminates ($4CaO.Al_2O_3.13H_2O$), hydrated calcium sulfoaluminates ($3CaO.Al_2O_3.CaSO_4.12H_2O$) or unhydrated tricalcium aluminates ($3CaO.Al_2O_3$) and forms ettringite ($3CaO.Al_2O_3.3CaSO_4.32H_2O$), which is shown in Eq. 1.16, Eq. 1.17 and Eq. 1.18 [17, 45].

$$4CaO.Al_2O_3.13H_2O + 3(CaSO_4.2H_2O) + 14H_2O \rightarrow 3CaO.Al_2O_3.3CaSO_4.32H_2O + Ca(OH)_2 \quad (1.16)$$

$$3CaO.Al_2O_3.CaSO_4.12H_2O + 2(CaSO_4.2H_2O) + 16H_2O \rightarrow 3CaO.Al_2O_3.3CaSO_4.32H_2O \quad (1.17)$$

$$3CaO.Al_2O_3 + 3(CaSO_4.2H_2O) + 26H_2O \rightarrow 3CaO.Al_2O_3.3CaSO_4.32H_2O \quad (1.18)$$

The formation of ettringite (Eq. 1.16 to Eq. 1.18) primarily leads to an increase in solid volume greater than the original constituents. The increase in volume causes expansion, which is attributed to the pressure exerted by the growth of ettringite crystals and to the swelling due to the absorption of water by poorly crystalline ettringite [17, 18, 45].

Action of sulfate ions on calcium silicate hydrate:

In addition to the formation of expansive ettringite and gypsum, sulfate ions can also react with the calcium silicate hydrate (C-S-H) formed in the hydration of dicalcium

silicate and tricalcium silicate. The decalcification of C-S-H occurs only due to the effect of magnesium sulfate and the reactions are as follows;

$$3CaO.2SiO_2.3H_2O + 3MgSO_4 + 8H_2O \rightarrow 3(CaSO_4.2H_2O) + 3Mg(OH)_2 + 2SiO_2H_2O \quad (1.19)$$

The reaction shown in Eq. 1.19 produces more gypsum, which would react with the calcium aluminates (Eq. 1.16 to Eq. 1.18) to produce more ettringite. The magnesium hydroxide ($Mg(OH)_2$) and the silica hydrate ($SiO_2.H_2O$) formed from reaction shown in Eq. 1.19 can react together to form non-cementitious magnesium silicate hydrate (M-S-H) as shown in Eq. 1.20 [17, 45].

$$4Mg(OH)_2 + SiO_2.nH_2O \rightarrow 4MgO.SiO_2.8.5H_2O + (n-4.5)H_2O \quad (1.20)$$

The decalcification of C-S-H into non-cementitious M-S-H is possible only due the attack of $MgSO_4$. Thus, magnesium sulfate has more damaging effect on concrete than sodium sulfate.

1.10 BEHAVIOUR OF CONCRETE IN CONJOINT CHLORIDE-SULFATE ENVIRONMENT

The environmental and geomorphical conditions in the coastal areas contribute to a reduction in the service life of concrete structures; particularly due to contamination of soil and groundwater with chloride and sulfate salts [19]. Both chloride and sulfate salts are present in seawater and groundwater. In the conjoint presence of chloride and sulfate ions, the mechanism of deterioration of concrete becomes complex due to the simultaneous interaction of these ions with hydrated cement phases. The presence of sulfate ions may influence the chloride attack and similarly the presence of chloride ions may affect the sulfate attack in concrete. Further, the cation type associated with these aggressive ions makes the mechanism even more complex. When chloride ions are present in the concrete, they chemically combine with C_3A phase of cement and forms calcium chloroaluminate (Friedel's salt) as shown in Eq. 1.21 [47], thereby reducing their deleterious effect on promoting corrosion of steel reinforcement. If sulfate ions are also present along with chloride ions, then they compete with chloride ions to react with C_3A and produce ettringite (as shown in Eq. 1.22 and Eq. 1.23) that results in disruptive expansion and disintegration of concrete into non-cohesive granular mass [18].

$$3CaO.Al_2O_3 + Ca(OH)_2 + 2Cl^- + 10H_2O \rightarrow 3CaO.Al_2O_3.CaCl_2.10H_2O + 2OH^- \quad (1.21)$$

$$Ca(OH)_2 + SO_4^{2-} + 2H_2O \rightarrow CaSO_4.2H_2O + 2OH^- \quad (1.22)$$

$$3CaO.Al_2O_3 + 3CaSO_4 + 32H_2O \rightarrow 3CaO.Al_2O_3.3CaSO_4.32H_2O \quad (1.23)$$

A higher proportion of C_3A in cement would reduce the corrosion inducing free chloride from the pore solution of concrete thereby reducing the risk of corrosion. On the other hand, it would pose a serious concrete durability problem in terms of sulfate attack.

1.11 NEED AND OBJECTIVES OF PRESENT RESEARCH WORK

The corrosion of steel reinforcement in concrete is a complex process. The presence of aggressive ions like chloride ions significantly affect the corrosion behaviour of steel reinforcement in concrete. Further, in the presence of both chloride and sulfate ions the corrosion behaviour of steel reinforcement may vary significantly as compared to that in the presence of only chloride ions, which may be attributed to the simultaneous interaction of these ions with hydrated cement phases in concrete. Similarly, the behaviour of concrete against sulfate attack in the presence of only sulfate ions may vary significantly as compared to that in the conjoint presence of both chloride and sulfate ions. Also, the effect of sulfate ions on performance of concrete and on chloride induced corrosion of steel reinforcement may vary with the cation type associated with sulfate ions. From the detailed literature review presented in Chapter 2, it is observed that different research works have been reported in the literature on corrosion behaviour of steel reinforcement in simulated concrete pore solution environment, and in concrete subjected to various exposure conditions. It is observed from the literature review that, the research work on corrosion behaviour of steel reinforcement in concrete powder solution extracts admixed with composite chloride-sulfate ions is very scanty. In addition, from the studies reported in literature on the effect of conjoint chloride and sulfate ions on steel reinforcement corrosion in concrete, the researchers have presented different opinions regarding the performance of concrete in composite chloride and sulfate environment. Keeping these observations in view, there is a need to carry out a study on the effect of conjoint presence of chloride and sulfate ions on electrochemical behaviour of steel reinforcement in electrolytic concrete powder solution extracts and also in concrete. Further, it is necessary to study the effect of chemical composition of the electrolytic concrete powder solution extracts on corrosion behaviour of steel

reinforcement. Also to analyze the changes in phase composition of hardened concrete in the presence of chloride and sulfate ions, there is a need to carry out microstructural studies. In addition, it is also necessary to evaluate the effect of cation type associated with sulfate ion on steel reinforcement corrosion and on the performance of concrete in composite chloride-sulfate environment with varying concentrations of chloride and sulfate ions.

Keeping in view the abovementioned research needs, the objectives of the present research work have been formulated as follows:

1a) To evaluate the effect of chloride and conjoint chloride-sulfate contamination on compressive strength of concrete.

b) To investigate the microstructure of concrete admixed with varying concentrations of chloride and sulfate ions through X-ray diffraction (XRD), Fourier transform infrared (FTIR) spectroscopy and Field emission scanning electron microscopy (FESEM) analyses.

c) To study the influence of varying concentrations of admixed chloride and sulfate ions on ionic concentration, pH and conductivity of electrolytic concrete powder solution (ECPS).

2a) To determine the ranges of potential values for different zones of corrosion namely active zone, passive zone and pitting zone of steel reinforcement through potentiodynamic polarization study in electrolytic concrete powder solutions contaminated with chloride and conjoint chloride-sulfate ions.

b) To study the effect of steel type, cement type, water-cement ratio (w/c ratio) and cation type associated with sulfate ions on passivity of steel reinforcement in electrolytic concrete powder solutions contaminated with varying concentrations of chloride and conjoint chloride-sulfate ions.

c) To assess the corrosion performance of steel reinforcement in electrolytic concrete powder solutions preapred from different types of cement, w/c ratio and contaminated with different concentrations of chloride ions and conjoint chloride-sulfate ions by measuring corrosion potential and corrosion current density.

3) To evaluate the effect of binder type and steel type on corrosion behaviour of steel reinforcement embedded in concrete in the presence of different concentrations of

conjoint chloride-sulfate ions by determining corrosion potential and corrosion current density.

4) To study the effect of binder type, w/b ratio, concentration of sulfate ions and associated cation type on variation in compressive strength of concrete exposed to sulfate and chloride-sulfate environment.

1.12 ORGANIZATION OF THESIS

The research work carried out in this investigation has been organized in eight chapters. In **Chapter 1**, introduction about the research area, need and objectives of the present research work are presented. **Chapter 2** describes the review of literature of the research work on corrosion behaviour of steel reinforcement in simulated concrete pore solution and that embedded in concrete in the presence of chloride and sulfate ions and on the performance of concrete in sulfate and chloride-sulfate environment. **Chapter 3** describes about the detailed experimental program adopted in the present research work for evaluating the corrosion behaviour of steel reinforcement and performance evaluation of concrete. **Chapter 4** presents and discusses the results on the effect of different concentrations of chloride and conjoint chloride-sulfate contaminations on 28 day compressive strength and microstructure of concrete. Further, the results of pH, conductivity and ionic concentration of electrolytic concrete powder solution (ECPS) are presented and discussed in this chapter. The results of potential ranges of different zones of corrosion of steel reinforcement in electrolytic concrete powder solution (ECPS) are presented in **Chapter 5**. Further, the influence of different concentrations of chloride and conjoint chloride-sulfate ions on passivity range, corrosion potential and corrosion current density of steel reinforcement in electrolytic concrete powder solution are presented and discussed in **Chapter 5**. In **Chapter 6**, the results of corrosion potential and corrosion current density of steel embedded in concrete admixed and subsequently exposed to conjoint chloride-sulfate ions are presented and discussed. **Chapter 7** presents and discusses the results about the role sulfate ions and conjoint chloride-sulfate ions on the performance of concrete in terms of change in weight and compressive strength. Finally, the conclusions obtained from the present research work and suggestions for further research are presented in **Chapter 8**.

CHAPTER 2

LITERATURE REVIEW

2.1 GENERAL

In this chapter, a detailed literature review on the research work carried out by various researchers on corrosion behaviour of steel reinforcement in concrete and in simulated concrete pore solution exposed to chloride and sulfate environment is presented. In addition, the reported research work on behaviour of concrete in sulfate and composite chloride-sulfate environment is also presented. The literature review is divided into following sections: (i) effect of chloride and sulfate contamination on concrete pore solution chemistry, (ii) corrosion behaviour of steel reinforcement in simulated concrete pore solution contaminated with chloride and sulfate ions; (iii) corrosion behaviour of steel reinforcement in concrete contaminated with chloride and sulfate ions; and (iv) deterioration of concrete in chloride and sulfate environment.

2.2 EFFECT OF CHLORIDE AND SULFATE CONTAMINATION ON CONCRETE PORE SOLUTION CHEMISTRY

Concrete pore solution composition is useful in understanding the deleterious reactions responsible for deterioration of concrete and in developing durability solutions [48]. The composition of the concrete pore solution reflects the ongoing hydration processes of cement and determines which solid phases are stable and may precipitate, and which phases are unstable and may dissolve. The study of concrete pore solution chemistry therefore contributes to the understanding of the mechanisms as well as the kinetics of cement hydration [49] and also of the stability of different phases in relation to various deterioration processes occurring in concrete. Various authors have investigated concrete pore solution chemistry under different conditions.

Gjorv and Vennesland [50] through their study had investigated the effect of sea salt concentration on the pH of saturated solution of $Ca(OH)_2$ and extracts of hydrated Portland cement. The extracts were prepared by rigorously mixing ordinary Portland cement and water in 1:1 proportion by weight for 30 minutes and kept for 3 hours for

hydration and settling, and then the liquid phase was filtered. The salt solutions were prepared by mixing $Ca(OH)_2$ solution or cement extracts with 20% salt suspension to a total volume of 100 ml. The results of the experimental investigation indicated that the sea salt concentrations up to 1% and 4% in saturated $Ca(OH)_2$ solutions and in the extracts of hydrated Portland cement respectively did not lower the pH to more than about 12.0 and subsequent increase of sea salt concentration of more than 2% and 6% respectively resulted in a sharp reduction of pH to about 10. However, further increase in sea salt concentration reduced the pH at a very slow rate. In addition, the authors found that the effect of sea salt on pH depends on the availability and amount of reserve basisity present in the solution. It is also observed that, as much as 20% NaCl did not reduce the pH of saturated $Ca(OH)_2$ solutions.

Yonezawa et al. [51] have studied the pore solution composition and effect of chloride ion on corrosion of steel in concrete. Ordinary Portland cement and water to cement ratio of 0.5 were used in the preparation of specimens. Cylindrical mortar specimens of 22 mm diameter and 100 length with a centrally embedded 8 mm diameter mild steel electrode were used for studying the electrochemical behaviour of steel. To extract the pore solution, cylindrical mortar specimens of 40 mm diameter and 100 mm length were used in the study. Two conditions were adopted to examine the electrochemical behaviour of steel electrode; first, the steel electrode embedded in the mortar specimen and second, the steel electrode directly immersed in the saturated $Ca(OH)_2$ solution or 0.4 M KOH + 0.2 M NaOH solution. The varying concentrations of NaCl [0, 0.52 M (3%), and 2.84 M (15%)] were added in the $Ca(OH)_2$ immersion test. The same concentrations of NaCl as that was added in the $Ca(OH)_2$ solution was added to the mixing water while preparing the mortar specimens. After 14 days of demoulding, the mortar specimens were immersed in the $Ca(OH)_2$ solution containing varying concentrations of NaCl. Corrosion potential and polarization resistance were measured by polarizing the steel cathodically to 10 mV from the corrosion potential at a sweep rate of 10 mV/min. During testing, the solutions were aerated using moistened and decarbonated air. After testing the mortar specimens, the steel electrodes embedded in the mortar were removed by splitting the mortar and their surfaces and the interface between the steel and the partly remaining mortar were examined by scanning electron microscope. For pore solution extraction, the mortar specimens were demoulded after one day and then immersed in the test solution, and in case of test on the specimens without immersion, the mortar specimens were placed for

aging in a polypropylene container in a completely sealed condition. The pore solution of the mortar specimens was extracted using the high pressure technique. The concentrations of OH^- and Cl^- ions in the expressed solution were analyzed. From the results, the authors reported that the passivity of steel in mortar is sustained at much higher $[Cl^-]/[OH^-]$ ratios in the pore solution as compared to the steel immersed directly in alkaline solutions. It is found from the results that, one of the protective mechanisms provided by mortar is the dissolution of calcium hydroxide crystals at the steel-mortar interface of an actively corroded electrode and it serves to restrain the pH drop on the steel surface. For the protective mechanism provided by mortar to operate, the adhesion between steel and mortar is necessary and the formation of voids at steel-mortar interface is necessary for active corrosion to steel reinforcement. The authors also reported that the critical threshold chloride content is not determined simply by a parameter of the pore solution such as $[Cl^-]/[OH^-]$ ratio, it depends on the steel-mortar interface conditions.

Andersson et al. [52] through their study have determined the chemical composition of pore solutions extracted from seven different cement pastes (viz. Swedish standard Portland cement, French standard Portland cement, sulfate resistant, blast furnace slag, fly ash, silica, and high alumina cements). Cylindrical specimens of 45 mm diameter and 80 mm height were prepared. Water/cement ratio of 0.5 was used in the study. The pore solution was obtained by applying high pressure to cylindrical cement paste specimens. The cations (Al, Ca, Fe, K, Mg, Na, Si) in the pore solution were determined by flame atomic absorption spectrometry and pH of the pore solution was also measured. The results indicated that the cement pore solutions had fairly high ionic strengths (up to 0.3 M) and pH in the range of 12.4 – 13.5. The authors found that the dominating cation in the pore solution extracted from these cement pastes were Na and K, except for the high alumina cement in which dominating cations were Na and Al. The concentrations of Si and Fe were low in all the pore solutions extracted from these cement pastes.

Goni and Andrade [53] have studied the synthetic concrete pore solution chemistry in the presence of chlorides. Synthetic saturated $Ca(OH)_2$ solutions with different $[Cl^-]/[OH^-]$ ratios were prepared from distilled decarbonated water. $Ca(OH)_2$ of 2 g/l was used in all the solutions. The OH^- concentrations were obtained by adding 0, 0.2 and 0.5 M KOH. Chloride ions (0.1, 0.5, 0.75 and 1 N) were added as NaCl and $CaCl_2$. The concentration of Ca^{2+} was determined by complexometric titration with 0.01 M EDTA and that of OH^- by titration with 0.01 M HCl. The conductivity and pH of the solutions were also

measured. From the results, the authors found that the difference in pH value of the solutions is a function of cation Na^+ or Ca^{2+} associated with chloride ions. The $[Cl^-]/[OH^-]$ ratio was higher in the solutions containing $CaCl_2$ due to lower pH as compared to the solutions containing NaCl. It was observed that addition of $CaCl_2$ produces a decrease in pH, due to the known common ion effect, which displaces the chemical equilibrium of the $Ca(OH)_2$ towards its precipitation. In the presence of $CaCl_2$, the pH values varied between 11.24 and 12.66 according to the amount of $CaCl_2$ added, despite the high concentration of KOH that was present. When NaCl was added, only small changes in the pH value was observed because it only influenced the ionic strength.

Dehwah et al. [54] have conducted a study to evaluate the influence of cement alkalinity on the pore solution chemistry and chloride-induced reinforcement corrosion. Two types of cements were used i.e. sulfate resistance Portland cement (SRPC) and ordinary Portland cement (OPC). Effective water-cement ratio of 0.45 was adopted. Cylindrical cement paste specimens of 49 mm diameter and 75 mm height were used in the study. All the paste specimens were admixed with fixed quantity of sodium chloride i.e. 0.8% Cl^- by weight of cement and varying alkalinity was adjusted to 0.4, 0.6, 0.8, 1.0, 1.2 and 1.4 % (Na_2O equivalent). The cement pastes were poured into plastic cylindrical vials and stored. The pore solution in the cement-paste specimens was extracted using high pressure pore solution expression device after 100 days of casting. The expressed pore solution was analyzed to determine OH^-, Cl^- and SO_4^{2-} ion concentrations. From the results the authors reported that the concentrations of OH^-, Cl^- and SO_4^{2-} ions in the pore solution of SRPC and OPC increased with increasing alkali content of the cements. The Cl^-/OH^- ratio decreased with increasing alkali content up to 0.8% Na_2O equivalent, then increased with a further increase in the alkalinity. The authors attributed the increase in Cl^- and SO_4^{2-} ion concentrations due to increasing alkalinity, to the solubility of calcium chloroaluminate hydrate and calcium sulfoaluminate hydrate at high alkalinities. The authors also studied the effect of alkalinity on chloride-induced reinforcement corrosion by measuring corrosion potentials and corrosion current density. For this purpose, reinforced concrete cylindrical specimens of size 75 mm diameter and 150 mm height with a 12 mm steel bar placed centrally were used. The specimens were exposed to 5% NaCl and varying alkalinities (0.4, 0.6, 0.8, 1.0, 1.2 and 1.4 % Na_2O equivalent). The level of the solution was adjusted so that only 85 mm to 90 mm from bottom of the specimen was in the solution. Corrosion potentials were measured using high impedance

voltmeter with respect to saturated calomel electrode. Corrosion current density was measured using linear polarization resistance method. The steel was polarized to ±20 mV of the corrosion potential. From the results the authors reported that the time-to-initiation of reinforcement corrosion in the SRPC and OPC concretes increased with increasing alkalinity up to 0.8% Na_2O equivalent. When the alkalinity was more than 0.8% Na_2O equivalent, decrease in the time-to-initiation of reinforcement corrosion was noted. The corrosion current density in SRPC and OPC concrete specimens was lowest when the alkalinity was 0.8% Na_2O equivalent. However, it was increased with further increase in alkalinity. Based on the test results, the authors suggested that the alkali content of cement can be increased to 0.8% Na_2O equivalent to increase the corrosion resistance of concrete.

Through another study Dehwah et al. [55] have investigated the effect of cation type associated with sulfate ions in the presence of chloride ions on pore solution chemistry. The major test variables were six types of cements viz. sulfate resisting Portland cement (SRPC; C_3A: 3.6%), ordinary Portland cement (OPC-A; C_3A: 8.5% and OPC-B; C_3A: 9.65%), 20% fly ash, 10% silica fume, and 70% blast furnace slag as replacement by weight of OPC-A cement. A water-to-cementitious material ratio of 0.45 was used in the study. Cylindrical paste specimens of 49 mm diameter and 75 mm height were prepared. The specimens were admixed with fixed quantity of chloride (0.8% Cl^-) and varying dosages of sulfate salts (1%, 2.5% and 4% SO_4^{2-}). Sodium chloride was used as source of Cl^- ions and $MgSO_4$ and Na_2SO_4 were used as the source of SO_4^{2-} ions. High-pressure pore solution expression device was used to extract pore solution after 100 days of casting to determine OH^-, Cl^- and SO_4^{2-} ion concentrations. From the results, the authors reported that the OH^- concentration was more in pore solution of plain and blended cements, when the specimen was exposed to NaCl plus Na_2SO_4 as compared to that exposed to NaCl plus $MgSO_4$ and increased with increase in the sulfate concentration. The OH^- concentration was lower in the blended cements as compared to that in the plain cements, which is due to the reaction between $Ca(OH)_2$ and pozzolanic material. The Cl^- and SO_4^{2-} ion concentrations of the pore solution were more in the specimens exposed to NaCl plus Na_2SO_4 than the specimens exposed to NaCl and NaCl plus $MgSO_4$ and increased with increase in the sulfate concentration in all the plain and blended cements. It was also reported that the Cl^- and SO_4^{2-} ion concentrations were lower in the blended cements as compared to plain cements. The presence of sulfate and chloride influences the alkalinity

of the pore solution and enhances the reinforcement corrosion. Thus, the authors concluded that to improve the durability of concrete and to reduce reinforcement corrosion, sulfate and chloride contamination should be controlled.

2.3 CORROSION BEHAVIOUR OF STEEL REINFORCEMENT IN SIMULATED CONCRETE PORE SOLUTION CONTAMINATED WITH CHLORIDE AND SULFATE IONS

The research works carried out by various researchers on corrosion behaviour of steel reinforcement in simulated concrete pore solutions are presented in this section.

Henriksen [56] through his study on the corrosion and protection of steel in saturated $Ca(OH)_2$ solution contaminated with NaCl, found that for the protection against nucleation of pits, the potential of steel must be below the pitting potential. The pitting potential varied with the chloride concentration, pH, temperature and oxygen content of the solution.

Al-Tayyib et al. [57] have carried out an experimental investigation to study the effect of sulfate ion on the corrosion mechanism of steel in simulated concrete pore solution. The simulated concrete pore solution was prepared from saturated $Ca(OH)_2$ with pH value of 12.5 and different concentrations of Na_2SO_4 (0.1% - 1%) was added to study the effect of sulfate ion on rebar corrosion. Carbon steel specimens of 0.635 cm diameter and 1.27 cm length was used in the study. Experiments were conducted at two temperatures i.e. at laboratory temperature of 22° C and at elevated temperature of 50° C to evaluate the effect of elevated temperature on corrosion rate. A.C impedance technique and linear polarization resistance test were conducted on the steel specimen. From the results, the authors reported that there is an increase in the corrosion rate and decrease in polarization resistance as the sulfate concentration increased from 0% to 0.5%. From the obtained Nyquist plots at different concentrations of Na_2SO_4, it was observed that the corrosion of the reinforcing steel in concrete is not only dependent on the modification of the environment in contact with the passive film but also dependent on the modification of the film itself. Further, it was observed that the combined action of sulfate ions and elevated temperature is more corrosive than that of chloride ions at normal temperature i.e. the combined effect of sulfate ions and elevated temperature results in seven fold increase in corrosion rate compared to that of the chloride ions at normal temperature.

Pistorius and Burstein [58] have studied the effect of dilute sulphate on metastable and stable pitting of type 304 stainless steel in chloride solution. The results indicated that addition of 0.1M SO_4^{2-} to a pH 0.7 solution containing 1M Cl^- solution affects both, the initiation and propagation of pits. It was also observed that the pit initiation is partially inhibited in sulphate anions, but at high potentials this inhibitory action is lost. In the presence of sulphate, the pit propagates at lower current density.

From another study conducted by Pistorius and Burstein [59] on the effect of chloride concentration and pH on the frequency of occurrence of metastable pits on the surface of stainless steel, it was reported that the rate of occurrence of metastable pits in chloride solution decreases with decrease in chloride concentration and electrolyte pH has no observable effect on the frequency of metastable pitting.

Bertolini et al. [60] have carried out an experimental investigation to assess the localized corrosion behaviour of stainless steel in solutions simulating the pore liquid of alkaline and carbonated concrete contaminated with chloride ions at temperatures of 20 °C and 40 °C. The major test variables were AISI 304, AISI 304L, AISI 316, and AISI 316L austenitic stainless steels, 23Cr4Ni duplex stainless steel, 254 SMO superaustenitic stainless steel, AISI 410 martensitic stainless steel and carbon steel. To evaluate the pitting potential, potentiodynamic test was conducted using an ASTM cell with saturated calomel electrode (SCE) and two platinum counter electrodes in saturated $Ca(OH)_2$ solution. The steel specimens were exposed to the saturated $Ca(OH)_2$ solution for 48 hours before testing and chloride ions were added only after 24 hours of passivation. Polarization curves were obtained at a scan rate of 20 mV per minute, starting at 200 mV (SCE) below the free corrosion potential and were interrupted when the anodic current density reached to 0.5 mA/cm^2. To evaluate the critical chloride content, potentiostatic polarization test at 200 mV (SCE) was conducted in these solutions; (i) saturated $Ca(OH)_2$, (ii) 0.9 M NaOH with pH 13.9, simulating the pore solution in concrete with a high alkaline content, (iii) 0.015 M $NaHCO_3$ and 0.005 M Na_2CO_3 with pH 9, simulating carbonated concrete, iv) 0.3 M $NaHCO_3$ and 0.1 M Na_2CO_3 with pH 9, to evaluate the effect of high levels of carbonates and bicarbonates and (v) tap water containing 35 parts of $CaCO_3$ in 100000 parts of water and a pH of about 7.6, simulating an environment in which the steel reinforcement is locally not covered by concrete. The tests were carried out simultaneously on 8 specimens connected to the same potentiostat with a reference saturated calomel electrode positioned in the center and an activated titanium mesh as

counter electrode placed at the bottom of test cell. The flow of current in each specimen was monitored and chloride concentration of 0.5% in the form of NaCl was added at every 48 hours, till a concentration of 10% was reached. When the anodic current density flowing in the specimen exceeded 0.5 mA/cm^2, the corrosion was considered to be initiated. From the results of potentiodynamic test, the authors found that stainless steel reinforcement can be in the passive condition even in the presence of a high concentration of chloride ions whereas, low chloride content is sufficient to produce localized corrosion on carbon steel. Thus, the stainless steel reinforcement can delay the initiation of corrosion to a significant extent as compared to carbon steel. From the results of potentiostatic tests, the authors found the beneficial effect of alkalinity on chloride induced localized corrosion of both carbon steel and stainless steels. In saturated $Ca(OH)_2$ solution, the stainless steels exhibited a critical chloride content for corrosion initiation in the range from 2% for low chromium AISI 410 to a minimum value of 5% for austenitic and austenoferritic stainless steels. In the solutions simulating the carbonated concrete pore liquid, the critical chloride concentration decreased especially for steels with low chromium content. The authors found that in the alkaline solutions, nickel plays a beneficial role in preventing the localized corrosion. Further, superaustenitic 254 SMO steel was not affected by localized attack under all experimental conditions.

Saremi and Mahallati [61] have studied the effect of chloride ions on passivity breakdown of steel in simulated concrete pore solution by conducting cyclic potentiodynamic polarization test. The authors observed that at $[Cl^-/OH^-]$ ratio of 0 to 0.3, repassivation of the pits on the surface of steel can be performed. At $[Cl^-/OH^-]$ equal to 0.6, repair of pits is impossible and at $[Cl^-/OH^-]$ equal to 1, many pits were formed and localized corrosion occurred. Further, localized corrosion was replaced by generalized corrosion at $[Cl^-/OH^-]$ ratio greater than 1.

Moreno et al. [62] have studied the effect of carbonation and chloride content on corrosion of reinforcing steel in simulated pore solutions. The simulated solutions with different values of pH and various chloride concentrations were used to simulate the pore solution of alkaline and carbonated concrete and the effect of different levels of chloride contamination. Potentiodynamic polarization and linear polarization resistance tests were carried out in the study. From the results, the authors found that the carbon steel remains passive in high alkaline solutions and in more concentrated carbonate plus bicarbonate solution even if the potential is raised up to the potential range of oxygen evolution, but it

showed generalized corrosion at all potentials higher than the free corrosion potential in the presence of low levels of carbonates and bicarbonates. In high alkaline solution and in more concentrated carbonate plus bicarbonate solution, chloride-induced pitting resulted in a significance increase in the corrosion rate, whereas the pitting initiation has no noticeable effect on the instantaneous corrosion rate in less concentrated carbonate plus bicarbonate solution. From the potentiodynamic test, critical chloride concentration was evaluated as 1% in the solution with pH 13.9 and decreased significantly to 0.02% in the saturated $Ca(OH)_2$ solution at pH 12.5. The authors concluded that an increase in pH coupled with high percentage of carbonate and bicarbonate has a beneficial effect on the chloride threshold and improves the corrosion resistance of carbon steel reinforcement against localized corrosion.

Mammoliti and Hansson [63] have investigated the influence of sulfate cation (Na^+ or Mg^{++}) on behaviour of reinforcing steel in high-pH sulfate solutions. Two solutions of varying compositions viz. lime water solution containing calcium hydroxide [$Ca(OH)_2$] and synthetic concrete pore solutions containing 0.6 M potassium hydroxide (KOH) and 0.3 M sodium hydroxide (NaOH) with and without $Ca(OH)_2$ were used in the study. Sodium sulfate and magnesium sulfate were added in the solutions ranging from 1.25% to 6.25% by mass of added $Ca(OH)_2$. Deformed black reinforcing steel was used as the steel reinforcement. Linear polarization resistance test was conducted by polarizing the steel to ±20 mV of the open circuit potential and cyclic polarization measurements were performed by polarizing the steel from +500 mV to -1000mV at a scan rate of 1 mV/s with respect to saturated calomel electrode. From the results, the authors found that corrosion is more dependent on the cation type associated with the sulfate anion rather than the sulfate itself. It is reported that the solutions containing SO_4^{2-} ions as Na_2SO_4 in lime water are hardly able to induce reinforcement corrosion, whereas considerable corrosion was occurred in all the solutions containing SO_4^{2-} as $MgSO_4$. Thus, the authors concluded that, cations associated with the sulfate ions influence the corrosion behaviour of reinforcing steel in simulated pore solution.

Pradhan and Bhattacharjee [64] have conducted potentiostatic study on reinforcing steel in chloride contaminated concrete powder solution extracts to identify different zones of corrosion. The major test variables used were steel type, cement type, w/c ratio, admixed chloride content and test condition (i.e., with and without deaeration). Bare steel specimens of 12 mm diameter and 60 mm in length with 4 mm exposed length were used

in the study. Potentiostatic linear sweeping test was carried out by polarizing the bare steel specimen in chloride contaminated concrete powder solution extracts from 0 mV to 1500 mV with offset from corrosion potential at a sweep rate of 50 mV per minute. Free chloride content, total chloride content and pH of chloride contaminated concrete powder solution extracts were also determined. From the results the authors reported that both free chloride content and total chloride content increased with increase in admixed chloride content and also the free chloride bears linear relationship with total chloride. It was also found that pH values of concrete do not vary with cement type, w/c ratio, and admixed chloride content. Further, the authors have identified the ranges of potential for different zones of corrosion namely semi-immune zone, active zone, passive zone, and pitting zone at various chloride concentrations and reported that the chloride content has the strongest influence in defining different zones of corrosion of steel reinforcement as compared to other parameters like steel type, cement type, w/c ratio and test condition.

Aal et al. [65] have measured the pitting corrosion current density of steel in $Ca(OH)_2$ solutions in the presence of aggressive ions such as chloride ions in the form of NaCl and sulfate ions in the form of Na_2SO_4. From the study, the authors observed that the pitting corrosion current starts to flow after an induction period that depends on the concentration of both aggressive anions and passivating $Ca(OH)_2$. Further, the pitting corrosion current density reached the steady-state values that varied with the concentration of counter acting anions. In addition, the authors observed that the corrosive action of the aggressive anions decreased in the order: $SO_4^{2-} > Cl^-$.

Zhang et al. [66] have investigated the correlation of localized corrosion behaviour and microstructure of steel reinforcement in simulated concrete pore solutions. The solutions that contained 0.6 mol/l KOH, 0.2 mol/l NaOH and saturation of $Ca(OH)_2$ were prepared as simulated concrete pore solutions (SPS) in the study. NaCl and $NaHCO_3$ were used for adding Cl^- ion and adjusting the pH of simulated pore solutions. To investigate the corrosion behaviour and interfacial structure of steel/solution, potentiodynamic polarization and EIS (Electrochemical impedance spectroscopy) measurements were conducted. The authors have also conducted ex-situ characterization using optical microscopy, SEM/EDS and SKPFM (Scanning Kelvin probe force microscopy); and in-situ optical microscopy and AFM (atomic force microscopy) measurements of steel reinforcement. For Potentiodynamic polarization measurement, potential sweep rate of 10 mV/min was applied with respect to Ag/AgCl reference electrode. From the results of

SEM/EDS analysis, the authors observed that most of ferrite, minor amount of pearlite and some inclusion of MnS existed on the surface of steel reinforcement. The results of SKPFM indicated a higher corrosion tendency at ferrite grain boundaries, pearlite grains and MnS inclusions. From the corrosion study, it was observed that the corrosion potential shifts towards a lower value with a higher chloride concentration and lower pH. It was also observed that the passivity breakdown potential or pitting potential is lower with higher chloride concentration. The higher pH of the solution facilitates the passivation of steel, whereas the higher concentration of Cl^- leads to a passivity breakdown at relatively lower potential. Further, the in-situ optical observations and AFM images provided detailed information of the localized corrosion behaviour of steel reinforcement, which were in good agreement with the results obtained from other measurements carried out in the study.

Ghods et al. [67] have investigated the growth of oxide film on steel surface in saturated calcium hydroxide solution with different amounts of NaOH, KOH and $Ca(SO)_4$. The pH of the solutions varied between 12.3 and 13.3. Anodic polarization test was carried out on bare steel specimens at three immersion periods i.e. after 5 days, 8 days and 14 days of immersion to see the oxide film development. The authors reported that the ions present in the pore solution i.e. Ca^{2+}, Na^+, K^+ and SO_4^{2-} has an effect on the protective properties of passive oxide layer. It was observed that the presence of SO_4^{2-} ions in the pore solution has a significant negative effect on the protective properties of the passive oxide film. The authors suggested that 8 days immersion is the ideal period for the oxides to stabilize.

Chen et al. [68] have studied the corrosion behaviour of reinforcing steel in simulated concrete pore solutions by using in-situ Raman spectroscopy, electrochemical impedance spectroscopy and polarization curves. Saturated $Ca(OH)_2$ solution with pH of 12.5 was used as the simulated concrete pore solution. NaCl concentration of 0.5 M was added to study the effect of chloride ions on corrosion behaviour of reinforcing steel. For electrochemical polarization measurement, potentiodynamic anodic polarization curves of steel in simulated concrete pore solution were obtained at a scan rate of 1 mV/s from the corrosion potential to more positive potentials until the polarization current density increased rapidly and reached 150 $\mu A/cm^2$. Linear polarization method was used to measure corrosion rate of steel reinforcement. To study the morphology change of the reinforcing steel in simulated concrete pore solution without and with NaCl, scanning

electron microscopy (SEM) analysis was also carried out in the study. The results of anodic polarization and linear polarization measurements indicated that the reinforcing steel remains passive in the chloride free simulated concrete pore solution (saturated $Ca(OH)_2$ solution) and the corrosion current density of the steel was very low. Further the results of Raman spectroscopy, electrochemical measurements and SEM observations showed that, the corrosion behaviour of the reinforcing steel varied considerably in the simulated concrete pore solution with 0.5 M NaCl. In the presence of chloride ions, the reinforcing steel did not exhibit a stable passive region and the corrosion current density exceeded 0.1 $\mu A/cm^2$. The steel surface was unstable with chloride attack and localized corrosion appeared with $FeCO_3$ and Fe_2O_3 as the main corrosion products on its surface.

Haleem et al. [69] have investigated the effect of chloride and sulfate ions on the rate of breakdown of passive oxide film formed on the surface of reinforcing steel in naturally aerated $Ca(OH)_2$ solutions. From the results, the authors reported that the initiation of pitting corrosion on reinforcing steel by chloride and sulfate ions takes place by the way of an adsorption mechanism. Chloride and sulfate ions compete with OH^- ions for adsorption sites on the oxide covered steel surface. The threshold concentrations of both Cl^- and SO_4^{2-} anions in $Ca(OH)_2$ solutions decreased the rate of oxide film thickening and finally caused the destruction of passivity and initiation of visible pits.

Moser et al. [70] have studied the chloride induced corrosion resistance of austenitic, duplex, and martensitic high-strength stainless steels and a pearlitic prestressing steel in simulated alkaline solution and carbonated concrete pore solutions by carrying out cyclic potentiodynamic polarization test. The chloride ion was added to the simulated pore solutions at concentrations of up to 1.0 M to simulate marine exposures. From their study the authors found that in alkaline solutions, all the high-strength stainless steels exhibited high corrosion resistance at chloride concentrations from 0 to 0.25 M. However, in carbonated solutions the corrosion resistance of all the steels reduced except for the duplex steel grades.

Alhozaimy et al. [71] have carried out an experimental investigation to study the effect of simulated concrete pore solution chemistry, chloride ion and temperature on the passive layer formed on steel reinforcement. Steel reinforcing bars of 32 mm diameter were used in the study. Two test solutions viz. simulated pore solution (SPS) made with NaOH and KOH and simulated pore solution saturated with lime (SPSL) i.e. made with NaOH, KOH and $Ca(OH)_2$ were used in the study. The thickness and phases of the passive film formed

on the surface of steel reinforcement were determined using x-ray photoelectron spectroscopy (XPS). To identify the phases of the passive film, Raman spectroscopy was conducted. From the results, the authors found that the nature of the passive film formed on the steel reinforcement bar is substantially altered by changing the parameters of the surroundings, such as pore solution chemistry, temperature and chloride ion concentration. The results of XPS, Raman spectroscopy, microscopy and electrochemical studies indicated that the changes in the nature of the passive film on the steel surface under different conditions can produce a large variation in the corrosion and pitting tendency of steel reinforcement. The presence of lime in the pore solution can significantly improve the protection properties of the passive film. It was observed that the phases of unstable oxides developed in the passive film due to adsorption of chloride ions onto the stable passive film. Further, the stable oxide phases were transformed into unstable oxides in the passive film due to increase in temperature.

Tang et al. [72] have studied the metastable pitting potential and its relation to the pitting potential for different types of steel in chloride containing solutions. From the results the authors reported that, for all types of steel used in the investigation, linear relationship exist between the metastable pitting potential and pitting potential i.e. as the chloride concentration changes, the metastable pitting potential and pitting potential values change in the same order. Further, it was observed that the passivity of metals in the chloride containing solutions plays the key role in both the nucleation processes of metastable pitting and stable pitting.

Padilla and Alfantazi [73] have investigated the corrosion performance of galvanized steel in sulfate-chloride solutions by studying the surface area changes, film breakdown susceptibility, and protectiveness of the corrosion products by conducting potentiodynamic polarization, cyclic voltammetry, cyclic polarization and electrochemical impedance spectroscopy. The test solutions were prepared by dissolving sodium chloride (NaCl), magnesium chloride ($MgCl_2$), calcium chloride ($CaCl_2$), potassium acetate (CH_3CO_2K) and sodium sulfate (Na_2SO_4) in deionized distilled water. The pH, conductivity, ionic strength and oxygen concentration of all the solutions were measured before conducting electrochemical test. From the results, the authors found that most severe corrosion damage in terms of corrosion rate and degradation of the corrosion film formed on the surface was observed when galvanized steel was immersed in NaCl + Na_2SO_4 solution whereas the best performance was observed in $MgCl_2$ + Na_2SO_4

solution. The authors attributed the better performance of steel specimens in $MgCl_2$ + Na_2SO_4 solution to the lower corrosion kinetics and greater surface coverage by the corrosion products.

Zhang and Poursaee [74] have studied the effect of both tensile and compressive stresses on the formation of passive film in simulated concrete alkaline environment and on depassivation in the presence of chloride ions. The authors reported that the steel specimens immersed in chloride-free pore solution under tensile loading passivate more rapidly as compared with those under compressive loading. However, in chloride-contaminated solution, the steel specimen under tensile stress exhibited more corrosion than the steel specimen under compressive stress or under no load.

Liu et al. [75] have studied the influence of carbonation on chloride-induced reinforcement corrosion in simulated concrete pore solution. Two simulated concrete pore solutions i.e. $Ca(OH)_2$ + KOH + NaOH solution and cement extract were used in the investigation. To simulate different levels of carbonation, different concentrations of bicarbonate ions were added in the solutions. Open-circuit potential measurement was carried out to determine the initiation of pitting corrosion and corrosion current density was determined from EIS curves. The results indicated that in $Ca(OH)_2$ + KOH + NaOH simulated concrete pore solution, high concentration of HCO_3^- ions enhances the stability of passive film and corrosion resistance of steel, whereas low concentration of HCO_3^- ions accelerates the corrosion. However, the HCO_3^- concentration in cement extract shortened the corrosion initiation time of steel reinforcement. The authors found that the cement extract is more suitable than $Ca(OH)_2$ + KOH + NaOH solution to simulate the concrete pore solution for carrying out investigation on chloride induced steel reinforcement corrosion.

Liu et al. [76] have investigated the corrosion behaviour and chloride threshold value (CTV) of reinforcing steels exposed to chloride and sulphate attack in simulated concrete pore solutions. The authors have conducted electrochemical measurements of open circuit potential, linear polarization resistance and electrochemical impedance spectroscopy (EIS). The corrosion initiation was determined by combining half-cell potential with corrosion current density and EIS curves. The HRB335 steel specimens of 16 mm diameter and 10 mm length were used in the experimental investigation. The saturated $Ca(OH)_2$ solution was prepared using distilled water, in which some $Ca(OH)_2$ remained

as insoluble. Sodium chloride (NaCl), sodium sulfate (Na_2SO_4) and NaCl plus Na_2SO_4 were added to saturated $Ca(OH)_2$ solution stepwise, 0.01 mol/l each day, as the source of chloride and sulphate ions. The results indicated that there is a good correlation between open circuit potential, linear polarization resistance and EIS measurements in monitoring corrosion behavior of steel. The chloride threshold value was 0.5 to 0.6 mol/l in simulated concrete pore solution contaminated with NaCl whereas the corrosion threshold content of sulphate ions was in the range of 0.02 to 0.03 mol/l in pore solution contaminated with Na_2SO_4. The concomitant presence of chloride and sulphate ions leads to higher corrosion current density as compared to the specimens exposed to chloride ions at the corresponding concentration, which indicated that corrosion rate of steel specimen accelerates when both chloride and sulphate are present in the simulated concrete pore solution.

Scott and Alexander [77] have investigated the effect of supplementary cementitious materials (SCMs) on the pore solution chemistry and corrosion of steel in alkaline environments. The pore solution compositions of paste samples produced with ordinary Portland cement (PC), ground granulated blast furnace slag at replacement ratios of 25% (SL), 50% (SM), 70% (SH), fly ash (FA) 30%, condensed silica fume (SF) 7%, and a ternary blend (TR) of 50% PC, 43% slag and 7% SF, were determined. Further, the impact of changes in the pore solution chemistry of cement pastes with SCMs on the passivation and corrosion of steel was investigated with mild steel in simulated pore solutions (SPS). From the results, the hydroxyl ion concentrations at 28 and 90 days were found to be the in decreasing order, PC > SL > SM > FA > SH > TR ≈ SF, ranging from 0.32 M (PC) to 0.060 M (SF) at 90 days. In PC, the hydroxyl ion concentration increased by 2.5 times from 7 to 90 days while for SF there was a reduction of 35% in the hydroxyl ion concentration. The non-silica fume containing mixes showed an increase in hydroxyl ion concentration with time while the silica fume containing mixes were found to maintain or slightly reduce the hydroxyl ion concentration. It was also found that sufficiently high hydroxyl ion concentration is essential for establishing the passive layer around the reinforcing steel and maintaining its protection in the presence of chloride ions. The initial pore solution results indicated the presence of significant concentrations of sulphides and thiosulphate in the slag-containing specimens. In case of 25% replacement of cement with slag, the redox potential was > 200 mV more negative compared to Portland cement (PC). The dissolved oxygen concentration and redox

potential values generally decreased with increase in levels of total reduced sulphur species. Considerable variability was observed in the chloride concentration required to initiate corrosion, with the Cl^-/OH^- ratio ranging from 0.3 to 1.7. The inclusion of sulphides in the simulated pore solution prior to chloride addition resulted in the formation of a passive layer under a reducing environment, which may be more susceptible to chloride attack resulting in a lower chloride threshold concentration required to initiate active corrosion as compared to the sulphide-free solutions. It was observed that 4.6 times decrease in the hydroxyl ion concentration at 0.2 M Cl resulted in a 55 times increase in the average rate of corrosion. The effects of sulphides were evident with up to 7 times increase in average corrosion rate for the sulphide containing SPS as compared to sulphide free solutions. Sulphides and thiosulphates, typically found in slag bearing pastes, appeared to reduce the chloride threshold concentration and increase the rate of corrosion in SPS.

2.4 CORROSION BEHAVIOUR OF STEEL REINFORCEMENT IN CONCRETE CONTAMINATED WITH CHLORIDE AND SULFATE IONS

The studies conducted by various researchers to investigate the corrosion behaviour of steel reinforcement embedded in concrete in chloride and sulfate exposure conditions are presented in this section.

Cheng et al. [78] have investigated the role of chloride and sulfate ions on reinforcing steel corrosion in artificial sea water and concentrated sulfate solution. Cylindrical concrete specimens of 50 mm diameter and 100 mm length with a centrally embedded low carbon steel bar were prepared using Type I or Type V Portland cement and water/cement ratio of 0.5. The cylindrical concrete specimens embedded with the steel bar were exposed to two types of simulated corrosive environments viz. artificial sea water and concentrated sulfate solution. Open circuit potential and corrosion rate by AC impedance spectroscopy technique were measured. From the obtained results, the authors reported that the chloride ions are more aggressive than sulfate ions, as the open circuit potentials in chloride solution were more active than that in concentrated sulfate solution. The results of AC impedance spectroscopy indicated that the sulfate ions can change the mechanistic parameters of surface film more significantly and sulfate induced corrosion problems may be more severe.

Al-Tayyib and Khan [79] have studied the effect of sulfate ions on corrosion of rebar embedded in concrete. ASTM Type V (sulfate-resistant) Portland cement and water-to-cement ratio (w/c) of 0.5 were used in the study. Three sets of reinforced concrete specimens of size 63 mm × 100 mm × 300 mm with a 12.5 mm diameter rebar embedded centrally were prepared. The first set of specimens were free from sulfate and chloride ions. The second set of specimens were admixed with three dosages of sulfate ions viz. 0.6, 1.2 and 1.8 kg/m^3. The third set of specimens were admixed with three dosages of chloride ions viz. 0.6, 1.2 and 1.8 kg/m^3. Sodium sulfate and sodium chloride were used as the source of sulfate and chloride ions respectively. The specimens were cured in the potable water for a period of 28 days and then stored in the laboratory condition for a period of four months. Then, all the specimens were immersed in the potable water for a period of 808 days. After that, the first set of specimens were exposed to the potable water, the second set of specimens were exposed to 3% SO_4^{2-} solution and third set of specimens were exposed to 3% Cl^- solution for a period of 60 days. To monitor corrosion, half-cell potential measurement and corrosion rate by linear polarization resistance measurement were carried out. From the results, the authors reported that the sulfate ions are corrosive to reinforcing steel but their corrosivity is less than that of chloride ions. The corrosion rate of chloride-contaminated concrete specimens was 23 - 35% higher than that of sulfate-contaminated specimens.

Al-Amoudi and Maslehuddin [19] have investigated the effect of chloride, sulfate and chloride-sulfate solutions on corrosion of steel reinforcement embedded in ordinary Portland cement paste specimens. Specimens of size 31 mm × 31 mm × 152 mm with a centrally embedded 6 mm diameter steel bar were used in the study. The specimens were cured in the potable water for a period of 14 days and were then exposed to the four different test solutions viz. 15.7% Cl^-, 2.1% SO_4^{2-}, 0.55% SO_4^{2-} + 15.7% Cl^- and 2.1% SO_4^{2-} + 15.7% Cl^-. Sodium chloride was used to provide chloride ions, while sodium sulfate and magnesium sulfate were used to provide sulfate ions. Reinforcement corrosion was monitored by evaluating the time to initiation of corrosion and by measuring corrosion current density. Corrosion potentials were measured using a high impedance voltmeter, with respect to saturated calomel electrode. Corrosion current density was measured at regular intervals using linear polarization resistance test. The steel was polarized to ±10 mV of the corrosion potential at a scan rate of 0.1mV/s. The water-soluble chlorides and sulfates were also determined. The corrosion current density of steel

reinforcement in the specimens placed in 15.7% Cl^- solution was 70 times that of the specimens placed in 2.1% SO_4^{2-} solution. The water-soluble sulfate ions increased with increase in the concentration of salts in the solutions. The results indicated that the steel reinforcement corrosion due to chlorides is not influenced by lower concentration of water-soluble sulfates i.e. less than 0.18% by weight of cement. For sulfate concentration higher than 0.18%, the corrosion activity was significantly enhanced. It was observed that the paste specimens placed in pure sulfate solution (2.1% SO_4^{2-}) showed lower corrosion current density. This indicated that the sulfate ions do not influence reinforcement corrosion activation. The presence of chloride ions is necessary for the initiation and propagation of reinforcement corrosion. The concomitant presence of sulfate and chloride ions may significantly affect the rate of corrosion. The reinforcement corrosion activity was found to be higher in the specimens immersed in sulfate-chloride solution as compared to those immersed in pure chloride solution. The corrosion rate was observed to be doubled when the sulfate concentration in 15.7% Cl^- solution was raised from 0.55% to 2.1%.

Al-Amoudi et al. [80] have evaluated the relationship between the early-age properties such as compressive strength, pulse velocity, porosity and permeability, and the long-term corrosion resistance of plain and blended cement concretes. The blended cements were prepared by using two ASTM C 618 class F fly ashes and one class N natural pozzolan each with replacement of 20% by weight and granulated blast furnace slag with 60% replacement by weight. Water-cementitious material ratio of 0.45 was used in the preparation of specimens. For determining compressive strength and pulse velocity, cube specimens of size 150 mm × 150 mm × 150 mm were used. Similarly for determining the porosity, cylindrical specimens of size 25 mm diameter and 50 mm height and for determining permeability, cylindrical specimens of size 70 mm diameter and 100 mm height were used. For monitoring corrosion, prismatic concrete specimens of size 100 mm × 62.5 mm × 300 mm with a 12 mm diameter steel bar placed centrally with an effective cover of 25 mm at the bottom were used in the study. The prismatic concrete specimens were cured in potable water for a period of 28 days and were then immersed in 5% NaCl solution. The level of the solution was adjusted so that only 150 mm of the specimen is immersed in it. The corrosion activity was monitored by measuring the corrosion potential with respect to saturated calomel electrode and determining corrosion current density by linear polarization resistance test. From the results, the authors reported that

blending of plain cement with mineral admixtures such as pozzolan and industrial by-products like fly ash and blast furnace slag reduces the permeability and porosity and increases the pulse velocity of concrete. The long-term corrosion performance in terms of corrosion rate of steel in blended cement concrete specimens was better than that in plain cement concrete specimens after 7 years of exposure to chloride solution. The rate of corrosion of steel in blended cement concrete specimens was about one-half to one-twelfth of that in plain cement concrete specimens. Further, the statistical analyses of the experimental results indicated very good correlation between permeability and corrosion rate, and between porosity and corrosion rate, whereas poor correlation was obtained between pulse velocity and corrosion rate, and between compressive strength and corrosion rate.

An experimental investigation was carried out by Al-Amoudi [81] to assess the performance of reinforced concrete in mixed magnesium sulfate-sodium sulfate environment. The major test variables were ASTM C 150 Type I, Type II, and Type V Portland cements, 10% silica fume (SF) and 20% class F fly ash (FA) as replacement by weight of Type I and Type V cement, and 60% blast furnace slag as replacement by weight of Type I cement. Effective water-to-cementitious materials (w/cm) ratios of 0.35 and 0.5 were used in the study. Cylindrical specimens of 75 mm diameter and 150 mm height with a centrally embedded reinforcing steel bar of 12 mm diameter were used in the study. The embedded reinforcing steel bar was coated with epoxy coating at the concrete-air interface and at the embedded end to avoid crevice corrosion. The specimens were cured in the potable water for a period of 14 days and were then exposed to test solutions. The test solutions were maintained at 2.1% SO_4^{2-} concentration. Sodium sulfate (Na_2SO_4) and magnesium sulfate ($MgSO_4$) were used to provide 50% of the sulfate concentration from each of them. The specimens were immersed in the solution up to their mid height for a period of 44 months. The physical deterioration due to sulfate attack was evaluated in terms of reduction/increase in weight of the reinforced concrete specimens. The corrosion of steel reinforcement was monitored by measuring corrosion potential and polarization resistance by linear polarization resistance technique. The obtained results indicated that the plain cement (Type I, II and V) concretes irrespective of their C_3A content performed fairly well in terms of sulfate resistance whereas they showed poor performance against steel reinforcement corrosion. The blended cement concrete mixtures made with fly ash and blast furnace slag showed advanced degree of

deterioration due to both sulfate attack and steel reinforcement corrosion. On the other hand, the silica fume cement concrete exhibited best performance against reinforcement corrosion despite of its inferior performance with respect to sulfate attack. Further, it was observed that a reduction in w/cm ratio was detrimental against sulfate attack in both plain and blended cement concretes.

Asrar et al. [82] have investigated the effect of microsilica on chloride permeability and corrosion behaviour of rebar exposed to sodium chloride and seawater environment. The test variables were two types of cement namely ordinary Portland cement (OPC) ASTM Type I and sulfate resistant cement (SRC) ASTM Type V. The concrete mixes were prepared with and without densified or undensified microsilica. Cylindrical specimens of diameter 76 mm and height 152 mm with a centrally embedded steel reinforcement bar of diameter 14 mm were used in the study. Two exposure conditions namely 5% sodium chloride (NaCl) solution and seawater immersion were used. Different tests carried out were salt fog test for periods of 3, 9, 18 and 24 months to find out the corrosion products formed on the surface of rebar, salt ingress test carried out for a period of 800 days to find the amount of chloride ion ingress in the concrete and open circuit potential measurement using saturated calomel reference electrode to monitor the corrosion process. In addition, rapid chloride permeability (RCP) test was also carried out. From the test results the authors reported that, in the chloride environment, the blending of OPC with microsilica decreases the corrosion of rebar, whereas it enhances the corrosion in seawater environment due to presence of SO_4^{2-} and Mg^{2+} ions. The blending of SRC with microsilica suppresses the corrosion of steel reinforcement in seawater environment. In addition, the blending of microsilica resulted in drastic reduction in permeability of chloride ions in both OPC and SRC concretes. Further, the authors observed that the concrete made with densified microsilica provided better corrosion protection to the steel reinforcement than that made with undensifed microsilica.

Alonso et al. [83] have carried out an experimental investigation to find out the chloride threshold values corresponding to depassivation of reinforcing bars embedded in standardized OPC mortar. Smoothed and ribbed bars were used as the steel reinforcement. Chloride ions were added in the mixing water as NaCl and $CaCl_2$. In the study, chloride thresholds in cement mortar were determined based on corrosion current measurements. From the results, the authors found that the chloride thresholds values were in the range of 1.24% to 3.08 % and 0.39% to1.16 %, by weight of cement for total

and free chlorides respectively and the threshold [Cl^-/OH^-] ratio varied from 1.17 to 3.98. It was also reported that the active corrosion is considered when the mean corrosion rate current is higher than 0.1 $\mu A/cm^2$. Further, it was observed that there is no significant influence of steel type on the chloride threshold value except for ribbed bars after depassivation, for which the mean corrosion current was slightly higher.

Dehwah et al. [84] have conducted a study to assess the effect of sulfate ions and its associated cation type on chloride induced-reinforcement corrosion in Portland cement concrete. Ordinary Portland cements (OPC-A; C_3A: 8.5% and OPC-B; C_3A: 9.65%) and sulfate resisting Portland cement (SRPC; C_3A: 3.6%) were used in the preparation of specimens. An effective water-cement ratio of 0.45 was adopted. Reinforced concrete specimens of size 75 mm diameter and 150 mm height with a 12 mm diameter steel bar centrally embedded with an effective cover of 25 mm at the bottom were prepared. The steel bar was coated with epoxy coating at the concrete-air interface and at the embedded end to avoid the crevice corrosion. The specimens were cured in the potable water for a period of 28 days. After that, the specimens were kept at room temperature for one week and were then placed in containers containing exposure solutions. All the exposure solutions contained 5% sodium chloride and varying concentrations (1%, 2.5% and 4% SO_4^{2-}) of sodium sulfate (Na_2SO_4) and (1%, 2.5% and 4% SO_4^{2-}) magnesium sulfate ($MgSO_4$). The specimens were immersed in the solution and the level of the solution was adjusted so that only 85 - 90 mm from bottom of the specimen was in the solution for a period of 1200 days. The reinforcement corrosion was monitored by measuring corrosion potential (with respect to saturated calomel electrode), and corrosion current density by linear polarization resistance method. From the results, the authors found that the presence of sulfate ions in chloride environment did not influence the time-to-initiation of reinforcement corrosion. The time-to-initiation of reinforcement corrosion in the ordinary Portland cement concrete specimens was marginally higher than that in the sulfate-resisting Portland cement concrete specimens. Further, it was reported by authors that the corrosion current density increased with increase in concentration of sodium sulfate. In the concrete specimens exposed to sodium chloride plus sodium sulfate, the corrosion current density was 1.1 – 2.0 times of that in the concrete specimens exposed to only sodium chloride. Similarly, the corrosion current density increased with increase in magnesium sulfate concentration up to 2.5% SO_4^{2-} concentration and then decreased when SO_4^{2-} concentration increased from 2.5% to 4%. In the concrete specimens exposed

to sodium chloride plus magnesium sulfate, the corrosion current density was 1.1 – 2.2 times of that in the concrete specimens exposed to only sodium chloride. The corrosion current density increased with increase in exposure period. Further, it was observed that the corrosion current density decreased with increase in C_3A content in the cement, which was attributed to the increase in chloride binding with increase in C_3A content thereby resulting in higher electrical resistivity of concrete. The rate of chloride-induced steel reinforcement corrosion in the concrete exposed to sodium chloride plus magnesium sulfate solutions was higher than that in the concrete exposed to sodium chloride plus sodium sulfate solutions.

Turkmen and Gavgali [85] have carried out an experimental investigation to evaluate the effect of mineral admixtures on physical and mechanical properties of concrete and on reinforcement corrosion in sulfate solution. Different binders namely Portland cement (PC), silica fume (SF) and blast furnace slag (BFS) and three water-binder ratios viz. 0.35, 0.4 and 0.45 were used in the study. Reinforced concrete cube specimens of size 70 mm with a 10 mm diameter and 200 mm height steel bar placed centrally were prepared. After casting, the specimens were kept in air-conditioned environment for 24 hours and were then kept in lime saturated water for 13 days and further cured for 14 days in an atmosphere of 75 - 80% humidity and temperature of 30 °C. The specimens were then cured in 5% Na_2SO_4 solution. The workability, dry unit weight, compressive strength and capillarity coefficient of the samples without steel reinforcement were determined. The corrosion current density was evaluated by the linear polarization technique on 28^{th}, 75^{th}, 150^{th} and 250^{th} days. From the results, the authors reported that the slump of the concrete increased with increasing water-binder ratio and decreased by the use of BFS and SF mineral admixtures. The dry unit weight of the concrete decreased with increasing water-binder ratio and by the use of BFS and SF mineral admixtures. The concrete specimens made with 10% SF + 20% BFS showed highest compressive strength and the lowest capillarity coefficient. The corrosion current density values of specimens made with BFS were lower than those made with SF and PC. The specimens made with 10% SF + 40% BFS with water-binder ratio of 0.35 showed lowest corrosion current density, which was attributed to higher electrical resistivity, lower chloride diffusion rate and OH^- concentration of the solution.

Sakr [86] has investigated the effect of different percentages of C_3A (tricalcium-aluminate) of cement on the corrosion of embedded reinforcing steel bars in the presence

of chloride and sulfate solutions. The major test variables were five types of ASTM C 150 Portland cements namely Type I (C_3A: 2%), Type II (C_3A: 6%), Type III (C_3A: 10%), Type IV (C_3A: 8%) and Type V (C_3A: 4%). The exposure solutions used were 5% sodium chloride (NaCl) and 5% magnesium sulphate ($MgSO_4$) solutions. For conducting compressive strength test, cement paste cube specimens of size 70 mm were prepared. For corrosion measurements, cylindrical specimens of 60, 85 and 110 mm in diameter and 100, 113 and 125 mm in height respectively were prepared with a reinforcing steel bar of 10 mm diameter placed at distances of 25, 38 and 50 mm from the bottom and sides of the specimens respectively. Corrosion tests namely half-cell potential measurement, impressed voltage method and impressed current method were conducted in the study. From the results, the author observed that the compressive strength of cement specimens immersed in 5% NaCl solution was decreased by 7 - 10% and that in 5% $MgSO_4$ solution was decreased by 15 - 20%. Further, it was observed that in 5% NaCl solution, as the C_3A content of cement increased from 2% to 10%, the steel reinforcement corrosion decreased proportionately. The rate of corrosion decreased as the C_3A content in the cement increased from 2% to 6% and rapidly accelerated in the cements containing 6% to 10% of C_3A content in 5% $MgSO_4$ solution. The optimum percentage of C_3A to control corrosion of reinforcing steel in both chloride and sulphate containing media is 6%. It was also reported that the cover thickness to the steel bar and its diameter also affect the corrosion rate of steel reinforcement.

Pradhan and Bhattacharjee [32] have investigated the role of steel and cement type on chloride-induced corrosion in concrete. The major test variables used were three types of cement, three types of steel, three water-cement ratios and four levels of admixed chloride concentrations. Three types of cement viz. ordinary Portland cement (OPC), Portland pozzolana cement (PPC) and Portland slag cement (PSC), three types of steel viz. cold twisted deformed (CTD) bars, Tempcore TMT (thermomechanically treated) bars and Thermex TMT bars; and three water-cement (w/c) ratios viz. 0.45, 0.5 and 0.55 were used in the study. Four different levels of sodium chloride concentrations used were 0%, 1.5%, 3% and 4.5% by mass of cement content. For measuring 28 day compressive strength, cube specimens of size 150 mm × 150 mm × 150 mm were prepared. For conducting corrosion tests, slab specimens of size 300 mm × 300 mm × 52 mm with a centrally embedded steel of 12 mm diameter were prepared in the study. The specimens were moist cured till the age of 28 days and were then kept in the ambient laboratory condition till

the age of 60 days. Free chloride content, total chloride content and pH value of concrete were also determined. The corrosion tests were performed on the slab specimens at the age of 60 days. From the results, the authors reported that the chloride binding was more in PSC concrete than that in OPC and PPC concretes. Linear relationship between free chloride and total chloride concentrations was observed in all the three types of cement used in the study. From the results of chloride content, pH, half-cell potential, relative resistivity and corrosion current density, the authors found that the corrosion performance of steel reinforcement in PPC and PSC concrete was better than that in OPC concrete. Further, it was reported that PSC is likely to improve the corrosion performance of reinforcing bar in concrete in the corrosion initiation period as compared to PPC and OPC, whereas PPC is likely to improve the corrosion performance of reinforcing bar in the propagation period as compared to PSC and OPC in chloride contaminated concrete. Tempcore TMT steel showed higher chloride tolerance and lower corrosion current density values than Thermex TMT and CTD steels. Thus, the authors concluded that PSC performed best in increasing the corrosion initiation period while PPC performed best in extending the propagation period among the cement types and among the steel types used in the study, Tempcore TMT steel performed best both in the initiation and propagation periods.

Maslehuddin et al. [87] have evaluated the effect of chloride concentration in soil on reinforcement corrosion in plain and blended cement concretes. Cements namely, Type I, Type V and Type I plus silica fume (7% replacement by weight of Type I cement) and water-to-cementitious ratio of 0.4 were used in the preparation of specimens. Cylindrical specimens of 75 mm diameter and 150 mm height with a centrally embedded steel bar of 12 mm diameter were used in the study. Concrete-air interface and bottom of the steel bars were coated with epoxy coating to avoid crevice corrosion. The specimens were exposed to the soil contaminated with varying concentrations of chloride viz. 0.05%, 0.1%, 0.2%, 0.5%, 1.0%, 2.0%, and 3.0%, in the container up to their mid height for a period of 18 months. Corrosion potential and corrosion current density were measured to monitor the reinforcement corrosion. Corrosion potentials were measured with respect to saturated calomel electrode and corrosion current density was evaluated by linear polarization resistance measurement. Further, gravimetric weight loss of steel reinforcement due to corrosion was also assessed. From the results, the authors reported that the time-to-initiation of reinforcement corrosion in Type V cement concrete in the

soil was noted when it was exposed to 0.1% or higher chloride concentration, whereas in Type I cement concrete specimens, the initiation of corrosion was noted for exposure to 0.5% or higher chloride concentration and in the specimens made with silica fume, the corrosion initiation was observed when it was exposed to 1% or higher chloride concentration. The reinforcement corrosion initiation time decreased with increase in chloride concentration in the soil. Further, the authors observed that the corrosion current density increased with increase in chloride concentration in the soil. The corrosion current density of steel in Type I and Type V cement concrete specimens were more than 0.3 $\mu A/cm^2$ when exposed to the soil contaminated with more than 0.5% of chloride concentration. The corrosion current density of steel in the silica fume cement concrete specimens was more than 0.3 $\mu A/cm^2$, when exposed to the soil contaminated with chloride concentration of 1% or more. For a particular chloride concentration, least reinforcement corrosion was noted in the silica fume cement concrete followed by Type I and Type V cement concrete. Further it was reported that, gravimetric weight loss in Type V cement concrete specimens exposed to the soil was observed at a chloride concentration of 0.1% or more whereas that was observed at a chloride concentration of 0.5% or more in Type I cement concrete specimens. In silica fume cement concrete specimens, the gravimetric weight loss was observed when the specimens were exposed to a chloride concentration of 1% or more.

Pradhan and Bhattacharjee [33] have carried out an experimental investigation to evaluate the performance of rebar in chloride contaminated concrete by corrosion rate. The test variables used in the study were three types of cement namely ordinary Portland cement (OPC), Portland pozzolana cement (PPC) and Portland slag cement (PSC), three types of rebar namely cold twisted deformed (CTD) bars, Tempcore TMT bars and Thermex TMT bars, and three water-cement (w/c) ratios namely 0.45, 0.5 and 0.55. Slab specimens of size 300 mm × 300 mm × 52 mm with a centrally embedded steel reinforcement of 12 mm diameter were prepared. Varying NaCl concentrations admixed in the concrete at the time of its preparation were 0%, 1.5%, 3% and 4.5% by mass of cement content. Linear polarization resistance (LPR) test was conducted at the age of 60 days and 1 year and AC impedance spectroscopy test was conducted at the age of 60 days on the slab specimens to determine the corrosion current density. Further, gravimetric (mass loss) measurement was conducted at the age of 1 year. From the results, the authors reported that the values of corrosion current density obtained by linear polarization resistance (LPR) technique

with guard ring arrangement were in close agreement with those obtained by gravimetric method. Further, the corrosion current density values obtained by AC impedance spectroscopy were slightly lower than those obtained by LPR measurement. From the results of corrosion rate of steel reinforcement obtained by three techniques, it was concluded that the blended cements (PPC and PSC) performed better as compared to OPC and amongst steel type, Tempcore TMT steel showed lower corrosion rate as compared to Thermex steel followed by CTD steel against chloride induced rebar corrosion in concrete. Further from the results of analysis of variance (ANOVA), the authors reported that chloride content has the strongest effect on corrosion rate followed by cement type, steel type and w/c ratio. In addition, the corrosion rate remained almost constant with age of testing adopted in the study, which was further corroborated by the results of ANOVA.

Pradhan [88] has studied the corrosion behaviour of steel reinforcement in concrete exposed to chloride and composite chloride-sulfate environment. The concrete mixes were prepared from two types of cement i.e. OPC and PPC and four w/c ratios i.e. 0.45, 0.50, 0.55 and 0.60. The corrosion behaviour of steel was evaluated by measuring half-cell potential, relative resistivity and corrosion current density. The corrosion tests were performed on slab specimens with a centrally embedded steel bar of 12 mm diameter. The exposure solutions were prepared with varying concentrations of sodium chloride, sodium chloride plus sodium sulfate and sodium chloride plus magnesium sulfate. From the results the author reported that the specimens made with PPC exhibited higher values of relative resistivity and lower values of corrosion current density as compared to those made with OPC in all exposure solutions. Further, the author observed the opposite behaviour between composite solutions of sodium chloride plus sodium sulfate and sodium chloride plus magnesium sulfate in terms of variations in relative resistivity and corrosion current density for both OPC and PPC. From the results of analysis of variance (ANOVA), the author reported that except concentration of sulfate ions; cement type, w/c ratio and chloride ion concentration affect both relative resistivity and corrosion current density in composite solutions of sodium chloride and magnesium sulfate. In composite solutions of sodium chloride and sodium sulfate, chloride ions and sulfate ions did not have significant effect on the variations in relative resistivity, whereas chloride ion concentration along with cement type and w/c ratio have significant effect on corrosion current density of steel reinforcement in concrete.

Kwon et al. [89] have investigated the long-term corrosion performance of blended cement concrete in the marine environment. Ordinary Portland cement (OPC), Portland pozzolona cement (PPC), Portland slag cement (PSC) and water cement ratio (W/C) of 0.55 were used in the preparation of concrete specimens. To measure the physicochemical properties of concrete such as compressive strength, alkalinity, free chloride content and sulphate content and bio-fouling attachment, cube specimens of size 150 mm were prepared. For conducting AC-impedance and potentiodynamic polarization tests, cubes of 150 mm size with two rebars of 12 mm diameter and 70 mm length embedded parallelly just opposite to each other at a cover of 40 mm were prepared. Corrosion rate of rebar was determined by gravimetric weight loss method. After 28 days of water curing, the concrete cubes were exposed to three field exposure conditions such as atmospheric zone (AZ), immersion zone (IZ) and splash zone (SZ). XRD and SEM analyses were also carried out on concrete samples exposed under various zones. Offshore Platform Marine Electrochemistry Center (OPMEC), Tuticorin, Tamil Nadu, India was selected as an exposure station. The ambient temperature of the atmospheric zone was ranging from 25 °C to 35 °C. In the immersion zone (IZ), the concrete cubes were immersed in the sea at a depth of 5 m. The pH value of the sea water at the place of IZ was ranging from 7.9 to 8.2 and the chloride and sulphate concentrations were ranging from 2200 to 2600 ppm. In the splash zone (SZ), the cubes were subjected to natural wave alternate wetting and drying conditions. The wetting of cubes was achieved by sea water having a chloride and sulphate concentrations ranging from 16000 to 18000 ppm and the drying was achieved in the atmospheric temperature ranging from 25 °C to 35 °C. The concrete cubes were exposed over the period of 10 years. From the results, the authors reported that strength and alkalinity of the blended cement concretes were relatively equal to that of OPC concrete. In addition, the pH values of the blended cement concretes were above the threshold limit recommended for depassivation. It was also reported that the chloride ion penetration was significantly reduced for blended cement concretes than that of OPC concrete. XRD analysis also showed a very similar trend. Blended cements exhibited very high amount of bio-fouling attachment. Further from electrochemical studies, it was found that the blended cement concretes have higher corrosion resistance in all three exposure zones as compared to OPC concrete. The authors observed that the blended cement concretes are sustainable from the durability point of view and highly recommended for aggressive marine environments than OPC concrete.

2.5 DETERIORATION OF CONCRETE IN CHLORIDE AND SULFATE ENVIRONMENT

The deterioration of concrete exposed to chloride and sulfate environment is a major concern for the service life of concrete structures. In this section, the literature review on the effect of chloride and sulfate ions on physical, mechanical, durability and microstructural properties of concrete are presented.

Cohen and Bentur [45] have studied the durability of Portland cement-silica fume pastes in magnesium sulfate and sodium sulfate solutions. The major test variables used in the study were ASTM Type I and Type V Portland cements, 15% silica fume as replacement of Type I and Type V Portland cements. The results indicated that silica fume addition to Portland cement can improve resistance to sodium sulfate attack, but it significantly reduced the resistance to magnesium sulfate attack. The authors attributed the greater damaging effects of magnesium sulfate solution on the Portland cement and Portland cement + silica fume specimens to the decomposition of C-S-H gel to non-cementitious M-S-H (magnesium silicate hydrate). Further, it was observed that intensity of magnesium attack was greater on Portland cement + silica fume specimens as compared to Portland cement specimens and this was attributed to the absence of magnesium hydroxide in the Portland cement + silica fume paste, which makes the C-S-H gel more prone to magnesium sulfate attack.

Harrison [90] has investigated the effect of chloride in mix ingredients on the sulphate resistance of concrete. The resistance to sulphate attack of concrete and mortar with and without chloride additions was assessed by immersing the cube specimens in solutions of magnesium sulphate and sodium sulphate. The specimens were prepared by using ordinary Portland cement (OPC 832) and sulphate-resisting Portland cement (SRPC 762). The mortar cube specimens of size 12.5 mm and concrete cube specimens of size 100 mm were prepared in the study. Varying levels of chloride were introduced either as sodium chloride or calcium chloride in the mixing water i.e. 0 - 4.5% of chloride by weight of cement was added in mortar specimens and 0 - 3.3% of chloride by weight of cement was added in concrete specimens. The specimens were cured in the water till the age of 28 days. After that, the mortar and concrete cube specimens were immersed in water as a control exposure and in four different sulphate solutions i.e. 1.5% SO_3 and 0.35% SO_3 concentrations each of magnesium sulphate and sodium sulphate. The deterioration was monitored by comparing the strength of cubes in sulphate solutions with that of similar

cubes immersed in water for a period of 7 years for concrete and 1 year of immersion for mortar specimens. The 28-day compressive strength was also determined. In addition, the concrete cubes were also visually assessed at the age of 3 and 7 years. From the results the author reported that, in chloride admixed mortar specimens after 1 year of exposure to sulphate solutions, the chloride had either negligible or generally beneficial effect on the resistance to sulphate attack in both OPC and SRPC. In strong sulphate solutions (1.5% SO_3, magnesium or sodium sulphate), sodium chloride addition in OPC and SRPC concretes had very little effect on sulphate resistance. However, addition of calcium chloride in concrete particularly below 0.5% chloride by weight of cement, significantly increased the degree of attack on OPC concrete and to a lesser extent on SRPC concrete in strong sulphate solution i.e. in some concretes containing calcium chloride and exposed to strong sulphate solution, the sulfate resistance of concrete was considerably reduced.

Bonen [91] has evaluated the effect of magnesium sulfate on plain and silica fume-bearing Portland cement mortar through chemical and microstructural study. The mortar beam specimens of size 5 mm × 15 mm × 80 mm were prepared using ASTM Type I Portland cement and Portland cement with silica fume (10% replacement by mass of cement). After demoulding, the specimens were cured in the saturated lime water for a period of 6 days. After that, the Portland cement mortar specimens were immersed in 4.2% magnesium sulfate solution and Portland cement with silica fume mortar specimens were immersed in 2.1% and 4.2% magnesium sulfate solutions for a period of one year at room temperature. After one year of exposure, backscatter SEM analysis was conducted on the mortar. The author reported that Portland cement mortars were more susceptible to magnesium sulfate attack and less durable as compared to their counterpart pastes as indicated by greater surface deterioration, greater depth of sulfate ingress, greater gypsum deposition and higher degree of decalcification of C-S-H gel. The Portland cement mortar specimens indicated massive deposition of gypsum around aggregate, in air voids and other cavities. The Portland cement with silica fume mortar specimens indicated less amount of gypsum deposition due to reduced rate of ingress of sulfates. However, the mortar prepared with silica fume exhibited greater decalcification of C-S-H than that in plain mortar.

Rasheeduzzafar et al. [46] have investigated the performance of plain and blended cements in the mixed magnesium-sodium sulfate environment. XRD and SEM analyses were carried out on cement paste specimens to identify the morphology and composition

of deteriorated products. Signs of deterioration on mortar cubes were visually observed. The reduction in compressive strength of mortar cubes was determined in terms of sulfate deterioration factor (SDF). The authors found that the sulfate deterioration in plain and blended cements was characterized by scaling, spalling, and softening rather than expansion and cracking. The deterioration was observed in all the cements after 2 years of exposure to mixed magnesium-sodium sulfate solution and more pronounced deterioration was observed in blast-furnace-slag and silica-fume cements than that in plain and fly ash blended cements. In the mixed magnesium-sodium sulfate environment, the strength reduction exceeded 70% in all cements after 24 months of exposure. The XRD and SEM analyses indicated that the inferior performance of the blended cements made with silica fume and blast furnace slag may be attributed to the depletion of calcium hydroxide as a result of pozzolanic reaction. In the absence of calcium hydroxide, magnesium ions react more extensively with the cementitious calcium silicate hydrate and produce gypsum and non-cementitious M-S-H.

Akoz et al. [92] have investigated the effect of sodium sulfate concentration on the sulfate resistance of mortars with and without silica fume. Portland cement (PC) and Portland cement-silica fume (PC-SF, 10% replacement by mass of cement) and water/cementitious material ratio of 0.5 were used in the preparation of specimens. The specimens were cured in lime saturated water at 20°C till the age of 28 days. After that except control specimens, all the other specimens were exposed to sodium sulfate solutions containing varying sulfate (SO_4^{2-}) concentration of 2700, 18000 and 72000 mg/l. Various physical and mechanical properties of mortar were determined at different ages up to 300 days of exposure. From the results, the authors reported that low sulfate concentrations not exceeding 18000 mg/l did not show any significant effect on the compressive strength and flexural strength of mortars whereas at sulfate concentrations of 18000 mg/l, volume density and volumetric water absorption indicated beginning of rapid deterioration of mortar at the critical exposure period. Further, the authors observed that at sulfate concentration of 72000 mg/l, both compressive strength and flexural strength decreased sharply between 90 and 180 days. Silica fume replacement at 10% caused a significant increase in sulfate resistance of mortar specimens even at higher concentration of sulfate ions.

Lee et al. [93] have studied the sulfate attack and role of silica fume in resisting strength loss of mortar. Ordinary Portland cement (OPC) and silica fume (SF) with replacement

levels of 5%, 10%, and 15% by mass of cement and water/cementitious materials ratios (w/cm) of 0.35, 0.45 and 0.55 were used in the preparation of mortar specimens. The test solutions used for supplying sulfate ions were 5% sodium sulfate (Na_2SO_4) and 5% magnesium sulfate ($MgSO_4$). The authors conducted compressive strength test and X-ray diffraction (XRD) analysis on mortar samples. Differential scanning calorimetry (DSC) test was conducted on paste samples. From the results, the authors reported that presence of silica fume had a beneficial effect against strength loss due to sodium sulfate attack. The best resistance to sodium sulfate attack was obtained with a SF replacement of 5-10%, but even then, a strength loss of 15-20% can be expected. However, the mortars specimens with silica fume were severely damaged in the magnesium sulfate environment. The larger the amount of SF content, the greater was the strength loss in magnesium sulfate environment. The formation of various expansive compounds in mortar in sulfate environment was also confirmed from XRD results. It was also found that the w/cm ratio is the most critical parameter influencing the sulfate resistance of concrete.

Al-Amoudi [43] has reviewed the studies conducted on sulfate attack on plain and blended cements exposed to aggressive environments and based on the review, the author elucidated the effect of cation type associated with the sulfate anions on concrete deterioration and the role of chloride ions on sulfate attack. From the review of various studies, the author has reported that blended cements particularly those prepared with silica fume and blast furnace slag cements were observed to be highly resistant to sodium sulfate (Na_2SO_4) attck in terms of strength reduction and weight loss of concrete. But these blended cements showed inferior performance when exposed to magnesium sulfate ($MgSO_4$) solution, which is attributed to the conversion of calcium silicate hydrate (C-S-H) to non-cementitious, non-crystalline, and fibrous M-S-H. The concomitant presence of chlorides with sulfate ions tends to mitigate sodium sulfate attack due to increased solubility of gypsum and ettringite, thereby inhibiting their expansive characteristics. In magnesium sulfate exposures, the chlorides reduce the gypsum attack in a way similar to that in sodium sulfate environment. However, the presence chloride ions in magnesium sulfate environment does not hinder the magnesium sulfate attack on C-S-H.

Zuquan et al. [94] have conducted a study to evaluate the effect of sulfate on chloride penetration and diffusivity and the effect of chloride on deterioration of concrete due to sulfate attack. The authors also studied the damage process of concrete caused by mixed

chloride and sulfate ions. Chinese standard 42.1 R (II) Portland cement similar to ASTM type I ordinary Portland cement and 20% and 30% replacements of cement with class F fly ash were used in the study. Water-to-binder ratios (W/B ratios) of 0.35 and 0.45 were used in the preparation of specimens. Concrete specimens of size 40 mm × 40 mm × 160 mm were prepared and cured in a condition of 20 ± 3 °C temperature and 95% of relative humidity for a period of 60 days. Two corrosion regimes were used in the study to investigate the damage process of concrete viz. naturally immersion regime and accelerated regime. The concrete specimens were submerged in corrosion solutions viz. 21 g/l Cl^- solution (3.5% by mass of NaCl), 33.8 g/l SO_4^{2-} solution (5% by mass of Na_2SO_4) and a composite solution of 3.5% NaCl and 5% Na_2SO_4 at room temperature for a period of about 800 days for naturally immersion regime. For accelerated regime, the concrete specimens were subjected to drying-immersion cycles in the same corrosion solutions, which were used for naturally immersion regime. Water soluble chloride content was determined at different depth intervals from the concrete surface to the inner section, and X-ray diffraction (XRD) and SEM analyses were performed on the collected powder samples. The relative dynamic modulus of elasticity (RDME) of specimens was determined. From the results, the authors reported that the presence of sulfate in the composite solution increased the resistance to chloride ingress into concretes at early exposure period, but the opposition was observed at latter exposure period. Further, it was observed that the damage process of concrete naturally submerged in 5% Na_2SO_4 for a period of 830 days is classified into three periods according to RDME: (I) linearly increased period; (II) steady period; and (III) declining stage. However, comparatively only pro-stage II was occurred in composite solution, which indicated that the presence of chloride ions in composite solution will reduce the number of stages at the same exposure period, and will prolong the interval of each stage. The damage process of concrete exposed to drying-immersion cycles in 5% Na_2SO_4 for a period of 500 days can be classified into four stages: (I) firstly decreased stage; (II) linearly increased stage; (III) slowly decreased stage; and (IV) accelerating failure stage. For the composite solution, only pro-stage III occurred for 500 days of accelerated corrosion period. The deterioration was found to be severe in 5% Na_2SO_4 solution as compared to that in composite solution. This indicates that the presence of chloride in composite solution prolonged the interval of each stage and the deterioration due to sulfate ions was retarded. The authors also reported that addition of fly ash increased the ingress of chloride ions into concrete at the

early exposure period but reduced it at the latter period. Concrete with low W/B ratio and suitable content of fly ash could retard the deterioration of concrete due to sulfate ions. The XRD results indicated the formation of more amount of gypsum and ettringite in the surface layer as compared to that in the core of the concrete. Further, the formation of these products (gypsum and ettringite) was confirmed from the SEM images.

Lee et al. [95] have carried out an experimental study on the mitigating effect of chloride ions on sulfate attack of cement mortars with and without silica fume. The major test variables used were ordinary Portland cement (OPC) and silica fume (SF) at replacement levels of 5%, 10%, and 15% by mass of cement. The water–binder ratio (w/b) of 0.45 was used for the preparation of specimens. Two types of specimens were prepared i.e. mortar specimens and paste specimens. Mortar cube specimens of size 50 mm were used for compressive strength measurement and prismatic specimens of size 25 mm × 25 mm × 285 mm were used for expansion measurement. A polycarbonic acid-based superplasticizer was used in all the mortar mixtures to obtain the suitable workability. The paste specimens were prepared using 100 g of total binder materials (OPC+SF) and 45 g of deionized water without superplasticizer in plastic cylinders of 13 mm diameter. The paste samples were used for conducting X-ray diffraction analysis and mercury intrusion porosimetry (MIP). The test solutions used were sulfate solution and sulfate-chloride solution. Sulfate solutions were prepared using 33800 ppm as SO_4^{2-} ions (Na_2SO_4) and sulfate-chloride solutions were prepared by using 33800 ppm as SO_4^{2-} ions (Na_2SO_4) and 3.5% NaCl. The mortar specimens were demoulded after 24 hours of casting and were then cured in water for 6 days and then kept in the test solutions. The paste specimens were demoulded after 24 hours of casting and cured in water for 6 days and then epoxy coated on all the surfaces except the upper surface and were then kept in the test solutions. Visual examination of mortar specimens exposed to test solutions was also carried out. From the results, the authors reported that OPC mortar mixtures with a higher w/b ratio showed the mitigating effect of sulfate attack in the presence of chloride ions. This may be due to the increased solubility of ettringite and gypsum in the chloride-bearing solution leading to reduction in the amount of ettringite and gypsum formed in the cement paste and the ettringite formed in the sulfate-chloride solution is less expansive. Further, it was observed that even low replacement of silica fume has a beneficial effect in terms of controlling the surface damage, compressive strength loss.

and expansion of plain mortar specimens due to its strong pozzolanic reaction and consequently less amount of $Ca(OH)_2$.

Aye and Oguchi [96] have evaluated the resistance of plain and blended cement mortars exposed to severe sulfate attack. Normal Portland cement (NPC), sulfate-resisting Portland cement (SRPC) and three blended cements 25% fly ash (FA), 8% silica fume (SF), and 8% diatomaceous earth (DE) replaced by weight of normal Portland cement were used in the preparation of mortar specimens. Naphthalene sulphonate-based superplasticizer, 0.8% by mass of binder was added in the mortar mixture made with water-cement (w/c) ratio of 0.45. Mortar cube specimens of size 5 cm and prismatic specimens of size 5 cm × 5 cm × 12 cm were prepared in the study. The test solutions of 10% Na_2SO_4 and 10% $MgSO_4$ concentration were used in the study. Four exposure regimes were used to evaluate the sulfate attack viz. exposure I: specimens continuously submerged in each sulfate solution, exposure II: specimens exposed to cyclic drying and wetting in each sulfate solution, the cycle consists of immersion, drying and cooling phases, exposure III: specimens continuously subjected to partial immersion in each sulfate solution for a depth of 3 cm and exposure IV: specimens partially immersed in sulfate solution and exposed to wetting and drying cycles. The performance of specimens in each exposure regime was visually inspected throughout the test. To find the degree of deterioration, compressive strength and weight loss measurements were carried out at the end of exposure period and X-ray diffraction (XRD) analysis was conducted on powder samples. To assess the pore characteristics of the mortars, mercury intrusion porosimetry (MIP) test was conducted. From the results, the authors reported that the addition of pozzolan improved the resistance of mortar to Na_2SO_4 solution, however, it increased the magnitude of $MgSO_4$ attack from the standpoint of chemical attack. The obtained XRD patterns indicated the formation of compounds such as ettringite, gypsum, mirabilite and thenardite in different exposure conditions. Further, it was observed that the performance of blended cement mortars with fine pore structure was relatively poor under the cyclic wetting and drying exposure regimes in Na_2SO_4 environment. However, the physical attack by $MgSO_4$ was not apparent in both plain and blended cement mortars. Overall, it was found that with respect to chemical attack, $MgSO_4$ is more damaging than Na_2SO_4 and in case of physical attack, Na_2SO_4 was more harmful than $MgSO_4$.

Sotiriadis et al. [97] have investigated the sulfate resistance of limestone cement concrete exposed to combined chloride and sulfate environment at low temperature. Normal

Portland cement and Portland limestone cements containing 15% and 35% w/w limestone produced by intergrinding clinker, limestone and gypsum in a pilot plant ball mill and water to cement ratio (W/C) of 0.52 were used for the preparation of concrete specimens. Visual inspection, mass change and compressive strength of concrete cube specimens immersed in chloride-sulfate and sulfate solutions stored at 5 ± 1 °C temperature were investigated in the study. The solutions were prepared using commercial NaCl and $MgSO_4.7H_2O$ salts. For the identification of the degradation products formed as a result of sulfate attack, XRD analysis was carried out. From the results, the authors found that the imestone cement concrete suffered from thaumasite form of sulfate attack, along with the formation of brucite and secondary gypsum. Further, it was observed that concrete with limestone cement exhibited higher degree of deterioration as compared to that made without limestone cement. The higher the limestone content of cement used, the disintegration of limestone cement concrete was more severe and rapid. It was also found that deterioration of concrete due to sulfate attack is more intensive for the specimens stored in sulfate environment, as compared to those stored in the combined chloride-sulfate environment, thereby indicating that the presence of chloride ions reduces the effect of sulfate attack on deterioration of concrete.

Màes and Belie [98] have studied the influence of chlorides on magnesium sulphate attack at two different temperatures (5 °C and 20 °C). In the study, mortar specimens were prepared with ordinary Portland cement (OPC), high-sulphate resistant Portland cement (HSR) and 50% blast-furnace slag (BFS) as replacement of ordinary Portland cement. Mortar cube specimens of size of 20 mm were prepared and were immersed in the test solutions at the age of 28 days. Test solutions used were 50 g/l Na_2SO_4, 42.5 g/l $MgSO_4$, 50 g/l Na_2SO_4 +50 g/l NaCl and 42.5 g/l $MgSO_4$ + 50 g/l NaCl. Visual inspection and mass change of specimens were evaluated to examine the influence of Cl^- on sulphate attack, and XRD analysis was conducted to identify the phase changes. From the results, the authors reported that the influence of Cl^- on $MgSO_4$ attack depends on the temperature and binder type. It was observed that at temperature of 20 °C, chlorides have no effect on deterioration due to magnesium sulphate attack in ordinary Portland cement and high-sulphate resistant Portland cement mortar. The small amount of deterioration was attributed to the formation gypsum and ettringite. However, in BFS mortar the degree of deterioration was significantly increased when exposed to magnesium sulphate solution with added chlorides. The presence of BFS decreases the formation of a protecting brucite

layer and favours decomposition of calcium silicate hydrates to magnesium silicate hydrates. Further, it was observed that at 5 °C, the presence of chlorides in a magnesium sulphate environment causes increased deterioration, regardless of the binder type. The combined attack of magnesium sulphate and chlorides at low temperatures leads to significant increase in deterioration of cementitious materials with OPC and HSR (as binder) as compared to the deterioration at 20 °C. In addition, for mortar containing BFS as a cement replacement, the deterioration was slightly decreased at temperature of 5 °C as compared to the deterioration at 20 °C. At 5 °C, the degradation results in thaumasite formation, and was found to be almost equal for the different binders used in the study and quite severe. Overall, it was observed that chlorides mitigate sulphate attack when ettringite and gypsum are the main reaction products causing deterioration. When thaumasite is formed due to sulphate attack, chlorides induce an increased deterioration.

Chen et al. [99] have investigated the resistance of concrete against combined attack of chloride and sulfate under drying-wetting cycles. The cements used were ordinary Portland cement; and fly ash (FA) and grounded blast furnace slag (GBFS) as 30% and 50% replacement by weight of cement respectively. Concrete specimens of size 70 mm× 70 mm × 280 mm were prepared and used for evaluating mass change, dynamic modulus of elasticity and total chloride content. Paste specimens were prepared to conduct XRD and TG/DSC analyses. Concrete and paste specimens were exposed to 5% NaCl and 5% Na_2SO_4 solutions and combined solutions of 5% NaCl and 5% Na_2SO_4 and 5% NaCl and 10% Na_2SO_4. The concrete specimens were first immersed in the exposure solutions at the room temperature for 21 h, followed by 3 h drying in the air. Then, they were dried at a temperature of 60 °C for 45 h, followed by cooling down in the air at the room temperature for 3 h. This period of three days (72 h) represented a drying-wetting cycle. From the results, the authors reported that addition of mineral admixture such as FA and GBFS in concrete resulted in lower chloride ingress when exposed to the 5% NaCl + 5% Na_2SO_4 solution under drying-wetting cycles. The presence of SO_4^{2-} ions in combined solutions can retard the chloride ingress in ordinary Portland cement concrete. It was observed that the concrete samples with mineral admixture addition have lower porosity than plain concrete samples after 150 days exposure in the 5% NaCl + 5% Na_2SO_4 solution under drying-wetting cycles. It was also observed that, the peaks for Friedel's salt in XRD patterns was almost disappeared for the samples exposed to 5% NaCl + 10% Na_2SO_4 solution, indicating that the presence of SO_4^{2-} ions in the chloride solution

retards the formation of Friedel's salt. Further from the comparison of exposure to combined solution with that to only sulfate solution, the authors observed that sulfate solution results in the formation of ettringite, whereas the presence of Cl^- ions in the sulfate solution may retard the formation of sulfate products, such as ettringite.

Wang et al. [100] have studied the durability of concrete containing fly ash and silica fume against combined freezing-thawing and sulfate attack. In the present study, concrete specimens were prepared with fly ash FA (10%, 15% and 25% by weight) and silica fume SF (5%, 8% and 11% by weight) as partial replacement of Portland cement (PC) at w/b ratios of 0.33 and 0.38 and were exposed to 5% and 10% sodium sulfate solutions under freezing-thawing cycles. Compressive strength, relative dynamic elastic modulus (RDEM) and scanning electron microscopy (SEM) analysis of concrete subjected to sulfate attack and freezing-thawing cycles in water and in the sulfate solutions were evaluated. From the results, it was found that, both fly ash and silica fume improve the resistance to sulfate attack when exposed to 5% sodium sulfate solution. Further, the performance of silica fume concrete was better than that of fly ash concrete. The concrete deterioration was attributed to the interaction between freezing-thawing and sulfate attack. It was found that the resistance of concrete without any admixture against combined freezing-thawing and sulfate attack increased up to 125 freezing-thawing cycles and then decreased. Fly ash and silica fume as concrete admixture improved the resistance of concrete against the combined freezing-thawing and sulfate attack at 25% fly ash and 5-8% silica fume by weight replacement level of cementitious materials, leading to significant improvement in concrete durability. The SEM images of concrete specimens at a depth of 5 mm exposed to sodium sulfate solutions showed the formation of gypsum and ettringite (in the form of needle-like crystals) in the concrete. The 10% sodium sulfate solution improved freezing-thawing resistance of concrete made with 25% fly ash by weight replacement level of cementitious materials than that in 5% sodium sulfate solution, while 5% and 10% sodium sulfate solution had the similar improvements in freezing-thawing resistance of concrete made with 8% silica fume by weight replacement level of cementitious materials.

2.6 SUMMARY OF LITERATURE REVIEW

From the review of literature carried out for the present research work, it is observed that various researchers have conducted investigations on corrosion behaviour of steel

reinforcement in simulated concrete pore solution environment, and in concrete subjected to different exposure conditions. For studying the corrosion behaviour, the researchers have carried out different corrosion tests on steel reinforcement in simulated pore solutions contaminated with chloride ions or sulfate ions. In addition, few studies have been reported in the literature to evaluate the microstructural changes in concrete in the conjoint presence of chloride and sulfate ions. Further, very less research work has been reported in the literature on the corrosion behaviour of steel reinforcement in concrete powder solution extracts contaminated with only chloride ions. However, the research work on corrosion behaviour of steel reinforcement in concrete powder solutions extracts admixed with conjoint chloride-sulfate ions is very scanty. The concrete powder from which the aqueous solution is extracted, is a mixture of cement hydrates, coarse aggregates and fine aggregates and thus the aqueous solution may represent the electrolytic pore solution of concrete more closely as compared to other simulated pore solution such as saturated calcium hydroxide solution. Keeping this in view, there is a need to carry out a comprehensive experimental investigation to study the effect of conjoint presence of chloride and sulfate ions on electrochemical behaviour of steel reinforcement in electrolytic concrete powder solution extracts by incorporating different types of cement, steel and water-cement (w/c) ratio, through potentiodynamic polarization study and corrosion rate measurement. In addition, it is also required to evaluate the effect of cation type associated with sulfate ions on corrosion behaviour of steel reinforcement in concrete powder solution extracts in the presence of chloride ions. Further to analyze the effect of chemical composition of the electrolytic concrete powder solution extracts on corrosion behaviour of steel reinforcement, it is necessary to determine the ionic concentration, pH and conductivity of the concrete powder solutions. In addition from the literature review, it is observed that limited studies have been carried out to investigate the effect of conjoint chloride and sulfate ions on steel reinforcement corrosion in concrete. From these studies, it is observed that the researchers have presented different opinions regarding the performance of concrete in combined chloride and sulfate exposure conditions. Hence, there is a need to carry out a comprehensive experimental investigation on reinforcing steel corrosion in concrete by incorporating different types of binder and steel reinforcement in composite chloride-sulfate environment with varying concentrations of chloride and sulfate ions. In addition, it is also required to evaluate the effect of cation type associated with sulfate ions on steel reinforcement corrosion and on variation in compressive strength of concrete in the presence of chloride ions. Further, for

the purpose of analyzing the changes in phase composition of hardened concrete in the presence of chloride and sulfate ions, there is a need to carry out various microstructural techniques such as X-ray diffraction (XRD), Field emission scanning electron microscopy (FESEM), and Fourier transform infrared (FTIR) spectroscopy analyses. Based on these inferences, the objectives of the present research work have been formulated and are already presented in Chapter 1.

CHAPTER 3

EXPERIMENTAL METHODOLOGY OF RESEARCH

3.1 GENERAL

This chapter describes about the details of materials, specimens, exposure conditions and test procedures adopted to achieve the objectives of the present research work.

3.2 MATERIALS USED

3.2.1 Cementitious Materials

Three types of cementitious materials used in the preparation of concrete mixes are ordinary Portland cement (OPC) satisfying IS: 12269 – 1987 [101] and ASTM Type I [102]; Portland pozzolana cement (PPC) satisfying IS: 1489 – 1991 [103] and ASTM Type IP [104]; and ASTM C 618 [105] class F fly ash (FA). Fly ash was used at 20% and 30% replacement by mass of binder content (OPC + fly ash). The chemical composition of OPC, PPC and fly ash determined by X-ray fluorescence (XRF) analysis are presented in Table 3.1.

Table 3.1: Chemical composition of OPC, PPC and fly ash determined by X-ray Fluorescence (XRF) analysis

Constituent (wt. %)	Ordinary Portland Cement (OPC)	Portland Pozzolana Cement (PPC)	Fly ash (FA)
Calcium oxide (CaO)	65.2	64.7	16.57
Silicon dioxide (SiO_2)	19.2	20.52	53.24
Aluminium oxide (Al_2O_3)	5.2	4.2	25.3
Ferric oxide (Fe_2O_3)	2.4	3.4	1.2
Magnesium oxide (MgO)	3.4	1.55	1.15
Sodium oxide (Na_2O)	0.3	0.35	0.13
Potassium oxide (K_2O)	0.62	1.31	0.4
Titanium dioxide (TiO_2)	0.23	0.87	0.53
Phosphorus pentoxide (P_2O_5)	0.31	0.18	0.39
sulphur trioxide (SO_3)	1.5	1.6	0.2
Loss on ignition	1.4	1.2	0.6

3.2.2 Aggregates

Locally available river sand was used as fine aggregate in the preparation of concrete. The specific gravity of sand was determined using the pycnometer in accordance with IS: 2386 – 1963 (part III) [106]. The obtained value of specific gravity of sand was 2.61. The sieve analysis of sand was carried out as per the guidelines of IS: 2386 – 1963 (part I) [107]. From the cumulative percentage passing values of sieve analysis it is observed that, the sand is conforming to grading zone II as per IS: 383 – 1970 [108], and as per ASTM C33/C33M-13 [109]. The grading curve of sand is shown in Fig. 3.1.

Coarse aggregates of quartzite origin were used in the preparation of different concrete mixes. The coarse aggregates of size 20 mm MSA (maximum size aggregate) and 10 mm MSA were used in the proportion of 1.941:1 by mass of total coarse aggregate content to satisfy the overall grading requirement of coarse aggregate as per IS: 383-1970 [108] and ASTM C33/C33M-13 [109]. The specific gravity of coarse aggregate was determined using pycnometer and wire basket method for 10 mm MSA and 20 mm MSA coarse aggregates respectively in accordance with IS: 2386 – 1963 (part III) [106]. The obtained values of specific gravity of 10 mm MSA and 20 mm MSA coarse aggregates are 2.63 and 2.64 respectively. The sieve analysis of 10 mm MSA and 20 mm MSA coarse aggregates was carried out as per the guidelines of IS: 2386 – 1963 (part I) [107] and the grading curves are shown in Fig. 3.2 and Fig. 3.3.

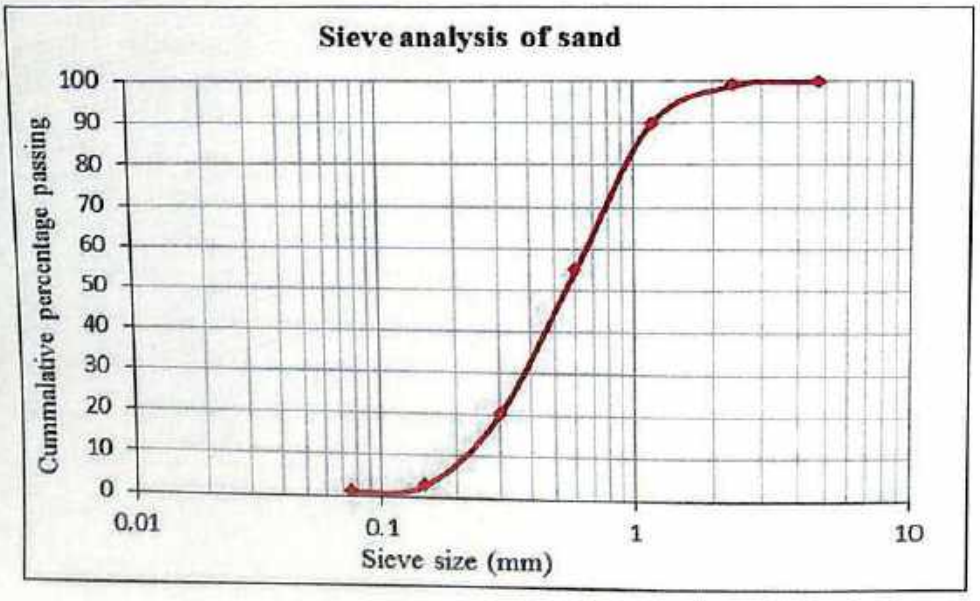

Fig. 3.1 Grading curve of sand

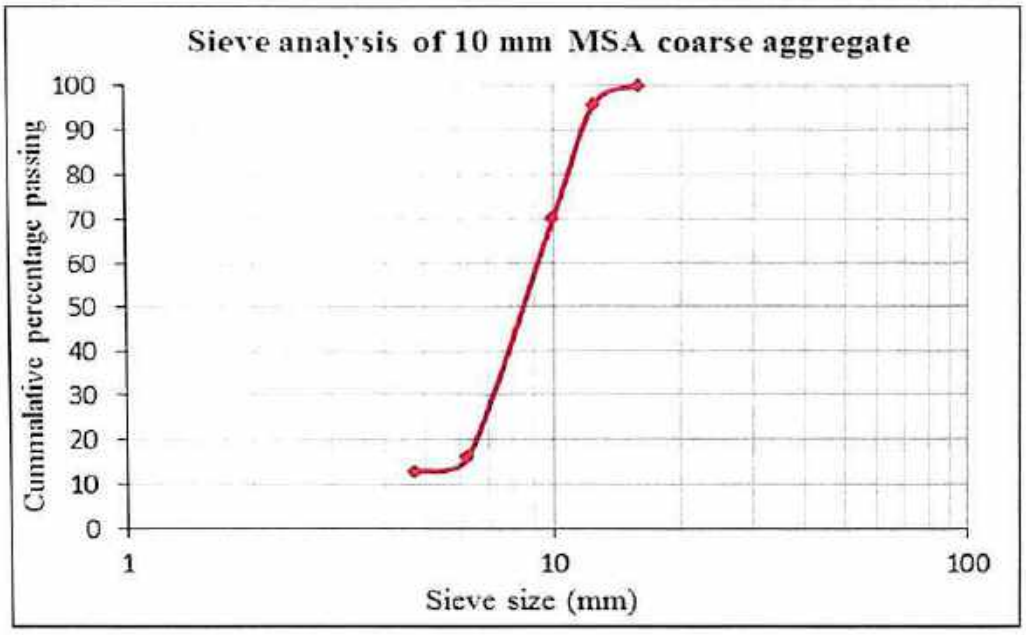

Fig. 3.2 Grading curve of 10 mm MSA coarse aggregate

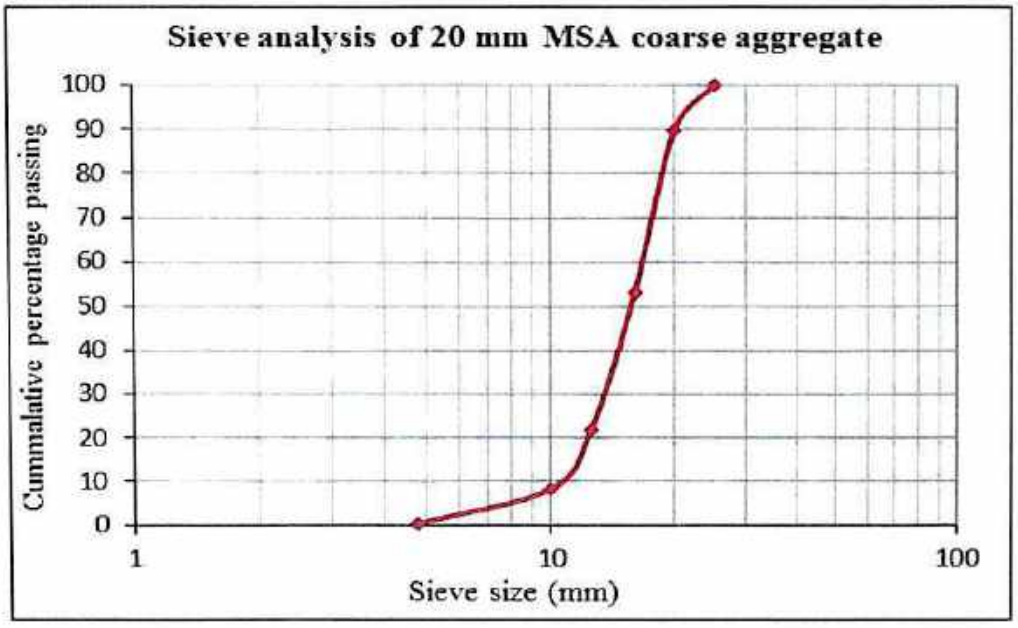

Fig. 3.3 Grading curve of 20 mm MSA coarse aggregate

3.2.3 Reinforcing Steel

Tempcore TMT (Thermomechanically treated) steel and Thermex TMT steel of diameter 12 mm were used as steel reinforcement. The chemical composition of Tempcore TMT steel and Thermex TMT steel as determined by Energy-dispersive x-ray (EDX) analysis are presented in Table 3.2.

Table 3.2: Chemical composition of steel in wt %, determined by Energy-Dispersive X-ray (EDX) analysis

Steel type	Mn (%)	Si (%)	Ni (%)	Cr (%)	Cu (%)	S (%)	P (%)	C (%)	Fe (%)
Tempcore TMT	1.2	0.6	0.2	0.2	0.1	0.2	0.1	<0.1	Balance
Thermex TMT	1.3	0.5	0.1	0.3	0.01	0.03	0.01	<0.1	Balance

The entire experimental program is divided into three series.

3.3 SERIES I

In this series, the effect of chloride and composite chloride-sulfate contamination on 28 day compressive strength and microstructural changes occurred in concrete due to the presence of chloride and composite chloride-sulfate ions has been investigated. Further, the effect of chloride and composite chloride-sulfate ions on ionic concentration, pH and conductivity of electrolytic concrete powder solution (ECPS); and corrosion behaviour of steel reinforcement in ECPS has also been investigated.

3.3.1 Specimen Preparation

Cube specimens of size 150 mm were prepared using ordinary Portland cement (OPC) and Portland pozzolana cement (PPC) from different concrete mixes i.e. from control mix and mixes contaminated with varying concentrations of chloride and composite chloride-sulfate salts. Chloride and sulfate salts were admixed at the time of preparation of concrete in the mixing water as percentage by mass of cement content. Sodium chloride (NaCl) was used as the source of chloride ions, whereas sodium sulfate (Na_2SO_4) and magnesium sulfate ($MgSO_4$) were used as the sources of sulfate ions. Sodium chloride (NaCl) is normally present in seawater and in contaminated soil and groundwater in varying concentrations. As already stated in Chapter 1, the chloride ions may also enter into fresh concrete at the time of its preparation through chloride contaminated mixing water, aggregates and chloride bearing admixtures. Further, in seawater and contaminated groundwater, sulfate salts mostly in the form of sodium sulfate and magnesium sulfate are also present along with chloride salts. On the basis of these factors, in the present work, lower to higher concentrations of NaCl, Na_2SO_4 and $MgSO_4$ were used. The concentrations of NaCl used were 3%, 5% and 7% and those of Na_2SO_4 and $MgSO_4$ were 3%, 6% and 12% each, by mass of cement content. The different combinations of the

salts admixed in concrete are presented in Table 3.3. The concrete mixes were prepared at water-cement ratios (w/c ratio) of 0.45 and 0.5. The water content in all the concrete mixes was kept at 195 Kg/m^3 and all the concrete mixes were designed for workability with slump varying from 20 to 50 mm. The mix proportioning of concrete was carried out using DOE method (British mix design method) with some modification []. The concrete mix proportion is presented in Table 3.4. Tap water from the laboratory was used as mixing water in the preparation of concrete mixes. After 24 hours of casting, the cube specimens were demoulded and subjected to moist curing till the age of 28 days from the day of preparation. After that, the specimens were removed from curing tank and kept in laboratory exposure condition till the period of crushing for obtaining concrete powder. Separate cubes specimens were also prepared to determine the 28 day compressive strength of different concrete mixes.

Table 3.3: Combination of chloride and sulfate salts admixed in concrete mixes by mass of cement content

Concentration of admixed salts	Abbreviation	Group
3% NaCl	3NC	Sodium chloride
5% NaCl	5NC	
7% NaCl	7NC	
3% NaCl + 3% Na_2SO_4	3NC + 3NS	Sodium chloride plus sodium sulfate
5% NaCl+ 3% Na_2SO_4	5NC + 3NS	
7% NaCl+ 3% Na_2SO_4	7NC + 3NS	
3% NaCl + 6% Na_2SO_4	3NC + 6NS	
5% NaCl+ 6% Na_2SO_4	5NC + 6NS	
7% NaCl+ 6% Na_2SO_4	7NC + 6NS	
3% NaCl + 12% Na_2SO_4	3NC + 12NS	
5% NaCl+ 12% Na_2SO_4	5NC + 12NS	
7% NaCl+ 12% Na_2SO_4	7NC + 12NS	
3% NaCl + 3% $MgSO_4$	3NC + 3MS	Sodium chloride plus magnesium sulfate
5% NaCl+ 3% $MgSO_4$	5NC + 3MS	
7% NaCl+ 3% $MgSO_4$	7NC + 3MS	
3% NaCl + 6%$MgSO_4$	3NC + 6MS	
5% NaCl+ 6% $MgSO_4$	5NC + 6MS	
7% NaCl+ 6% $MgSO_4$	7NC + 6MS	
3% NaCl + 12% $MgSO_4$	3NC + 12MS	
5% NaCl+ 12% $MgSO_4$	5NC + 12MS	
7% NaCl+ 12% $MgSO_4$	7NC + 12MS	

Table 3.4: Mixture proportion of concrete for OPC and PPC

Water-cement ratio	0.45	0.5
Water content (kg/m^3)	195	195
Cement content (kg/m^3)	433.33	390
Fine aggregate (kg/m^3)	614.83	648
Coarse aggregate (kg/m^3)	1141.84	1152

3.3.2 Preparation of Electrolytic Concrete Powder Solution (ECPS)

The concrete cube specimens were crushed at the age of 56 days from the day of preparation in the compression testing machine followed by further crushing in abrasion testing machine. The collected powder was sieved through a sieve having square mesh of size 150 μm. The sieved concrete powder was then stored in air tight plastic containers. Fig 3.4 shows photograph of stored concrete powder samples. To prepare electrolytic concrete powder solution (ECPS), the concrete powder was mixed with distilled water in 1:1 proportion by mass in a beaker. The mixture was then stirred for half an hour and then boiled for 15 – 20 minutes. After that the solution was allowed to settle and cool to the room temperature. The solution was then filtered through Whatman no. 1 filter paper. The obtained filtered concrete powder aqueous solution nearly represents all the species in the vicinity of steel reinforcement in the concrete as it is extracted from concrete powder, which is a mixture of cement hydrates, coarse aggregate, fine aggregate and admixed concentrations of chloride and composite chloride-sulfate ions. The process of stirring, heating and filtration of the solution is shown in Fig 3.5. The electrolytic concrete powder solution was chemically analyzed to determine its ionic concentration, pH and conductivity. The electrochemical tests on steel specimen were conducted in this electrolytic concrete powder solution.

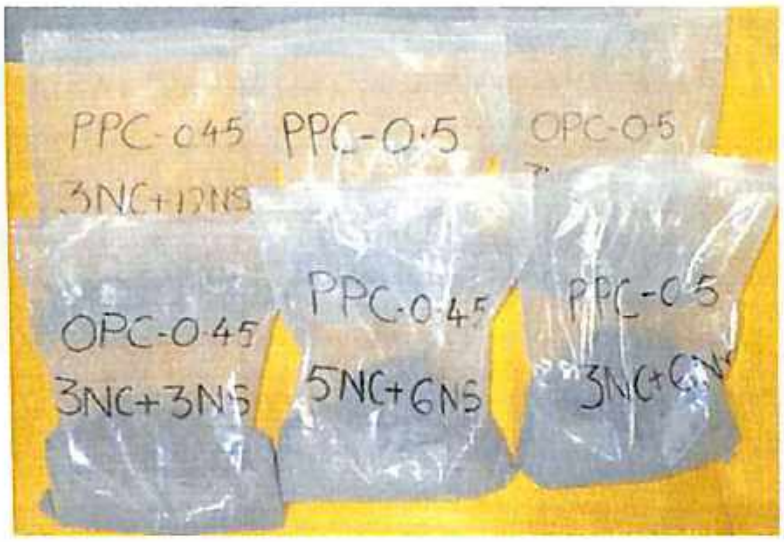

Fig 3.4 Collected and stored concrete powder samples in air tight plastic containers

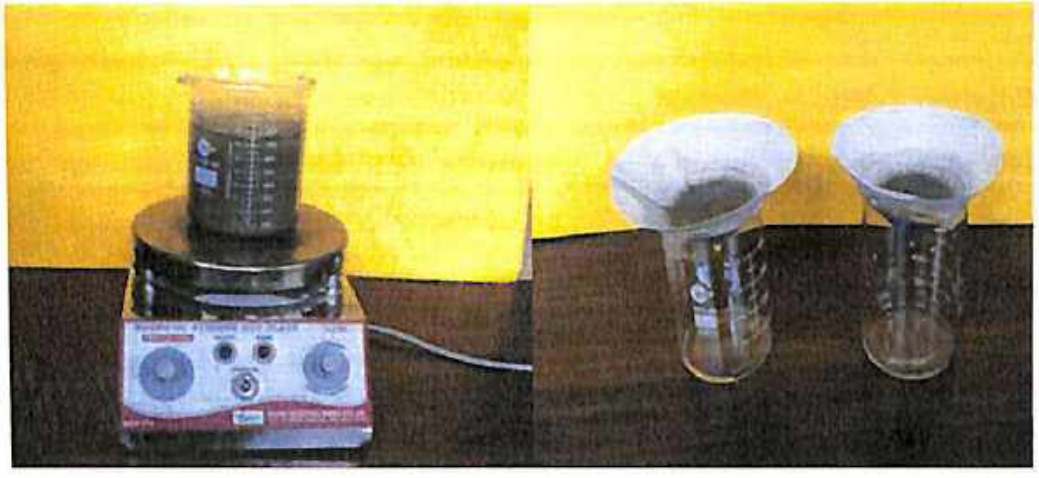

Fig 3.5 Stirring, heating and filtration of electrolytic concrete powder solution extracted from concrete powder

3.3.3 Preconditioning of Bare Steel Specimens

As already stated, Tempcore TMT and Thermex TMT steel bars of 12 mm diameter were used as steel reinforcement in the experimental investigation. The steel bars were cut to a length of 70 mm. These specimens were drilled and threaded at one end to be mounted to the working electrode node of the corrosion monitoring instrument. The steel specimens were cleaned with wire brush to remove any surface scale. After that, the specimens were coated with epoxy, leaving an exposed length of 5 mm at the opposite end of the drilled one. The exposed surface area of the steel specimen is 1.884 cm^2. The schematic diagram of preconditioned steel specimen is shown in Fig. 3.6.

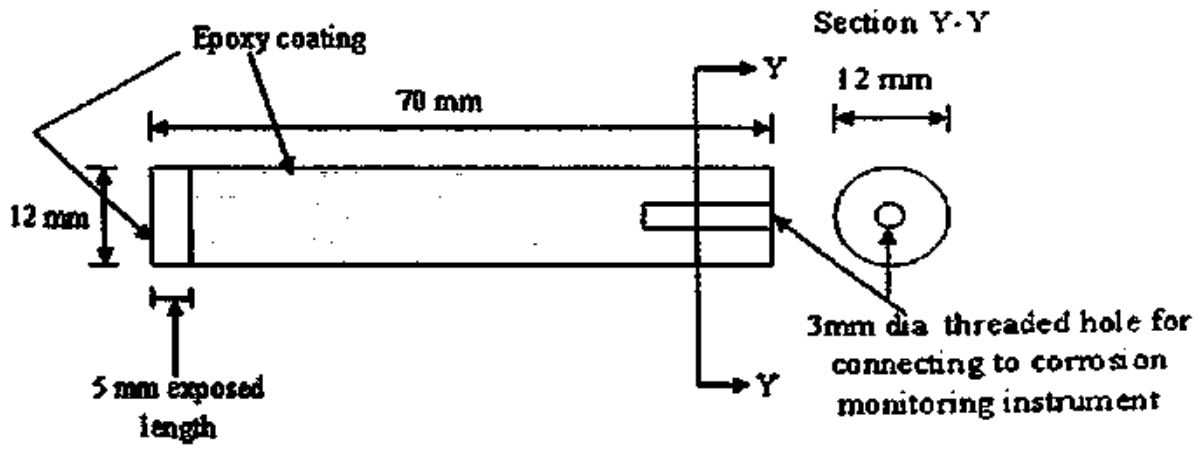

Fig. 3.6 Schematic diagram of steel specimen

3.3.4 Test Techniques

3.3.4.1 Compressive Strength Test

The effect of admixed chloride and composite chloride-sulfate ions on compressive strength of concrete was evaluated by conducting compressive strength test on cube specimens of size 150 mm made from different concrete mixes at the age of 28 days. As already stated, the cube specimens were cured in water till the age of 28 days in a curing tank. The specimens were then taken out from the curing tank and tested as per IS: 516 – 1959 [110] in a hydraulically operated compression testing machine. Three replicate cube specimens of each concrete mix were tested and the average value was reported.

3.3.4.2 Microstructural Study of Concrete Powder

3.3.4.2.1 X-ray Diffraction (XRD) Analysis

In the present investigation, XRD analysis was carried out to determine the effect of chloride and sulfate ions on phase composition of hardened concrete. Powder X-ray diffraction was performed on Bruker D-8 Advance X-ray diffractometer with Cu Kα radiation (λ = 1.5405 Å). Diffraction patterns were generated on a vertical goniometer attached to a board focus X-ray tube with a copper target operating at 40 kV and 40 mA. The concrete powder samples, which were obtained from different concrete mixes and stored after passing through 150 μm sieve were used to conduct XRD analysis. The concrete powder sample filled into the sample holder and was scanned from 5° to 55° (2θ) at a sampling interval of 0.05° 2θ per second. After obtaining the XRD patterns, the phase

identification process involves the calculation of the most likely match score for a given phase based on peak intensity and peak position, when compared with the database of standard phases.

3.3.4.2.2 Fourier Transform Infrared (FTIR) Spectroscopy

In the present investigation, FTIR spectroscopy was performed to identify functional groups associated with different products formed in concrete. Fourier transform infrared spectrum of concrete powder sample was collected in the transmission mode using Thermo fisher scientific Nicolet iS10 FTIR spectrometer. The sample pallets were prepared by mixing 250 mg of potassium bromide (KBr) with 3 mg of concrete powder sample. Fifteen scans were recorded over a range of 4000 cm^{-1} to 400 cm^{-1}. Before scanning the sample, the background spectrum was collected at ambient atmosphere to eliminate the atmospheric effect.

3.3.4.2.3 Field Emission Scanning Electron Microscopy (FESEM)

Microstructural changes occurred in the concrete mixes contaminated with NaCl, Na_2SO_4 and $MgSO_4$ was evaluated by field emission scanning electron microscopy. This study was conducted on field emission scanning electron microscope (make: Zeiss model: Sigma) to examine the morphology of concrete. The concrete powder sample was sprayed on double sided carbon tape kept on the stub top and then pressed with a clean glass plate to reduce the number of loose grains. The concrete powder is coated with a thin layer of electrically conductive material before scanning i.e. coated with gold by means of high resolution sputter coater to protect the concrete powder from charging.

3.3.4.3 pH Measurement of Electrolytic Concrete Powder Solution

The pH values of uncontaminated electrolytic concrete powder solution and of that contaminated with chloride and composite chloride-sulfate ions were measured using a digital pH meter with pH range 0 – 14. The pH meter was calibrated before carrying out the measurement of electrolytic concrete powder solution.

3.3.4.4 Conductivity Measurement of Electrolytic Concrete Powder Solution

The conductivity of concrete depends on the presence of different ions such as Na^+, K^+, Ca^{++}, OH^-, SO_4^{2-} and Cl^- in the concrete pore solution. The conductivity of electrolytic concrete powder solutions uncontaminated and contaminated with chloride and composite chloride-sulfate ions were measured using a digital conductivity meter. The conductivity meter was calibrated before measuring the conductivity of electrolytic concrete powder solution.

3.3.4.5 Chemical Analysis of Electrolytic Concrete Powder Solution

The chemical composition of electrolytic concrete powder solution extracted from concrete powder depends on binder type, water-cement ratio and concentration of admixed chloride and sulfate ions. The electrolytic concrete powder solutions prepared from OPC and PPC at water-cement ratios of 0.45 and 0.5 and admixed with varying dosages of chloride and sulfate ions are analyzed to determine the concentrations of cations i.e. sodium (Na^+), calcium (Ca^{++}), potassium (K^+), and anions i.e. chloride (Cl^-) and sulfate (SO_4^{2-}).

The concentrations of sodium (Na^+), calcium (Ca^{++}) and potassium (K^+) ions present in the electrolytic concrete powder solution were determined using Flame photometer by preparing the appropriate dilute solutions in accordance with the Standard Methods for the examination of water and wastewater published by the American Public Health Association (APHA) [111]. In the flame photometer, the solution under analysis is sprayed as a mist into a non-luminous flame, which becomes coloured according to the characteristic emission of elements (Na: 589 nm, K: 786 nm and Ca: 622 nm). The flame is monitored by a photo detector through a narrow band optical filter that only passes the wavelengths centered around the characteristic emission of the selected element. For analyzing the electrolytic concrete powder solution for Na^+, Ca^{++} and K^+ ions, first the automatic capillary tube of flame photometer was dipped in distilled water. Then, the flame photometer was calibrated with standard solutions of Na^+ (10 ppm), Ca^{++} (100 ppm) and K^+ (10 ppm). After calibration, the concentrations of sodium (Na^+), calcium (Ca^{++}) and potassium (K^+) ions were measured.

The water soluble or free chloride ion (Cl^-) concentration in electrolytic concrete powder solution was determined by argentometric method as described in the Standard Methods

for the examination of water and wastewater published by APHA [111]. To measure free Cl^- ion concentration, first the titrant for blank was determined. For this purpose, 25 ml of the distilled water was taken in conical flask and 1 ml of potassium chromate indicator was added to it, followed by titrating against silver nitrate ($AgNO_3$) solution, till the colour changes to reddish-brown. After that, the electrolytic concrete powder solution was diluted and 1 ml of potassium chromate indicator was added to it. This solution was then titrated against $AgNO_3$. The water soluble or free Cl^- ion concentration was determined by using the following equation.

$$Cl^-(mg/l) = \frac{(A-B)\times N\times 35450}{25\ ml} \qquad (3.1)$$

Where, A is titrant for electrolytic concrete powder solution (ml), B is titrant for blank (ml) and N is normality of $AgNO_3$ taken as 0.141.

The sulfate ion (SO_4^{2-}) concentration in the electrolytic concrete powder solution was determined by turbidimetric method as described in the Standard Methods for the examination of water and wastewater published by APHA [111]. The standard sulfate solution was prepared. The electrolytic concrete powder solution was diluted and 20 ml of buffer solution (prepared by dissolving 30 g magnesium chloride ($MgCl_2 . 6H_2O$), 5 g sodium acetate ($CH_3COONa . 3H_2O$) 1.0 g potassium nitrate (KNO_3) and 20 ml acetic acid (CH_3COOH) in 500 ml distilled water and make up to 1000 ml) was added to it and mixed by stirring. While stirring the solution, one spoon full of barium chloride ($BaCl_2$) crystals was added and stirred for one minute. Then, the solution was poured in turbidity cell of the turbidity meter to measure the turbidity. The SO_4^{2-} ion concentration in electrolytic concrete powder solution was then determined by comparing the turbidity reading with a calibration curve, prepared by using standard sulfate solution.

3.3.4.6 Potentiodynamic Polarization Test

The corrosion behaviour of steel reinforcement was evaluated by obtaining different zones of corrosion from anodic polarization curves. For this purpose, potentiodynamic polarization test was conducted on bare steel specimen immersed in electrolytic concrete powder solution (ECPS) obtained from control mix and that contaminated with chloride and sulfate ions, in an electrochemical cell. The electrochemical cell consists of three electrodes, namely working electrode (WE), reference electrode (RE), and auxiliary

electrode (AE). Bare steel specimen was used as the working electrode. A saturated calomel electrode (SCE) and a platinum electrode were used as reference electrode and auxiliary electrode respectively. The potentiodynamic polarization test was performed on steel specimens using a corrosion monitoring instrument (make: ACM, Gill AC serial no. 1542 sequencer). The electrolytic concrete powder solution was poured in the electrochemical cell and the electrodes were immersed in the solution. The electrodes were connected to the corrosion monitoring instrument that automatically maintains the desired potential between working electrode and auxiliary electrode by passing the appropriate current between them and plots the polarization curves. The potentiodynamic polarization test was conducted on the steel specimen by applying the potential scan from 0 mV to 1500 mV with an offset from corrosion potential at a sweep rate of 50 mV per minute. The schematic diagram and photograph of experimental set-up are shown in Fig. 3.8 and Fig. 3.9 respectively. Two replicate steel specimens were tested for a given electrolytic concrete powder solution to observe the reproducibility. The photograph of some of the tested steel specimens is shown in Fig. 3.10.

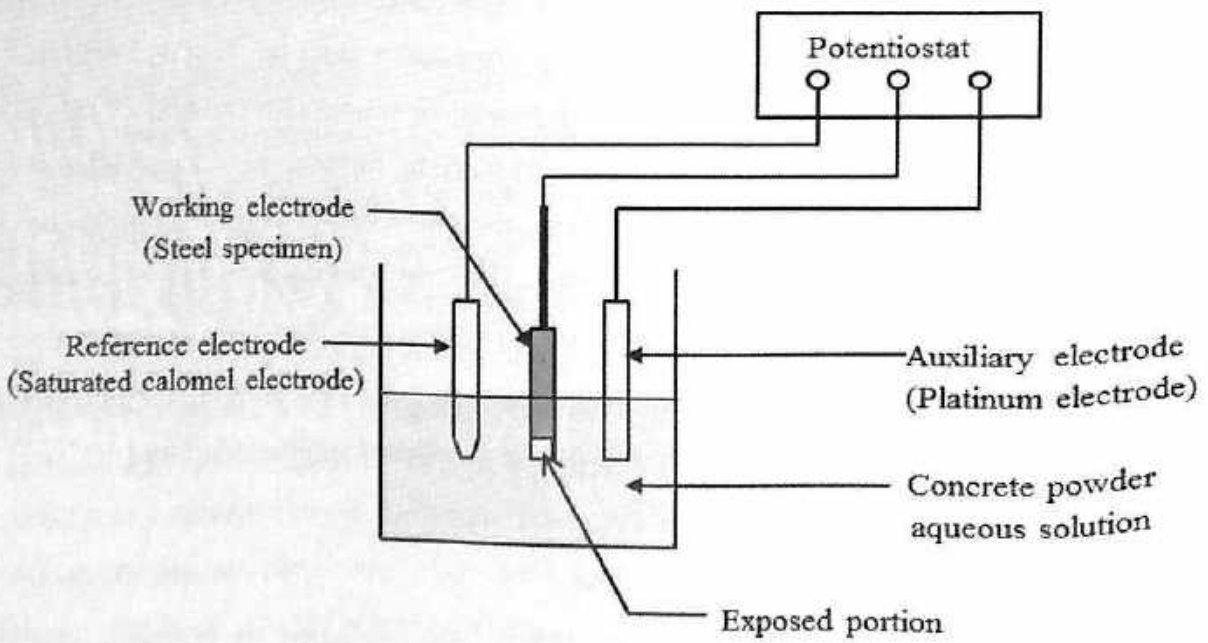

Fig. 3.7 Schematic diagram of electrochemical test set-up

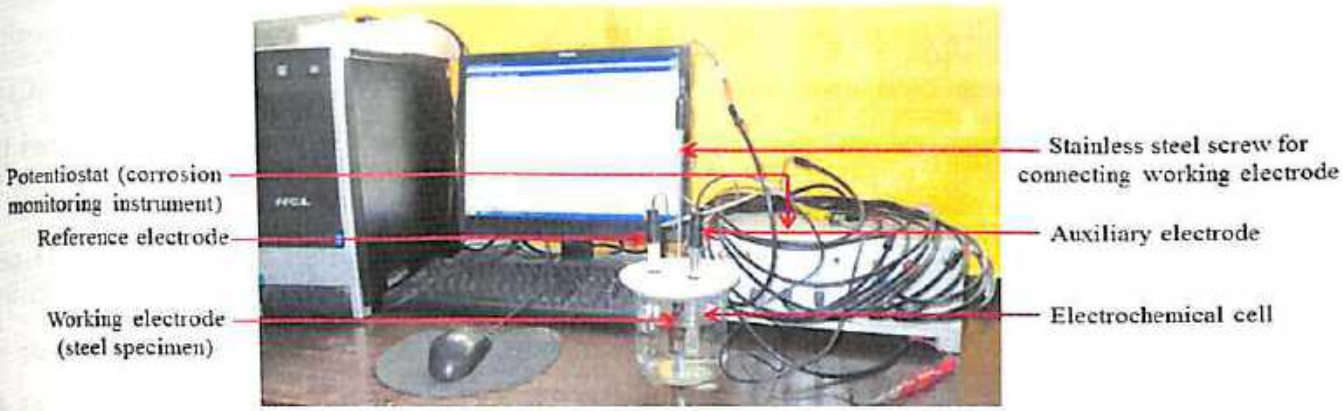

Fig. 3.8 Photograph of electrochemical test set-up

Fig. 3.9 Photograph of steel specimens after completion of potentiodynamic polarization test in contaminated electrolytic concrete powder solution

3.3.4.7 Linear Polarization Resistance (LPR) Test

In the present research work, the performance of different types of cement and steel reinforcement against corrosion in electrolytic concrete powder solution contaminated with different concentrations of chloride and sulphate ions was evaluated by measuring corrosion potential and corrosion current density. The corrosion potential provides information about the probability of occurrence of steel reinforcement corrosion, whereas the quantitative estimation of corrosion rate of steel reinforcement is obtained from corrosion current density.

The corrosion current density of steel reinforcement was determined by linear polarization resistance (LPR) technique. For measuring corrosion potential and corrosion current density of reinforcing steel in electrolytic concrete powder solution, the same test

set-up (Fig. 3.8), as in case of potentiodynamic polarization test, was used. The corrosion potential of steel was measured with reference to saturated calomel electrode (SCE). During the LPR measurement, the working electrode (steel specimen) was polarized by applying a potential scan of ±20 mV from the corrosion potential at a scan rate of 6 mV per minute. The corrosion current density was then determined by using the Stern-Geary equation [112-115].

$$I_{corr} = \frac{B}{R_p} \tag{3.2}$$

Where, I_{corr} is the corrosion current density, B is the Stern-Geary constant and R_p is the polarization resistance of steel reinforcement.

The Stern-Geary constant 'B' is given by;

$$B = \frac{\beta_a \times \beta_c}{2.3(\beta_a + \beta_c)} \tag{3.3}$$

Where β_a and β_c are anodic and cathodic Tafel constants respectively. The value of B equal to 26 mV for steel in active condition and 52 mV for steel in passive condition are normally used [22, 114]. In the present research work, the value of B is taken as 26 mV, considering the steel in active condition. Two replicate steel specimens were tested for a given electrolytic concrete powder solution to observe the reproducibility and the average values of corrosion potential and corrosion current density are reported.

3.4 SERIES II

In this series, the effects of binder type and steel type on corrosion behaviour of steel reinforcement in concrete admixed with varying concentrations conjoint chloride-sulfate ions and subsequently exposed externally to these ions have been investigated.

3.4.1 Specimen Preparation

Prismatic reinforced concrete specimens of size 72 mm × 72 mm × 300 mm were prepared using different types of binders such as ordinary Portland cement (OPC), Portland pozzolana cement (PPC) and OPC plus fly ash at different replacement levels (20% and 30% by mass of binder content) at a w/b ratio of 0.5. The binder content, water content and aggregate contents of the concrete mix were same as that of the concrete mix (Table 3.4) used for obtaining concrete powder. The prismatic reinforced concrete

specimens were prepared with a steel bar of 12 mm diameter embedded centrally wi... concrete cover of 30 mm on all the sides and at the bottom. Tempcore TMT and Thermex TMT steel bars were used as steel reinforcement. The steel bars were cut to a length of 320 mm and cleaned with wire brush to remove any surface scale. In order to prevent crevice corrosion, the steel specimens were wrapped with insulating tap followed by application of epoxy coating at the locations where there is discontinuity of steel bar with the surrounding concrete. The schematic diagram of preconditioned steel specimen is shown in Fig. 3.11. The prismatic reinforced concrete specimens were prepared from different concrete mixes i.e. from control mix and mixes contaminated with varying concentrations of composite chloride-sulfate salts. For composite chloride-sulfate contamination, the concrete mixes were admixed with different concentrations of sodium chloride plus sodium sulfate and sodium chloride plus magnesium sulfate. The admixed concentrations of sodium chloride were 3%, 5% and 7% by mass of binder content. Similarly the admixed concentrations of sodium sulfate and magnesium sulfate, each were 3% and 6% by mass of binder content. The required quantities of these salts were dissolved in the mixing water during the preparation of concrete mixes. The different combinations of the salts admixed in concrete are presented in Table 3.5. All the specimens were moist cured in a curing tank till the period of 28 days from the day of preparation. The schematic diagram of the prismatic reinforced concrete specimen is shown in Fig. 3.12. The exposed length of the steel bar inside the prismatic specimen is 150 mm.

Table 3.5: Combinations of chloride and sulfate salts admixed in the concrete mixes by mas
binder content

Concentration of admixed salts	Abbreviation	Group
3% NaCl + 3% Na_2SO_4	3NC + 3NS	Sodium chloride plus sodium sulfate
5% NaCl+ 3% Na_2SO_4	5NC + 3NS	
7% NaCl+ 3% Na_2SO_4	7NC + 3NS	
3% NaCl + 6% Na_2SO_4	3NC + 6NS	
5% NaCl+ 6% Na_2SO_4	5NC + 6NS	
7% NaCl+ 6% Na_2SO_4	7NC + 6NS	
3% NaCl + 3% $MgSO_4$	3NC + 3MS	Sodium chloride plus magnesium sulfate
5% NaCl+ 3% $MgSO_4$	5NC + 3MS	
7% NaCl+ 3% $MgSO_4$	7NC + 3MS	
3% NaCl + 6%$MgSO_4$	3NC + 6MS	
5% NaCl+ 6% $MgSO_4$	5NC + 6MS	
7% NaCl+ 6% $MgSO_4$	7NC + 6MS	

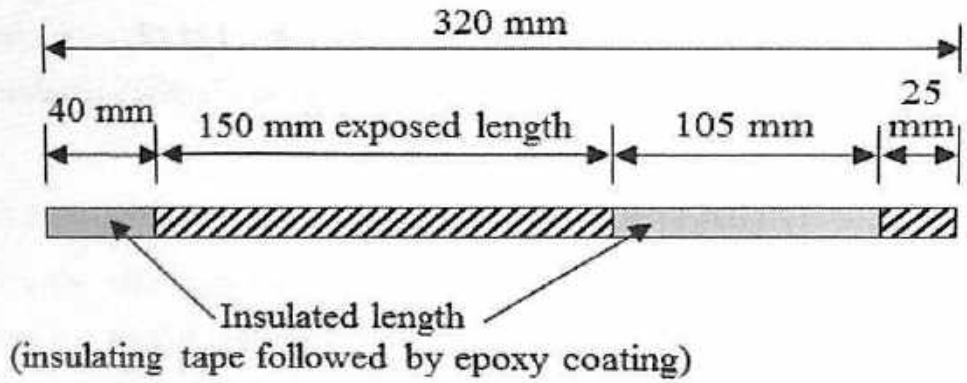

Fig. 3.10 Schematic diagram of preconditioned reinforcing steel specimen

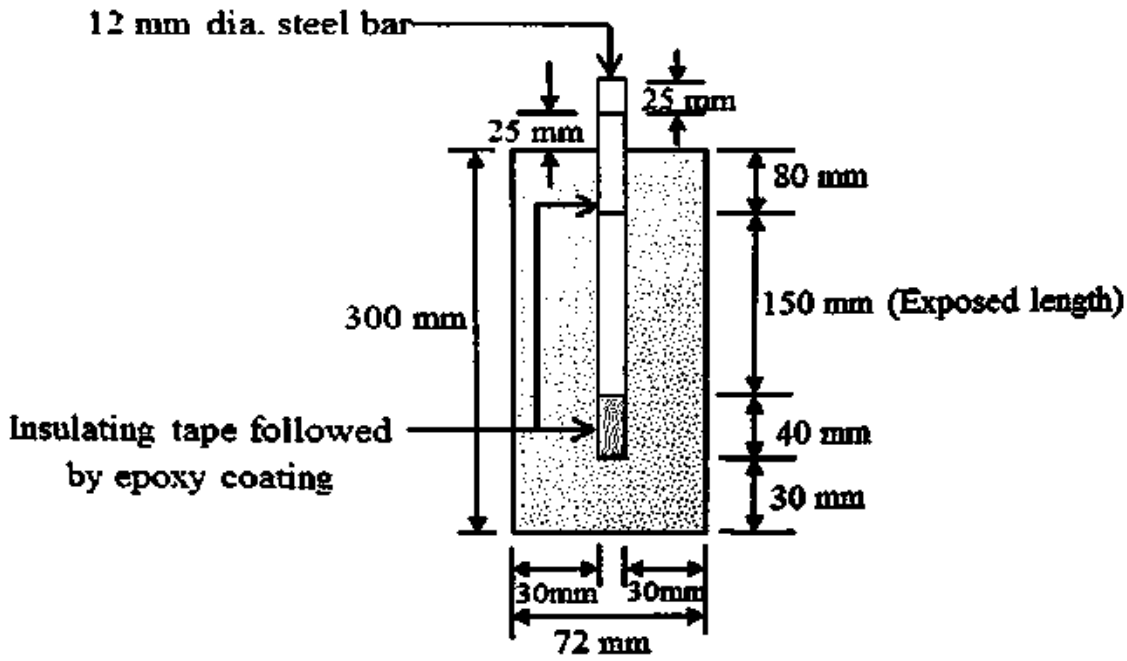

Fig. 3.11 Schematic diagram of prismatic reinforced concrete specimen (72 mm × 72 mm × 300 mm) centrally embedded with a steel bar

3.4.2 Exposure Condition

After 28 days of moist curing, the prismatic reinforced concrete specimens were removed from the curing tank and were kept in laboratory exposure condition for a period of 90 days from the day of preparation. After that, the specimens prepared from control mix i.e. uncontaminated concrete mix were exposed to normal water and those prepared from contaminated concrete mix i.e. admixed with chloride and sulfate salts were exposed to composite chloride-sulfate solutions. The composite chloride-sulfate solutions were prepared by adding sodium chloride plus sodium sulfate and sodium chloride plus magnesium sulfate in water at same concentrations (%) as that was admixed during the preparation of concrete mixes. It is to be noted that these salts were added as % by mass of water for preparing the exposure solutions. The prismatic reinforced concrete specimens were subjected to exposure solutions with alternate wetting-drying cycles, after laboratory exposure, till a period of 270 days from the day of preparation. The alternate wetting-drying cycles comprised of 7 days of partial immersion of the prismatic specimens in the exposure solutions in plastic tanks up to a height of 230 mm from the bottom of the specimen followed by 14 days of drying in the laboratory condition. The level of solution in the plastic tank was monitored at regular intervals and maintained up

to the height of 230 mm from the bottom of the specimen. The plastic tanks were covered with polythene sheets to prevent evaporation. Photograph of some of the reinforced concrete prismatic specimens during wetting and drying is shown in Fig. 3.13. It is to be noted that three replicate prismatic specimens from each concrete mix were prepared for a given exposure solution.

Fig. 3.12 Photograph of reinforced concrete prismatic specimens during wetting and drying

3.4.3 Corrosion Monitoring of Steel Reinforcement in Concrete

The corrosion of steel reinforcement embedded in prismatic specimens admixed with composite chloride-sulfate ions and subsequently exposed to chloride-sulfate solutions was monitored by measuring corrosion potential and corrosion current density at the age of 90, 180 and 270 days from the day of preparation of the specimens. In the present investigation, linear polarization resistance (LPR) technique was used to determine the corrosion current density of steel reinforcement embedded in concrete. Saturated calomel electrode (SCE) was used as reference electrode and a pair of stainless steel plates were used as auxiliary electrode. The schematic diagram of the experimental set-up is shown in Fig. 3.14. The prismatic specimen, reference electrode and auxiliary electrode were immersed in the test solution (corresponding exposure solution), as shown in Fig. 3.14. The steel reinforcement embedded in concrete as working electrode, reference electrode and auxiliary electrode were connected to the corrosion monitoring instrument. The corrosion potential of steel reinforcement embedded in the prismatic specimen was measured with reference to saturated calomel electrode. During LPR measurement, the

steel bar embedded in prismatic specimen was polarized to ±20 mV from the corrosion potential at a scan rate of 6 mV per minute. The corrosion current density was then determined by using Stern-Geary equation as mentioned in Eq. 3.3. From a given concrete mix three replicate prismatic specimens were tested for each exposure solution and the average values of corrosion potential and corrosion current density are reported. The photograph of the test set-up is shown in Fig. 3.15.

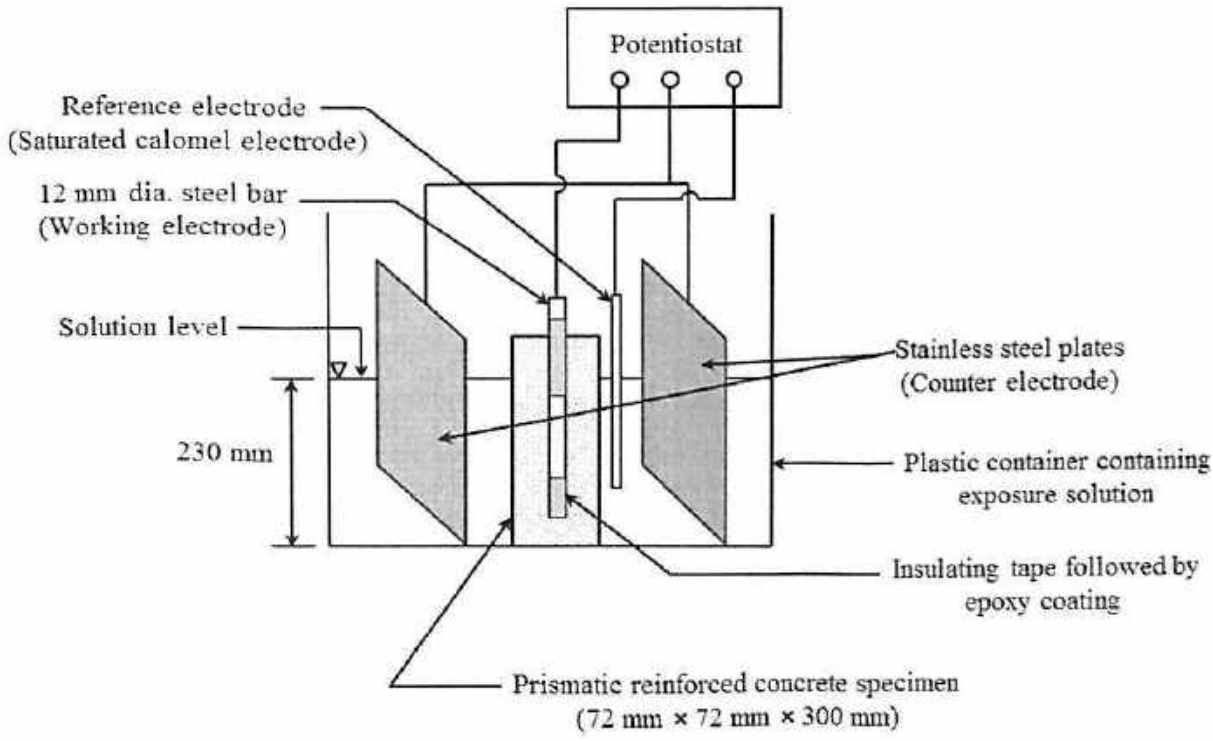

Fig. 3.13 Schematic diagram of test set-up for corrosion potential and corrosion current density measurement

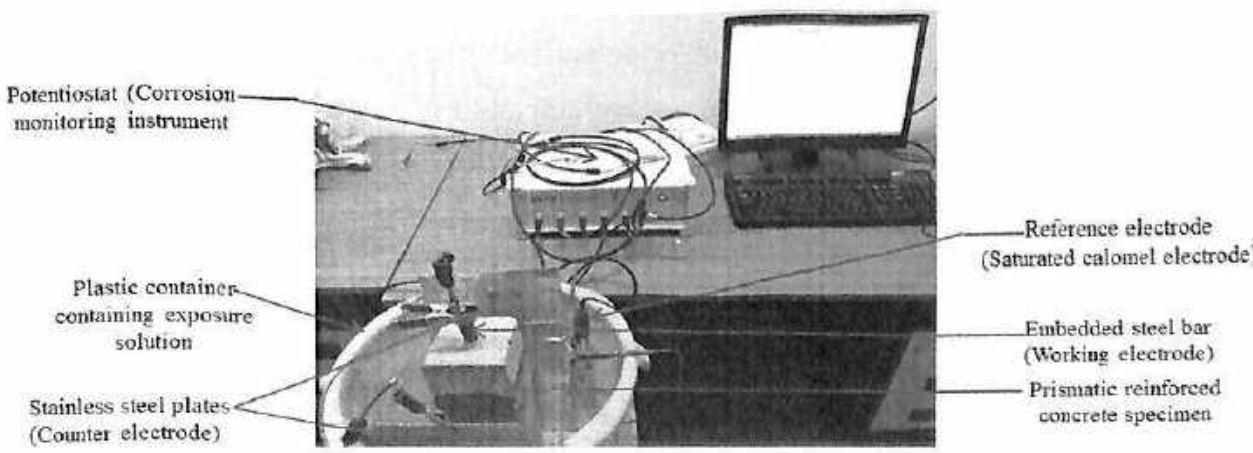

Fig. 3.14 Photograph of test set-up for corrosion potential and corrosion current density measurement

3.5 SERIES III

In this series, the effect of sulfate ions and that of composite chloride-sulfate ions on deterioration of concrete have been investigated through the measurement of change in weight and compressive strength of concrete specimens after 360 days of exposure to these aggressive agents.

3.5.1 Specimen Preparation

Cube specimens of size 150 mm were prepared from different concrete mixes. The concrete mixes were prepared with different types of binder such as OPC, PPC and OPC plus fly ash at different replacement levels (20% and 30% by mass of binder content) at w/b ratios of 0.45 and 0.5. The binder content, water content and aggregate contents of the concrete mixes were same as that of the concrete mixes shown in Table 3.4. Six replicate cube specimens were prepared from each concrete mix for a given exposure solution. After 24 hours of casting, the cube specimens were demoulded and moist cured in curing tank till the age of 28 days from the day of preparation.

3.5.2 Exposure Condition

After completion of moist curing, the cube specimens were removed from the curing tank and were then kept in the laboratory condition for a period of 7 days. After that, the specimens were exposed to normal water, sulfate solutions and composite chloride-sulfate solutions for a period of 360 days. The sulfate solutions were prepared by adding sodium sulfate and magnesium sulfate separately, each at concentrations of 3%, 6% and 12% (by mass of water). Similarly composite chloride-sulfate solutions were prepared by adding sodium chloride plus sodium sulfate and sodium chloride plus magnesium sulfate in water. The concentrations of sodium chloride in composite solutions were 3% and 5% (by mass of water) and the concentrations of sodium sulfate and magnesium sulfate were same as that added for preparation of only sulfate solutions. The concentrations and combinations of different exposure solutions are presented in Table 3.6. The weight of each cube specimen was measured before immersing in the exposure solution. Out of six replicate cube specimens prepared from each concrete mix, three cubes were subjected to alternate wetting-drying cycles with 7 days of full immersion in the exposure solution in plastic tanks followed by 14 days of drying in the laboratory condition. Remaining three cubes were fully immersed in the exposure solution continuously till the end of exposure

period. After completion of exposure period i.e. 360 days, the weight and compressive strength of each cube specimen were measured. The level of the exposure solution in the plastic tanks was monitored at regular intervals and adjusted, so that all the specimens were immersed fully in the expsoure solutions. To prevent evaporation, the plastic tanks were covered with polythene sheets. Photograph of some of the cube specimens during wetting and drying are shown in Fig. 3.16.

Table 3.6: Concentrations and combinations of exposure solutions

Concentration of exposure solutions	Abbreviation	Category
3% Na_2SO_4	3NS	Sodium sulfate
6% Na_2SO_4	6NS	
12% Na_2SO_4	12NS	
3% $MgSO_4$	3MS	Magnesium sulfate
6% $MgSO_4$	6MS	
12% $MgSO_4$	12MS	
3% NaCl + 3% Na_2SO_4	3NC + 3NS	Sodium chloride plus sodium sulfate
3% NaCl + 6% Na_2SO_4	3NC + 6NS	
3% NaCl + 12% Na_2SO_4	3NC + 12NS	
5% NaCl + 3% Na_2SO_4	5NC + 3NS	
5% NaCl + 6% Na_2SO_4	5NC + 6NS	
5% NaCl + 12% Na_2SO_4	5NC + 12NS	
3% NaCl + 3% $MgSO_4$	3NC + 3MS	Sodium chloride plus magnesium sulfate
3% NaCl + 6% $MgSO_4$	3NC + 6MS	
3% NaCl + 12% $MgSO_4$	3NC + 12MS	
5% NaCl + 3%$MgSO_4$	5NC + 3MS	
5% NaCl + 6% $MgSO_4$	5NC + 6MS	
5% NaCl + 12% $MgSO_4$	5NC + 12MS	

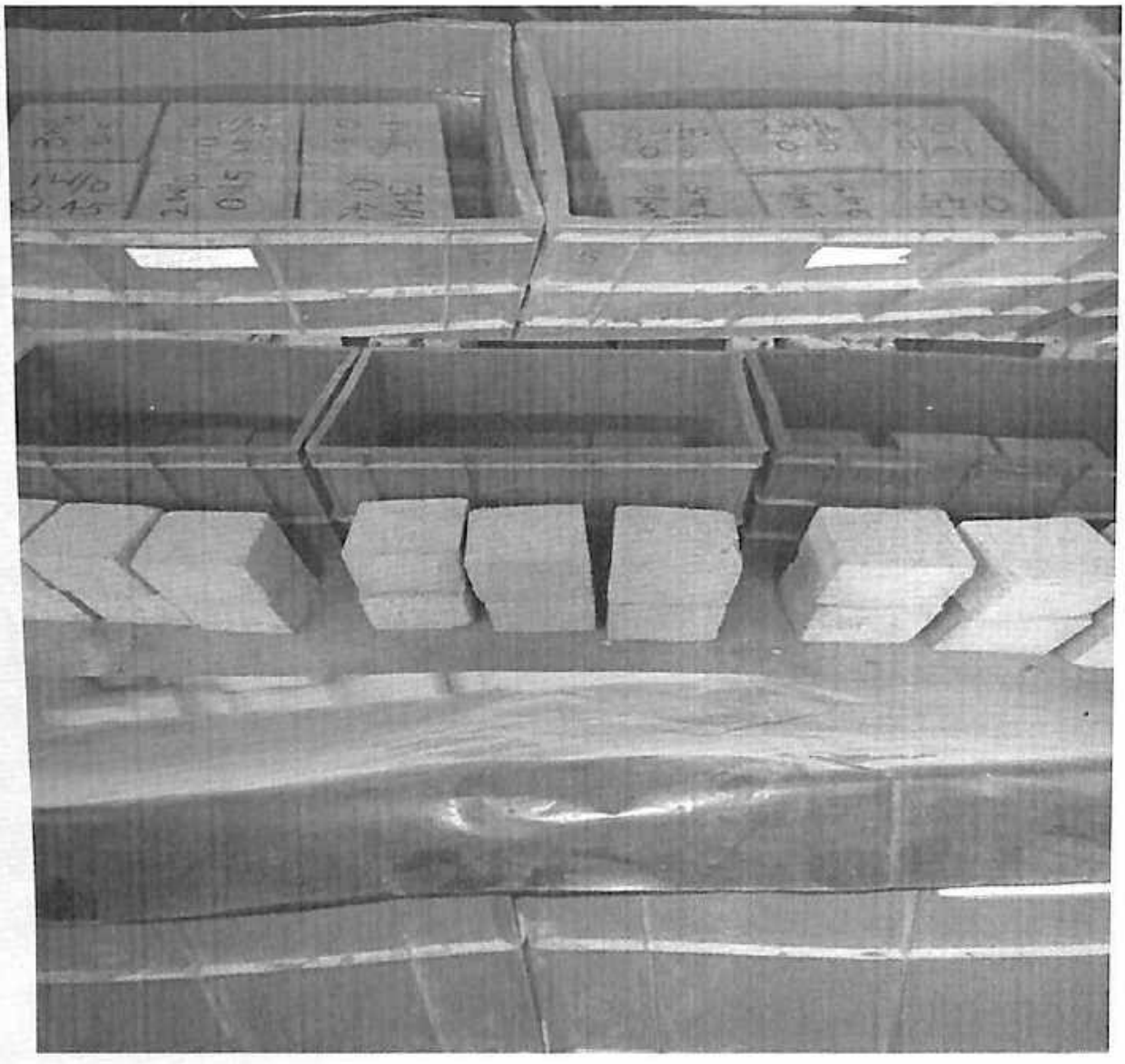

Fig. 3.15 Photograph of cube specimens under continuous full immersion and alternate wetting and drying condition

3.5.3 Test Procedures

3.5.3.1 Change in Weight of Concrete

The degree of physical deterioration due to sulfate ion and that due to composite chloride-sulfate ions was evaluated in terms of change (gain or reduction) in weight of concrete cube specimens after 360 days of exposure to the aggressive solutions. As already mentioned, the weight of each cube specimen was measured as initial weight before immersing in the exposure solution. After 360 days of exposure to different exposure solutions, the cube specimens were air-dried in the laboratory, and subsequently cleaned

and weighed. The average change in weight of cube specimen was calculated as a percentage with respect to its initial weight and is shown below.

$$\text{Average change in weight (\%)} = \left[\frac{W_i - W_t}{W_i}\right] \times 100 \quad (3.4)$$

Where, W_i = average initial weight (kg) of three replicate cubes and W_t = average weight (kg) of three replicate cubes after the exposure period.

3.5.3.2 Change in Compressive Strength of Concrete

To evaluate the extent of deterioration due to sulfate attack and combined chloride-sulfate attack, the change in compressive strength of concrete was determined after 360 days of exposure to sulfate and composite chloride-sulfate solutions. Companion cube specimens exposed to normal water were also tested for compressive strength after the exposure period. Three replicate cube specimens from each concrete mix were tested and the average value of compressive strength was reported. The average change in compressive strength of cube specimens of a given concrete mix after completion of exposure to a given solution was determined as a percentage with respect to its compressive strength for the exposure to normal water and is shown by the following relationship.

$$\text{Average change in compressive strength (\%)} = \left[\frac{A - B}{A}\right] \times 100 \quad (3.5)$$

Where, A = average compressive strength (N/mm^2) of three replicate cube specimens exposed to normal water and B = average compressive strength (N/mm^2) of three replicate cube specimens exposed to sulfate or composite chloride-sulfate solutions.

3.5.3.3 Microstructure Analysis

In order to examine the effect of sulfate ions and conjoint sulfate-chloride ions on the microstructure of hardened concrete, X-ray diffraction (XRD) and Field emission scanning electron microscopy (FESEM) analyses were carried out on concrete powder samples. After determining the compressive strength at the end of exposure period, the cube specimens were further crushed in the compression testing machine. The crushed material was then passed through a sieve of square mesh size 150 μm. The sieved concrete powder sample was then stored in air tight containers and used for microstructural analysis. The procedure as mentioned in Section 3.3.4.2.1 and 3.3.4.2.3

were used for carrying out X-ray diffraction (XRD) and Field emission scanning electron microscopy (FESEM) analyses respectively. It is to be noted that in the XRD analysis the obtained concrete powder was scanned from 5° to 50° (2θ).

CHAPTER 4

EFFECT OF CHLORIDE AND CONJOINT CHLORIDE-SULFATE CONTAMINATION ON MICROSTRUCTURE OF CONCRETE AND ELECTROLYTIC CONCRETE POWDER SOLUTION (ECPS) CHEMISTRY

4.1 GENERAL

In this chapter, the results obtained from the experimental investigation on the effect of chloride and conjoint chloride-sulfate contamination on 28-day compressive strength of concrete are presented and discussed. In order to study the microstructural changes occurred in concrete due to contamination of chloride and conjoint chloride-sulfate ions, X-ray diffraction (XRD) analysis, Fourier transform infrared (FTIR) spectroscopy and Field emission scanning electron microscopy (FESEM) were conducted on concrete powder samples and the obtained results are presented and discussed. Further, the results obtained from the chemical composition of electrolytic concrete powder solution prepared from different concrete mixes are discussed.

4.2 COMPRESSIVE STRENGTH

The effect of chloride and conjoint chloride-sulfate ions on mechanical property of concrete was evaluated by conducting compressive strength test at the curing age of 28 days on cube specimens of size 150 mm prepared from OPC and PPC at w/c ratios of 0.45 and 0.5. Three replicate cube specimens from each concrete mix were tested and the average value of compressive strength along with standard deviation was reported.

4.2.1 Effect of Chloride Contamination on Compressive Strength of Concrete

The average 28 day-compressive strength values along with standard deviation for OPC and PPC cube specimens made from control mix (i.e. without addition of any salts) and admixed with varying dosages of sodium chloride at w/c ratios of 0.45 and 0.5 are presented in Table 4.1 and Table 4.2 respectively.

From the compressive strength values presented in Table 4.1 and Table 4.2, it is observed that the control mix (uncontaminated) specimens made with PPC exhibited lower

compressive strength as compared to those made with OPC at both w/c ratios i.e. at 0.45 and 0.5. The lower compressive strength exhibited by PPC concrete indicates that the pozzolanic reaction was not effective till the age of 28 days of curing in enhancing the compressive strength of concrete. However, there is no significant difference in the compressive strength between OPC and PPC concrete made at w/c of 0.5.

From compressive strength values presented in Table 4.1 and Table 4.2, it is observed that compressive strength of chloride contaminated concrete specimens was lower than that of uncontaminated concrete specimens. The reduction in compressive strength due to the presence of chloride ions may be attributed to salt crystallization in the pores of concrete. Further, the specimens made from chloride contaminated OPC concrete showed lower compressive strength as compared to those made from chloride contaminated PPC concrete at all levels of NaCl concentration and at both w/c ratios. The crystallization of calcium chloroaluminate (formed due to reaction of chloride ions with hydrated tricalcium aluminate) in the pores of OPC concrete to a greater extent as compared to that in PPC concrete might have resulted a reduction in compressive strength of OPC concrete. However, there is no significant difference in compressive strength between OPC and PPC concrete contaminated with chloride ions at w/c of 0.5 as observed from Table 4.2. The formation of calcium chloroaluminate (Friedel's salt) in the chloride contaminated concrete is evident from the XRD profiles shown in Figures (Fig. 4.1 to Fig. 4.4) for both OPC and PPC. Although theses XRD profiles are obtained from the samples of 56 days old concrete, the formation of Friedel's salt at the age of 28 days can be envisaged from the fact that it starts forming at the age of day 1 [116].

From Table 4.1 and Table 4.2, it is observed that the compressive strength of concrete specimens increased with increase in admixed NaCl concentration up to 5% and then decreased at 7% NaCl concentration in both OPC and PPC concrete at both w/c ratios 0.45 and 0.5. The increase in compressive strength up to 5% NaCl may be attributed to filling of pores with calcium chloroaluminate and non-expansive ettringite. As stated earlier, calcium chloroaluminate is formed due to reaction of chloride ions with hydrated C_3A [6, 117, 118]. The non-expansive ettringite is formed due to reaction of C_3A with gypsum, which is added in the manufacturing process to control early setting and hardening behaviour of Portland cement. This non-expansive ettringite is termed as primary ettringite [119]. It is formed as weakly developed crystals in small quantities [120] and fills the pores of concrete. Therefore the compressive strength of concrete

increased with increase in NaCl concentration up to 5%. However in the presence of higher amount of chloride ions (i.e. at 7% NaCl), ettringite becomes unstable and more amount of calcium chloroaluminate is formed [47, 121] owing to reaction of chloride ion with C_3A. This might have resulted in crystallization of calcium chloroaluminate in the pores of concrete to a greater extent, leading to tensile stresses causing expansion and hence reduction in compressive strength of concrete. Thus, the compressive strength was reduced in the presence of higher concentration of chloride ions (7% NaCl) in both OPC and PPC concrete at both w/c ratios.

Table 4.1: Average 28 day compressive strength along with standard deviation values of OPC and PPC concrete prepared with and without admixed NaCl at w/c of 0.45

Cement type	Concentration of NaCl (% by weight of cement) added at the time of preparation of concrete	Compressive strength (N/mm^2)	Standard deviation (N/mm^2)
OPC	0% NaCl	45.41	0.03
	3% NaCl	37.2	1.0
	5% NaCl	39.1	1.3
	7% NaCl	36.7	0.8
PPC	0% NaCl	40.4	0.02
	3% NaCl	39.6	1.1
	5% NaCl	40.2	0.1
	7% NaCl	39.1	0.2

Table 4.2: Average 28 day compressive strength along with standard deviation values of OPC and PPC concrete prepared with and without admixed NaCl at w/c of 0.5

Cement type	Concentration of NaCl (% by weight of cement) added at the time of preparation of concrete	Compressive strength (N/mm^2)	Standard deviation (N/mm^2)
OPC	0% NaCl	39.0	0.01
	3% NaCl	35.8	1.1
	5% NaCl	37.6	1.2
	7% NaCl	34.7	0.5
PPC	0% NaCl	38.0	0.04
	3% NaCl	36.7	1.2
	5% NaCl	37.8	0.2
	7% NaCl	35.5	0.6

4.2.2 Effect of Conjoint Chloride-Sulfate Contamination on Compressive Strength of Concrete

The average compressive strength along with standard deviation values of OPC and PPC cube specimens made from concrete admixed with varying dosages of sodium chloride plus sodium sulfate and sodium chloride plus magnesium sulfate at water-cement ratios of 0.45 and 0.5 are presented in Table 4.3 and Table 4.4 respectively.

From compressive strength values presented in Table 4.3 and Table 4.4, it is observed that for sodium chloride plus sodium sulfate contamination, OPC concrete showed lower compressive strength as compared to PPC concrete almost at all levels of chloride-sulfate contamination. Sulfate ions react with calcium hydroxide (portlandite) produced during hydration process and forms gypsum, which then reacts with tricalcium aluminate (C_3A) and forms ettringite [6]. The ettringite that is formed by the reaction of sulfate ions is termed as secondary ettringite, which is characterized by expansion and cracking [40]. As PPC concrete possesses less reserve of calcium hydroxide, it mitigates the production of expansive ettringite. However, in OPC concrete due to more availability of calcium hydroxide as compared to that in PPC concrete, more amounts of gypsum and ettringite are formed in the presence of sulfate ions, which may exert swelling pressure in the pores of concrete and results in expansion and strength reduction of OPC concrete in the conjoint presence of sodium chloride and sodium sulfate.

Further from Table 4.3 and Table 4.4, it is observed that in concrete specimens admixed with 3% NaCl and 5% NaCl with varying concentrations of Na_2SO_4, the compressive strength mostly increased with increase in Na_2SO_4 concentration up to 6% followed by a decrease at 12% in both OPC and PPC concretes at both w/c ratios 0.45 and 0.5. The increase in compressive strength of concrete with increase in Na_2SO_4 concentration up to 6% may be attributed to the filling of pores of concrete with calcium chloroaluminate formed in the presence of chloride ions and ettringite formed in the presence of sulfate ions. It may be noted that there is formation of higher amount of ettringite in OPC due to preferential reaction of sulfate ions with C_3A whereas in PPC the preferential reaction of chloride ions with C_3A results in formation of higher amount calcium chloroaluminate in the conjoint presence of sodium chloride and sodium sulfate and this observation is confirmed through the obtained XRD profiles, which are presented and discussed afterward in Section 4.3.1.2. At 12% Na_2SO_4 concentration, the reduction in compressive strength may be attributed to the crystallization in the pores of concrete to a greater extent

due to formation of higher amount of ettringite in the presence of higher concentration of sulfate ion and also due to conversion of calcium chloroaluminate to ettringite [122, 123] in the presence of higher dosage of Na_2SO_4 at a given NaCl concentration.

For OPC, the variation in compressive strength with varying concentrations of Na_2SO_4 at 7% NaCl is different from that in case of 3% NaCl and 5% NaCl at both w/c ratios. At 7% NaCl concentration, the compressive strength decreased with increase in Na_2SO_4 dosage. At higher dosage of NaCl (i.e. at 7%), the formation of relatively higher amount of calcium chloroaluminate and formation of higher amount of ettringite with increasing sulfate ion concentration might have resulted in crystallization to a greater extent in the pores of OPC concrete, thereby resulting in reduced compressive strength. However in PPC, opposite behaviour was observed i.e. compressive strength mostly increased with increase in Na_2SO_4 dosage at 7% NaCl concentration. The increase in compressive strength with increase in sulfate ion concentration up to 6% Na_2SO_4 in PPC may be attributed to the filling of pores of concrete with calcium chloroaluminate formed in the presence of chloride ions and ettringite formed in the presence of sulfate ions. Further, the higher compressive strength at 12% Na_2SO_4 may be due to dominant effect of pozzolanic reaction, that might have accelerated at higher chloride ion concentration (7% NaCl) leading to increased compressive strength. This indicates that at 12% Na_2SO_4, the reduction in compressive strength due to sulfate deterioration is mitigated in the presence of higher chloride ion concentration (7% NaCl).

In concrete specimens admixed with sodium chloride plus magnesium sulfate, the compressive strength decreased with increase in magnesium sulfate concentration in both OPC and PPC concrete at both w/c ratios as observed from Table 4.3 and Table 4.4. In OPC concrete, the decrease in compressive strength with increase in $MgSO_4$ concentration may be attributed to more crystallization in the pores of concrete due to dominant effect of gypsum and magnesium hydroxide whereas in PPC concrete the decrease in compressive strength with increase in $MgSO_4$ concentration may be due to dominant effect of formation of higher amount of non-cementitious magnesium silicate hydrate (M-S-H). In PPC concrete, due to less availability of calcium hydroxide as result of its consumption in the pozzolanic reaction, magnesium sulfate attack is directed extensively towards C-S-H gel and converts it to non-cementitious M-S-H. Further from average compressive strength and standard deviation values, it is observed that at 3%, 5% and 7% NaCl concentrations, compressive strength in PPC is higher as compared to that

in OPC for 3% and 6% $MgSO_4$ concentrations at w/c ratios of 0.45 and 0.5, which may be attributed to formation of denser microstructure as a result of production of more C-S-H. However at 12% $MgSO_4$, mostly lower compressive strength in PPC as compared to that in OPC is attributed to the formation of significant amount of non-cementitious M–S–H in the presence of higher concentration of $MgSO_4$. While analyzing the effect of w/c ratio, it is inferred that the compressive strength of concrete was higher at w/c ratio of 0.45 as compared that at w/c ratio of 0.5 in the presence of NaCl plus Na_2SO_4 and NaCl plus $MgSO_4$ for both OPC and PPC, as observed from Table 4.3 and Table 4.4.

Table 4.3: Average 28 day compressive strength along with standard deviation values of OPC and PPC concrete at w/c ratio of 0.45 and contaminated with chloride-sulfate ions

Cement type	Admixed chloride salt		NaCl					
			3%		5%		7%	
	Admixed sulfate salts		Compressive strength (N/mm^2)	Standard deviation (N/mm^2)	Compressive strength (N/mm^2)	Standard deviation (N/mm^2)	Compressive strength (N/mm^2)	Standard deviation (N/mm^2)
OPC	Na_2SO_4	3%	34.5	0.2	30.5	0.2	33.3	0.5
		6%	36.3	0.4	34.8	0.3	30.1	0.2
		12%	24.6	0.1	25.6	1	27.6	0.5
	$MgSO_4$	3%	35.7	0.3	37.3	0.4	37.8	0.5
		6%	28.2	0.4	32.7	0.1	30.3	0.3
		12%	21	0.8	26.8	0.2	29	0.1
PPC	Na_2SO_4	3%	38.1	0.7.	31.4	1.2	44.3	0.7
		6%	37.8	0.6	34.8	0.3	33	0.3
		12%	32.7	0.5	33.9	0.2	35.1	0.2
	$MgSO_4$	3%	36.1	0.2	38.3	0.4	40.6	0.2
		6%	32.9	0.4	34	0.2	31.1	0.3
		12%	23.9	0.2	25.6	0.3	20.9	0.1

Table 4.4: Average 28 day compressive strength along with standard deviation values of OPC and PPC concrete at w/c ratio of 0.5 and contaminated with chloride-sulfate ions

Cement type	Admixed chloride salt		NaCl					
			3%		5%		7%	
	Admixed sulfate salts		Compressive strength (N/mm^2)	Standard deviation (N/mm^2)	Compressive strength (N/mm^2)	Standard deviation (N/mm^2)	Compressive strength (N/mm^2)	Standard deviation (N/mm^2)
OPC	Na_2SO_4	3%	28.9	0.4	30	0.5	30.3	0.7
		6%	35.9	1.1	33.3	0.6	27	0.5
		12%	24.6	1.1	31.8	1.2	25.6	1.2
	$MgSO_4$	3%	30.1	1.3	32.6	1	33.7	0.6
		6%	23.6	0.6	29.8	1.1	25.8	0.3
		12%	19.7	1	25.4	0.4	21.3	0
PPC	Na_2SO_4	3%	35.7	0.9	34.4	1.1	32.2	0.9
		6%	36.6	0.4	35.1	0.4	34.8	0.7
		12%	28.9	0.5	33.5	0.2	37.8	0.3
	$MgSO_4$	3%	30.5	0.9	32.2	1.4	36.7	0
		6%	28.8	0.8	30.3	0.3	27.6	0.3
		12%	21.2	0.2	23	1	19.9	0

4.2.3 Comparison of the Effects of Chloride and Conjoint Chloride-Sulfate Contaminations on Compressive Strength of Concrete

From Table 4.1 to Table 4.4, it is observed that for both OPC and PPC, the specimens admixed with varying concentrations of sodium chloride exhibited higher compressive strength as compared to those admixed with varying concentrations of conjoint sodium chloride plus sodium sulfate and sodium chloride plus magnesium sulfate at w/c ratios of 0.45 and 0.5, except at 7% NaCl plus 3% Na_2SO_4 and 7% NaCl plus 3% $MgSO_4$ contamination in OPC and PPC made with w/c of 0.45. The reduction in compressive strength in the conjoint presence of chloride and sulfate ions as compared to that in the presence of only chloride ions is attributed to the crystallization of expansive gypsum and ettringite (formed in the presence of sulfate ions) in the pores of concrete to a greater extent. However, the higher compressive strength at higher NaCl concentration (7%) in the presence of 3% sodium sulfate or 3% magnesium sulfate indicates that in the presence of lower concentration of sulfate ions, the deleterious effect of gypsum and ettringite is mitigated in the presence of higher chloride ion concentration. While observing the effect

of cation type associated with sulfate ions on compressive strength of OPC and PPC concrete, the specimens admixed with sodium chloride plus magnesium sulfate showed lower compressive strength as compared to those admixed with sodium chloride plus sodium sulfate, except for OPC concrete in the presence of 3% $MgSO_4$ at both w/c ratios. The lower compressive strength in concrete admixed with sodium chloride plus magnesium sulfate may be attributed to salt crystallization in the pores of concrete as a result of formation of higher amount of gypsum and magnesium hydroxide in OPC and formation of higher amount of non-cementitious M-S-H in PPC in the presence of magnesium sulfate. However, the higher compressive strength of OPC concrete in the presence of 3% $MgSO_4$ as compared to that in the presence of 3% Na_2SO_4 at all concentrations of NaCl may be attributed to the dominant effect of formation of lower amount of gypsum and magnesium hydroxide.

4.3 EFFECT OF CHLORIDE AND CONJOINT CHLORIDE-SULFATE CONTAMINATION ON MICROSTRUCTURE OF CONCRETE

To analyze the changes in the phase composition of hardened concrete due to contamination of chloride and conjoint chloride-sulfate ions, X-ray diffraction (XRD) analysis was carried out on concrete powder samples. Fourier transform infrared (FTIR) spectroscopy was also conducted on the concrete powder samples to find out the functional groups associated with the products formed in concrete. Further, morphological changes occurred in the concrete due to the presence of chloride and conjoint chloride-sulfate ions was examined by field emission scanning electron microscopy (FESEM).

4.3.1 X-ray Diffraction (XRD) Analysis

4.3.1.1 XRD Analysis of Concrete Contaminated with NaCl

The X-ray diffraction profiles of concrete contaminated with 3%, 5% and 7% sodium chloride are shown in Fig. 4.1 and Fig. 4.2 for OPC and PPC respectively at w/c ratio of 0.45 and in Fig. 4.3 and Fig. 4.4 respectively at w/c ratio of 0.5. The XRD profiles shown in Fig. 4.1 to Fig. 4.4 indicate the peaks of gypsum (G), ettringite (E), calcium hydroxide (CH), calcium carbonate (CC), quartz (Q), thaumasite (T) and calcium chloroaluminate (CCA), which are formed in concrete. The formation of calcium chloroaluminate (Friedel's salt) was indicated through the peaks at 11.2° 2θ and 23° 2θ in the concrete

contaminated with sodium chloride as shown in Fig. 4.1 to Fig. 4.4. From these figures, it is observed that peak intensity of calcium chloroaluminate was more in OPC as compared to that in PPC admixed with sodium chloride. This indicates more chloride binding in OPC than that in PPC, which may be attributed to higher C_3A content in OPC as compared to that in PPC. Gypsum peaks were identified at 32.1° 2θ and 50.5° 2θ and the presence of this primary gypsum may be attributed to its addition to Portland cement clinker during manufacturing, to prevent flash setting of cement. Gypsum when combines with C_3A, forms ettringite. The peaks ettringite were found at 8.8° 2θ, 15.75° 2θ, 25.6° 2θ, and 27.5° 2θ as observed from Fig. 4.1 to Fig. 4.4. It is noted that the peak intensity of ettringite was less in OPC concrete as compared to that in PPC concrete at all levels of admixed NaCl. This is due to the preferential reaction of chloride ions with C_3A to form more amounts of calcium chloroaluminate in OPC, resulting in lesser availability of C_3A to react with gypsum to form a lower amount of ettringite. Thus, the peak intensity of calcium chloroaluminate was more in OPC concrete as compared to that in PPC concrete.

From the XRD profiles shown in Fig. 4.1 to Fig. 4.4, it is observed that OPC concrete showed precipitation of calcium hydroxide through well-defined peaks at 18.08° 2θ, 34.1° 2θ, and 36.5° 2θ, whereas in PPC concrete, the peaks of calcium hydroxide are less intense at all levels of admixed NaCl. This is attributed to consumption of calcium hydroxide in pozzolanic reaction in PPC concrete. Further peaks of quartz were found at 20.85° 2θ, 26.65° 2θ, 39.45° 2θ, 42.5° 2θ and 50.1° 2θ, as shown in Fig. 4.1 to Fig. 4.4, which is mostly due to the presence of aggregates in the concrete. Similarly, the peaks of thaumasite and calcium carbonate were found at 27.9° 2θ and 29.4° 2θ respectively.

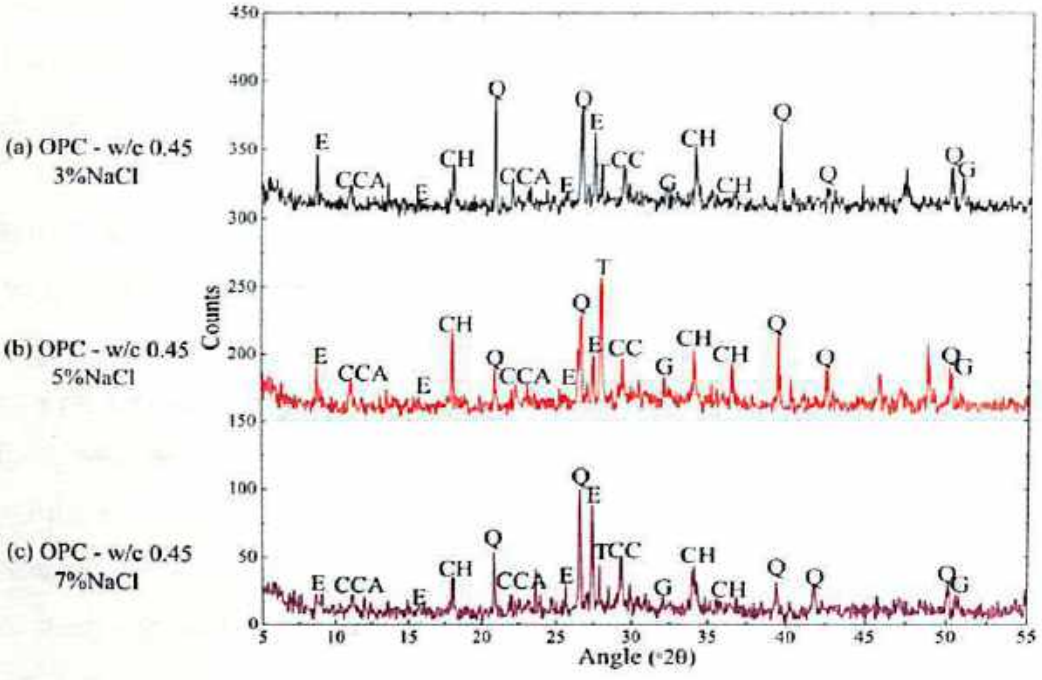

Fig. 4.1 XRD profiles of OPC concrete admixed with (a) 3% NaCl, (b) 5% NaCl and (c) 7% NaCl, at w/c ratio of 0.45

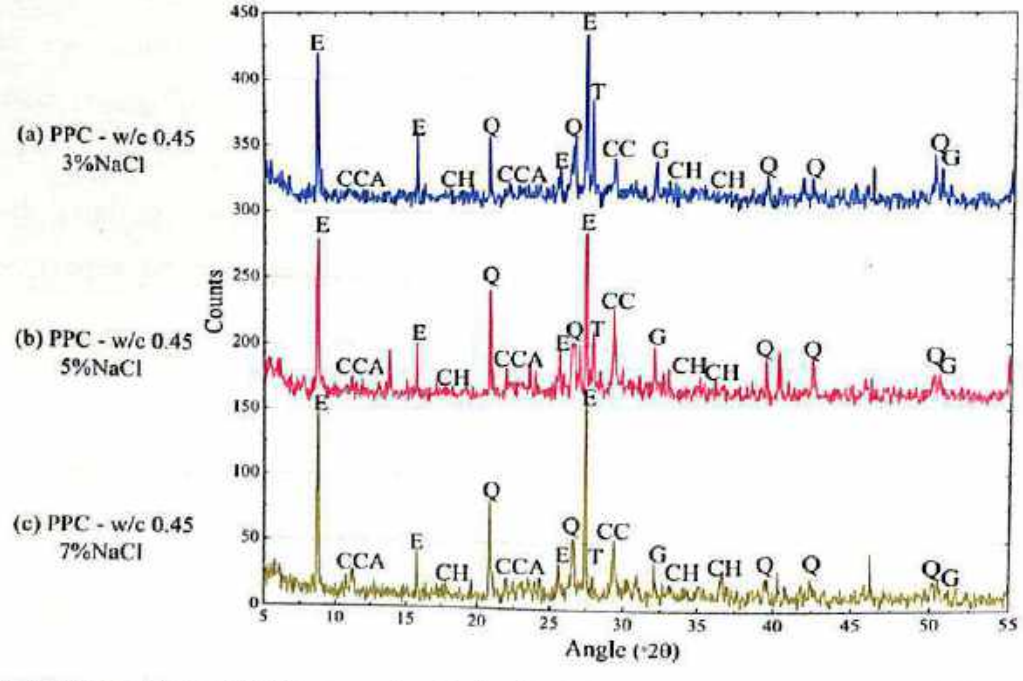

Fig. 4.2 XRD profiles of PPC concrete admixed with (a) 3% NaCl, (b) 5% NaCl and (c) 7% NaCl, at w/c ratio of 0.45

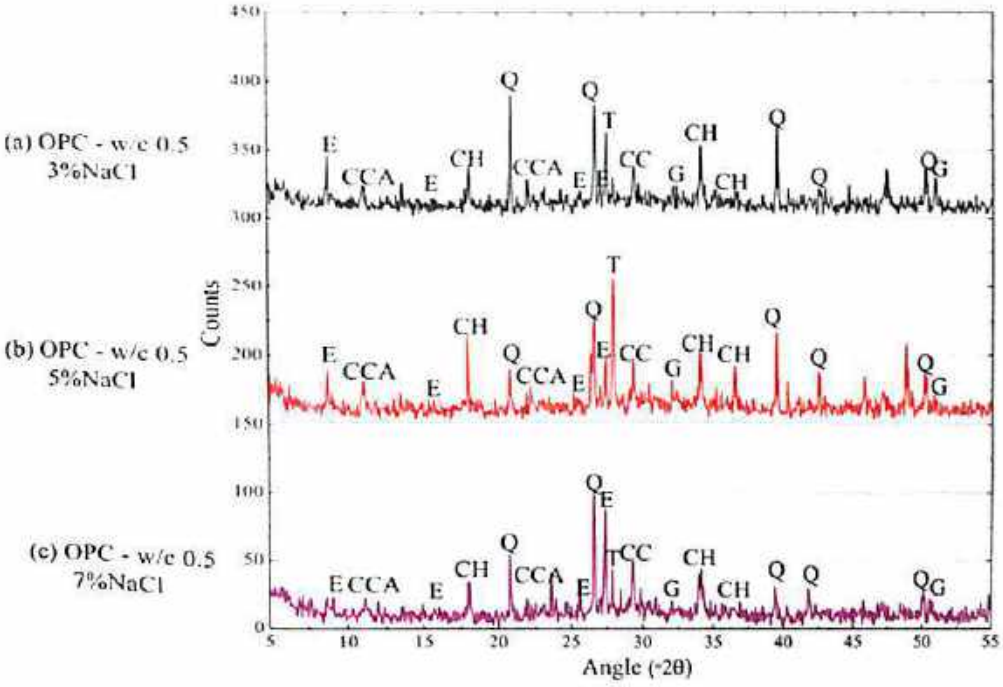

Fig. 4.3 XRD profiles of OPC concrete admixed with (a) 3% NaCl, (b) 5% NaCl and (c) 7% NaCl, at w/c ratio of 0.5

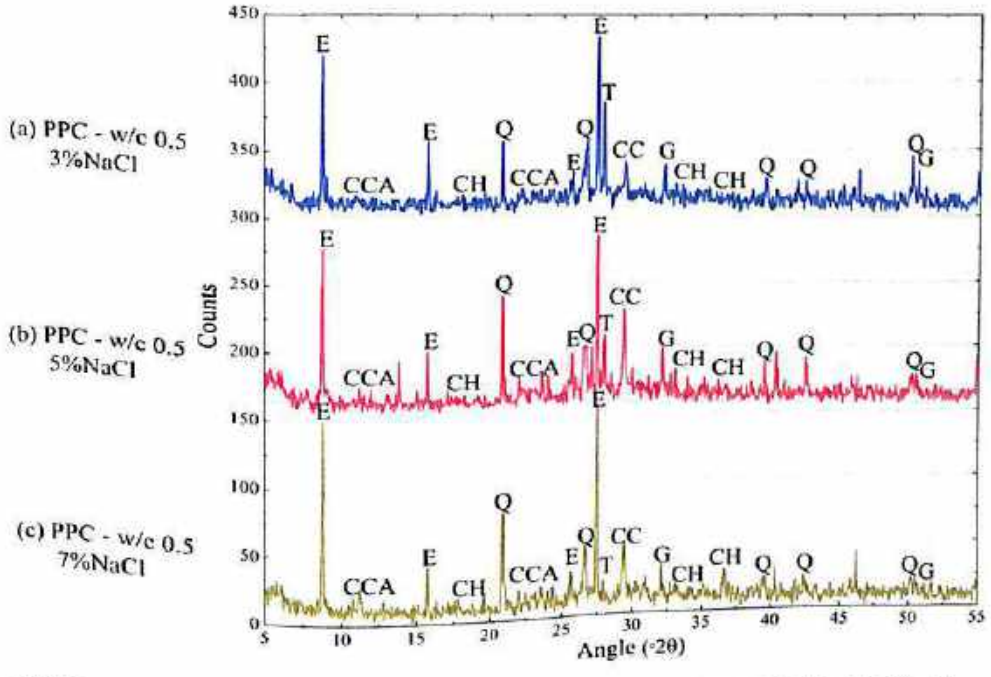

Fig. 4.4 XRD profiles of PPC concrete admixed with (a) 3% NaCl, (b) 5% NaCl and (c) 7% NaCl, at w/c ratio of 0.5

4.3.1.2 XRD Analysis of Concrete Contaminated with NaCl plus Na_2SO_4

The X-ray diffraction profiles of OPC concrete made with w/c ratio of 0.45 and contaminated with varying concentrations (3%, 5% and 7%) of sodium chloride plus 3% sodium sulfate, 6% sodium sulfate and 12% sodium sulfate are shown in Fig. 4.5, Fig. 4.6 and Fig. 4.7 respectively and in Fig. 4.8, Fig. 4.9 and Fig. 4.10 respectively for PPC concrete. Similarly, X-ray diffraction profiles of OPC concrete made with w/c ratio of 0.5 and contaminated with varying concentrations (3%, 5% and 7%) of sodium chloride plus 3% sodium sulfate, 6% sodium sulfate and 12% sodium sulfate are shown in Fig. 4.11, Fig. 4.12 and Fig. 4.13 respectively and in Fig. 4.14, Fig. 4.15 and Fig. 4.16 respectively for PPC concrete. The XRD profiles shown in Fig. 4.5 to Fig. 4.10 for concrete powder samples contaminated with different concentrations of NaCl plus Na_2SO_4 for OPC and PPC at w/c ratio of 0.45 indicate the peaks of gypsum (G) at 32.1° 2θ and 50.5° 2θ, and that of ettringite (E) at 8.8° 2θ, 15.75° 2θ, 25.6° 2θ, and 27.5° 2θ in the conjoint presence of chloride and sulfate ions.

From Fig. 4.5 to Fig. 4.10, it is observed that OPC concrete at w/c ratio of 0.45 showed presence of small amount of ettringite through less intense peaks, however it indicated the presence of higher amount of gypsum through more intense peaks as compared to PPC concrete at all concentrations of NaCl plus Na_2SO_4 contamination. The presence of less amount of gypsum in PPC concrete may be due to the consumption of calcium hydroxide in the pozzolanic reaction thereby resulting in its lesser availability to react with Na_2SO_4 to produce gypsum and sodium hydroxide.

The XRD profiles of concrete powder samples contaminated with varying concentrations of NaCl plus Na_2SO_4 at w/c ratio of 0.5 showed more intense peaks of gypsum and ettringite in OPC concrete as compared to that in PPC concrete as observed from Fig. 4.11 to Fig. 4.16. The availability of higher amount of $Ca(OH)_2$ in OPC has resulted in the formation of more amount of gypsum in the presence of sulfate ions, thus showing intense peaks of gypsum in OPC as compared to that in PPC. Further in OPC, the preferential reaction of sulfate ions with C_3A has resulted in formation of higher amount of ettringite as compared to that in PPC in the conjoint presence of Na_2SO_4 and NaCl, thus showing intense peaks of ettringite in OPC at w/c ratio of 0.5. The reasons for formation of lower amounts of gypsum and ettringite in PPC as compared to that in OPC at w/c ratio of 0.5 in the conjoint presence of Na_2SO_4 and NaCl are: in the first stage, sodium sulfate reacts with calcium hydroxide liberated during the hydration reaction and

forms calcium sulfate and sodium hydroxide. This stage is hindered in PPC due to less reserve of calcium hydroxide leading to less formation of gypsum, thus showing its less intense peaks in XRD profiles. In the second stage, gypsum produced (in the first stage) reacts with C_3A to form expansive ettringite. The amount of ettringite formation is reduced in PPC due to less availability of gypsum and C_3A (diluted due to replacement of part of Portland cement clinker by fly ash in PPC), thus showing less intense peaks of ettringite in PPC.

In Fig. 4.5 to Fig. 4.16, the calcium chloroaluminate (CCA) peaks were found at 11.2° 2θ and 23° 2θ. At w/c ratio of 0.45, the peaks of calcium chloroaluminate are more intense in OPC as compared to that in PPC at all NaCl plus Na_2SO_4 contaminations, as observed from Fig. 4.5 to Fig. 4.10, which is attributed to more chloride binding with hydrated C_3A in OPC than that in PPC. On the other hand, the peak intensity of calcium chloroaluminate was more in PPC than that in OPC at w/c ratio of 0.5 at all NaCl plus Na_2SO_4 contaminations, as observed from Fig. 4.11 to Fig. 4.16. In PPC, the preferential reaction of chloride ions with C_3A has led to higher chloride binding, thus resulting in formation of more amount of calcium chloroaluminate. This indicates that the w/c ratio of concrete affects the variation in formation of calcium chloroaluminate in the presence of composite chloride and sulfate ions.

From XRD profiles shown in Fig. 4.5 to Fig. 4.16, it is noted that the peaks of calcium hydroxide (CH) were found at 18.08° 2θ, 34.1° 2θ, and 36.5° 2θ. The intensity of calcium hydroxide peak in XRD profile is less in PPC as compared to that in OPC at all levels of chloride-sulfate contaminations, which is attributed to consumption of $Ca(OH)_2$ in pozzolanic reaction in PPC concrete. Further, peaks of quartz (Q) were found at 20.85° 2θ, 26.65° 2θ, 39.45° 2θ, 42.5° 2θ and 50.1° 2θ, as shown in Fig. 4.5 to Fig. 4.16, which is mostly due to the presence of aggregates in the concrete. The peak of thaumasite (T) was found at 27.9° 2θ. Thaumasite may be formed as a result of the reaction between C-S-H, calcium carbonate and calcium sulfate in the presence of water. It may also be formed through woodfordite route due to the reaction between C-S-H, ettringite and calcium carbonate in the presence of water [124, 125]. The peak of calcium carbonate (CC) in concrete was found at 29.4° 2θ.

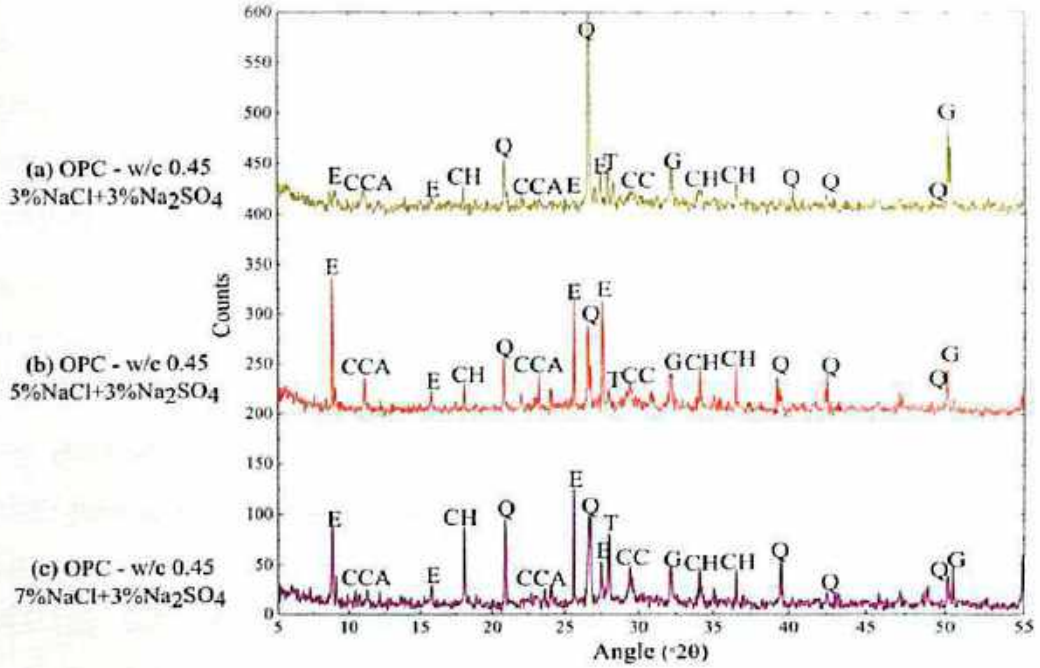

Fig. 4.5 XRD profiles of OPC concrete admixed with (a) 3% NaCl + 3% Na_2SO_4, (b) 5% NaCl + 3% Na_2SO_4 and (c) 7% NaCl + 3% Na_2SO_4, at w/c ratio of 0.45

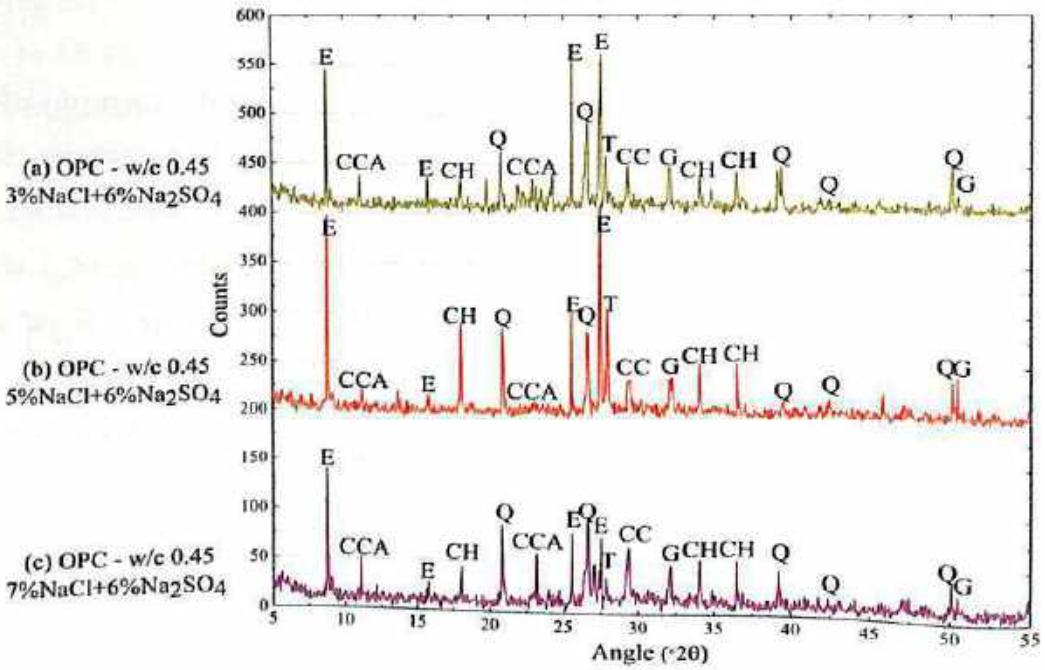

Fig. 4.6 XRD profiles of OPC concrete admixed with (a) 3% NaCl + 6% Na_2SO_4, (b) 5% NaCl + 6% Na_2SO_4 and (c) 7% NaCl + 6% Na_2SO_4, at w/c ratio of 0.45

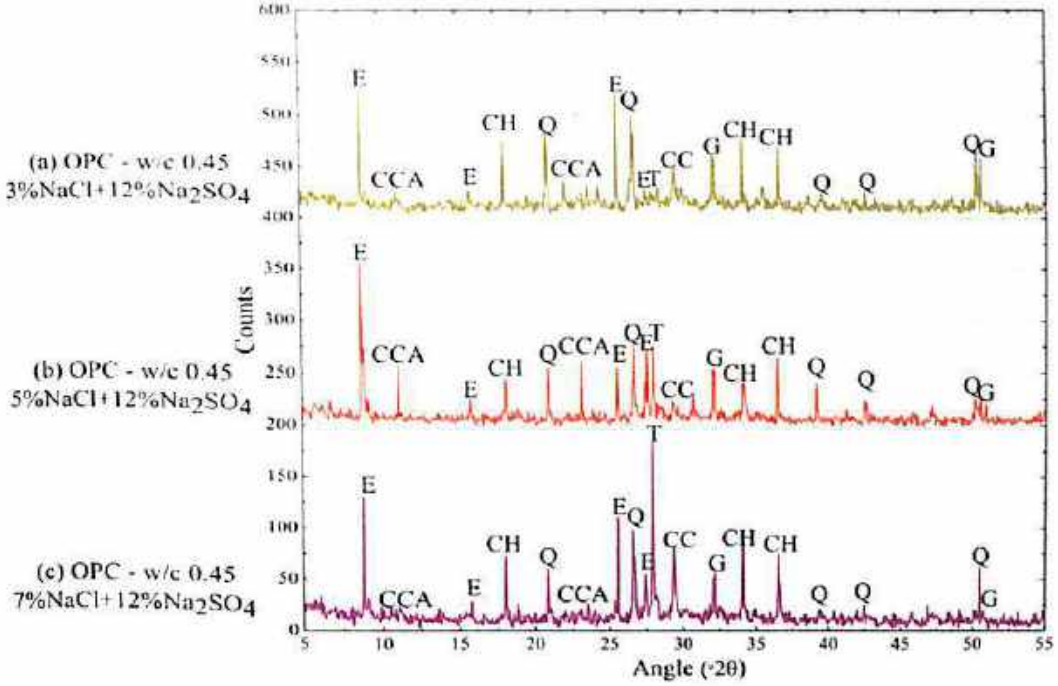

Fig. 4.7 XRD profiles of OPC concrete admixed with (a) 3% NaCl + 12% Na_2SO_4, (b) 5% NaCl + 12% Na_2SO_4 and (c) 7% NaCl + 12% Na_2SO_4, at w/c ratio of 0.45

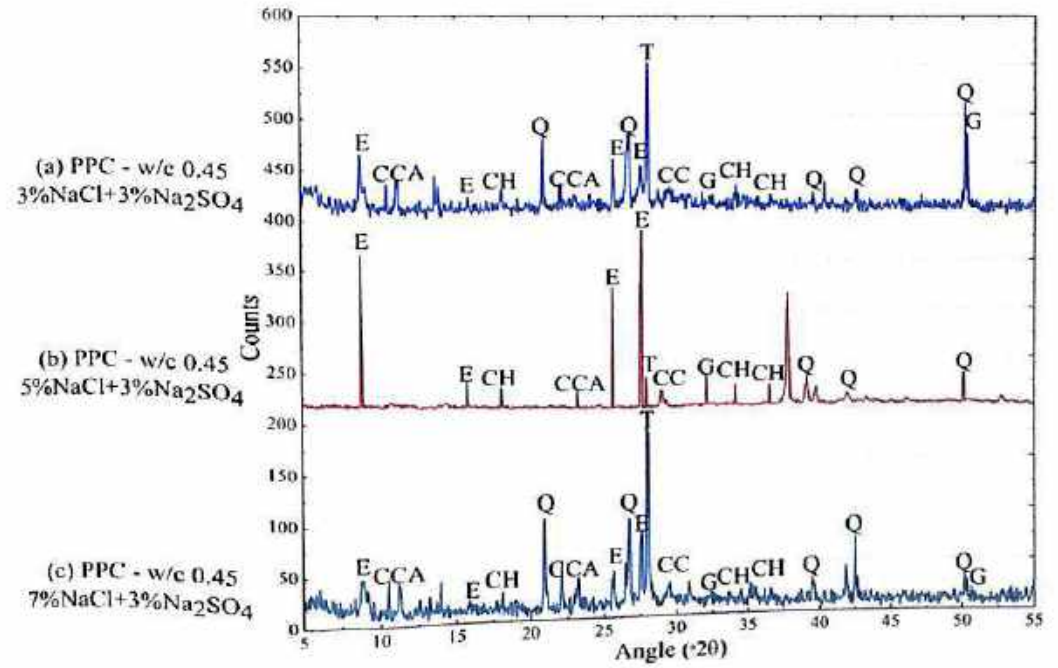

Fig. 4.8 XRD profiles of PPC concrete admixed with (a) 3% NaCl + 3% Na_2SO_4, (b) 5% NaCl + 3% Na_2SO_4 and (c) 7% NaCl + 3% Na_2SO_4, at w/c ratio of 0.45

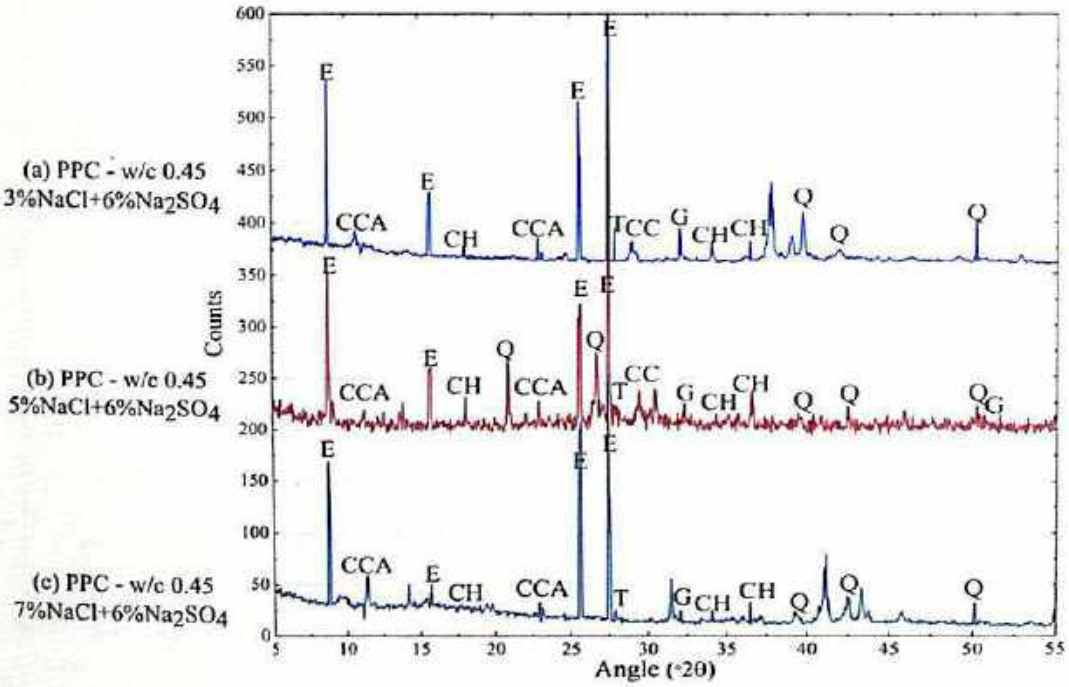

Fig. 4.9 XRD profiles of PPC concrete admixed with (a) 3% NaCl + 6% Na_2SO_4, (b) 5% NaCl + 6% Na_2SO_4 and (c) 7% NaCl + 6% Na_2SO_4, at w/c ratio of 0.45

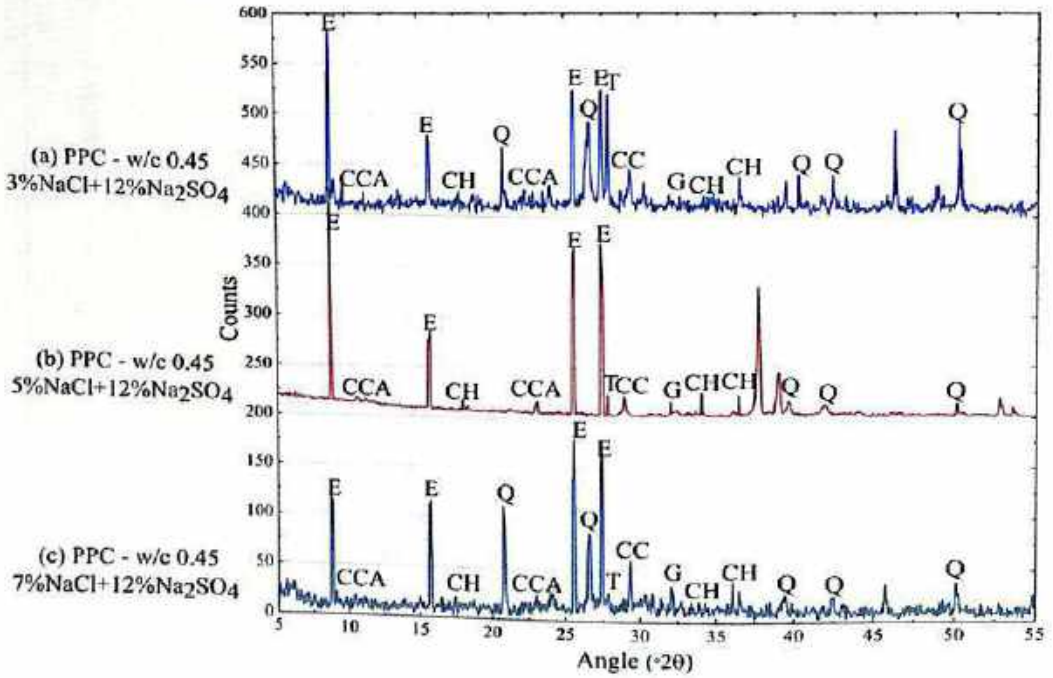

Fig. 4.10 XRD profiles of PPC concrete admixed with (a) 3% NaCl + 12% Na_2SO_4, (b) 5% NaCl + 12% Na_2SO_4 and (c) 7% NaCl + 12% Na_2SO_4, at w/c ratio of 0.45

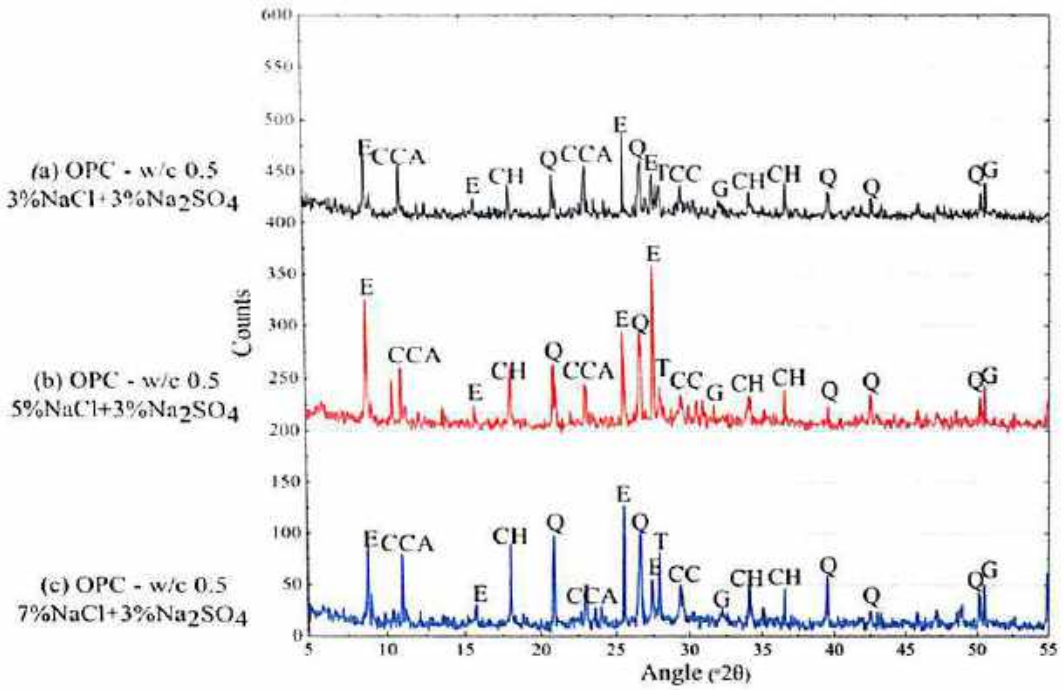

Fig. 4.11 XRD profiles of OPC concrete admixed with (a) 3% NaCl + 3% Na_2SO_4, (b) 5% NaCl + 3% Na_2SO_4 and (c) 7% NaCl + 3% Na_2SO_4, at w/c ratio of 0.5

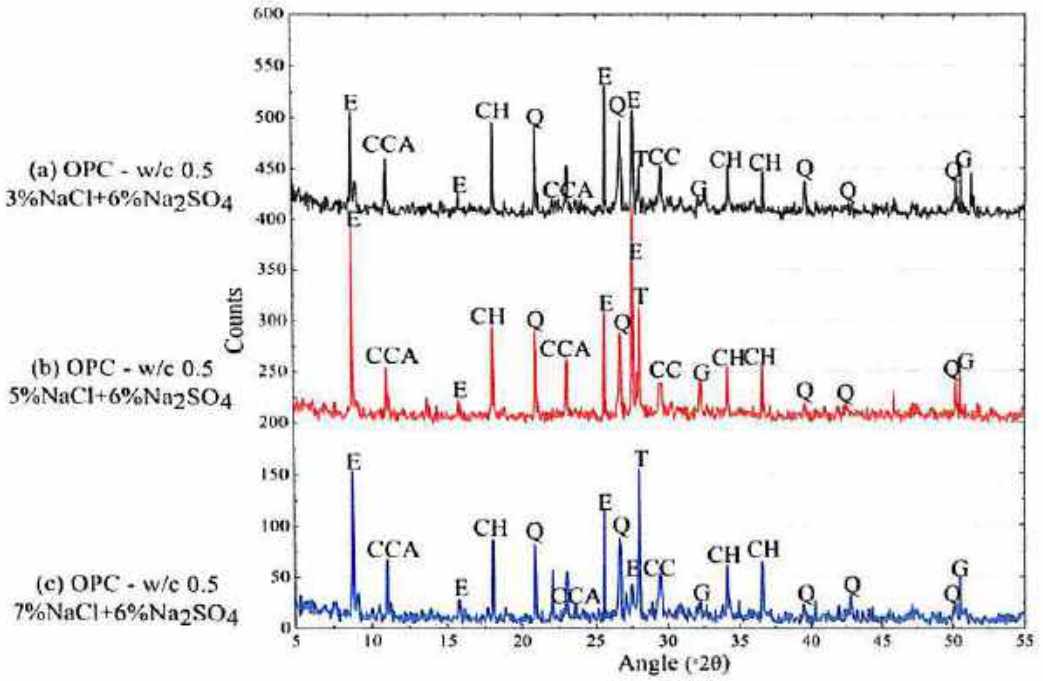

Fig. 4.12 XRD profiles of OPC concrete admixed with (a) 3% NaCl + 6% Na_2SO_4, (b) 5% NaCl + 6% Na_2SO_4 and (c) 7% NaCl + 6% Na_2SO_4, at w/c ratio of 0.5

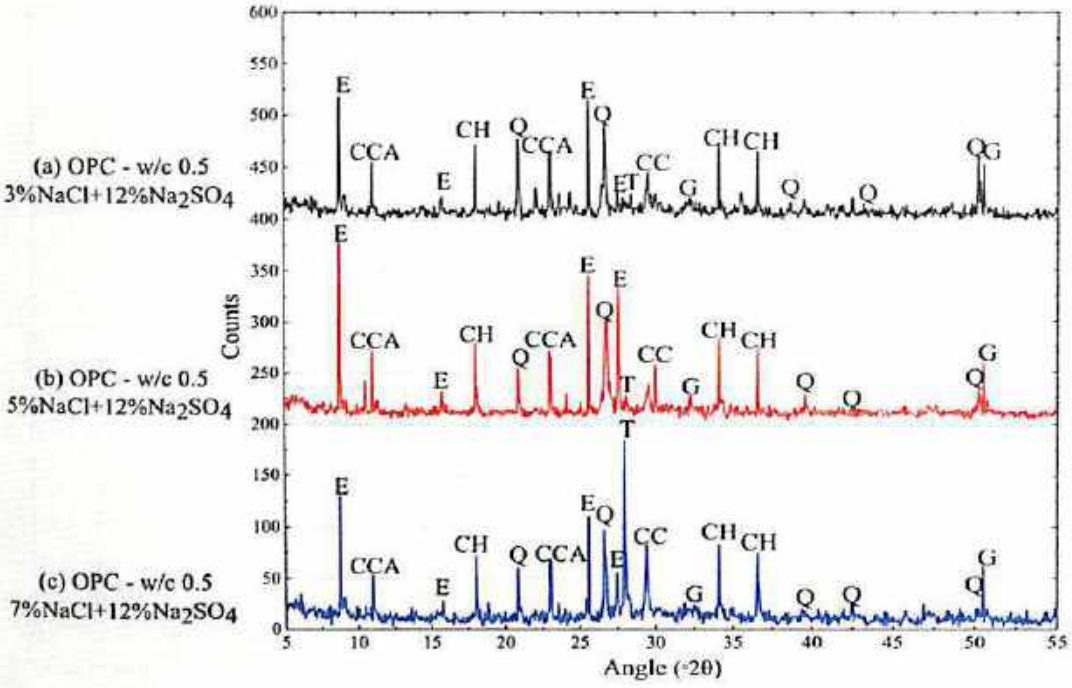

Fig. 4.13 XRD profiles of OPC concrete admixed with (a) 3% NaCl + 12% Na_2SO_4, (b) 5% NaCl + 12% Na_2SO_4 and (c) 7% NaCl + 12% Na_2SO_4, at w/c ratio of 0.5

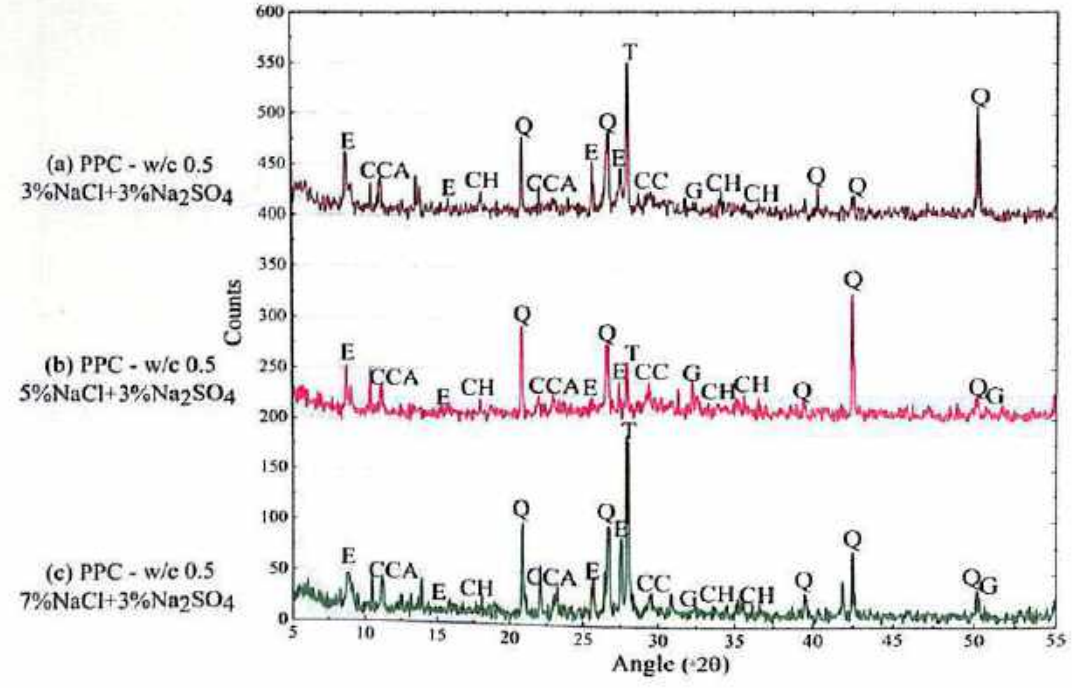

Fig. 4.14 XRD profiles of PPC concrete admixed with (a) 3% NaCl + 3% Na_2SO_4, (b) 5% NaCl + 3% Na_2SO_4 and (c) 7% NaCl + 3% Na_2SO_4, at w/c ratio of 0.5

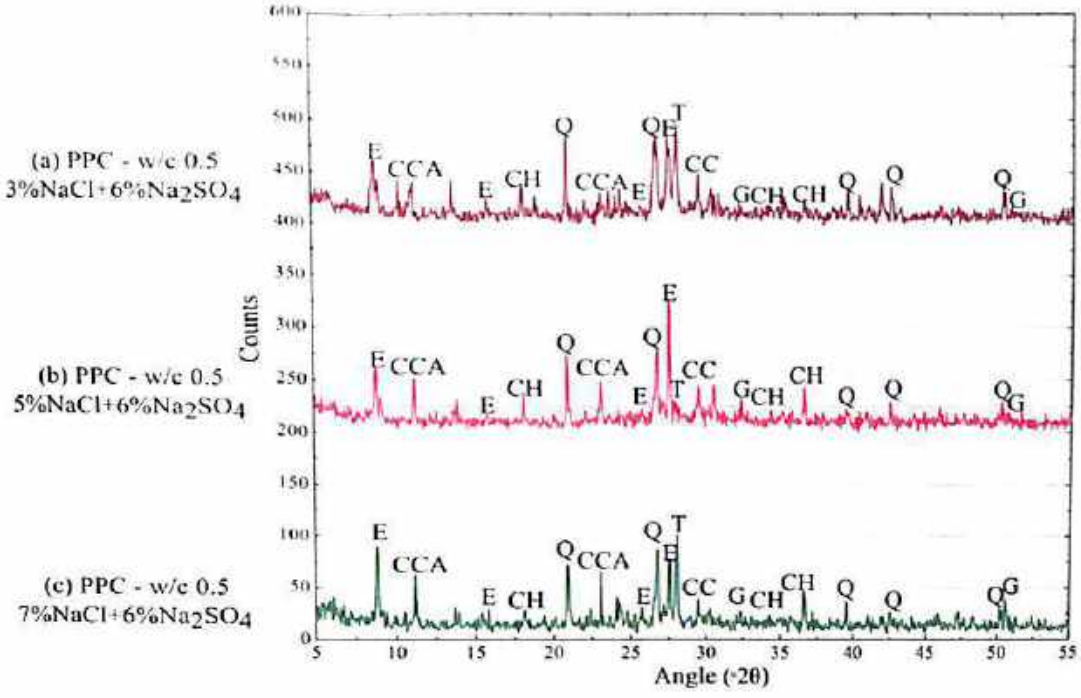

Fig. 4.15 XRD profiles of PPC concrete admixed with (a) 3% NaCl + 6% Na_2SO_4, (b) 5% NaCl + 6% Na_2SO_4 and (c) 7% NaCl + 6% Na_2SO_4, at w/c ratio of 0.5

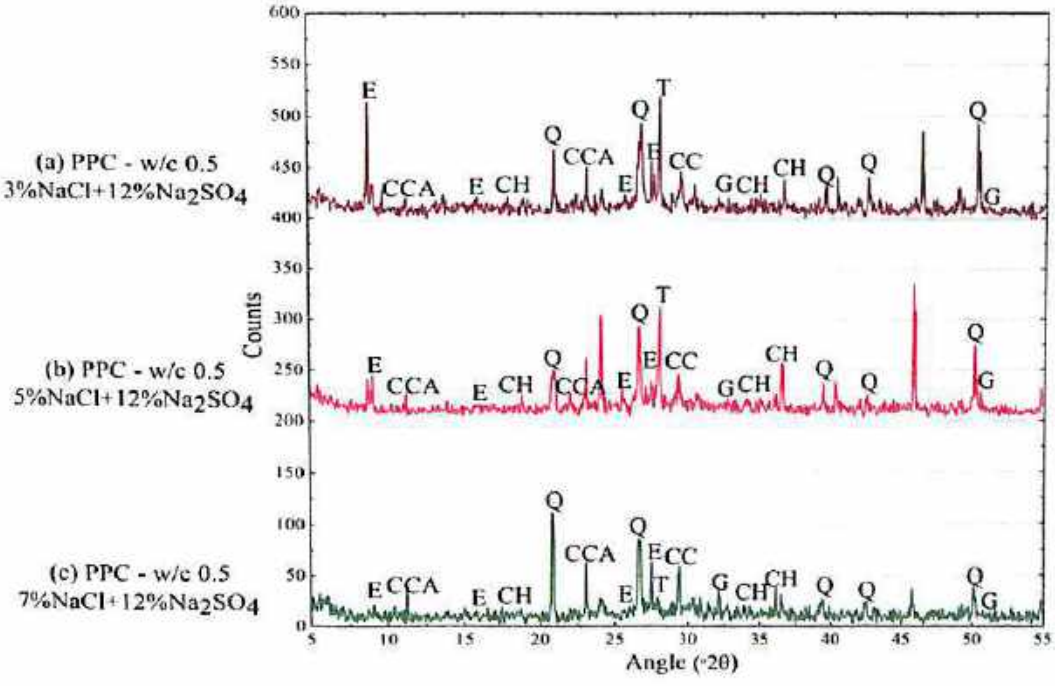

Fig. 4.16 XRD profiles of PPC concrete admixed with (a) 3% NaCl + 12% Na_2SO_4, (b) 5% NaCl + 12% Na_2SO_4 and (c) 7% NaCl + 12% Na_2SO_4, at w/c ratio of 0.5

4.3.1.3 XRD Analysis of Concrete Contaminated with NaCl plus $MgSO_4$

The X-ray diffraction profiles of OPC concrete contaminated with varying concentrations (3%, 5% and 7%) of sodium chloride plus 3% magnesium sulfate, 6% magnesium sulfate and 12% magnesium sulfate are shown in Fig. 4.17, Fig. 4.18 and Fig. 4.19 respectively and in Fig. 4.20, Fig. 4.21 and Fig. 4.22 respectively for PPC concrete, at w/c ratio of 0.45. Similarly at w/c ratio of 0.5, the X-ray diffraction profiles of OPC concrete contaminated with varying concentrations (3%, 5% and 7%) of sodium chloride plus 3% magnesium sulfate, 6% magnesium sulfate and 12% magnesium sulfate are shown in Fig. 4.23, Fig. 4.24 and Fig. 4.25 respectively and in Fig. 4.26, Fig. 4.27 and Fig. 4.28 respectively for PPC concrete. The compounds identified from the peaks of XRD profiles shown in Fig. 4.17 to Fig. 4.28 are ettringite (E), gypsum (G), calcium chloroaluminate (CCA), calcium hydroxide (CH), quartz (Q), thaumasite (T), calcium carbonate (CC) and magnesium hydroxide (MH).

From the XRD profiles shown in Fig. 4.17 to Fig. 4.28, the peaks of calcium hydroxide were found at 18.08° 2θ, 34.1° 2θ, and 36.5° 2θ and those of magnesium hydroxide (brucite) were found at 33.9° 2θ for both OPC and PPC at all levels of NaCl and $MgSO_4$ contaminations. From these figures it is observed that peak intensities of both $Ca(OH)_2$ (calcium hydroxide) and magnesium hydroxide (MH) are less in PPC as compared to that in OPC. The lower calcium hydroxide reserve in PPC concrete is due to its consumption in pozzolanic reaction, thus showing its less intense peaks. The lower amount of calcium hydroxide in PPC has resulted in the formation of lower amount of magnesium hydroxide in the presence of magnesium sulfate, thus showing less intense peaks in PPC as compared to that in OPC.

The XRD profiles (Fig. 4.17 to Fig. 4.28) show peaks of gypsum at 32.1° 2θ and 50.5° 2θ, peaks of ettringite at 8.8° 2θ, 15.75° 2θ, 25.6° 2θ, and 27.5° 2θ, and calcium chloroaluminate peaks at 11.2° 2θ and 23° 2θ in the conjoint presence of chloride and sulfate ions. From Fig. 4.17 to Fig. 4.28, it is observed that the peak intensities of gypsum and ettringite are more in PPC as compared to that in OPC in the conjoint presence of NaCl and $MgSO_4$ at both w/c ratios. The formation of higher amount of gypsum in PPC may be attributed to Mg-oriented attack on C-S-H because of less reserve of calcium hydroxide in PPC, thus showing more intense peaks of gypsum. The more intense peaks of ettringite in PPC as compared to that in OPC may be due to the reaction of gypsum with hydrated aluminate phases in concrete to a greater extent. Further, the peak intensity

of calcium chloroaluminate was more in OPC as compared to that in PPC at w/c ratio of 0.45 whereas the opposite variation was observed at w/c ratio of 0.5. This variation in formation of calcium chloroaluminate with change in w/c ratio in OPC and PPC may be attributed to the change in extent of reaction of chloride ions with the cement hydrates. From the XRD profiles shown in Fig. 4.17 to Fig. 4.28, the peaks of quartz were identified at 20.85° 2θ, 26.65° 2θ, 39.45° 2θ, 42.5° 2θ and 50.1° 2θ, and that of calcium carbonate and thaumasite were identified at 29.4° 2θ and 27.9° 2θ respectively in all concrete mixes contaminated with varying dosages of sodium chloride plus magnesium sulfate.

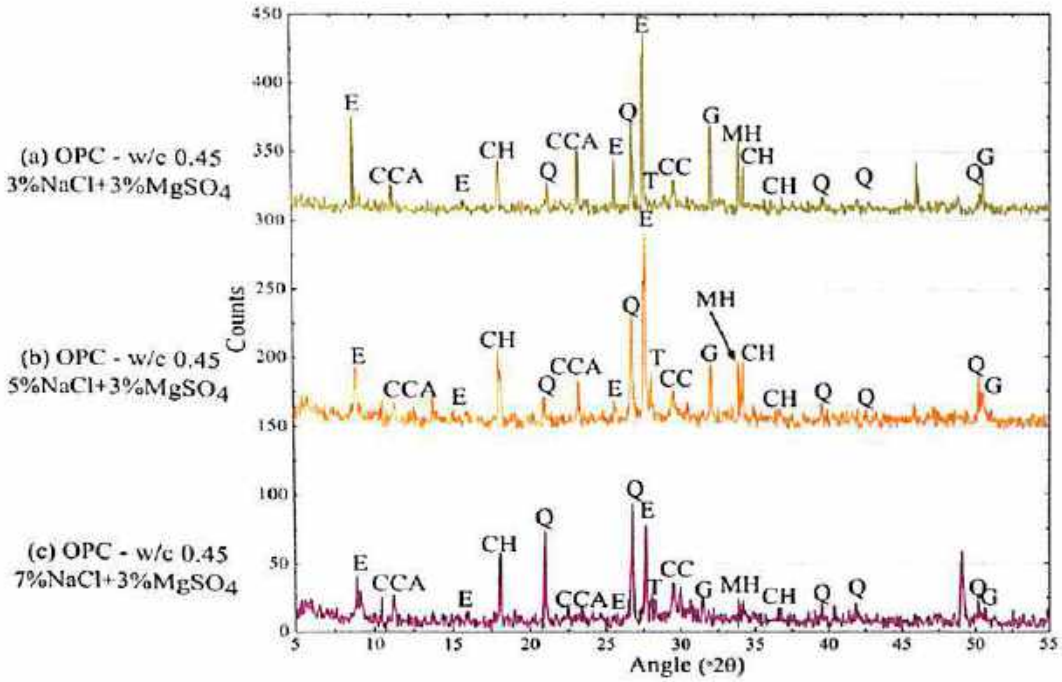

Fig. 4.17 XRD profiles of OPC concrete admixed with (a) 3% NaCl + 3% $MgSO_4$, (b) 5% NaCl + 3% $MgSO_4$ and (c) 7% NaCl + 3% $MgSO_4$, at w/c ratio of 0.45

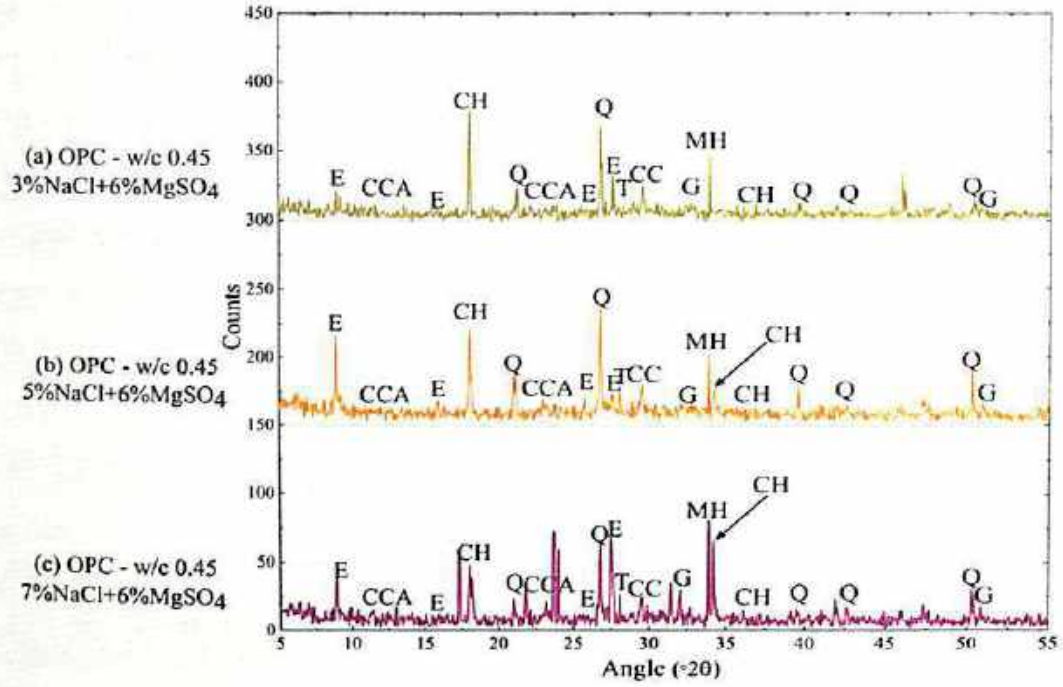

Fig. 4.18 XRD profiles of OPC concrete admixed with (a) 3% NaCl + 6% $MgSO_4$, (b) 5% NaCl + 6% $MgSO_4$ and (c) 7% NaCl + 6% $MgSO_4$, at w/c ratio of 0.45

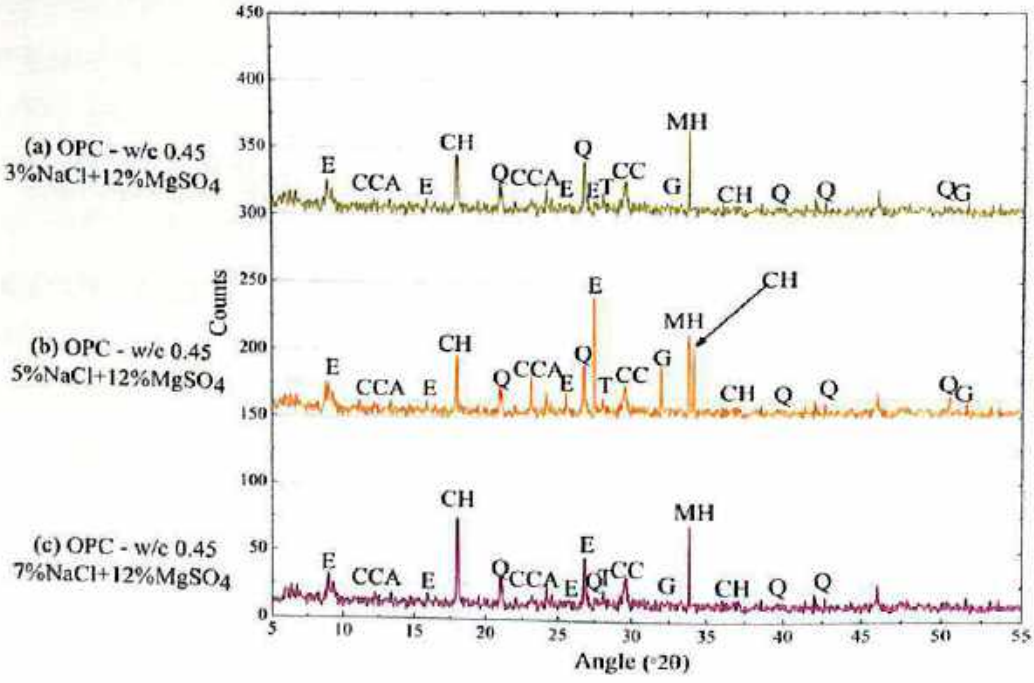

Fig. 4.19 XRD profiles of OPC concrete admixed with (a) 3% NaCl + 12% $MgSO_4$, (b) 5% NaCl + 12% $MgSO_4$ and (c) 7% NaCl + 12% $MgSO_4$, at w/c ratio of 0.45

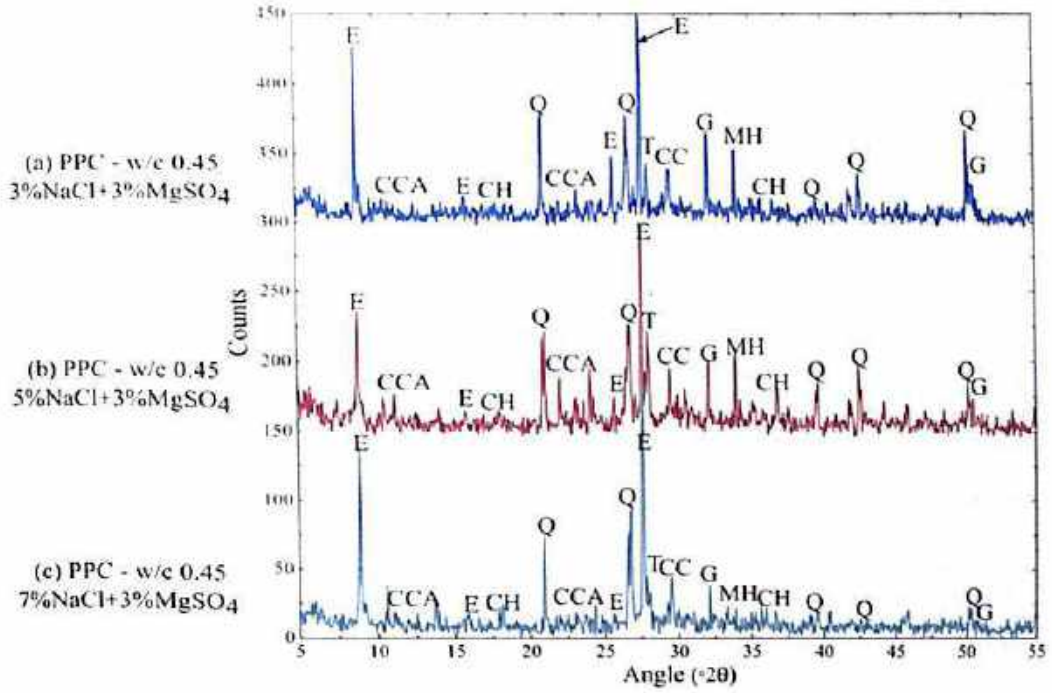

Fig. 4.20 XRD profiles of PPC concrete admixed with (a) 3% NaCl + 3% $MgSO_4$, (b) 5% NaCl + 3% $MgSO_4$ and (c) 7% NaCl + 3% $MgSO_4$, at w/c ratio of 0.45

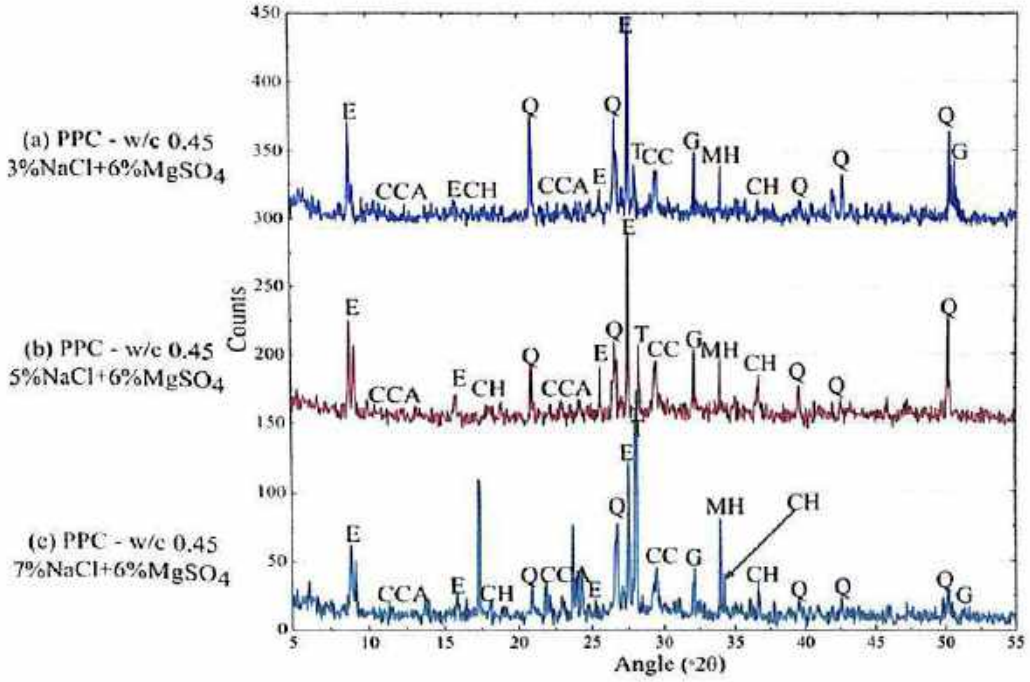

Fig. 4.21 XRD profiles of PPC concrete admixed with (a) 3% NaCl + 6% $MgSO_4$, (b) 5% NaCl + 6% $MgSO_4$ and (c) 7% NaCl + 6% $MgSO_4$, at w/c ratio of 0.45

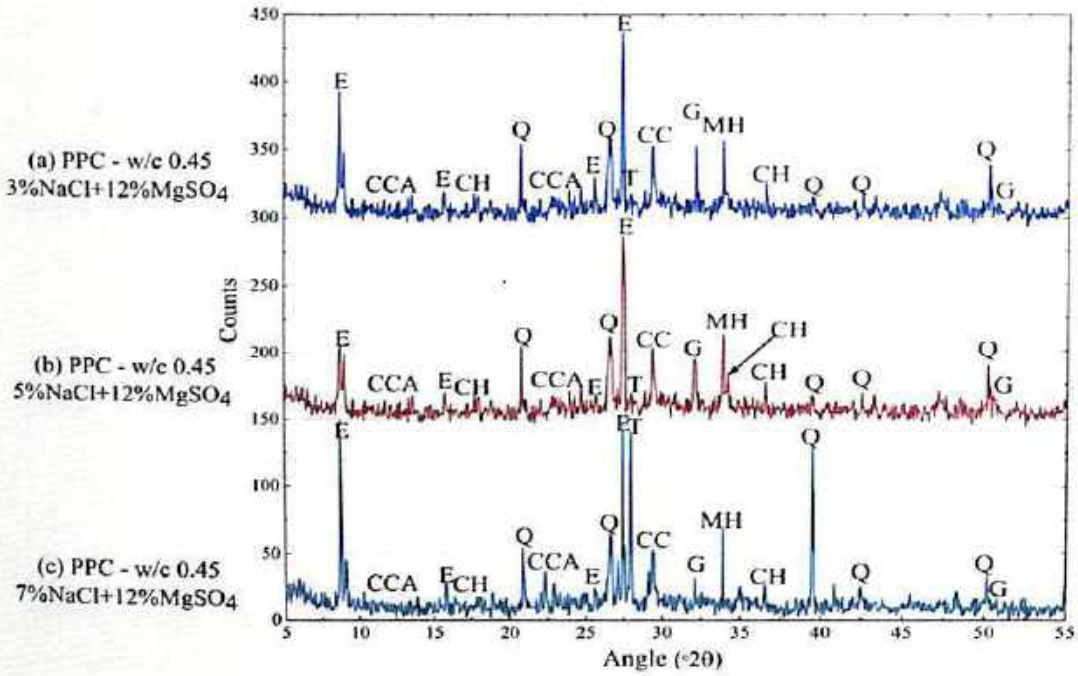

Fig. 4.22 XRD profiles of PPC concrete admixed with (a) 3% NaCl + 12% $MgSO_4$, (b) 5% NaCl + 12% $MgSO_4$ and (c) 7% NaCl + 12% $MgSO_4$, at w/c ratio of 0.45

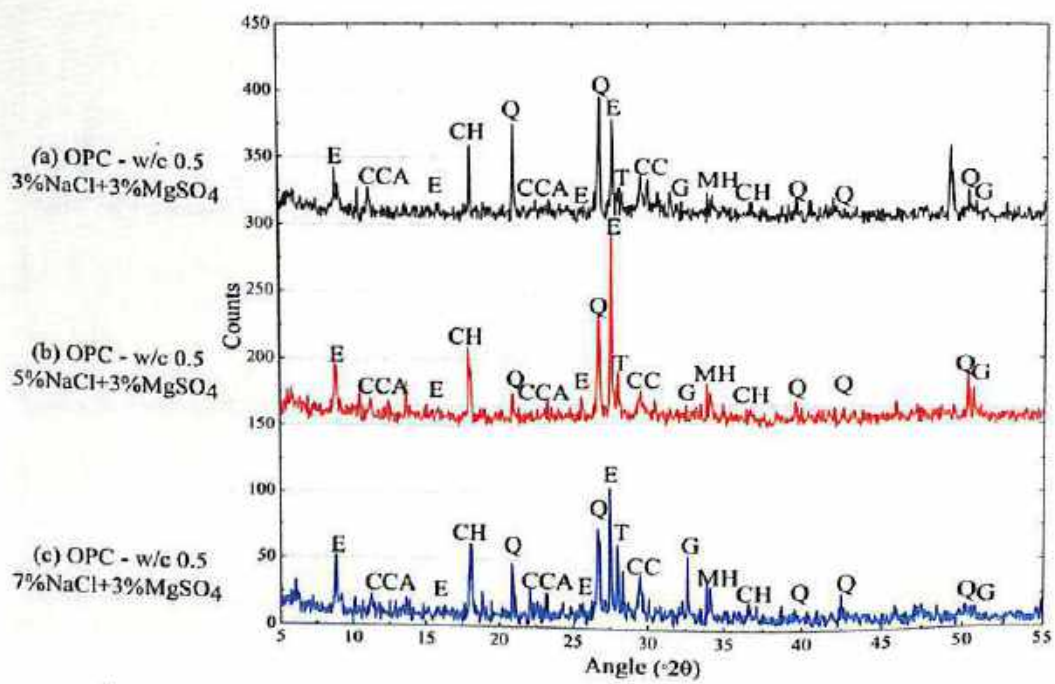

Fig. 4.23 XRD profiles of OPC concrete admixed with (a) 3% NaCl + 3% $MgSO_4$, (b) 5% NaCl + 3% $MgSO_4$ and (c) 7% NaCl + 3% $MgSO_4$, at w/c ratio of 0.5

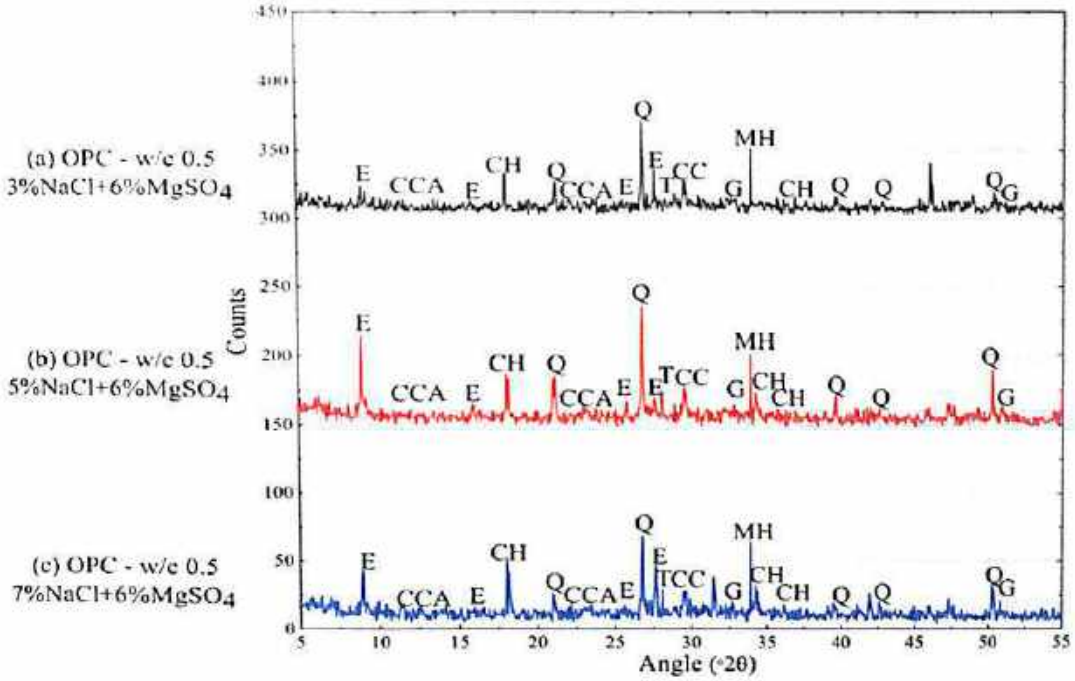

Fig. 4.24 XRD profiles of OPC concrete admixed with a) 3% NaCl + 6% $MgSO_4$, (b) 5% NaCl + 6% $MgSO_4$ and (c) 7% NaCl + 6% $MgSO_4$, at w/c ratio of 0.5

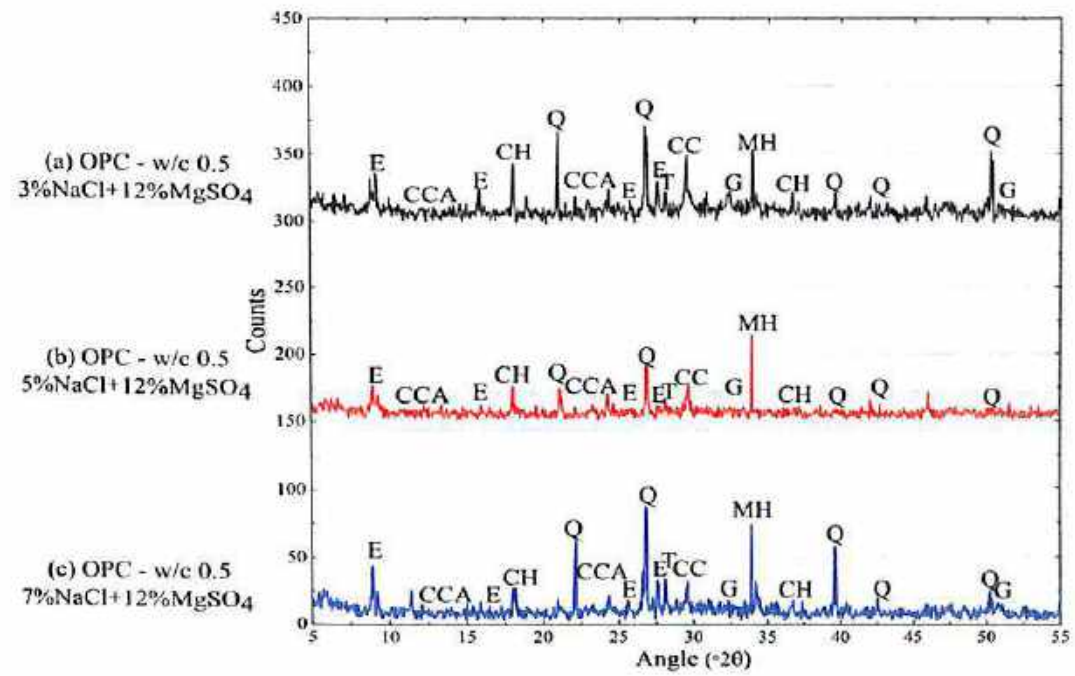

Fig. 4.25 XRD profiles of OPC concrete admixed with (a) 3% NaCl + 12% $MgSO_4$, (b) 5% NaCl + 12% $MgSO_4$ and (c) 7% NaCl + 12% $MgSO_4$, at w/c ratio of 0.5

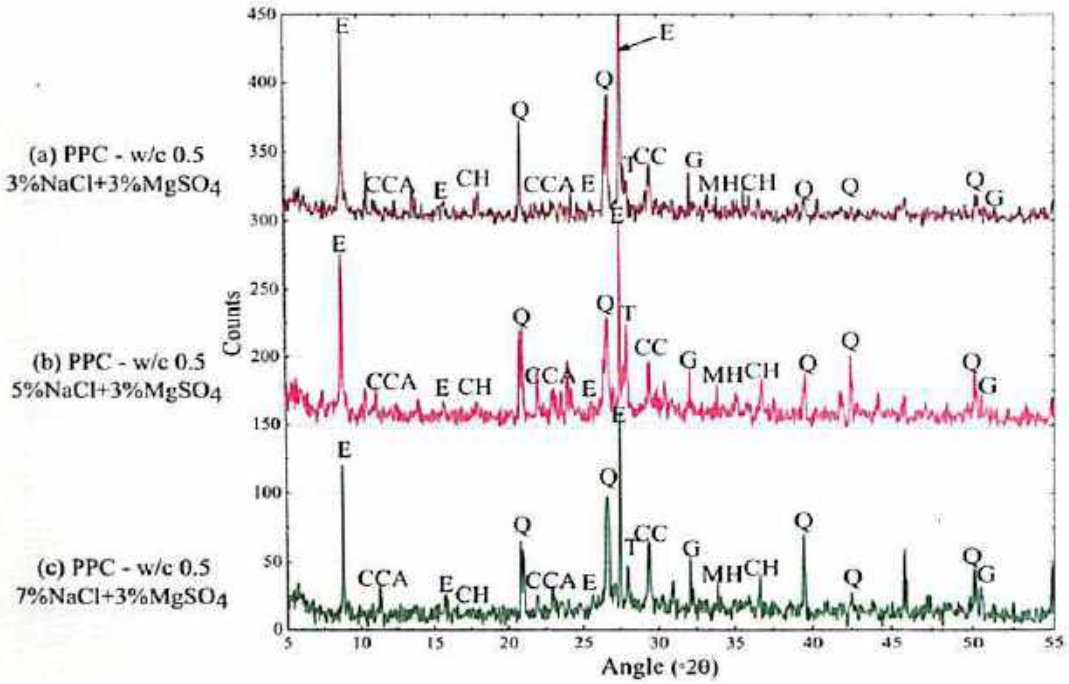

Fig. 4.26 XRD profiles of PPC concrete admixed with (a) 3% NaCl + 3% $MgSO_4$, (b) 5% NaCl + 3% $MgSO_4$ and (c) 7% NaCl + 3% $MgSO_4$, at w/c ratio of 0.5

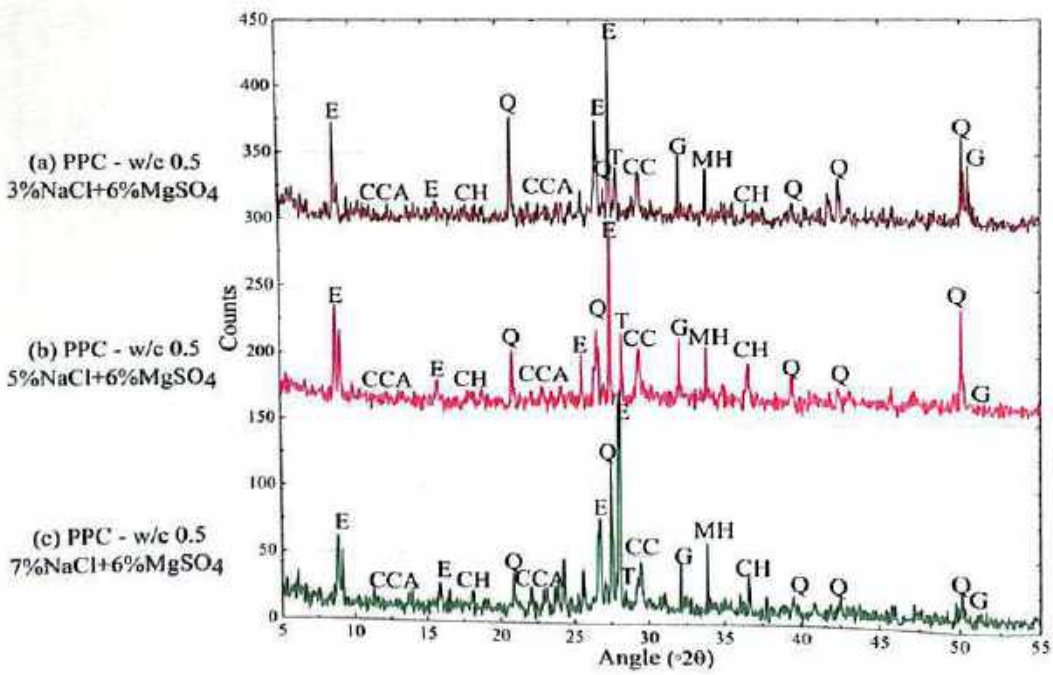

Fig. 4.27 XRD profiles of PPC concrete admixed with (a) 3% NaCl + 6% $MgSO_4$, (b) 5% NaCl + 6% $MgSO_4$ and (c) 7% NaCl + 6% $MgSO_4$, at w/c ratio of 0.5

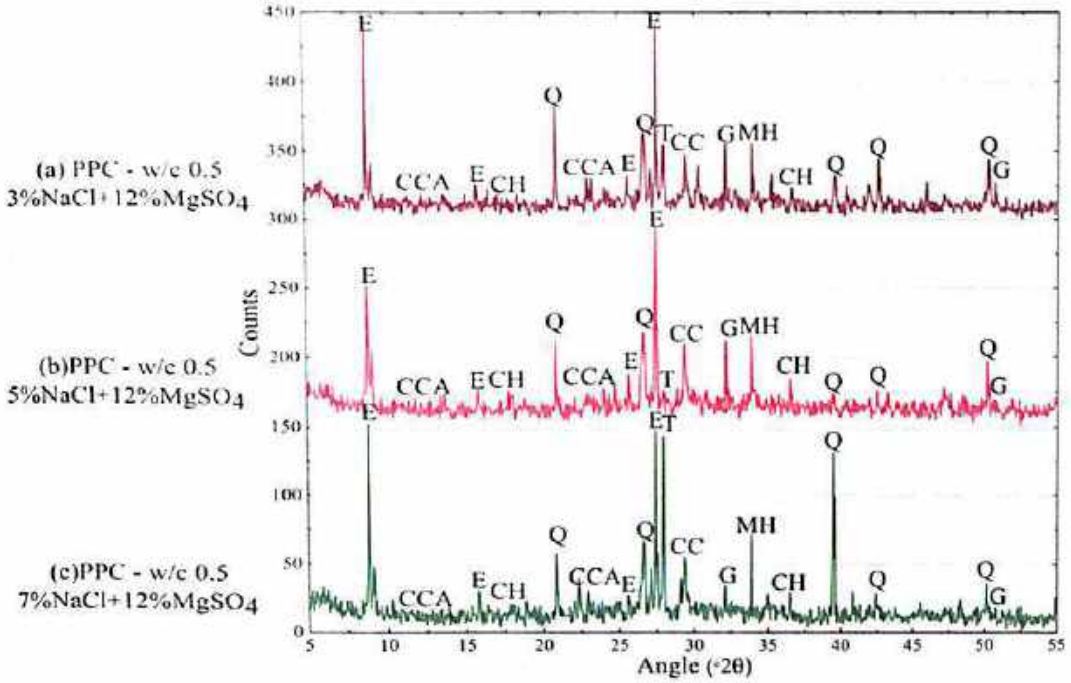

Fig. 4.28 XRD profiles of PPC concrete admixed with (a) 3% NaCl + 12% $MgSO_4$, (b) 5% NaCl + 12% $MgSO_4$ and (c) 7% NaCl + 12% $MgSO_4$, at w/c ratio of 0.5

.3.2 Fourier Transform Infrared (FTIR) Spectroscopy

4.3.2.1 FTIR Spectroscopy of Concrete Contaminated with NaCl

The FTIR spectra of concrete contaminated with sodium chloride concentrations of 3%, 5% and 7% are shown in Fig. 4.29 and Fig. 4.30 for OPC and PPC respectively at w/c ratio of 0.45 and in Fig. 4.31 and Fig. 4.32 respectively at w/c ratio of 0.5. The functional groups associated with different products formed in the concrete as identified from the transmittance band positions in FTIR spectra shown in Fig. 4.29 to Fig. 4.32 are O-H, SO_4^{2-}, CO_3^{2-} and Al-O.

From the FTIR spectra shown in Fig. 4.29 and Fig. 4.30 at w/c ratio of 0.45, it is observed that the bands ranging from 3445 cm^{-1} to 3447 cm^{-1} and 1638 cm^{-1} to 1649 cm^{-1} for OPC and those ranging from 3282 cm^{-1} to 3394 cm^{-1} and 1594 cm^{-1} to 1647 cm^{-1} for PPC irrespective of admixed sodium chloride dosage are caused by stretching and bending bands of O-H group particularly contributed from gypsum [126, 127, 128]. Further, the XRD profiles shown earlier indicate the presence of calcium carbonate in concrete at 29.4° 2θ, which is substantiated by infrared spectra showing CO_3^{2-} bands ranging from 1424 cm^{-1} to 1432 cm^{-1} for OPC and ranging from 1388 cm^{-1} to 1594 cm^{-1} for PPC [126,

129, 130] as shown in Fig. 4.29 and Fig. 4.30. The bands ranging from 996 cm^{-1} to 1004 cm^{-1} and 601 cm^{-1} to 778 cm^{-1} for OPC and ranging from 940 cm^{-1} to 1003 cm^{-1} and 618 cm^{-1} to 778 cm^{-1} for PPC represent ν_1 and ν_4 vibrations of SO_4^{2-} bands contributed by the presence of gypsum [126, 127, 128]. The formation of ettringite as indicated by XRD profiles was corroborated by FTIR spectra through the presence of Al-O bands ranging from 534 cm^{-1} to 536 cm^{-1} and 872 cm^{-1} to 874 cm^{-1} [126, 130] for OPC and at 536 cm^{-1} and 537 cm^{-1} and ranging from 824 cm^{-1} to 874 cm^{-1} for PPC, as shown in Fig. 4.29 and Fig. 4.30.

From the FTIR spectra shown in Fig. 4.31 and Fig. 4.32 at w/c ratio of 0.5, it is observed that the bands ranging from 3445 cm^{-1} to 3452 cm^{-1} and 1642 cm^{-1} to 1649 cm^{-1} for OPC and those at 3394 cm^{-1} and ranging from 1594 cm^{-1} to 1598 cm^{-1} for PPC irrespective of admixed sodium chloride dosage are caused by stretching and bending bands of O-H group contributed from gypsum. Further, the CO_3^{2-} bands ranging from 1424 cm^{-1} to 1432 cm^{-1} for OPC and ranging from 1388 cm^{-1} to 1399 cm^{-1} for PPC are observed from Fig. 4.31 and Fig. 4.32. The bands ranging from 996 cm^{-1} to 1004 cm^{-1} and 776 cm^{-1} to 778 cm^{-1} for OPC and at 940 cm^{-1} and ranging from 725 cm^{-1} to 730 cm^{-1} for PPC represent ν_1 and ν_4 vibrations of SO_4^{2-} bands contributed by the presence of gypsum. The Al-O peak at 872 cm^{-1} for OPC and at 824 cm^{-1} for PPC show the presence of ettringite in concrete as observed from Fig. 4.31 and Fig. 4.32.

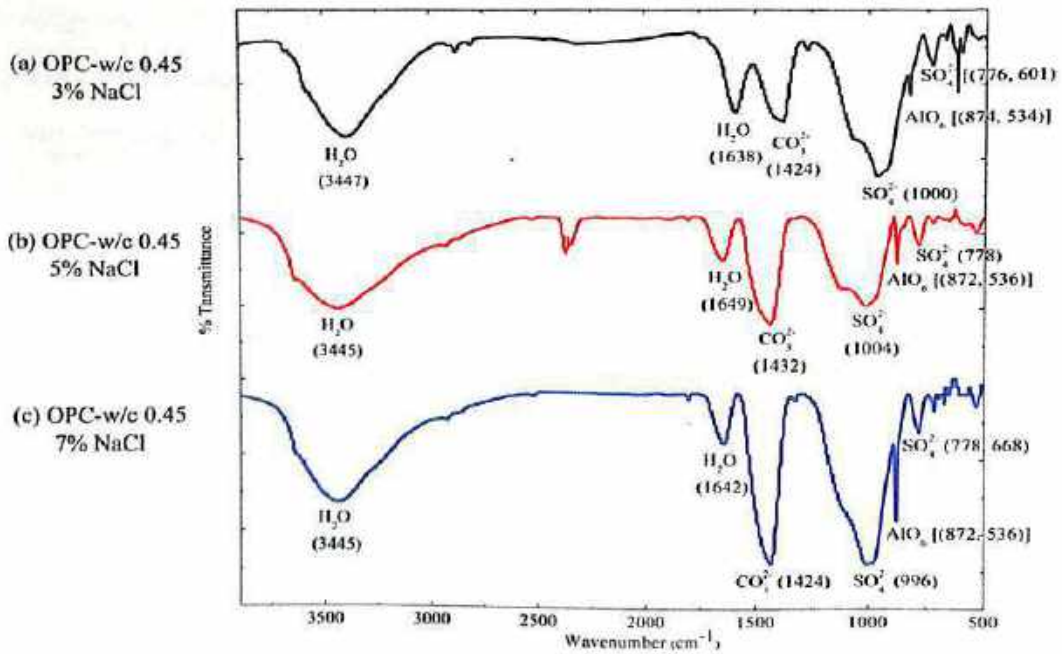

Fig. 4.29 FTIR spectra of OPC concrete admixed with (a) 3% NaCl, (b) 5% NaCl and (c) 7% NaCl, at w/c ratio of 0.45

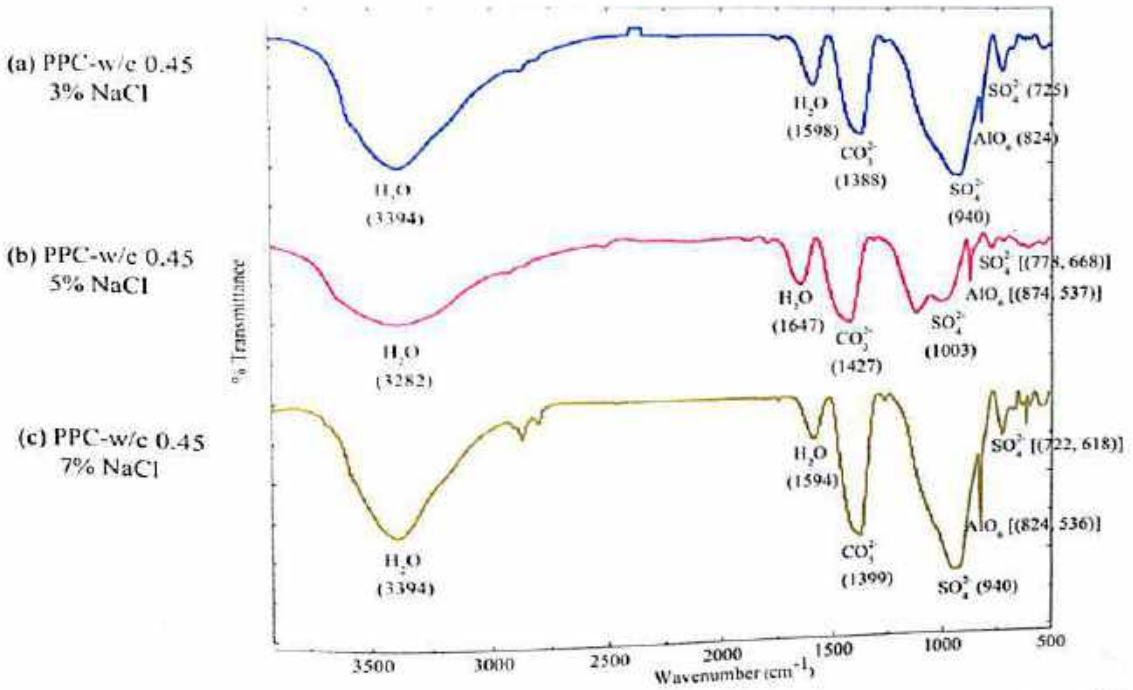

Fig. 4.30 FTIR spectra of PPC concrete admixed with (a) 3% NaCl, (b) 5% NaCl and (c) 7% NaCl, at w/c ratio of 0.45

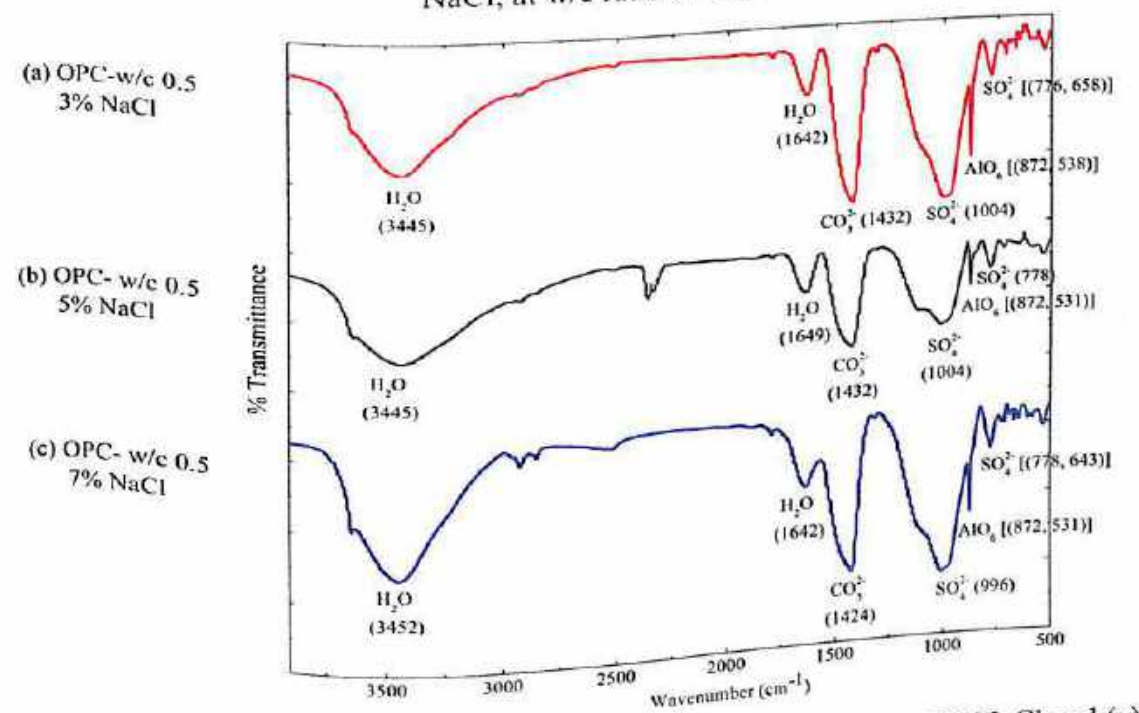

Fig. 4.31 FTIR spectra of OPC concrete admixed with (a) 3% NaCl, (b) 5% NaCl and (c) 7% NaCl, at w/c ratio of 0.5

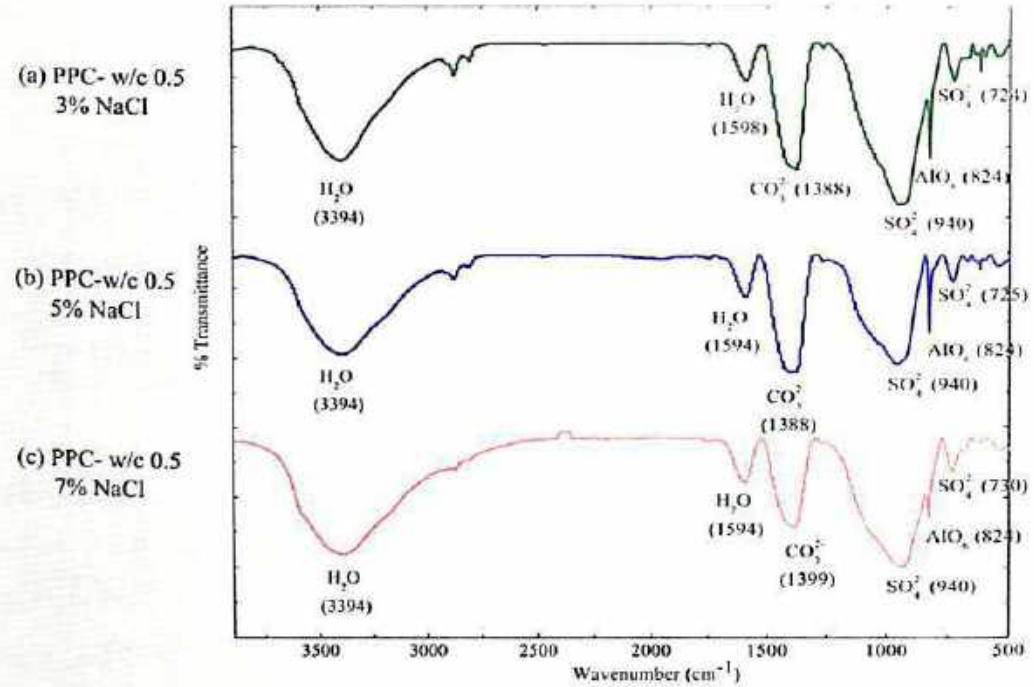

Fig. 4.32 FTIR spectra of PPC concrete admixed with (a) 3% NaCl, (b) 5% NaCl and (c) 7% NaCl, at w/c ratio of 0.5

4.3.2.2 FTIR Spectroscopy of Concrete Contaminated with NaCl plus Na_2SO_4

The FTIR spectra of OPC concrete contaminated with varying concentrations of sodium chloride (3%, 5% and 7%) plus sodium sulfate (3%, 6% and 12%) are shown in Fig. 4.33, Fig. 4.34 and Fig. 4.35 and that of PPC concrete are shown in Fig. 4.36, Fig. 4.37 and Fig. 4.38 at w/c ratio of 0.45. Similarly at w/c ratio of 0.5, the FTIR spectra of concrete contaminated with varying concentrations sodium chloride plus sodium sulfate are shown in Fig. 4.39, Fig. 4.40 and Fig. 4.41 for OPC and in Fig. 4.42, Fig. 4.43 and Fig. 4.44 for PPC. The functional groups associated with different products formed in the concrete as identified from the transmittance band positions shown in FTIR spectra (Fig. 4.33 to Fig. 4.44) are O-H, SO_4^{2-}, CO_3^{2-} and Al-O.

From the FTIR spectra of OPC (Fig. 4.33 to Fig. 4.35) and PPC (Fig. 4.36 to Fig. 4.38) concrete contaminated with conjoint sodium chloride and sodium sulfate at w/c ratio of 0.45, it is observed that the bands ranging from 3376 cm^{-1} to 3447 cm^{-1} and 1646 cm^{-1} to 1650 cm^{-1} for OPC and those ranging from 3354 cm^{-1} to 3445 cm^{-1} and 1632 cm^{-1} to 1647 cm^{-1} for PPC irrespective of admixed NaCl and Na_2SO_4 dosage are caused by stretching and bending bands of O-H group contributed from gypsum. Similarly, the bands ranging from 986 cm^{-1} to 1003 cm^{-1} and 600 cm^{-1} to 781 cm^{-1} for OPC and those ranging from

975 cm^{-1} to 1003 cm^{-1} and 600 cm^{-1} to 781 cm^{-1} for PPC due to v_1 and v_4 vibrations of SO_4^{2-} are also associated with gypsum. The presence of ettringite was further confirmed by the stretching bands of Al-O ranging from 870 cm^{-1} to 875 cm^{-1} and 527 cm^{-1} to 538 cm^{-1} for OPC and those ranging from 860 cm^{-1} to 875 cm^{-1} and 527 cm^{-1} to 538 cm^{-1} for PPC irrespective of admixed NaCl and Na_2SO_4 concentration. The CO_3^{2-} bands ranging from 1415 cm^{-1} to 1439 cm^{-1} for OPC and those ranging from 1426 cm^{-1} to 1451 cm^{-1} for PPC as observed from Fig. 4.33 to Fig. 4.38 indicate the presence of calcium carbonate in concrete.

The FTIR spectra (Fig. 4.39 to Fig. 4.41 for OPC and Fig. 4.42 to Fig. 4.44 for PPC) of concrete at w/c ratio of 0.5 and contaminated with conjoint sodium chloride and sodium sulfate indicate the presence of gypsum through the bands ranging from 3445 cm^{-1} to 3449 cm^{-1} and 1637 cm^{-1} to 1641 cm^{-1} for OPC and those ranging from 3418 cm^{-1} to 3449 cm^{-1} and from 1638 cm^{-1} to 1645 cm^{-1} for PPC irrespective of admixed NaCl and Na_2SO_4 dosage correspond to the stretching and bending bands of O-H group contributed from gypsum. Further, the bands ranging from 1003 cm^{-1} to 1011 cm^{-1} and from 648 cm^{-1} to 779 cm^{-1} for OPC and those ranging from 967 cm^{-1} to 1006 cm^{-1} and from 600 cm^{-1} to 779 cm^{-1} for PPC represent v_1 and v_4 vibrations of SO_4^{2-} bands contributed by the presence of gypsum for sodium chloride plus sodium sulfate contaminations. The presence of ettringite as indicated by XRD profiles was substantiated through Al-O bands at 873 cm^{-1} and 874 cm^{-1} and that at 533 cm^{-1} and 534 cm^{-1} for OPC and those ranging from 873 cm^{-1} to 875 cm^{-1} and from 533 cm^{-1} to 536 cm^{-1} for PPC as observed from Fig. 4.39 to Fig. 4.44. The presence of calcium carbonate in concrete is also corroborated by the FTIR spectra showing CO_3^{2-} bands ranging from 1425 cm^{-1} to 1448 cm^{-1} for OPC and those ranging from 1424 cm^{-1} to 1468 cm^{-1} for PPC as observed from Fig. 4.39 to Fig. 4.44.

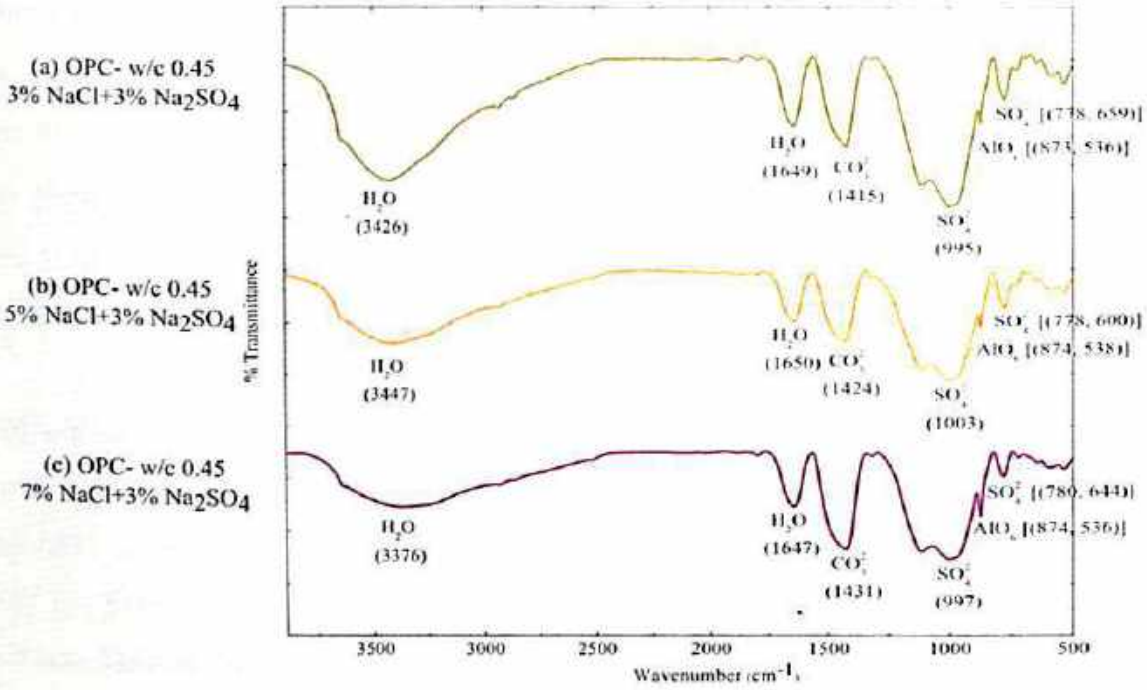

Fig. 4.33 FTIR spectra of OPC concrete admixed with (a) 3% NaCl + 3% Na_2SO_4, (b) 5% NaCl + 3% Na_2SO_4 and (c) 7% NaCl + 3% Na_2SO_4, at w/c ratio of 0.45

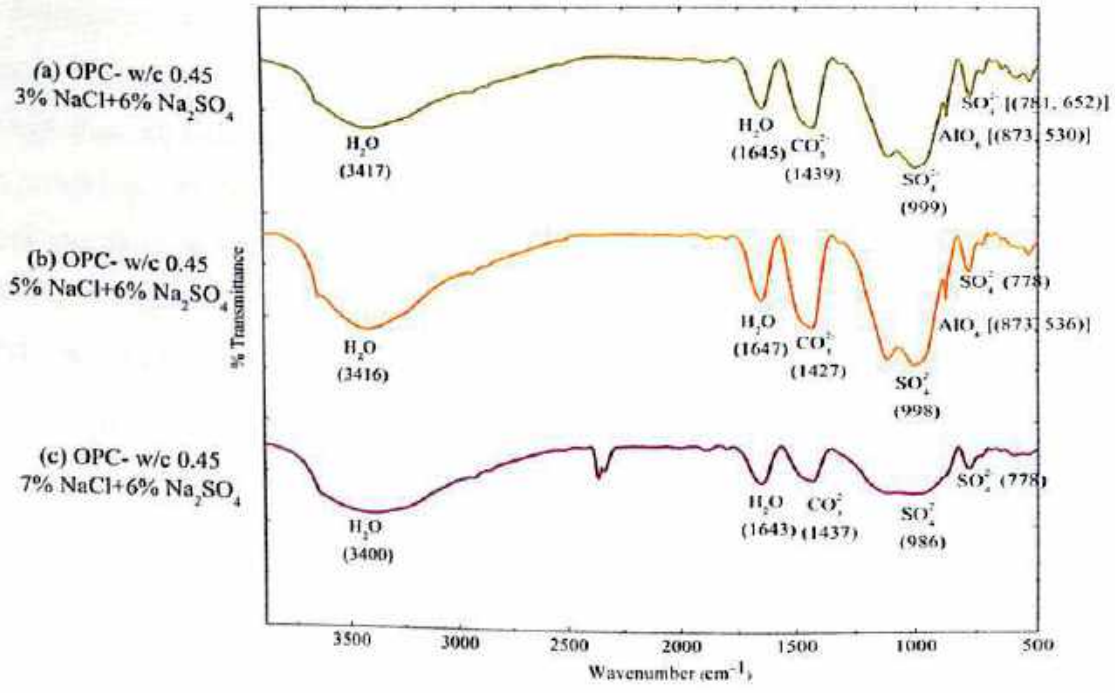

Fig. 4.34 FTIR spectra of OPC concrete admixed with (a) 3% NaCl + 6% Na_2SO_4, (b) 5% NaCl + 6% Na_2SO_4 and (c) 7% NaCl + 6% Na_2SO_4, at w/c ratio of 0.45

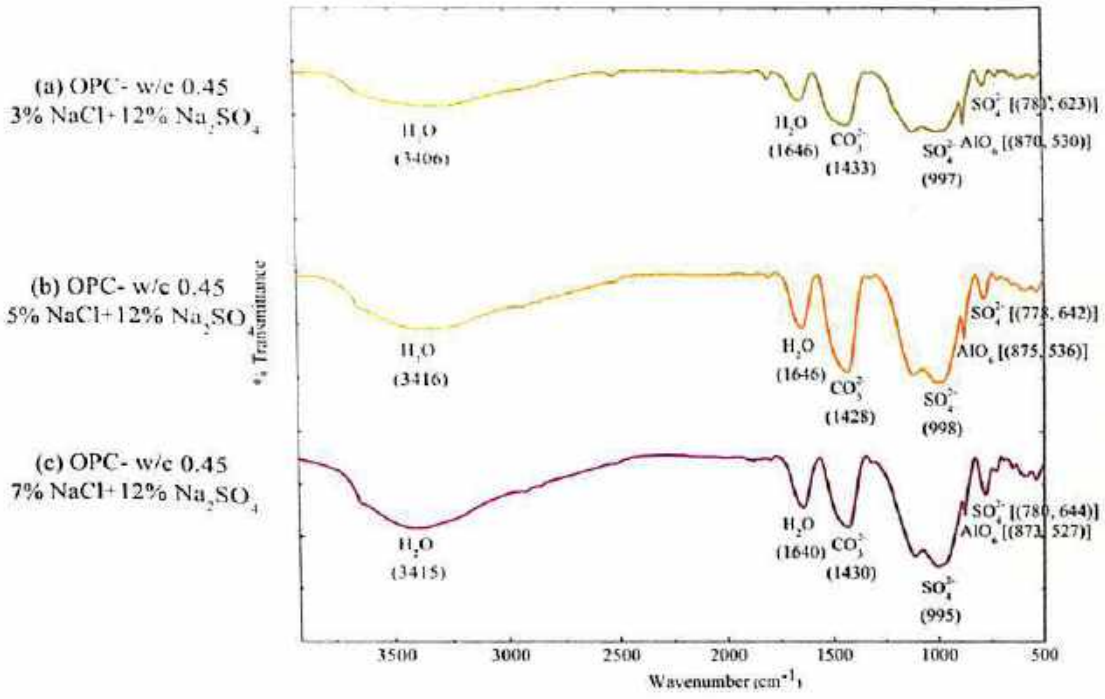

Fig. 4.35 FTIR spectra of OPC concrete admixed with (a) 3% NaCl + 12% Na_2SO_4, (b) 5% NaCl + 12% Na_2SO_4 and (c) 7% NaCl + 12% Na_2SO_4, at w/c ratio of 0.45

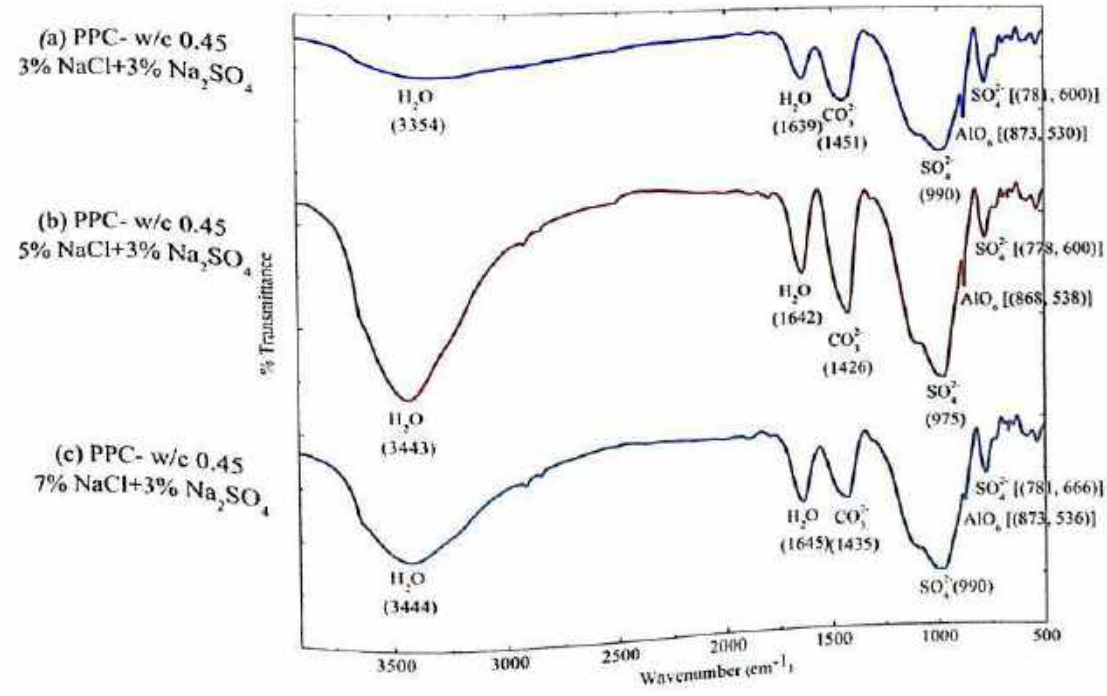

Fig. 4.36 FTIR spectra of PPC concrete admixed with (a) 3% NaCl + 3% Na_2SO_4, (b) 5% NaCl + 3% Na_2SO_4 and (c) 7% NaCl + 3% Na_2SO_4, at w/c ratio of 0.45

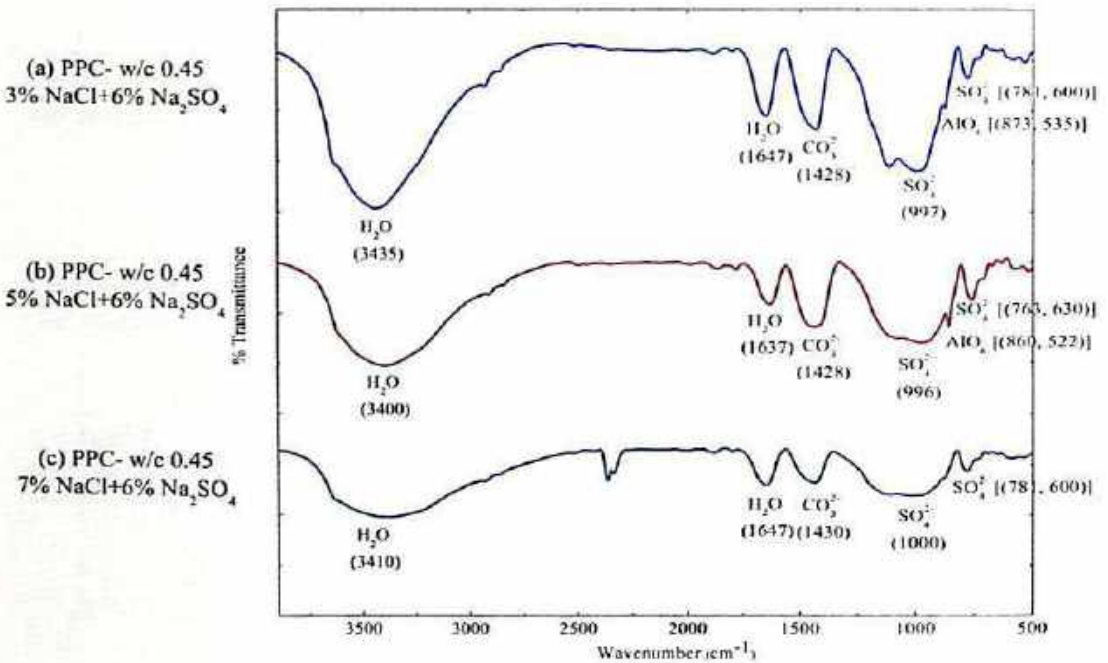

Fig. 4.37 FTIR spectra of PPC concrete admixed with (a) 3% NaCl + 6% Na_2SO_4, (b) 5% NaCl + 6% Na_2SO_4 and (c) 7% NaCl + 6% Na_2SO_4, at w/c ratio of 0.45

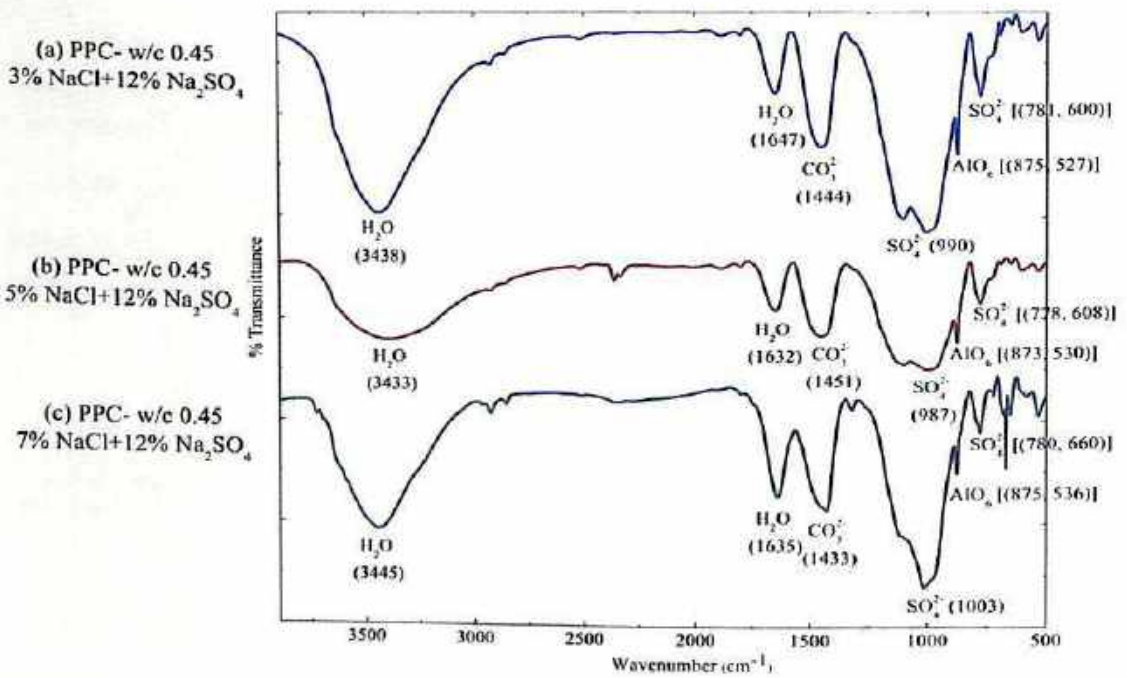

Fig. 4.38 FTIR spectra of PPC concrete admixed with (a) 3% NaCl + 12% Na_2SO_4, (b) 5% NaCl + 12% Na_2SO_4 and (c) 7% NaCl + 12% Na_2SO_4, at w/c ratio of 0.45

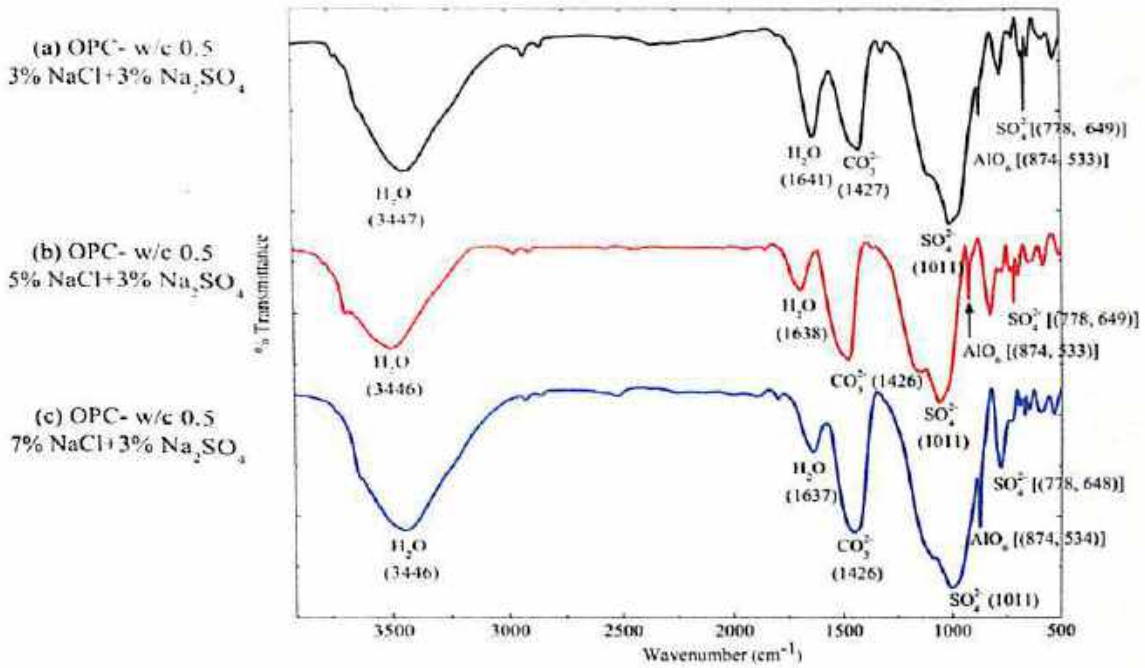

Fig. 4.39 FTIR spectra of OPC concrete admixed with (a) 3% NaCl + 3% Na_2SO_4, (b) 5% NaCl + 3% Na_2SO_4 and (c) 7% NaCl + 3% Na_2SO_4, at w/c ratio of 0.5

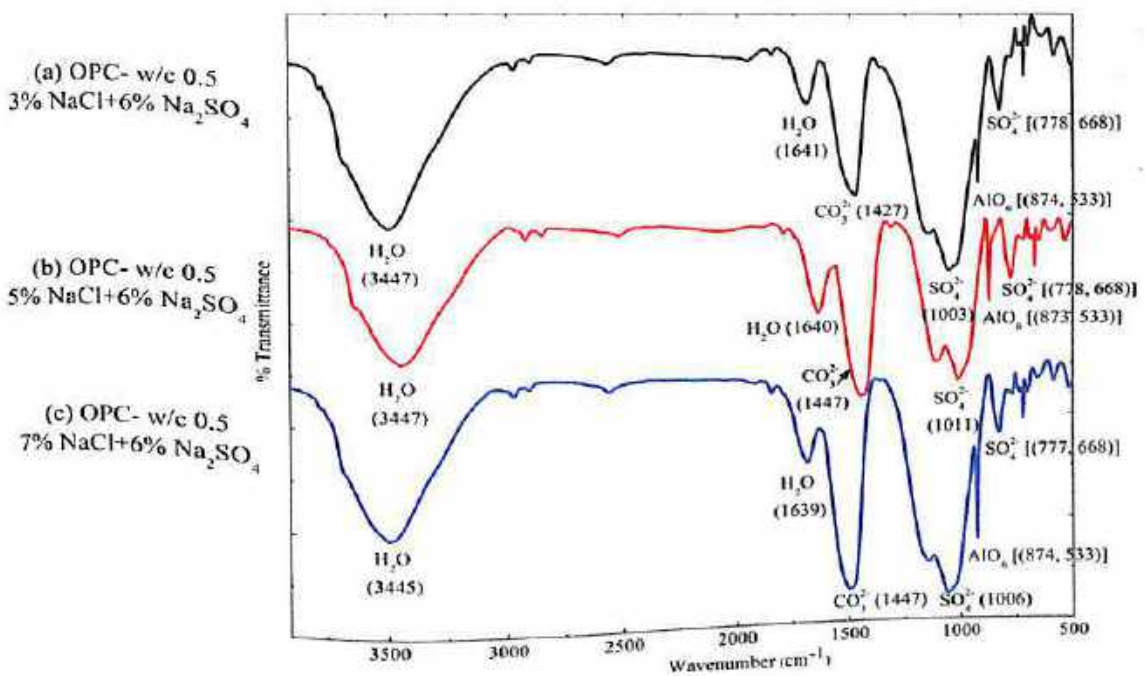

Fig. 4.40 FTIR spectra of OPC concrete admixed with (a) 3% NaCl + 6% Na_2SO_4, (b) 5% NaCl + 6% Na_2SO_4 and (c) 7% NaCl + 6% Na_2SO_4, at w/c ratio of 0.5

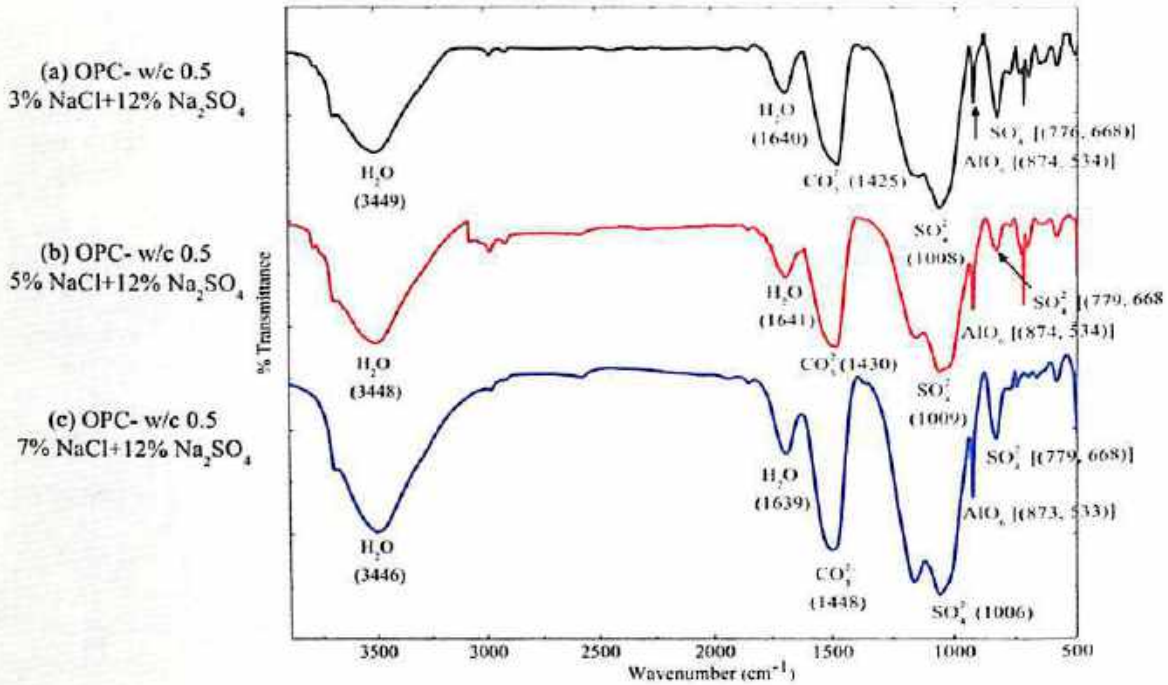

Fig. 4.41 FTIR spectra of OPC concrete admixed with (a) 3% NaCl + 12% Na_2SO_4, (b) 5% NaCl + 12% Na_2SO_4 and (c) 7% NaCl + 12% Na_2SO_4, at w/c ratio of 0.5

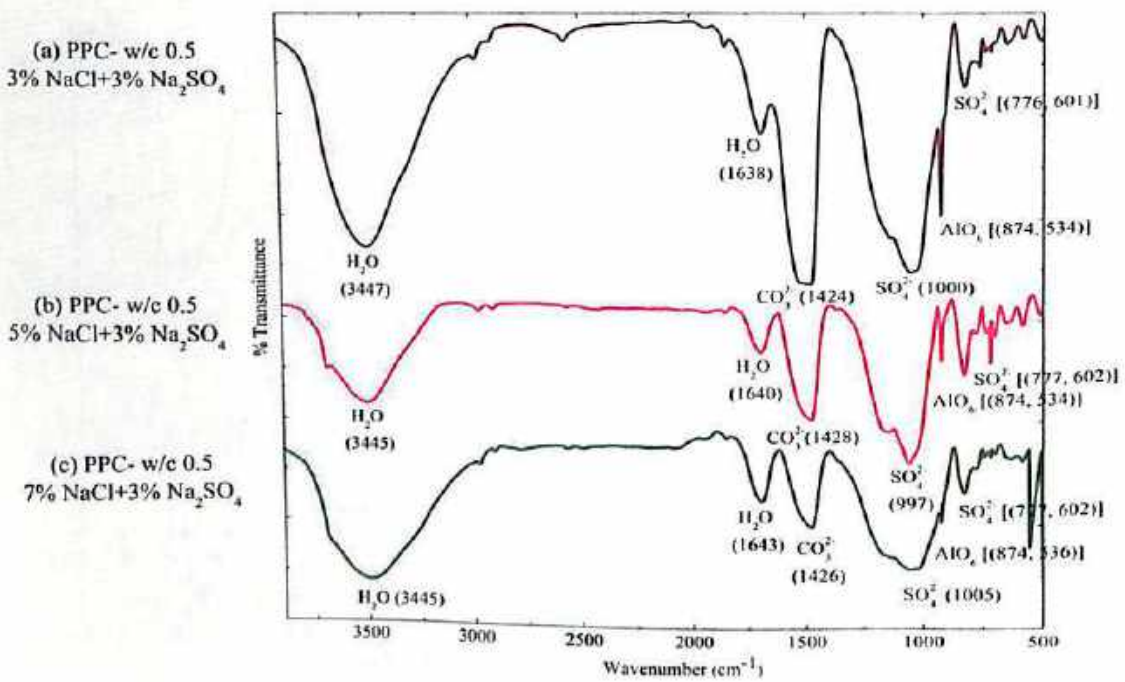

Fig. 4.42 FTIR spectra of PPC concrete admixed with (a) 3% NaCl + 3% Na_2SO_4, (b) 5% NaCl + 3% Na_2SO_4 and (c) 7% NaCl + 3% Na_2SO_4, at w/c ratio of 0.5

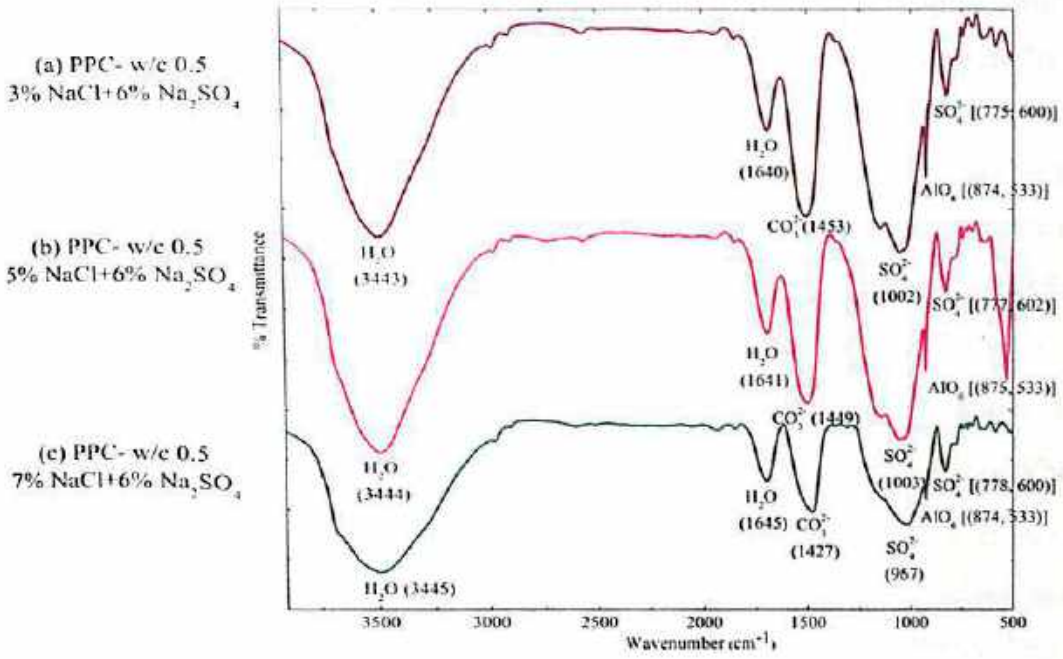

Fig. 4.43 FTIR spectra of PPC concrete admixed with (a) 3% NaCl + 6% Na_2SO_4, (b) 5% NaCl + 6% Na_2SO_4 and (c) 7% NaCl + 6% Na_2SO_4, at w/c ratio of 0.5

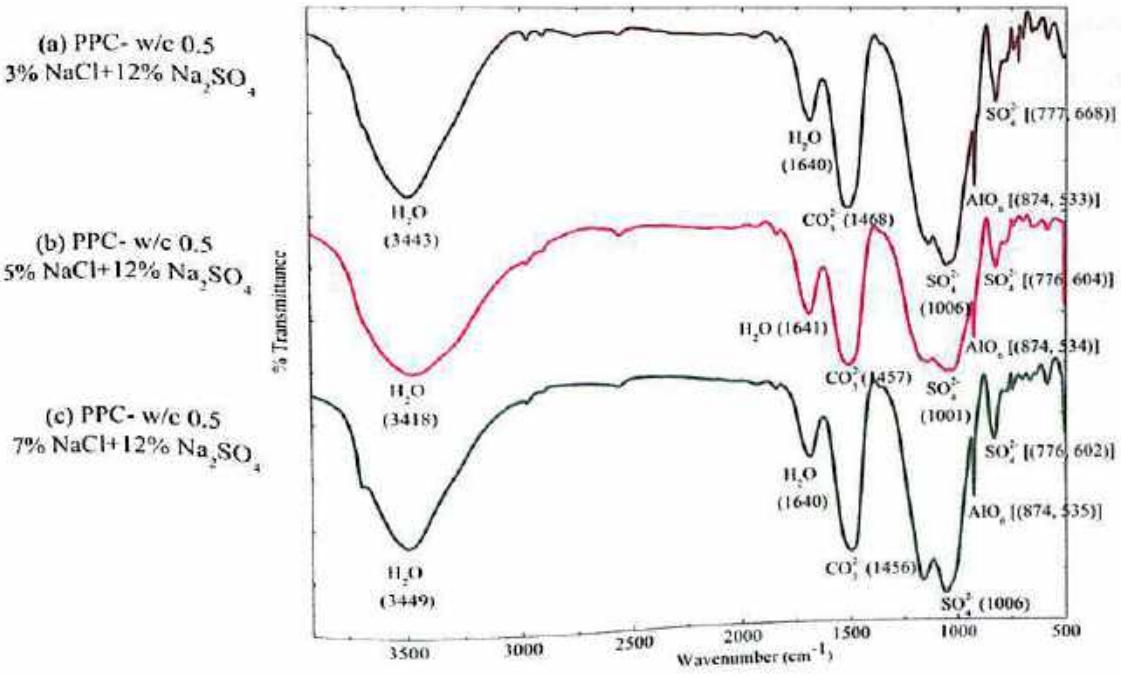

Fig. 4.44 FTIR spectra of PPC concrete admixed with (a) 3% NaCl + 12% Na_2SO_4, (b) 5% NaCl + 12% Na_2SO_4 and (c) 7% NaCl + 12% Na_2SO_4, at w/c ratio of 0.5

4.3.2.3 FTIR Spectroscopy of Concrete Contaminated with NaCl plus $MgSO_4$

For conjoint sodium chloride plus magnesium sulfate contamination, the FTIR spectra of concrete admixed with varying concentrations of sodium chloride (3%, 5% and 7%) plus magnesium sulfate (3%, 6% and 12%) are shown in Fig. 4.45, Fig. 4.46 and Fig. 4.47 for OPC and in Fig. 4.48, Fig. 4.49 and Fig. 4.50 for PPC at w/c ratio of 0.45. Similarly at w/c ratio of 0.5, the FTIR spectra of concrete admixed with varying concentrations of sodium chloride plus magnesium sulfate are shown in Fig. 4.51, Fig. 4.52 and Fig. 4.53 for OPC and in Fig. 4.54, Fig. 4.55 and Fig. 4.56 for PPC. The FTIR spectra shown in Fig. 4.45 to Fig. 4.56 indicate functional groups such as O-H, SO_4^{2-}, CO_3^{2-} and Al-O, which are associated with different products formed in concrete.

In the concrete made with w/c ratio of 0.45 and contaminated with sodium chloride plus magnesium sulfate, the bands ranging from 3289 cm^{-1} and 3438 cm^{-1} and from 1636 cm^{-1} to 1654 cm^{-1} for OPC (Fig. 4.45 to Fig. 4.47) and those ranging from 3391 cm^{-1} to 3443 cm^{-1} and from 1635 cm^{-1} to 1654 cm^{-1} for PPC (Fig. 4.48 to Fig. 4.50) irrespective of admixed NaCl and $MgSO_4$ dosage correspond to stretching and bending bands of O-H group contributed from gypsum. Further for sodium chloride plus magnesium sulfate contaminations, the bands ranging from 982 cm^{-1} to 1003 cm^{-1} and from 601 cm^{-1} to 781 cm^{-1} for OPC and those ranging from 979 cm^{-1} to 1005 cm^{-1} and from 600 cm^{-1} to 784 cm^{-1} for PPC are due to v_1 and v_4 vibrations of SO_4^{2-} associated with gypsum. The presence of ettringite in sodium chloride plus magnesium sulfate admixed concrete was confirmed by the stretching bands of Al-O ranging from 868 cm^{-1} to 877 cm^{-1} and from 526 cm^{-1} to 536 cm^{-1} for OPC and those ranging from 873 cm^{-1} to 879 cm^{-1} and from 526 cm^{-1} to 537 cm^{-1} for PPC as observed from FTIR spectra shown in Fig. 4.45 to Fig. 4.50. Similarly the presence of calcium carbonate in concrete was substantiated by the infrared spectra showing CO_3^{2-} bands ranging from 1420 cm^{-1} to 1444 cm^{-1} for OPC and those ranging from 1414 cm^{-1} to 1446 cm^{-1} for PPC.

The FTIR spectra shown in Fig. 4.51 to Fig. 4.53 and Fig. 4.54 to Fig. 4.56 for OPC and PPC concrete respectively at w/c ratio of 0.5 indicate the bands ranging from 3428 cm^{-1} to 3447 cm^{-1} and from 1637 cm^{-1} to 1641 cm^{-1} for OPC and those ranging from 3416 cm^{-1} to 3456 cm^{-1} and from 1639 cm^{-1} to 1659 cm^{-1} for PPC irrespective of admixed NaCl and $MgSO_4$ concentration correspond to stretching and bending bands of O-H group contributed from gypsum. Similarly, the bands ranging from 998 cm^{-1} to 1010 cm^{-1} and

from 608 cm^{-1} to 779 cm^{-1} for OPC and those ranging from 955 cm^{-1} to 1003 cm^{-1} and from 600 cm^{-1} to 777 cm^{-1} for PPC are due to v_1 and v_4 vibrations of SO_4^{2-} associated with gypsum. The Al-O stretching bands associated with ettringite are found at 874 cm^{-1} and from 534 cm^{-1} to 536 cm^{-1} for OPC and those ranging from 871 cm^{-1} to 875 cm^{-1} and at 534 cm^{-1} and 535 cm^{-1} for PPC, as observed from FTIR spectra shown in Fig. 4.51 to Fig. 4.56. Similarly, the CO_3^{2-} bands in FTIR spectra ranging from 1420 cm^{-1} to 1448 cm^{-1} for OPC and those ranging from 1424 cm^{-1} to 1498 cm^{-1} for PPC indicate the presence of calcium carbonate in concrete.

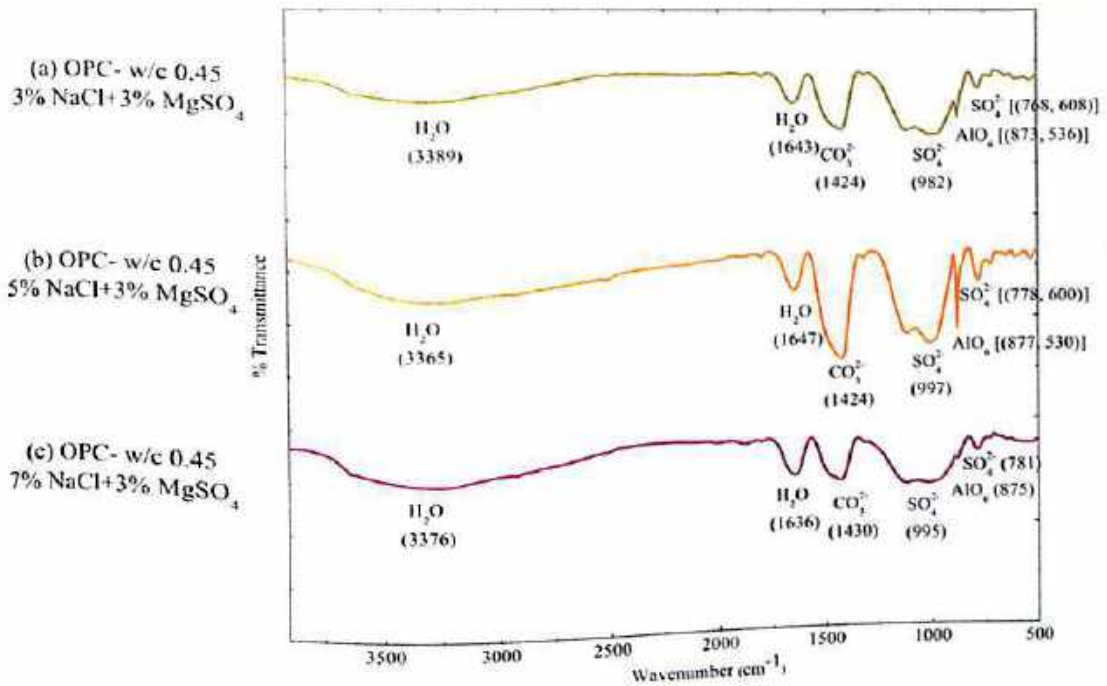

Fig. 4.45 FTIR spectra of OPC concrete admixed with (a) 3% NaCl + 3% $MgSO_4$, (b) 5% NaCl + 3% $MgSO_4$ and (c) 7% NaCl + 3% $MgSO_4$, at w/c ratio of 0.45

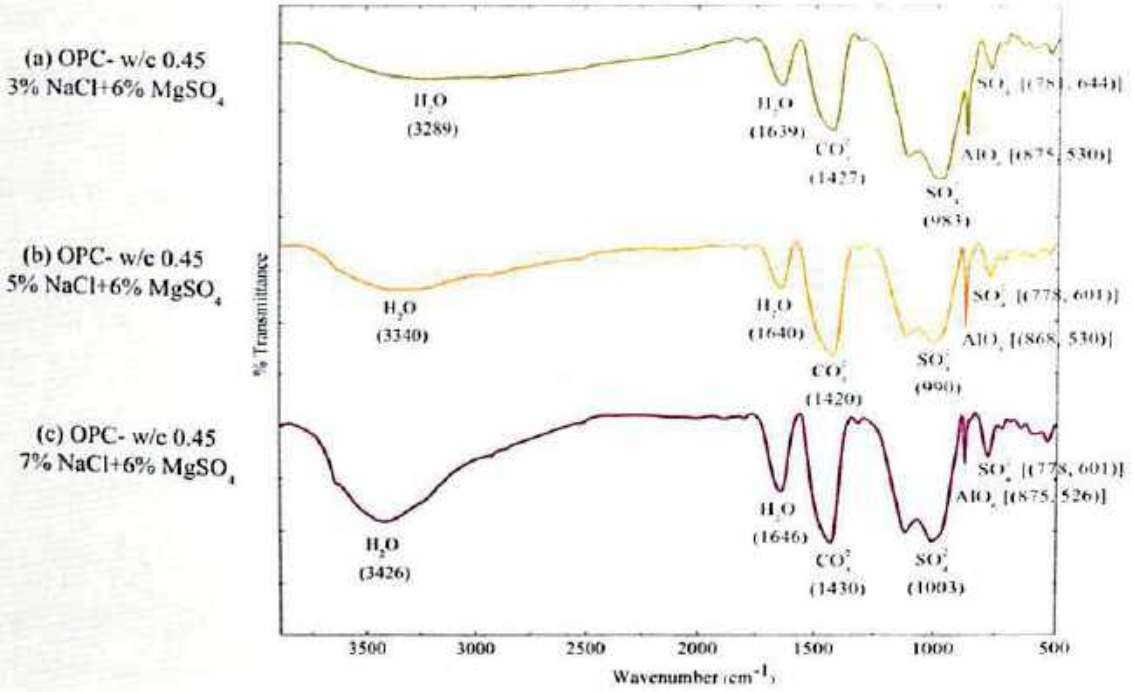

Fig. 4.46 FTIR spectra of OPC concrete admixed with (a) 3% NaCl + 6% $MgSO_4$, (b) 5% NaCl + 6% $MgSO_4$ and (c) 7% NaCl + 6% $MgSO_4$, at w/c ratio of 0.45

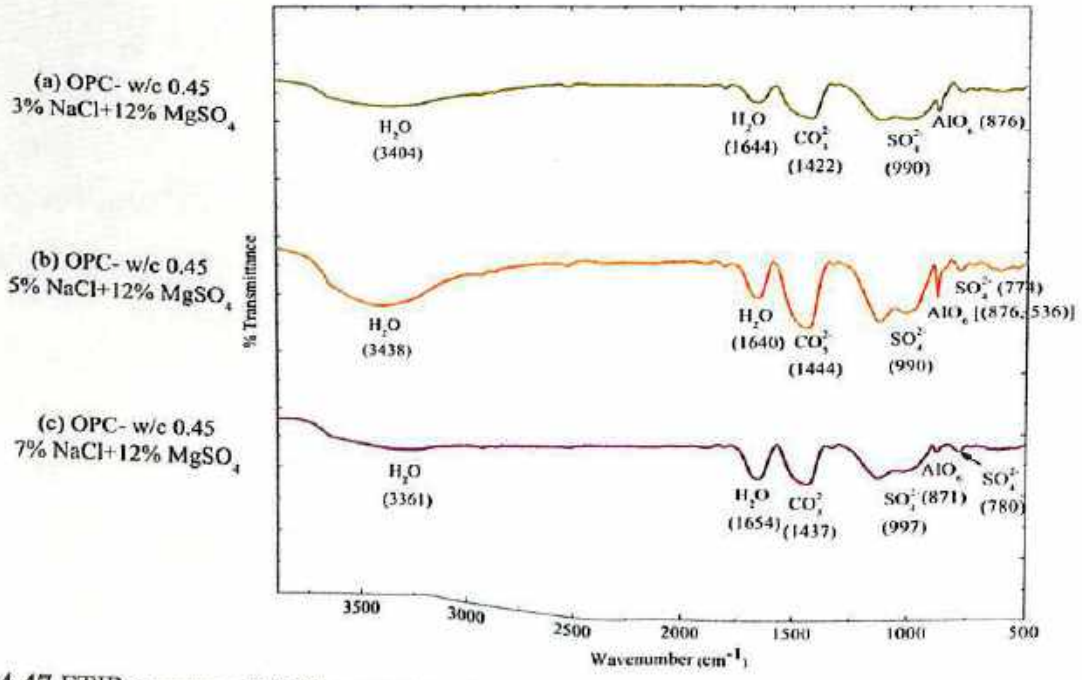

Fig. 4.47 FTIR spectra of OPC concrete admixed with (a) 3% NaCl + 12% $MgSO_4$, (b) 5% NaCl + 12% $MgSO_4$ and (c) 7% NaCl + 12% $MgSO_4$, at w/c ratio of 0.45

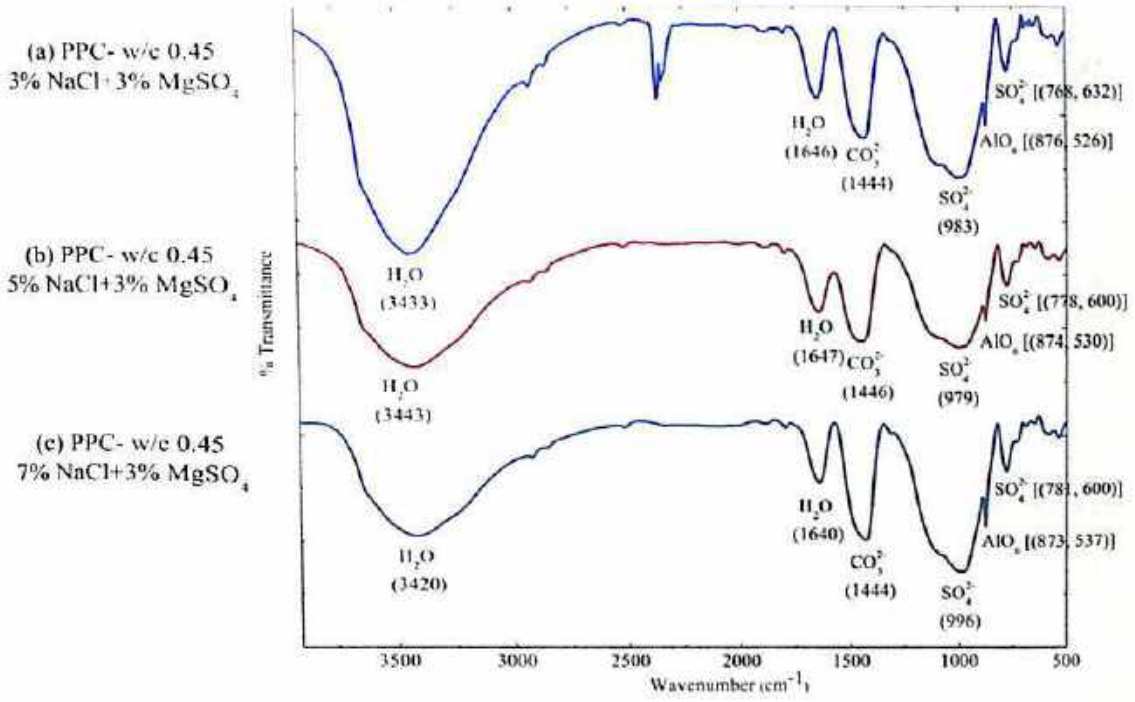

Fig. 4.48 FTIR spectra of PPC concrete admixed with (a) 3% NaCl + 3% $MgSO_4$, (b) 5% NaCl + 3% $MgSO_4$ and (c) 7% NaCl + 3% $MgSO_4$, at w/c ratio of 0.45

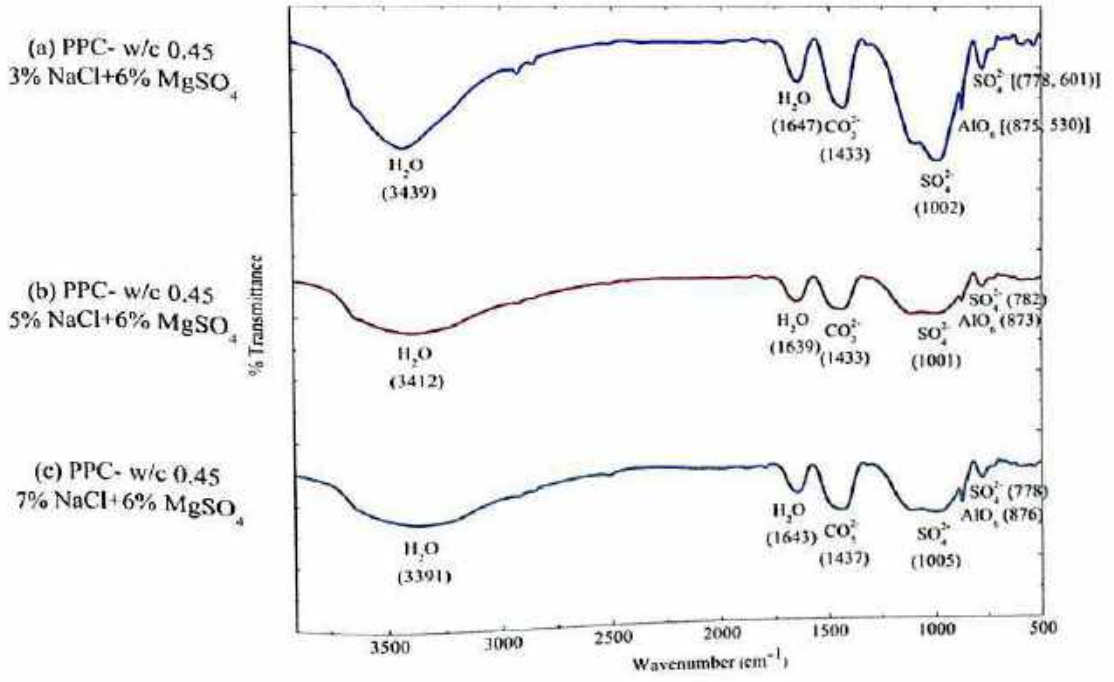

Fig. 4.49 FTIR spectra of PPC concrete admixed with (a) 3% NaCl + 6% $MgSO_4$, (b) 5% NaCl + 6% $MgSO_4$ and (c) 7% NaCl + 6% $MgSO_4$, at w/c ratio of 0.45

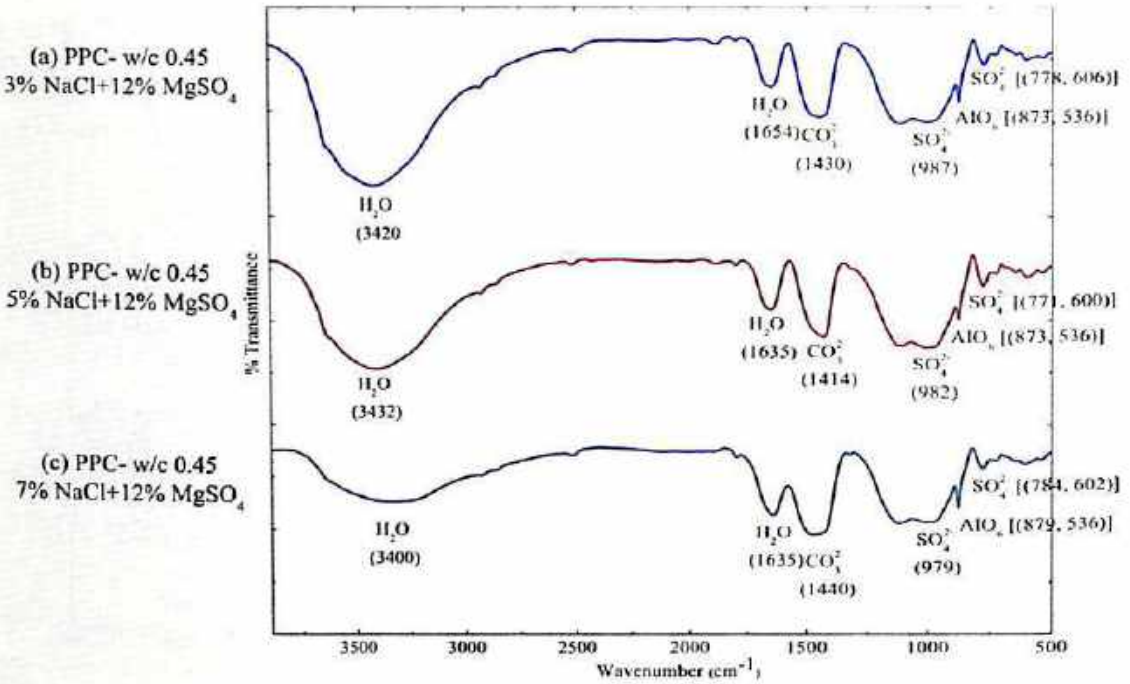

Fig. 4.50 FTIR spectra of PPC concrete admixed with (a) 3% NaCl + 12% $MgSO_4$, (b) 5% NaCl + 12% $MgSO_4$ and (c) 7% NaCl + 12% $MgSO_4$, at w/c ratio of 0.45

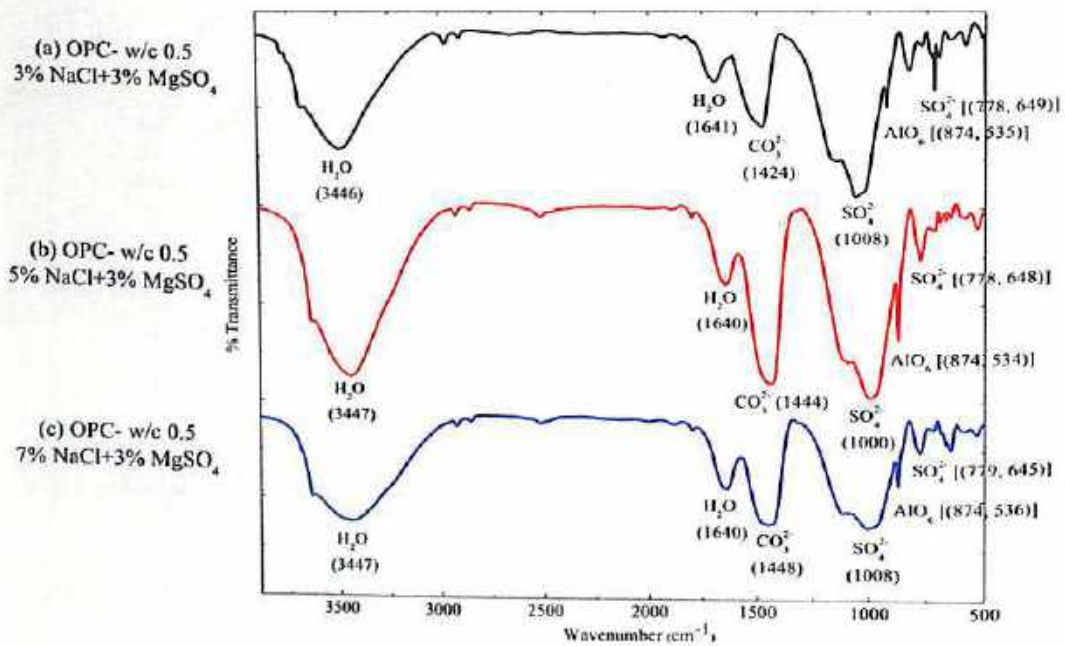

Fig. 4.51 FTIR spectra of OPC concrete admixed with (a) 3% NaCl + 3% $MgSO_4$, (b) 5% NaCl + 3% $MgSO_4$ and (c) 7% NaCl + 3% $MgSO_4$, at w/c ratio of 0.5

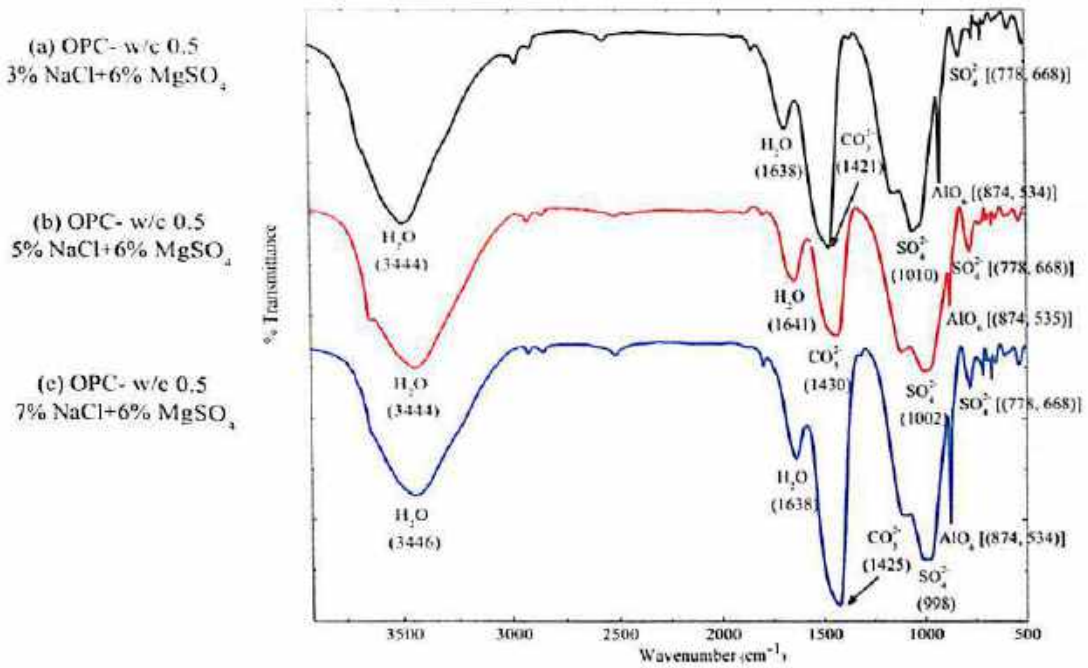

Fig. 4.52 FTIR spectra of OPC concrete admixed with (a) 3% NaCl + 6% $MgSO_4$, (b) 5% NaCl + 6% $MgSO_4$ and (c) 7% NaCl + 6% $MgSO_4$, at w/c ratio of 0.5

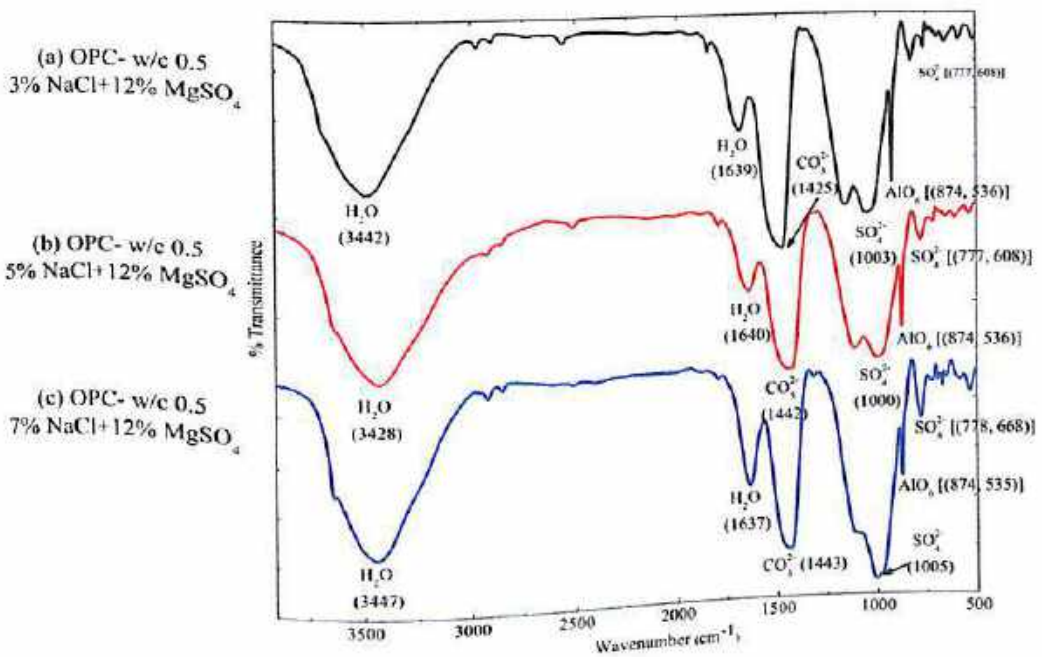

Fig. 4.53 FTIR spectra of OPC concrete admixed with (a) 3% NaCl + 12% $MgSO_4$, (b) 5% NaCl + 12% $MgSO_4$ and (c) 7% NaCl + 12% $MgSO_4$, at w/c ratio of 0.5

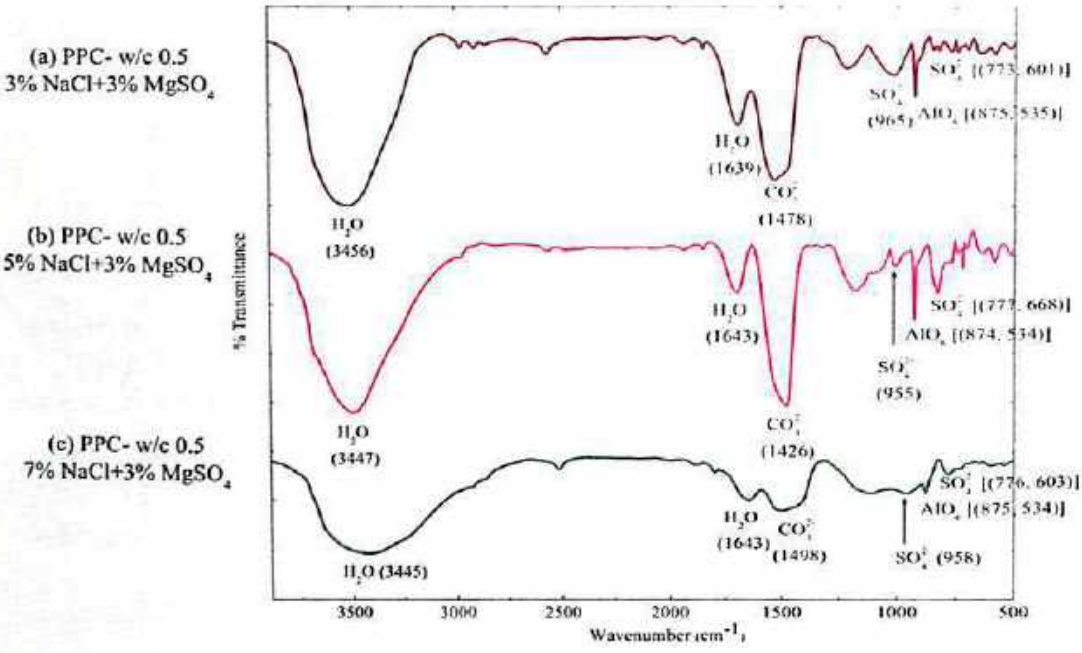

Fig. 4.54 FTIR spectra of PPC concrete admixed with (a) 3% NaCl + 3% $MgSO_4$, (b) 5% NaCl + 3% $MgSO_4$ and (c) 7% NaCl + 3% $MgSO_4$, at w/c ratio of 0.5

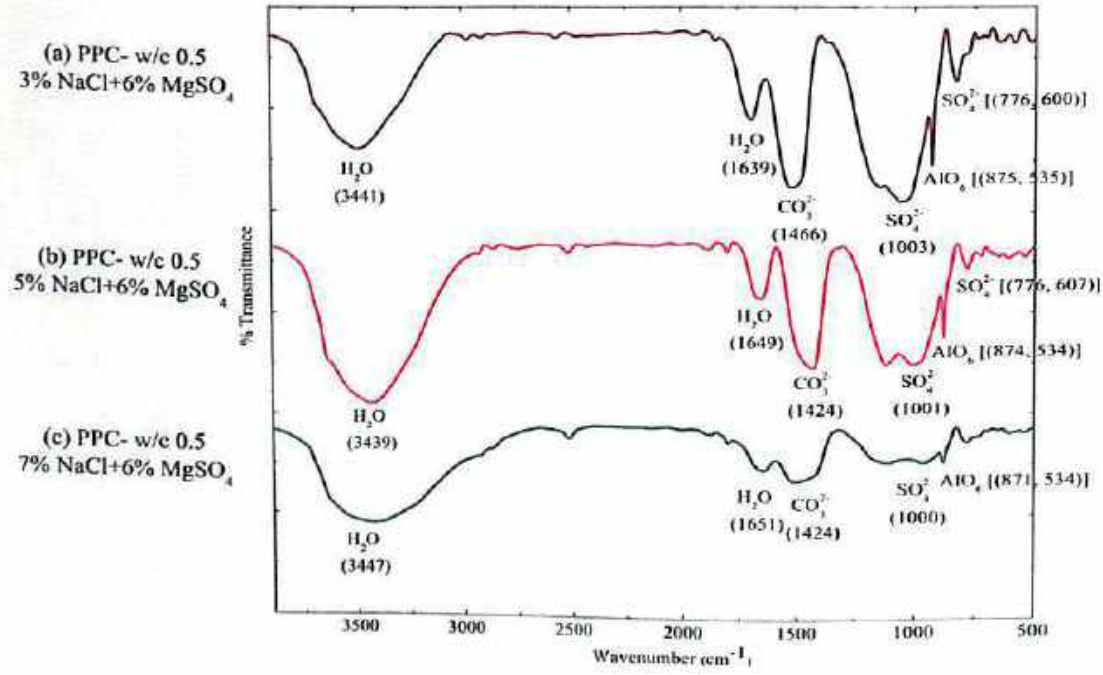

Fig. 4.55 FTIR spectra of PPC concrete admixed with (a) 3% NaCl + 6% $MgSO_4$, (b) 5% NaCl + 6% $MgSO_4$ and (c) 7% NaCl + 6% $MgSO_4$, at w/c ratio of 0.5

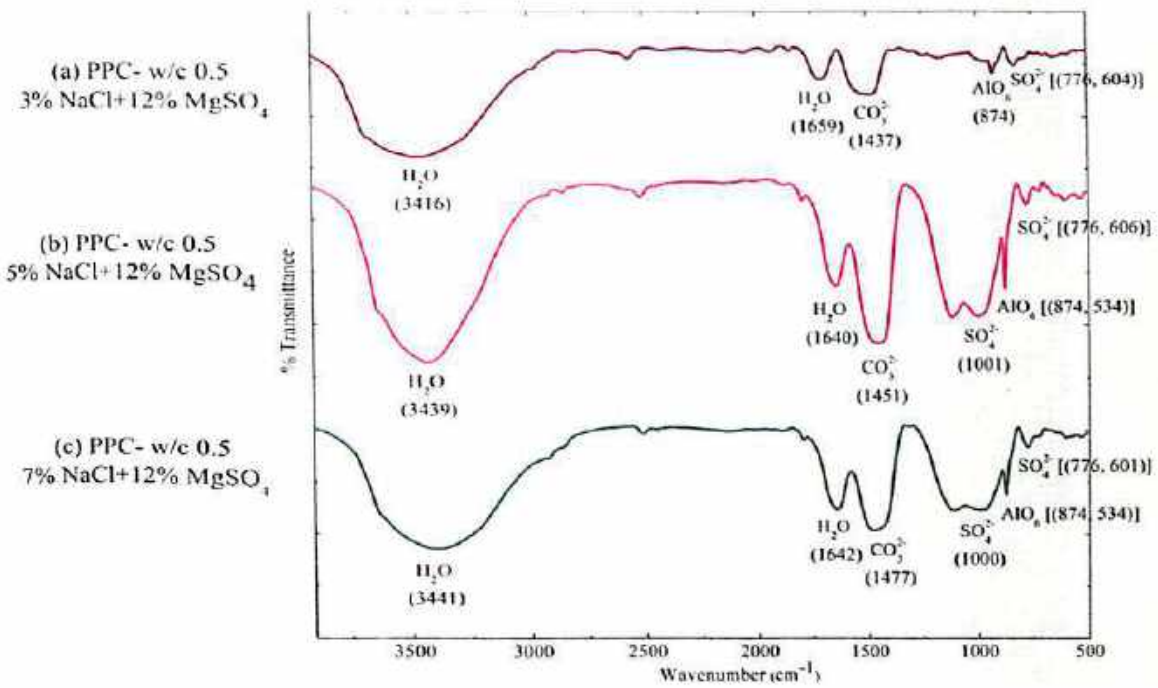

Fig. 4.56 FTIR spectra of PPC concrete admixed with (a) 3% NaCl + 12% $MgSO_4$, (b) 5% NaCl + 12% $MgSO_4$ and (c) 7% NaCl + 12% $MgSO_4$, at w/c ratio of 0.5

4.3.3 Field Emission Scanning Electron Microscopy (FESEM)

In the present research work, FESEM analysis was used to study the microstructure of hardened concrete admixed with chloride and sulfate ions. Fig. 4.57 and Fig. 4.58 show the typical FESEM micrographs for OPC and PPC concrete respectively at w/c ratio of 0.45 and contaminated with sodium chloride. Similarly, typical FESEM micrographs of chloride admixed concrete at w/c ratio of 0.5 are shown in Fig. 4.59 and Fig. 4.60 for OPC and PPC respectively. The FESEM micrographs of chloride admixed concrete shown in Fig. 4.57 to Fig. 4.60 for both types of cement indicate the formation of C-S-H, and calcium chloroaluminate (Friedel's salt). The formation of calcium chloroaluminate, which was observed by XRD profiles in chloride contaminated concrete, is further corroborated through the SEM micrographs. Further, the formation of calcium hydroxide in concrete as observed from XRD profiles is confirmed through FESEM micrographs (Fig. 4.57 to Fig. 4.60), as indicated by hexagonal crystals. The formation of ettringite in concrete is also observed from the FESEM micrograph of OPC concrete shown in Fig. 4.57.

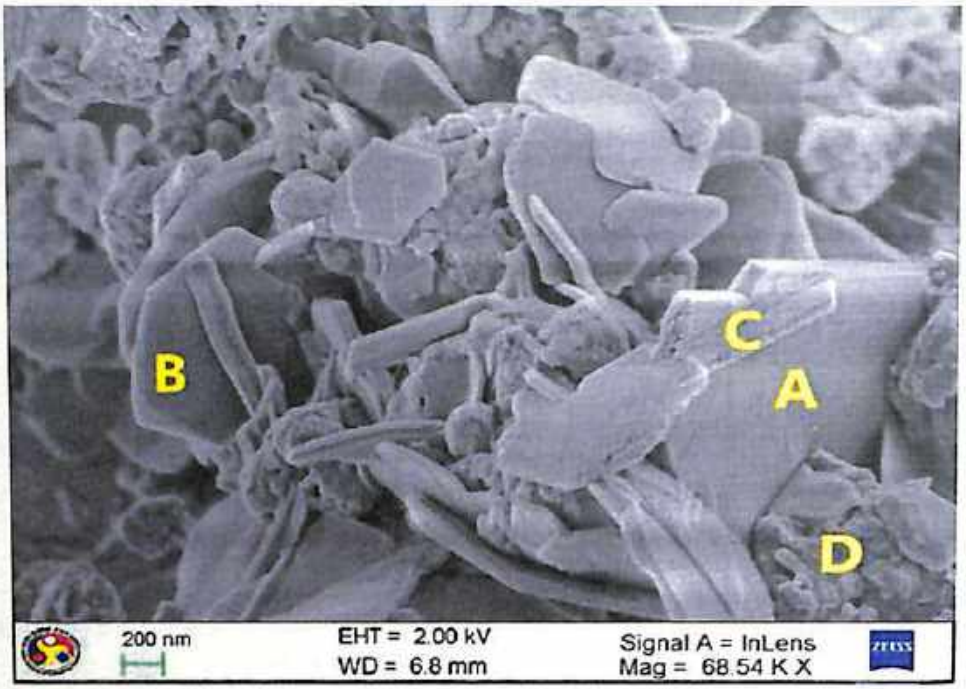

Fig. 4.57 FESEM micrograph of OPC concrete made at w/c ratio of 0.45 and admixed with 7% NaCl: (A) Calcium chloroaluminate, (B) Calcium hydroxide, (C) Ettringite and (D) C-S-H gel

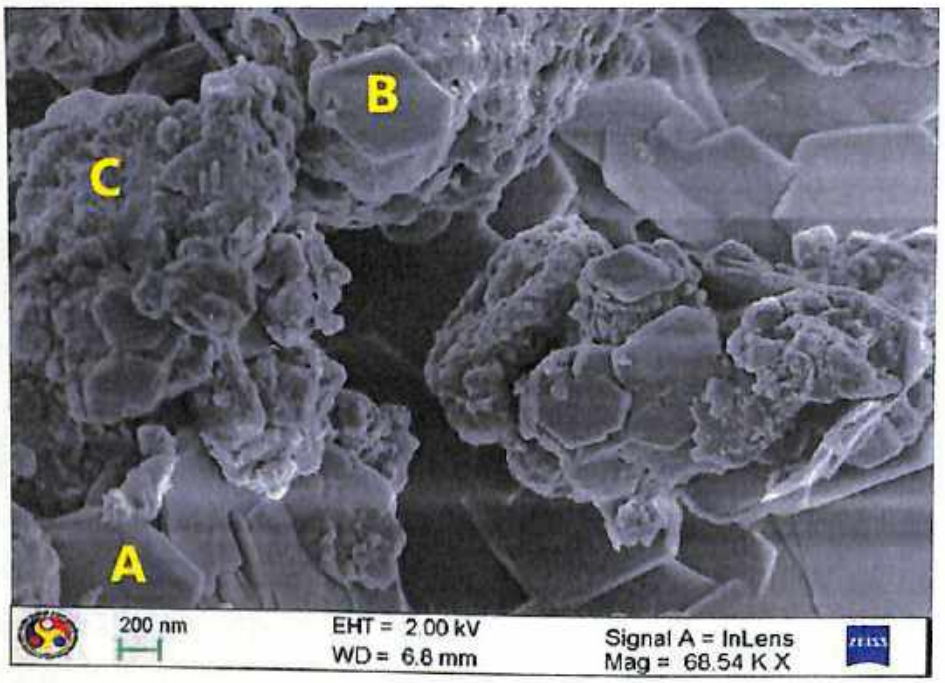

Fig. 4.58 FESEM micrograph of PPC concrete made at w/c ratio of 0.45 and admixed with 7% NaCl: (A) Calcium chloroaluminate, (B) Calcium hydroxide and (C) C-S-H gel

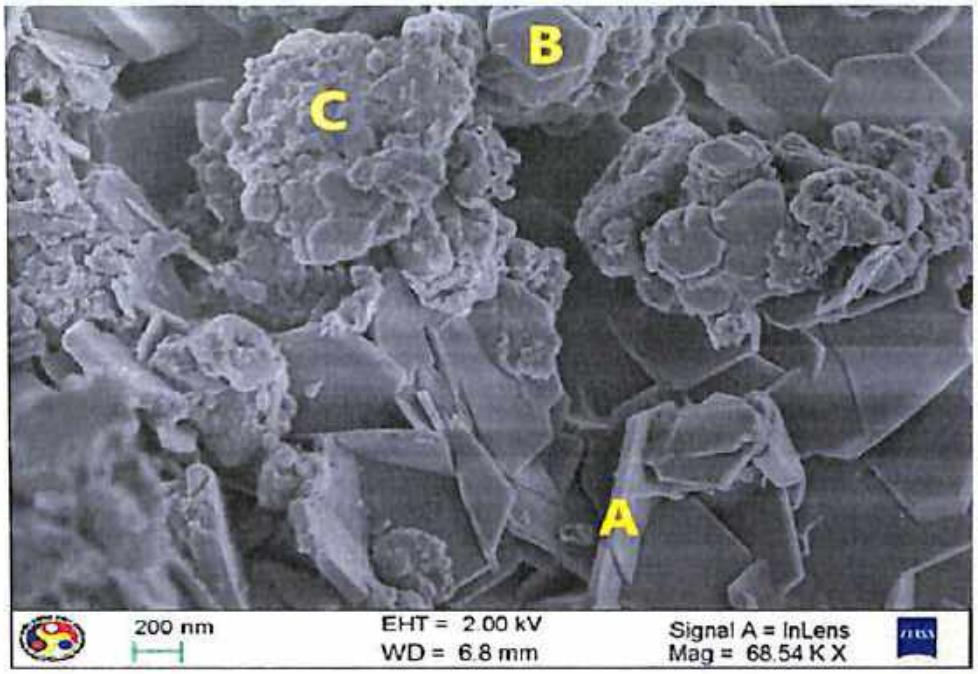

Fig. 4.59 FESEM micrograph of OPC concrete made at w/c ratio of 0.5 and admixed with 7% NaCl: (A) Calcium chloroaluminate, (B) Calcium hydroxide and (C) C-S-H gel

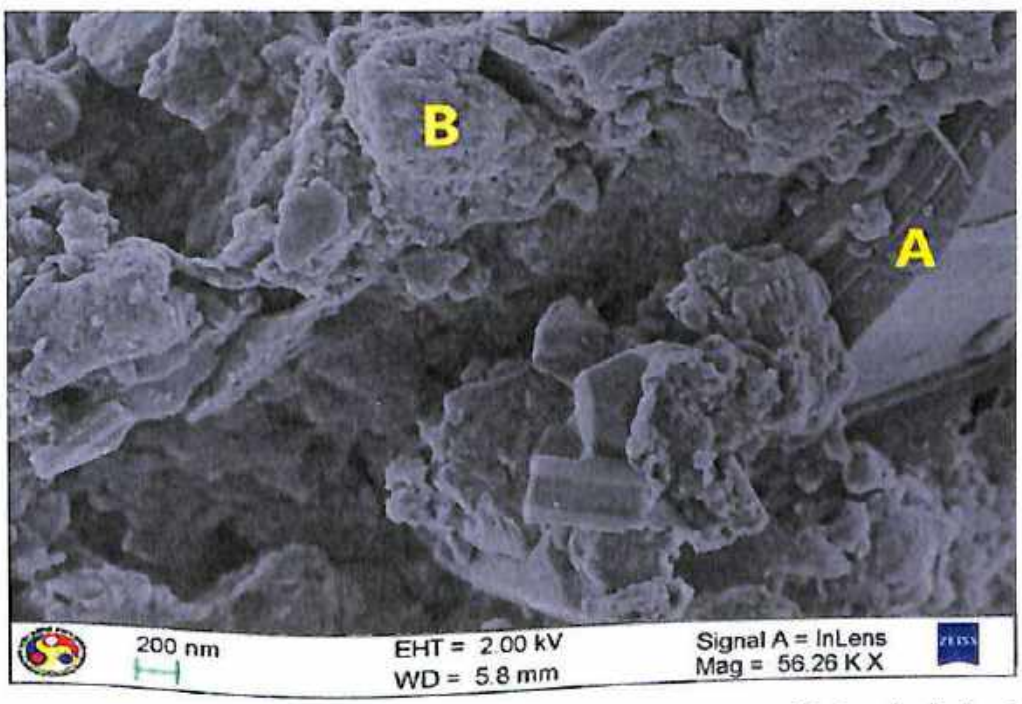

Fig. 4.60 FESEM micrograph of PPC concrete made at w/c ratio of 0.5 and admixed with 7% NaCl: (A) Calcium chloroaluminate and (B) C-S-H gel

For concrete admixed with sodium chloride plus sodium sulfate, the typical FESEM micrographs are shown in Fig. 4.61 and Fig. 4.62 for OPC and PPC concrete respectively at w/c ratio of 0.45. Similarly, Fig. 4.63 and Fig. 4.64 show the typical FESEM micrographs of concrete contaminated with sodium chloride plus sodium sulfate at w/c ratio of 0.5. The micrographs shown in Fig. 4.61 to Fig. 4.64 for both types of cement indicate the formation of C-S-H in concrete. Sulfate ions when associated with Na^+ cation react with different cement hydrates in concrete and forms gypsum and ettringite. The formation of ettringite in conjoint chloride-sulfate contaminated concrete is clearly indicated by needle-like crystals in FESEM micrographs as shown in Fig. 4.61 to Fig. 4.64. It may be noted that, the formation of ettringite was also observed through its peaks in XRD profile, which was discussed earlier for concrete admixed with sodium chloride plus sodium sulfate.

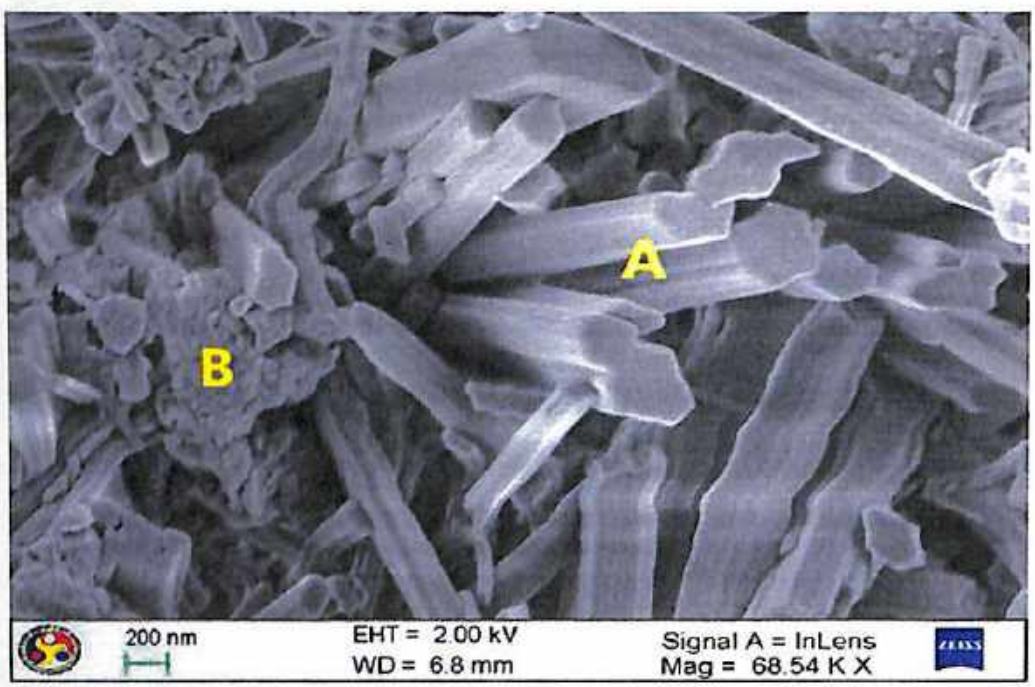

Fig.4. 61 FESEM micrograph of OPC concrete made at w/c ratio of 0.45 and admixed with 7% NaCl plus 12% Na_2SO_4: (A) Ettringite and (B) C-S-H gel

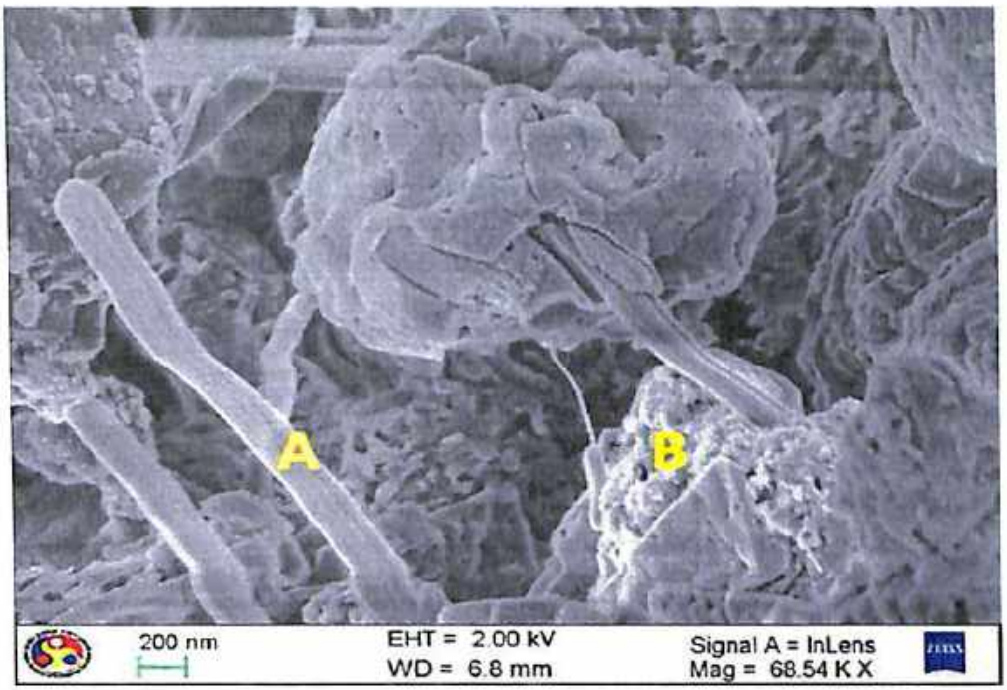

Fig. 4.62 FESEM micrograph of PPC concrete made at w/c ratio of 0.45 and admixed with 7% NaCl plus 12% Na_2SO_4: (A) Ettringite and (B) C-S-H gel

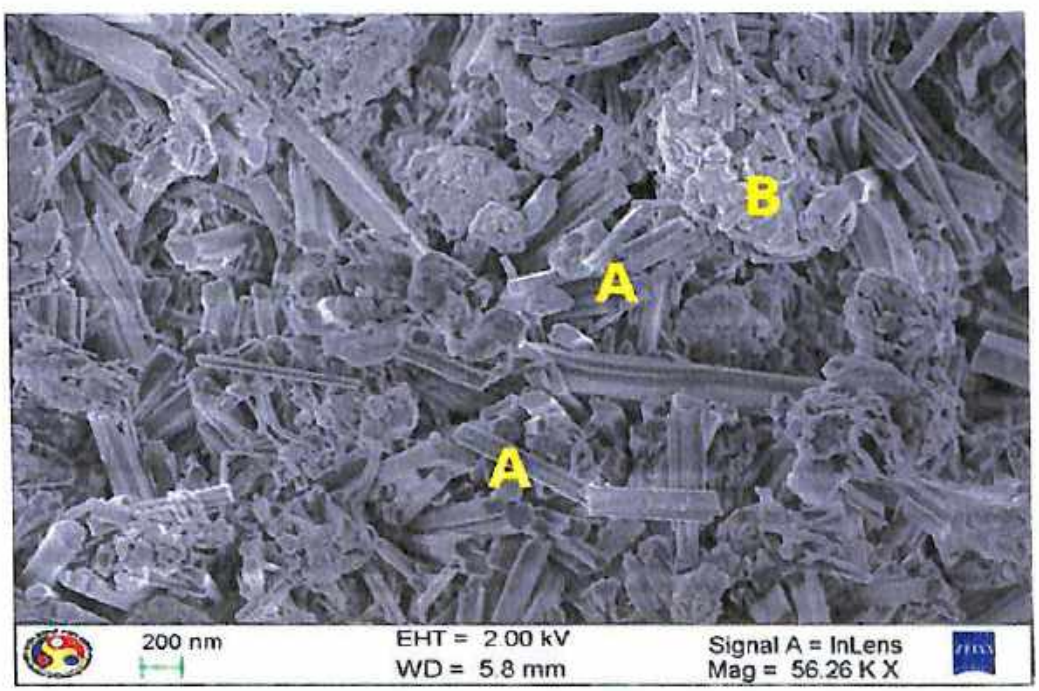

Fig. 4.63 FESEM micrograph of OPC concrete made at w/c ratio of 0.5 and admixed with 7% NaCl plus 12% Na_2SO_4: (A) Ettringite and (B) C-S-H gel

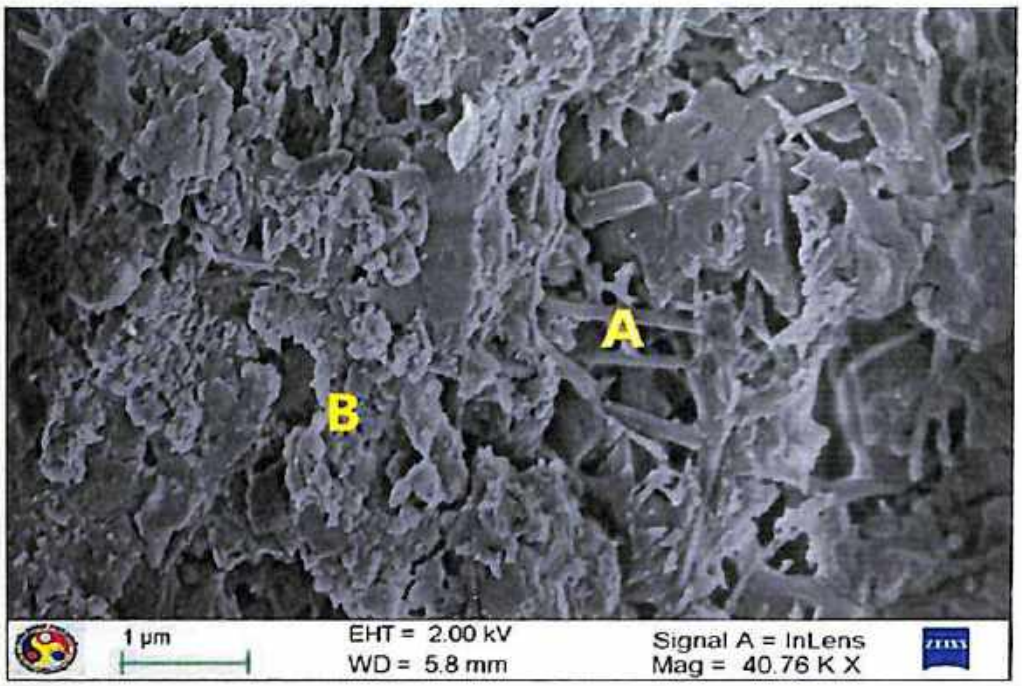

Fig. 4.64 FESEM micrograph of PPC concrete made at w/c ratio of 0.5 and admixed with 7% NaCl plus 12% Na_2SO_4: (A) Ettringite and (B) C-S-H gel

Fig. 4.65 (a, b) and Fig. 4.66 show the FESEM micrographs for OPC and PPC respectively at w/c ratio of 0.45 for concrete contaminated with sodium chloride plus magnesium sulfate. Similarly, FESEM micrographs at w/c ratio of 0.5 are shown in Fig. 4.67 and Fig. 4.68. For both types of cement, the micrographs shown in Fig. 4.65 to Fig. 4.68 indicate the formation of gypsum, ettringite and magnesium hydroxide along with significant presence of M-S-H. The formation of these products in concrete admixed with sodium chloride and magnesium sulfate were also indicated by XRD profiles of concrete discussed earlier. In the FESEM micrographs, the C-S-H is noticeably reduced, indicating its conversion to non-cementitious M-S-H due to magnesium sulfate attack.

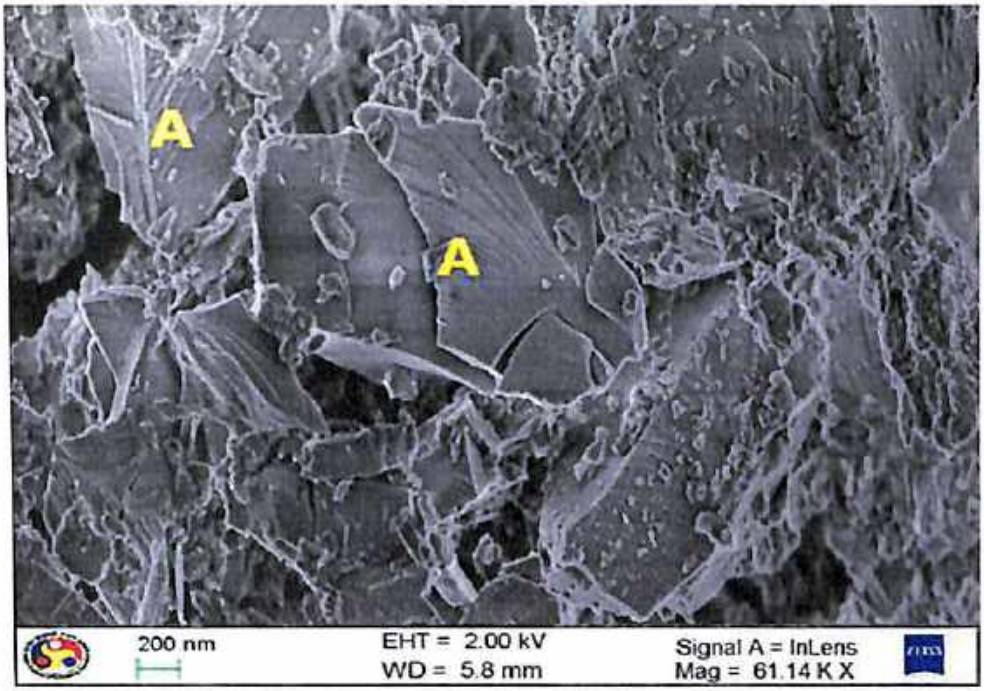

Fig. 4.65 (a) FESEM micrograph of OPC concrete made at w/c ratio of 0.45 and admixed with 7% NaCl plus 12% $MgSO_4$: (A) Magnesium hydroxide

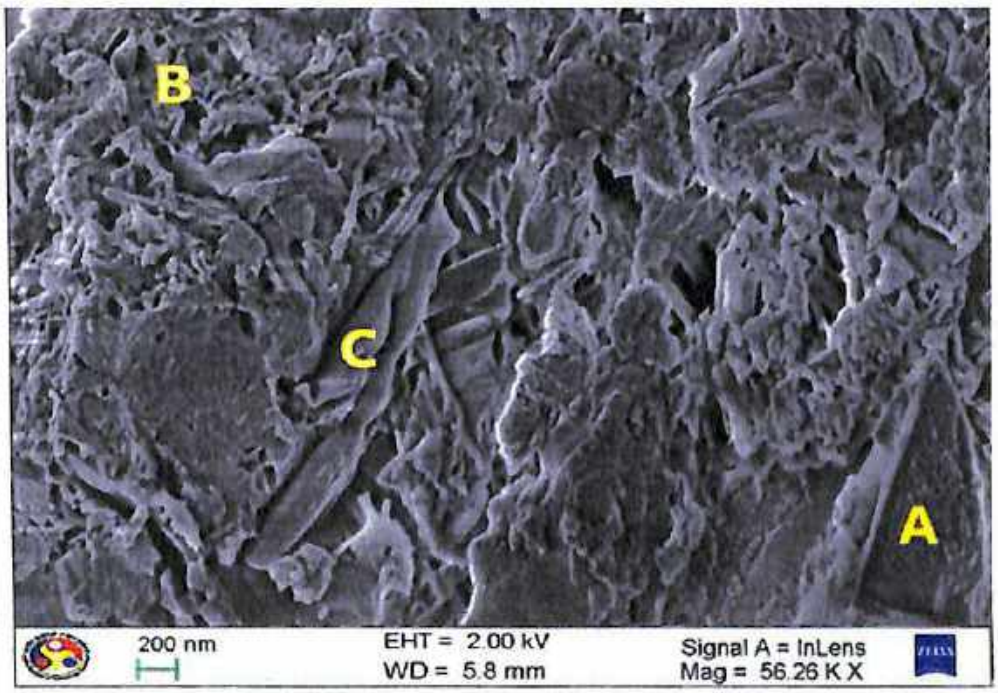

Fig. 4.65 (b) FESEM micrograph of OPC concrete made at w/c ratio of 0.45 and admixed with 7% NaCl plus 12% $MgSO_4$: (A) Magnesium hydroxide, (B) Fibrous M-S-H gel and (C) Gypsum

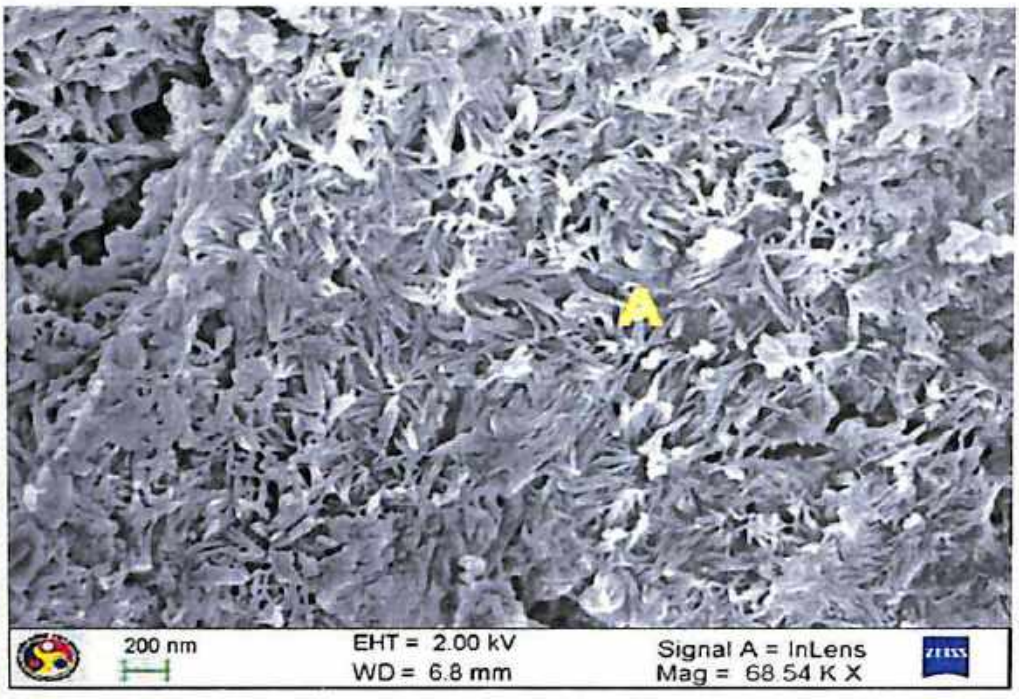

Fig. 4.66 FESEM micrograph of PPC concrete made at w/c ratio of 0.45 and admixed with 7% NaCl plus 12% $MgSO_4$: (A) Fibrous M-S-H gel

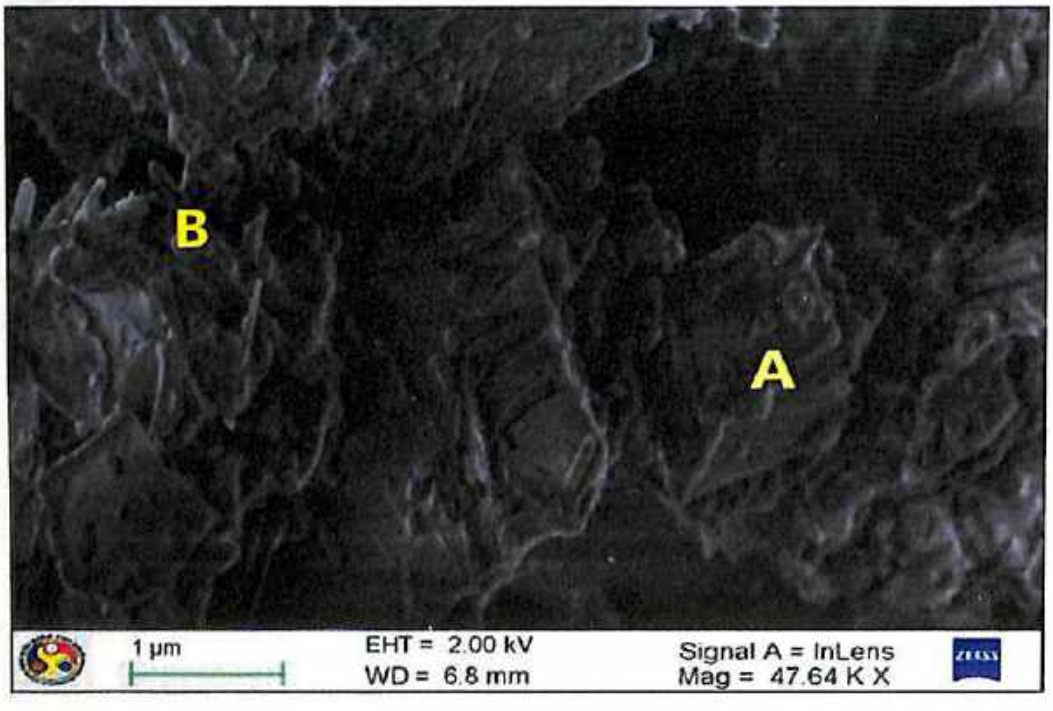

Fig. 4.67 FESEM micrograph of OPC concrete made at w/c ratio of 0.5 and admixed with 7% NaCl plus 12% $MgSO_4$: (A) Magnesium hydroxide and (B) Ettringite

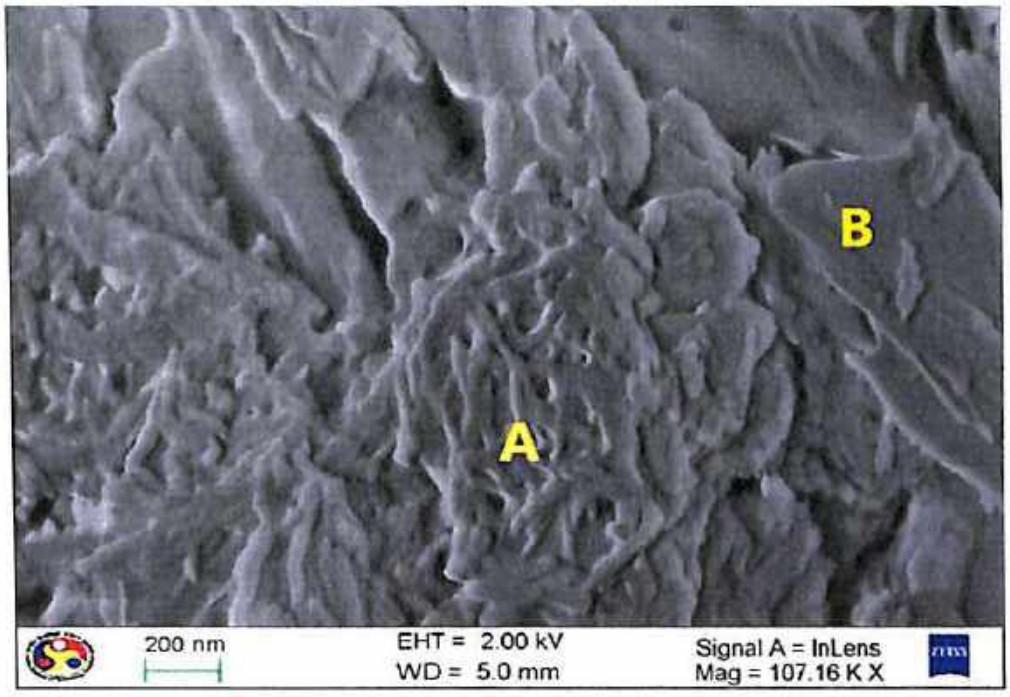

Fig. 4.68 FESEM micrograph of PPC concrete made at w/c ratio of 0.5 and admixed with 7% NaCl plus 12% $MgSO_4$: (A) Fibrous M-S-H gel and (B) Gypsum

4.4 ELECTROLYTIC CONCRETE POWDER SOLUTION (ECPS) CHEMISTRY

The electrolytic concrete powder solution was chemically analyzed to determine chloride (Cl^-), sulfate (SO_4^{2-}), sodium (Na^+), calcium (Ca^{++}) and potassium (K^+) ion concentrations. In addition, the pH and conductivity of contaminated and uncontaminated electrolytic concrete powder solutions were also measured.

4.4.1 Chemical Composition of Chloride Contaminated Electrolytic Concrete Powder Solution

The chemical composition of electrolytic concrete powder solution prepared from control mix and chloride contaminated concrete mixes made with OPC and PPC are presented in Table 4.5 and Table 4.6 at w/c ratios of 0.45 and 0.5 respectively. In addition, the measured pH and conductivity values of the solutions are also presented in these tables. From Table 4.5 and Table 4.6, it is observed that the concentrations of Cl^-, SO_4^{2-}, Na^+, Ca^{++} and K^+ ions are mostly higher in control mix made with w/c ratio of 0.45 as compared to that made with w/c ratio of 0.5 for both OPC and PPC. This variation in the concentrations of ions with w/c ratio may be attributed to the variations in the extent of

formation of cement hydrates in concrete. Further, it is observed that the pH value was lower at w/c ratio of 0.45 as compared to that at w/c ratio of 0.5. In addition, the conductivity was higher in control mix at w/c ratio of 0.45 than that at w/c ratio of 0.5. Further from Table 4.5 and Table 4.6, it is observed that the conductivity of electrolytic concrete powder solution made from control mix was higher in PPC as compared to that in OPC, which may be attributed to higher concentrations of cations i.e. Na^+, Ca^{++} and K^+ in PPC than that in OPC at both w/c ratios.

From Table 4.5 and Table 4.6, it is observed that the concentration of free chloride ion i.e. Cl^- ion increased with increase in admixed NaCl dosage in both OPC and PPC at both w/c ratios i.e. 0.45 and 0.5. Further, chloride ion concentration was lower in OPC as compared to that in PPC in the presence of admixed NaCl at both w/c ratios. This may be attributed to higher chloride binding with C_3A in OPC as compared to that in PPC as a result of higher C_3A content in OPC. The higher chloride binding in OPC as compared to that in PPC is also corroborated from the XRD profiles (presented and discussed in Section 4.3.1.1), wherein the peak intensity of calcium chloroaluminate was more in OPC as compared to that in PPC. Further, chloride ion concentration was higher at w/c ratio of 0.45 as compared to that at 0.5 for both OPC and PPC as observed from Table 4.5 and 4.6.

The concentration of sulfate ion was higher in OPC as compared to that in PPC at both w/c ratios as observed from Table 4.5 and Table 4.6. It may be noted that sulfate ion present in the concrete powder solution (made form control mix and chloride contaminated concrete mix) is due to presence of the gypsum added in the manufacturing process to control early setting and hardening behaviour of Portland cement. The higher concentration of SO_4^{2-} ion in OPC as compared to that in PPC may be due to the preferential reaction of chloride ion than gypsum with C_3A in OPC. Further, the conductivity of chloride contaminated electrolytic concrete powder solution made from PPC was higher than that made from OPC at both w/c ratios, which may be due to higher concentration of Cl^- ion in PPC as compared that in OPC. In addition, the concentration of cations i.e. Ca^{++} and K^+ were also higher in PPC as compared to that in OPC as observed from Table 4.5 and Table 4.6. The higher concentrations of Ca^{++} and K^+ ions in PPC may be attributed to the alteration in the extent of hydration of cement compounds due to pozzolanic reaction in PPC concrete and also due to change in reactivity of the alkali compounds. The concentration of Na^+ ion was higher in OPC as compared that in

PPC at both w/c ratios 0.45 and 0.5, which may be attributed to reaction of chloride ions with hydrated C_3A to a greater extent in OPC in the presence of admixed NaCl, thereby resulting in higher concentration of Na^+ ion in the electrolytic concrete powder solution. The presence of sodium chloride decreased the pH of electrolytic concrete powder solution as observed from Table 4.5 and Table 4.6. However, there was no significant difference in pH value of electrolytic concrete powder solution with different concentrations of admixed NaCl and also between OPC and PPC, although the pH value was slightly higher in OPC as compared to that in PPC.

Table 4.5: Chemical composition, pH and conductivity of electrolytic concrete powder solution prepared from control concrete and concrete mix admixed with varying concentrations of NaCl for both OPC and PPC at w/c ratio of 0.45

Cement type	Admixed salts concentration (% by weight of cement)	pH	Conductivity (mS/cm)	Cl^- (mmol/l)	SO_4^{2-} (mmol/l)	Na^+ (mmol/l)	Ca^{++} (mmol/l)	K^+ (mmol/l)
OPC	Control mix (without salt contamination)	12.9	6.6	28.8	0.8	251.7	60.0	14.8
PPC	Control mix (without salt contamination)	12.84	8.2	29.6	0.3	284.7	86.5	17.3
OPC	3% NC	12.54	24.6	84.6	8.2	313.0	110.7	18.0
	5% NC	12.48	30.3	149.5	8.8	367.4	184.5	20.7
	7% NC	12.42	34.8	180.5	10.5	390.3	199.6	35.0
PPC	3% NC	12.45	26.2	90.3	5.5	269.1	139.4	22.9
	5% NC	12.41	31.6	156.5	7.8	337.4	189.3	24.0
	7% NC	12.27	36.5	189.5	10.0	351.1	239.5	40.8

Table 4.6: Chemical composition, pH and conductivity of electrolytic concrete powder solution prepared from control concrete and concrete mix admixed with varying concentrations of NaCl for both OPC and PPC at w/c ratio of 0.5

Cement type	Admixed salts concentration (% by weight of cement)	pH	Conductivity (mS/cm)	Cl^- (mmol/l)	SO_4^{2-} (mmol/l)	Na^+ (mmol/l)	Ca^{++} (mmol/l)	K^+ (mmol/l)
OPC	Control mix (without salt contamination)	13.4	5.5	2.8	0.22	12.8	25.2	11.2
PPC	Control mix (without salt contamination)	13.2	6.6	5.6	0.3	17.1	88.6	349.1
OPC	3% NC	12.39	22.2	67.7	1.5	155.2	62.4	15.5
	5% NC	12.36	27.3	138.2	1.7	174.6	94.7	16.6
	7% NC	12.34	33.8	169.2	2.2	227.4	126	23.5
PPC	3% NC	12.36	24.4	73.3	1.3	113.7	514.6	33.9
	5% NC	12.34	28.2	146.7	1.5	138.9	791.7	35.3
	7% NC	12.32	34.6	172.1	1.7	184.2	1058.7	35.8

4.4.2 Chemical Composition of Electrolytic Concrete Powder Solution Contaminated with Sodium Chloride plus Sodium Sulfate

The measured ionic concentration along with pH and conductivity of electrolytic concrete powder solutions prepared from OPC and PPC and contaminated with conjoint NaCl plus Na_2SO_4 are presented in Table 4.7 and Table 4.8 at w/c ratios of 0.45 and 0.5 respectively. From these tables, it is observed that the concentration of Cl^- ion increased with an increase in admixed NaCl concentration for both types of cement and w/c ratios at all admixed concentrations of Na_2SO_4.

From Table 4.7, it is observed that in the conjoint presence of NaCl plus Na_2SO_4 in OPC concrete at w/c ratio of 0.45, the concentration of Cl^- ion increased whereas that of SO_4^{2-} ion decreased with an increase in Na_2SO_4 dosage up to 6% and then the concentration of Cl^- ion decreased whereas that of SO_4^{2-} ion increased at 12% Na_2SO_4 dosage. This may be attributed to the variation in preferential reactions of chloride and sulfate ions with C_3A hydrates with increase in dosage of Na_2SO_4. From Table 4.8, it is observed that in the

conjoint presence of NaCl plus Na_2SO_4 in OPC concrete at w/c ratio of 0.5, the concentration of Cl^- ion increased whereas that of SO_4^{2-} ion decreased with an increase in Na_2SO_4 dosage. This may be due to lower chloride binding as a result of preferential reaction of sulfate ions than chloride ions, with C_3A hydrates resulting in higher Cl^- ion and lower SO_4^{2-} ion concentrations in the presence of NaCl plus Na_2SO_4. Further from Table 4.7 and Table 4.8, it is observed that in the presence of NaCl plus Na_2SO_4 in PPC concrete at w/c ratio of 0.45, the concentration of Cl^- ion increased whereas that of SO_4^{2-} ion decreased with an increase in Na_2SO_4 dosage and at w/c ratio of 0.5, the opposite variation is observed. This is attributed to change in chloride binding as a result of variation in preferential reaction of chloride and sulfate ions with C_3A hydrates at different w/c ratios (0.45 and 0.5) in the conjoint presence of NaCl plus Na_2SO_4 in concrete.

While analyzing the effect of cement type on the concentration of Cl^- and SO_4^{2-} ions in the ECPS contaminated with varying concentrations of NaCl plus Na_2SO_4, it is noted that at w/c ratio of 0.45, OPC concrete exhibited lower Cl^- ion concentration and higher SO_4^{2-} ion concentration as compared to PPC concrete as observed from Table 4.7. This is attributed to higher chloride binding and lower sulfate binding as a result of preferential reaction of chloride ions than sulfate ions, with C_3A hydrates resulting in lower Cl^- ion and higher SO_4^{2-} ion concentrations in OPC. This observation is further substantiated by the XRD profiles shown in Fig. 4.5 to Fig. 4.10, which indicate more intense peaks of calcium chloroaluminate and less intense peaks of ettringite in OPC concrete as compared to that in PPC concrete. From Table 4.8 it is observed that at w/c ratio of 0.5, OPC concrete mostly showed higher Cl^- ion concentration and lower SO_4^{2-} ion concentration as compared to PPC concrete. This is attributed to lower chloride binding and higher sulfate binding in OPC as compared to that in PPC. This observation is also corroborated from XRD profiles shown in Fig. 4.11 to Fig. 4. 16, which showed more intense peaks of ettringite in OPC concrete as compared to that in PPC concrete indicating the preferential reaction of sulfate ions with C_3A in OPC as compared to that in PPC. Further, the lower chloride binding in OPC was corroborated by lower peak intensity of calcium chloroaluminate (Fig. 4.11 to Fig. 4. 16) in OPC than that in PPC at all NaCl plus Na_2SO_4 concentrations.

Table 4.7: Chemical composition, pH and conductivity of electrolytic concrete powder solution prepared from concrete mix admixed with varying concentrations of NaCl and Na_2SO_4 for both types of cement at w/c ratio of 0.45

Cement type	Admixed salts concentration (% by weight of cement)	pH	Conductivity (mS/cm)	Cl^- (mmol/l)	SO_4^{2-} (mmol/l)	Na^+ (mmol/l)	Ca^{++} (mmol/l)	K^+ (mmol/l)
OPC	3% NaCl + 3% Na_2SO_4	12.64	40.8	45.1	83.8	348.3	205.8	37.1
	3% NaCl + 6% Na_2SO_4	12.56	44.6	80.4	74.6	458.0	242	39.6
	3% NaCl + 12% Na_2SO_4	12.62	49.5	73.3	92.3	507.0	263.5	48.1
PPC	3% NaCl + 3% Na_2SO_4	12.56	42.4	73	71.1	338.3	230.8	29.2
	3% NaCl + 6% Na_2SO_4	12.51	45.8	82	64.5	387.0	298.2	63.2
	3% NaCl + 12% Na_2SO_4	12.5	50.2	87	63.1	465.2	342.2	83.4
OPC	5% NaCl + 3% Na_2SO_4	12.58	42	126.9	69.4	518.7	250.6	48.5
	5% NaCl + 6% Na_2SO_4	12.46	46.1	141	56.7	523.9	292.9	69.6
	5% NaCl + 12% Na_2SO_4	12.54	50.8	136.8	70.2	663.9	317.9	79.0
PPC	5% NaCl + 3% Na_2SO_4	12.47	49.7	130	60.4	378.3	279.7	30.9
	5% NaCl + 6% Na_2SO_4	12.45	50.8	147	58.9	408.7	359.8	73.4
	5% NaCl + 12% Na_2SO_4	12.43	51.3	152	52.3	535.7	409.6	117.1
OPC	7% NaCl + 3% Na_2SO_4	12.57	45	150.9	56.4	666.1	296.7	51.7
	7% NaCl + 6% Na_2SO_4	12.4	48.3	169.2	48.4	695.7	344.1	76.8
	7% NaCl + 12% Na_2SO_4	12.43	52.2	166.1	58.9	754.3	391.5	98.7
PPC	7% NaCl + 3% Na_2SO_4	12.4	51.6	169	50.6	392.6	334.0	34.1
	7% NaCl + 6% Na_2SO_4	12.38	52.3	178	46.2	471.3	396.2	75.7
	7% NaCl + 12% Na_2SO_4	12.33	52.9	186	45.0	726.1	424.4	128.4

Table 4.8: Chemical composition, pH and conductivity of electrolytic concrete powder solution prepared from concrete mix admixed with varying concentrations of NaCl and Na_2SO_4 for both types of cement at w/c ratio of 0.5

Cement type	Admixed salts concentration (% by weight of cement)	pH	Conductivity (mS/cm)	Cl^- (mmol/l)	SO_4^{2-} (mmol/l)	Na^+ (mmol/l)	Ca^{++} (mmol/l)	K^+ (mmol/l)
OPC	3% NaCl + 3% Na_2SO_4	12.66	38.4	42	51.6	224.4	130.6	9.0
	3% NaCl + 6% Na_2SO_4	12.6	41.6	54	40.7	233.7	134.4	9.9
	3% NaCl + 12% Na_2SO_4	12.57	47.4	62	29.4	242.2	147.2	10.1
PPC	3% NaCl + 3% Na_2SO_4	12.48	40	71	40.1	150.4	1120.3	31.5
	3% NaCl + 6% Na_2SO_4	12.64	38.7	65	44.8	194.8	872.4	28.6
	3% NaCl + 12% Na_2SO_4	12.72	39.7	56	59.4	221.7	717.2	25.6
OPC	5% NaCl + 3% Na_2SO_4	12.62	39.7	124	30.5	230.7	160.6	11.1
	5% NaCl + 6% Na_2SO_4	12.58	42.3	133	19.1	284.6	176.2	11.1
	5% NaCl + 12% Na_2SO_4	12.55	49.2	135	18.7	285.9	196.9	11.3
PPC	5% NaCl + 3% Na_2SO_4	12.44	42.81	121	23.4	159.1	1033.0	38.8
	5% NaCl + 6% Na_2SO_4	12.61	40.2	116	33.2	219.0	627.4	37.2
	5% NaCl + 12% Na_2SO_4	12.68	40.4	113	44.8	269.6	504.5	36.2
OPC	7% NaCl + 3% Na_2SO_4	12.61	40.3	144	13.7	298.0	188.4	12.0
	7% NaCl + 6% Na_2SO_4	12.56	45.7	158	7.0	349.1	199.1	12.3
	7% NaCl + 12% Na_2SO_4	12.44	50.2	164	5.8	455.2	235.5	12.3
PPC	7% NaCl + 3% Na_2SO_4	12.18	47.4	138	13.2	192.2	908.2	48.0
	7% NaCl + 6% Na_2SO_4	12.58	42.4	135	23.4	238.3	593.2	42.2
	7% NaCl + 12% Na_2SO_4	12.65	41.6	118	40.6	314.4	492.2	40.5

The concentrations of Ca^{++} and K^{+} ions in electrolytic concrete powder solution made from PPC were higher than that in the solution made from OPC in the conjoint presence of NaCl plus Na_2SO_4 at both w/c ratios as observed from Table 4.7 and Table 4.8. The higher concentration of Ca^{++} and K^{+} ions in PPC may be due to change in the extent of hydration reaction due to the pozzolanic activity and also as a result of change in reactivity of the alkali compounds. The concentration of Na^{+} ion was higher in electrolytic concrete powder solution contaminated with NaCl plus Na_2SO_4 in OPC than that in PPC at both w/c ratios. In NaCl plus Na_2SO_4 contamination, the higher concentration of Na^{+} ion in OPC than that in PPC may be attributed to the reaction of sodium sulfate with calcium hydroxide to a greater extent, thereby resulting in higher concentration of Na^{+} ion.

Further, from Table 4.7 and Table 4.8, it is observed that the conductivity of ECPS increased with an increase in admixed NaCl concentration for OPC and PPC at all levels of admixed Na_2SO_4 for both w/c ratios, which may be attributed to increase in Cl^{-} concentration. It is also observed that the conductivity of the solution made from OPC and PPC increased with increase in admixed Na_2SO_4 concentration at both w/c ratios except in case of PPC in the conjoint presence of NaCl plus Na_2SO_4 at w/c ratio 0.5 wherein the conductivity mostly decreased with increase in admixed Na_2SO_4 concentration. These variations in conductivity of electrolytic concrete powder solution (ECPS) made from OPC and PPC in the conjoint presence of NaCl plus Na_2SO_4 may be attributed to the variations in both Cl^{-} ion and SO_4^{2-} ion concentrations as observed from Table 4.7 and Table 4.8. On observing the effect of cement type i.e. OPC and PPC on conductivity of electrolytic concrete powder solution, it is found that PPC showed mostly higher conductivity as compared to OPC at both w/c ratios in the conjoint presence of NaCl plus Na_2SO_4. The reason for higher conductivity of PPC in the conjoint presence of NaCl plus Na_2SO_4 may be attributed to higher concentrations of Ca^{++}, K^{+} and Cl^{-} ions in PPC as compared to that in OPC.

From Table 4.7 and Table 4.8, it is observed that the ECPS contaminated with NaCl plus Na_2SO_4 showed higher pH values in OPC than that in PPC at w/c ratio of 0.45 whereas mostly the opposite variation was observed at w/c ratio of 0.5. The change in pH of electrolytic concrete powder solution with w/c ratio may be attributed to the variation in the availability of calcium hydroxide and sodium hydroxide in OPC and PPC concrete in the presence of NaCl plus Na_2SO_4.

4.4.3 Chemical Composition of Electrolytic Concrete Powder Solution Contaminated with Sodium Chloride plus Magnesium Sulfate

The measured ionic concentration, pH and conductivity of electrolytic concrete powder solutions prepared from OPC and PPC and contaminated with conjoint NaCl plus $MgSO_4$ are presented in Table 4.9 and Table 4.10 at w/c ratios of 0.45 and 0.5 respectively. From these tables it is observed that in the conjoint presence of NaCl plus $MgSO_4$, the concentration of Cl^- ion increased with an increase in admixed NaCl concentration for both types of cement and w/c ratio.

From Table 4.9 and Table 4.10, it is observed that the concentration of SO_4^{2-} ion decreased whereas that of Cl^- ion increased with an increase in $MgSO_4$ dosage in both OPC and PPC at both w/c ratios of 0.45 and 0.5 in the conjoint presence of NaCl plus $MgSO_4$. This may be attributed to higher sulfate binding as compared to chloride binding, with cement hydration products in the presence of $MgSO_4$ in concrete. On comparing the effect of cement type on the concentration of Cl^- and SO_4^{2-} ions in the conjoint presence of NaCl plus $MgSO_4$, it is observed that the concentration of Cl^- ions is lower in OPC as compared to that in PPC whereas the concentration of SO_4^{2-} ions is higher in OPC as compared to that in PPC at both w/c ratios as evident from Table 4.9 and Table 4.10. This may be attributed to increased chloride binding and reduced sulfate binding with cement hydrates in the conjoint presence of NaCl plus $MgSO_4$ in OPC concrete as compared to that in PPC concrete. The reduced sulfate binding in OPC concrete in the conjoint presence of NaCl plus $MgSO_4$ is also substantiated from XRD results shown earlier in Fig. 4.17 to Fig. 4.28, which indicated lower peak intensity of ettringite in OPC as compared to that in PPC. The increased chloride binding in OPC was also confirmed from XRD profiles (Fig. 4.17 to Fig. 4.28) through more intense peaks of calcium chloroaluminate at w/c ratio of 0.45, whereas at w/c ratio of 0.5, XRD profiles showed less peak intensity of calcium chloroaluminate in OPC, although the Cl^- ion concentration was less in OPC as compared to that in PPC, which may be attributed to the more dominant effect of physical binding of chloride ions as compared to that of chemical binding.

The concentrations of Na^+, Ca^{++} and K^+ ions in electrolytic concrete powder solution made from PPC were higher than that in the solution made from OPC in the conjoint presence of NaCl plus $MgSO_4$ at both w/c ratios as observed from Table 4.9 and Table

4.10. The change in the extent of hydration reaction due to the pozzolanic reaction in PPC and also change in reactivity of the alkali compounds might have resulted in higher concentration of these ions in PPC.

From Table 4.9 and Table 4.10, it is observed that the conductivity of electrolytic concrete powder solution increased with an increase in admixed NaCl concentration for OPC and PPC at all levels of $MgSO_4$ concentration for both w/c ratios, which is attributed to the increase in Cl^- ion concentration. Further the conductivity of the solution made from OPC and PPC increased with an increase in admixed $MgSO_4$ concentration at both w/c ratios. On observing the effect of cement type i.e. OPC and PPC on conductivity of electrolytic concrete powder solution, it is found that PPC showed mostly higher conductivity as compared to OPC at both w/c ratios in the conjoint presence of NaCl plus $MgSO_4$ as observed from Table 4.9 and Table 4.10. The higher conductivity of PPC in the conjoint presence of NaCl plus $MgSO_4$ is attributed to the higher concentrations of Na^+, Ca^{++}, K^+ and Cl^- ions in PPC as compared to that in OPC.

From Table 4.9 and Table 4.10, it is noted that the electrolytic concrete powder solution admixed with NaCl plus $MgSO_4$ showed higher pH values in OPC as compared to that in PPC at both w/c ratios. The lower pH in PPC concrete may attributed to the conversion of C-S-H to non-cementitious M-S-H to a greater extent because magnesium sulfate attack is directed extensively towards C-S-H gel due to less availability of calcium hydroxide in PPC as result of its consumption in the pozzolanic reaction.

Table 4.9: Chemical composition, pH and conductivity of electrolytic concrete powder solution prepared from concrete mix admixed with varying concentrations of NaCl and $MgSO_4$ for both types of cement at w/c ratio of 0.45

Cement type	Admixed salts concentration (% by weight of cement)	pH	Conductivity (mS/cm)	Cl^- (mmol/l)	SO_4^{2-} (mmol/l)	Na^+ (mmol/l)	Ca^{++} (mmol/l)	K^+ (mmol/l)
OPC	3% NaCl + 3% $MgSO_4$	12.49	46.3	90	28.6	297.0	213.2	50.4
	3% NaCl + 6% $MgSO_4$	12.36	49.5	96	29.1	330.4	272.5	67.8
	3% NaCl + 12% $MgSO_4$	12.3	50.1	106	23.4	375.9	331.6	93.2
PPC	3% NaCl + 3% $MgSO_4$	12.21	48.9	93	27.0	337.0	246.6	153.7
	3% NaCl + 6% $MgSO_4$	12.05	50.6	100	25.8	390.7	299.5	185.5
	3% NaCl + 12% $MgSO_4$	12.01	52.8	107	22.8	395.7	359.3	204.6
OPC	5% NaCl + 3% $MgSO_4$	12.42	51.6	155	22.6	321.7	250.9	62.7
	5% NaCl + 6% $MgSO_4$	12.32	52.8	164	18.2	374.3	306.9	74.2
	5% NaCl + 12% $MgSO_4$	12.24	55.3	168	15.6	464.5	442.8	100.6
PPC	5% NaCl + 3% $MgSO_4$	11.89	53.5	158	20.0	417.4	315.9	159.7
	5% NaCl + 6% $MgSO_4$	11.79	54.4	167	17.0	436.7	410.7	197.4
	5% NaCl + 12% $MgSO_4$	11.76	56.7	169	13.9	476.5	462.7	226.1
OPC	7% NaCl + 3% $MgSO_4$	12.37	56.2	189	19.4	382.6	318.1	78.5
	7% NaCl + 6% $MgSO_4$	12.29	58.0	194	15.6	433.0	385.1	85.0
	7% NaCl + 12% $MgSO_4$	12.19	60.2	197	10.4	582.3	456.6	105.9
PPC	7% NaCl + 3% $MgSO_4$	11.57	58.3	192	15.9	459.8	353.3	168.2
	7% NaCl + 6% $MgSO_4$	11.42	60.3	195	15.6	523.7	438.0	202.0
	7% NaCl + 12% $MgSO_4$	11.37	62.5	209	10.5	619.3	478.2	229.8

Table 4.10: Chemical composition, pH and conductivity of electrolytic concrete powder solution prepared from concrete mix admixed with varying concentrations of NaCl and $MgSO_4$ for both types of cement at w/c ratio of 0.5

Cement type	Admixed salts concentration (% by weight of cement)	pH	Conductivity (mS/cm)	Cl^- (mmol/l)	SO_4^{2-} (mmol/l)	Na (mmol/l)	Ca^{++} (mmol/l)	K^+ (mmol/l)
OPC	3% NaCl + 3% $MgSO_4$	12.36	41.4	73	10.26	103.5	132.1	20.7
	3% NaCl + 6% $MgSO_4$	12.24	44.2	76	3.68	110.2	171.2	20.2
	3% NaCl + 12% $MgSO_4$	12.01	48.5	85	2.77	135.4	172.9	19.6
PPC	3% NaCl + 3% $MgSO_4$	12.27	44.9	79	8.2	104.8	859.3	30.7
	3% NaCl + 6% $MgSO_4$	12.18	46.6	85	3.86	113.7	658.6	31.2
	3% NaCl + 12% $MgSO_4$	12.04	51.3	90	1.6	146.3	592.9	30.8
OPC	5% NaCl + 3% $MgSO_4$	12.32	43.6	141	5.13	193.5	166.9	15.9
	5% NaCl + 6% $MgSO_4$	12.21	45.1	147	3.49	193.5	176.2	15.5
	5% NaCl + 12% $MgSO_4$	11.97	50.4	158	1.86	198.9	194.4	14.3
PPC	5% NaCl + 3% $MgSO_4$	12.23	46.2	152	4.25	194.8	814.2	33.3
	5% NaCl + 6% $MgSO_4$	12.15	49.7	161	3.37	215.4	609.6	35.0
	5% NaCl + 12% $MgSO_4$	11.84	51.8	169	1.36	221.8	492.2	35.1
OPC	7% NaCl + 3% $MgSO_4$	12.28	47.8	164	4.17	204.4	199.2	13.6
	7% NaCl + 6% $MgSO_4$	12.17	48.3	175	2.86	226.1	207.0	12.7
	7% NaCl + 12% $MgSO_4$	11.78	52.6	178	1.6	247.8	221.1	12.3
PPC	7% NaCl + 3% $MgSO_4$	12.21	48.7	181	4.01	210.0	754.0	35.4
	7% NaCl + 6% $MgSO_4$	12.1	50.8	183	2.81	237.0	509.0	37.9
	7% NaCl + 12% $MgSO_4$	11.33	54.5	186	0.43	243.5	404.2	38.3

4.4.4 Effect of Cation Type Associated with Sulfate ion on Chemical Composition of Electrolytic Concrete Powder Solution

While comparing the effect of cation type associated with sulfate ion, it is observed that the Cl^- ion concentration was higher whereas SO_4^{2-} ion concentration was lower in electrolytic concrete powder solution admixed with NaCl plus $MgSO_4$ as compared to that admixed with NaCl plus Na_2SO_4 for both types of cement and w/c ratio, as evident from Table 4.7 to Table 4.10. This may be attributed to reduced chloride binding and increased sulfate binding with cement hydrates in the presence of $MgSO_4$ in concrete. Further, it is observed that the concentration of Na^+ ion was mostly higher in ECPS contaminated with NaCl plus Na_2SO_4 as compared to that contaminated with NaCl plus $MgSO_4$ for both OPC and PPC and at both w/c ratios. In addition, the concentrations of Ca^{++} and K^+ ions were lower in ECPS contaminated with NaCl plus Na_2SO_4 as compared to that contaminated with NaCl plus $MgSO_4$ made from both types of cement at w/c ratio of 0.45 as observed from Table 4.7 to Table 4.10. However at w/c ratio of 0.5, the concentrations of Ca^{++} and K^+ ions were higher in ECPS contaminated with NaCl plus Na_2SO_4 as compared to that contaminated with NaCl plus $MgSO_4$ in PPC whereas the opposite variation was observed in OPC. These variations in the concentrations of Na^+, Ca^{++} and K^+ ions in the ECPS contaminated with NaCl plus Na_2SO_4 and NaCl plus $MgSO_4$ may be attributed to the variations in the extent of reaction of the alkali compounds in concrete in the conjoint presence of chloride and sulfate salts.

From Table 4.7 to Table 4.10, it is observed that the conductivity of electrolytic concrete powder solution was higher in the conjoint presence of NaCl plus $MgSO_4$ as compared to that in conjoint presence of NaCl plus Na_2SO_4. This indicates that the presence of sulfate ion when associated with magnesium cation increases the conductivity in the presence of NaCl. In addition, it is inferred that the electrolytic concrete powder solution contaminated with NaCl plus Na_2SO_4 showed higher pH as compared to that contaminated with NaCl plus $MgSO_4$ for both OPC and PPC and at both w/c ratios as observed from these tables. The higher pH in the presence of sodium sulfate may be attributed to the formation of sodium hydroxide (as result of the reaction between calcium hydroxide and sodium sulfate), which increases the pH value. In the presence of magnesium sulfate, magnesium hydroxide that is formed due to reaction between calcium hydroxide and magnesium sulfate has very low solubility and low pH value [3] that has resulted a reduction in pH value of the ECPS admixed with NaCl plus $MgSO_4$. While

analyzing the effect of w/c ratio, it is observed that the concentrations of both Cl^- and SO_4^{2-} ions are higher at w/c ratio of 0.45 as compared to that at 0.5 in the conjoint presence of both NaCl plus Na_2SO_4 and NaCl plus $MgSO_4$ for both types of cement and w/c ratio, as evident from Table 4.7 to Table 4.10. The higher concentrations of Cl^- and SO_4^{2-} ions at lower w/c ratio (0.45) may be attributed to the variations in chloride and sulfate binding as a result of variation in preferential reaction of chloride and sulfate ions with cement hydrates in the concrete in the conjoint presence of chloride and sulfate ions, although the chloride binding in concrete made at lower w/c ratio (0.45) would have been more due of higher cement content.

4.5 SUMMARY

The results of 28-day compressive strength of cube specimens prepared from OPC and PPC concrete and admixed with chloride and chloride-sulfate ions at w/c ratios of 0.45 and 0.5 indicated that the varying concentrations of chloride and chloride-sulfate ions have significant effect on compressive strength of concrete. The specimens prepared from OPC concrete mostly showed lower compressive strength as compared to those made from PPC concrete at all levels of chloride and chloride-sulfate contaminations for both w/c ratios. The concrete specimens admixed with varying concentrations of sodium chloride exhibited higher compressive strength as compared to those admixed with varying concentrations of sodium chloride plus sodium sulfate and sodium chloride plus magnesium sulfate at w/c ratios of 0.45 and 0.5 and for both OPC and PPC. Further, it is found that the concrete admixed with sodium chloride plus magnesium sulfate showed lower compressive strength as compared to those admixed with sodium chloride plus sodium sulfate.

The obtained results on microstructural changes in concrete due to chloride and chloride-sulfate contamination (studied through XRD, FTIR and FESEM analyses) indicated the variations in the formation of various compounds in concrete due to the effect of cement type, w/c ratio and concentrations of chloride ions and sulfate ions along with the associated cation type. The obtained XRD profiles of concrete in the presence of NaCl, NaCl plus Na_2SO_4 and NaCl plus $MgSO_4$ for different types of cement and w/c ratio showed variations in the formation of ettringite, gypsum, calcium chloroaluminate and calcium hydroxide as indicated by their respective peak intensities. The XRD profiles

indicating the formation of different compounds in concrete in the presence of chloride and sulfate ions were consistent with functional groups associated with those compounds as observed from FTIR spectrum analysis. The FESEM micrographs of concrete contaminated with sodium chloride, sodium chloride plus sodium sulfate and sodium chloride plus magnesium sulfate for OPC and PPC indicated the formation of C-S-H, gypsum, ettringite, and calcium chloroaluminate (Friedel's salt). In addition to this, the micrographs also indicated the formation of magnesium hydroxide (brucite) and non-cementitious M-S-H in the concrete admixed with sodium chloride plus magnesium sulfate.

The discussion of the results obtained from the measurement of ionic concentration (Cl^-, SO_4^{2-}, Na^+, Ca^{++} and K^+ ions), pH and conductivity of electrolytic concrete powder solution (ECPS) indicated that cement type (OPC and PPC), w/c ratio (0.45 and 0.5) and the varying concentrations of admixed NaCl, NaCl plus Na_2SO_4 and NaCl plus $MgSO_4$ significantly affect the characteristics of electrolytic concrete powder solution.

CHAPTER 5

ELECTROCHEMICAL BEHAVIOUR OF STEEL REINFORCEMENT IN ELECTROLYTIC CONCRETE POWDER SOLUTION

5.1 GENERAL

In this chapter, the results obtained from the study on electrochemical behaviour of steel reinforcement in electrolytic concrete powder solution (ECPS) contaminated with varying concentrations of sodium chloride, sodium chloride plus sodium sulfate and sodium chloride plus magnesium sulfate are presented and discussed. The electrochemical behaviour of steel reinforcement was evaluated by conducting potentiodynamic polarization test on bare steel specimens in electrolytic concrete powder solutions, from which the anodic polarization curves were obtained. From the anodic polarization curves, boundary potential values of different zones of corrosion namely active zone, passive zone and pitting zone were determined to study the effect of chloride and sulfate ions on zones of corrosion of steel reinforcement. Further, to evaluate the effect of varying concentrations of chloride and conjoint chloride-sulfate ions on corrosion of steel reinforcement in electrolytic concrete powder solution, corrosion potential and corrosion current density were determined by conducting potential and linear polarization resistance (LPR) measurements.

5.2 ELECTROCHEMICAL BEHAVIOUR OF STEEL IN ELECTROLYTIC CONCRETE POWDER SOLUTION (ECPS)

Portland cement concrete provides both chemical and physical protection to the reinforcing steel. The chemical protection is provided by the highly alkaline nature of the pore solution (pH > 13) of concrete. At this pH value, the steel reinforcement is passivated in the presence of oxygen presumably due to the formation of a sub-macroscopically thin γ-Fe_2O_3 layer [18]. The physical protection is provided by the dense impermeable structure of concrete, which retards the diffusion of the aggressive species, like chlorides, sulfates, carbon dioxide, and moisture to the steel-concrete interface. Depassivation of steel reinforcement occurs due to reduction in the pore solution pH as result of carbonation or by ingress of chloride ions to the steel-concrete interface [16, 18].

Chloride ions break down the passive layer and play a dominant role in initiating steel reinforcement corrosion. However, the concomitant presence of chloride and sulfate ions could influence the kinetics of steel reinforcement corrosion and the mechanism of deterioration may become even more complex.

In the present study, the effect of chloride and sulfate ions on electrochemical behavior of steel in electrolytic concrete powder solution prepared from OPC and PPC concrete at w/c ratios of 0.45 and 0.5 has been evaluated by conducting potentiodynamic polarization test and monitoring the steel reinforcement corrosion by measuring corrosion potential and corrosion current density.

5.2.1 Corrosion Zones of Steel Reinforcement

The anodic polarization curves were obtained through potentiodynamic polarization test performed on the bare steel specimens in electrolytic concrete powder solutions extracted from different concrete mixes. The polarization curves were obtained for two types of steel viz. Tempcore TMT and Thermex TMT, for two types of cement viz. OPC and PPC, for two w/c ratios viz. 0.45 and 0.5 and for varying concentrations of sodium chloride (NaCl), sodium chloride plus sodium sulfate ($NaCl + Na_2SO_4$) and sodium chloride plus magnesium sulfate ($NaCl + MgSO_4$). The anodic polarization curves of Tempcore TMT steel in electrolytic concrete powder solution made from OPC and PPC at w/c ratio of 0.45 for control mix (without salt contamination) are shown in Fig. 5.1 and those at w/c ratio of 0.5 are shown in Fig. 5.2. Similarly, the anodic polarization curves for Thermex TMT steel in electrolytic concrete powder solution made from OPC and PPC at w/c ratio of 0.45 for control mix are shown in Fig. 5.3 and those at w/c ratio of 0.5 are shown in Fig. 5.4. In these curves (Fig. 5.1 to Fig. 5.4), different zones of corrosion of steel reinforcement namely active zone, passive zone and transpassivity zone are shown. At potentials more positive than corrosion potential (E_{corr}), iron has tendency to oxidation corresponding to dissolution of Fe at the anode ($Fe \rightarrow Fe^{2+} + 2e^-$). The zone of corrosion below corrosion potential (E_{corr}) is termed as immune zone [26]. At potential values below corrosion potential, steel is thermodynamically unable to undergo anodic reactions and thus in a condition of immunity. The zone of corrosion, which lies above corrosion potential is termed as active zone [34, 71]. In active zone, passive film does not form spontaneously, leading to a significant increase in current density with small change in potential. The zone above the active zone is known as passive zone. In this zone, the

anodic current is very less, as the steel is covered by a very thin film of iron oxide (passive film). Thus in passive zone, the change in current density is very less with significant increase in potential. The zone above the passive zone is termed as transpassivity zone. Above the passive range, the steel is in the condition of transpassivity. In transpassivity zone, oxygen may be produced on steel surface as per the anodic reaction of oxygen evolution ($2H_2O \rightarrow O_2 + 4H^+ + 4e^-$) that produces acidity [20]. However, in the presence of chloride ions the transpassivity zone is termed as pitting zone. In this zone due to oxygen evolution, the anodic current density increases significantly leading to localized dissolution of steel in the presence of chloride ions. From obtained anodic polarization curves, corrosion potential (E_{corr}), potential at the point of transition from active to passive state i.e. act/pass zone boundary potential and that from passive to transpassive state i.e. pass/transpass zone boundary potential were determined for the steel reinforcement as shown in Fig 5.1 to Fig. 5.4. In the presence of chloride ions, the potential at the point of transition from passive to pitting state (i.e. pass/pitt boundary potential) is termed as breakdown potential or pitting potential. The boundary potential values for control mix are presented in Table 5.1.

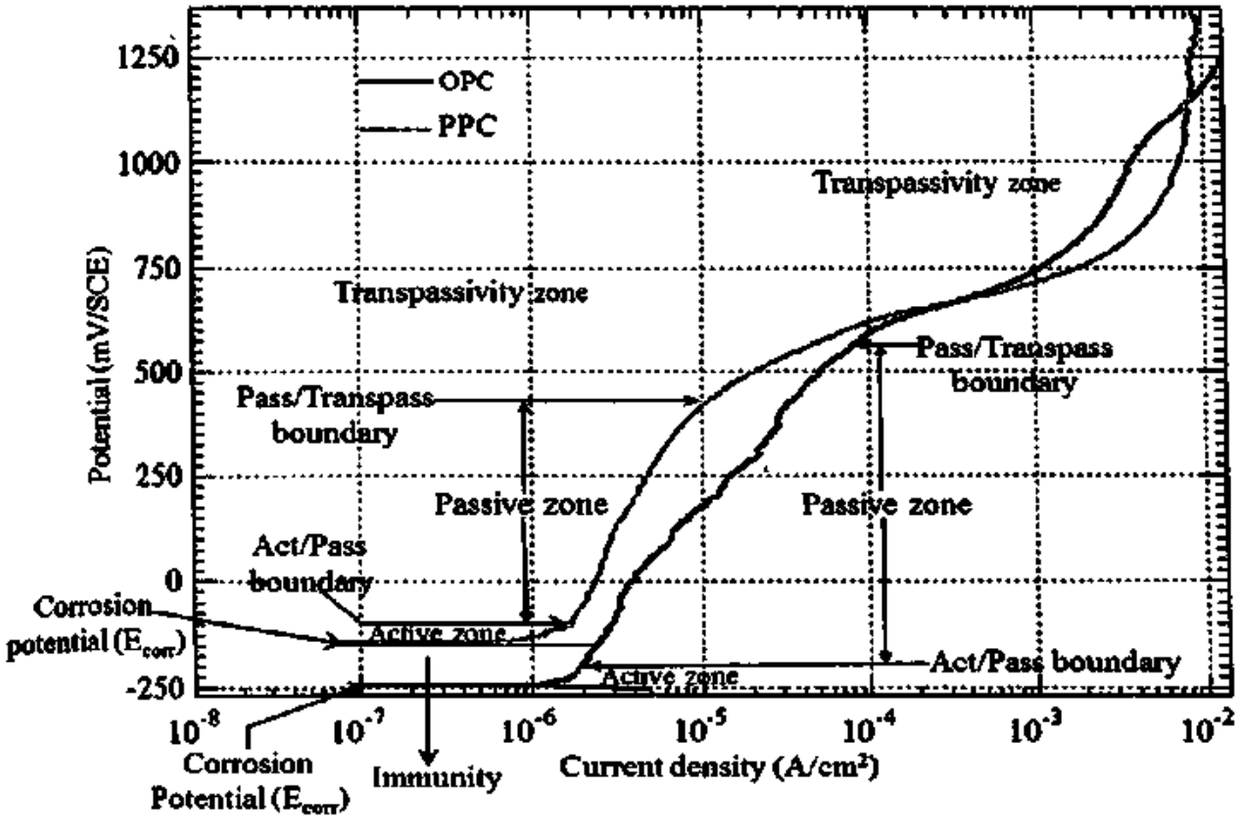

Fig. 5.1 Anodic polarization curves of Tempcore TMT steel in ECPS prepared from control mix for OPC and PPC at w/c ratio of 0.45

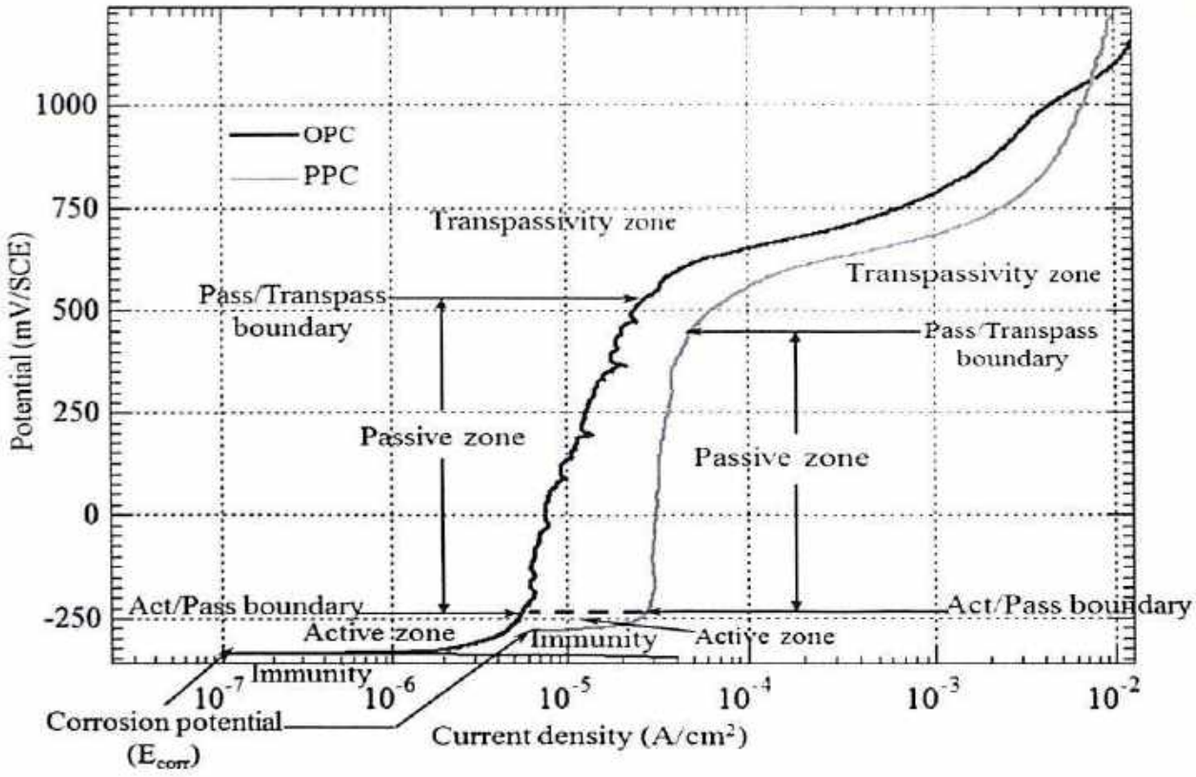

Fig. 5.2 Anodic polarization curves of Tempcore TMT steel in ECPS prepared from control mix for OPC and PPC at w/c ratio of 0.5

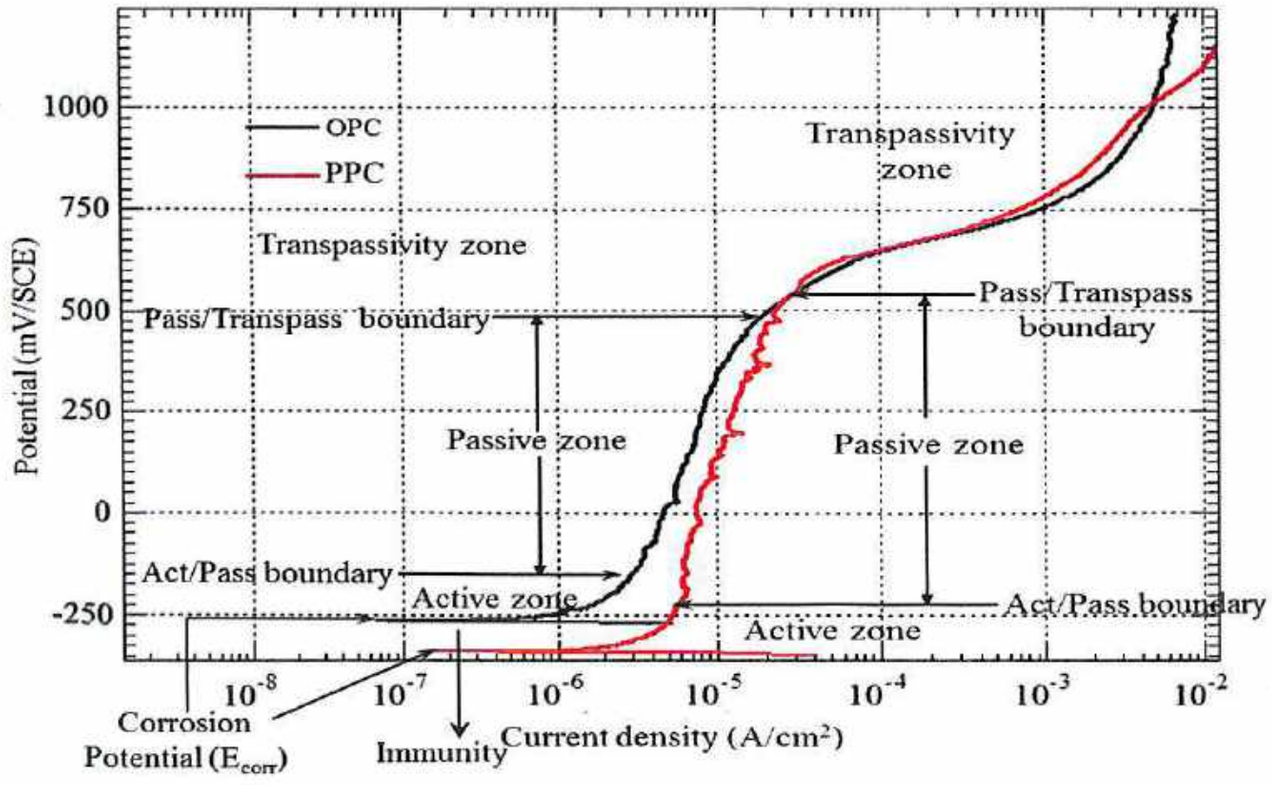

Fig. 5.3 Anodic polarization curves of Thermex TMT steel in ECPS prepared from control mix for OPC and PPC at w/c ratio of 0.45

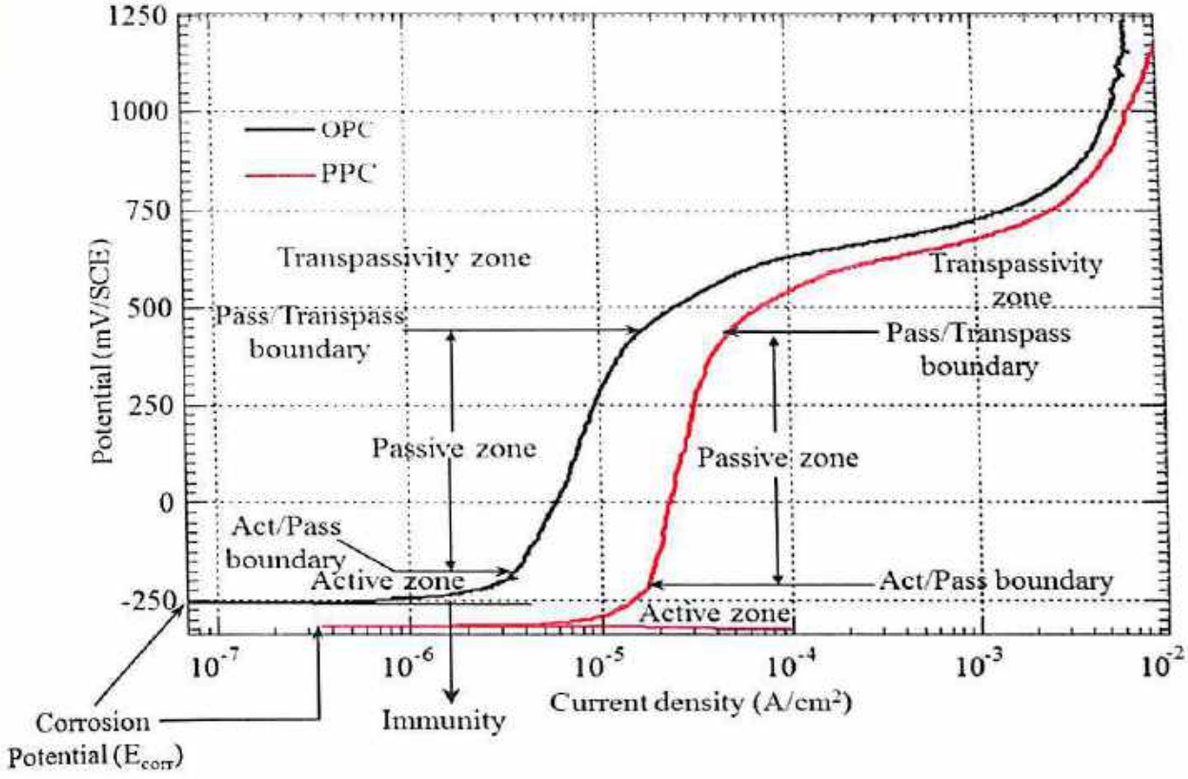

Fig. 5.4 Anodic polarization curves of Thermex TMT steel in ECPS prepared from control mix for OPC and PPC at w/c ratio of 0.5

From the anodic polarization curves shown in Fig. 5.1 and Fig. 5.2, it is observed that the range of passive zone of Tempcore TMT steel is more in OPC as compared to that in PPC at both w/c ratios of 0.45 and 0.5, which may be attributed to more alkalinity due to availability of more amount of calcium hydroxide in OPC concrete. From the anodic polarization curves shown in Fig. 5.3 and Fig. 5.4, it is observed that the range of passive zone of Thermex TMT steel is more in PPC as compared to that in OPC at both w/c ratios. Although the alkalinity of PPC concrete is less than that of OPC, but Thermex TMT steel exhibited more passivity in PPC concrete as compared to that in OPC concrete. This indicates that the passivity of steel not only depends on the alkalinity of concrete but also on the surface microstructure and chemical composition of the steel reinforcement. Further while comparing the steel type, it is observed that the range of passive zone is more in Tempcore TMT steel as compared to that in Thermex TMT steel in both OPC and PPC at both w/c ratios. This indicates that Tempcore TMT steel reinforcement showed higher passivity range as compared to Thermex TMT steel reinforcement in control concrete (i.e. without salt contamination).

5.2.1.1 Effect of Chloride Contamination in Electrolytic Concrete Powder Solution on Passivity of Steel Reinforcement

As stated earlier in Chapter 3, two replicate steel specimens were tested for a given electrolytic concrete powder solution to observe the reproducibility and a typical plot showing the polarization curves of replicate steel specimens for a given electrolytic concrete powder solution is shown in Fig. A1 (Appendix). From the obtained polarization curves of replicates, it is observed that there is not much difference between the profiles of polarization curves of both replicates.

The anodic polarization curves of Tempcore TMT steel and Thermex TMT steel in electrolytic concrete powder solution (ECPS) contaminated with varying concentrations of sodium chloride i.e. 3%, 5% and 7% NaCl for OPC and PPC at w/c ratios of 0.45 and 0.5 are shown in Fig. A2 to Fig. A9 (Appendix). From these anodic polarization curves, corrosion potential (E_{corr}), act/pass boundary potential and pass/pitt boundary potential (pitting potential) values were obtained and are presented in Table 5.1. The boundary potential values presented in Table 5.1 are the average value of two replicate steel specimens for a given electrolytic concrete powder solution.

From the boundary potential values obtained from anodic polarization curves shown in Fig. A2 to Fig. A9, it is observed that the range of passive zone of Tempcore TMT steel is more as compared to that of Thermex TMT steel in the presence of chloride ions for both types of cement and w/c ratio. This may be due to the effect of improved surface microstructure of Tempcore TMT steel than that of Thermex TMT steel. This indicates that Tempcore TMT steel maintains passivity to a greater degree as compared to Thermex TMT steel in the presence of chloride ions. Further from the results it is observed that, the range of passive zone of steel reinforcement in uncontaminated electrolytic concrete powder solution is more as compared to that in chloride contaminated electrolytic concrete powder solution. This indicates that the presence of chloride ions in concrete reduces the passivity of steel reinforcement. The plots of boundary potential values versus free chloride ion (Cl^- ion) concentration for electrolytic concrete powder solutions contaminated with 0%, 3%, 5% and 7% NaCl are shown in Fig. 5.5 to Fig. 5.8 and in Fig. 5.9 to Fig. 5.12 for Tempcore TMT steel and Thermex TMT steel respectively.

Table 5.1: Corrosion potential and boundary potentials of steel reinforcement in ECPS prepared from control concrete (without addition of salt) and concrete admixed with NaCl for OPC and PPC at w c ratios of 0.45 and 0.5

Steel type	w/c ratio	Cement type	Admixed salt concentration (% by weight of cement)	Corrosion potential (mV/SCE)	Act/pass boundary potential (mV/SCE)	Pass/transpass boundary potential (for control mix) and Pass/pitt boundary potential (pitting potential) (mV/SCE)
Tempcore TMT	0.45	OPC	Control mix	-252	-74	546
		PPC	Control mix	-151	-94	418
		OPC	3% NaCl	-449	-329	-136
			5% NaCl	-382	-198	-85
			7% NaCl	-364	-197	-93
		PPC	3% NaCl	-362	-223	-129
			5% NaCl	-403	-258	-170
			7% NaCl	-418	-313	-240
	0.5	OPC	Control mix	-346	-216	523
		PPC	Control mix	-280	-211	430
		OPC	3% NaCl	-326	-236	-34
			5% NaCl	-349	-283	-105
			7% NaCl	-393	-342	-178
		PPC	3% NaCl	-338	-267	-83
			5% NaCl	-360	-304	-145
			7% NaCl	-363	-334	-186
Thermex TMT	0.45	OPC	Control mix	-259	-189	348
		PPC	Control mix	-311	-234	495
		OPC	3% NaCl	-330	-201	-102
			5% NaCl	-347	-166	-72
			7% NaCl	-361	-199	-116
		PPC	3% NaCl	-374	-222	-146
			5% NaCl	-407	-356	-293
			7% NaCl	-398	-242	-196
	0.5	OPC	Control mix	-260	-191	390
		PPC	Control mix	-322	-217	378
		OPC	3% NaCl	-310	-169	-34
			5% NaCl	-385	-224	-96
			7% NaCl	-349	-210	-127
		PPC	3% NaCl	-336	-90	15
			5% NaCl	-355	-183	-102
			7% NaCl	-350	-197	-118

From Fig. 5.5 to Fig. 5.12, it is observed that the range of passive zone (calculated from the difference of pass/pitt boundary potential and act/pass boundary potential) of steel reinforcement decreased with increase in free Cl^- ion concentration in the electrolytic concrete powder solution admixed with varying dosages of NaCl for both types of cement, steel reinforcement and w/c ratio. Further, it is inferred that the change in range of active zone (which is calculated from the difference of act/pass boundary potential and corrosion potential) with Cl^- ion concentration is not systematic with increase in Cl^- ion concentration with respect to cement type, steel type and w/c ratio. This variation in active zone with Cl^- ion concentration may be attributed to the dominant effect of its proximity to the equilibrium condition. In addition, the pitting potential of steel reinforcement was more negative in the presence of chloride ions as compared to the control mix as observed from Table 5.1 and the pitting potential mostly decreased i.e. became more negative with increase in Cl^- ion concentration.

From the potential values presented in Table 5.1, it is observed that the values of E_{corr}, act/pass boundary potential and pass/pitt boundary potential for Tempcore TMT steel lie in the ranges of -326 mV to -449 mV, -197 mV to -342 mV, and -34 mV to -178 mV with reference to saturated calomel electrode respectively in the electrolytic concrete powder solution prepared from chloride contaminated OPC concrete irrespective of admixed NaCl dosage and w/c ratio. Similarly in PPC, the values E_{corr}, act/pass boundary potential and pass/pitt boundary potential for Tempcore TMT steel lie in the ranges of -338 mV to -418 mV, -223 mV to -334 mV, and -83 mV to -240 mV respectively irrespective of admixed NaCl dosage and w/c ratio. For Thermex TMT steel, the values of E_{corr}, act/pass boundary potential and pass/pitt boundary potential range from -310 mV to -385 mV, -166 mV to -224 mV, and -34 mV to -127 mV respectively in the electrolytic concrete powder solution prepared from chloride contaminated OPC concrete irrespective of admixed NaCl dosage and w/c ratio. Similarly in the ECPS prepared from chloride contaminated PPC concrete irrespective of admixed NaCl dosage and w/c ratio, the values E_{corr}, act/pass boundary potential and pass/pitt boundary potential for Thermex TMT steel range from -336 mV to -407 mV, -90 mV to -356 mV, and +15 mV to -293 mV respectively. From the boundary potential values presented in Table 5.1 and also from Fig. 5.5 to Fig. 5.12, it is found that for both Tempcore TMT and Thermex TMT steel, the range of passive zone is more in electrolytic concrete powder solution prepared from OPC concrete as compared to that prepared from PPC concrete at all levels of

admixed NaCl and at both w/c ratios of 0.45 and 0.5. The higher passivity range of steel reinforcement in OPC concrete as compared to that in PPC concrete is attributed to more chloride binding in OPC as compared to that in PPC, which resulted in lower Cl^- ion concentration in the electrolytic concrete powder solution prepared from OPC than that prepared from PPC (Chapter 4, Table 4.5 and 4.6). The higher chloride binding in OPC as compared to that in PPC was also conformed from XRD profiles shown in Fig. 4.1 to Fig. 4.4 (Chapter 4), in which the peak intensity of calcium chloroaluminate (CCA) was more in OPC as compared to that in PPC at all concentrations of NaCl. Further, it is observed that both Tempcore TMT steel and Thermex TMT steel showed higher passivity range in the electrolytic concrete powder solutions prepared from w/c ratio of 0.5 as compared to those made from w/c ratio of 0.45 at all concentrations of admixed NaCl and for both types of cement. The higher range of passivity of steel reinforcement in electrolytic concrete powder solution prepared from w/c ratio of 0.5 is attributed to lower Cl^- ion concentration as compared that at w/c ratio of 0.45 (observed from Table 4.5 and 4.6).

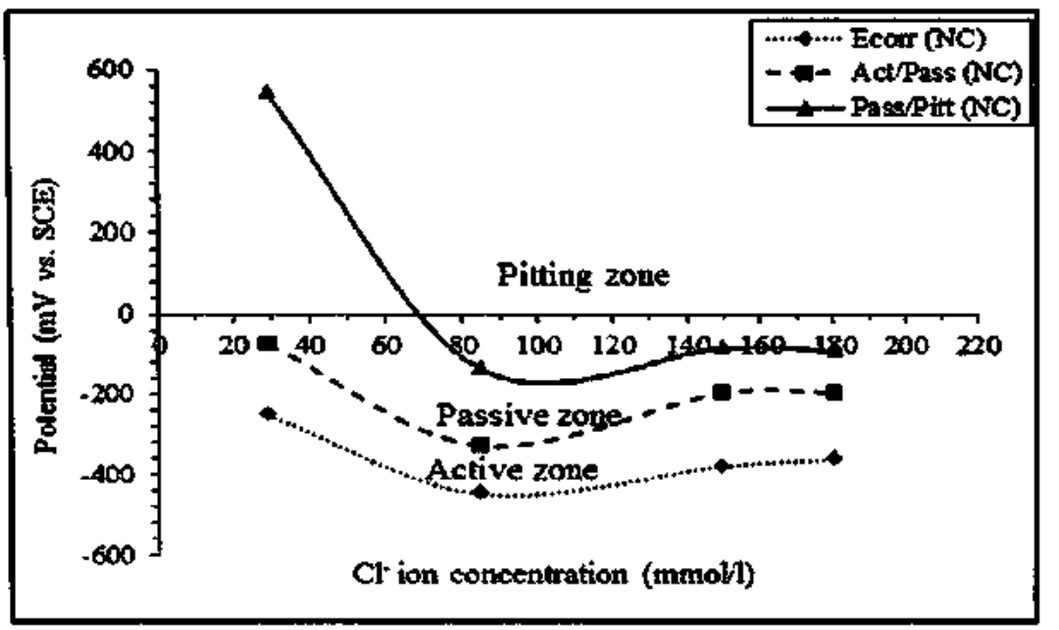

Fig. 5.5 Potential vs. Cl^- ion concentration of Tempcore TMT steel in ECPS prepared from OPC and w/c ratio of 0.45 at varying dosages of NaCl admixed by mass of cement

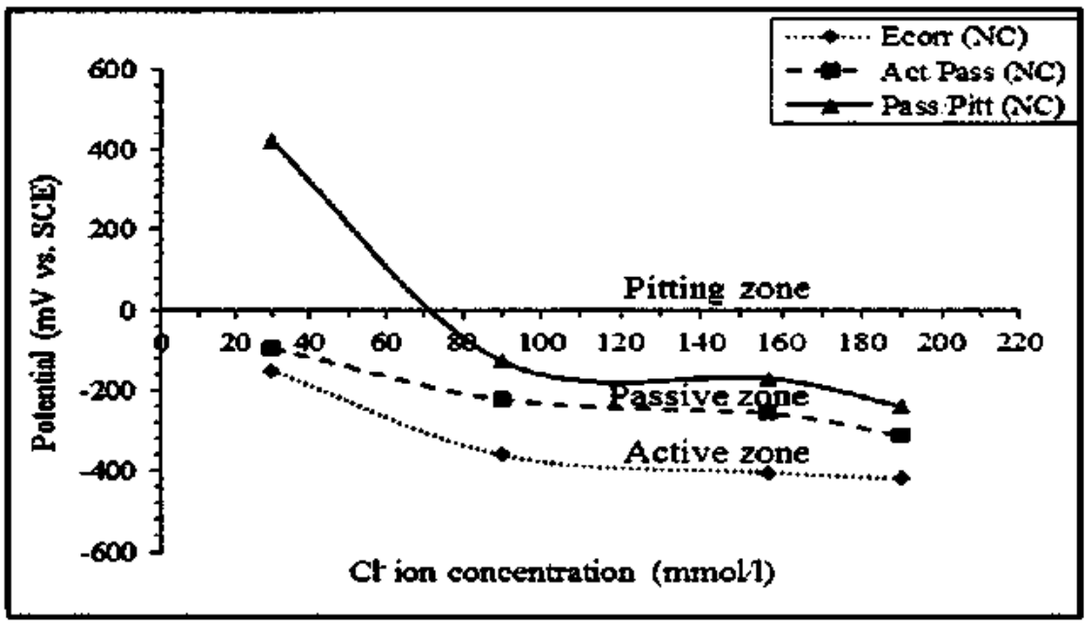

Fig. 5.6 Potential vs. chloride concentration of Tempcore TMT steel in ECPS prepared from PPC and w/c ratio of 0.45 at varying dosages of NaCl admixed by mass of cement

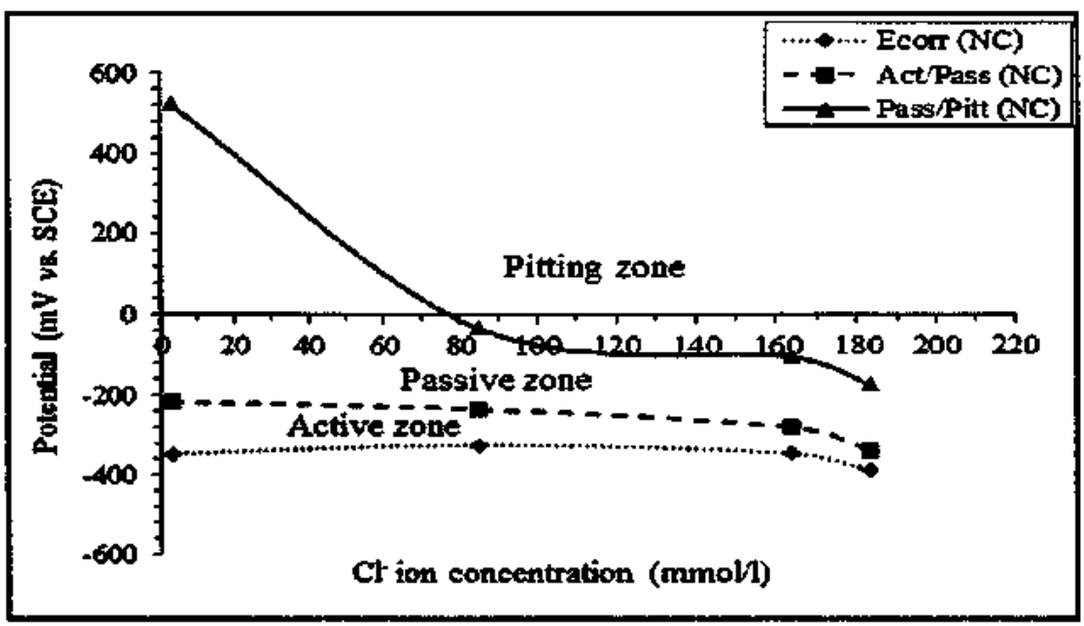

Fig. 5.7 Potential vs. chloride concentration of Tempcore TMT steel in ECPS prepared from OPC and w/c ratio of 0.5 at varying dosages of NaCl admixed by mass of cement

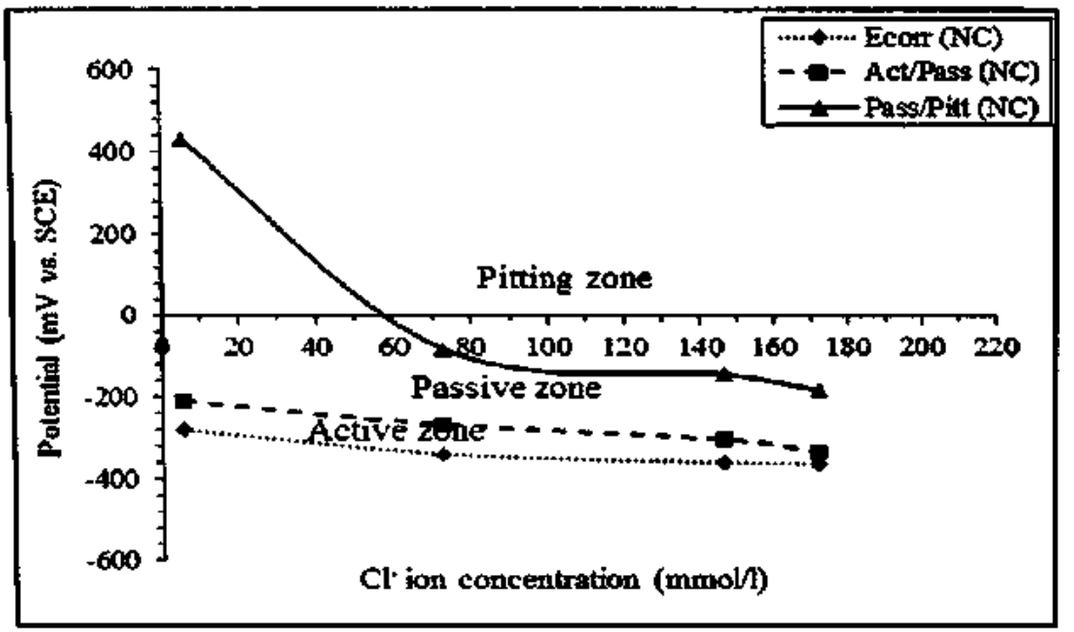

Fig. 5.8 Potential vs. chloride concentration of Tempcore TMT steel in ECPS prepared from PPC and w/c ratio of 0.5 at varying dosages of NaCl admixed by mass of cement

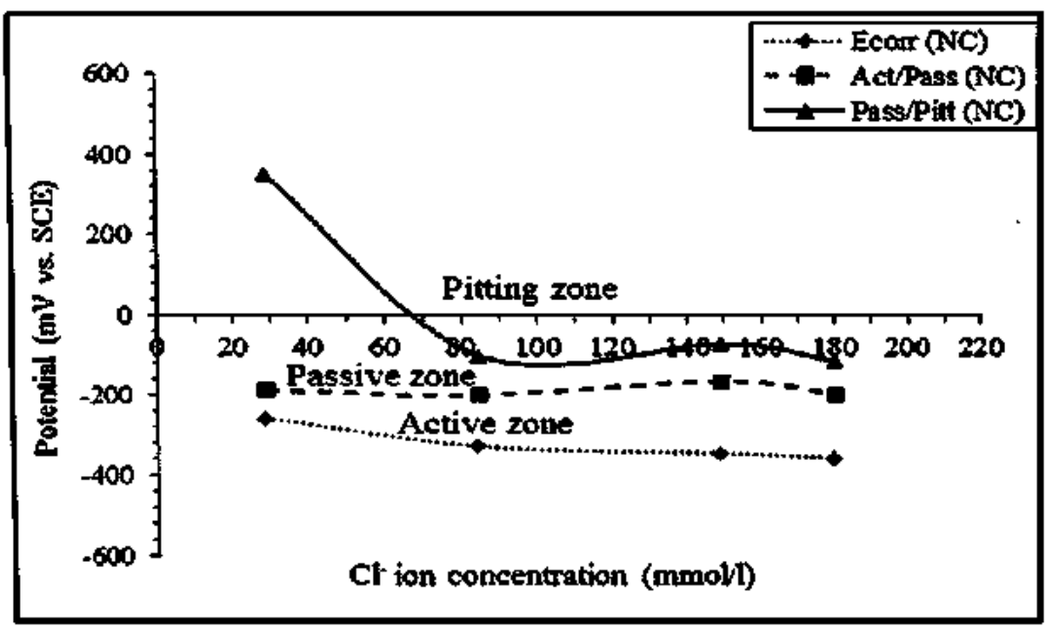

Fig. 5.9 Potential vs. chloride concentration of Thermex TMT steel in ECPS prepared from OPC and w/c ratio of 0.45 at varying dosages of NaCl admixed by mass of cement

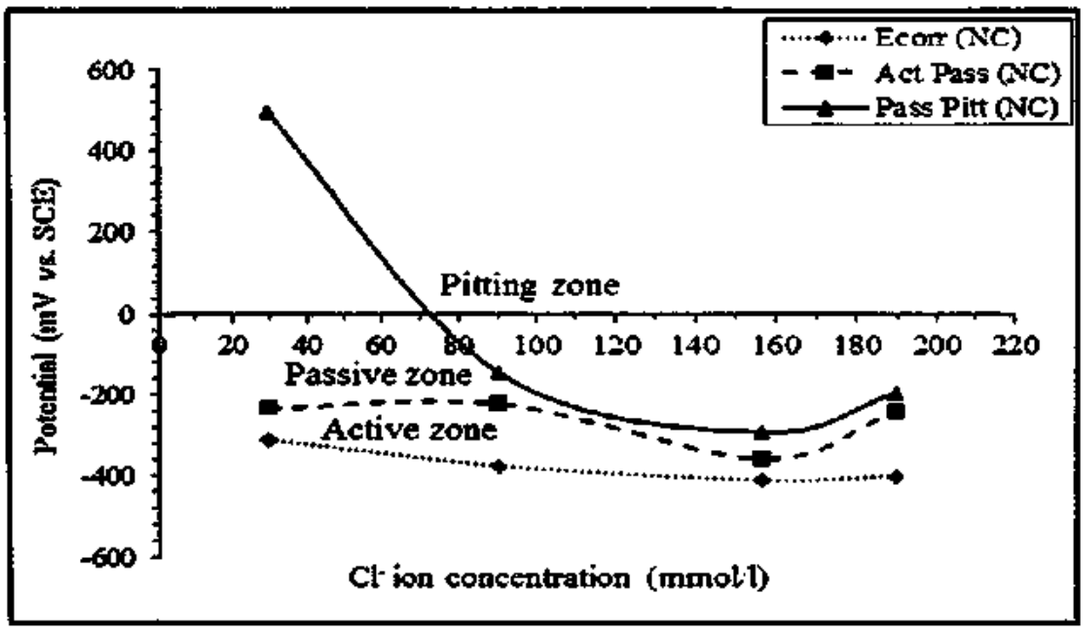

Fig. 5.10 Potential vs. chloride concentration of Thermex TMT steel in ECPS prepared from PPC and w/c ratio of 0.45 at varying dosages of NaCl admixed by mass of cement

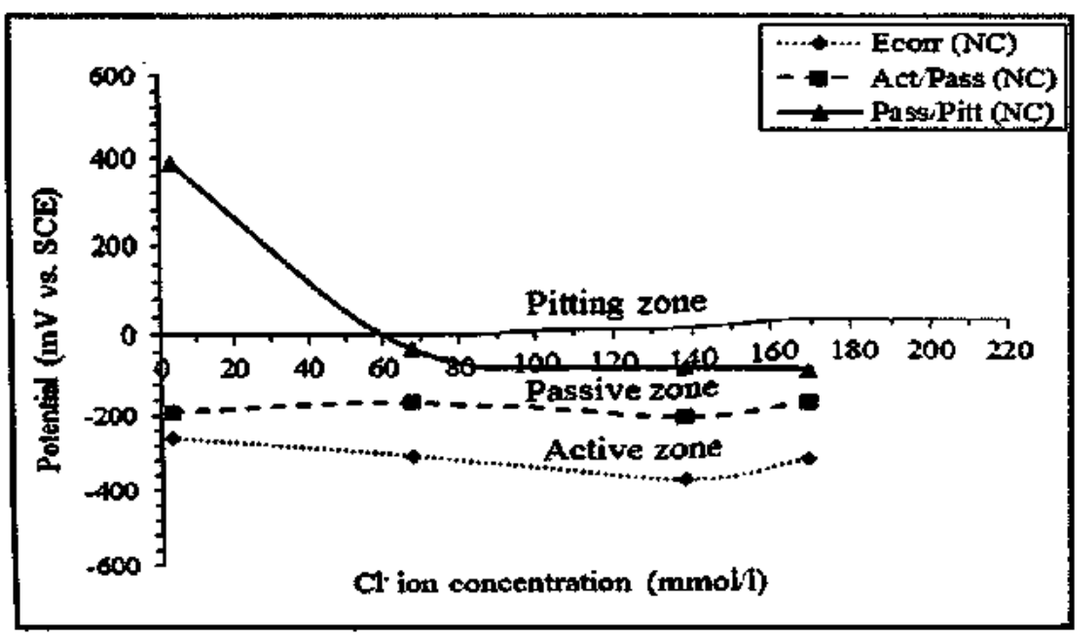

Fig. 5.11 Potential vs. chloride concentration of Thermex TMT steel ECPS prepared from OPC and w/c ratio of 0.5 at varying dosages of NaCl admixed by mass of cement

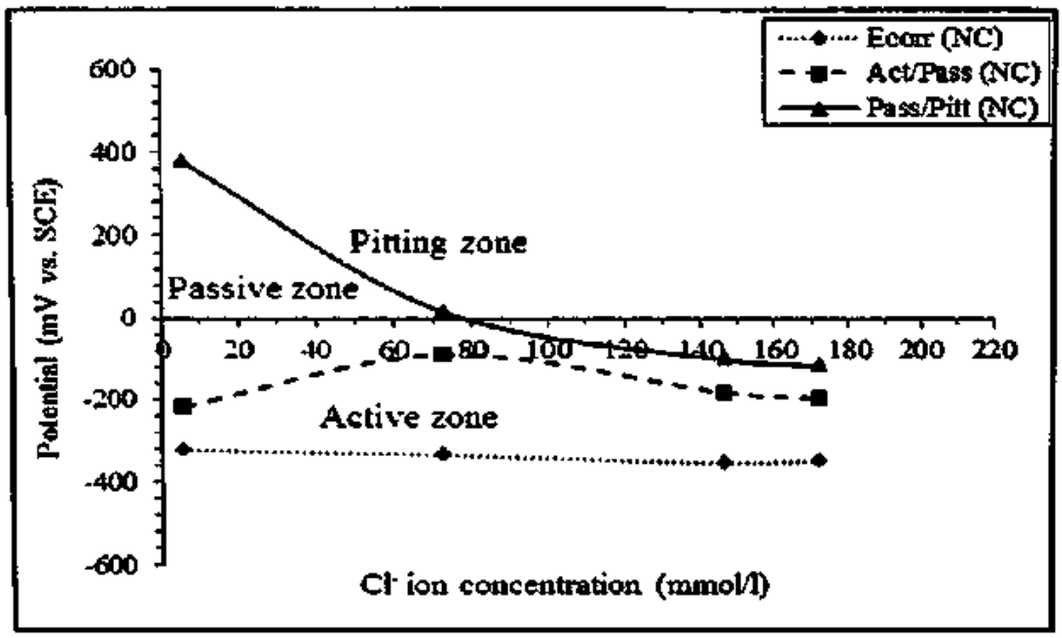

Fig. 5.12 Potential vs. chloride concentration of Thermex TMT steel in ECPS prepared from PPC and w/c ratio of 0.5 at varying dosages of NaCl admixed by mass of cement

5.2.1.2 Effect of Conjoint Chloride-Sulfate Contamination in Electrolytic Concrete Powder Solution on Passivity of Steel Reinforcement

The anodic polarization curves obtained by conducting potentiodynamic polarization test for Tempcore TMT steel and Thermex TMT steel in electrolytic concrete powder solutions contaminated with varying concentrations of sodium chloride (NaCl) plus sodium sulfate (Na_2SO_4) are shown in Fig. A10 to Fig. A17 and in that contaminated with sodium chloride (NaCl) plus magnesium sulfate ($MgSO_4$) are shown in Fig. A18 to Fig. A25 (Appendix) for both types of cement and w/c ratio. From these anodic polarization curves of Tempcore TMT steel and Thermex TMT steel, the values of corrosion potential (E_{corr}), act/pass boundary potential and pass/pitt boundary potential were obtained and are presented in Table 5.2, Table 5.3 and Table 5.4 respectively for both OPC and PPC at w/c ratios of 0.45 and 0.5. The boundary potential values presented in these tables are the average value of two replicate steel specimens for a given electrolytic concrete powder solution. Further, the variations in boundary potentials with Cl^- ion concentration were plotted for various concentrations of admixed chloride and sulfate ions. The variations in boundary potentials with free Cl^- ion concentration for Tempcore TMT steel in the ECPS contaminated with varying concentrations of NaCl plus Na_2SO_4 and that contaminated with NaCl plus $MgSO_4$ are shown in Fig. 5.13 to Fig. 5.24 for both types of cement and

w/c ratio. Similarly the, variations in boundary potentials with Cl⁻ ion concentration for Thermex TMT steel are shown in Fig. 5.25 to Fig. 5.36.

Table 5.2: Corrosion potential of steel reinforcement in ECPS prepared from concrete mix admixed with varying concentrations of NaCl plus Na_2SO_4 and NaCl plus $MgSO_4$ for OPC and PPC at w/c ratios of 0.45 and 0.5

Steel type	w/c ratio	Cement type	OPC			PPC		
		Admixed sulfate salts	Admixed chloride salt (NaCl)					
			3%	5%	7%	3%	5%	7%
Tempcore TMT	0.45	3% Na_2SO_4	-401	-315	-386	-404	-329	-333
		6% Na_2SO_4	-400	-394	-420	-312	-324	-384
		12% Na_2SO_4	-301	-344	-334	-399	-345	-293
	0.5	3% Na_2SO_4	-322	-344	-333	-362	-440	-361
		6% Na_2SO_4	-328	-426	-381	-318	-315	-356
		12% Na_2SO_4	-356	-409	-346	-354	-328	-324
	0.45	3% $MgSO_4$	-342	-417	-383	-389	-337	-350
		6% $MgSO_4$	-236	-309	-424	-427	-397	-334
		12% $MgSO_4$	-369	-378	-414	-414	-370	-375
	0.5	3% $MgSO_4$	-204	-320	-286	-415	-366	-398
		6% $MgSO_4$	-361	-384	-366	-266	-285	-418
		12% $MgSO_4$	-396	-396	-436	-466	-436	-376
Thermex TMT	0.45	3% Na_2SO_4	-356	-368	-343	-389	-397	-317
		6% Na_2SO_4	-340	-346	-339	-367	-364	-419
		12% Na_2SO_4	-324	-400	-320	-358	-361	-450
	0.5	3% Na_2SO_4	-319	-367	-347	-339	-315	-405
		6% Na_2SO_4	-452	-361	-393	-379	-350	-353
		12% Na_2SO_4	-326	-342	-391	-357	-389	-385
	0.45	3% $MgSO_4$	-349	-411	-391	-377	-416	-410
		6% $MgSO_4$	-352	-382	-397	-415	-373	-405
		12% $MgSO_4$	-486	-366	-381	-427	-389	-430
	0.5	3% $MgSO_4$	-476	-452	-358	-403	-356	-414
		6% $MgSO_4$	-415	-375	-411	-367	-367	-384
		12% $MgSO_4$	-376	-430	-423	-411	-361	-467

Table 5.3: Active/Passive boundary potential of steel reinforcement in ECPS prepared from concrete mix admixed with varying concentrations of NaCl plus Na_2SO_4 and NaCl plus $MgSO_4$ for OPC and PPC at w/c ratios of 0.45 and 0.5

Steel type	w/c ratio	Cement type	Admixed sulfate salts	OPC			PPC		
				Admixed chloride salt (NaCl)					
				3%	5%	7%	3%	5%	7%
Tempcore TMT	0.45	Na_2SO_4	3%	-316	-244	-269	-278	-245	-219
			6%	-350	-270	-306	-210	-237	-187
			12%	-208	-214	-231	-296	-246	-242
	0.5		3%	-202	-306	-258	-284	-408	-310
			6%	-248	-363	-318	-265	-289	-302
			12%	-305	-379	-290	-212	-250	-268
	0.45	$MgSO_4$	3%	-283	-358	-312	-276	-236	-216
			6%	-180	-247	-303	-333	-243	-175
			12%	-267	-241	-296	-366	-222	-316
	0.5		3%	-172	-212	-172	-380	-289	-344
			6%	-269	-294	-291	-213	-236	-360
			12%	-338	-325	-348	-407	-338	-340
Thermex TMT	0.45	Na_2SO_4	3%	-269	-287	-290	-199	-335	-242
			6%	-271	-289	-313	-320	-313	-387
			12%	-240	-319	-303	-263	-338	-416
	0.5		3%	-217	-278	-202	-240	-255	-346
			6%	-380	-244	-276	-304	-281	-309
			12%	-236	-264	-222	-270	-342	-335
	0.45	$MgSO_4$	3%	-311	-397	-253	-354	-255	-219
			6%	-265	-191	-240	-389	-222	-373
			12%	-455	-227	-189	-273	-227	-257
	0.5		3%	-446	-429	-338	-374	-291	-395
			6%	-399	-337	-346	-298	-345	-361
			12%	-307	-383	-397	-346	-206	-328

Table 5.4: Passive/Pitting boundary potential of steel reinforcement in ECPS prepared from concrete mix admixed with varying concentrations of NaCl plus Na_2SO_4 and NaCl plus $MgSO_4$ for OPC and PPC at w/c ratios of 0.45 and 0.5

Steel type	w/c ratio	Cement type		OPC			PPC		
		Admixed sulfate salts		Admixed chloride salt (NaCl)					
				3%	5%	7%	3%	5%	7%
Tempcore TMT	0.45	Na_2SO_4	3%	-85	-78	-155	-122	-126	-121
			6%	-194	-151	-193	-70	-124	-99
			12%	-14	-62	-100	-79	-130	-166
	0.5		3%	369	-34	-83	-54	-189	-152
			6%	27	-141	-168	59	-33	-83
			12%	-80	-197	-168	120	18	-42
	0.45	$MgSO_4$	3%	-97	-223	-209	-98	-136	-127
			6%	-28	-117	-230	-185	-159	-106
			12%	-137	-165	-227	-241	-152	-254
	0.5		3%	16	-36	-9	-219	-133	-201
			6%	-90	-134	-143	-76	-90	-229
			12%	-179	-181	-230	-281	-268	-240
Thermex TMT	0.45	Na_2SO_4	3%	30	-110	-131	268	-91	-26
			6%	-27	-139	-172	-49	-92	-226
			12%	-75	-189	-218	-25	-198	-287
	0.5		3%	118	-89	-34	278	12	-106
			6%	-110	-91	-129	65	-46	-138
			12%	-41	-126	-122	-21	-192	-201
	0.45	$MgSO_4$	3%	-90	-267	-148	-217	-164	-140
			6%	-119	-88	-148	-261	-143	-304
			12%	-315	-129	-105	-178	-129	-193
	0.5		3%	-222	-292	-213	-262	-196	-309
			6%	-222	-203	-242	-166	-256	-288
			12%	-143	-273	-300	-242	-122	-258

5.2.1.2.1 Effect of Conjoint NaCl plus Na_2SO_4 Contamination in Electrolytic Concrete Powder Solution on Passivity of Steel Reinforcement

From the corrosion potential values presented in Table 5.2, it is observed that the range of corrosion potential of Tempcore TMT steel in electrolytic concrete powder solution contaminated with sodium chloride plus sodium sulfate varied from -301 mV to -426 mV and -293 mV to -440 mV for OPC and PPC respectively, and for Thermex TMT steel the corrosion potential varied from -319 mV to -452 mV and -315 mV to -450 mV respectively for OPC and PPC irrespective of NaCl concentration, Na_2SO_4 concentration and w/c ratio. From Table 5.3 it is observed that the range of act/pass boundary potential for Tempcore TMT steel in electrolytic concrete powder solution varied from -202 mV to -379 mV and -187 mV to -408 mV and for Thermex TMT steel, it varied from -202 mV to -380 mV and -199 mV to -416 mV for OPC and PPC respectively, irrespective of NaCl concentration, Na_2SO_4 concentration and w/c ratio. Similarly, the range of pass/pitt boundary potential for Tempcore TMT steel varied from +369 mV to -197 mV and +120 mV to -189 mV and for Thermex TMT steel, the boundary potential varied from +118 mV to -218 mV and +278 mV to -287 mV for OPC and PPC respectively, irrespective of admixed salt concentration and w/c ratio as observed from Table 5.4. The range of passive zone calculated from the difference of pass/pitt boundary potential and act/pass boundary potential values presented in Table 5.4 and Table 5.3 respectively indicated that in the conjoint presence of NaCl plus Na_2SO_4, Tempcore steel mostly showed higher passivity range as compared to Thermex TMT steel in OPC, whereas in PPC the opposite variation was observed i.e. Thermex steel mostly exhibited higher passivity range than Tempcore TMT steel, at both w/c ratios. While comparing with the uncontaminated electrolytic concrete powder solution, it is observed that the range of passive zone of steel reinforcement is reduced in the conjoint presence of NaCl and Na_2SO_4.

From Fig. 5.13 to Fig. 5.36, it is observed that the range of passive zone of both Tempcore TMT steel and Thermex TMT steel decreased with an increase in concentration of Cl^- ion irrespective of admixed Na_2SO_4 concentration in both OPC and PPC and at both w/c ratios. The decrease in passivity range with increase in Cl^- ion concentration is attributed to increase in conductivity of electrolytic concrete powder solution (Table 4.7 and 4.8, Chapter 4). Further, it is observed that the change in range of active zone with Cl^- ion concentration is not systematic in the presence of sulfate ions with respect to steel type, cement type and w/c ratio. The unsystematic variation in the

range of active zone in the conjoint presence of NaCl and Na_2SO_4 with respect to cement type, steel type and w/c ratio may be attributed to the alteration in the corrosion potential and the passivity of steel reinforcement in the conjoint presence of chloride and sulfate ions. The pitting potential of steel reinforcement was more negative in the conjoint presence of chloride and sulfate ions as compared to that in the uncontaminated mix for both types of cement, steel and w/c ratio, as observed from Fig. 5.13 to Fig. 5.36. In addition, the variation in pitting potential of steel reinforcement was not systematic for both types of cement, steel and w/c ratio. The unsystematic variation in the pitting potential in ECPS contaminated with NaCl and Na_2SO_4 with respect to cement type, steel type and w/c ratio may be attributed to alteration in the extent of passive zone due to the combined effect of chloride and sulfate ions.

From Fig. 5.13 to Fig. 5.18 it is inferred that the range of passive zone of Tempcore TMT steel in electrolytic concrete powder solution contaminated with varying concentrations of NaCl plus Na_2SO_4 decreased with an increase in admixed Na_2SO_4 concentration up to 6% followed by an increase at 12% Na_2SO_4 concentration irrespective of NaCl dosage for OPC and PPC at w/c ratio of 0.45. This indicates that at w/c ratio of 0.45, higher concentration of sulfate ions (12% Na_2SO_4) mitigated the chloride attack on the passivity of reinforcing steel, thereby increasing the range of passive zone. The passivity range of Tempcore TMT steel in electrolytic concrete powder solution prepared from OPC at w/c ratio of 0.5 decreased with an increase in Na_2SO_4 concentration at all levels of NaCl contaminations as observed from Fig. 5.19 to Fig. 5.21. This may be attributed to increase in Cl^- ion concentration and drop in pH of the solution with increase in Na_2SO_4 concentration in the presence of NaCl (as observed from Table 4.8, Chapter 4). The opposite behavior was observed for Tempcore TMT steel in electrolytic concrete powder solution made from PPC concrete at w/c ratio of 0.5 i.e. the passivity range of steel increased with an increase in Na_2SO_4 concentration at all levels of NaCl contaminations as observed from Fig. 5.22 to Fig. 5.24. The increase in range of passive zone in PPC may be due to the decrease in Cl^- ion concentration and increase in pH of the solution with increase in Na_2SO_4 concentration in the presence of NaCl (as observed from Table 4.8, Chapter 4). This indicates that the passivity range of steel, which depends on the variations in the act/pass boundary potential and pitting potential is a function of Cl^- ion concentration in the concrete pore solution, which in turn depends on the concentration of Na_2SO_4 and is also influenced by the pH value of the electrolytic concrete powder

solution. From Fig. 5.25 to Fig. 5.36 it is observed that, in electrolytic concrete powder solution contaminated with varying concentrations of NaCl plus Na_2SO_4, the range of passive zone of Thermex TMT steel decreased with an increase in admixed Na_2SO_4 dosage in both OPC and PPC concrete at w/c ratios of 0.45 and 0.5. These variations in the passivity range with Na_2SO_4 concentration for different types of steel indicate that the passivity range of steel in concrete pore solution not only depends on the concentration of chloride and sulfate ions but also on the surface microstructure of steel reinforcement in the conjoint presence of NaCl and Na_2SO_4.

While observing the effect of w/c ratio on passivity of steel reinforcement (for both Tempcore TMT and Thermex TMT steel) in the conjoint presence of NaCl and Na_2SO_4, it is observed that the range of passive zone is higher in electrolytic concrete powder solution made from w/c ratio of 0.5 as compared to that made from w/c ratio of 0.45 for both OPC and PPC at all concentrations of sodium chloride plus sodium sulfate as observed from Fig. 5.13 to Fig. 5.36. This is attributed to lower Cl^- ion concentration in electrolytic concrete powder solution made from w/c ratio of 0.5 as compared to that made from w/c ratio of 0.45, as observed from Table 4.7 and Table 4.8 (Chapter 4).

While analyzing the effect of cement type on the passivity range of steel reinforcement, it is observed from Fig. 5.13 to Fig. 5.18 that, Tempcore TMT steel in the electrolytic concrete powder solution made from OPC showed higher range of passivity as compared to that made from PPC at w/c ratio of 0.45 in the conjoint presence of sodium chloride and sodium sulfate. From the XRD profiles presented in Section 4.3.1.2 (Chapter 4), it is observed that OPC concrete showed more intense peaks of calcium chloroaluminate (CCA) as compared to PPC concrete at w/c ratio of 0.45. This is because, in the conjoint presence of sodium chloride and sodium sulfate, the preferential reaction of chloride ions with hydrated C_3A phase of cement has resulted in formation of higher amount of CCA in OPC than that in PPC, whereas in PPC the preferential reaction of sulfate ions with hydrated C_3A has resulted in the formation of higher amount of ettringite, which is corroborated by more intense peaks of ettringite in PPC than that in OPC as observed from XRD profiles (presented in Section 4.3.1.2, Chapter 4). Due to higher chloride binding as a result of formation of more amount of calcium chloroaluminate in OPC (lower Cl^- ion concentration), the range of passive zone is higher in OPC than that in PPC in the conjoint presence of NaCl and Na_2SO_4 at w/c ratio of 0.45.

From Fig. 5.19 to Fig. 5.24 it is observed that at w/c ratio of 0.5, the range of passive zone of Tempcore TMT steel is higher in OPC as compared to that in PPC at 3% Na_2SO_4 concentration, whereas PPC showed higher passivity range as compared to OPC at 6% and 12% Na_2SO_4 concentrations for all dosages of admixed NaCl. From the results of Cl^- ion concentration (Table 4.8, Chapter 4), it is observed that for 3% Na_2SO_4 dosage, the Cl^- ion concentration was significantly higher in PPC as compared to that in OPC at 3% NaCl, whereas there was a minor difference in Cl^- ion concentration between OPC and PPC at 5% and 7% NaCl concentrations. However at 6% and 12% Na_2SO_4 concentrations, Cl^- ion concentration was mostly higher in electrolytic concrete powder solution made from OPC than that in PPC at all dosages of admixed NaCl. This indicates that higher range of passivity in OPC at lower Na_2SO_4 concentration (i.e. 3%) and that in PPC at higher Na_2SO_4 concentrations (i.e. 6% and 12%) may be attributed to higher chloride binding resulting in lower Cl^- ion concentration at corresponding Na_2SO_4 concentrations in the presence of NaCl. From Fig. 5.25 to Fig. 5.36, it is observed that Thermex TMT steel in electrolytic concrete powder solution made from PPC concrete showed higher range of passivity as compared to that made from OPC concrete at both w/c ratios of 0.45 and 0.5 in the conjoint presence of sodium chloride and sodium sulfate. This indicates that the performance of Thermex TMT steel in PPC is better than that in OPC in maintaining the passivity of steel reinforcement. The variation in the passivity range with steel type in the conjoint presence of sodium chloride and sodium sulfate is not only affected by cement type and w/c ratio but also by the surface microstructure of steel reinforcement.

5.2.1.2.2 Effect of Conjoint NaCl plus $MgSO_4$ Contamination in Electrolytic Concrete Powder Solution on Passivity of Steel Reinforcement

From the corrosion potential values presented in Table 5.2, it is observed that the range of corrosion potential values of Tempcore TMT steel in electrolytic concrete powder solution admixed with sodium chloride plus magnesium sulfate varied from -204 mV to -436 mV and -266 mV to -466 mV for OPC and PPC respectively and for Thermex TMT steel, varied from -349 mV to -486 mV and -356 mV to -467 mV respectively for OPC and PPC irrespective of NaCl and $MgSO_4$ concentrations and w/c ratio. The range of act/pass boundary potential values of Tempcore TMT steel in electrolytic concrete powder solution varied from -172 mV to -358 mV and -175 mV to -407 mV and for

Thermex TMT steel, varied from -189 mV to -455 mV and -206 mV to -395 mV respectively for OPC and PPC irrespective of NaCl and $MgSO_4$ concentrations and w/c ratio as observed from Table 5.3. Similarly, from Table 5.4 it is observed that the range of pass/pitt boundary potential values of Tempcore TMT steel varied from +16 mV to -230 mV and -76 mV to -281 mV and for Thermex TMT steel, varied from -88 mV to -315 mV and +143 mV to -309 mV for OPC and PPC respectively irrespective of NaCl and $MgSO_4$ concentrations and w/c ratio. The range of passive zone calculated from the boundary potential values presented in Table 5.3 and Table 5.4 indicated that in the conjoint presence of NaCl plus $MgSO_4$, Tempcore steel mostly showed higher range of passivity as compared to Thermex TMT steel for both types of cement and w/c ratio.

From Fig. 5.13 to Fig. 5.36, it is observed that the range of passive zone decreased with an increase in admixed NaCl concentration irrespective of admixed $MgSO_4$ concentration for both types of cement, steel and w/c ratio. The decrease in the passivity range due to increase in admixed NaCl concentration is attributed to increase in Cl^- ion concentration and drop in pH (as mentioned in Table 4.9 and Table 4.10, Chapter 4) of electrolytic concrete powder solution. Further, there is no systematic variation in the range of active zone with admixed NaCl and $MgSO_4$ concentrations for both types of cement, steel reinforcement and w/c ratio. In addition, the conjoint presence of chloride and sulfate ions resulted in a decrease in the pitting potential as compared to the uncontaminated concrete mix irrespective of cement type, steel type and w/c ratio, as observed from Fig. 5.13 to Fig. 5.36. However, the variation in pitting potential of steel reinforcement was not systematic for both types of cement, steel and w/c ratio in the conjoint presence of NaCl and $MgSO_4$.

Further from Fig. 5.13 to Fig. 5.36, it is inferred that the range of passive zone decreased with increase in admixed $MgSO_4$ concentration at all levels of admixed NaCl for both types of cement, steel reinforcement and w/c ratio. This may be due to increase in Cl^- ion concentration and reduction in pH of the electrolytic concrete powder solution with increase in $MgSO_4$ dosage (Table 4.9 and 4.10, Chapter 4). The increase in Cl^- ion concentration with increase in admixed magnesium sulfate concentration may be due to lower chloride binding as a result of the preferential reaction of sulfate ions as compared to chloride ions, with hydrated C_3A in concrete. The increase in Cl^- ion concentration leads to increase in conductivity of electrolytic concrete powder solution. The reduction in pH of electrolytic concrete powder solution with increase in $MgSO_4$ concentration may

be attributed to the formation low soluble magnesium hydroxide ($Mg(OH)_2$) that is formed as a result of reaction of magnesium sulfate with calcium hydroxide. This indicates that the presence of sulfate ion associated with magnesium cation enhanced the chloride attack on the passivity of reinforcing steel, thereby decreasing the range of passive zone with increase in magnesium sulfate concentration. On comparison with uncontaminated electrolytic concrete powder solution, it is observed that the passivity range of steel reinforcement decreased in the conjoint presence of NaCl and $MgSO_4$.

While examining the effect of w/c ratio on the passivity range of steel reinforcement, it is observed that the range of passive zone is higher in electrolytic concrete powder solution made at w/c ratio of 0.5 as compared to that made at w/c ratio of 0.45 for both types of cement and steel reinforcement at all concentrations of sodium chloride plus magnesium sulfate. The lower Cl^- ion concentration at w/c ratio of 0.5 as compared to that at w/c ratio of 0.45 as observed from Table 4.9 and Table 4.10 (Chapter 4) has resulted in higher passivity range at w/c ratio of 0.5.

While analyzing the effect of cement type on the passivity of steel reinforcement, it is observed that (Fig. 5.13 to Fig. 5.36) for both Tempcore TMT and Thermex TMT steel, the range of passive zone is higher in electrolytic concrete powder solution prepared from OPC as compared to that prepared from PPC at all concentrations of sodium chloride plus magnesium sulfate and at both w/c ratios, which indicates that OPC maintains the passivity of reinforcing steel to a greater extent than PPC in the conjoint presence of NaCl and $MgSO_4$. This is attributed to lower Cl^- ion concentration observed in OPC as compared to that in PPC at all concentrations of admixed NaCl plus $MgSO_4$ (Table 4.9 and 4.10, Chapter 4). Further, decrease in passivity range of steel in PPC in the conjoint presence of NaCl and $MgSO_4$ can also be attributed to its susceptibility to Mg-oriented attack. Magnesium sulfate reacts with calcium hydroxide liberated in hydration reaction of calcium silicates (C_3S and C_2S) and forms calcium sulfate (gypsum) and magnesium hydroxide (brucite) [42]. In PPC due to less reserve of calcium hydroxide, which acts as the first defensive material to react with magnesium sulfate, the magnesium sulfate attack is therefore directed extensively towards C-S-H gel, ultimately forming more amounts of gypsum and non-cementitious magnesium silicate hydrate (M-S-H) [43]. Thus, the passivity of steel in electrolytic concrete powder solution prepared from PPC in the presence of NaCl plus $MgSO_4$ is decreased due to increase in the conductivity of electrolytic concrete powder solution as a result of more Cl^- ion concentration and

formation of more amount of non-cementitious M-S-H. The formation of more amount of gypsum due to Mg-oriented attack on C-S-H because of less reserve of calcium hydroxide and formation of more amount of ettringite due to the reaction of gypsum with hydrated aluminate phases in concrete to a greater extent in PPC as compared to that in OPC is also corroborated from XRD profiles (presented in Section 4.3.1.3, Chapter 4), which showed more intense peaks of gypsum and ettringite in PPC as compared to that in OPC in the conjoint presence of NaCl and $MgSO_4$.

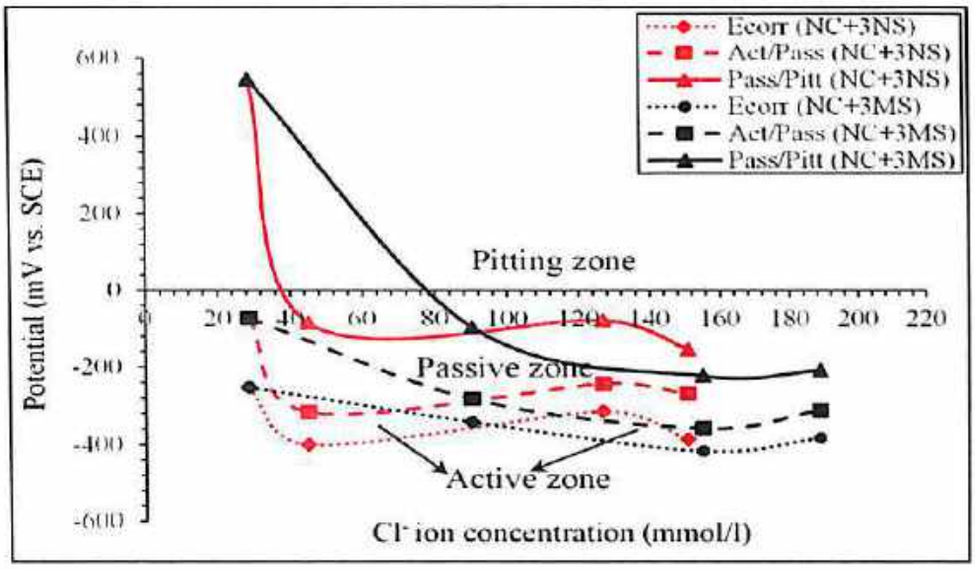

Fig. 5.13 Potential vs. Cl^- ion concentration of Tempcore TMT steel in ECPS prepared from OPC and w/c ratio of 0.45 and admixed with 0%, 3%, 5% and 7% NaCl plus 3% Na_2SO_4 and 3% $MgSO_4$ (added by mass of cement)

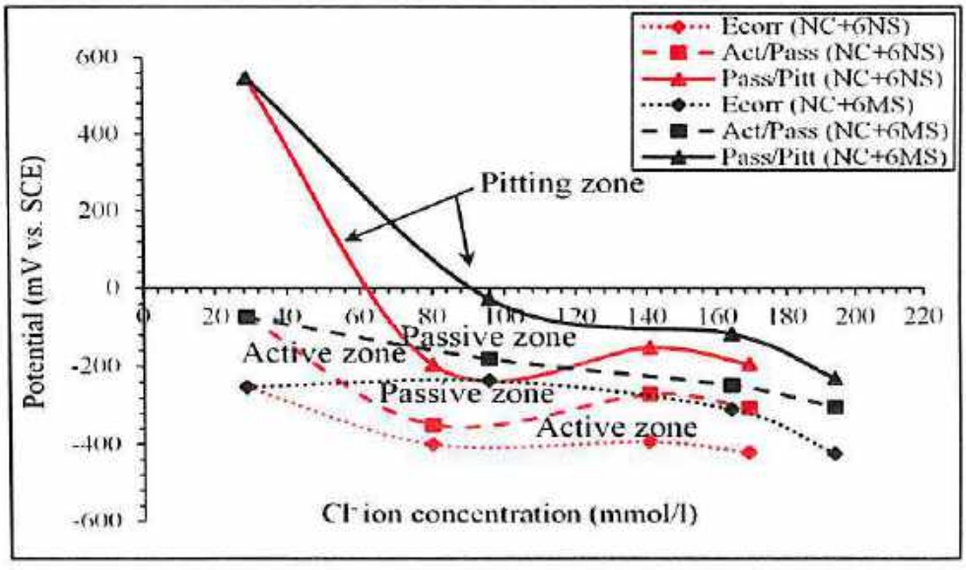

Fig. 5.14 Potential vs. Cl^- ion concentration of Tempcore TMT steel in ECPS prepared from OPC and w/c ratio of 0.45 and admixed with 0%, 3%, 5% and 7% NaCl plus 6% Na_2SO_4 and 6% $MgSO_4$ (added by mass of cement)

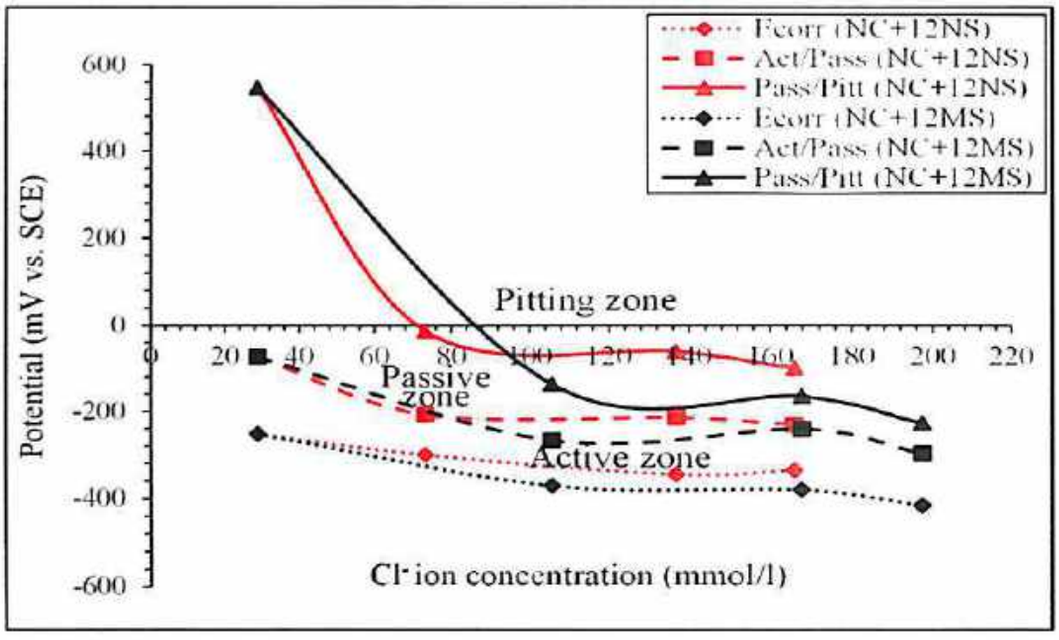

Fig. 5.15 Potential vs. Cl^- ion concentration of Tempcore TMT steel in ECPS prepared from OPC and w/c ratio of 0.45 and admixed with 0%, 3%, 5% and 7% NaCl plus 12% Na_2SO_4 and 12% $MgSO_4$ (added by mass of cement)

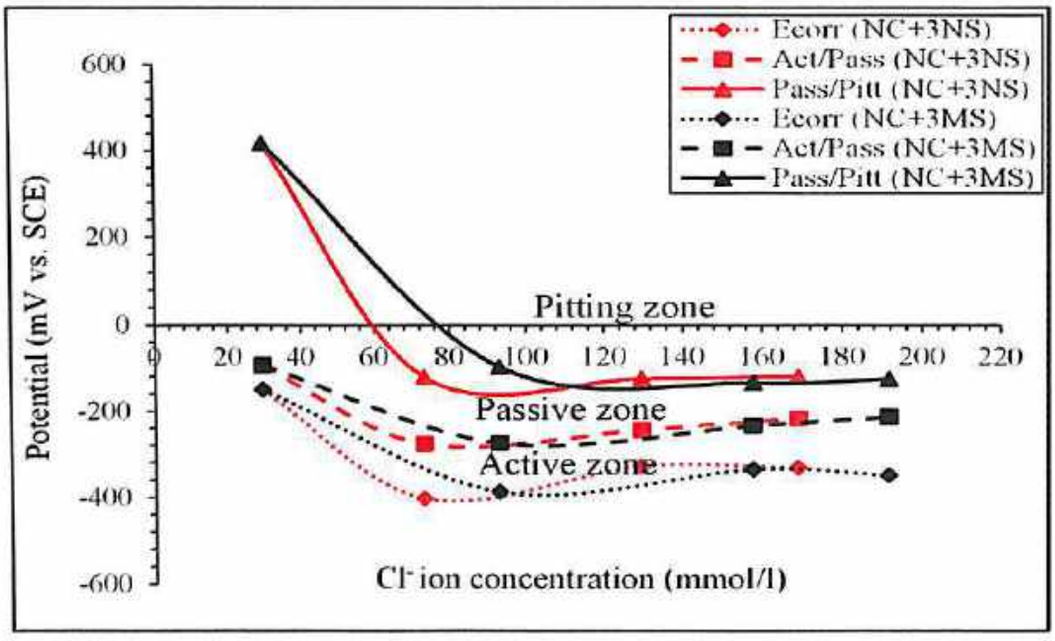

Fig. 5.16 Potential vs. Cl^- ion concentration of Tempcore TMT steel in ECPS prepared from PPC and w/c ratio of 0.45 and admixed with 0%, 3%, 5% and 7% NaCl plus 3% Na_2SO_4 and 3% $MgSO_4$ (added by mass of cement)

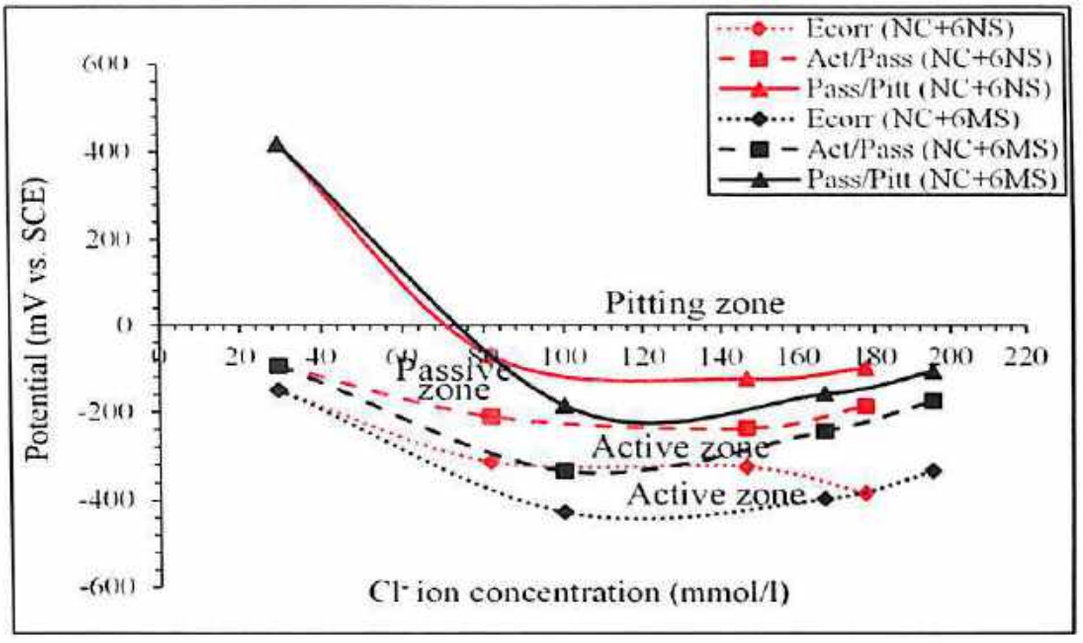

Fig. 5.17 Potential vs. Cl^- ion concentration of Tempcore TMT steel in ECPS prepared from PPC and w/c ratio of 0.45 and admixed with 0%, 3%, 5% and 7% NaCl plus 6% Na_2SO_4 and 6% $MgSO_4$ (added by mass of cement)

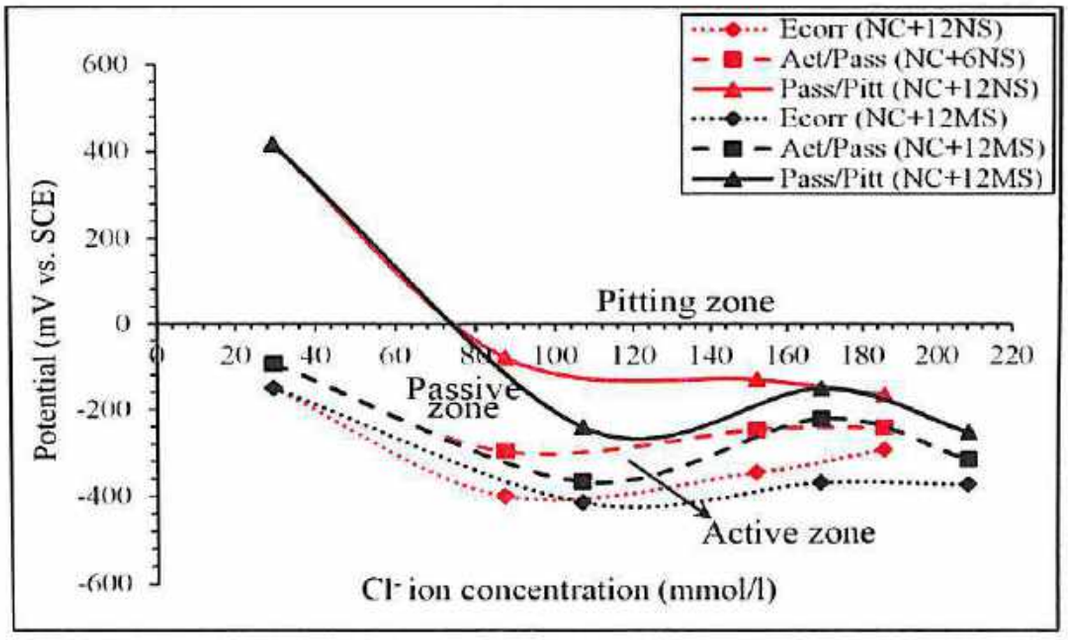

Fig. 5.18 Potential vs. Cl^- ion concentration of Tempcore TMT steel in ECPS prepared from PPC and w/c ratio of 0.45 and admixed with 0%, 3%, 5% and 7% NaCl plus 12% Na_2SO_4 and 12% $MgSO_4$ (added by mass of cement)

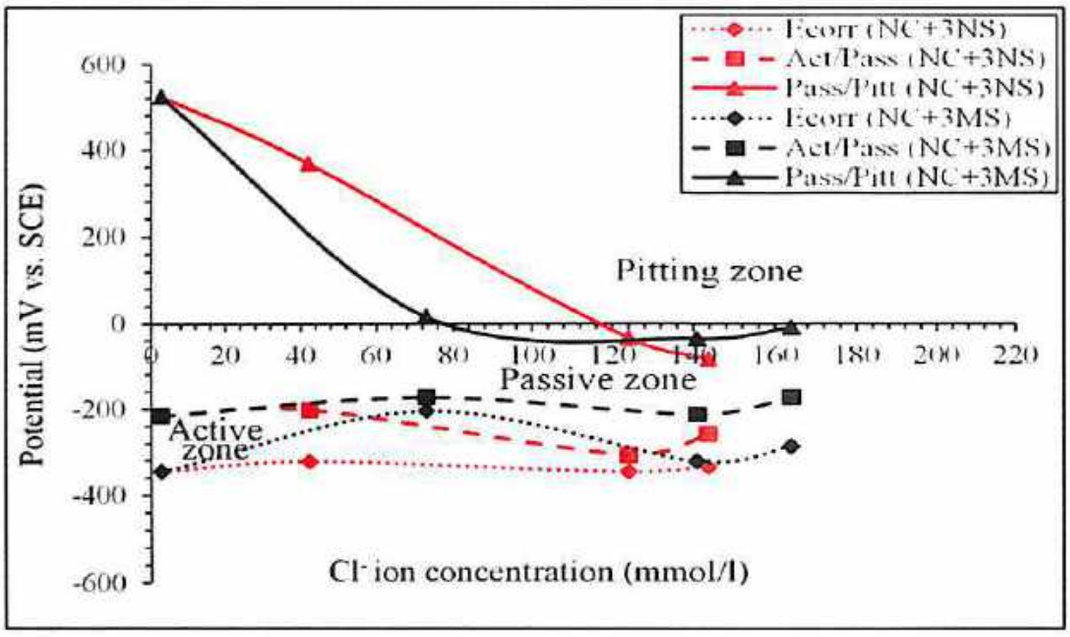

Fig. 5.19 Potential vs. Cl^- ion concentration of Tempcore TMT steel in ECPS prepared from OPC and w/c ratio of 0.5 and admixed with 0%, 3%, 5% and 7% NaCl plus 3% Na_2SO_4 and 3% $MgSO_4$ (added by mass of cement)

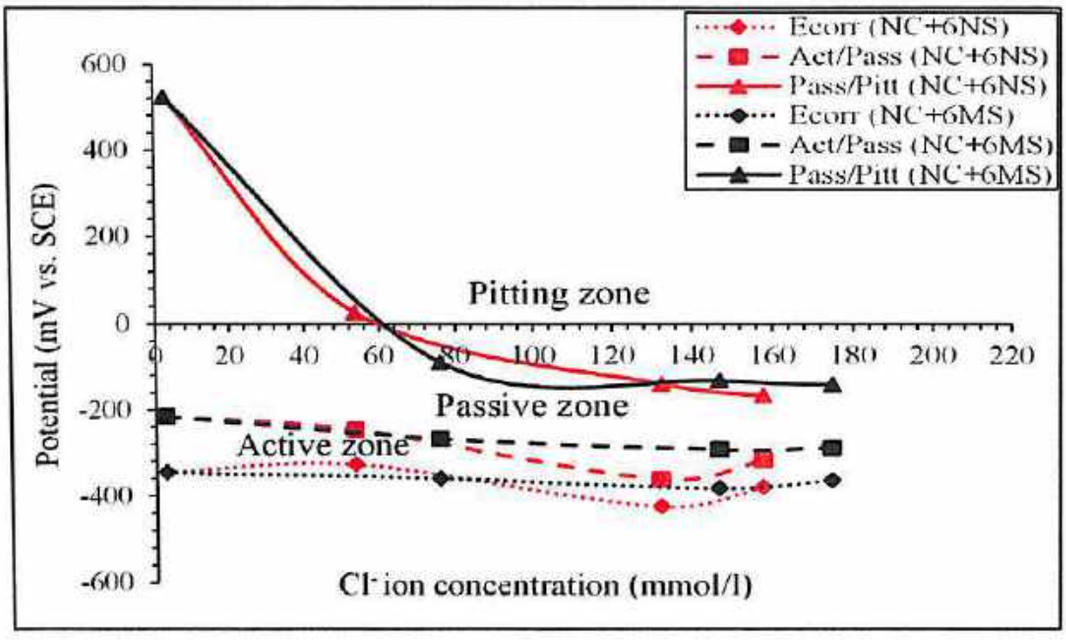

Fig. 5.20 Potential vs. Cl^- ion concentration of Tempcore TMT steel in ECPS prepared from OPC and w/c ratio of 0.5 and admixed with 0%, 3%, 5% and 7% NaCl plus 6% Na_2SO_4 and 6% $MgSO_4$ (added by mass of cement)

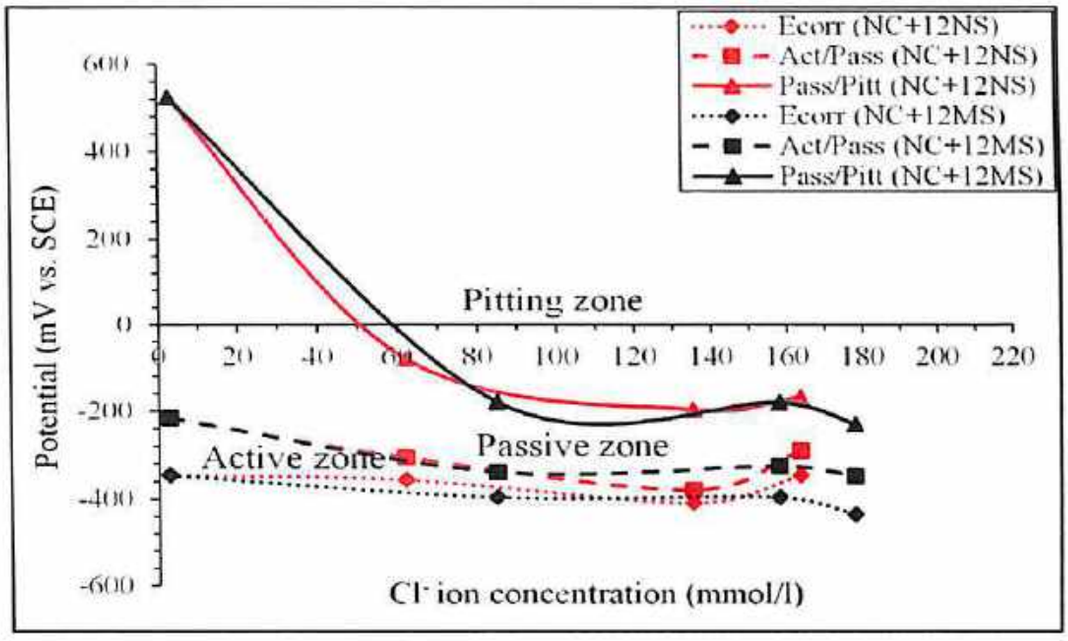

Fig. 5.21 Potential vs. Cl^- ion concentration of Tempcore TMT steel in ECPS prepared from OPC and w/c ratio of 0.5 and admixed with 0%, 3%, 5% and 7% NaCl plus 12% Na_2SO_4 and 12% $MgSO_4$ (added by mass of cement)

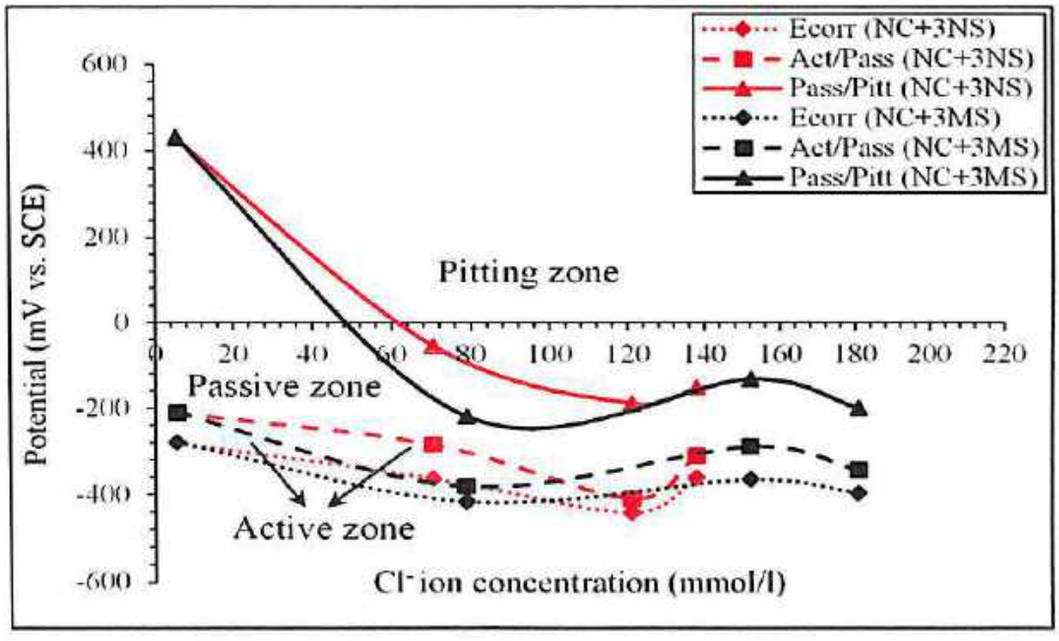

Fig. 5.22 Potential vs. Cl^- ion concentration of Tempcore TMT steel in ECPS prepared from PPC and w/c ratio of 0.5 and admixed with 0%, 3%, 5% and 7% NaCl plus 3% Na_2SO_4 and 3% $MgSO_4$ (added by mass of cement)

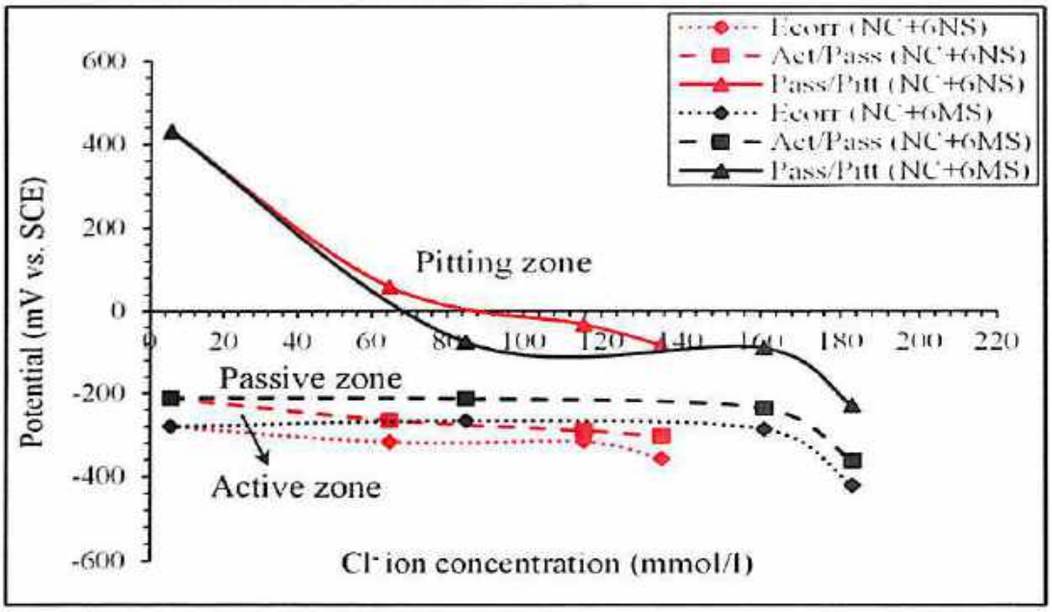

Fig. 5.23 Potential vs. Cl^- ion concentration of Tempcore TMT steel in ECPS prepared from PPC and w/c ratio of 0.5 and admixed with 0%, 3%, 5% and 7% NaCl plus 6% Na_2SO_4 and 6% $MgSO_4$ (added by mass of cement)

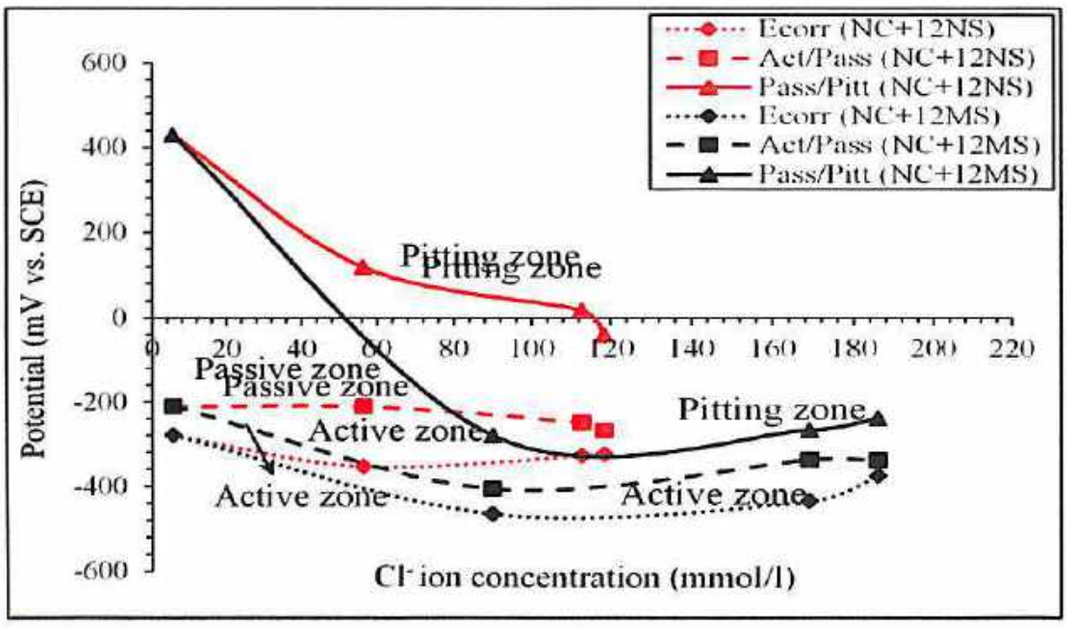

Fig. 5.24 Potential vs. Cl^- ion concentration of Tempcore TMT steel in ECPS prepared from PPC and w/c ratio of 0.5 and admixed with 0%, 3%, 5% and 7% NaCl plus 12% Na_2SO_4 and 12% $MgSO_4$ (added by mass of cement)

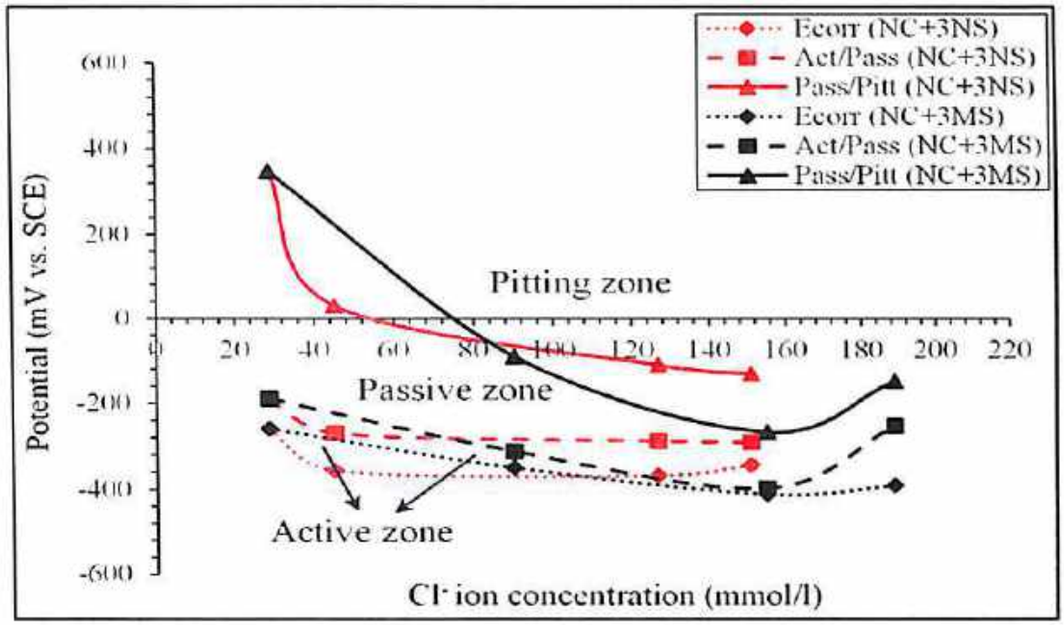

Fig. 5.25 Potential vs. Cl^- ion concentration of Thermex TMT steel in ECPS prepared from OPC and w/c ratio of 0.45 and admixed with 0%, 3%, 5% and 7% NaCl plus 3% Na_2SO_4 and 3% $MgSO_4$ (added by mass of cement)

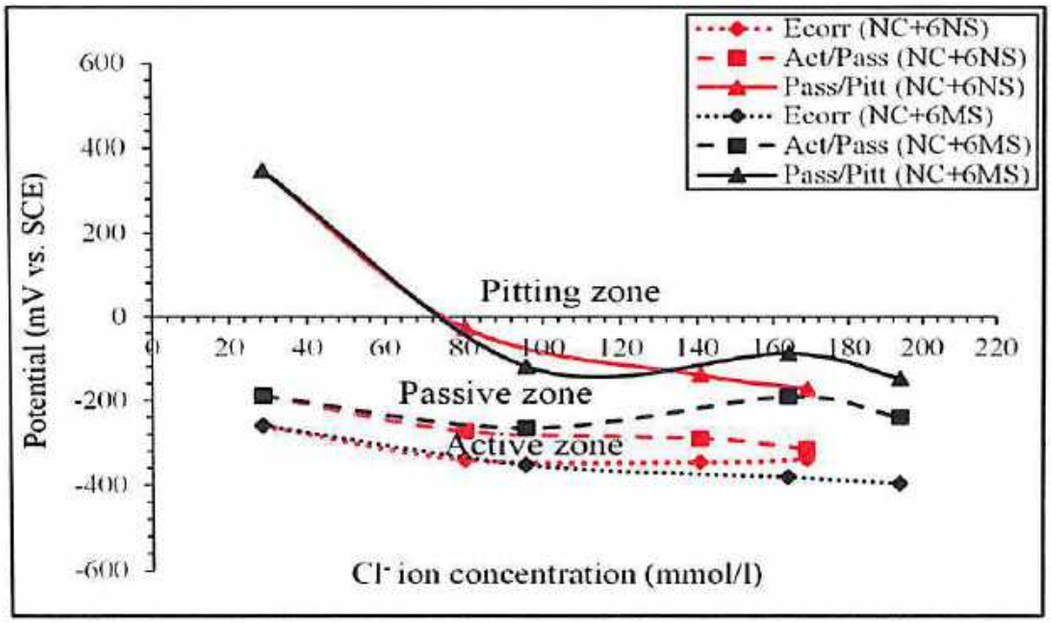

Fig. 5.26 Potential vs. Cl^- ion concentration of Thermex TMT steel in ECPS prepared from OPC and w/c ratio of 0.45 and admixed with 0%, 3%, 5% and 7% NaCl plus 6% Na_2SO_4 and 6% $MgSO_4$ (added by mass of cement)

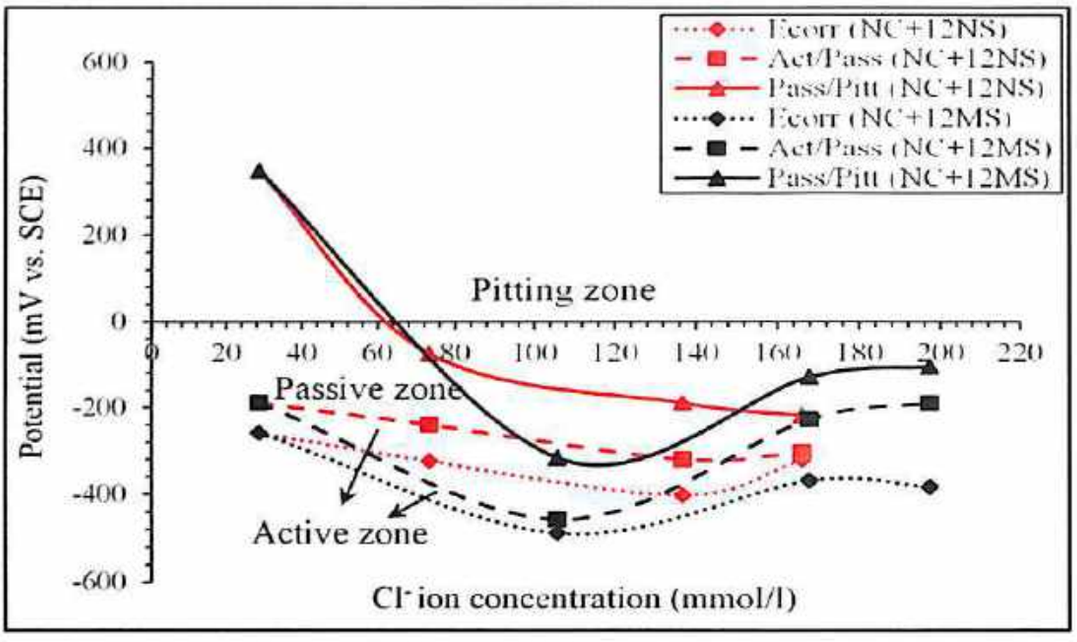

Fig. 5.27 Potential vs. Cl^- ion concentration of Thermex TMT steel in ECPS prepared from OPC and w/c ratio of 0.45 and admixed with 0%, 3%, 5% and 7% NaCl plus 12% Na_2SO_4 and 12% $MgSO_4$ (added by mass of cement)

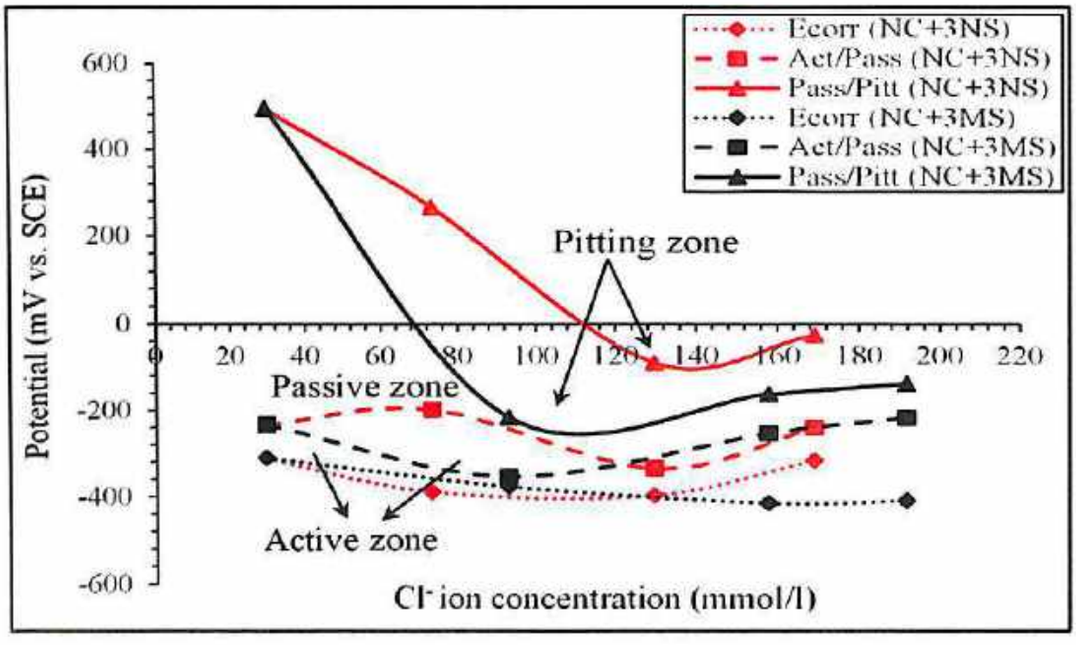

Fig. 5.28 Potential vs. Cl^- ion concentration of Thermex TMT steel in ECPS prepared from PPC and w/c ratio of 0.45 and admixed with 0%, 3%, 5% and 7% NaCl plus 3% Na_2SO_4 and 3% $MgSO_4$ (added by mass of cement)

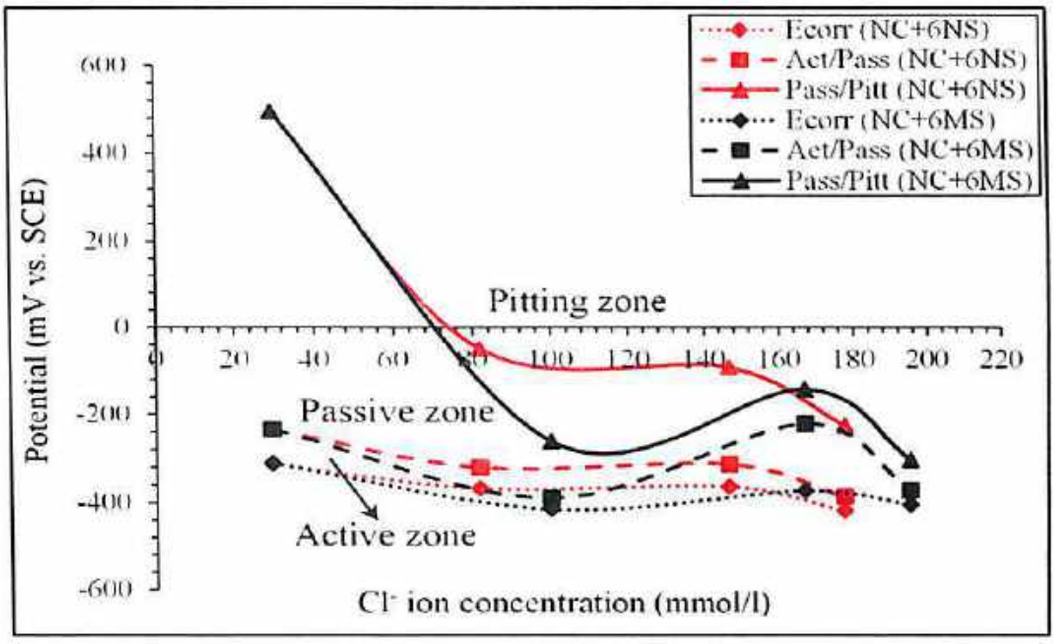

Fig. 5.29 Potential vs. Cl^- ion concentration of Thermex TMT steel in ECPS prepared from PPC and w/c ratio of 0.45 and admixed with 0%, 3%, 5% and 7% NaCl plus 6% Na_2SO_4 and 6% $MgSO_4$ (added by mass of cement)

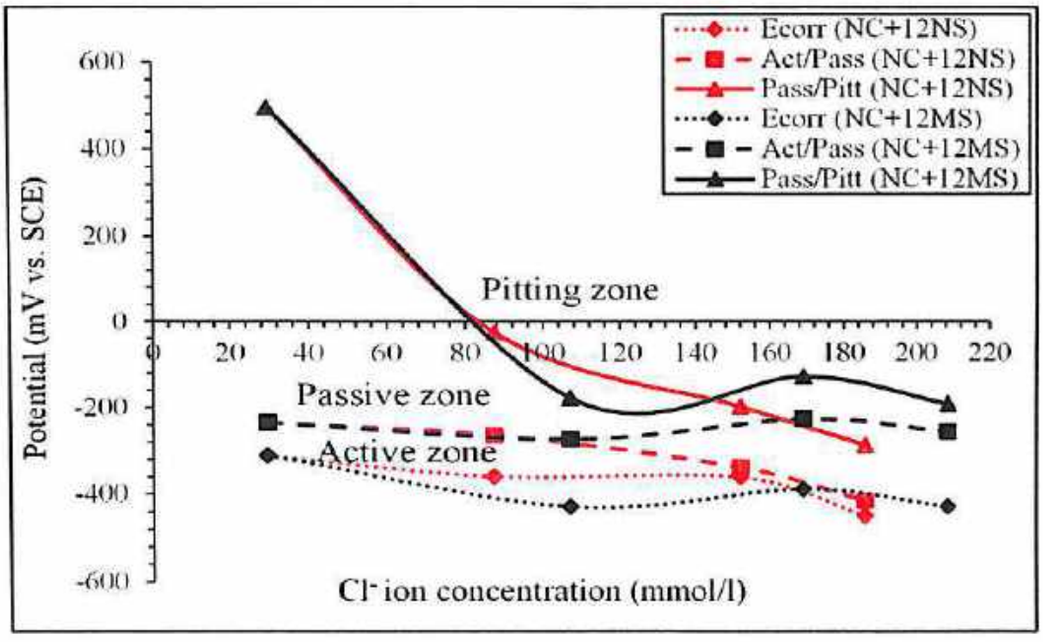

Fig. 5.30 Potential vs. Cl^- ion concentration of Thermex TMT steel in ECPS prepared from PPC and w/c ratio of 0.45 and admixed with 0%, 3%, 5% and 7% NaCl plus 12% Na_2SO_4 and 12% $MgSO_4$ (added by mass of cement)

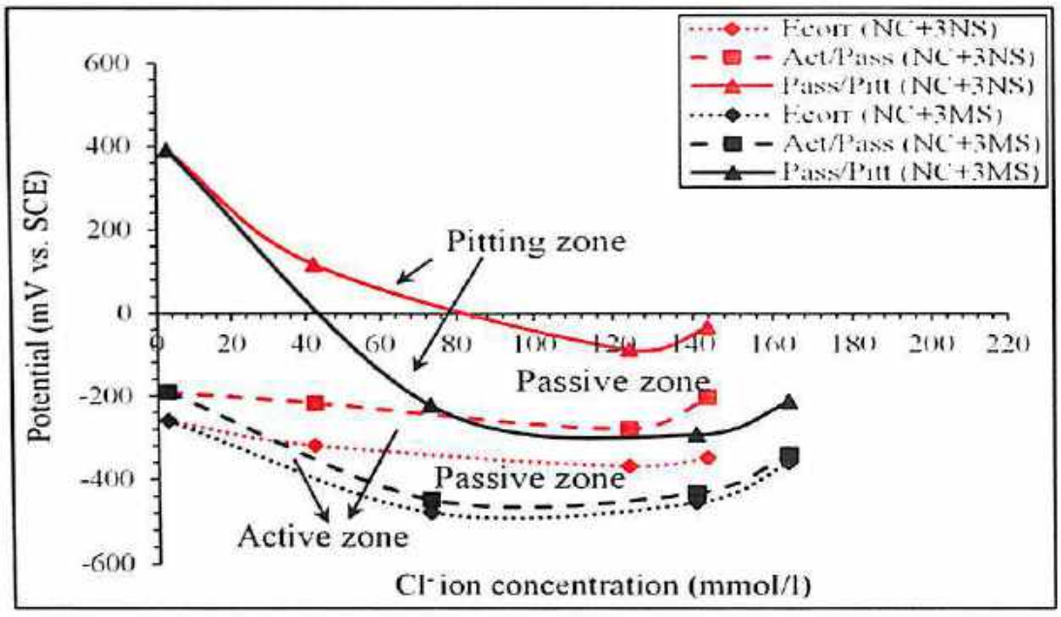

Fig. 5.31 Potential vs. Cl^- ion concentration of Thermex TMT steel in ECPS prepared from OPC and w/c ratio of 0.5 and admixed with 0%, 3%, 5% and 7% NaCl plus 3% Na_2SO_4 and 3% $MgSO_4$ (added by mass of cement)

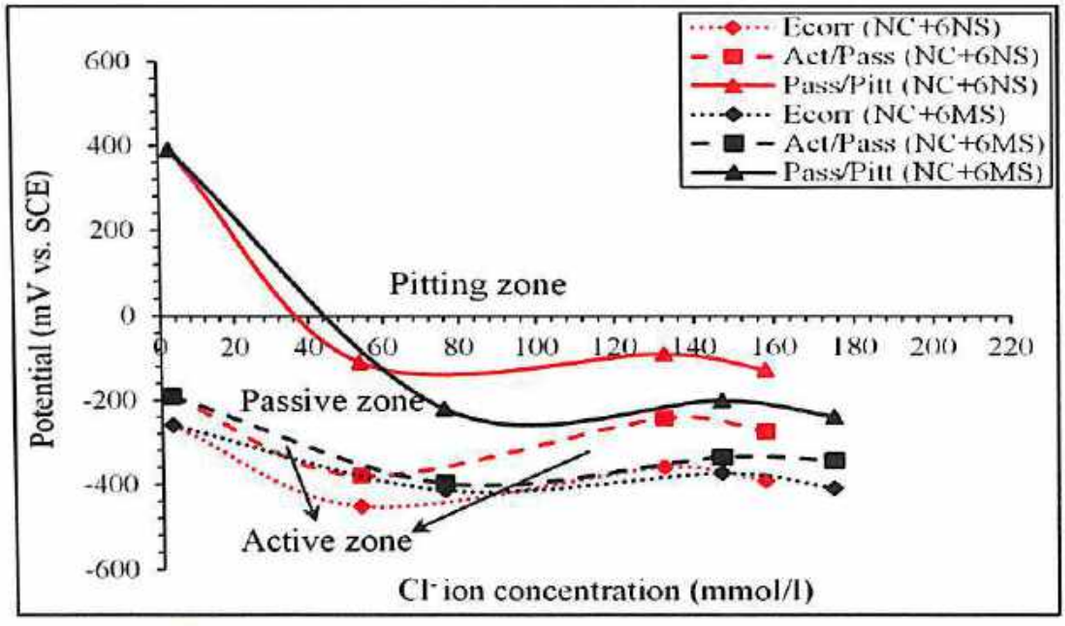

Fig. 5.32 Potential vs. Cl^- ion concentration of Thermex TMT steel in ECPS prepared from OPC and w/c ratio of 0.5 and admixed with 0%, 3%, 5% and 7% NaCl plus 6% Na_2SO_4 and 6% $MgSO_4$ (added by mass of cement)

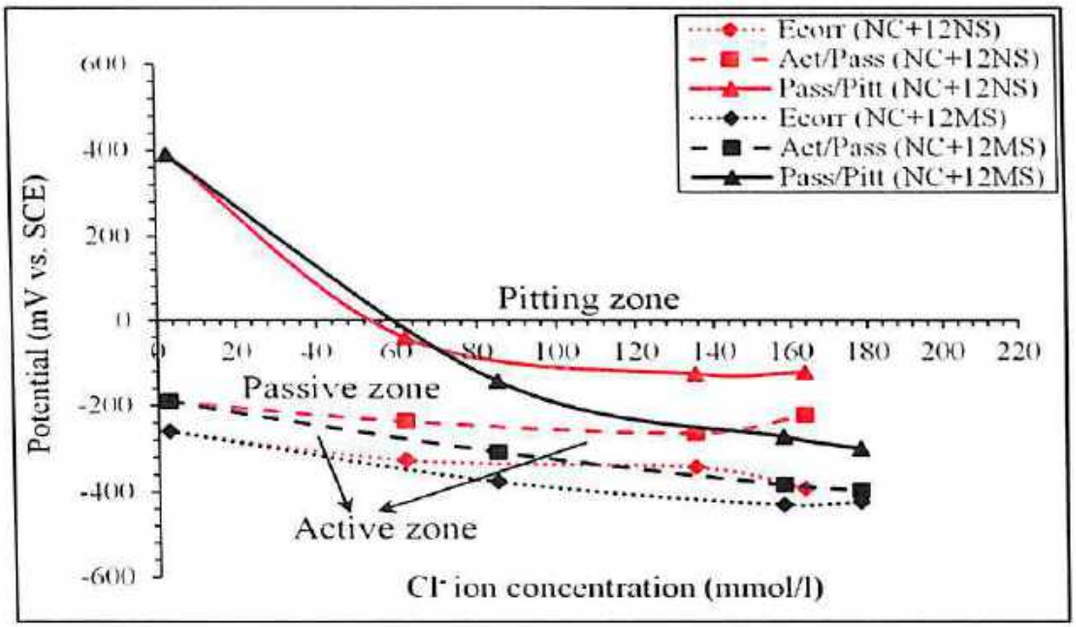

Fig. 5.33 Potential vs. Cl^- ion concentration of Thermex TMT steel in ECPS prepared from OPC and w/c ratio of 0.5 and admixed with 0%, 3%, 5% and 7% NaCl plus 12% Na_2SO_4 and 12% $MgSO_4$ (added by mass of cement)

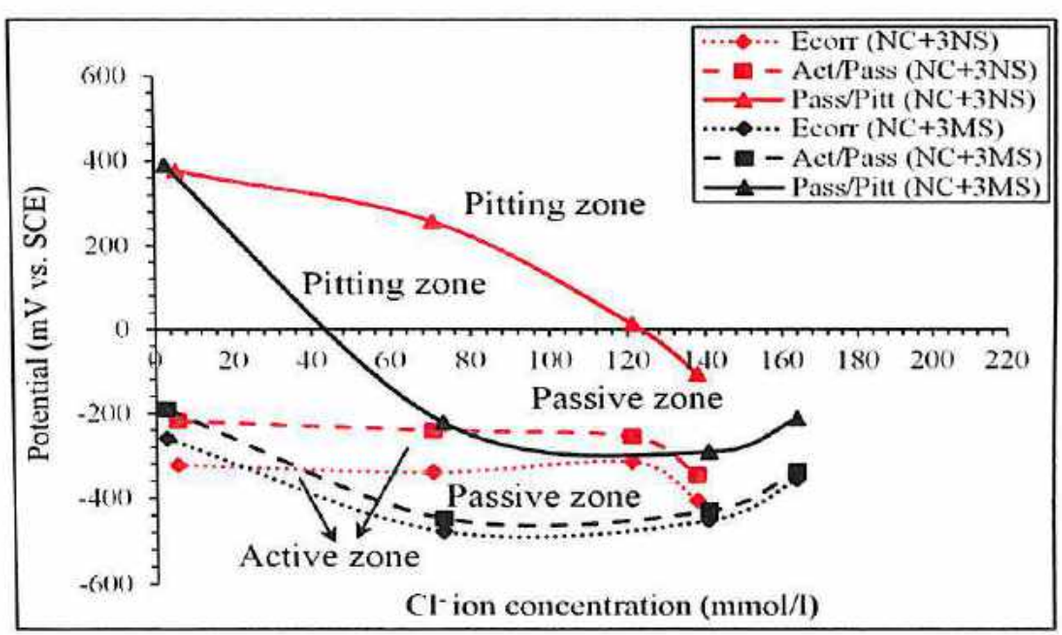

Fig. 5.34 Potential vs. Cl^- ion concentration of Thermex TMT steel in ECPS prepared from PPC and w/c ratio of 0.5 and admixed with 0%, 3%, 5% and 7% NaCl plus 3% Na_2SO_4 and 3% $MgSO_4$ (added by mass of cement)

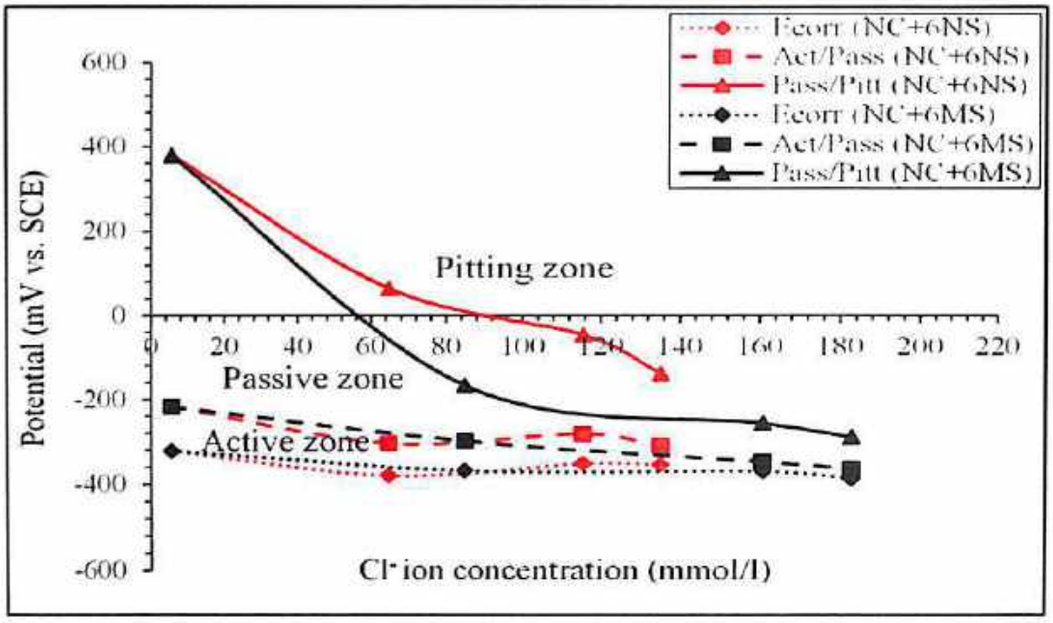

Fig. 5.35 Potential vs. Cl^- ion concentration of Thermex TMT steel in ECPS prepared from PPC and w/c ratio of 0.5 and admixed with 0%, 3%, 5% and 7% NaCl plus 6% Na_2SO_4 and 6% $MgSO_4$ (added by mass of cement)

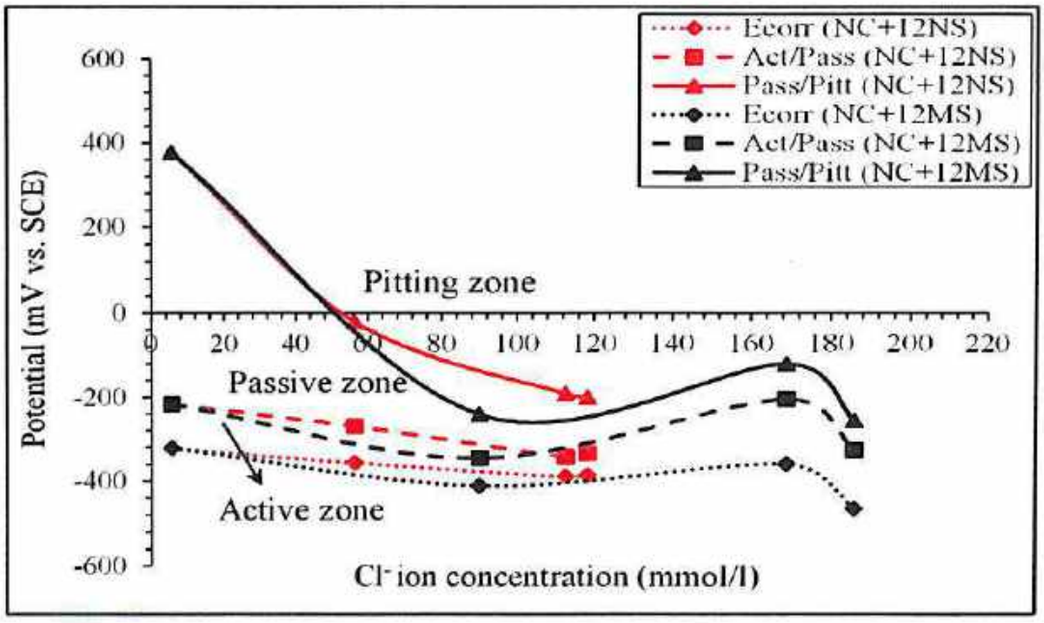

Fig. 5.36 Potential vs. Cl^- ion concentration of Thermex TMT steel in ECPS prepared from PPC and w/c ratio of 0.5 and admixed with 0%, 3%, 5% and 7% NaCl plus 12% Na_2SO_4 and 12% $MgSO_4$ (added by mass of cement)

5.2.1.2.3 Comparison between Chloride Contamination and Conjoint Chloride-Sulfate Contamination in ECPS on Passivity of Steel Reinforcement

For Tempcore TMT steel, the range of passive zone in the electrolytic concrete powder solution (ECPS) contaminated with only sodium chloride is less as compared to that in the ECPS contaminated with sodium chloride plus sodium sulfate in both OPC and PPC and at both w/c ratios. The similar behaviour was also observed for Thermex TMT steel. This indicates that the presence of sodium sulfate in chloride environment has mitigated the effect of chloride ions on reducing the passivity of reinforcing steel. Further, for Tempcore TMT steel the range of passive zone is more in the ECPS contaminated with only sodium chloride as compared to that in the conjoint presence of sodium chloride and magnesium sulfate. This indicates that the presence of magnesium sulfate in chloride environment has stimulated the effect of chloride ions on reducing the passivity of steel reinforcement. It may be also noted that lower Cl^- ion concentration was found in the concrete mixes contaminated with NaCl plus Na_2SO_4 whereas higher Cl^- ion concentration was found in the concrete mixes contaminated with NaCl plus $MgSO_4$ as compared to that contaminated with only NaCl. For Thermex TMT steel, the range of passive zone is less in the electrolytic concrete powder solution contaminated with only sodium chloride as compared to that in the conjoint presence of sodium chloride and magnesium sulfate. This indicates that Thermex TMT steel performed better in the conjoint presence of NaCl and $MgSO_4$ in maintaining the passivity as compared to that in the presence of only NaCl. Although higher Cl^- ion concentration was found in the concrete mixes contaminated with NaCl plus $MgSO_4$ as compared to that in the concrete mixes contaminated with only NaCl, the better performance of Thermex TMT steel in the conjoint presence of NaCl plus $MgSO_4$ may be attributed to its surface microstructure. On comparing the effect of cation type (Na^+ and Mg^{++}) associated with sulfate ions, it is observed that the range of passive zone of both Tempcore TMT and Thermex TMT steel is more in NaCl plus Na_2SO_4 environment as compared to that in NaCl plus $MgSO_4$ environment for both types of cement and w/c ratio. This implies that Mg-oriented sulfate attack is more aggressive in the presence of chloride ions in reducing the passivity of steel reinforcement as compared to Na-oriented sulfate attack.

5.2.2 Corrosion Parameters of Steel Reinforcement in Electrolytic Concrete Powder Solution from LPR Measurement

The linear polarization resistance (LPR) measurement was carried out on steel reinforcement in electrolytic concrete powder solutions and the details about the experimental work are already presented in Chapter 3. During LPR measurement, the corrosion potential of steel reinforcement was measured with reference to saturated calomel electrode (SCE) and the corrosion current density was determined using Stern-Geary equation. Two replicate steel specimens were tested for a given electrolytic concrete powder solution to observe the reproducibility and the average value of two replicate steel specimens was reported as the representative value.

5.2.2.1 Corrosion Potential

The corrosion potential provides qualitative information about the occurrence of steel reinforcement corrosion. As per ASTM C 876 [133], the threshold potential for occurrence of steel reinforcement corrosion is –270 mV (SCE) / –350 mV (CSE). The corrosion potential values more negative than -270 mV (SCE) indicate greater than 90% probability of occurrence of steel reinforcement corrosion in concrete. The corrosion potential of Tempcore TMT steel in uncontaminated electrolytic concrete powder solution prepared from control mix are -150 mV and -251 mV for OPC and PPC respectively at w/c ratio of 0.45 and -173 mV and -180 mV respectively at w/c ratio of 0.5. Similarly for Thermex TMT steel, the corrosion potentials in electrolytic concrete powder solution prepared from control mix are -186 mV and -195 mV respectively for OPC and PPC at w/c ratio of 0.45 and those at w/c ratio of 0.5 are -206 mV and -225 mV respectively. Thus the corrosion potential values of Tempcore TMT and Thermex TMT steel in uncontaminated electrolytic concrete powder solution made from control mix are less negative than -270 mV (SCE) for both types of cement and at both w/c ratios, which indicates lower probability of occurrence of steel reinforcement corrosion in uncontaminated concrete.

5.2.2.1.1 Effect of Sodium Chloride Contamination on Corrosion Potential of Steel Reinforcement in Electrolytic Concrete Powder Solution

The corrosion potential values of Tempcore TMT steel in electrolytic concrete powder solution (ECPS) prepared from OPC and PPC and admixed with 3%, 5% and 7% NaCl are shown in Fig. 5.37 and Fig. 5.38 respectively for w/c ratios of 0.45 and 0.5 and for Thermex TMT steel, the corrosion potential values are shown in Fig. 5.39 and Fig. 5.40 for w/c ratios of 0.45 and 0.5 respectively. In these figure, the corrosion potentials of steel in uncontaminated (0% admixed NaCl) electrolytic concrete powder solutions are also shown.

From the corrosion potential values shown in Fig. 5.37 to Fig. 5.40, it is observed that, the steel reinforcement in chloride contaminated electrolytic concrete powder solution exhibited more negative potentials as compared to that in uncontaminated electrolytic concrete powder solution. This indicates that the presence of Cl^- ions in the ECPS increased the probability of occurrence of corrosion of steel reinforcement. Further from Fig. 5.37 to Fig. 5.40 it is observed that, in the electrolytic concrete powder solutions admixed with varying concentrations of NaCl, the corrosion potentials were more negative than -270 mV (SCE) for both types of steel, cement and w/c ratio, thus indicating greater probability of occurrence of corrosion in the presence of chloride ions. Further, the corrosion potential values became more negative with increase in admixed NaCl concentration, which is attributed to increase in Cl^- ion concentration in the electrolytic concrete powder solution with increase in NaCl dosage.

While observing the effect of cement and steel type, it is found that OPC and Tempcore TMT steel showed less negative potential values as compared to PPC and Thermex TMT steel respectively at both w/c ratios in the presence of chloride ions. While observing the effect of w/c ratio, it is found that the corrosion potential values are marginally more negative at w/c ratio of 0.45 as compared to that at w/c ratio of 0.5 in most of the cases for both types of cement and steel reinforcement.

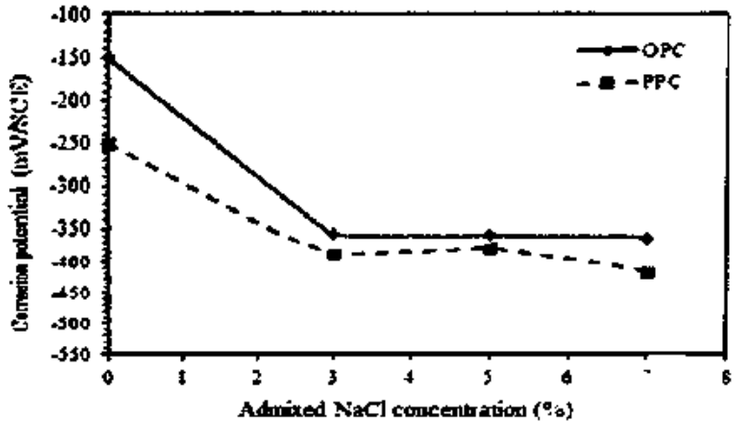

Fig. 5.37 Corrosion potential of Tempcore TMT steel in uncontaminated and contaminated (with varying concentrations of NaCl by mass of cement) ECPS prepared from OPC and PPC at w/c of 0.45

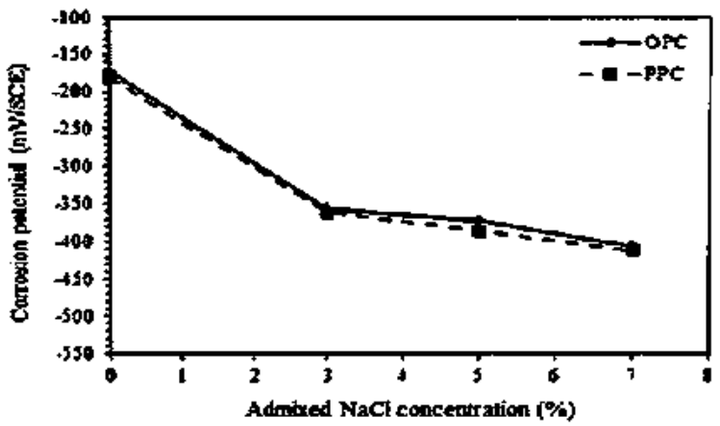

Fig. 5.38 Corrosion potential of Tempcore TMT steel in uncontaminated and contaminated (with varying concentrations of NaCl by mass of cement) ECPS prepared from OPC and PPC at w/c of 0.5

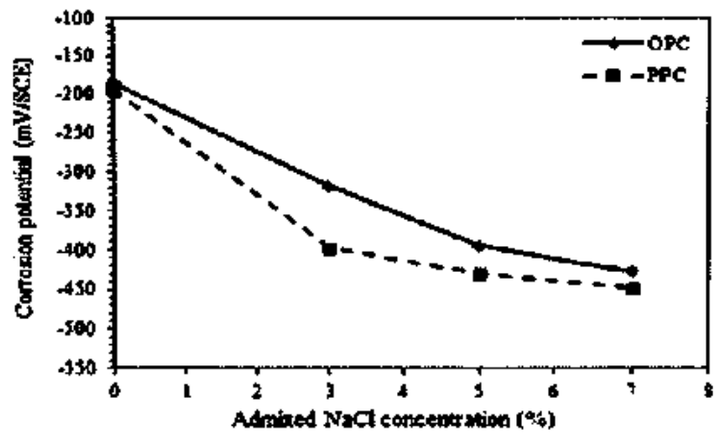

Fig. 5.39 Corrosion potential of Thermex TMT steel in uncontaminated and contaminated (with varying concentrations of NaCl by mass of cement) ECPS prepared from OPC and PPC at w/c of 0.45

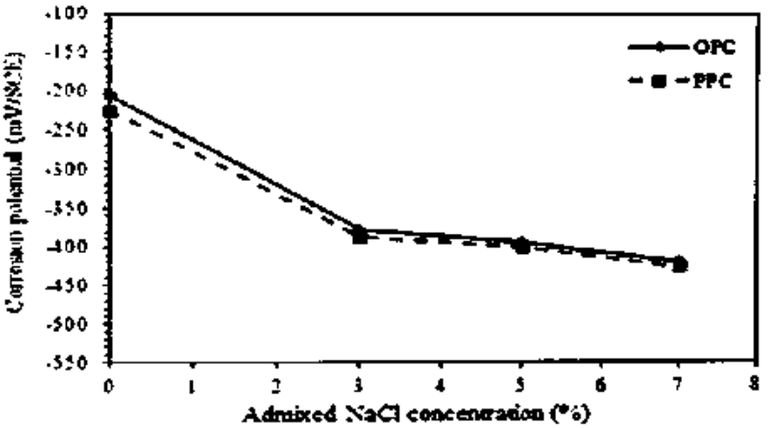

Fig. 5.40 Corrosion potential of Thermex TMT steel in uncontaminated and contaminated (with varying concentrations of NaCl by mass of cement) ECPS prepared from OPC and PPC at w/c of 0.5

5.2.2.1.2 Effect of Conjoint Sodium Chloride and Sodium Sulfate Contamination on Corrosion Potential of Steel Reinforcement in Electrolytic Concrete Powder Solution

The corrosion potential values of Tempcore TMT steel in electrolytic concrete powder solution (ECPS) prepared from OPC and PPC and admixed with varying concentrations of sodium chloride plus sodium sulfate are shown in Fig. 5.41 and Fig. 5.42 at w/c ratios of 0.45 and 0.5 respectively. Similarly, the corrosion potential values of Thermex TMT steel in electrolytic concrete powder solution admixed with varying concentrations of sodium chloride plus sodium sulfate at w/c ratios of 0.45 and 0.5 are shown in Fig. 5.43 and Fig. 5.44 respectively.

From the obtained corrosion potential values, it is observed that the steel reinforcement in sodium chloride plus sodium sulfate contaminated ECPS exhibited more negative potentials as compared to that in uncontaminated ECPS. This indicates that there is higher probability of occurrence of steel reinforcement corrosion in concrete in the presence of NaCl and Na_2SO_4 as compared to that in control concrete. Further, the corrosion potential values were more negative than -270 mV (SCE) for both types of cement, steel and w/c ratio at all concentrations of NaCl plus Na_2SO_4 as observed from Fig. 5.41 to Fig. 5.44, thus showing active state of corrosion of steel reinforcement in concrete.

From Fig. 5.41 to Fig. 5.44, it is observed that the corrosion potential of both Tempcore TMT and Thermex TMT steel became more negative with an increase in admixed NaCl dosage for both OPC and PPC and at w/c ratios of 0.45 and 0.5 in the conjoint presence of NaCl plus Na_2SO_4. This is attributed to increase in Cl^- ion concentration with increase in

NaCl dosage (as mentioned in Table 4.7 and Table 4.8, Chapter 4) in the presence of $NaSO_4$, which leads to increase in the probability of occurrence of corrosion.

While examining the variations in corrosion potential of steel reinforcement with Na_2SO_4 concentration, it is observed from Fig. 5.41 that, the corrosion potential of Tempcore TMT steel became more negative with increase in Na_2SO_4 concentration up to 6% followed by less negative potential at 12% Na_2SO_4 concentration for both types of cement at w/c ratio of 0.45. This indicates that there is relatively lower probability of occurrence of corrosion of steel at higher dosage of Na_2SO_4 (12%) at w/c ratio of 0.45 in the conjoint presence of sodium chloride and sodium sulfate. At w/c ratio of 0.5, the corrosion potential of Tempcore TMT steel became more negative with increase in Na_2SO_4 concentration in electrolytic concrete powder solution prepared from OPC whereas the opposite behavior was observed in electrolytic concrete powder solution prepared from PPC i.e. the corrosion potential of Tempcore TMT steel became less negative with increase in Na_2SO_4 concentration in the conjoint presence of NaCl and Na_2SO_4 as observed from Fig. 5.42.

From Fig. 5.43 and Fig. 5.44, it is inferred that the corrosion potential of Thermex TMT steel became more negative with an increase in Na_2SO_4 concentration for both OPC and PPC and at both w/c ratios in the conjoint presence of NaCl plus Na_2SO_4. Further it is observed that the corrosion potential values of Thermex TMT steel are mostly more negative than those of Tempcore TMT steel in the presence of NaCl plus Na_2SO_4 except in PPC at w/c ratio of 0.45, wherein Thermex steel showed less negative potential values as compared to Tempcore TMT steel. This indicates that type of steel also plays a significant role in the initiation of corrosion of steel reinforcement in concrete.

While analyzing the effect of cement type on corrosion potential of steel reinforcement in the conjoint presence of NaCl and Na_2SO_4, it is observed (from Fig. 5.41 and Fig. 5.42) that at w/c ratio of 0.45 the corrosion potential of Tempcore TMT steel in electrolytic concrete powder solution prepared from PPC is more negative than that prepared from OPC, whereas at w/c ratio of 0.5, the corrosion potential of Tempcore TMT steel in PPC is less negative than that in OPC. This indicates that for Tempcore TMT steel, OPC performed better at w/c ratio of 0.45 whereas PPC performed better at w/c ratio of 0.5 in terms of probability of occurrence of steel reinforcement corrosion in the conjoint presence of NaCl and Na_2SO_4. From Fig. 5.43 and Fig. 5.44 it is observed that at both w/c ratios, the corrosion potential values of Thermex TMT steel in electrolytic concrete

powder solution prepared from OPC are more negative as compared to PPC. This indicates that PPC performed better as compared to OPC in terms of corrosion initiation of Thermex TMT steel. Further, it is observed that the corrosion potential values of steel reinforcement were mostly more negative at w/c ratio of 0.45 as compared to that at w/c ratio of 0.5 in the conjoint presence of NaCl and Na_2SO_4.

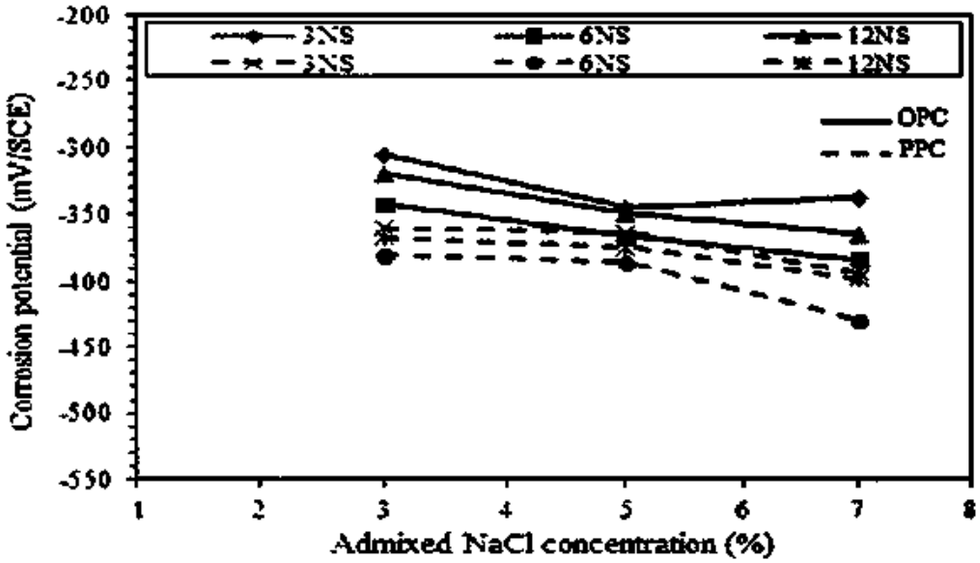

Fig. 5.41 Corrosion potentials of Tempcore TMT steel in ECPS prepared from OPC and PPC at w/c ratio of 0.45 and admixed with varying concentrations of NaCl plus Na_2SO_4 by mass of cement

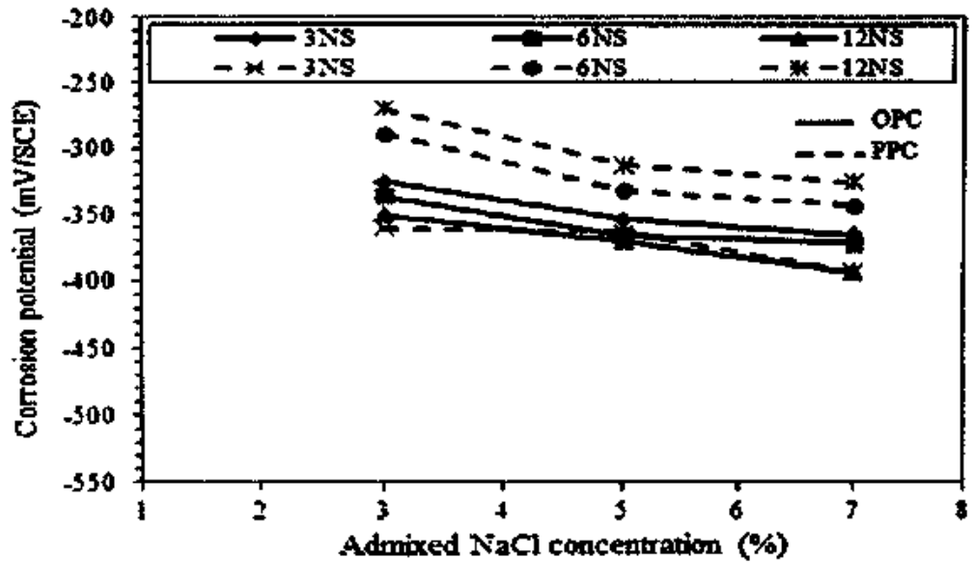

Fig. 5.42 Corrosion potentials of Tempcore TMT steel in ECPS prepared from OPC and PPC at w/c ratio of 0.5 and admixed with varying concentrations of NaCl plus Na_2SO_4 by mass of cement

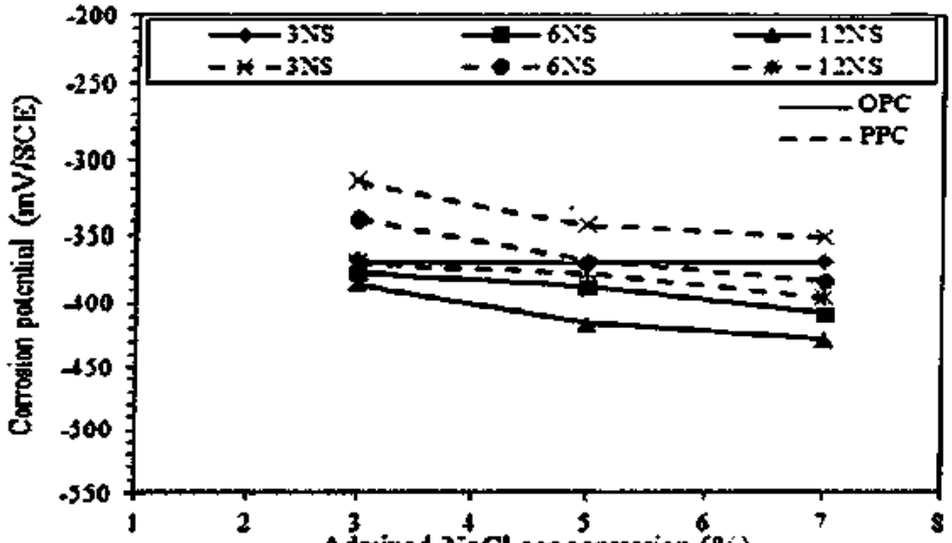

Fig. 5.43 Corrosion potentials of Thermex TMT steel in ECPS prepared from OPC and PPC at w/c ratio of 0.45 and admixed with varying concentrations of NaCl plus Na_2SO_4 by mass of cement

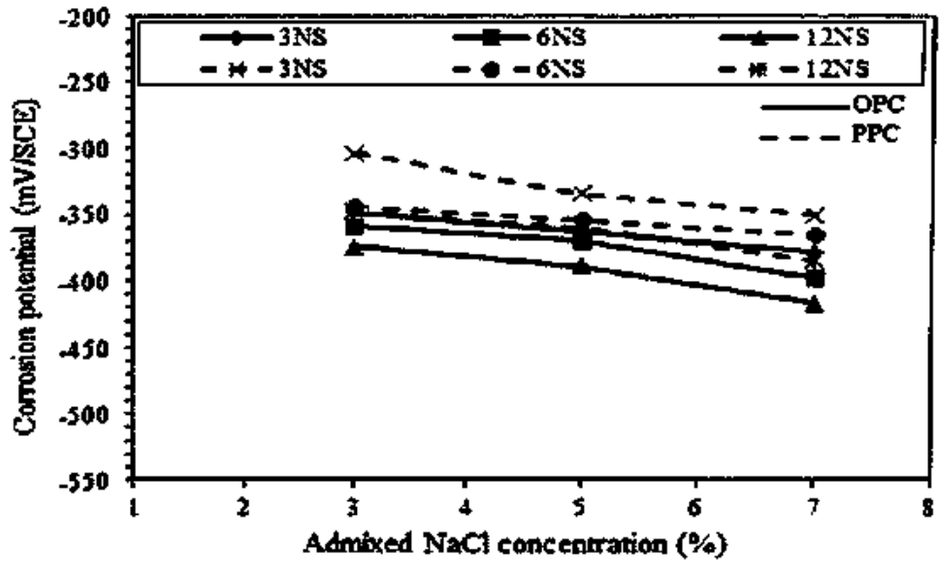

Fig. 5.44 Corrosion potentials of Thermex TMT steel in ECPS prepared from OPC and PPC at w/c ratio of 0.5 and admixed with varying concentrations of NaCl plus Na_2SO_4 by mass of cement

5.2.2.1.3 Effect of Conjoint Sodium Chloride and Magnesium Sulfate Contamination on Corrosion Potential of Steel Reinforcement in Electrolytic Concrete Powder Solution

The corrosion potential values of Tempcore TMT steel in electrolytic concrete powder solution (ECPS) prepared from OPC and PPC and contaminated with varying concentrations of sodium chloride plus magnesium sulfate are shown in Fig. 5.45 and Fig.

5.46 at w/c ratios of 0.45 and 0.5 respectively. Similarly the corrosion potential values of Thermex TMT steel are shown in Fig. 5.47 and Fig. 5.48 at w/c ratios of 0.45 and 0.5 respectively.

From Fig. 5.45 to Fig. 5.48, it is observed that, the steel reinforcement in sodium chloride plus magnesium sulfate contaminated ECPS exhibited more negative potential values as compared to that in uncontaminated ECPS, which indicates higher probability of occurrence of steel reinforcement corrosion in the conjoint presence of NaCl and $MgSO_4$. Further, it is inferred that the corrosion potential values were more negative than -270 mV (SCE) for both types of cement, steel and w/c ratio in the conjoint presence of sodium chloride and magnesium sulfate as evident from Fig. 5.45 to Fig. 5.48, which indicates that the steel reinforcement is in active state of corrosion in both OPC and PPC.

The corrosion potentials of both Tempcore TMT and Thermex TMT steel became more negative with an increase in NaCl dosage in both OPC and PPC at both w/c ratios in the conjoint presence of NaCl and $MgSO_4$ (as observed from Fig. 5.45 to Fig. 5.48), which is attributed to increase in Cl^- ion concentration with increase in NaCl dosage in the electrolytic concrete powder solution (as mentioned in Table 4.9 and Table 4.10, Chapter 4). In addition, from Fig. 5.45 to Fig. 5.48 it is observed that, the corrosion potential of both types of steel reinforcement became more negative with increase in $MgSO_4$ concentration in OPC and PPC at both w/c ratios. This indicates that the probability of occurrence of steel reinforcement corrosion increases with increase in $MgSO_4$ concentration in the conjoint presence of NaCl and $MgSO_4$.

While observing the effect of cement type it is found that both types of steel (Tempcore TMT and Thermex TMT) in PPC exhibited more negative corrosion potential values as compared to that in OPC at both w/c ratios and at all levels of NaCl plus $MgSO_4$ concentration. Similarly, the corrosion potential values of Thermex TMT steel were more negative as compared to that of Tempcore TMT steel at all levels of NaCl plus $MgSO_4$ concentrations. Thus, OPC and Tempcore TMT steel performed better as compared to PPC and Thermex TMT steel respectively in terms of probability of occurrence of steel reinforcement corrosion in the conjoint presence of NaCl and $MgSO_4$. Further, in the conjoint presence of NaCl and $MgSO_4$, the corrosion potential values of steel reinforcement were more negative at w/c ratio of 0.45 as compared to that at w/c ratio of 0.5 irrespective of cement type and steel type, as observed from Fig. 5.45 to Fig. 5.48.

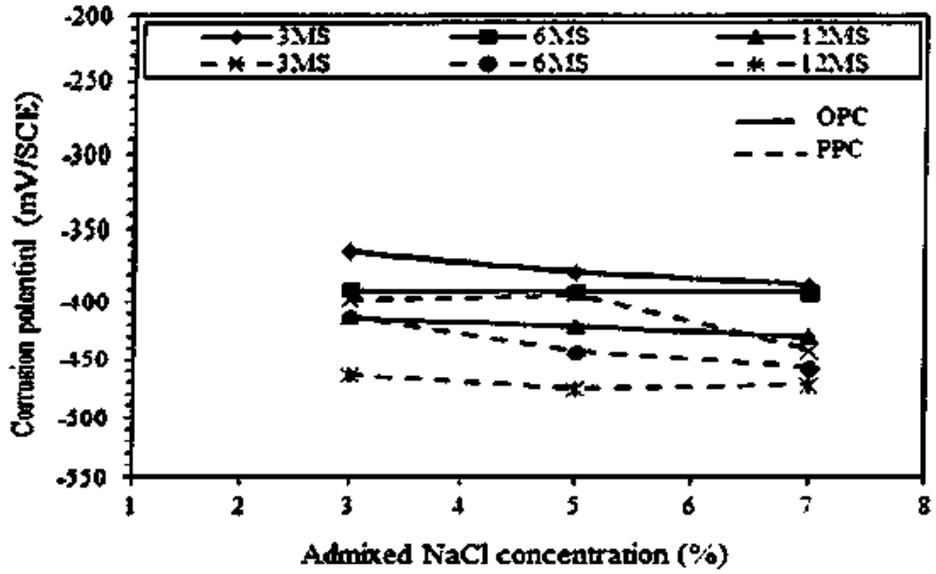

Fig. 5.45 Corrosion potentials of Tempcore TMT steel in ECPS prepared from OPC and PPC at w/c ratio 0f 0.45 and admixed with varying concentrations of NaCl plus $MgSO_4$ by mass of cement

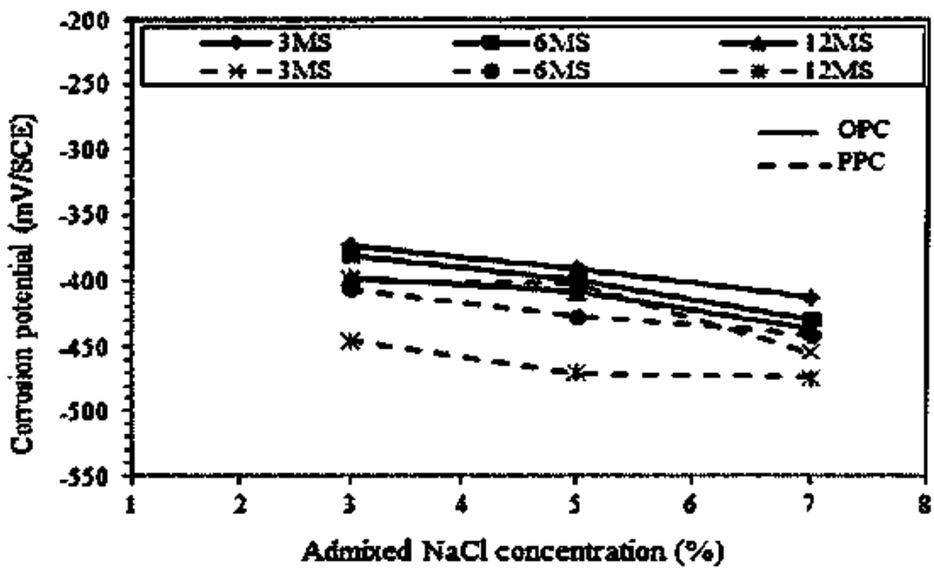

Fig. 5.46 Corrosion potentials of Tempcore TMT steel in ECPS prepared from OPC and PPC at w/c ratio 0f 0.5 and admixed with varying concentrations of NaCl plus $MgSO_4$ by mass of cement

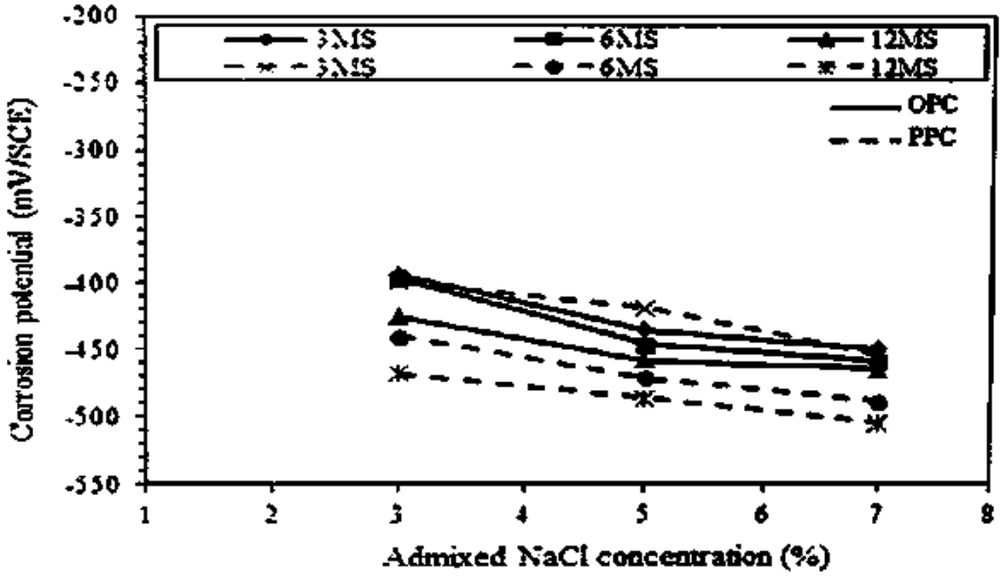

Fig. 5.47 Corrosion potentials of Thermex TMT steel in ECPS prepared from OPC and PPC at w/c ratio 0f 0.45 and admixed with varying concentrations of NaCl plus $MgSO_4$ by mass of cement

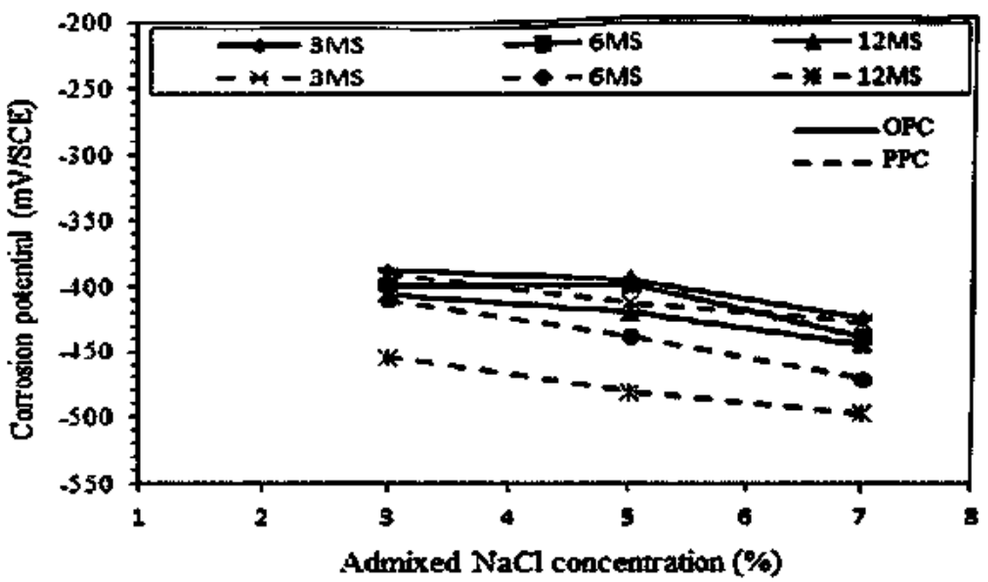

Fig. 5.48 Corrosion potentials of Thermex TMT steel in ECPS prepared from OPC and PPC at w/c ratio 0f 0.5 and admixed with varying concentrations of NaCl plus $MgSO_4$ by mass of cement

5.2.2.2 Corrosion Current Density

As stated earlier, linear polarization resistance (LPR) technique was used to determine the corrosion current density of steel reinforcement in electrolytic concrete powder solution. The corrosion current density values of Tempcore TMT steel reinforcement in electrolytic

concrete powder solution made from uncontaminated concrete are 0.05 $\mu A/cm^2$ and 0.07 $\mu A/cm^2$ respectively for OPC and PPC at w/c ratio of 0.45 and 0.03 $\mu A/cm^2$ and 0.06 $\mu A/cm^2$ respectively for OPC and PPC at w/c ratio of 0.5. Similarly for Thermex TMT steel, the corrosion current density values in uncontaminated electrolytic concrete powder solutions at w/c ratio of 0.45 are 0.2 $\mu A/cm^2$ and 0.12 $\mu A/cm^2$ respectively and at w/c ratio of 0.5 are 0.15 $\mu A/cm^2$ and 0.11 $\mu A/cm^2$ respectively for OPC and PPC. From these results, it is observed that the corrosion current density in PPC was higher than that in OPC for Tempcore TMT steel, whereas for Thermex TMT steel the corrosion current density in PPC was lower as compared to that in OPC in uncontaminated concrete. Further, Tempcore TMT steel exhibited lower values of corrosion current density as compared to Thermex TMT steel for both types of cement and w/c ratio. In addition, the corrosion current density of steel reinforcement was higher at w/c ratio of 0.45 as compared to that at w/c ratio of 0.5 in uncontaminated electrolytic concrete powder solutions prepared from both types of cement and for both types of steel reinforcement.

5.2.2.2.1 Effect of Sodium Chloride Contamination on Corrosion Current Density of Steel Reinforcement in Electrolytic Concrete Powder Solution

The variations in the corrosion current density of Tempcore steel in electrolytic concrete powder solutions prepared from OPC and PPC and contaminated with 3%, 5% and 7% NaCl are shown in Fig. 5.49 and Fig. 5.50 for w/c ratios of 0.45 and 0.5 respectively. Similarly, the variations in corrosion current density of Thermex TMT steel are shown in Fig. 5.51 and Fig. 5.52 for w/c ratios of 0.45 and 0.5 respectively. From these results, it is found that the corrosion current density of steel in chloride contaminated electrolytic concrete powder solutions is higher than that in uncontaminated electrolytic concrete powder solution, thus indicating increase in corrosion activity of steel reinforcement in chloride contaminated concrete.

From Fig. 5.49 to Fig. 5.52, it is observed that the corrosion current density of both Tempcore TMT and Thermex TMT steel increased with an increase in NaCl dosage in all concrete mixes. This is attributed to increase in Cl^- ion concentration in the electrolytic concrete powder solution with increase in NaCl dosage. The corrosion current density of Tempcore TMT steel varied from 6.9 $\mu A/cm^2$ to12.7 $\mu A/cm^2$ and that of Thermex TMT varied from 14.0 $\mu A/cm^2$ to 20.0 $\mu A/cm^2$ for different concentrations of NaCl irrespective of cement type and w/c ratio. From these values, it is observed Tempcore TMT steel

exhibited lower corrosion current density as compared to Thermex TMT steel in electrolytic concrete powder solution at all levels of NaCl contaminations. Thus Tempcore TMT steel is likely to show a longer corrosion propagation period.

While analyzing the effect of cement type, it is observed that the corrosion current density of steel in OPC was in the range of 6.9 $\mu A/cm^2$ to 18.2 $\mu A/cm^2$ and that in PPC was in the range of 9.6 $\mu A/cm^2$ to 18.8 $\mu A/cm^2$ irrespective of steel type and w/c ratio. The higher corrosion current density in PPC as compared to that in OPC for both types of steel and w/c ratio at all levels of NaCl contaminations may be attributed to higher conductivity in PPC concrete as compared to that in OPC concrete as result of higher Cl^- ion concentration in PPC than that in OPC (as observed from Table 4.5 and 4.6, Chapter 4). Thus, steel reinforcement in OPC is likely to exhibit longer propagation period as compared to that in PPC at both w/c ratios. Further from Fig. 5.49 to Fig. 5.52, it is observed that the corrosion current density is higher at w/c ratio of 0.45 as compared to that at w/c ratio of 0.5 for both types of cement and steel in electrolytic concrete powder solution admixed with NaCl. Thus from the results, it is inferred that the combination of Tempcore TMT steel and OPC at w/c ratio of 0.5 is likely perform better in terms of exhibiting longer corrosion propagation period in chloride contaminated concrete.'

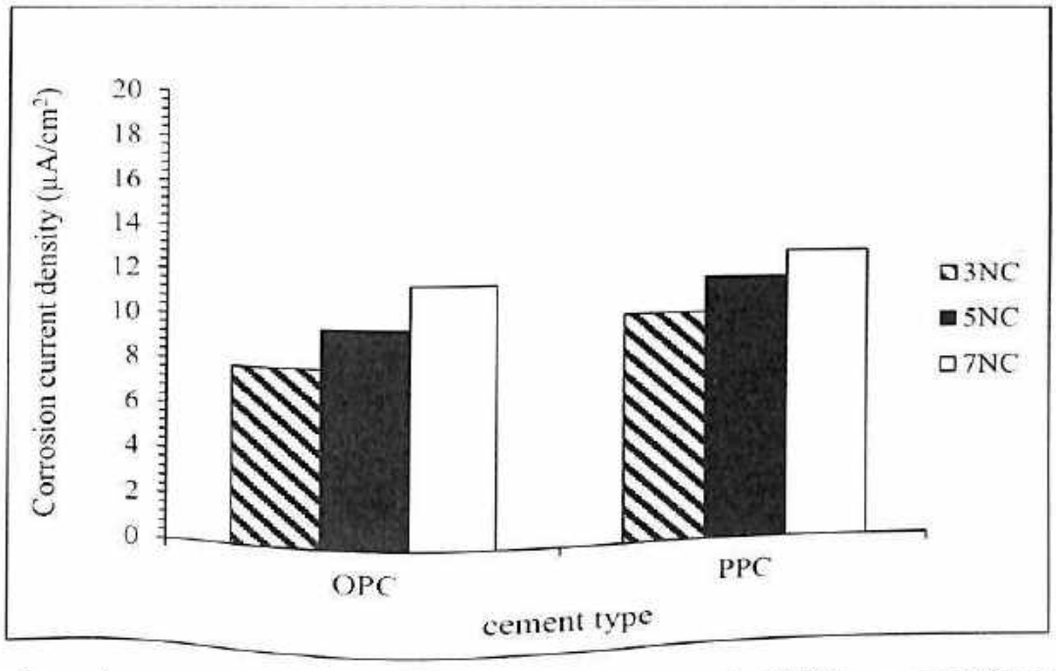

Fig. 5.49 Corrosion current density of Tempcore TMT steel in ECPS prepared from OPC and PPC at w/c of 0.45 and admixed with varying concentrations of NaCl by mass of cement

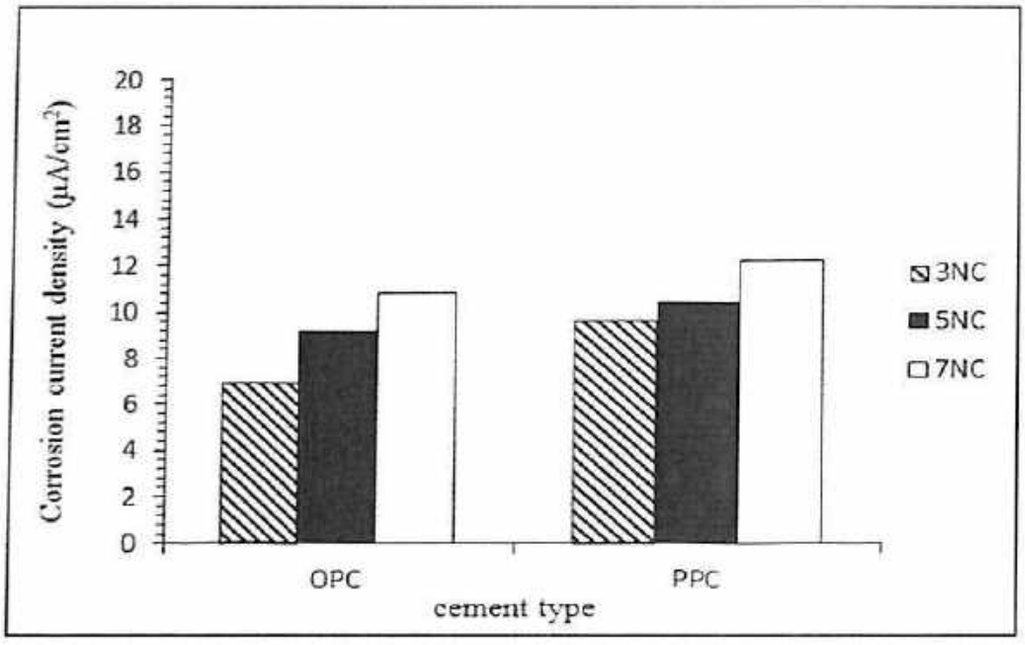

Fig. 5.50 Corrosion current density of Tempcore TMT steel in ECPS prepared from OPC and PPC at w/c of 0.5 and admixed with varying concentrations of NaCl by mass of cement

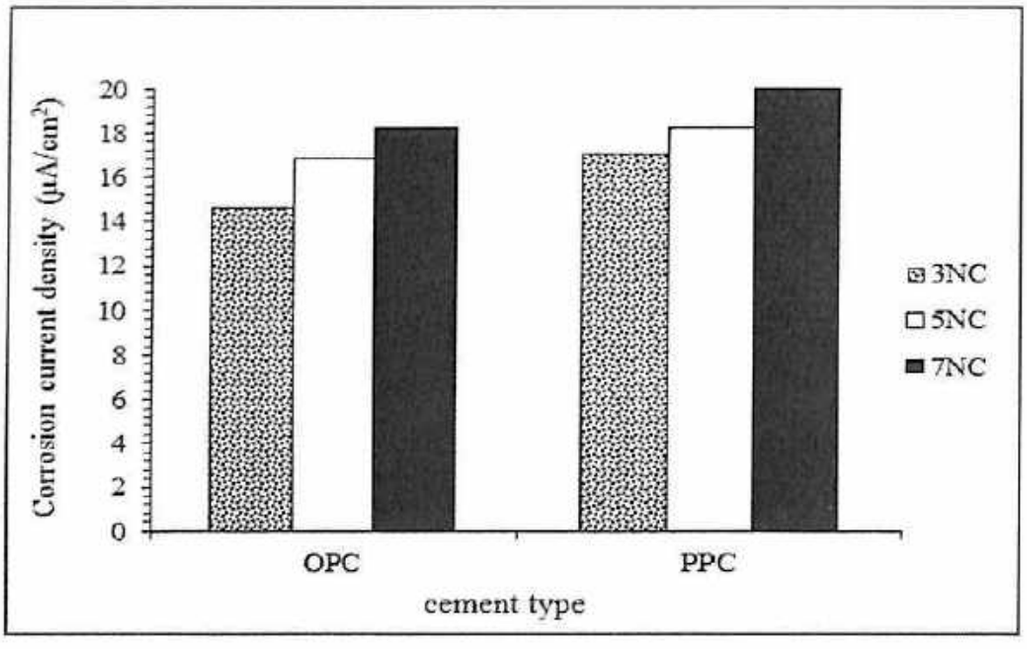

Fig. 5.51 Corrosion current density of Thermex TMT steel in ECPS prepared from OPC and PPC at w/c of 0.45 and admixed with varying concentrations of NaCl by mass of cement

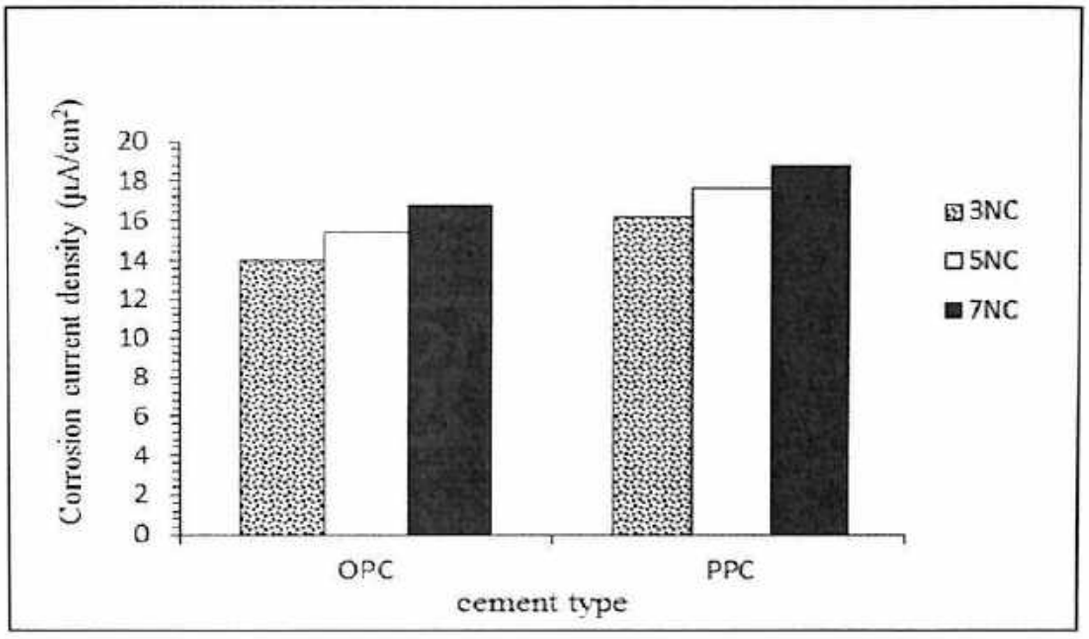

Fig. 5.52 Corrosion current density of Thermex TMT steel in ECPS prepared from OPC and PPC at w/c of 0.5 and admixed with varying concentrations of NaCl by mass of cement

5.2.2.2.2 Effect of Conjoint Sodium Chloride and Sodium Sulfate on Corrosion Current Density of Steel Reinforcement in Electrolytic Concrete Powder Solution

The variations in the corrosion current density of steel reinforcement in electrolytic concrete powder solutions prepared from OPC and PPC and contaminated with varying concentrations of sodium chloride plus sodium sulfate are shown in Fig. 5.53 and Fig. 5.54 at w/c ratios of 0.45 and 0.5 respectively for Tempcore TMT steel and in Fig. 5.55 and Fig. 5.56 for Thermex TMT steel. On comparison with uncontaminated electrolytic concrete powder solution, it is observed that the corrosion current density of steel reinforcement in sodium chloride plus sodium sulfate contaminated electrolytic concrete powder solution is higher than that in uncontaminated electrolytic concrete powder solution. This indicates increase in corrosion activity of steel reinforcement in the conjoint presence of chloride and sulfate ions in concrete.

From the results shown in Fig. 5.53 to Fig. 5.56, it is observed that the corrosion current density of both Tempcore TMT and Thermex TMT steel increased with an increase in NaCl concentration in the conjoint presence of NaCl and Na_2SO_4 for both types of cement and w/c ratio. This may be due to increase in conductivity of concrete as a result of increase in Cl^- ion concentration with increase in NaCl dosage (as observed from Table 4.7 and Table 4.8, Chapter 4).

While observing the effect of sodium sulfate concentration on corrosion current density of Tempcore TMT steel in ECPS contaminated with varying concentrations of NaCl and Na_2SO_4, it is observed that, the corrosion current density increased with increase in dosage of Na_2SO_4 up to 6% followed by a decrease at 12% Na_2SO_4 for both OPC and PPC at w/c ratio of 0.45, as evident from Fig. 5.53. This indicates that in the conjoint presence of NaCl and Na_2SO_4, higher concentration of Na_2SO_4 (12%) mitigated the corrosion activity of steel reinforcement in both OPC and PPC at w/c ratio of 0.45. From Fig. 5.54 it is observed that at w/c ratio of 0.5, the corrosion current density of Tempcore TMT steel in ECPS contaminated with varying concentrations of NaCl and Na_2SO_4 increased with increase in Na_2SO_4 concentration in OPC whereas the opposite behavior was observed in PPC i.e. the corrosion current density decreased with increase in Na_2SO_4 concentration. This indicates that at w/c ratio of 0.5, the presence of sulfate ions in OPC concrete has increased the conductivity as result of increase in Cl^- ion concentration with increase in dosage of Na_2SO_4 (as observed from Table 4.8, Chapter 4). However, in PPC concrete the presence of sulfate ions has mitigated the attack of chloride ions on steel reinforcement at w/c ratio of 0.5. This is attributed to decrease in conductivity of PPC concrete as a result of decrease in Cl^- ion concentration with increase in dosage of Na_2SO_4 (Table 4.8, Chapter 4).

From Fig. 5.55 and Fig. 5.56, it is observed that in the conjoint presence of NaCl and Na_2SO_4, the corrosion current density of Thermex TMT steel increased with an increase in Na_2SO_4 concentration for both types of cement and w/c ratio. The increase in corrosion current density of Thermex TMT steel with Na_2SO_4 concentration indicates that the presence of sulfate ions (associated with sodium cation) has stimulated the effect of chloride ion on corrosion of steel reinforcement in the conjoint presence of NaCl and Na_2SO_4. This indicates that the behavior of steel type i.e. Tempcore TMT and Thermex TMT is different in different types of cement and at different w/c ratios.

While analyzing the effect of steel type, it is observed that Tempcore TMT steel exhibited lower corrosion current density in all cases except in PPC at w/c ratio of 0.45, where Thermex TMT steel showed lower corrosion current density, as observed from Fig. 5.53 to Fig. 5.56. This variation in corrosion current density with steel type can be attributed to the effect of surface microstructure of steel and also to the variations in the concentrations of chloride and sulfate ions in ECPS prepared from different types of cement and w/c ratio.

From Fig. 5.53, it is found that the corrosion current density of Tempcore TMT steel in electrolytic concrete powder solution prepared from OPC is in the range of 5.8 $\mu A/cm^2$ to 10.1 $\mu A/cm^2$ and in that prepared from PPC is in the range of 6.7 $\mu A/cm^2$ to 10.5 $\mu A/cm^2$ at w/c ratio of 0.45 irrespective of NaCl and Na_2SO_4 concentrations. From these values, it is observed that OPC showed lower values of corrosion current density as compared to PPC at all levels of NaCl plus Na_2SO_4 concentration. This indicates that, in the conjoint presence of NaCl and Na_2SO_4, OPC is likely to show a longer propagation period as compared to PPC at w/c ratio of 0.45. From Fig. 5.54, it is observed that the corrosion current density of Tempcore TMT steel in electrolytic concrete powder solution prepared from OPC varied from 5.6 $\mu A/cm^2$ to 9.6 $\mu A/cm^2$ and in that prepared from PPC varied from 2.0 $\mu A/cm^2$ to 7.7 $\mu A/cm^2$ at w/c ratio of 0.5 irrespective of NaCl and Na_2SO_4 concentrations. From these values it is observed that OPC showed higher corrosion current density as compared to PPC at all levels NaCl plus Na_2SO_4 concentrations. Thus, for Tempcore TMT steel, PPC is likely to show longer corrosion propagation period as compared to OPC in the conjoint presence of NaCl and Na_2SO_4 at w/c ratio of 0.5.

From Fig. 5.55 and Fig. 5.56, it is observed that the corrosion current density of Thermex TMT steel in electrolytic concrete powder solutions prepared from OPC and PPC are in the ranges of 8.7 $\mu A/cm^2$ to 13.0 $\mu A/cm^2$ and 4.7 $\mu A/cm^2$ to 9.5 $\mu A/cm^2$ respectively at w/c ratio of 0.45 and those at w/c ratio of 0.5 are in the ranges of 6.7 $\mu A/cm^2$ to 12.3 $\mu A/cm^2$ and 3.4 $\mu A/cm^2$ to 8.8 $\mu A/cm^2$ respectively for OPC and PPC irrespective of NaCl and Na_2SO_4 concentrations. From these results it is found that for Thermex TMT steel, PPC performed better as compared to OPC in terms of reduced corrosion current density at both w/c ratios in the conjoint presence of NaCl and Na_2SO_4.

While evaluating the effect of w/c ratio on corrosion current density, it is inferred that the steel reinforcement showed lower corrosion current density at w/c ratio of 0.5 as compared to that at w/c ratio 0.45 in the conjoint presence of NaCl and Na_2SO_4 for both types of cement and steel, as observed from Fig. 5.53 to Fig. 5.56. The lower corrosion current density of steel reinforcement at w/c ratio of 0.5 is attributed to the presence of lower Cl^- ion concentration in ECPS prepared at w/c ratio of 0.5.

Further it is observed that (from Figs. 5.49, 5.50 and Figs. 5.53, 5.54), the corrosion current density of Tempcore TMT steel is lower in the electrolytic concrete powder solution contaminated with sodium chloride plus sodium sulfate as compared to that in the electrolytic concrete powder solution contaminated with only sodium chloride in both

OPC and PPC and at both w/c ratios. This indicates that the presence of sulfate ions (associated with sodium cation) in conjunction with chloride ions mitigated the effect of chloride ions on corrosion rate of steel reinforcement. The reduction in corrosion current density of steel reinforcement in the conjoint presence of sodium chloride plus sodium sulfate may be attributed to lower Cl^- ion concentration as compared that in the electrolytic concrete powder solution admixed with only NaCl (observed from Table 4.5, 4.6 and Table 4.7, 4.8). Further from these tables, it is observed that the conductivity was higher in the conjoint presence of NaCl plus Na_2SO_4 as compared to that in the presence of only NaCl, however, the pH value was lower in the presence of only NaCl as compared to that in the conjoint presence of NaCl plus Na_2SO_4 (Table 4.5, 4.6 and Table 4.7, 4.8). The effect of lower pH in the presence of only NaCl was more dominant than the lower conductivity thereby resulting in higher corrosion current density in the presence of only NaCl as compared to that in the conjoint presence of NaCl plus Na_2SO_4. Thermex TMT steel showed the similar variation in corrosion current density as Tempcore TMT steel, except in OPC at w/c ratio of 0.45 and 0.5, where, higher corrosion current density was observed in the conjoint presence of NaCl plus Na_2SO_4 as compared to that in the presence of only NaCl. This indicates that the steel type also affects the variation in corrosion current density.

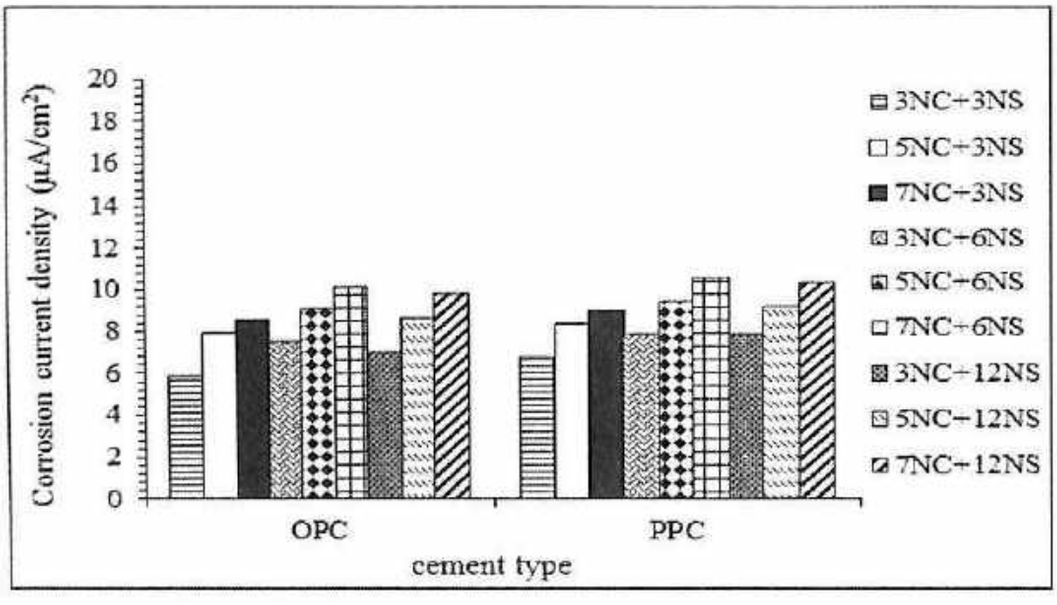

Fig. 5.53 Corrosion current density of Tempcore TMT steel in ECPS solutions prepared from OPC and PPC at w/c ratio of 0.45 and admixed with varying concentrations of NaCl plus Na_2SO_4 by mass of cement

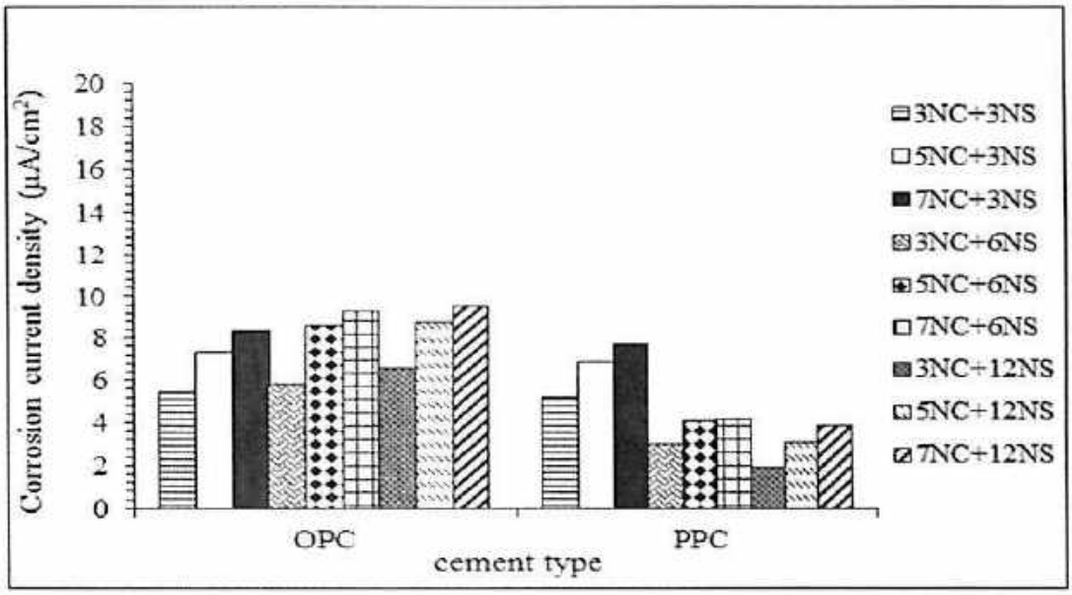

Fig. 5.54 Corrosion current density of Tempcore TMT steel in ECPS solutions prepared from OPC and PPC at w/c ratio of 0.5 and admixed with varying concentrations of NaCl plus Na_2SO_4 by mass of cement

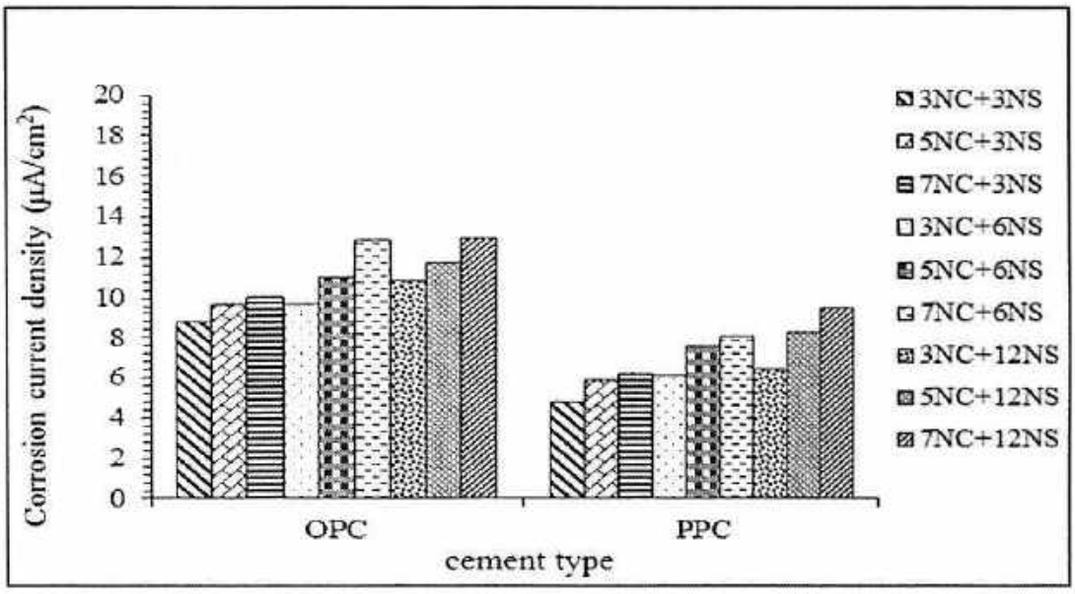

Fig. 5.55 Corrosion current density of Thermex TMT steel in ECPS solutions prepared from OPC and PPC at w/c ratio of 0.45 and admixed with varying concentrations of NaCl plus Na_2SO_4 by mass of cement

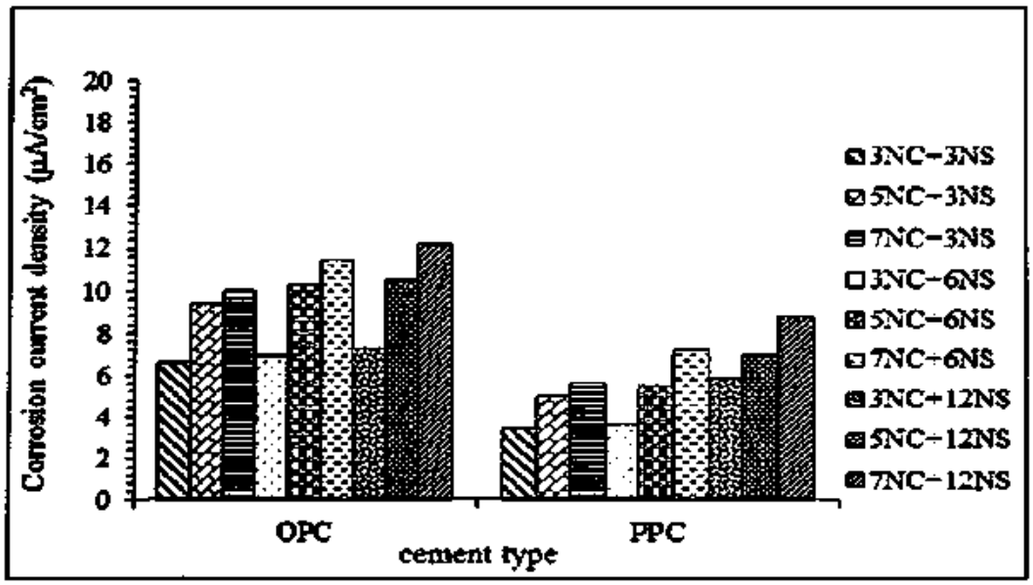

Fig. 5.56 Corrosion current density of Thermex TMT steel in ECPS solutions prepared from OPC and PPC at w/c ratio of 0.5 and admixed with varying concentrations of NaCl plus Na_2SO_4 by mass of cement

5.2.2.2.3 Effect of Conjoint Sodium Chloride and Magnesium Sulfate on Corrosion Current Density of Steel Reinforcement in Electrolytic Concrete Powder Solution

The variations in corrosion current density of Tempcore TMT steel reinforcement in electrolytic concrete powder solutions prepared from OPC and PPC and contaminated with varying concentrations of sodium chloride plus magnesium sulfate are shown in Fig. 5.57 at w/c ratio of 0.45 and that at w/c ratio of 0.5 are shown in Fig. 5.58. Similarly the variations in corrosion current density of Thermex steel are shown in Fig. 5.59 and Fig. 5.60 at w/c ratios of 0.45 and 0.50 respectively. While comparing the corrosion current density values shown in these figures with that of uncontaminated electrolytic concrete powder solution (ECPS), it is observed that the corrosion current density of steel reinforcement in sodium chloride plus magnesium sulfate contaminated electrolytic concrete powder solution is higher as compared to that in uncontaminated electrolytic concrete powder solution.

From Fig. 5.57 to Fig. 5.60, it is observed that the corrosion current density values of both Tempcore TMT and Thermex TMT steel increased with an increase in NaCl concentration in the conjoint presence of NaCl and $MgSO_4$ for both types of cement and w/c ratio. The increase in corrosion current density with increase in NaCl dosage may be attributed to increase in Cl^- ion concentration of the electrolytic concrete powder solution (as observed from Table 4.9 and 4.10, Chapter 4). While examining the effect of sulfate

ion (associated with magnesium cation) on corrosion current density, it is observed that the corrosion current density increased with an increase in $MgSO_4$ concentration in all the concrete mixes (OPC, PPC and w/c ratios of 0.45 and 0.5) for both types of steel reinforcement. The increase in corrosion current density with increase in $MgSO_4$ concentration indicates that SO_4^{2-} ions associated with magnesium cation accelerated the effect of chloride ions on corrosion rate of steel reinforcement. This is attributed to increase in conductivity of concrete in the conjoint presence of NaCl plus $MgSO_4$ as a result of increase in Cl^- ion concentration with increase in $MgSO_4$ dosage (as observed from Table 4.9 and 4.10, Chapter 4).

On evaluating the effect of steel type, it is inferred that Thermex TMT steel showed higher corrosion current density as compared to Tempcore TMT steel in both OPC and PPC and at both w/c ratios, as observed from Fig. 5.57 to Fig. 5.60. This indicates that Tempcore TMT steel is likely to exhibit longer corrosion propagation period as compared to Thermex TMT steel in conjoint sodium chloride plus magnesium sulfate exposure conditions.

From Fig. 5.57 and Fig. 5.58 it is observed that for Tempcore TMT steel, the corrosion current density in OPC at w/c ratio 0.45 is in the range of 8.5 $\mu A/cm^2$ to 12.5 $\mu A/cm^2$ and that at w/c ratio of 0.5 is in the range of 7.2 $\mu A/cm^2$ to 11.3 $\mu A/cm^2$. Similarly in PPC, the corrosion current density of Tempcore TMT steel is in the range of 10.5 $\mu A/cm^2$ to 15.9 $\mu A/cm^2$ at w/c ratio 0.45 and that at w/c ratio of 0.5 is in the range of 10.0 $\mu A/cm^2$ to 12.9 $\mu A/cm^2$. For Thermex TMT steel, the corrosion current density in OPC varied from 12.0 $\mu A/cm^2$ to 14.8 $\mu A/cm^2$ at w/c ratio of 0.45 and that at w/c ratio of 0.5 varied from 7.9 $\mu A/cm^2$ to 14.2 $\mu A/cm^2$, as observed from Fig. 5.59 and Fig. 5.60. Similarly in PPC, the corrosion current density of Thermex TMT steel varied from 12.4 $\mu A/cm^2$ to 18.1 $\mu A/cm^2$ and 12.1 $\mu A/cm^2$ to 18.2 $\mu A/cm^2$ at w/c ratios of 0.45 and 0.5 respectively. From these results it is inferred that both Tempcore TMT steel and Thermex TMT steel showed higher corrosion current density in PPC as compared to that in OPC at both w/c ratios and at all levels of NaCl and $MgSO_4$ concentration. The higher corrosion current density in PPC is attributed to higher conductivity of the electrolytic concrete powder solution as a result of higher Cl^- ion concentration in PPC as compared to that in OPC (as observed from Table 4.9 and Table 4.10, Chapter 4). The higher conductivity of PPC in the conjoint presence NaCl and $MgSO_4$ may also be attributed to its susceptibility to Mg-oriented attack. Further, it is found that the corrosion current density of steel

reinforcement was lower at w/c ratio of 0.5 as compared to that at w/c ratio of 0.45 in the conjoint presence of NaCl and $MgSO_4$ for both types of cement and steel, as observed from Fig. 5.57 to Fig. 5.60. Thus, it is inferred that the combination of Tempcore TMT steel and OPC at w/c ratio of 0.5 performed better as compared to other type of steel, cement and w/c ratio in the conjoint presence of NaCl and $MgSO_4$ and are likely to exhibit longer propagation period.

Further from the results it is found that the corrosion current density of Tempcore TMT steel is higher in the electrolytic concrete powder solution contaminated with sodium chloride plus magnesium sulfate as compared to that in the electrolytic concrete powder solution contaminated with only sodium chloride in both OPC and PPC and at both w/c ratios. This is attributed to lower chloride binding thereby resulting in higher chloride ion concentration in the conjoint presence of NaCl and $MgSO_4$ as compared to that in the presence of only NaCl (Table 4.5, 4.6 and Table 4.9, 4.10, Chapter 4). Subsequently, pH value of the electrolytic concrete powder solution was lower in the conjoint presence of NaCl and $MgSO_4$ as compared that in the presence of only NaCl. Thus, the presence of sulfate ions (associated with magnesium cation) along with chloride ions stimulated the effect of chloride ions on the extent of corrosion of Tempcore TMT steel reinforcement.

For Thermex TMT steel, it is found that the corrosion current density of steel reinforcement is lower in the electrolytic concrete powder solution contaminated with sodium chloride plus magnesium sulfate as compared to that in the electrolytic concrete powder solution contaminated with only sodium chloride in both types of cement and w/c ratio. This indicates that the conjoint presence of sulfate ions (associated with magnesium cation) and chloride ions mitigated the effect of chloride ions on extent of corrosion of Thermex TMT steel reinforcement. Thus, it is inferred that the effect of sulfate ions associated with magnesium cation on corrosion rate of steel reinforcement is different for different types of steel.

While analyzing the effect of cation type i.e. Na^+ and Mg^{++}, it is observed that, the corrosion current density of steel reinforcement in the electrolytic concrete powder solution contaminated with NaCl plus $MgSO_4$ is higher than that in the electrolytic concrete powder solution contaminated with NaCl plus Na_2SO_4 in both OPC and PPC and at both w/c ratios. This is due to higher conductivity of electrolytic concrete powder solution in the conjoint presence of NaCl plus $MgSO_4$ as compared to that in the conjoint presence of NaCl plus Na_2SO_4. The higher conductivity in the conjoint presence of NaCl

plus $MgSO_4$ is attributed to higher chloride ion concentration as compared to that in the conjoint presence of NaCl plus Na_2SO_4. In addition, the pH value of electrolytic concrete powder solution was lower in the conjoint presence of NaCl plus $MgSO_4$ as compared to that in the conjoint presence of NaCl plus Na_2SO_4 as observed from Table 4.7 to 4.10 (Chapter 4). Thus, it can be concluded that in chloride environment, the presence of sulfate ion associated with magnesium cation has more detrimental effect in terms of higher corrosion current density of steel reinforcement than that associated with sodium cation.

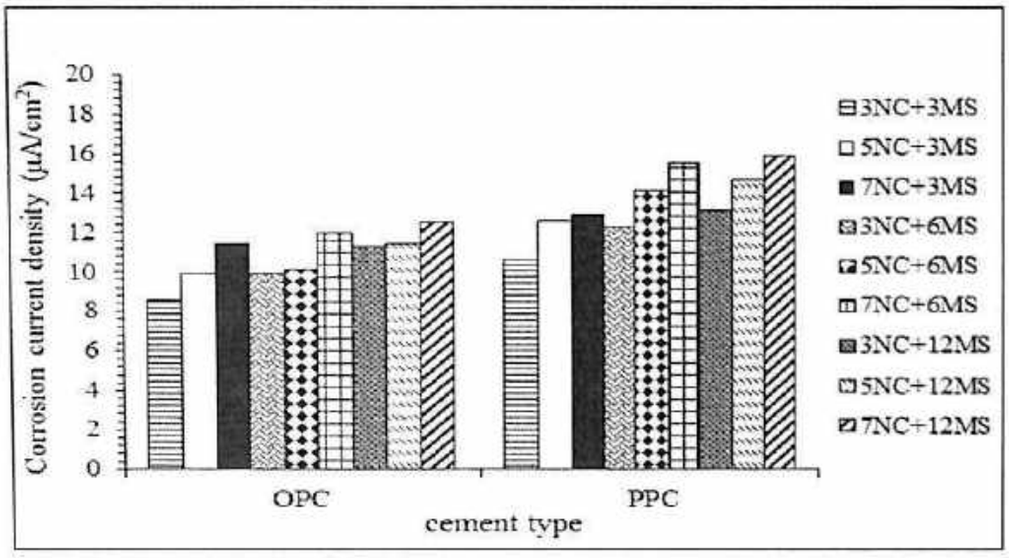

Fig. 5.57 Corrosion current density of Tempcore TMT steel in ECPS prepared from OPC and PPC at w/c ratio of 0.45 and admixed with varying concentrations of NaCl plus $MgSO_4$ by mass of cement

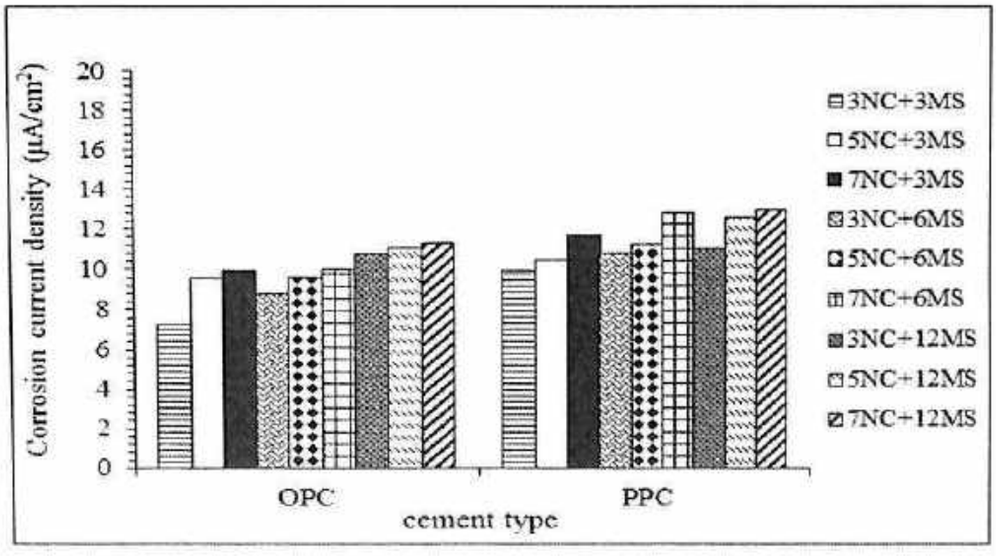

Fig. 5.58 Corrosion current density of Tempcore TMT steel in ECPS prepared from OPC and PPC at w/c ratio of 0.5 and admixed with varying concentrations of NaCl plus $MgSO_4$ by mass of cement

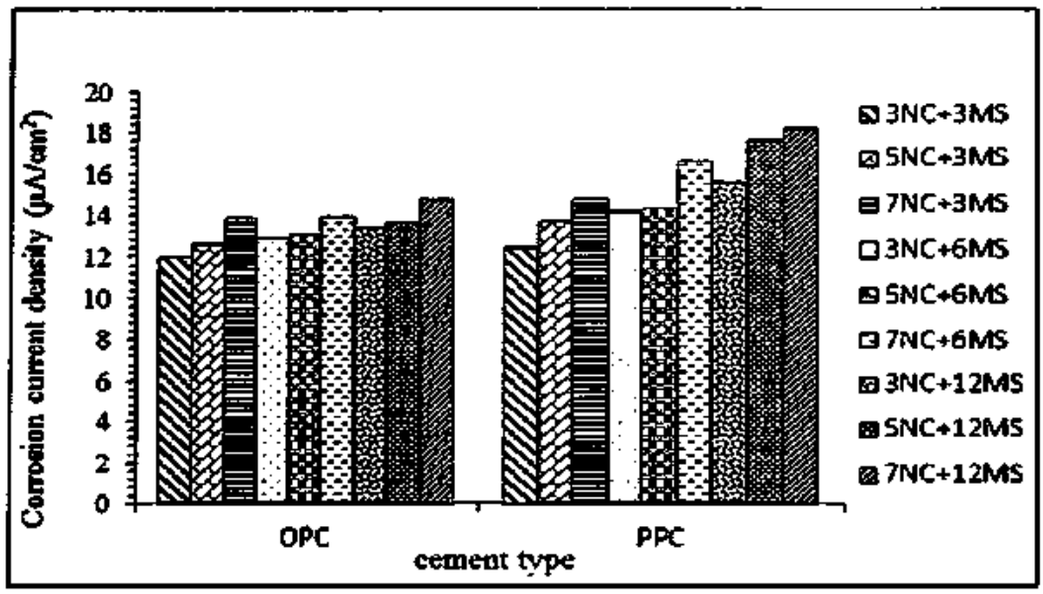

Fig. 5.59 Corrosion current density of Thermex TMT steel in ECPS prepared from OPC and PPC at w/c ratio of 0.45 and admixed with varying concentrations of NaCl plus $MgSO_4$ by mass of cement

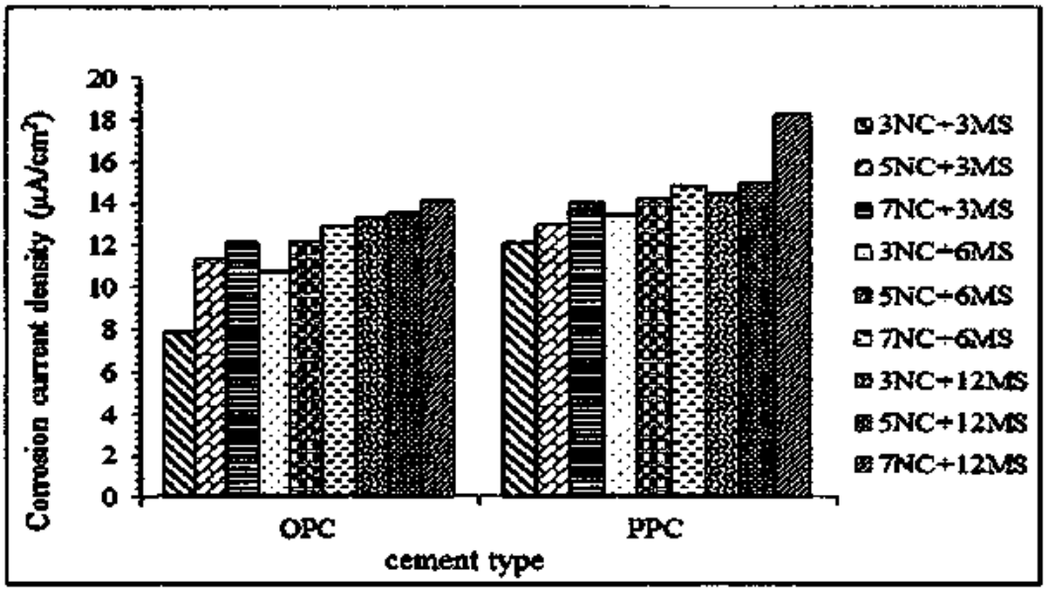

Fig. 5.60 Corrosion current density of Thermex TMT steel in ECPS prepared from OPC and PPC at w/c ratio of 0.5 and admixed with varying concentrations of NaCl plus $MgSO_4$ by mass of cement

5.3 SUMMARY

From the results of potentiodynamic polarization test, different zones of corrosion namely active zone, passive zone and pitting zone of steel reinforcement in electrolytic concrete powder solutions (ECPS) contaminated with varying concentrations of chloride and

conjoint chloride-sulfate ions were obtained. Tempcore TMT steel and w/c ratio of 0.5 showed higher range of passivity as compared to Thermex TMT steel and w/c ratio of 0.45 respectively in ECPS contaminated with chloride ions and composite chloride-sulfate ions (for both cations). The range of passive zone was more in ECPS prepared from OPC as compared to that prepared from PPC in the presence of only chloride ions for both types of steel and w/c ratios. In ECPS contaminated with NaCl plus Na_2SO_4, PPC mostly showed higher range of passivity as compared to OPC, whereas OPC showed higher range of passivity as compared to PPC in ECPS contaminated with NaCl plus $MgSO_4$. Further the range of passive zone of both types of steel reinforcement was more in ECPS contaminated with NaCl plus Na_2SO_4 as compared to that contaminated with NaCl plus $MgSO_4$ for both types of cement and w/c ratio. This indicates that Mg-oriented sulfate attack is more aggressive in reducing the passivity of steel reinforcement as compared to Na-oriented sulfate attack in the presence of chloride ions. For both Tempcore TMT and Thermex TMT steels, the passivity range in the electrolytic concrete powder solution (ECPS) contaminated with only sodium chloride was lower as compared to that in the ECPS contaminated with sodium chloride plus sodium sulfate in both OPC and PPC and at both w/c ratios. Thus, the presence of sodium sulfate in chloride environment has mitigated the effect of chloride ions on reducing the passivity of reinforcing steel. Further, the passivity range of Tempcore TMT steel was higher in the ECPS contaminated with only sodium chloride as compared to that in the conjoint presence of sodium chloride and magnesium sulfate. This indicated that the presence of magnesium sulfate in chloride environment has stimulated the effect of chloride ions on reducing the passivity for Tempcore steel reinforcement. However, the passivity range of Thermex TMT steel in the ECPS contaminated with only sodium chloride was lower as compared to that in the conjoint presence of sodium chloride and magnesium sulfate. This indicated that Thermex TMT steel performed better in the conjoint presence of NaCl and $MgSO_4$ as compared to that in the presence of only NaCl, in maintaining the passivity. Overall, the passivity of steel reinforcement was maintained to a greater degree in the electrolytic concrete powder solutions contaminated with NaCl plus Na_2SO_4 as compared to those contaminated with only NaCl and NaCl plus $MgSO_4$.

The results obtained from the corrosion parameters of steel reinforcement in electrolytic concrete powder solution indicated that the presence of chloride and conjoint chloride-sulfate ions increased the probability of occurrence of steel reinforcement corrosion for

both types of cement, steel and w/c ratio. Tempcore TMT steel and w/c ratio of 0.5 exhibited lower corrosion current density as compared to Thermex TMT steel and w/c ratio of 0.45 respectively in ECPS contaminated with NaCl, NaCl plus Na_2SO_4 and NaCl plus $MgSO_4$. On comparison between cement type, it is observed that PPC exhibited higher corrosion current density than OPC in the presence of chloride ions. In the conjoint presence NaCl plus Na_2SO_4, OPC mostly showed higher corrosion current density as compared to PPC whereas PPC showed higher corrosion current density as compared to OPC in the conjoint presence NaCl plus $MgSO_4$.

On comparing the variations in corrosion current density between chloride and conjoint chloride-sulfate ions, it is inferred that, the presence of sulfate ions associated with sodium cation has mitigated the effect of chloride ions on corrosion current density for both types of steel reinforcement. However, the presence of sulfate ions associated with magnesium cation has stimulated the effect of chloride ions on corrosion current density of Tempcore TMT steel whereas for Thermex TMT steel, the presence of sulfate ions associated with magnesium cation has mitigated the effect of chloride ions on corrosion current density.

While comparing the variations in passivity range of steel reinforcement and that in corrosion parameters (corrosion potential and corrosion current density), it is inferred that there exists a good correlation between the passivity range of steel reinforcement and the above corrosion parameters of steel reinforcement in sodium chloride, sodium chloride plus sodium sulfate and sodium chloride plus magnesium sulfate contaminated electrolytic concrete powder solutions.

CHAPTER 6

CORROSION BEHAVIOUR OF STEEL REINFORCEMENT IN CONCRETE AGAINST COMPOSITE CHLORIDE-SULFATE EXPOSURE

6.1 GENERAL

In this chapter, the results on corrosion behaviour of steel reinforcement embedded in concrete that is contaminated with varying concentrations of chloride-sulfate ions and further exposed to composite chloride-sulfate environment are presented and discussed. The corrosion behaviour of steel reinforcement embedded in prismatic reinforced concrete specimens was evaluated through corrosion potential and corrosion current density measurements. Further, to study the effect of exposure period, the corrosion potential and corrosion current density of steel reinforcement were measured at the ages of 90 days, 180 days and 270 days from the day of preparation of the specimens.

6.2 CORROSION PARAMETERS

As mentioned earlier, the corrosion parameters such as corrosion potential and corrosion current density of steel reinforcement were measured at the ages of 90 days, 180 days and 270 days from the day of preparation of prismatic reinforced concrete specimens. As already mentioned in Chapter 3, the prismatic reinforced concrete specimens were prepared from different types of binder such as OPC, PPC, OPC plus 20% fly ash (OPC+20FA) and OPC plus 30% fly ash (OPC+30FA) at a w/b ratio of 0.5. After 28 days of water curing, the specimens were kept in ambient laboratory exposure condition till the age of 90 days from the day of preparation. After that, the specimens were exposed to normal water, sodium chloride plus sodium sulfate solution, and sodium chloride plus magnesium sulfate solution with alternate wetting and drying cycles till the age of 270 days.

6.2.1 Corrosion Potential

The corrosion potential values of steel reinforcement in prismatic specimens made of control mix (uncontaminated) with different types of binders at different ages for Tempcore TMT steel and Thermex TMT steel and subsequently exposed to normal water are shown in Fig. 6.1 and Fig. 6.2 respectively.

From Fig. 6.1 and Fig. 6.2, it is observed that the corrosion potential values are more positive than -270 mV (SCE) for both types of steel in all binder types. As per ASTM C 876 criteria [133], the potential values more negative than -270 mV (SCE)/-350 mV ($Cu/CuSO_4$ electrode), correspond to greater than 90% probability of occurrence of steel reinforcement corrosion. This indicates that there is lower probability of occurrence of steel reinforcement corrosion in control mix made from all binders for both types of steel reinforcement.

From Fig. 6.1, it is observed that for Tempcore TMT steel the corrosion potential values varied from -40 mV to -177 mV at the age of 90 days, +51 mV to +111 mV at the age of 180 days and +86 mV to +209 mV at the age of 270 days irrespective of binder type. For Thermex TMT steel, the corrosion potential values varied from -51 mV to -180 mV at the age of 90 days, +12 mV to +104 mV at the age of 180 days and +51 mV to +129 mV at the age of 270 days irrespective of binder type as observed from Fig. 6.2. From these potential values, it is found that the corrosion potential values became less negative with increase in the exposure period for both types of steel in the control mix. Further from Fig. 6.1 and Fig. 6.2, it is observed that the corrosion potential values are more negative in OPC specimens as compared to other binders i.e. PPC, OPC+20FA and OPC+30FA for both types of steel and at all ages i.e. 90, 180 and 270 days.

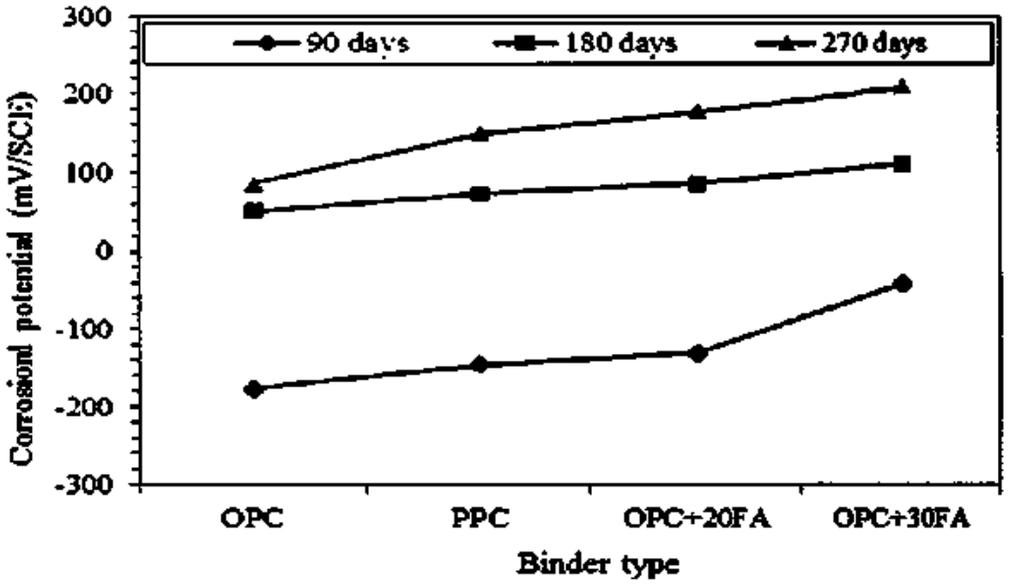

Fig. 6.1 Corrosion potential versus binder type for Tempcore TMT steel in control mix at different ages

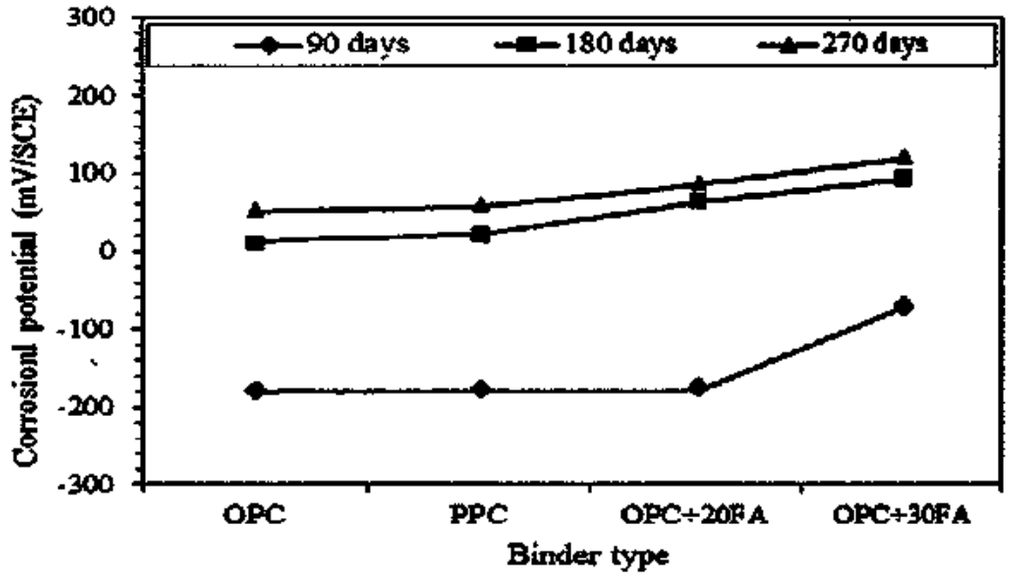

Fig. 6.2 Corrosion potential versus binder type for Thermex TMT steel in control mix at different ages

6.2.1.1 Corrosion potential of Steel Reinforcement Embedded in Contaminated Concrete Exposed to Sodium Chloride plus Sodium Sulfate Solutions

The corrosion potential values in the conjoint presence of sodium chloride (NaCl) and sodium sulfate (Na_2SO_4) for Tempcore TMT steel embedded in concrete specimens made with different types of binders viz. OPC, PPC, OPC+20FA and OPC+30FA at different ages i.e. 90 days, 180 days and 270 days are shown in Fig. 6.3, Fig. 6.4 and Fig. 6.5 respectively. Similarly, the corrosion potential values for Thermex TMT steel at 90 days,

180 days and 270 days are shown in Fig. 6.6, Fig. 6.7 and Fig. 6.8 respectively. From Fig. 6.3 to Fig. 6.8, it is observed that in the conjoint presence of NaCl plus Na_2SO_4, the corrosion potential values of Tempcore TMT and Thermex TMT in all types of binders i.e. OPC, PPC, OPC+20FA, OPC+30FA were more negative than the threshold potential of -270 mV (SCE) at all levels of NaCl plus Na_2SO_4 concentration and at all exposure ages. This indicates that the conjoint presence of sodium chloride plus sodium sulfate internally (admixed at the time of preparation) as well as external exposure has resulted in greater probability of occurrence of steel reinforcement corrosion. While comparing with the exposure of control specimens to the normal water, it observed that specimens admixed with NaCl and Na_2SO_4 and further exposed to composite solutions of NaCl and Na_2SO_4 exhibited more negative potential values for both types of steel and all types of binder.

Further from Fig. 6.3 to Fig. 6.8, it is noted that the corrosion potential values of both Tempcore TMT and Thermex TMT steel became more negative with an increase in NaCl dosage. This is possibly due to increase in Cl^- ion concentration in the vicinity of steel reinforcement embedded in concrete. While analyzing the influence of sulfate ion on corrosion potential of steel reinforcement in the conjoint presence of NaCl plus Na_2SO_4, it is found that the corrosion potential values became more negative with increase in concentration of Na_2SO_4. This indicates that the presence of Na_2SO_4 in combination with NaCl has increased the probability of occurrence of steel reinforcement corrosion in concrete.

The corrosion potential values of Tempcore TMT steel in the conjoint presence of NaCl plus Na_2SO_4 varied from -337 mV to -586 mV at the age of 90 days, -292 mV to -495 mV at the age of 180 days and -357 mV to -632 mV at the age of 270 days irrespective of binder type. Similarly for Thermex TMT steel, the corrosion potential values varied from -359 mV to -513 mV at the age of 90 days, -361 mV to -463 mV at the age of 180 days and -412 mV to -602 mV at the age of 270 days irrespective of binder type in the conjoint presence of NaCl plus Na_2SO_4. From these variations of corrosion potential values, it is observed that the potential values were less negative at the age of 180 days as compared to that at the age of 90 days and were more negative at the age of 270 days as compared to that at the age of 180 days. This indicates that after the exposure period of 180 days, the probability of occurrence of corrosion of steel reinforcement in the conjoint presence of NaCl plus Na_2SO_4 has increased.

Further from Fig. 6.3 to Fig. 6.8, it is observed that the corrosion potential values of Tempcore TMT steel in OPC, PPC, OPC+20FA and OPC+30FA concrete were in the ranges of -341 mV to -632 mV, -330 mV to -624 mV, -318 mV to -565 mV and -292 mV to -531 mV respectively irrespective of exposure period. For Thermex TMT steel, the corrosion potential values in OPC, PPC, OPC+20FA and OPC+30FA concrete varied from -388 mV to -602 mV, -381 mV to -592 mV, -380 mV to -517 mV and -359 mV to -514 mV respectively irrespective of exposure period in the conjoint presence of NaCl and Na_2SO_4. From these corrosion potential values, it is inferred that OPC concrete showed more negative potential values as compared to blended cements (PPC, OPC+20FA and OPC+30FA), thereby indicating higher probability of occurrence of corrosion in OPC in the conjoint presence of NaCl plus Na_2SO_4 for both types of steel. The comparatively lower probability of occurrence of corrosion in blended cement concrete specimens may be attributed to the formation of denser microstructure due to production of additional C-S-H because of pozzolanic reaction, thereby resulting in lower conductivity of concrete and retarding the penetration of aggressive ions and diffusion of oxygen to the steel reinforcement level in concrete.

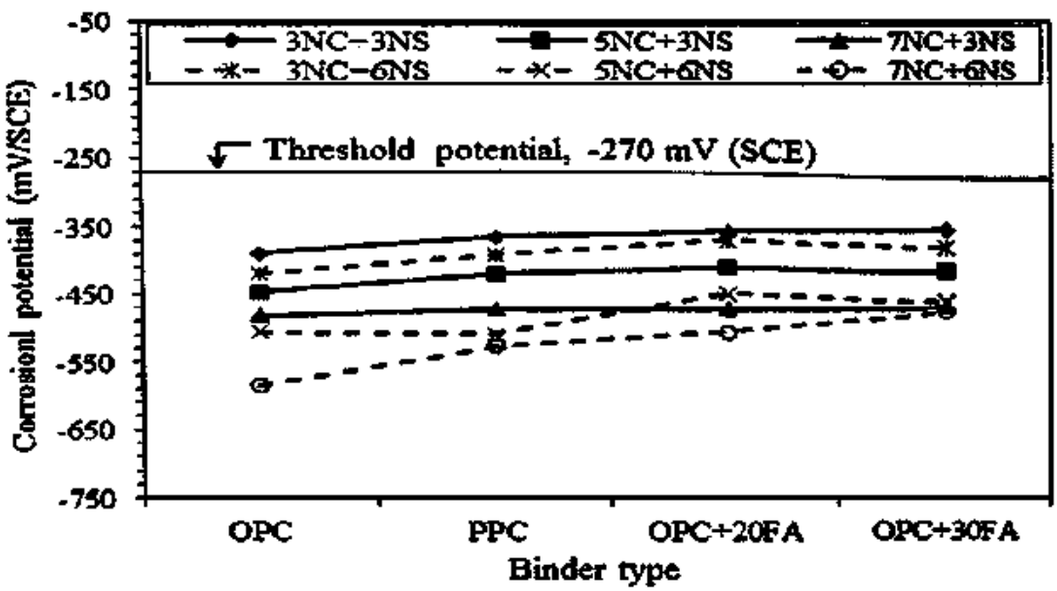

Fig. 6.3 Corrosion potential versus binder type for Tempcore TMT steel at the age of 90 days in different concrete mixes admixed with varying concentrations of NaCl plus Na_2SO_4

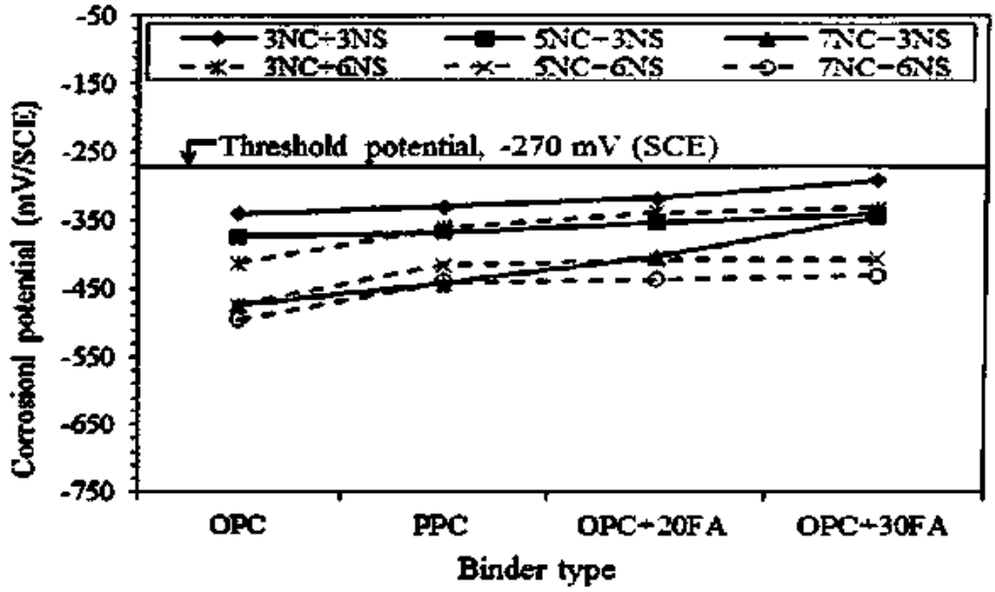

Fig. 6.4 Corrosion potential versus binder type for Tempcore TMT steel at the age of 180 days in different concrete mixes admixed with varying concentrations of NaCl plus Na_2SO_4 and further exposed to NaCl plus Na_2SO_4 solution with alternate wetting and drying cycles

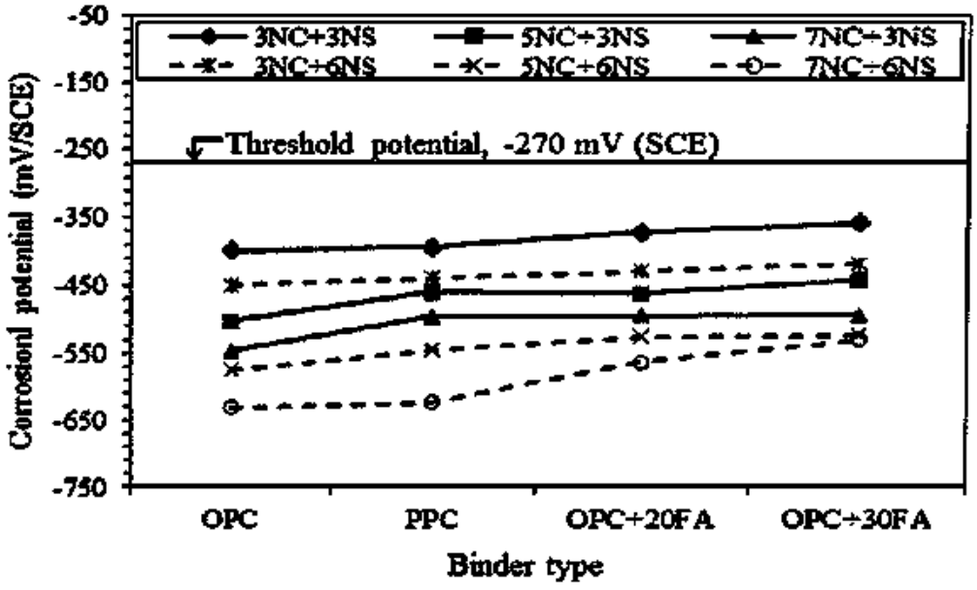

Fig. 6.5 Corrosion potential versus binder type for Tempcore TMT steel at the age of 270 days in different concrete mixes admixed with varying concentrations of NaCl plus Na_2SO_4 and further exposed to NaCl plus Na_2SO_4 solution with alternate wetting and drying cycles

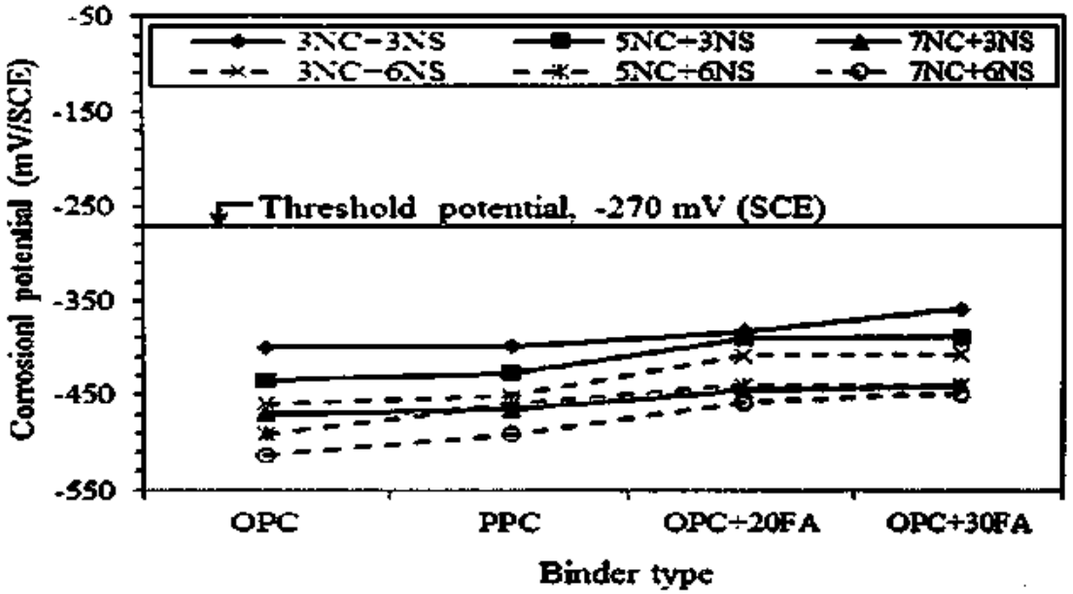

Fig. 6.6 Corrosion potential versus binder type for Thermex TMT steel at the age of 90 days in different concrete mixes admixed with varying concentrations of NaCl plus Na_2SO_4

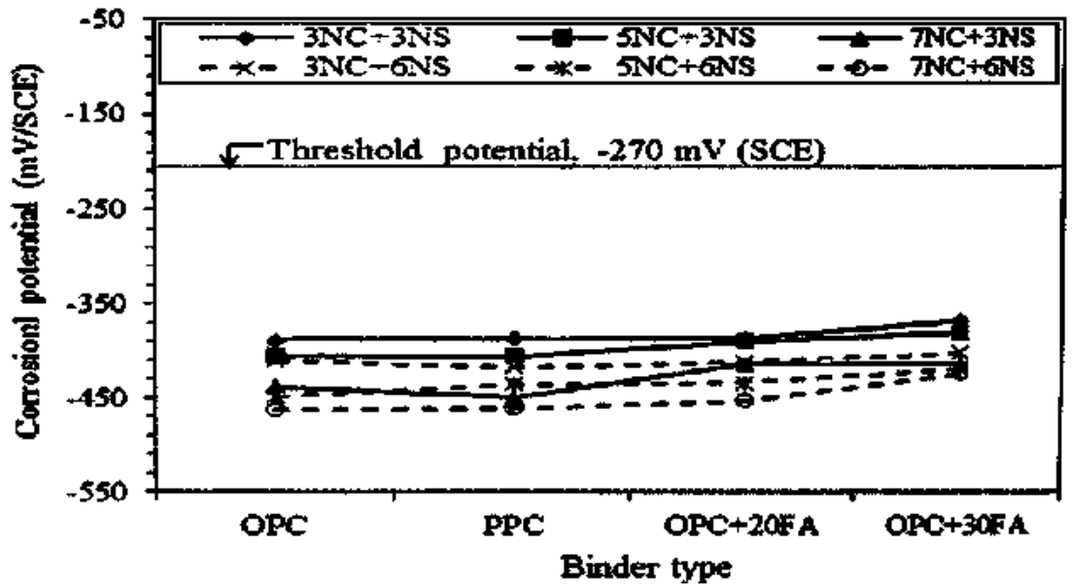

Fig. 6.7 Corrosion potential versus binder type for Thermex TMT steel at the age of 180 days in different concrete mixes admixed with varying concentrations of NaCl plus Na_2SO_4 and further exposed to NaCl plus Na_2SO_4 solution with alternate wetting and drying cycles

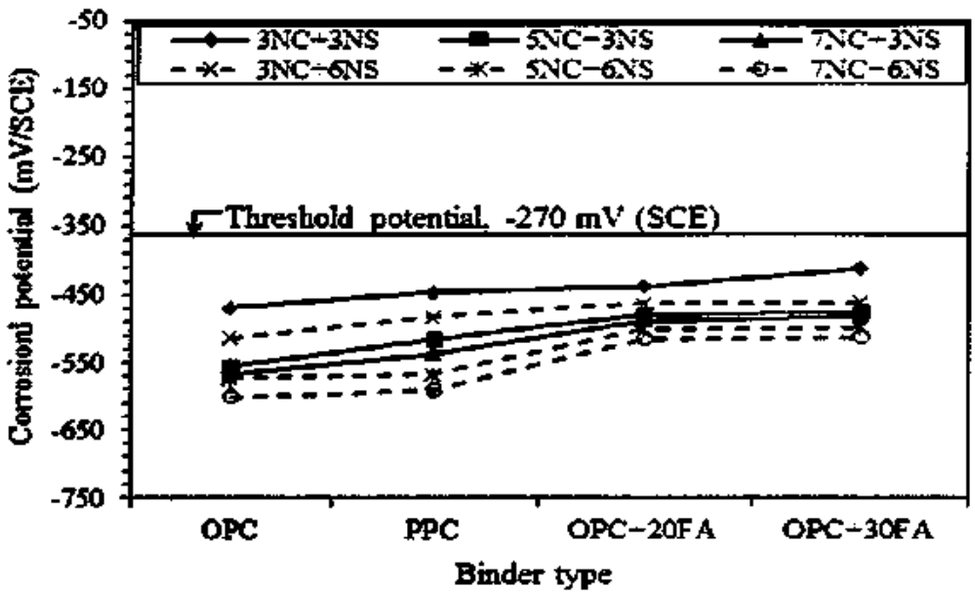

Fig. 6.8 Corrosion potential versus binder type for Thermex TMT steel at the age of 270 days in different concrete mixes admixed with varying concentrations of NaCl plus Na_2SO_4 and further exposed to NaCl plus Na_2SO_4 solution with alternate wetting and drying cycles

6.2.1.2 Corrosion potential of Steel Reinforcement Embedded in Contaminated Concrete Exposed to Sodium Chloride plus Magnesium Sulfate Solutions

The corrosion potential values in the conjoint presence of sodium chloride (NaCl) plus magnesium sulfate ($MgSO_4$) for Tempcore TMT steel embedded in concrete specimens made with different types of binder viz. OPC, PPC, OPC+20FA and OPC+30FA at different ages i.e. 90 days, 180 days and 270 days are shown in Fig. 6.9, Fig. 6.10 and Fig. 6.11 respectively. Similarly, the corrosion potential values for Thermex TMT steel embedded in concrete at different ages i.e. 90 days, 180 days and 270 days are shown in Fig. 6.12, Fig. 6.13 and Fig. 6.14 respectively in the conjoint presence of NaCl and $MgSO_4$.

From Fig. 6.9 to Fig. 6.14, it is observed that in the conjoint presence of NaCl plus $MgSO_4$, the corrosion potential values of both Tempcore TMT and Thermex TMT in all types of binders i.e. OPC, PPC, OPC+20FA, and OPC+30FA have exceeded the threshold potential of -270 mV (SCE) at all levels of NaCl plus $MgSO_4$ concentration and at all ages. This indicates that in the conjoint presence of sodium chloride and magnesium sulfate either admixed during preparation of concrete and/or penetrated into hardened concrete, there is greater probability of occurrence of steel reinforcement corrosion.

From Fig. 6.9 to Fig. 6.14, it is observed that the corrosion potential values of Tempcore TMT and Thermex TMT steel became more negative with an increase in NaCl and $MgSO_4$ dosage. In other words, the probability of occurrence of steel reinforcement corrosion in concrete increased with increase in concentrations of NaCl and $MgSO_4$. This may be attributed to increase in Cl^- ion concentration in the vicinity of steel reinforcement in concrete with increase in NaCl concentration in the presence of $MgSO_4$. Further from the results, it is observed that the control specimens exposed to normal water showed less negative potential as compared to those admixed and exposed to composite NaCl and $MgSO_4$ for both types of steel and in all concrete mixes.

The corrosion potential values of Tempcore TMT steel in NaCl plus $MgSO_4$ environment varied from -321 mV to -501 mV at the age of 90 days, -339 mV to -665 mV at the age of 180 days and -360 mV to -675 mV at the age of 270 days irrespective of binder type. Similarly for Thermex TMT steel, the corrosion potential values varied from -362 mV to -494 mV, -363 mV to -533 mV and -458 mV to -672 mV at the age of 90 days, 180 days and 270 days respectively irrespective of binder type. From these ranges of corrosion potential values, it is inferred that the potential values became more negative with increase in exposure period, which indicates that the probability of occurrence of steel reinforcement corrosion increased with an increase in exposure period in the conjoint presence of NaCl plus $MgSO_4$.

From Fig. 6.9 to Fig. 6.11, it is observed that in the conjoint presence of NaCl plus $MgSO_4$ the corrosion potential values of Tempcore TMT steel in OPC, PPC, OPC+20FA and OPC+30FA concrete varied from -321 mV to -551 mV, -336 mV to -513 mV, -347 mV to -535 mV and -352 mV to -665 mV respectively irrespective of exposure period. For Thermex TMT steel in the conjoint presence of NaCl plus $MgSO_4$, the corrosion potential values in OPC, PPC, OPC+20FA and OPC+30FA concrete were in the ranges of -363 mV to -569 mV, -381 mV to -551 mV, -392 mV to -637 mV and -396 mV to -672 mV respectively irrespective of exposure period as observed from Fig. 6.12 to Fig. 6.14. From these variations in corrosion potential values, it is inferred that OPC+30FA concrete showed more negative potential values whereas OPC concrete showed mostly less negative potential values as compared to other types of binder for both types of steel reinforcement. This implies that the probability of occurrence of steel reinforcement corrosion is more in OPC+30FA concrete and less in OPC concrete as compared to other types of binder in the conjoint presence of NaCl plus $MgSO_4$. The higher probability of

occurrence of steel reinforcement corrosion in blended cement concrete specimens as compared to that in OPC concrete specimens in the conjoint presence of NaCl and $MgSO_4$ may be attributed to its susceptibility to Mg-oriented attack due to lower availability of calcium hydroxide in blended cement concrete.

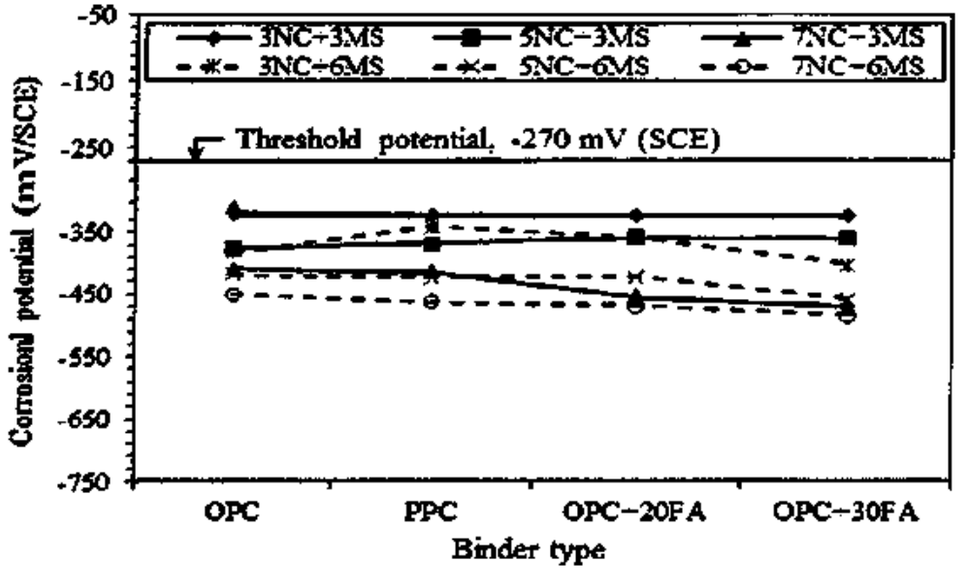

Fig. 6.9 Corrosion potential versus binder type for Tempcore TMT steel at the age of 90 days in different concrete mixes admixed with varying concentrations of NaCl plus $MgSO_4$

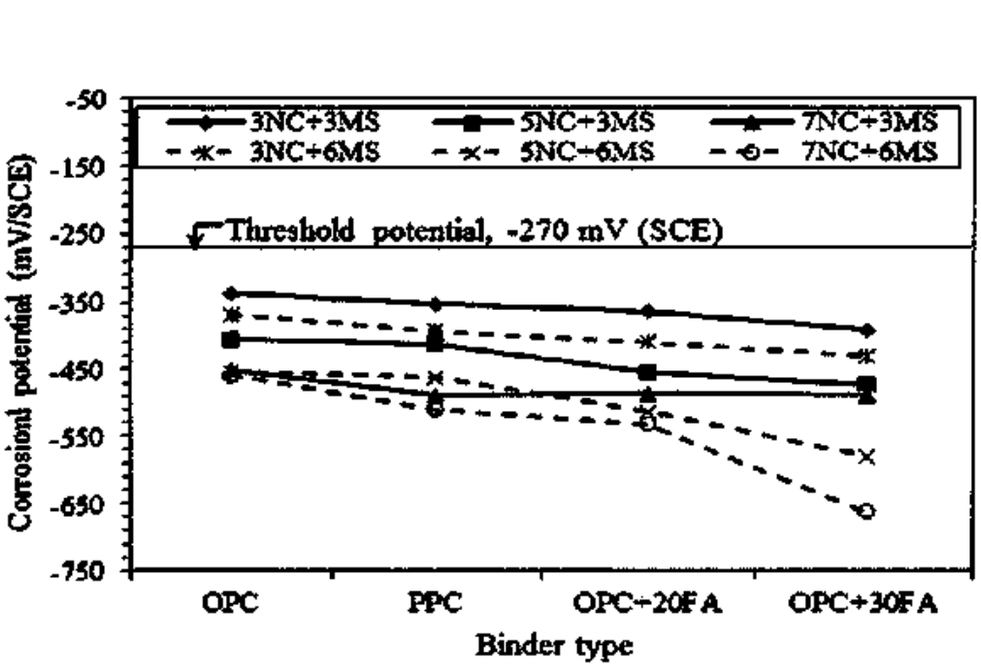

Fig. 6.10 Corrosion potential versus binder type for Tempcore TMT steel at the age of 180 days in different concrete mixes admixed with varying concentrations of NaCl plus $MgSO_4$ and further exposed to NaCl plus $MgSO_4$ solution with alternate wetting and drying cycles

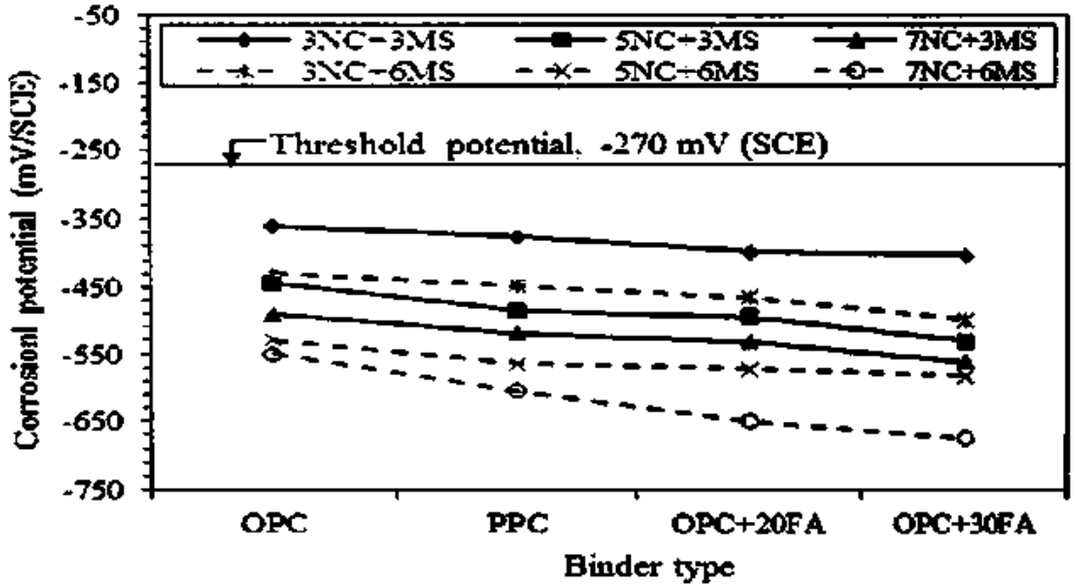

Fig. 6.11 Corrosion potential versus binder type for Tempcore TMT steel at the age of 270 days in different concrete mixes admixed with varying concentrations of NaCl plus $MgSO_4$ and further exposed to NaCl plus $MgSO_4$ solution with alternate wetting and drying cycles

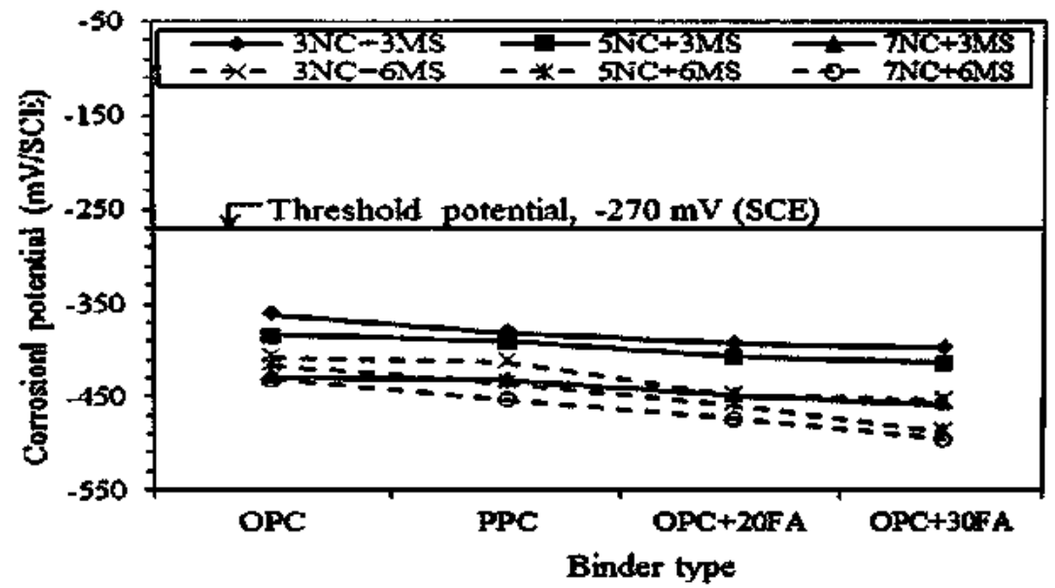

Fig. 6.12 Corrosion potential versus binder type for Thermex TMT steel at the age of 90 days in different concrete mixes admixed with varying concentrations of NaCl plus $MgSO_4$

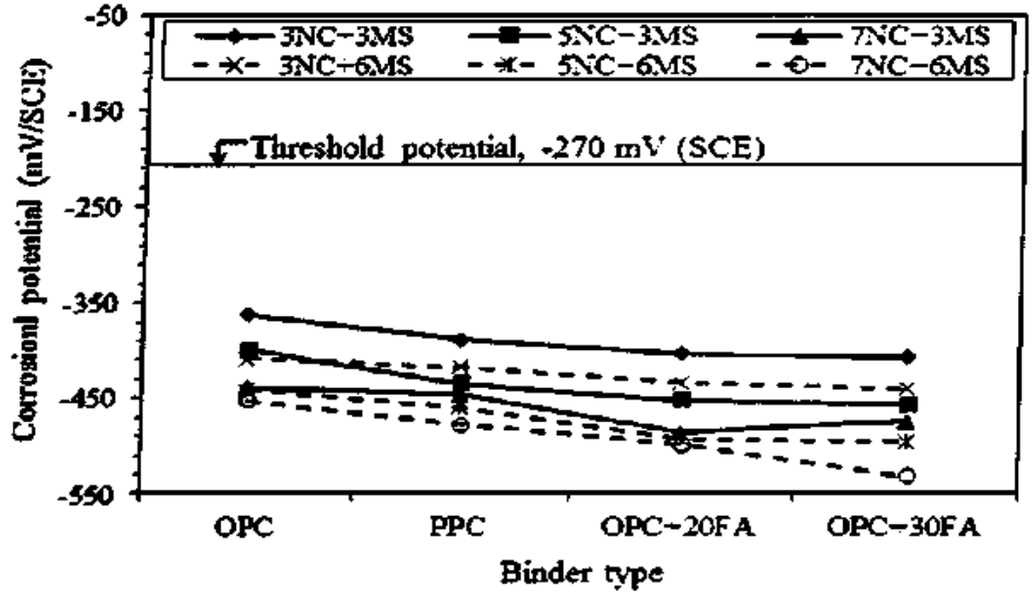

Fig. 6.13 Corrosion potential versus binder type for Thermex TMT steel at the age of 180 days in different concrete mixes admixed with varying concentrations of NaCl plus $MgSO_4$ and further exposed to NaCl plus $MgSO_4$ solution with alternate wetting and drying cycles

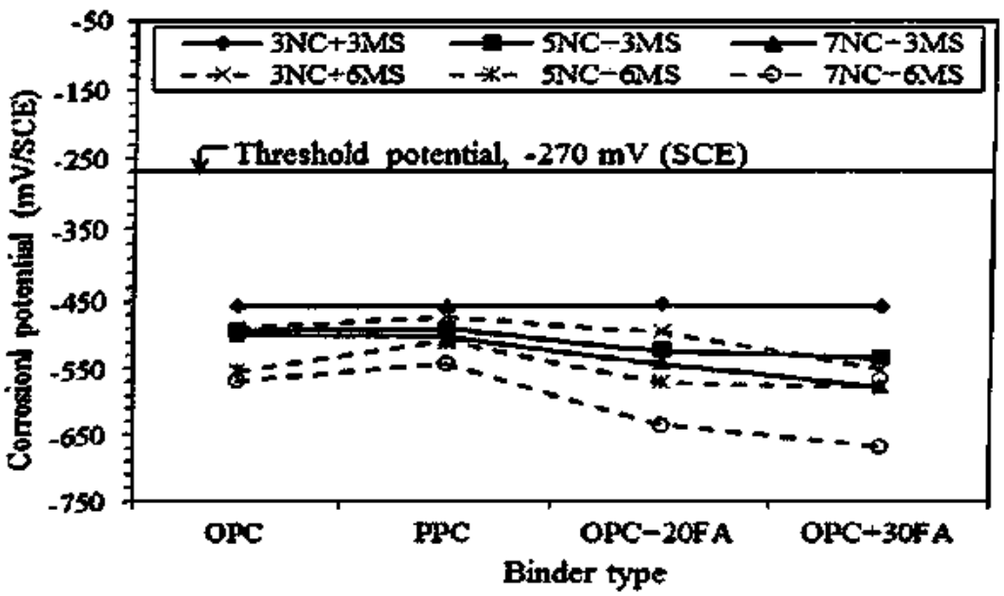

Fig. 6.14 Corrosion potential versus binder type for Thermex TMT steel at the age of 270 days in different concrete mixes admixed with varying concentrations of NaCl plus $MgSO_4$ and further exposed to NaCl plus $MgSO_4$ solution with alternate wetting and drying cycles

6.2.2 Corrosion Current Density

The quantitative information about steel reinforcement corrosion was obtained by determining corrosion current density (I_{corr}) of reinforced concrete specimens using linear polarization resistance (LPR) technique at the ages of 90, 180 and 270 days in the conjoint presence of NaCl plus Na_2SO_4 and NaCl plus $MgSO_4$. The detailed explanation of experimental procedure is already stated in chapter 3. The variations in corrosion current density with binder type for different exposure periods in control mix specimens exposed to normal water are shown in Fig. 6.15 and Fig. 6.16 for Tempcore TMT and Thermex TMT steel respectively.

From Fig. 6.15 and Fig. 6.16, it is observed that in control mix, the corrosion current density decreased with exposure period in normal water. The corrosion current density of Tempcore TMT steel in OPC, PPC, OPC+20FA and OPC+30FA concrete without any salt contamination (control concrete) varied from 0.008 $\mu A/cm^2$ to 0.07 $\mu A/cm^2$, 0.004 $\mu A/cm^2$ to 0.06 $\mu A/cm^2$, 0.003 $\mu A/cm^2$ to 0.025 $\mu A/cm^2$ and 0.002 $\mu A/cm^2$ to 0.023 $\mu A/cm^2$ respectively irrespective of exposure period. Similarly for Thermex TMT steel, the corrosion current density in OPC, PPC, OPC+20FA and OPC+30FA concrete varied from 0.063 $\mu A/cm^2$ to 0.084 $\mu A/cm^2$, 0.042 $\mu A/cm^2$to 0.066 $\mu A/cm^2$, 0.027 $\mu A/cm^2$ to 0.061 $\mu A/cm^2$ and 0.013 $\mu A/cm^2$ to 0.027 $\mu A/cm^2$ respectively irrespective of exposure period. From these variations in corrosion current density, it is observed that the specimens made from OPC concrete showed slightly higher values of corrosion current density as compared to those made from blended cement (PPC, OPC+20FA and OPC+30FA) concretes at all exposure periods. The lowest corrosion current density values were observed in the specimens made from OPC+30FA concrete for both types of steel i.e. Tempcore TMT and Thermex TMT. This is due to the formation of denser microstructure in OPC+30FA concrete, thereby resulting in higher resistivity concrete and retarding the diffusion of oxygen to steel reinforcement level in concrete.

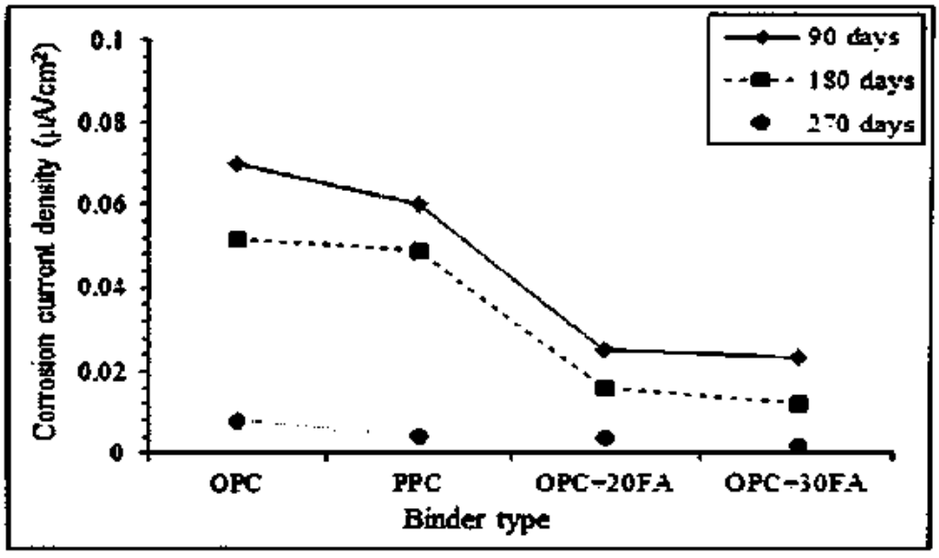

Fig. 6.15 Corrosion current density of Tempcore TMT steel in control mix made with different types of binder at different ages

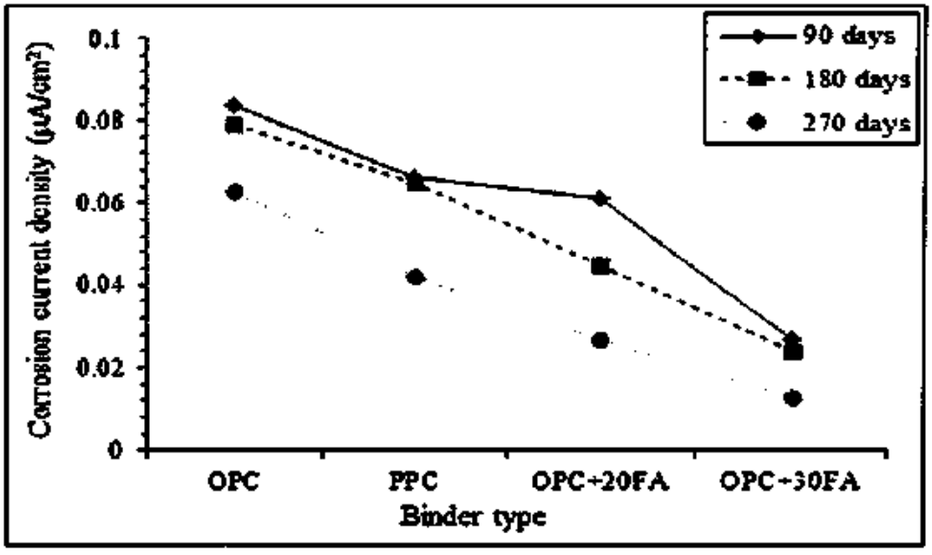

Fig. 6.16 Corrosion current density of Thermex TMT steel in control mix made with different types of binder at different ages

6.2.2.1 Effect of Composite Chloride and Sulfate Exposure on Corrosion Current Density of Steel Reinforcement Embedded in Contaminated Concrete

The values of corrosion current density (I_{corr}) of Tempcore TMT steel in OPC, PPC, OPC+20FA and OPC+30FA concrete specimens admixed with different concentrations of NaCl plus Na_2SO_4 and NaCl plus $MgSO_4$ at the age of 90 days are shown in Fig. 6.17 and Fig. 6.18. Further, the corrosion current density of Tempcore TMT steel in OPC, PPC, OPC+20FA and OPC+30FA concrete specimens admixed with different

concentrations of NaCl plus Na_2SO_4 and NaCl plus $MgSO_4$ and further subjected to these exposure environment are shown in Fig. 6.19 and Fig. 6.20 at the age of 180 days and in Fig. 6.21 and Fig. 6.22 at the age of 270 days. Similarly, the corrosion current density of Thermex TMT steel in OPC, PPC, OPC+20FA and OPC+30FA concrete specimens in NaCl plus Na_2SO_4 and NaCl plus $MgSO_4$ exposure environment are shown in Fig. 6.23 and Fig. 6.24 at the age of 90 days, in Fig. 6.25 and Fig. 6.26 at the age of 180 days and in Fig. 6.27 and Fig. 6.28 at the age of 270 days.

From Fig. 6.17 to Fig. 6.28, it is observed that the corrosion current density values increased with an increase in NaCl dosage in all types of binders and for both types of steel reinforcement irrespective of Na_2SO_4 and $MgSO_4$ concentration. The increase in corrosion current density with increase in NaCl dosage may be attributed to increase in Cl^- ion concentration at the rebar level, which results in increase in conductivity of concrete. Further, there was an increase in corrosion current density of steel reinforcement in concrete with increase in concentrations of Na_2SO_4 and $MgSO_4$ in the conjoint presence of NaCl plus Na_2SO_4 and NaCl plus $MgSO_4$ respectively. While comparing the effect of cation type associated with sulfate ions on corrosion current density, it is inferred that the steel reinforcement in NaCl plus $MgSO_4$ environment showed higher corrosion current density as compared to that in NaCl plus Na_2SO_4 environment for all binders and steel type. This indicates that not only the increase in concentration of sulfate ions but also the associated cation type affected the corrosion current density of steel reinforcement and sulfate ions associated with Mg^{++} cation has more deleterious effect than that associated with Na^+ cation on corrosion performance of steel reinforcement. On comparison of corrosion current density between control mix and those admixed and further exposed to composite sodium chloride plus sodium sulfate and sodium chloride plus magnesium sulfate, it is found that the control mix specimens exhibited lower values of corrosion current density as compared to those subjected to varying concentrations of NaCl plus Na_2SO_4 and NaCl plus $MgSO_4$.

From Fig. 6.17 to Fig. 6.22, it is observed that the corrosion current density of Tempcore TMT steel in prismatic concrete specimens in the conjoint presence of sodium chloride plus sodium sulfate were in the ranges of 0.13 $\mu A/cm^2$ to 0.68 $\mu A/cm^2$ at the age of 90 days, 0.024 $\mu A/cm^2$ to 0.56 $\mu A/cm^2$ at the age of 180 days and 0.16 $\mu A/cm^2$ to 1.05 $\mu A/cm^2$ at the age of 270 days, irrespective of binder type. Similarly in the conjoint presence of sodium chloride plus magnesium sulfate, the corrosion current density of

Tempcore TMT steel varied from 0.36 $\mu A/cm^2$ to 1.98 $\mu A\ cm^2$ at the age of 90 days, 0.37 $\mu A/cm^2$ to 4.64 $\mu A/cm^2$ at the age of 180 days and 0.52 $\mu A\ cm^2$ to 10.5 $\mu A/cm^2$ at the age of 270 days. Further from Fig. 6.23 to Fig. 6.28, it is observed that the corrosion current density of Thermex TMT steel in prismatic concrete specimens in the conjoint presence of sodium chloride plus sodium sulfate were in the ranges of 0.3 $\mu A/cm^2$ to 0.82 $\mu A/cm^2$, 0.13 $\mu A/cm^2$ to 0.72 $\mu A/cm^2$ and 0.3 $\mu A/cm^2$ to 2.23 $\mu A/cm^2$ at the ages of 90 days, 180 days and 270 days respectively, irrespective of binder type. Similarly, the corrosion current density of Thermex TMT steel in the conjoint presence of sodium chloride plus magnesium sulfate varied from 0.63 $\mu A/cm^2$ to 3.55 $\mu A/cm^2$, 1.12 $\mu A/cm^2$ to 5.2 $\mu A/cm^2$ and 1.14 $\mu A/cm^2$ to 11.8 $\mu A/cm^2$ at the ages of 90 days, 180 days and 270 days respectively. From these values, it is observed that the corrosion current density of steel reinforcement in concrete in the presence of NaCl plus Na_2SO_4 decreased with an increase in exposure period till 180 days and after that the corrosion current density increased at the age of 270 days for both types of steel reinforcement. It may be noted that the prismatic reinforced concrete specimens admixed with NaCl plus Na_2SO_4 were subjected to laboratory exposure condition till the age of 90 days and were then further exposed to NaCl plus Na_2SO_4 solutions with alternate wetting and drying cycles. The decrease in the corrosion current density of steel reinforcement at the age of 180 days may be attributed to filling of pores in concrete with calcium chloroaluminate and calcium sulphoaluminate (formed respectively as a result of reaction of admixed chloride and sulfate ions with hydrated C_3A), thereby retarding the diffusion of Cl^- and SO_4^{2-} ions to the rebar level in concrete. Further, with increase in exposure to the external solutions, there is increase in penetration of chloride ions to the rebar level through the pores of concrete due to higher rate of diffusion of chloride ions than that of the sulfate ions [134] and also due to increased solubility of ettringite in chloride solution [43]. As reported by Harrison [90], the solubility of ettringite in chloride solution is three times greater than that in water. Thus there is increase in corrosion current density of steel reinforcement at the exposure age of 270 days due to increase in Cl^- ion concentration at the rebar level. In NaCl plus $MgSO_4$ environment, the corrosion current density of steel reinforcement increased with an increase in exposure period. This is attributed to increase in conductivity of concrete due ingress of higher amount Cl^- ion to the rebar level because of conversion of C-S-H to non-cementitious M-S-H as result of reaction of $MgSO_4$ with C-S-H in the conjoint presence of NaCl and $MgSO_4$.

From Fig. 6.17 to Fig. 6.22, it is observed that the corrosion current density values of Tempcore TMT steel in OPC, PPC, OPC+20FA and OPC+30FA concrete were in the ranges of 0.09 $\mu A/cm^2$ to 1.05 $\mu A/cm^2$, 0.076 $\mu A/cm^2$ to 0.83 $\mu A/cm^2$, 0.046 $\mu A/cm^2$ to 0.76 $\mu A/cm^2$ and 0.024 $\mu A/cm^2$ to 0.53 $\mu A/cm^2$ respectively, in the conjoint presence of NaCl plus Na_2SO_4 irrespective of exposure period and NaCl plus Na_2SO_4 concentrations. Similarly, the corrosion current density values of Tempcore TMT steel in the conjoint presence of sodium chloride plus magnesium sulfate in OPC, PPC, OPC+20FA and OPC+30FA concrete varied from 0.36 $\mu A/cm^2$ to 5.36 $\mu A/cm^2$, 0.5 $\mu A/cm^2$ to 6.8 $\mu A/cm^2$, 0.58 $\mu A/cm^2$ to 8.2 $\mu A/cm^2$ and 0.64 $\mu A/cm^2$ to 10.5 $\mu A/cm^2$ respectively. For Thermex TMT steel, the corrosion current density in OPC, PPC, OPC+20FA and OPC+30FA concrete varied from 0.34 $\mu A/cm^2$ to 2.23 $\mu A/cm^2$, 0.31 $\mu A/cm^2$ to 1.94 $\mu A/cm^2$, 0.27 $\mu A/cm^2$ to 0.82 $\mu A/cm^2$ and 0.13 $\mu A/cm^2$ to 0.77 $\mu A/cm^2$ respectively in the conjoint presence of NaCl plus Na_2SO_4, whereas in the conjoint presence of NaCl plus $MgSO_4$, the corrosion current density in OPC, PPC, OPC+20FA and OPC+30FA concrete varied from 0.63 $\mu A/cm^2$ to 5.61 $\mu A/cm^2$, 0.69 $\mu A/cm^2$ to 6.87 $\mu A/cm^2$, 0.89 $\mu A/cm^2$ to 8.56 $\mu A/cm^2$ and 0.96 $\mu A/cm^2$ to 11.8 $\mu A/cm^2$ respectively for Thermex TMT steel, as observed from Fig. 6.23 to Fig. 6.28.

From the above corrosion current density values, it is inferred that, the corrosion current density of both types of steel in blended cement concrete specimens were lower than those in OPC concrete specimens in the conjoint presence of sodium chloride plus sodium sulfate, whereas the opposite variation was observed in the conjoint presence of sodium chloride plus magnesium sulfate i.e. the corrosion current density values in OPC concrete were lower than those in blended cement concrete specimens. The lower corrosion current density in blended cement concrete (PPC, OPC+20FA and OPC+30FA) as compared to that in OPC concrete in the conjoint presence of NaCl plus $NaSO_4$ may be attributed to relatively higher resistivity of blended cement concrete because of production of additional C-S-H and reduction in formation of gypsum and ettringite due to lower availability of calcium hydroxide in blended cement concrete. In the conjoint presence of NaCl plus $MgSO_4$, the lower corrosion current density in OPC concrete than that in blended cement concrete may be due to increase in resistivity of OPC concrete as a result of filling of pores with magnesium hydroxide (brucite) to a greater extent. In blended cement concrete, the higher corrosion density in the conjoint presence of NaCl

plus $MgSO_4$ may be attributed to lower resistivity as a result of formation of gypsum and non-cementitious magnesium silicate hydrate.

On comparing the steel type, it is observed that Tempcore TMT steel exhibited lower corrosion density as compared to Thermex TMT steel in all the binders and also in the conjoint presence of both NaCl plus Na_2SO_4 and NaCl plus $MgSO_4$. The improved performance of Tempcore TMT steel as compared to Thermex TMT steel in the conjoint presence of chloride and sulfate ions may be attributed to improved surface microstructure of Tempcore TMT steel.

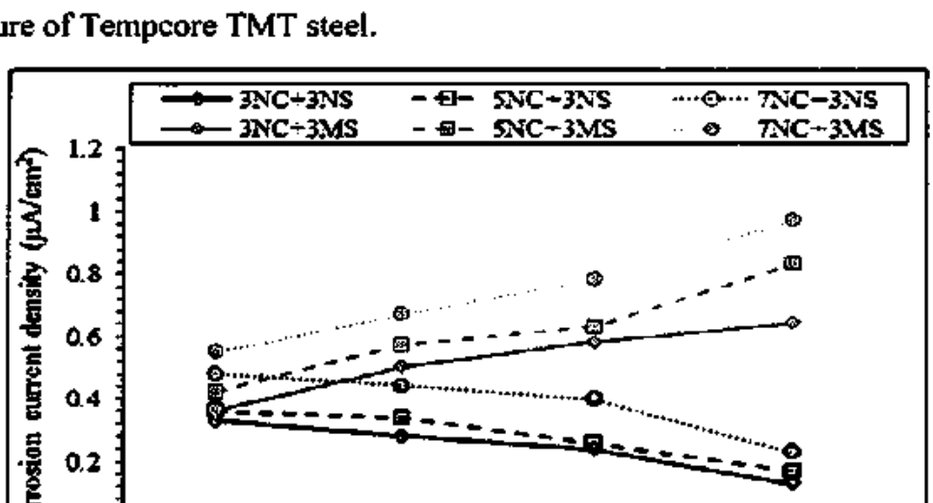

Fig. 6.17 Corrosion current density of Tempcore TMT steel at 90 days in different concrete mixes admixed with varying concentrations of NaCl plus 3% Na_2SO_4 and NaCl plus 3% $MgSO_4$

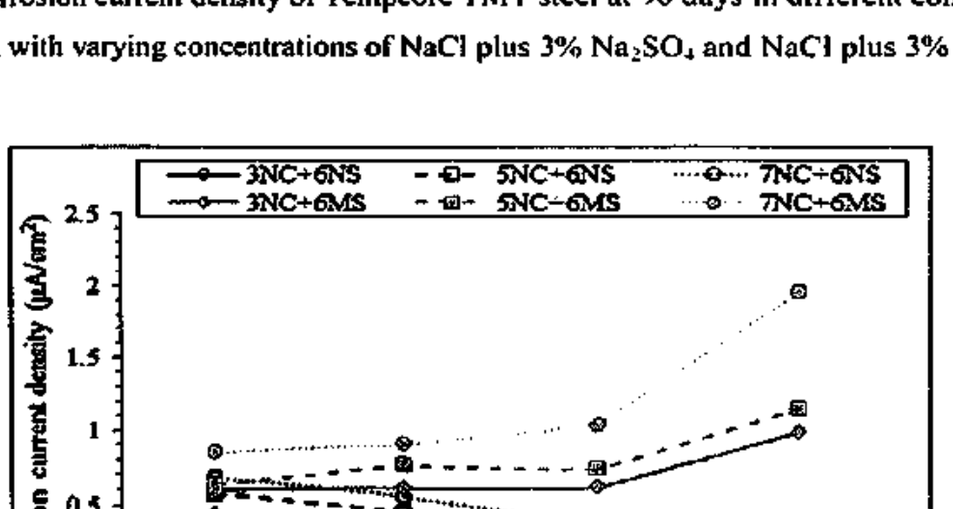

Fig. 6.18 Corrosion current density of Tempcore TMT steel at 90 days in different concrete mixes admixed with varying concentrations of NaCl plus 6% Na_2SO_4 and NaCl plus 6% $MgSO_4$

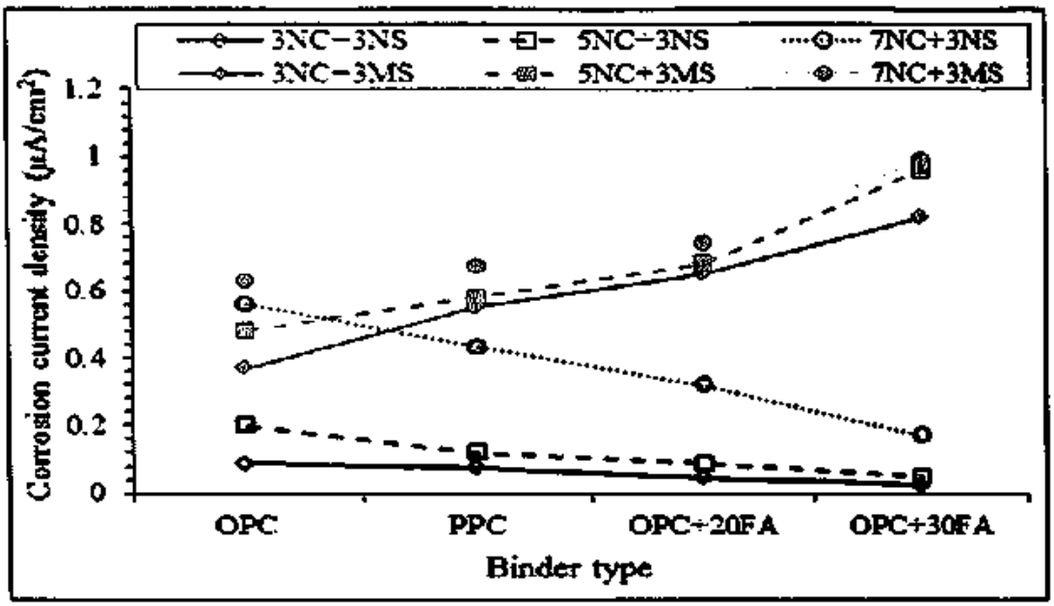

NC: NaCl; NS: Na_2SO_4; MS: $MgSO_4$

Fig. 6.19 Corrosion current density of Tempcore TMT steel at 180 days in different concrete mixes admixed and further exposed to varying concentrations of NaCl plus 3% Na_2SO_4 and NaCl plus 3% $MgSO_4$ with alternate wetting and drying cycles

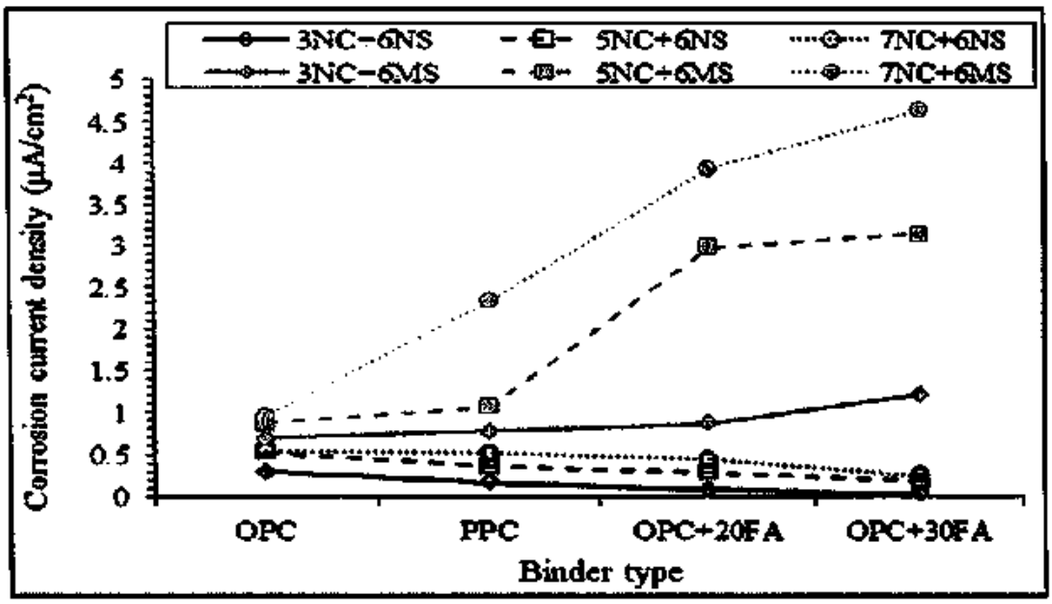

Fig. 6.20 Corrosion current density of Tempcore TMT steel at 180 days in different concrete mixes admixed and further exposed to varying concentrations of NaCl plus 6% Na_2SO_4 and NaCl plus 6% $MgSO_4$ with alternate wetting and drying cycles

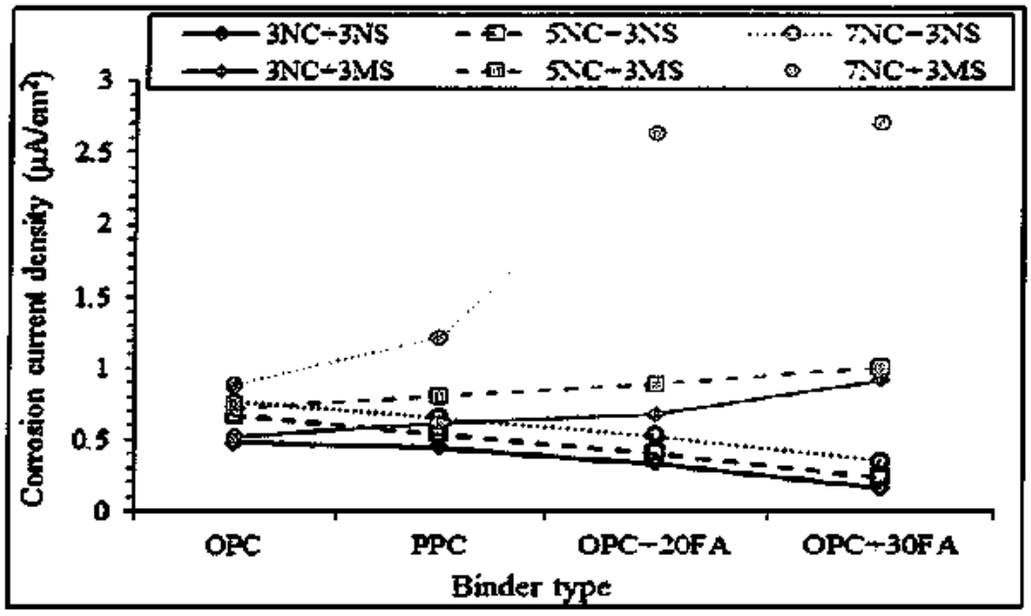

Fig. 6.21 Corrosion current density of Tempcore TMT steel at 270 days in different concrete mixes admixed and further exposed to varying concentrations of NaCl plus 3% Na_2SO_4 and NaCl plus 3% $MgSO_4$ with alternate wetting and drying cycles

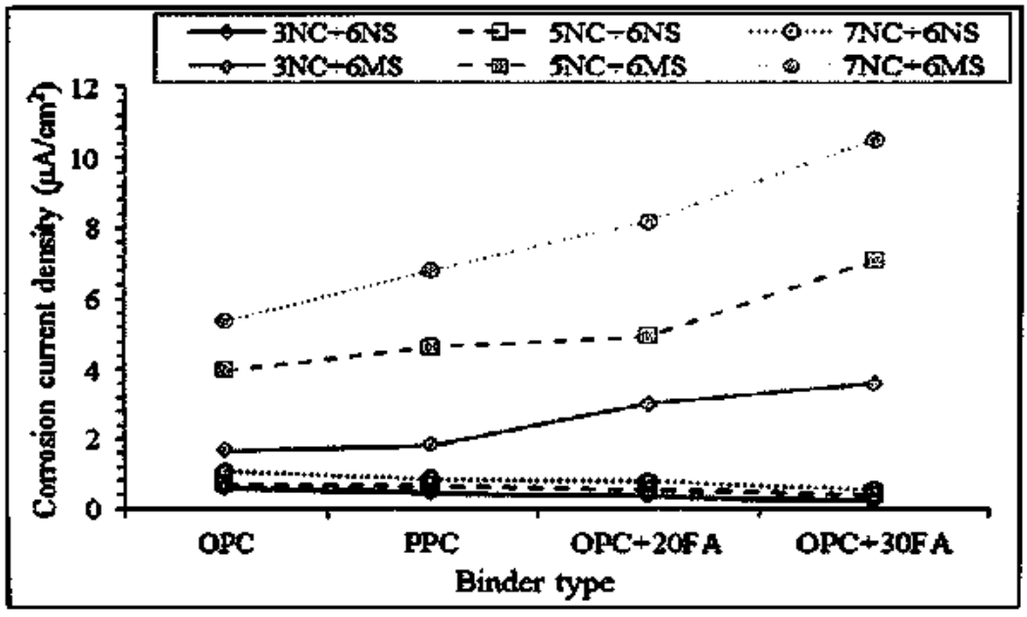

Fig. 6.22 Corrosion current density of Tempcore TMT steel at 270 days in different concrete mixes admixed and further exposed to varying concentrations of NaCl plus 6% Na_2SO_4 and NaCl plus 6% $MgSO_4$ with alternate wetting and drying cycles

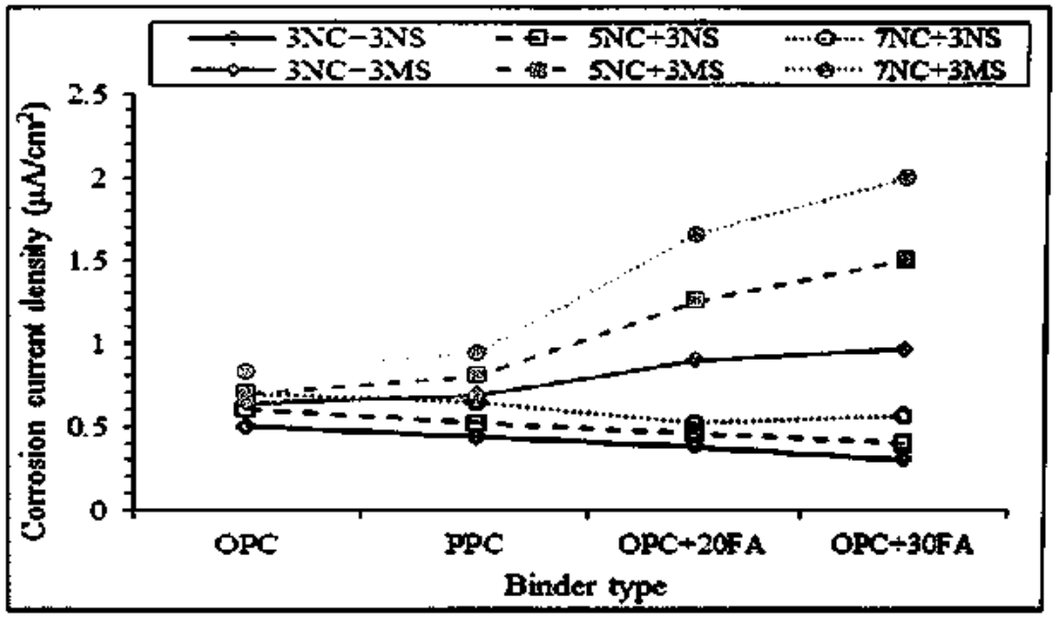

Fig. 6.23 Corrosion current density of Thermex TMT steel at 90 days in different concrete mixes admixed with varying concentrations of NaCl plus 3% Na_2SO_4 and NaCl plus 3% $MgSO_4$

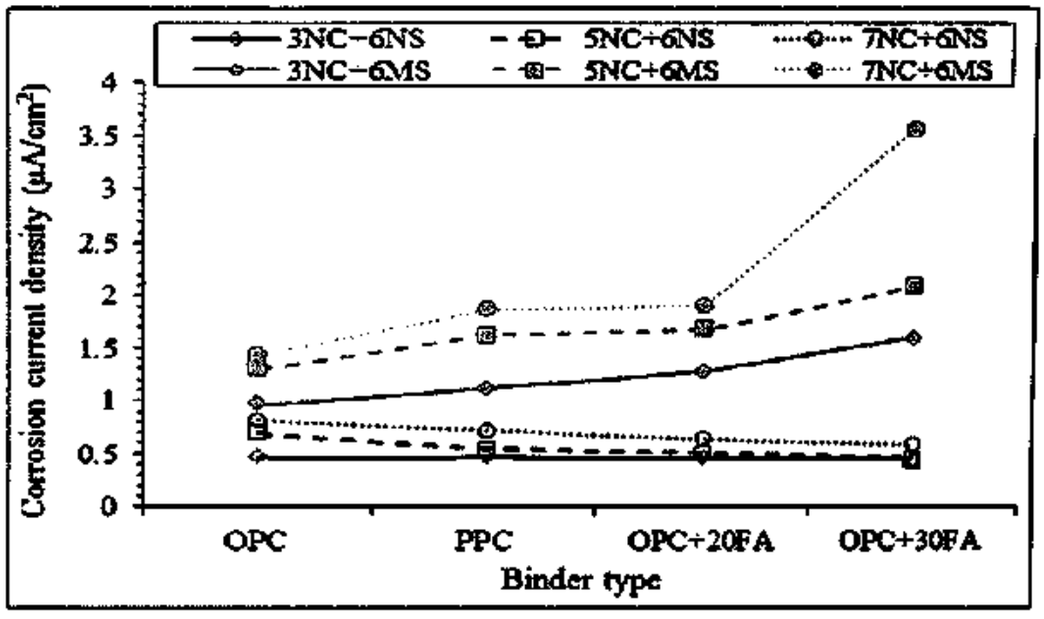

Fig. 6.24 Corrosion current density of Thermex TMT steel at 90 days in different concrete mixes admixed with varying concentrations of NaCl plus 6% Na_2SO_4 and NaCl plus 6% $MgSO_4$

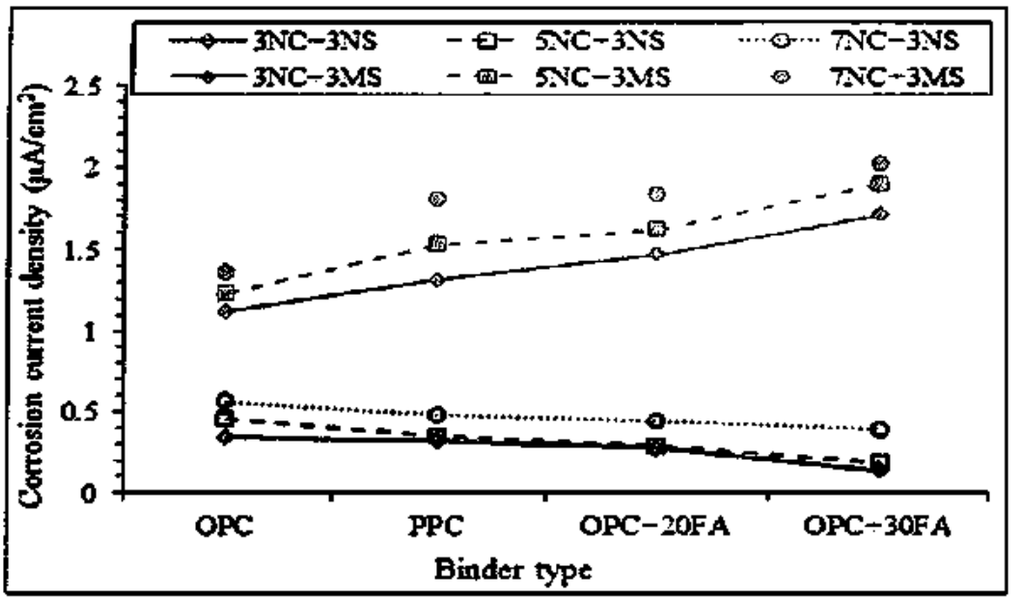

Fig. 6.25 Corrosion current density of Thermex TMT steel at 180 days in different concrete mixes admixed and further exposed to varying concentrations of NaCl plus 3% Na_2SO_4 and NaCl plus 3% $MgSO_4$ with alternate wetting and drying cycles

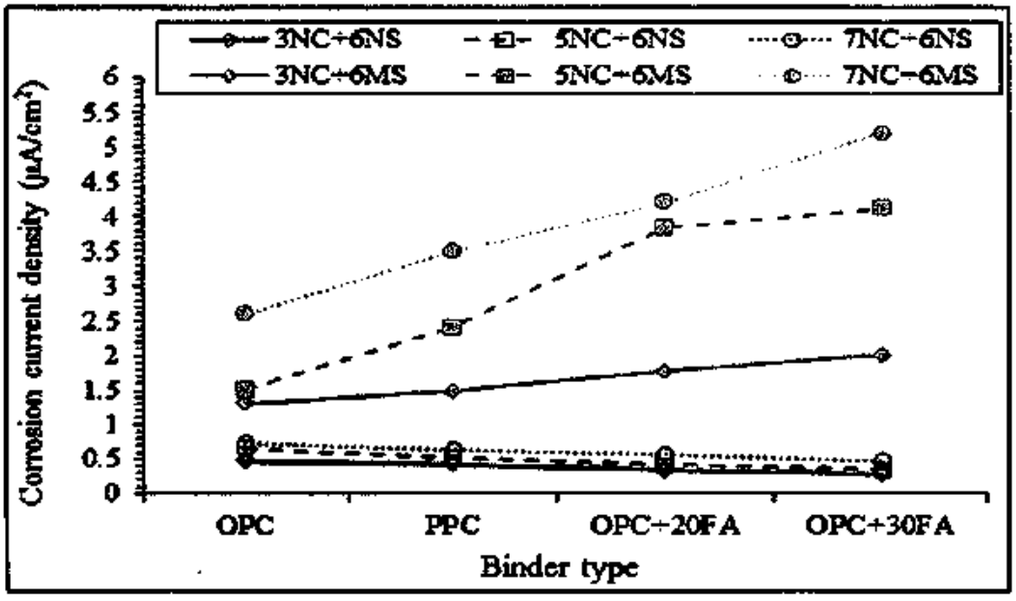

Fig. 6.26 Corrosion current density of Thermex TMT steel at 180 days in different concrete mixes admixed and further exposed to varying concentrations of NaCl plus 6% Na_2SO_4 and NaCl plus 6% $MgSO_4$ with alternate wetting and drying cycles

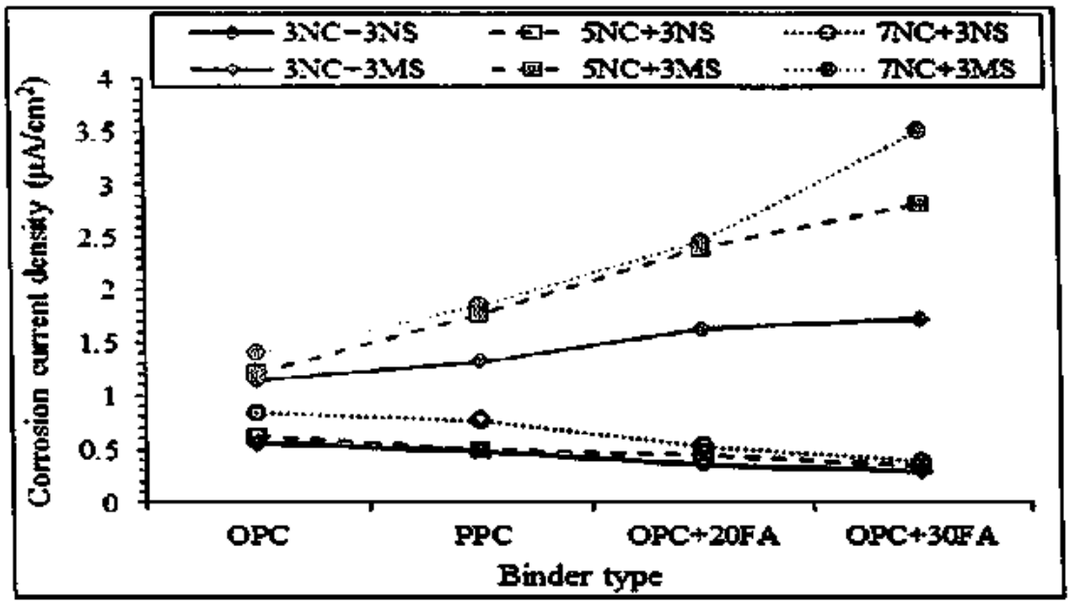

Fig. 6.27 Corrosion current density of Thermex TMT steel at 270 days in different concrete mixes admixed and further exposed to varying concentrations of NaCl plus 3% Na_2SO_4 and NaCl plus 3% $MgSO_4$ with alternate wetting and drying cycles

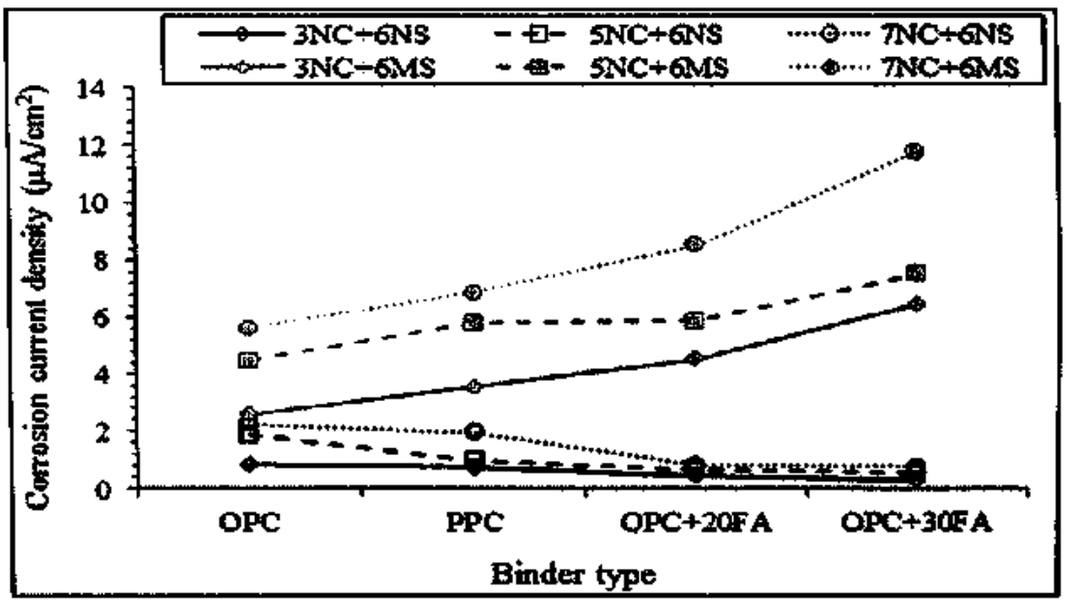

Fig. 6.28 Corrosion current density of Thermex TMT steel at 270 days in different concrete mixes admixed and further exposed to varying concentrations of NaCl plus 6% Na_2SO_4 and NaCl plus 6% $MgSO_4$ with alternate wetting and drying cycles

6.3 SUMMARY

The results obtained from corrosion potential measurement of steel reinforcement embedded in concrete admixed with chloride-sulfate ions and further exposed to these ions indicated that the probability of occurrence of steel reinforcement corrosion increased in the presence of chloride and sulfate ions (associated with sodium and magnesium cations) for all binders and steel type. Further, the corrosion potential values became more negative with increase in concentrations of NaCl, Na_2SO_4 and $MgSO_4$. Steel reinforcement in OPC concrete showed more negative potential values as compared to that in blended cement (PPC, OPC+20FA and OPC+30FA) concretes in the conjoint presence of NaCl plus Na_2SO_4, thereby indicating higher probability of occurrence of corrosion in OPC, whereas in the conjoint presence of NaCl plus $MgSO_4$, the probability of occurrence of steel reinforcement corrosion was higher in blended cements as compared to OPC for both types of steel reinforcement.

The results indicated that the corrosion current density of steel reinforcement increased with an increase in NaCl, Na_2SO_4 and $MgSO_4$ dosage for all types of binder and steel reinforcement. Further, the corrosion current density of steel reinforcement was higher in NaCl plus $MgSO_4$ environment as compared to that in NaCl plus Na_2SO_4 environment. The corrosion current density of both types of steel reinforcement in blended cement concrete specimens were lower than those in OPC concrete specimens in the conjoint presence of sodium chloride plus sodium sulfate, whereas the opposite variation was observed in the conjoint presence of sodium chloride plus magnesium sulfate i.e. the corrosion current density values in OPC concrete were lower than those in blended cement concrete specimens. On comparing the steel type, it is observed that Tempcore TMT steel exhibited lower corrosion density as compared to Thermex TMT steel in all binders and in the conjoint presence of NaCl plus Na_2SO_4 and NaCl plus $MgSO_4$. The variations in the corrosion current density of steel reinforcement embedded in concrete in the conjoint presence of NaCl plus Na_2SO_4 and NaCl plus $MgSO_4$ are consistent with the variations in corrosion current density of steel reinforcement in the electrolytic concrete powder solutions (presented in Chapter 5) contaminated with composite chloride and sulphate ions. Further, the variations in passivity of steel reinforcement in the electrolytic concrete powder solutions (presented in Chapter 5) are also consistent with that in the corrosion current density of steel reinforcement embedded in concrete in the conjoint presence of chloride and sulfate ions along with the associated cation type.

Overall, OPC+30FA and Tempcore TMT steel exhibited best performance against the combined effect of sodium chloride and sodium sulfate whereas OPC and Tempcore TMT showed best performance against the combined effect of sodium chloride and magnesium sulfate in terms of reduced corrosion current density as compared to other types of binder and steel.

CHAPTER 7

PERFORMANCE OF CONCRETE IN SULFATE AND CONJOINT CHLORIDE-SULFATE ENVIRONMENT

7.1 GENERAL

The deterioration of concrete and reduction in its compressive strength are caused due to its exposure to the aggressive ions like sulfate and chloride ions. The durability performance of concrete made with different types of binder namely OPC, PPC, OPC+20FA (20% fly ash) and OPC+30FA (30% fly ash) at water-binder ratios (w/b ratios) of 0.45 and 0.5 and exposed to sulfate and chloride-sulfate solutions for a period of 360 days was evaluated thorough visual inspection; measurements of change in weight and change in compressive strength of concrete cube specimens. Two exposure conditions were adopted viz. exposure I: continuous full immersion and exposure II: full immersion with alternate wetting and drying cycles. To elucidate the effect of sulfate and chloride ions on the microstructure of concrete, X-ray diffraction (XRD) analysis and Field emission scanning electron microscopy (FESEM) analysis were conducted. The results of these experimental investigations are presented and discussed in this chapter.

7.2 VISUAL APPEARANCE OF CONCRETE CUBE SPECIMENS

The visual appearance of concrete cube specimens before subjecting them to exposure solutions is shown in Fig. 7.1.

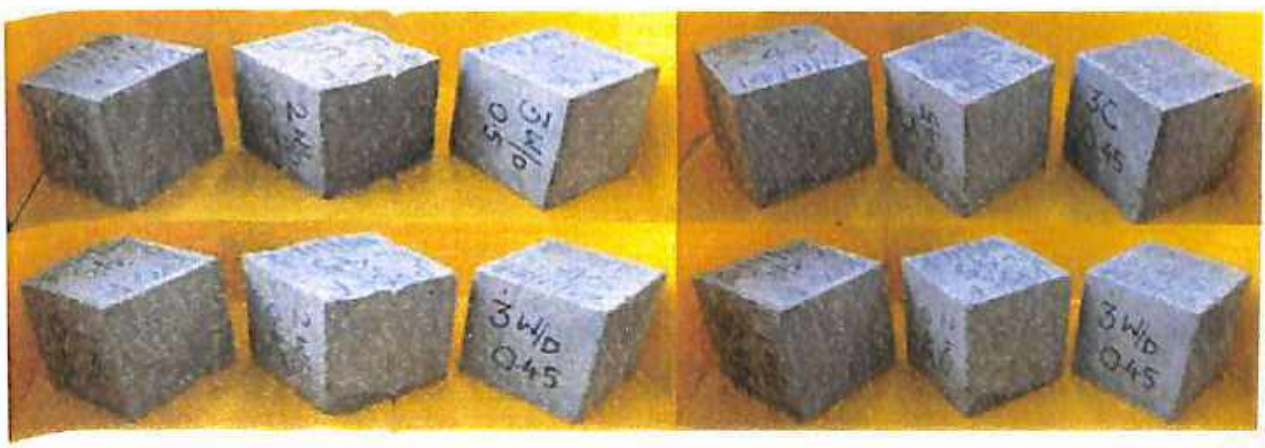

Fig. 7.1 Visual appearance of cubes before subjecting to exposure solutions

As already stated in Chapter 3, the concrete cube specimens made with different types of binder viz. OPC, PPC, OPC+20FA and OPC+30FA and w/b ratios of 0.45 and 0.5 were subjected to exposure solutions containing varying concentrations of sodium sulfate (Na_2SO_4), magnesium sulfate ($MgSO_4$), sodium chloride plus sodium sulfate (NaCl + Na_2SO_4) and sodium chloride plus magnesium sulfate (NaCl + $MgSO_4$).

The visual appreance of some of the cube specimens after exposure to sulfate solutions of 12% Na_2SO_4 and 12% $MgSO_4$ with alternate wetting and drying cycles are shown in Fig. 7.2 and Fig. 7.3 respectively. The signs of deterioration was observed on the surface of the cube specimens as evident from these figures. Further, there was no significant surface deterioration on the cube specimens at other concentrations (3% and 6%) of Na_2SO_4 and $MgSO_4$ solutions for both types of exposure condition (i.e. continuous and alternate wetting and drying).

Fig. 7.2 Visual appearance of concrete cube specimens exposed to 12% Na_2SO_4 solution with alternate wetting and drying cycles for a period of 360 days

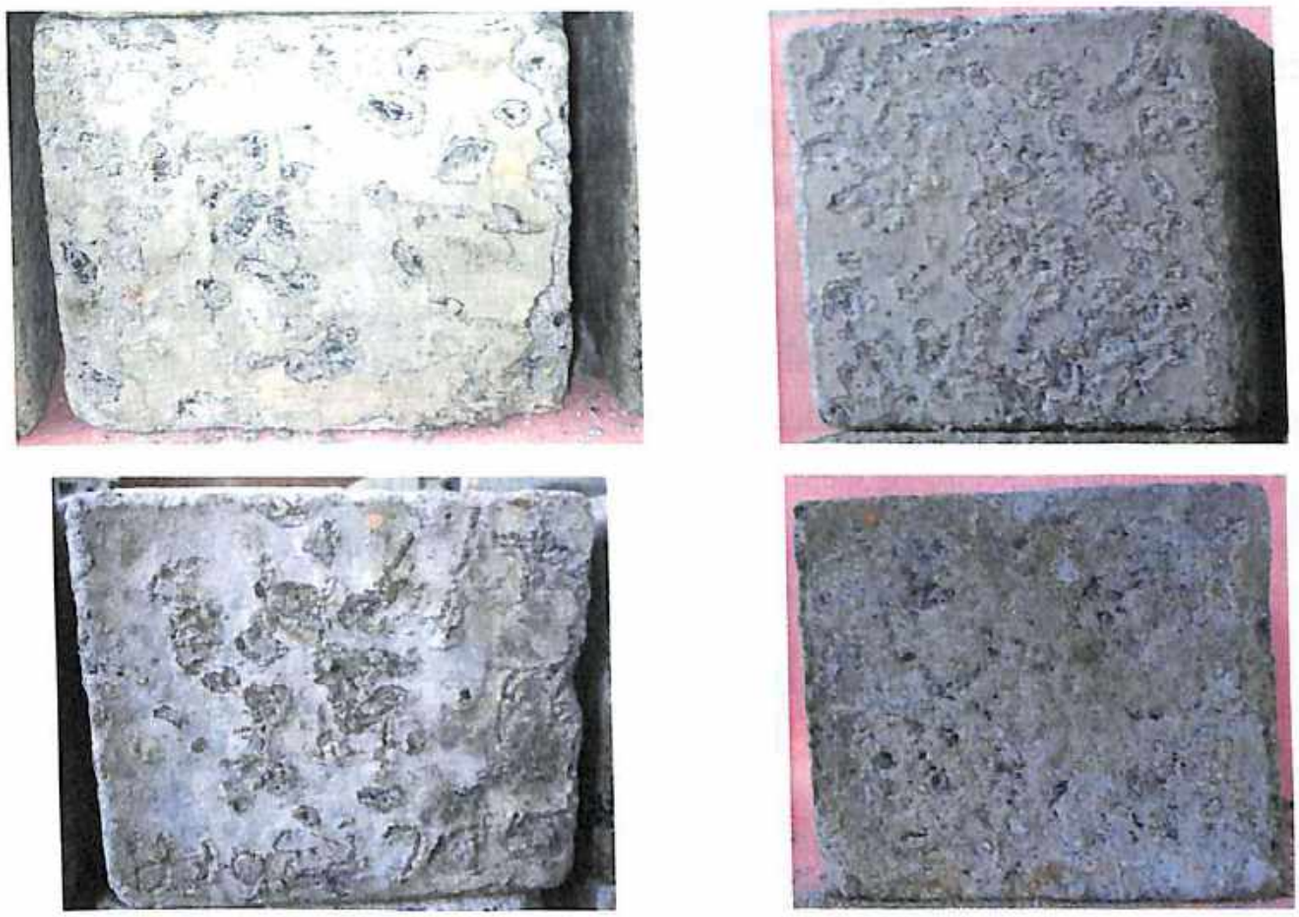

Fig. 7.3 Visual appearance of concrete cube specimens exposed to $MgSO_4$ solution with alternate wetting and drying cycles for a period of 360 days

From Fig. 7.2, it is observed that the concrete cube specimens exposed to Na_2SO_4 solution showed deterioration at the edges of the specimens. However, the cube specimens exposed to $MgSO_4$ solution showed deterioration in the form of peeling of the surface skin on all the faces of the cube specimens with the aggregates exposed as observed from Fig. 7.3. The peeling of surface skin of concrete in $MgSO_4$ solution is attributed to the loss of cohesiveness between the surface layer; and the inner cement matrix and the aggregates.

Further from visual examination, it is observed that there was no significant deterioration on surface of concrete cube specimens exposed to NaCl + Na_2SO_4 and NaCl + $MgSO_4$ solutions. This indicates that the degree of surface deterioration was mitigated in the specimens exposed to NaCl + Na_2SO_4 and NaCl + $MgSO_4$ solutions as compared to those exposed to only sulfate solutions. However, a crystalline salt deposition was observed on the surface of all the specimens exposed to sulfate and conjoint chloride-sulfate solutions.

7.3 CHANGE IN WEIGHT OF CONCRETE EXPOSED TO SULFATE ENVIRONMENT AND CONJOINT CHLORIDE-SULFATE ENVIRONMENT

The degree of deterioration was evaluated by measuring the change in weight of the concrete cube specimens. This method of monitoring the concrete cube specimens is a non-destructive means of checking the degree of deterioration of concrete. To evaluate the weight change (reduction/increase) due to the effect of sulfate ions and conjoint chloride-sulfate ions, the weight of all the specimens were measured before they were subjected to different exposure solutions. After the completion of the exposure period of 360 days, the cube specimens were weighed and subsequently the change in weight was calculated as the percentage of the original weight of the cube specimen (stated already in chapter 3). It is to be noted that, three replicate cube specimens of a concrete mix were subjected to a given exposure solution and accordingly the average change in weight (%) was calculated.

7.3.1 Change in Weight of Concrete Subjected to Exposure Solutions with Continuous Full Immersion and Full Immersion with Alternate Wetting and Drying Cycles

The average change in weight (%) of cube specimens are plotted for different types of binder (viz. OPC, PPC, OPC+20FA and OPC+30FA), w/b ratios (0.45 and 0.5) and different exposure solutions (viz. varying concentrations of Na_2SO_4 and $MgSO_4$). These plots are shown in Fig. 7.4 and Fig. 7.5 at w/b ratios of 0.45 and 0.5 respectively for continuous full immersion condition and in Fig. 7.6 and Fig. 7.7 respectively for full immersion with alternate wetting and drying cycles. It may be noted that replicate cube specimens from all the concrete mixes were also exposed to normal water for a period of 360 days with same exposure conditions.

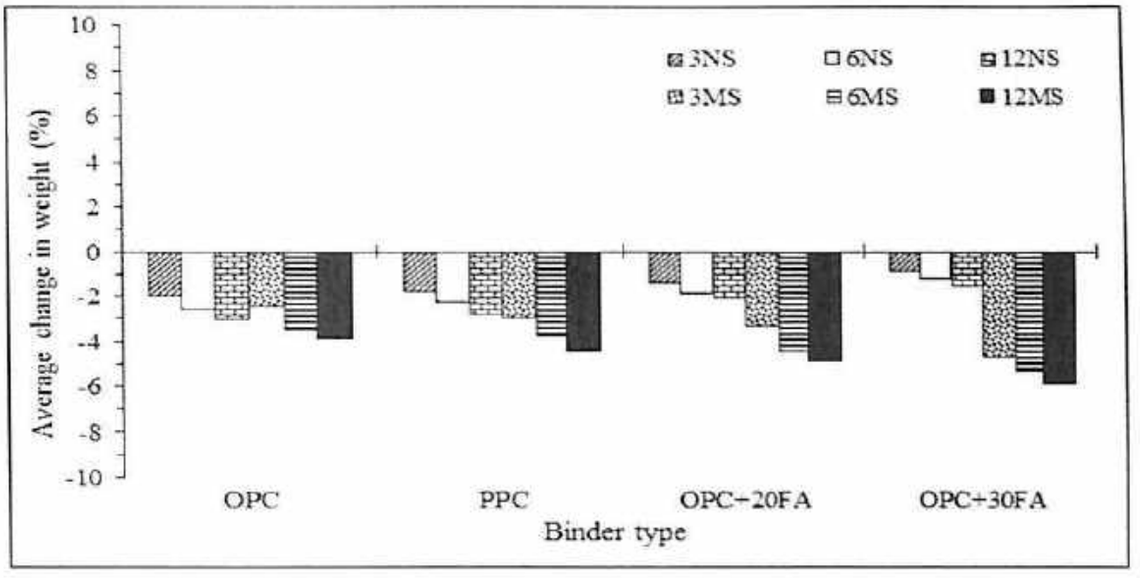

(3NS: 3% Na_2SO_4, 6NS: 6% Na_2SO_4, 12NS: 12% Na_2SO_4, 3MS: 3% $MgSO_4$, 6MS: 6% $MgSO_4$, and 12MS: 12% $MgSO_4$)

Fig. 7.4 Average change in weight (%) of concrete specimens made from different types of binder and w/b ratio of 0.45 and exposed to varying concentrations of Na_2SO_4 and $MgSO_4$ solutions for a period of 360 days under continuous full immersion condition

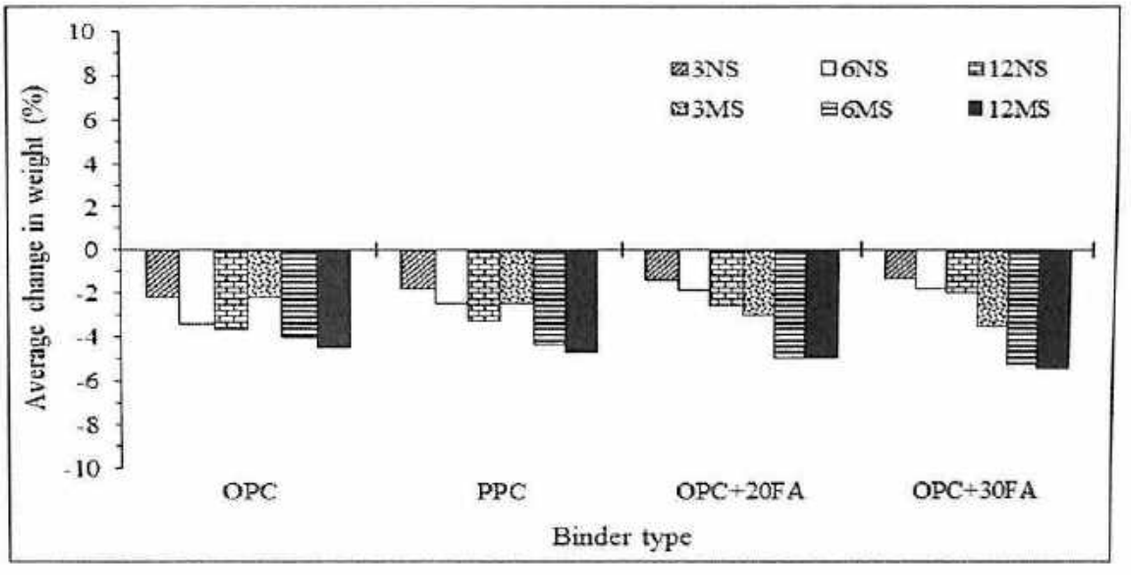

Fig. 7.5 Average change in weight (%) of concrete specimens made from different types of binder and w/b ratio of 0.5 and exposed to varying concentrations of Na_2SO_4 and $MgSO_4$ solutions for a period of 360 days under continuous full immersion condition

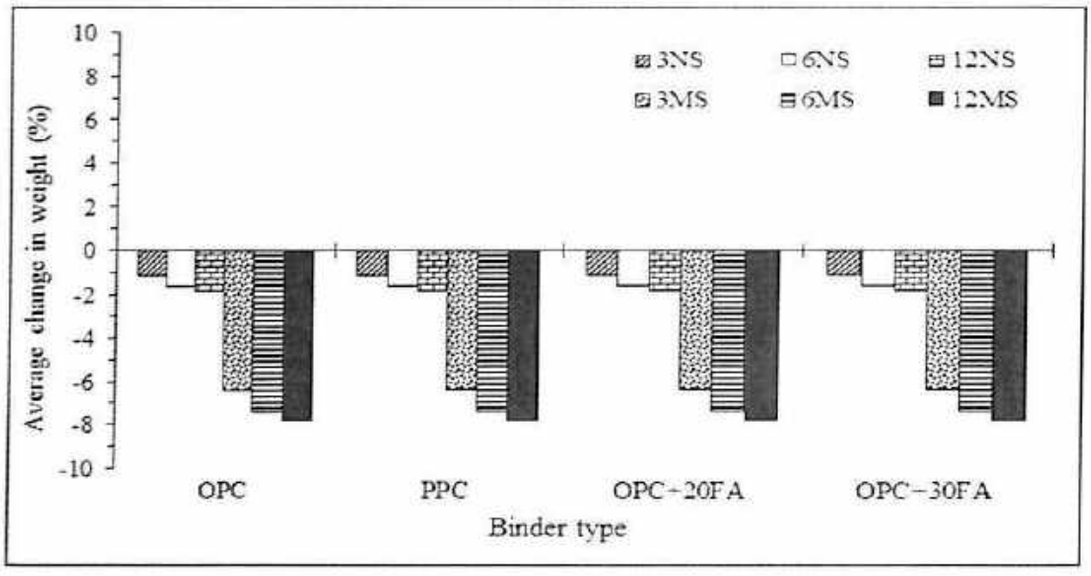

Fig. 7.6 Average change in weight (%) of concrete specimens made from different types of binder and w/b ratio of 0.45 and exposed to varying concentrations of Na_2SO_4 and $MgSO_4$ solutions for a period of 360 days under full immersion with alternate wetting and drying cycles

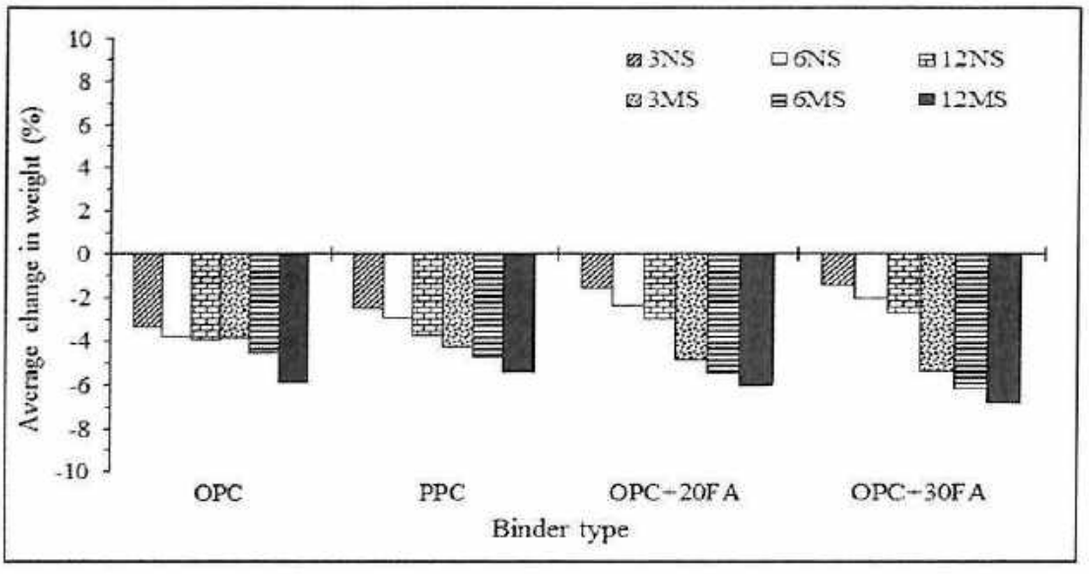

Fig. 7.7 Average change in weight (%) of concrete specimens made from different types of binder and w/b ratio of 0.5 and exposed to varying concentrations of Na_2SO_4 and $MgSO_4$ solutions for a period of 360 days under full immersion with alternate wetting and drying cycles

From Fig. 7.4 to Fig. 7.7, it is observed that the cube specimens exposed to varying concentrations of Na_2SO_4 and $MgSO_4$ showed negative change in weight percentage, which indicates that the weight of cube specimens reduced after exposure to the sulfate solutions. The loss in weight of cube specimens may be attributed to the deterioration of

concrete in the presence of sulfate ions. Further, it is found that the weight loss is higher in the specimens exposed to $MgSO_4$ solution as compared to those exposed to Na_2SO_4 solution at all concentrations, as observed from Fig. 7.4 to Fig. 7.7. The similar observation was reported by Jiang and Niu [134]. The higher weight loss of concrete specimens exposed to $MgSO_4$ solution may be attributed to the destabilization of calcium silicate hydrate (C-S-H) as the magnesium sulfate attack is directed extensively towards C-S-H gel, thereby converting it to non-cementitious magnesium silicate hydrate (M-S-H).

Further from Fig. 7.4 to Fig. 7.7, it is observed that the concrete specimens made with OPC exhibited higher weight loss percentage as compared to the other types of binder at both w/b ratios when exposed to Na_2SO_4 solution, whereas for exposure to $MgSO_4$ solution, the cube specimens made with OPC+30FA exhibited higher weight loss percentage as compared to the other types of binder at both w/b ratios. While evaluating the effect of w/b ratio, it is observed that the specimens made with w/b ratio of 0.5 exhibited higher weight loss as compared to those made with w/b ratio of 0.45 in Na_2SO_4 solutions whereas the opposite variation was observed in $MgSO_4$ solutions i.e. the specimens made with w/b ratio of 0.45 mostly showed higher weight loss as compared to those made with w/b ratio of 0.5. These variations in weight loss of concrete with binder type and w/b ratio in different sulfate solutions may be attributed to the variations in the extent of deterioration of concrete due to effect of sulfate ions along with the associated cation type (Na^+ and Mg^{++}).

The plots of average change in weight (%) of cube specimens made from different concrete mixes and exposed to varying concentrations of NaCl + Na_2SO_4 and NaCl + $MgSO_4$ solutions are shown in Fig. 7.8 and Fig. 7.9 at w/b ratios of 0.45 and 0.5 respectively for continuous full immersion condition and in Fig. 7.10 and Fig. 7.11 respectively for full immersion with alternate wetting and drying cycles.

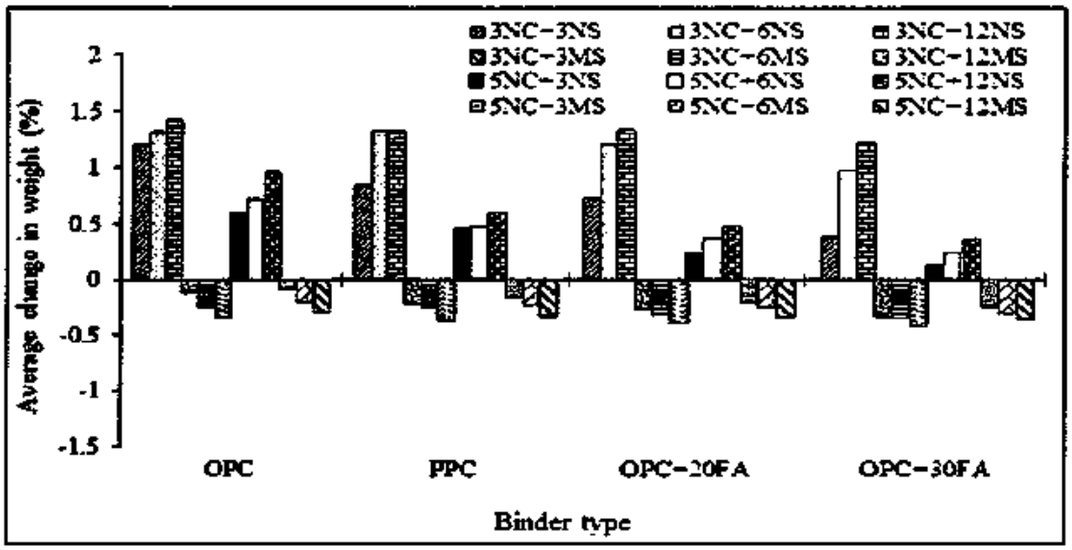

Fig. 7.8 Average change in weight (%) of concrete specimens made from different types of binder and w/b ratio of 0.45 and exposed to varying concentrations of $NaCl+Na_2SO_4$ and $NaCl+MgSO_4$ solutions for a period of 360 days under continuous full immersion condition

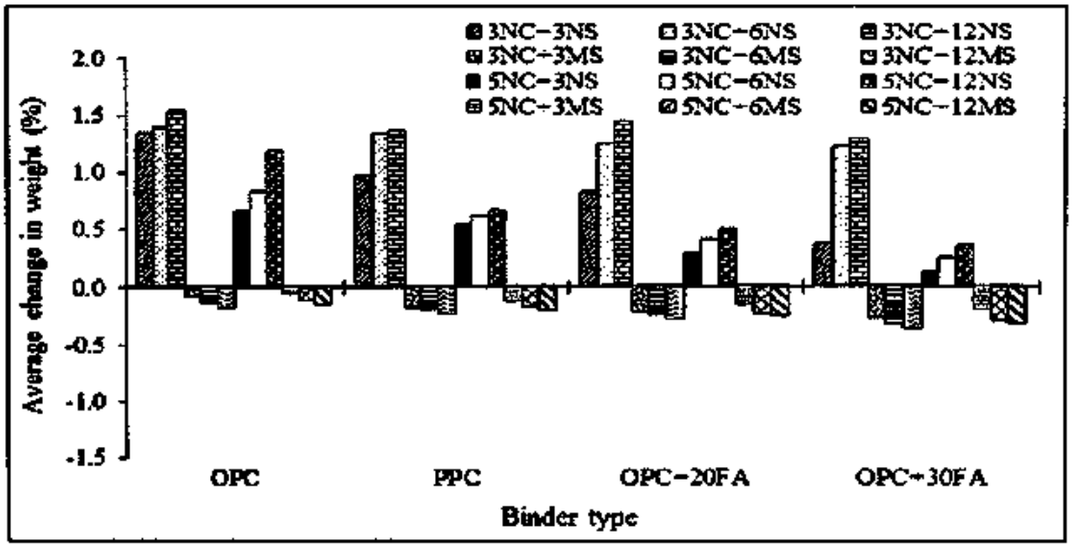

Fig. 7.9 Average change in weight (%) of concrete specimens made from different types of binder and w/b ratio of 0.5 and exposed to varying concentrations of $NaCl+Na_2SO_4$ and $NaCl+MgSO_4$ solutions for a period of 360 days under continuous full immersion condition

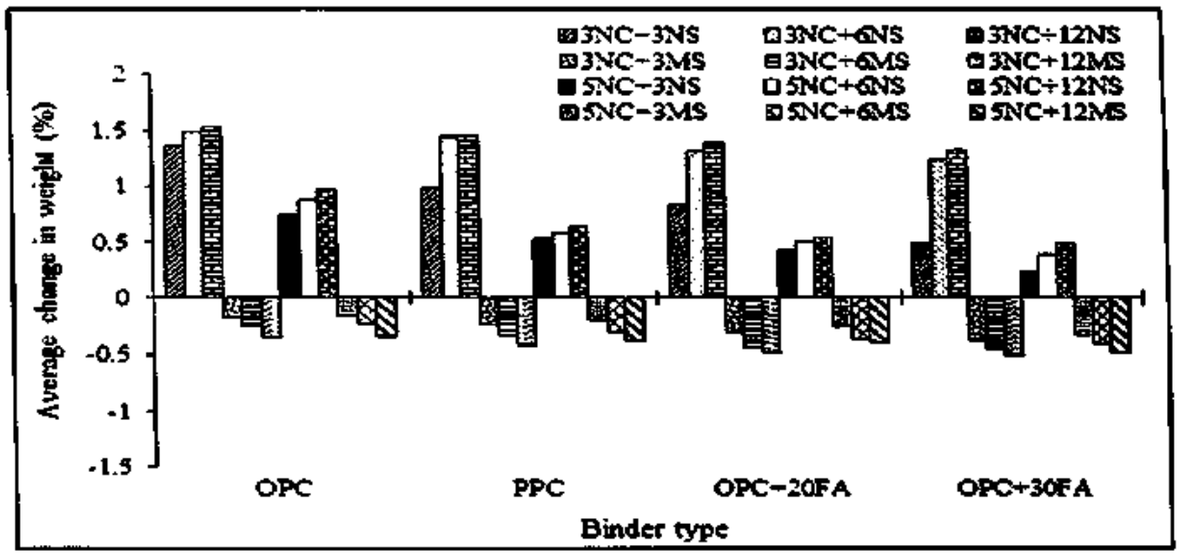

Fig. 7.10 Average change in weight (%) of concrete specimens made from different types of binder and w/b ratio of 0.45 and exposed to varying concentrations of $NaCl+Na_2SO_4$ and $NaCl+MgSO_4$ solutions for a period of 360 days under full immersion with alternate wetting and drying cycles

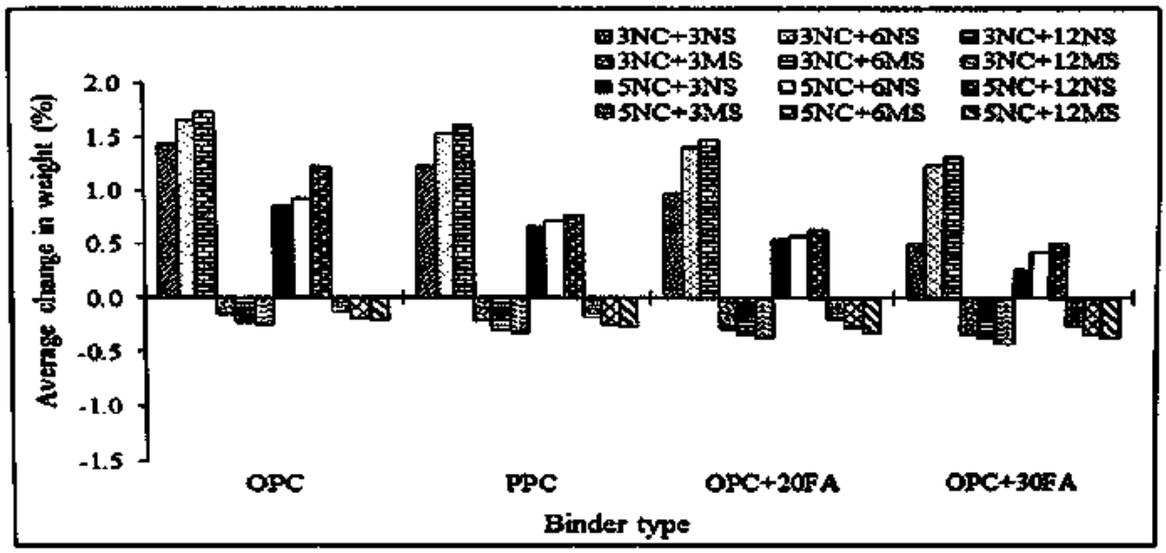

Fig. 7.11 Average change in weight (%) of concrete specimens made from different types of binder and w/b ratio of 0.5 and exposed to varying concentrations of $NaCl+Na_2SO_4$ and $NaCl+MgSO_4$ solutions for a period of 360 days under full immersion with alternate wetting and drying cycles

From Fig. 7.8 to Fig. 7.11, it is observed that the concrete specimens exposed to varying concentrations of NaCl + Na_2SO_4 showed positive change in weight percentage, which indicates that the weight of the concrete cube specimens increased after 360 days of exposure. The weight gain (although marginal) of the cube specimens exposed to NaCl + Na_2SO_4 environment may be attributed to the formation of products as result of reaction of the chloride and sulfate ions with hydrated cement phase. Further it is observed that the cube specimens exposed to NaCl + $MgSO_4$ environment showed negative change in weight percentage. This indicates that the specimens exposed to NaCl + $MgSO_4$ solutions showed a reduction in the weight of concrete. The reduction in weight (although marginal) of concrete may be due to the deleterious action of $MgSO_4$ on calcium silicate hydrate (C-S-H).

From Fig. 7.4 to Fig. 7.11, it is observed that the weight loss of concrete cube specimens exposed to only Na_2SO_4 and $MgSO_4$ solutions is higher as compared to those exposed to NaCl + Na_2SO_4 and NaCl + $MgSO_4$ solutions. This indicates that the presence of chloride ions along with sulfate ions might have mitigated the sulfate attack on concrete. While observing the effect of varying concentrations of NaCl + Na_2SO_4 on different types of binder, it is observed that the concrete specimens made with OPC showed maximum weight gain as compared to other types of binders at both w/b ratios. While analyzing the effect of varying concentrations of NaCl + $MgSO_4$ on different types of binder, it is observed that the concrete specimens made with OPC+30FA showed the maximum weight loss than other types of binder at both w/b ratios as evident from Fig. 7.8 to Fig. 7.11. On comparing the average change in weight (%) of concrete between different exposure conditions i.e. continuous full immersion and full immersion with alternate wetting and drying cycles, it is observed that the weight loss of concrete was higher in the specimens under wetting and drying exposure as compared to continuous full immersion exposure in all exposure solutions. The aforementioned discussions indicate that the effect of sulfate attack in terms of weight loss was more prominent in sulfate and conjoint chloride-sulfate solutions when the sulfate ion is associated with magnesium cation as compared to that associated with sodium cation.

7.4 COMPRESSIVE STRENGTH OF CONCRETE SUBJECTED TO SULFATE AND CONJOINT CHLORIDE-SULFATE ENVIRONMENT

The average compressive strength of concrete cube specimens after 360 days of exposure to normal water for different types of binder and w/b ratios are shown in Fig. 7.12 and Fig. 7.13 for continuous full immersion condition and full immersion with alternate wetting and drying cycles respectively. From these figures, it is inferred that the maximum compressive strength after 360 days of exposure to normal water was attained by OPC+30FA concrete followed by OPC+20FA, PPC and OPC concretes. This indicates that the presence of fly ash has resulted in development of higher compressive strength in concrete. The higher compressive strength in concrete mixes made with PPC, OPC+20FA and OPC+30FA as compared to that in OPC is attributed to the effect pozzolanic reaction producing additional C-S-H in concrete. Further, it is observed that the concrete specimens made with w/b ratio of 0.45 exhibited higher compressive strength as compared to those made with w/b ratio of 0.5.

While comparing the effect of different exposure conditions, it is observed that the concrete mixes made at w/b ratio of 0.45 exhibited lower compressive strength in continuous full immersion condition as compared to that in full immersion under alternate wetting and drying condition. However, the concrete mixes made at w/b ratio of 0.5 exhibited higher compressive strength in continuous full immersion as compared to that in full immersion under cyclic wetting and drying condition. This variation in compressive strength with exposure condition may be attributed to the variations in the extent of hydration and pozzolanic reactions in concrete at different w/b ratios.

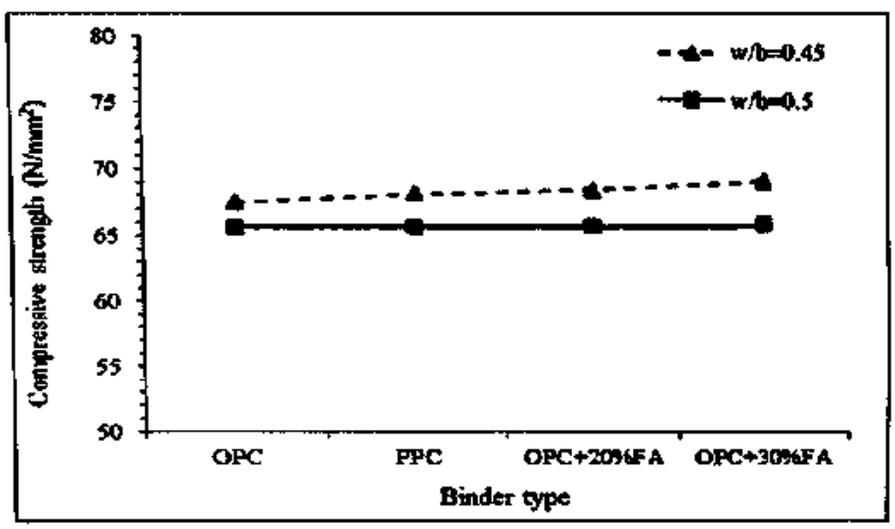

Fig. 7.12 Average compressive strength of concrete after exposure to normal water for a period of 360 days under continuous full immersion condition

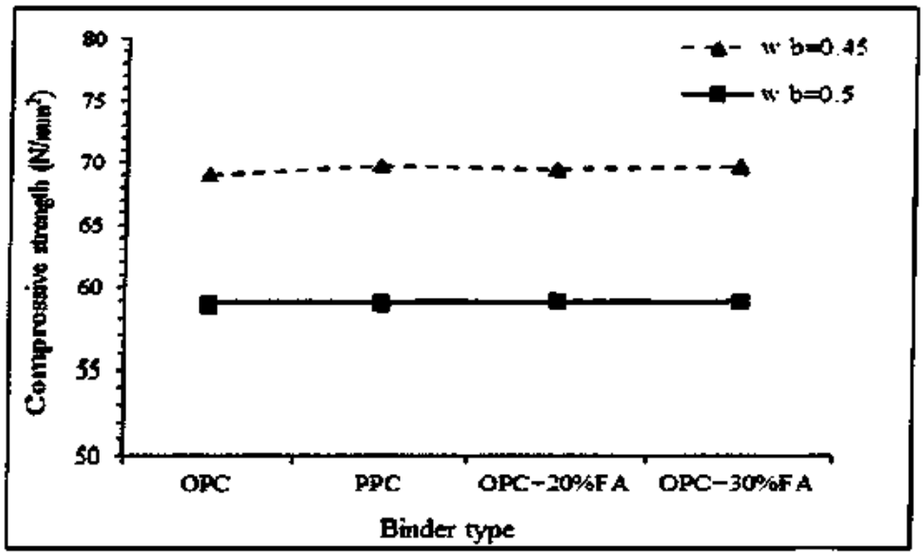

Fig. 7.13 Average compressive strength of concrete after exposure to normal water for a period of 360 days under full immersion with alternate wetting and drying cycles

The average compressive strength of concrete cube specimens after 360 days of exposure to sulfate and chloride-sulfate solutions are presented in Table 7.1 and Table 7.2 respectively at w/b ratios of 0.45 and 0.5 for continuous full immersion condition. Similarly, the average compressive strength of concrete for full immersion with alternate wetting and drying cycles are presented in Table 7.3 and Table 7.4 respectively at w/b ratios of 0.45 and 0.5. In addition, the compressive strength of concrete exposed to normal water is also presented in these tables.

Table 7.1: Average 360 day compressive strength of concrete made from OPC, PPC, OPC+20FA and OPC+30FA at w/b ratio of 0.45 and exposed to normal water and solutions containing varying concentrations of Na_2SO_4, $MgSO_4$, NaCl + Na_2SO_4 and NaCl + $MgSO_4$ under continuous full immersion condition

Exposure condition: Continuous full immersion					
w/b ratio	Exposure solutions	Average Compressive strength (N/mm^2)			
		OPC	PPC	OPC+20FA	OPC+30FA
0.45	Normal water	60.2	68.5	70.4	72.7
	3%Na_2SO_4	36.2	37.4	37.8	39.5
	6N%a_2SO_4	33.5	34.7	35	36.4
	12%Na_2SO_4	32.8	33.6	34.2	35.8
	3% $MgSO_4$	33.7	33.2	32.5	31.7
	6% $MgSO_4$	30.6	29.8	29.6	29.1
	12% $MgSO_4$	30	29.2	28.9	28.4
	3%NaCl + 3%Na_2SO_4	51.7	53.07	55.3	56.7
	3%NaCl + 6N%a_2SO_4	50.8	52.1	54.8	55.8
	3%NaCl + 12%Na_2SO_4	49.6	50.3	53.2	55.1
	5%NaCl + 3%Na_2SO_4	57.9	58	59.3	59.8
	5%NaCl + 6%Na_2SO_4	56.4	57.5	58	58.4
	5%NaCl + 12%Na_2SO_4	55.8	56.8	57.2	57.4
	3% NaCl + 3% $MgSO_4$	48.5	47.3	46.1	45.2
	3% NaCl + 6% $MgSO_4$	47	46.4	45.2	44.3
	3% NaCl + 12% $MgSO_4$	45.9	44.2	43.3	42.1
	5% NaCl + 3% $MgSO_4$	52.7	51.3	50.2	49.7
	5% NaCl + 6% $MgSO_4$	51.3	50.1	49	48.4
	5% NaCl + 12% $MgSO_4$	50.6	49.3	48.4	46.5

Table 7.2: Average 360 day compressive strength of concrete made from OPC, PPC, OPC+20FA and OPC+30FA at w/b ratio of 0.5 and exposed to normal water and solutions containing varying concentrations of Na_2SO_4, $MgSO_4$, NaCl + Na_2SO_4 and NaCl + $MgSO_4$ under continuous full immersion condition

Exposure condition: Continuous full immersion					
w/b ratio	Exposure solutions	Average Compressive strength (N/mm^2)			
		OPC	PPC	OPC+20FA	OPC+30FA
0.5	Normal water	65.6	66	66.4	67
	3%Na_2SO_4	35.1	36.7	36.3	38.6
	6N%a_2SO_4	32.4	33.6	34.8	36
	12%Na_2SO_4	31.7	32.9	33.9	35.2
	3% $MgSO_4$	34.8	34	33.7	33
	6% $MgSO_4$	31.2	30.7	30.1	29.3
	12% $MgSO_4$	30.8	30.1	29.6	28.7
	3%NaCl + 3%Na_2SO_4	51.1	52.8	54.7	56
	3%NaCl + 6N%a_2SO_4	50.3	51.7	53.3	55.7
	3%NaCl + 12%Na_2SO_4	49.2	50.1	52	54.8
	5%NaCl + 3%Na_2SO_4	56.4	57.5	58.6	59
	5%NaCl + 6%Na_2SO_4	55.8	56.6	57.1	58.1
	5%NaCl + 12%Na_2SO_4	54.7	55.2	56.4	56.6
	3% NaCl + 3% $MgSO_4$	49.3	48.4	47.3	46.1
	3% NaCl + 6% $MgSO_4$	48.4	47.3	46.4	45.2
	3% NaCl + 12% $MgSO_4$	47.2	46.1	45.5	44.7
	5% NaCl + 3% $MgSO_4$	54.8	53.2	52.6	51.6
	5% NaCl + 6% $MgSO_4$	53.4	52.1	51.5	50.7
	5% NaCl + 12% $MgSO_4$	52.6	51.5	50.4	49.6

Table 7.3: Average 360 day compressive strength of concrete made from OPC, PPC, OPC+20FA and OPC+30FA at w/b ratio of 0.45 and exposed to normal water and solutions containing varying concentrations of Na_2SO_4, $MgSO_4$, NaCl + Na_2SO_4 and NaCl + $MgSO_4$ under full immersion with alternate wetting and drying cycles

Exposure condition: Full immersion with alternate wetting and drying cycles					
w/b ratio	Exposure solutions	Average Compressive strength (N/mm^2)			
		OPC	PPC	OPC+20FA	OPC+30FA
0.45	Normal water	69	70	70.4	71
	3%Na_2SO_4	35.4	36	36.8	37.4
	6N%a$_2SO_4$	32.5	33.9	34.6	35.3
	12%Na_2SO_4	31.3	33	33.7	34.1
	3% $MgSO_4$	32.8	30.4	29.8	28.6
	6% $MgSO_4$	29.6	28.7	27.5	26.9
	12% $MgSO_4$	29	28	27	26.3
	3%NaCl + 3%Na_2SO_4	50.9	52.1	54.1	56
	3%NaCl + 6N%a$_2SO_4$	49.8	51.3	53.7	55.3
	3%NaCl + 12%Na_2SO_4	48.4	50	52.9	54.6
	5%NaCl + 3%Na_2SO_4	56.3	57	58	58.4
	5%NaCl + 6%Na_2SO_4	55.2	56.6	57.6	57.3
	5%NaCl + 12%Na_2SO_4	54.7	55.7	56.5	55.8
	3% NaCl + 3% $MgSO_4$	47.6	46.2	45	44
	3% NaCl + 6% $MgSO_4$	46.3	45.3	44.1	42.3
	3% NaCl + 12% $MgSO_4$	44.1	42	42.1	40.8
	5% NaCl + 3% $MgSO_4$	51.4	50.8	49.3	48
	5% NaCl + 6% $MgSO_4$	50.6	49.2	48.6	47.1
	5% NaCl + 12% $MgSO_4$	49.7	48.5	47.2	46

Table 7.4: Average 360 day compressive strength of concrete made from OPC, PPC, OPC+20FA and OPC+30FA at w/b ratio of 0.5 and exposed to normal water and solutions containing varying concentrations of Na_2SO_4, $MgSO_4$, NaCl + Na_2SO_4 and NaCl + $MgSO_4$ under full immersion with alternate wetting and drying cycles

Exposure condition: Full immersion with alternate wetting and drying cycles					
w/b ratio	Exposure solutions	Average Compressive strength (N/mm^2)			
		OPC	PPC	OPC+20FA	OPC+30FA
0.5	Normal water	58.8	59.4	60.6	61.4
	3%Na_2SO_4	34.7	35.2	35.5	36.2
	6N%a_2SO_4	31.2	32.6	33.1	34.7
	12%Na_2SO_4	30.6	31.8	32.5	33.8
	3% $MgSO_4$	34	33.6	33.2	32.5
	6% $MgSO_4$	30.9	30.2	29.8	29.1
	12% $MgSO_4$	30	29.7	29.3	28.4
	3%NaCl + 3%Na_2SO_4	50.5	51.3	53.8	56.2
	3%NaCl + 6N%a_2SO_4	49.6	50.4	52.4	54.3
	3%NaCl + 12%Na_2SO_4	48.8	49.8	51	53.7
	5%NaCl + 3%Na_2SO_4	55.3	56.2	57.6	58.7
	5%NaCl + 6%Na_2SO_4	53.2	54.6	56.1	57.7
	5%NaCl + 12%Na_2SO_4	52.2	54	55.4	56.2
	3% NaCl + 3% $MgSO_4$	48.2	47.8	46.2	45.2
	3% NaCl + 6% $MgSO_4$	47.1	46.4	45.1	44.3
	3% NaCl + 12% $MgSO_4$	46.3	45.3	44.3	43.8
	5% NaCl + 3% $MgSO_4$	53.6	52.1	51.3	50.2
	5% NaCl + 6% $MgSO_4$	52.3	51.1	50.2	49.1
	5% NaCl + 12% $MgSO_4$	50	50	49.1	48.3

From Table 7.1 to Table 7.4, it is observed that, the concrete specimens exposed to sulfate and conjoint chloride-sulfate solutions exhibited lower compressive strength as compared to those exposed to normal water. This indicates that the exposure of concrete to aggressive environment leads to reduction in its compressive strength. Further, it is noted that the concrete mixes made with OPC showed higher compressive strength as compared to blended cement concrete mixes (PPC, OPC+20FA and OPC+30FA) in $MgSO_4$ and NaCl + $MgSO_4$ environment at all concentrations whereas the opposite behaviour was observed in Na_2SO_4 and NaCl + Na_2SO_4 environment i.e. the blended cement concrete mixes (PPC, OPC+20FA and OPC+30FA) exhibited higher compressive strength as compared to OPC concrete at both w/b ratios.

7.4.1 Reduction in Compressive Strength of Concrete Subjected to Sulfate and Conjoint Chloride-Sulfate Environment

For evaluating the reduction in compressive strength of concrete exposed to sulfate and conjoint chloride-sulfate solutions, the average reduction in compressive strength (%) was calculated with respect to the compressive strength of concrete exposed to normal water with same exposure condition (already mentioned in Chapter 3). The average reduction in compressive strength (%) was calculated from the obtained compressive strength values presented in Table 7.1 to Table 7.4 for different exposure solutions and conditions.

For continuous full immersion condition, the average reduction in compressive strength (%) of concrete cube specimens made at w/b ratio of 0.45 and subjected to varying concentrations of Na_2SO_4, $MgSO_4$, NaCl + Na_2SO_4 and NaCl + $MgSO_4$ solutions are shown in Fig. 7.14, Fig. 7.15, Fig. 7.16 and Fig. 7.17 for OPC, PPC, OPC+20FA and OPC+30FA respectively. Similarly, the average reduction in compressive strength (%) of concrete cube specimens made at w/b ratio of 0.5 are shown in Fig. 7.18, Fig. 7.19, Fig. 7.20 and Fig. 7.21 for OPC, PPC, OPC+20FA and OPC+30FA respectively for continuous full immersion condition.

For full immersion with alternate wetting and drying cycles, the average reduction in compressive strength (%) of concrete made at w/b ratio of 0.45 and subjected to varying concentrations of Na_2SO_4, $MgSO_4$, NaCl + Na_2SO_4 and NaCl + $MgSO_4$ solutions are shown in Fig. 7.22, Fig. 7.23, Fig. 7.24 and Fig. 7.25 for OPC, PPC, OPC+20FA and OPC+30FA respectively. Similarly, the average reduction in compressive strength (%) of

concrete made at w/b ratio of 0.5 are shown in Fig. 7.26. Fig. 7.27. Fig. 7.28 and Fig. 7.29 respectively for full immersion with alternate wetting and drying cycles.

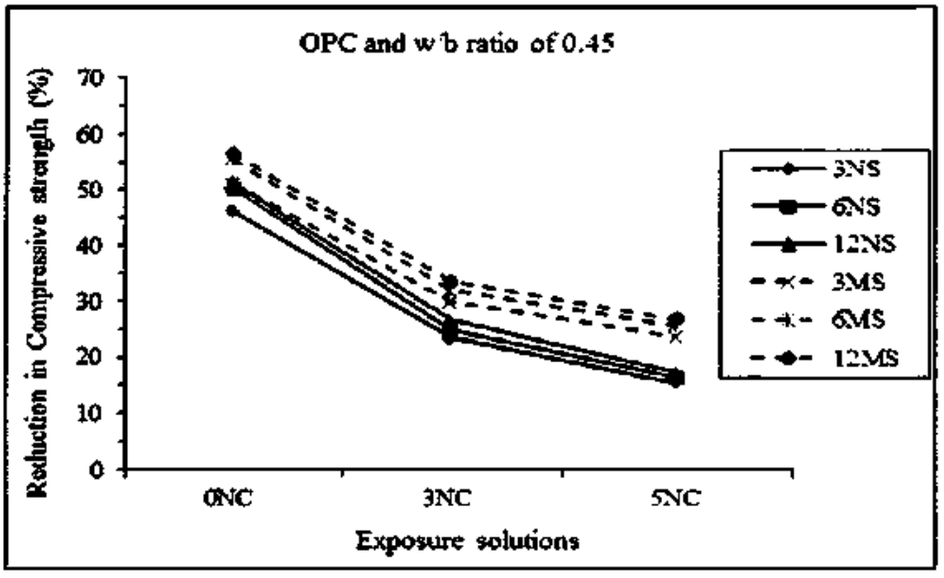

Fig. 7.14 Average reduction in compressive strength (%) of concrete made from OPC at w/b ratio of 0.45 and subjected to varying concentrations of Na_2SO_4, $MgSO_4$, NaCl+Na_2SO_4 and NaCl +$MgSO_4$ solutions for a period of 360 days under continuous full immersion condition

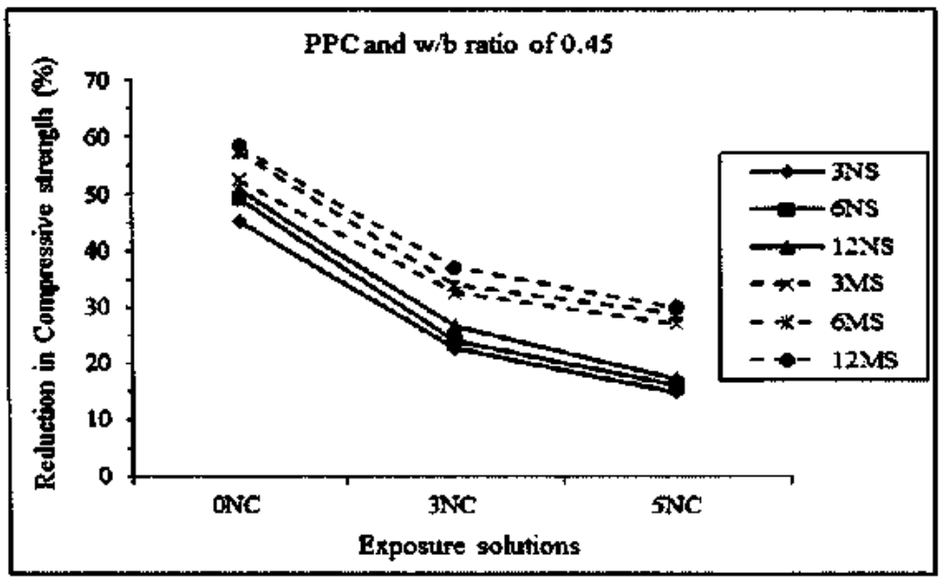

Fig. 7.15 Average reduction in compressive strength (%) of concrete made from PPC at w/b ratio of 0.45 and subjected to varying concentrations of Na_2SO_4, $MgSO_4$, NaCl+Na_2SO_4 and NaCl +$MgSO_4$ solutions for a period of 360 days under continuous full immersion condition

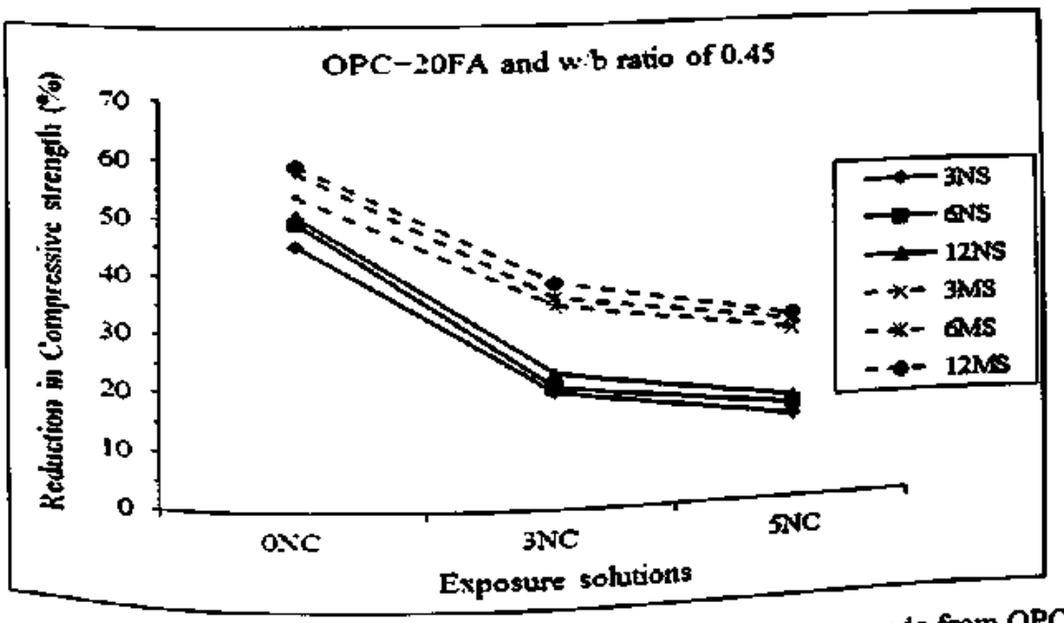

Fig. 7.16 Average reduction in compressive strength (%) of concrete made from OPC+20FA at w/b ratio of 0.45 and subjected to varying concentrations of Na_2SO_4, $MgSO_4$, $NaCl+Na_2SO_4$ and $NaCl+MgSO_4$ solutions for a period of 360 days under continuous full immersion condition

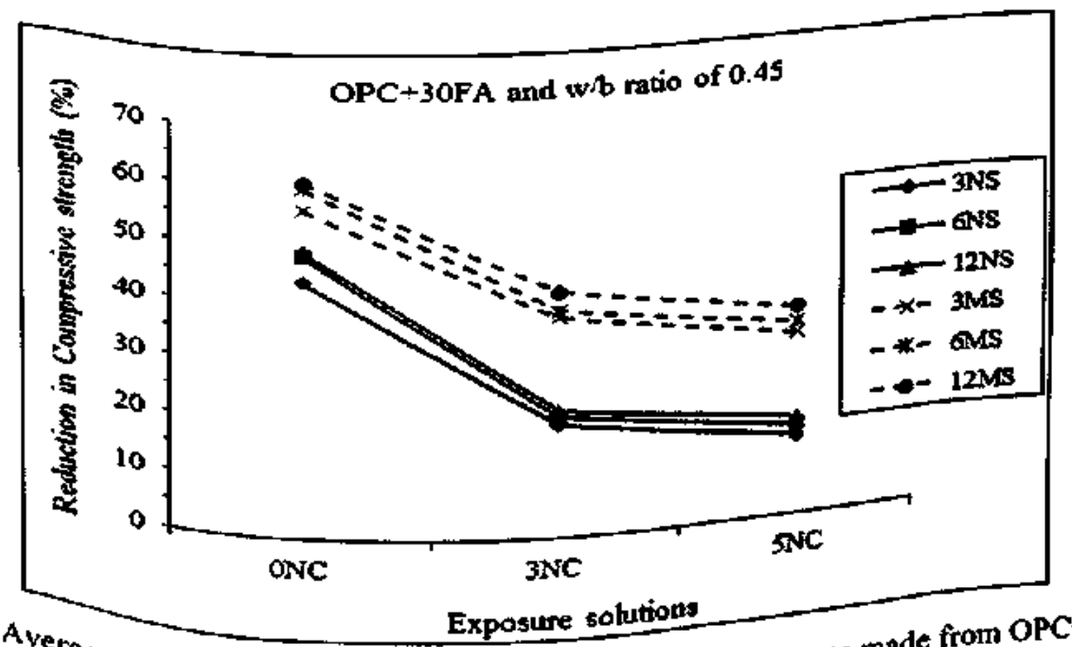

Fig. 7.17 Average reduction in compressive strength (%) of concrete made from OPC+30FA at w/b ratio of 0.45 and subjected to varying concentrations of Na_2SO_4, $MgSO_4$, $NaCl+Na_2SO_4$ and $NaCl+MgSO_4$ solutions for a period of 360 days under continuous full immersion condition

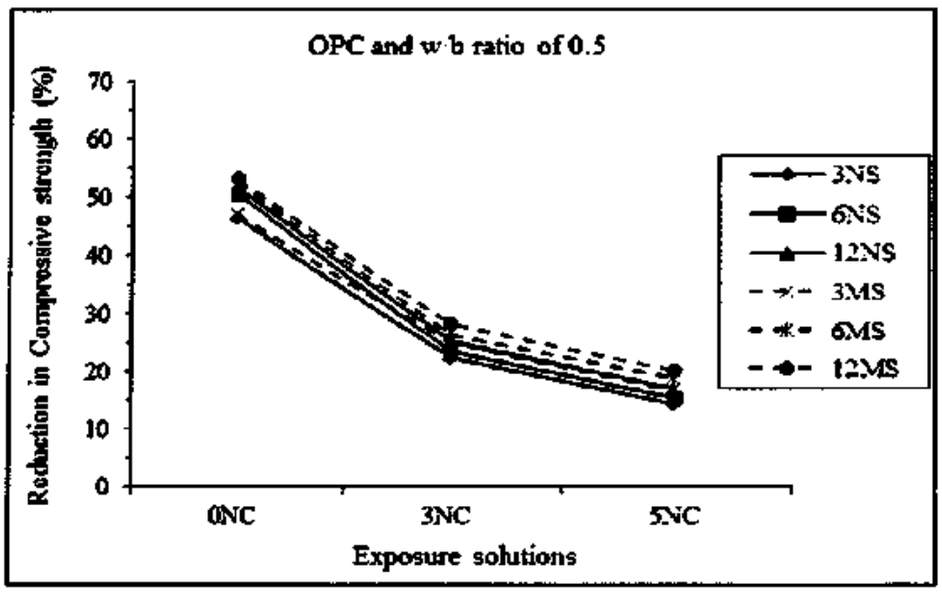

Fig. 7.18 Average reduction in compressive strength (%) of concrete made from OPC at w/b ratio of 0.5 and subjected to varying concentrations of Na_2SO_4, $MgSO_4$, NaCl+Na_2SO_4 and NaCl +$MgSO_4$ solutions for a period of 360 days under continuous full immersion condition

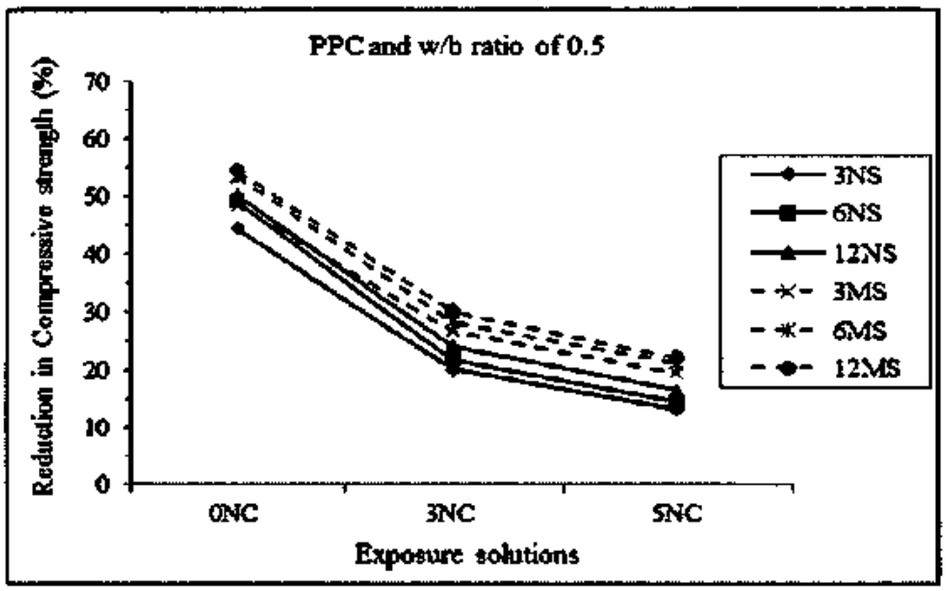

Fig. 7.19 Average reduction in compressive strength (%) of concrete made from PPC at w/b ratio of 0.5 and subjected to varying concentrations of Na_2SO_4, $MgSO_4$, NaCl+Na_2SO_4 and NaCl +$MgSO_4$ solutions for a period of 360 days under continuous full immersion condition

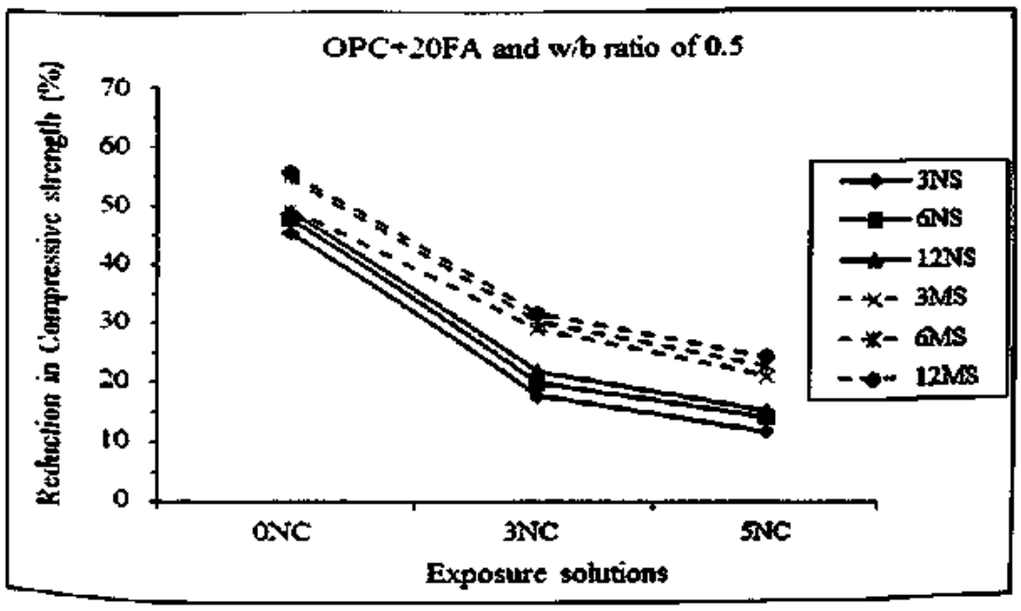

Fig. 7.20 Average reduction in compressive strength (%) of concrete made from OPC+20FA at w/b ratio of 0.5 and subjected to varying concentrations of Na_2SO_4, $MgSO_4$, NaCl+Na_2SO_4 and NaCl +$MgSO_4$ solutions for a period of 360 days under continuous full immersion condition

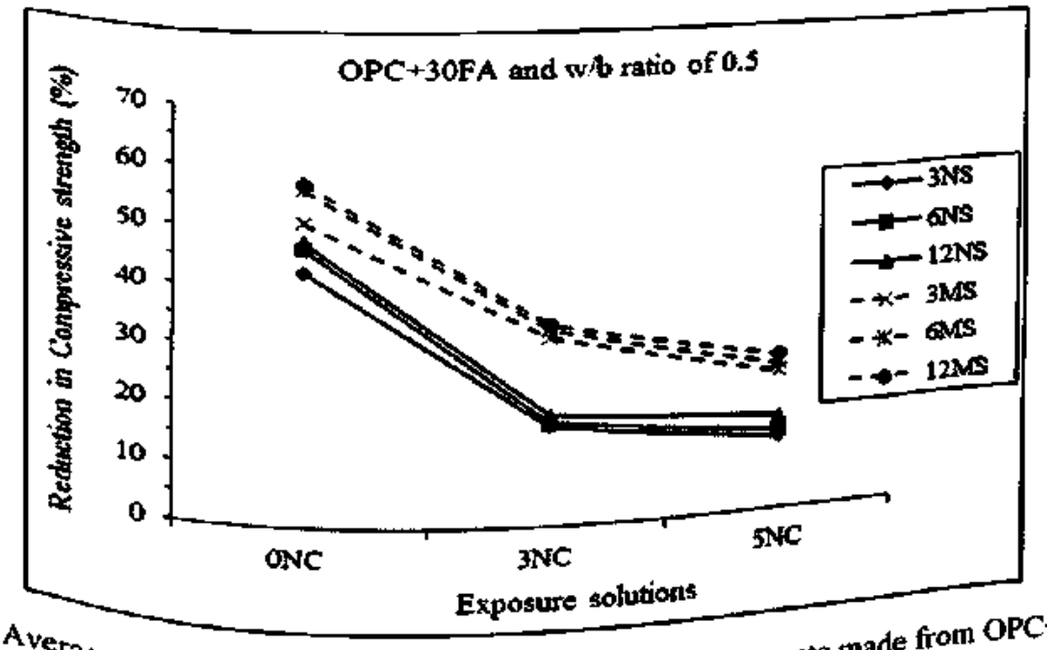

Fig. 7.21 Average reduction in compressive strength (%) of concrete made from OPC+30FA at w/b ratio of 0.5 and subjected to varying concentrations of Na_2SO_4, $MgSO_4$, NaCl+Na_2SO_4 and NaCl +$MgSO_4$ solutions for a period of 360 days under continuous full immersion condition

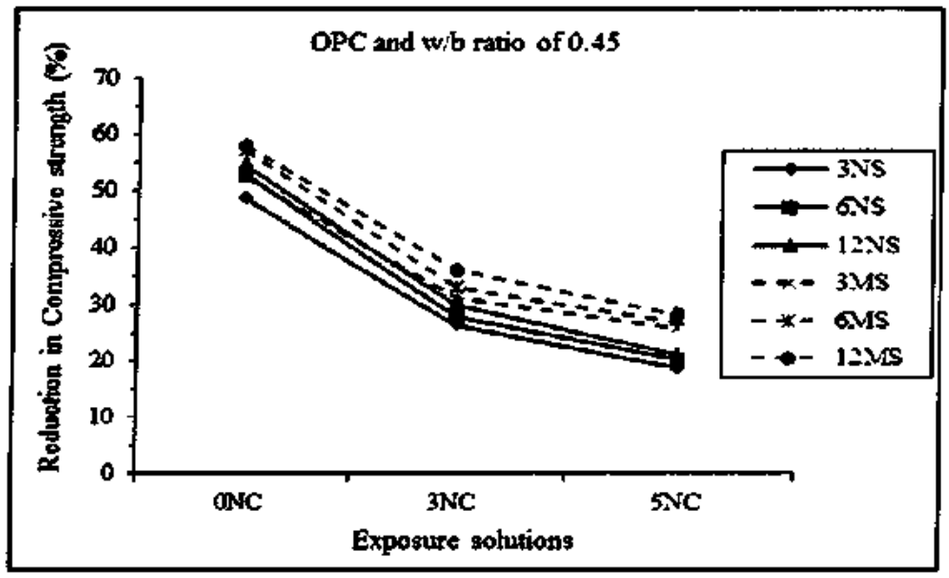

Fig. 7.22 Average reduction in compressive strength (%) of concrete made from OPC at w/b ratio of 0.45 and subjected to varying concentrations of Na_2SO_4, $MgSO_4$, NaCl+Na_2SO_4 and NaCl +$MgSO_4$ solutions for a period of 360 days under full immersion with alternate wetting and drying cycles

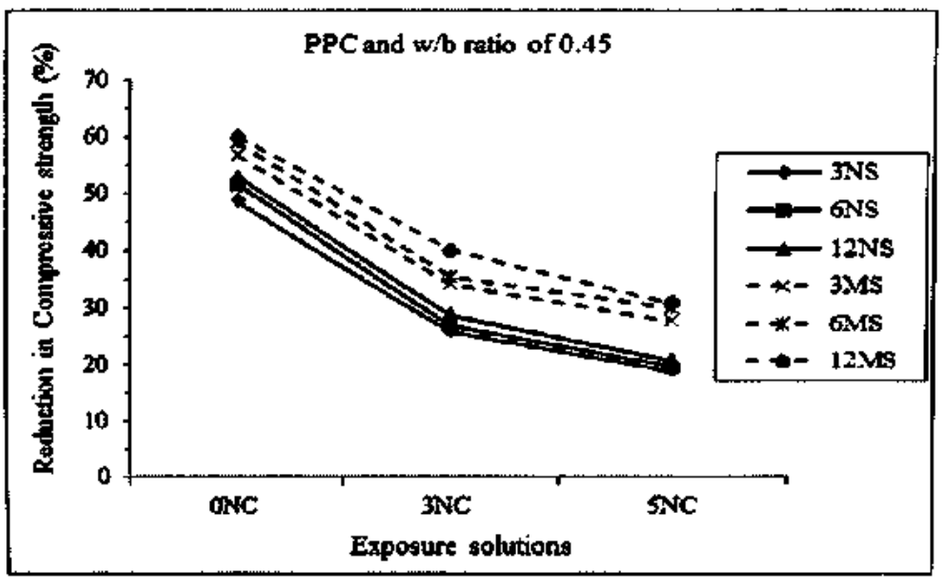

Fig. 7.23 Average reduction in compressive strength (%) of concrete made from PPC at w/b ratio of 0.45 and subjected to varying concentrations of Na_2SO_4, $MgSO_4$, NaCl+Na_2SO_4 and NaCl +$MgSO_4$ solutions for a period of 360 days under full immersion with alternate wetting and drying cycles

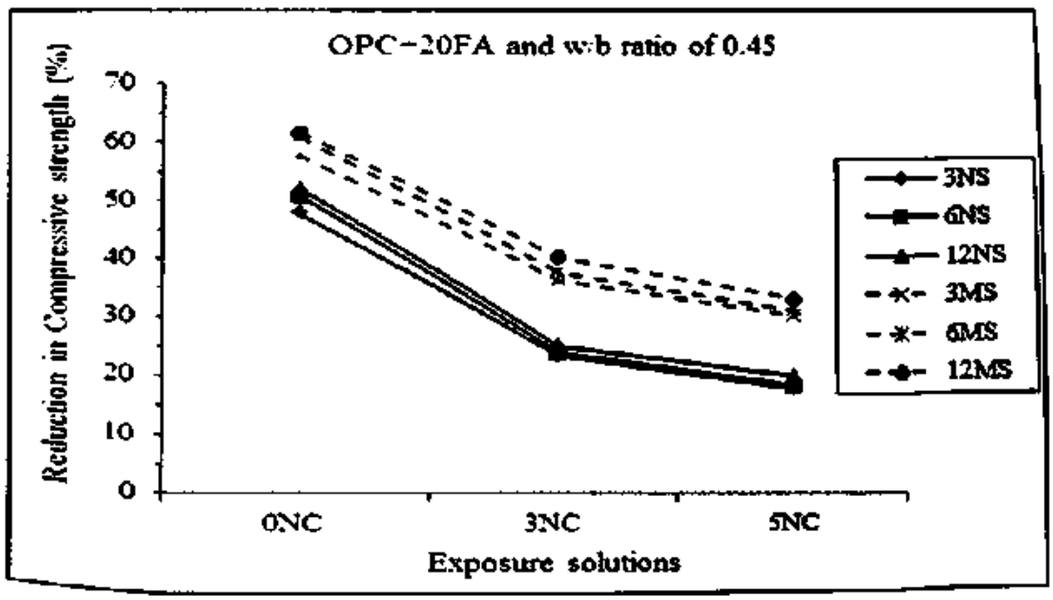

Fig. 7.24 Average reduction in compressive strength (%) of concrete made from OPC+20FA at w/b ratio of 0.45 and subjected to varying concentrations of Na_2SO_4, $MgSO_4$, NaCl+Na_2SO_4 and NaCl +$MgSO_4$ solutions for a period of 360 days under full immersion with alternate wetting and drying cycles

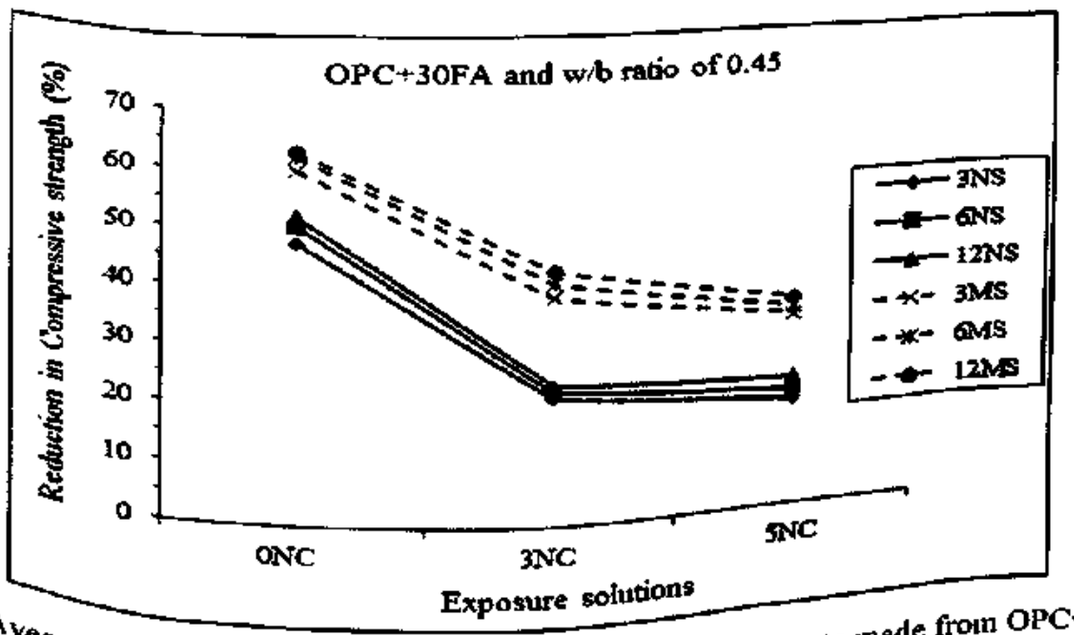

Fig. 7.25 Average reduction in compressive strength (%) of concrete made from OPC+30FA at w/b ratio of 0.45 and subjected to varying concentrations of Na_2SO_4, $MgSO_4$, NaCl+Na_2SO_4 and NaCl +$MgSO_4$ solutions for a period of 360 days under full immersion with alternate wetting and drying cycles

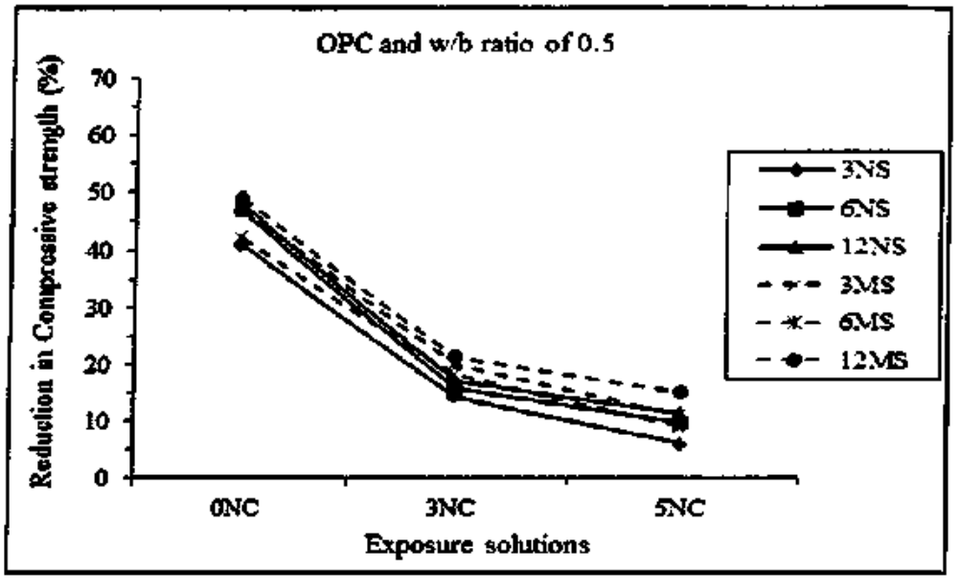

Fig. 7.26 Average reduction in compressive strength (%) of concrete made from OPC at w/b ratio of 0.5 and subjected to varying concentrations of Na_2SO_4, $MgSO_4$, $NaCl+Na_2SO_4$ and $NaCl+MgSO_4$ solutions for a period of 360 days under full immersion with alternate wetting and drying cycles

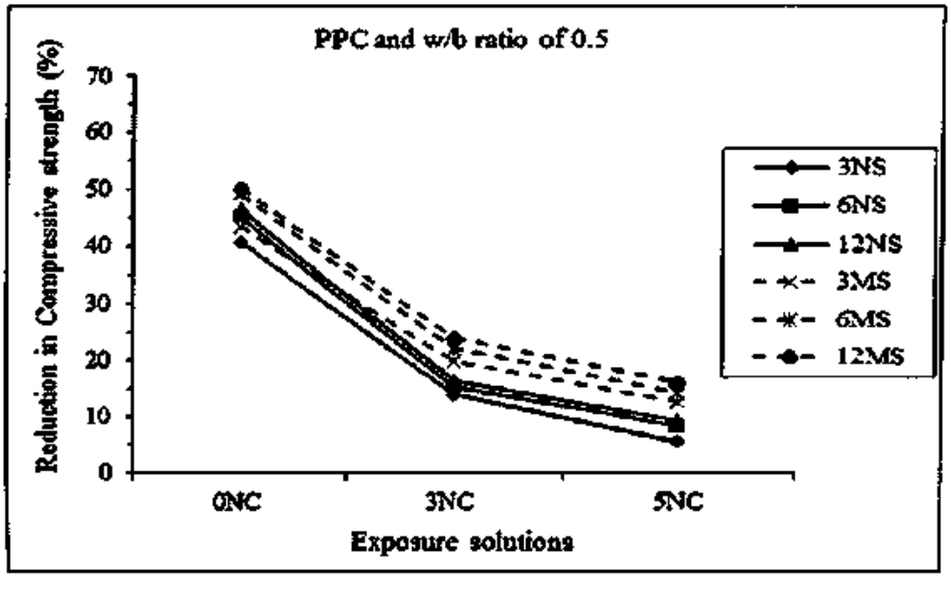

Fig. 7.27 Average reduction in compressive strength (%) of concrete made from PPC at w/b ratio of 0.5 and subjected to varying concentrations of Na_2SO_4, $MgSO_4$, $NaCl+Na_2SO_4$ and $NaCl+MgSO_4$ solutions for a period of 360 days under full immersion with alternate wetting and drying cycles

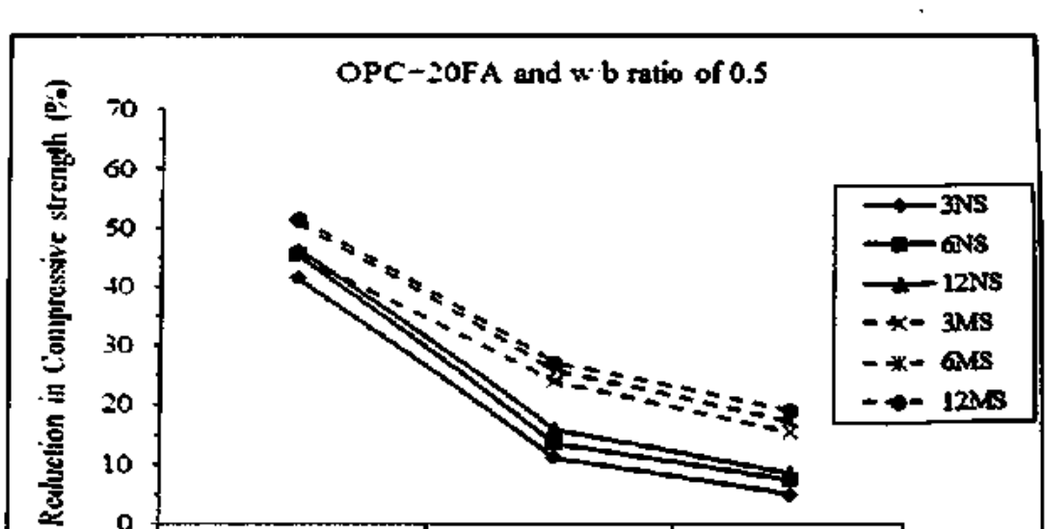

Fig. 7.28 Average reduction in compressive strength (%) of concrete made from OPC+20FA at w/b ratio of 0.5 and subjected to varying concentrations of Na_2SO_4, $MgSO_4$, $NaCl+Na_2SO_4$ and $NaCl+MgSO_4$ solutions for a period of 360 days under full immersion with alternate wetting and drying cycles

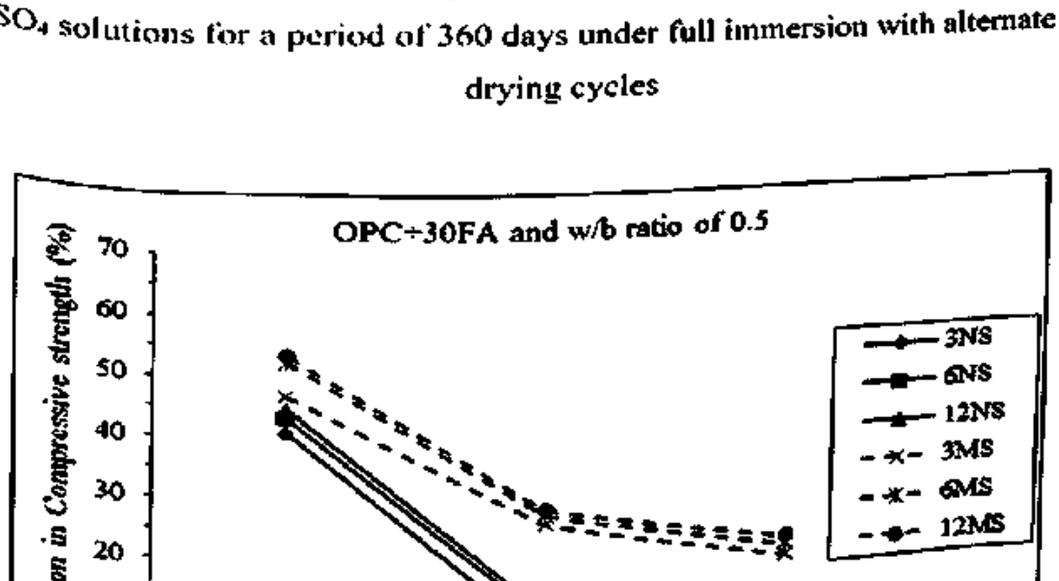

Fig. 7.29 Average reduction in compressive strength (%) of concrete made from OPC+30FA at w/b ratio of 0.5 and subjected to varying concentrations of Na_2SO_4, $MgSO_4$, $NaCl+Na_2SO_4$ and $NaCl+MgSO_4$ solutions for a period of 360 days under full immersion with alternate wetting and drying cycles

From Fig. 7.14 to Fig. 7.29, it is observed that the reduction in compressive strength of concrete varied with binder type, w/b ratio, exposure solution and exposure condition. After 360 days of exposure, the maximum compressive strength reduction of OPC, PPC, OPC+20FA and OPC+30FA concrete were 54.6%, 52.9%, 52.1% and 52.0% respectively in Na_2SO_4 solutions and 58.0%, 60.0%, 61.6% and 63.0% respectively in $MgSO_4$ solutions. Similarly, the maximum compressive strength reduction of OPC, PPC, OPC+20FA and OPC+30FA concrete were 29.9%, 28.6%, 24.9% and 23.1% respectively in NaCl + Na_2SO_4 solutions; and 36.1%, 40.0%, 40.2% and 42.5% respectively in NaCl + $MgSO_4$ solution irrespective of w/b ratio, exposure condition and concentrations of sodium chloride, sodium sulfate and magnesium sulfate. These values indicate that the compressive strength reduction in OPC was higher as compared to that in PPC, OPC+20FA and OPC+30FA in Na_2SO_4 and NaCl + Na_2SO_4 solutions, whereas the opposite variation was observed in $MgSO_4$ and NaCl + $MgSO_4$ solutions i.e. the reduction in compressive strength of concrete was higher in PPC, OPC+20FA and OPC+30FA as compared to that in OPC at all concentrations of sulfate and chloride salts; and for both w/b ratios and exposure conditions. This indicates that blended cement concretes (PPC, OPC+20FA and OPC+30FA) exhibited improved resistance to sodium sulfate attack whereas they showed poor resistance to magnesium sulfate attack as compared to OPC concrete. The similar observations were reported by Rasheeduzzafar et al. [46] and Al-Amoudi [135].

The improved resistance of blended cement concretes (PPC, OPC+20FA and OPC+30FA) in Na_2SO_4 and NaCl + Na_2SO_4 environment may be attributed to the formation of relatively denser microstructure as a result of production of additional C-S-H due to pozzolanic reaction and reduction in formation of gypsum and ettringite as result of less availability of calcium hydroxide and C_3A in blended cement concretes. The formation of lower amount of gypsum and ettringite in blended cement concretes as compared to that in OPC concrete is corroborated from the typical XRD profiles shown in Fig. 7.30, Fig 7.31, Fig. 7.32 and Fig. 7.33 for OPC, PPC, OPC+20FA and OPC+30FA concrete respectively at w/b ratio of 0.45 when exposed to 12% Na_2SO_4, 3% NaCl + 12% Na_2SO_4 and 5% NaCl + 12% Na_2SO_4 solutions with alternate wetting and drying cycles. The XRD profiles shown in these figures indicate the formation of gypsum (G) with peak at 32.1° 2θ, and ettringite (E) with peaks at 8.8° 2θ, 15.75° 2θ, 25.6° 2θ, and 27.5° 2θ. From these XRD profiles, it is observed that the blended cement concretes showed less

intense peaks of gypsum and ettringite as compared to OPC concrete. In Na_2SO_4 environment, the expansion and cracking due to formation of gypsum and ettringite are the primary cause of deterioration of concrete leading to reduction in compressive strength.

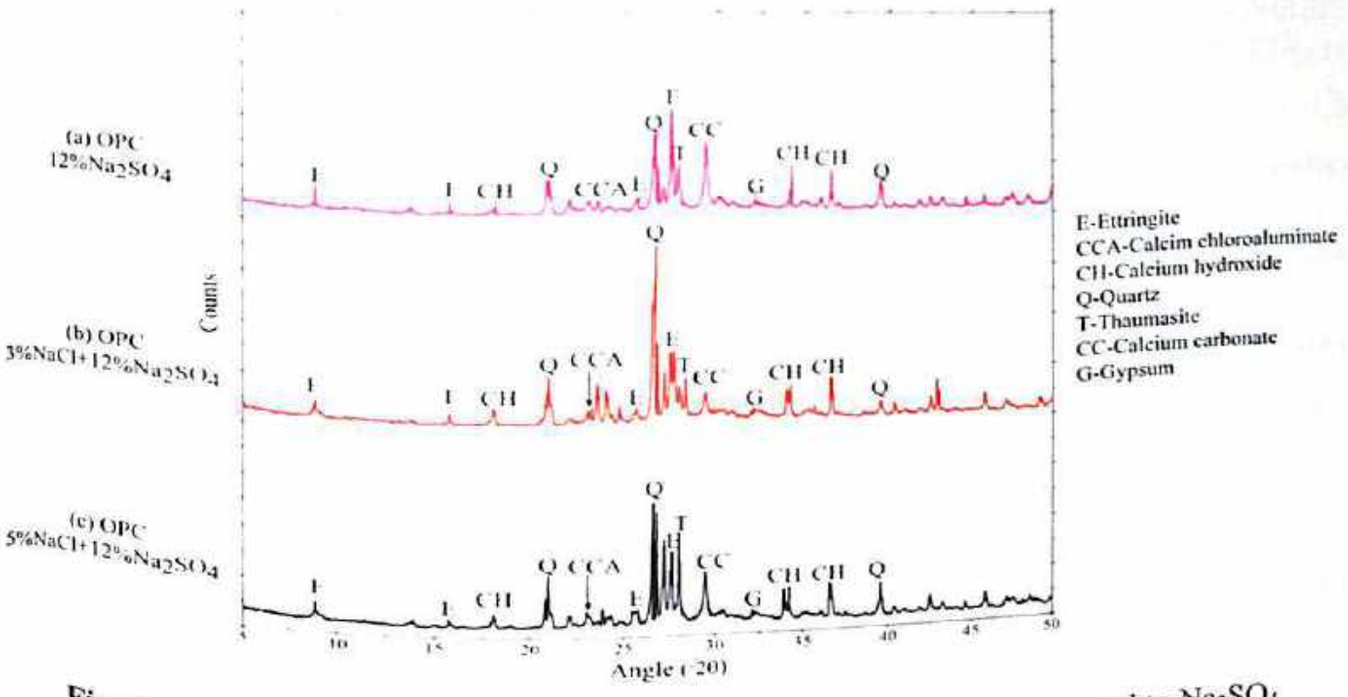

Fig. 7.30 XRD profile of OPC concrete at w/b ratio of 0.45 and exposed to Na_2SO_4 and $NaCl + Na_2SO_4$ solutions for a period of 360 days under full immersion with alternate wetting and drying cycles

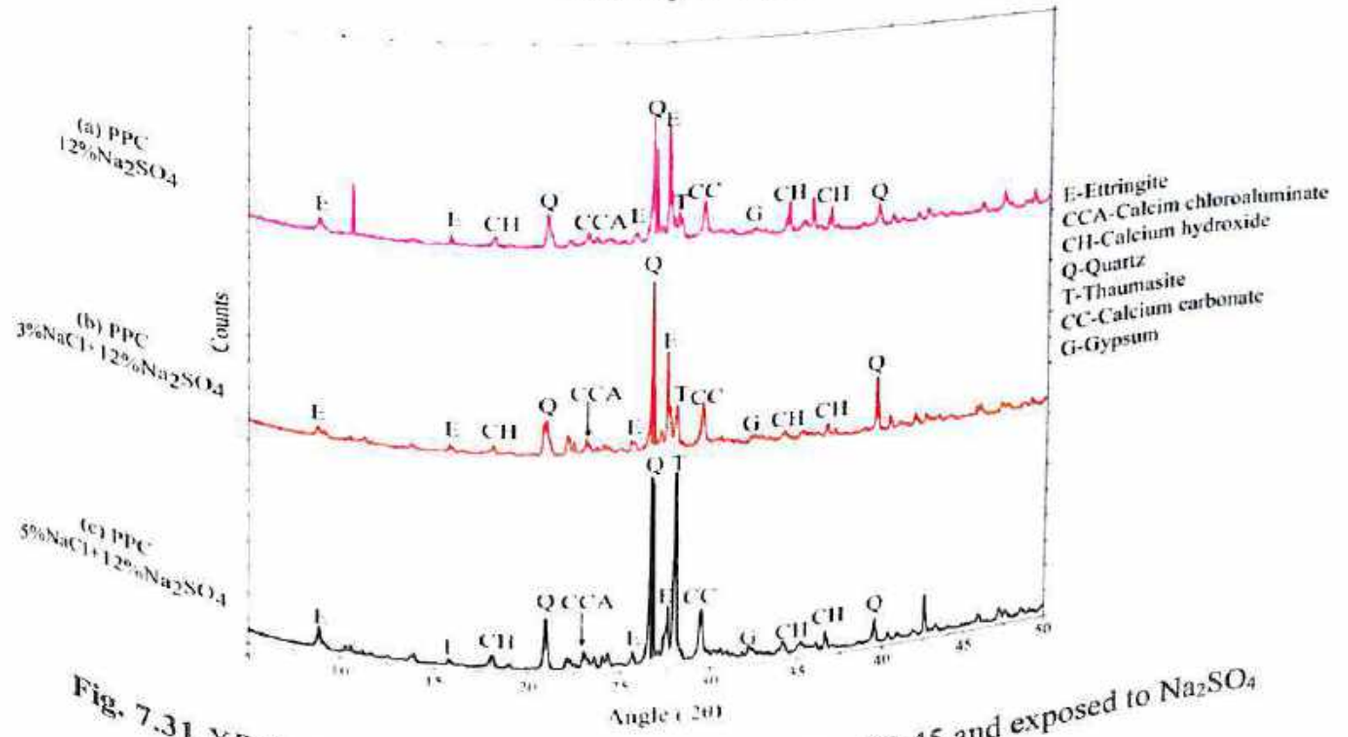

Fig. 7.31 XRD profile of PPC concrete at w/b ratio of 0.45 and exposed to Na_2SO_4

and $NaCl + Na_2SO_4$ solutions for a period of 360 days under full immersion with alternate wetting and drying cycles

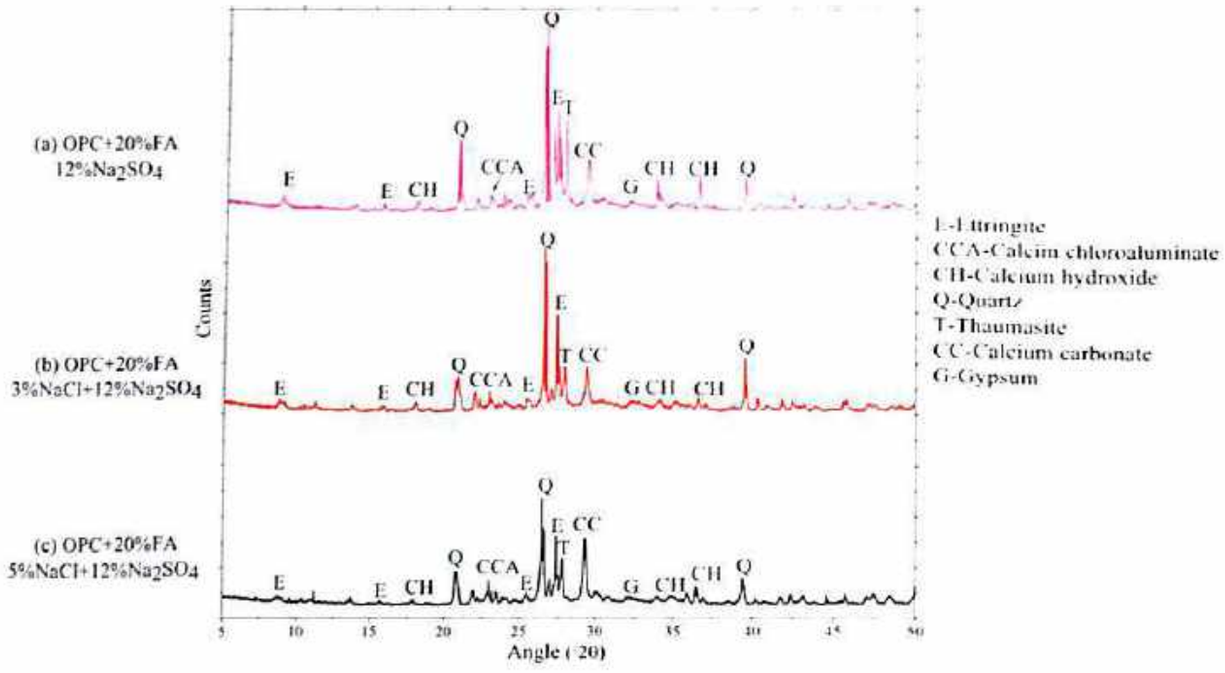

Fig. 7.32 XRD profile of OPC+20%FA concrete at w/b ratio of 0.45 and exposed to Na_2SO_4 and $NaCl + Na_2SO_4$ solutions for a period of 360 days under full immersion with alternate wetting and drying cycles

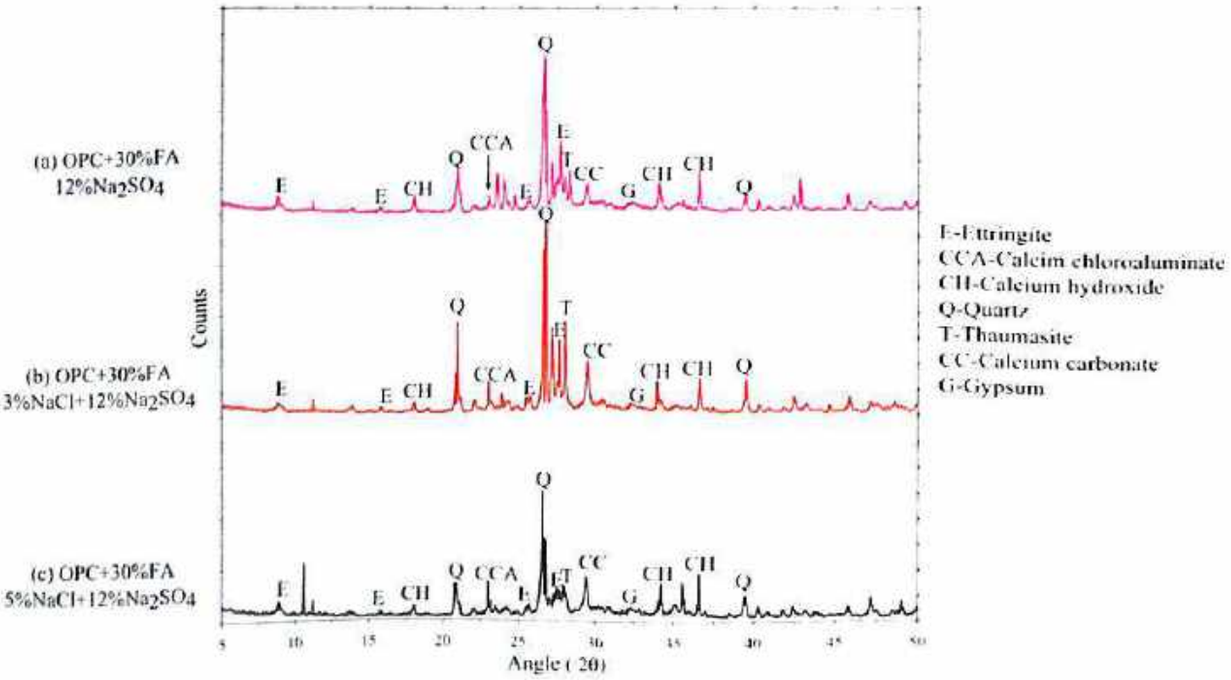

Fig. 7.33 XRD profile of OPC+30%FA concrete at w/b ratio of 0.45 and exposed to Na_2SO_4 and $NaCl + Na_2SO_4$ solutions for a period of 360 days under full immersion with alternate wetting and drying cycles

The XRD profiles shown in Fig. 7.30, Fig 7.31, Fig. 7.32 and 7.33 indicate the precipitation of calcium hydroxide (CH) through well-defined peaks at 18.04° 2θ and 34.1° 2θ in all the concrete mixes. The concrete mixes made with PPC, OPC+20FA and OPC+30FA showed less intense peaks of calcium hydroxide as compared to that made with OPC. The less peak intensity of calcium hydroxide in blended cement concretes is attributed to its consumption in the pozzolanic reaction. Further, the peaks of quartz (Q) were found at 20.85° 2θ, 26.65° 2θ and 39.45° 2θ as observed from Fig. 7.30 to Fig. 7.33, which is mostly due to the presence of aggregates in the concrete. Similarly, the peaks of thaumasite (T) and calcium carbonate (CC) were found at 27.9° 2θ and 29.4° 2θ respectively in the XRD profiles.

The formation of ettringite in the form of needle-like crystals in the concrete mixes exposed to Na_2SO_4 and NaCl + Na_2SO_4 solutions are indicated by the FESEM micrographs shown in Fig. 7.34, Fig. 7.35, Fig 7.36, and Fig. 7.37 respectively for OPC, PPC, OPC+20FA and OPC+30FA concrete mixes exposed to Na_2SO_4 solutions and in Fig. 7.38, Fig. 7.39, Fig 7.40, and Fig. 7.41 for the concrete mixes exposed to NaCl + Na_2SO_4 solutions with alternate wetting and drying cycles. In addition, the presence of C-S-H, calcium hydroxide, gypsum and calcium carbonate in concrete was also observed from these micrographs.

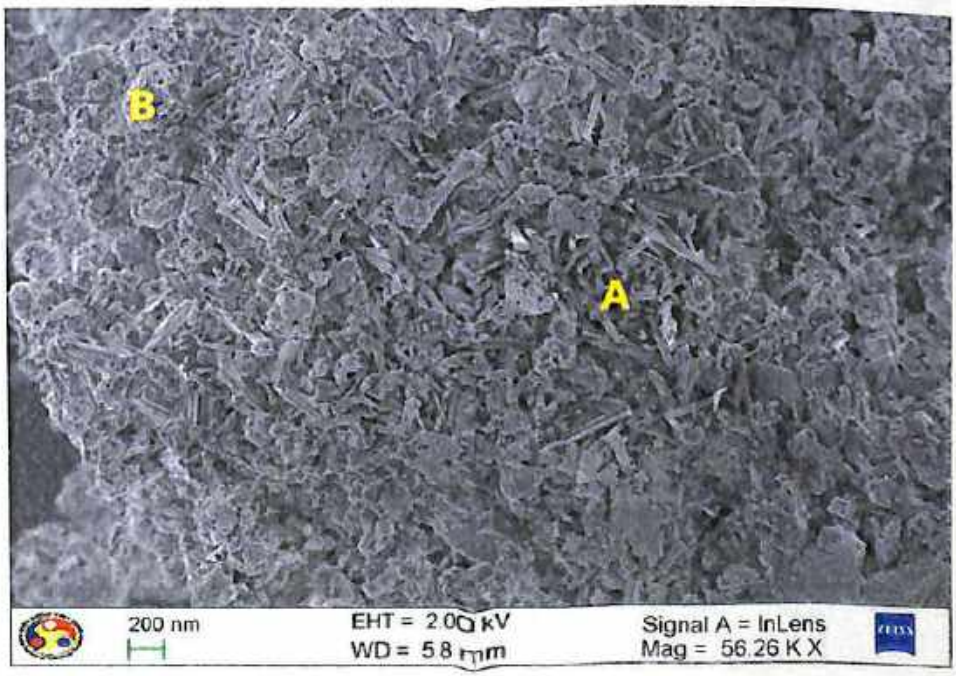

Fig.7.34 FESEM micrograph of OPC concrete made at w/b ratio of 0.45 and exposed to 12% Na_2SO_4 solution under full immersion with alternate wetting and drying cycles for a period of 360 days: (A) Ettringite and (B) Calcium hydroxide

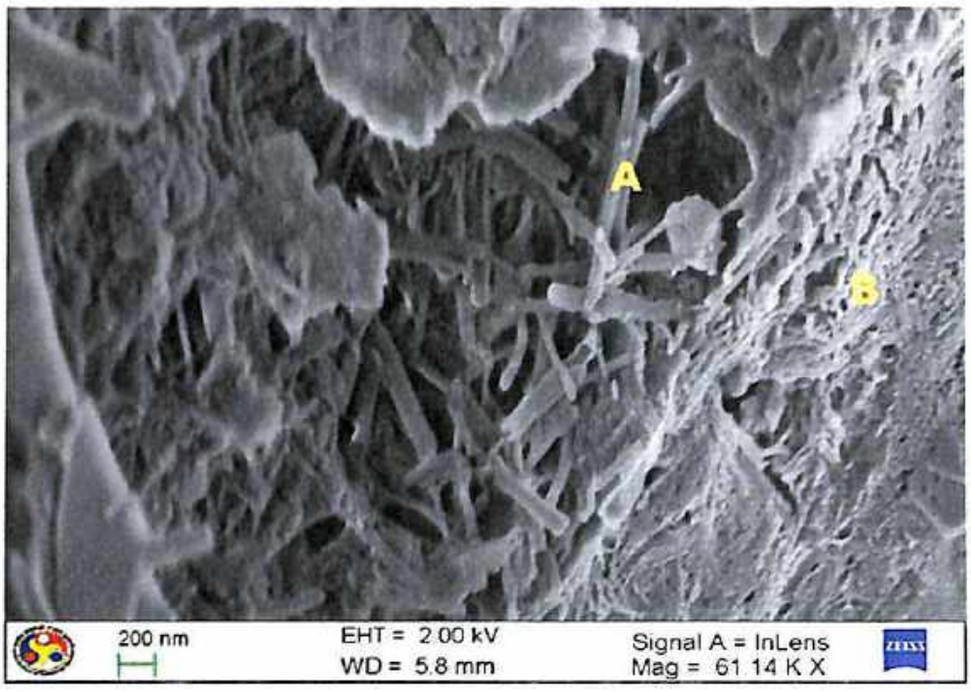

Fig.7.35 FESEM micrograph of PPC concrete made at w/b ratio of 0.45 and exposed to 12% Na_2SO_4 solution under full immersion with alternate wetting and drying cycles for a period of 360 days (A) Ettringite and (B) C-S-H

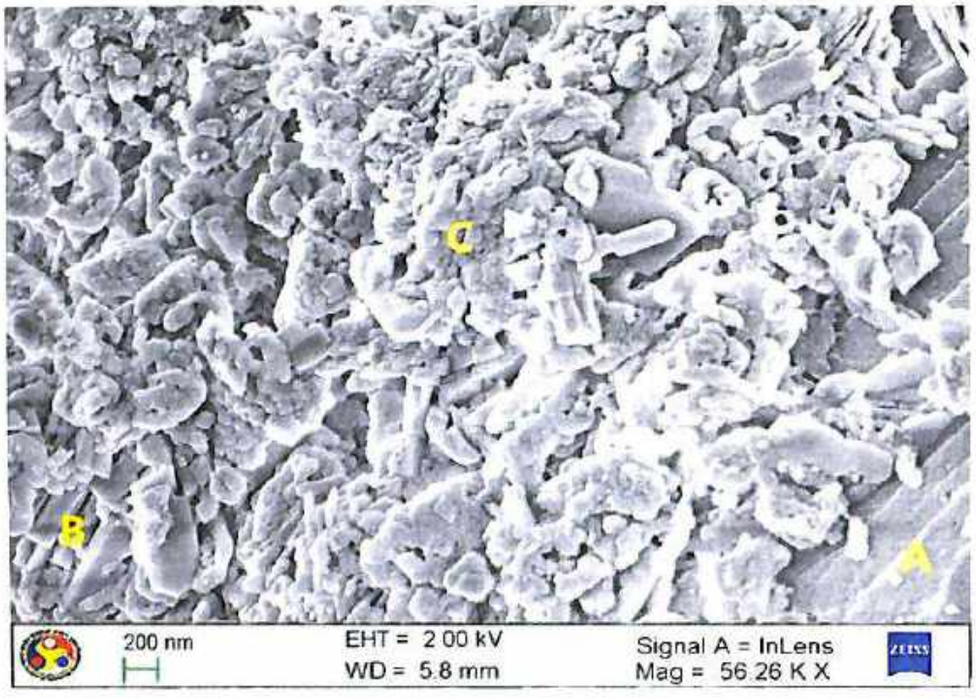

Fig.7.36 FESEM micrograph of OPC+20%FA concrete made at w/b ratio of 0.45 and exposed to 12% Na_2SO_4 solution under full immersion with alternate wetting and drying cycles for period of 360 days (A) Gypsum, (B) Ettringite and (C) C-S-H

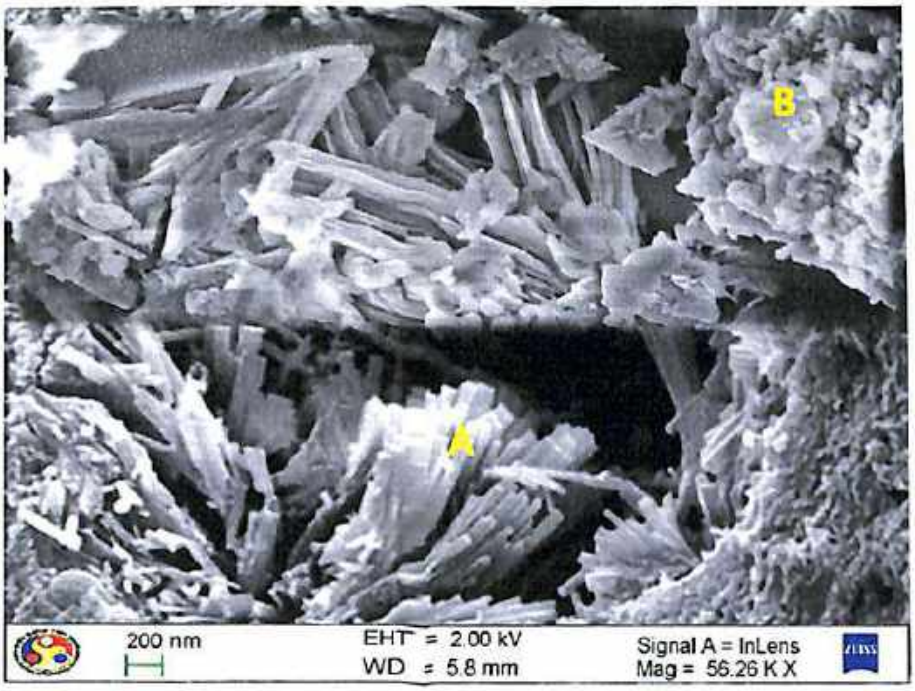

Fig. 7.37 FESEM micrograph of OPC+30%FA concrete made at w/b ratio of 0.45 and exposed to 12% Na_2SO_4 solution under full immersion with alternate wetting and drying cycles for a period of 360 days (A) Ettringite and (B) C-S-H

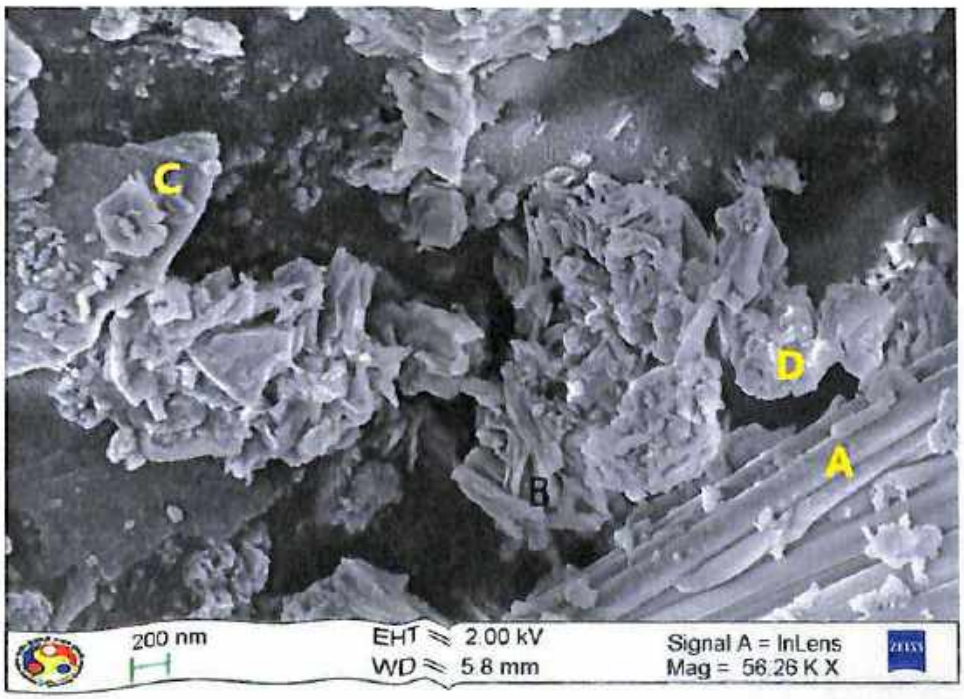

Fig.7.38 FESEM micrograph of OPC concrete made at w/b ratio of 0.45 and exposed to 5% NaCl + 12% Na_2SO_4 solution under full immersion with alternate wetting and drying cycles for a period of 360 days (A) Gypsum, (B) Ettringite, (C) Calcium hydroxide and (D) C-S-H

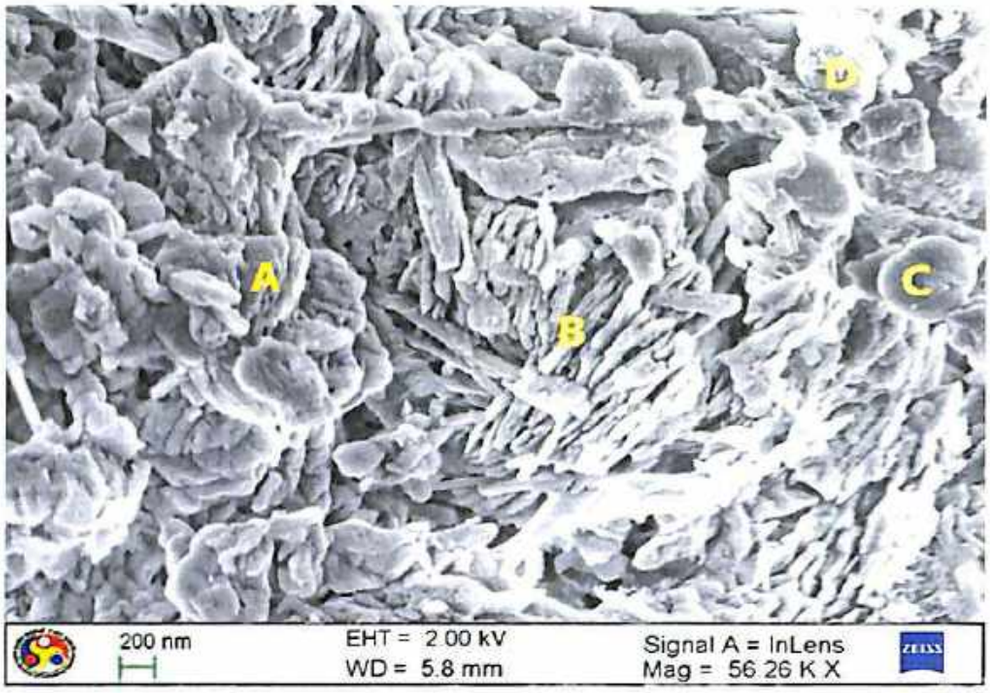

Fig. 7.39 FESEM micrograph of PPC concrete made at w/b ratio of 0.45 and exposed to 5% NaCl + 12% Na_2SO_4 solution under full immersion with alternate wetting and drying cycles for a period of 360 days

(A) Gypsum, (B) Ettringite, (C) Fly ash particle and (D) C-S-H

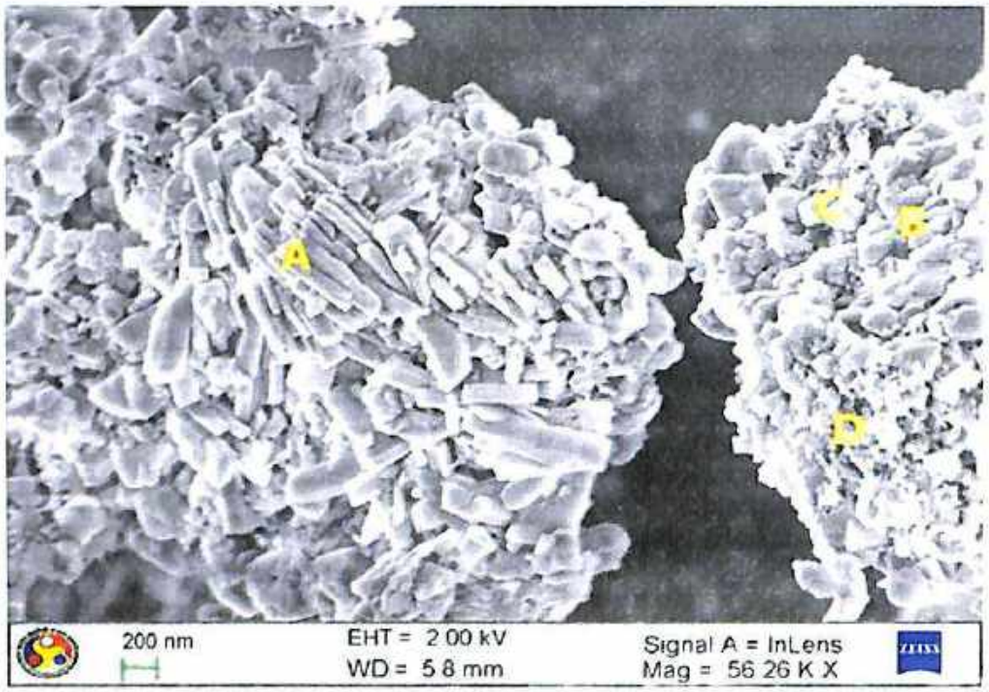

Fig. 7.40 FESEM of OPC+20%FA concrete made at w/b ratio of 0.45 and exposed to 5% NaCl + 12% Na_2SO_4 solution under full immersion with alternate wetting and drying cycles for a period of 360 days (A) Ettringite, (B) Calcium carbonate, (C) Calcium hydroxide and (D) C-S-H gel

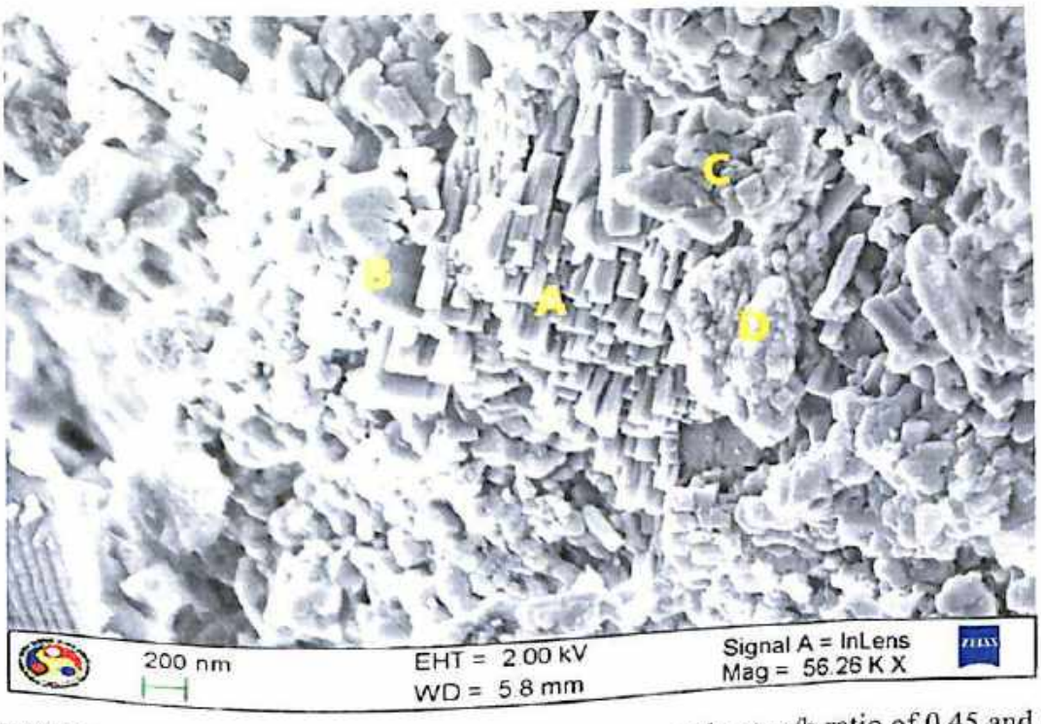

Fig. 7.41 FESEM micrograph of OPC+30%FA concrete made at w/b ratio of 0.45 and exposed to 5% NaCl + 12% Na_2SO_4 solution under full immersion with alternate wetting and drying cycles for a period of 360 days

(A) Ettringite, (B) Calcium hydroxide, (C) Calcium carbonate and (D) C-S-H

The poor resistance of blended cement concretes (PPC, OPC+20FA and OPC+30FA) as indicated by higher reduction in compressive strength as compared to that of OPC concrete when exposed to $MgSO_4$ and NaCl + $MgSO_4$ solutions may be attributed to the lower availability of $Ca(OH)_2$ and formation of more amount of gypsum in the blended cement concretes as compared to that in OPC concrete. In the blended cement concrete, due to lower availability of calcium hydroxide that acts as the first defensive material to react with magnesium sulfate, the magnesium sulfate attack is directed extensively towards C-S-H, ultimately forming more amount of gypsum and non-cementitious M-S-H. The formation of higher amount of gypsum in blended cement concretes as compared to that in OPC concrete is corroborated from XRD profiles presented in Fig. 7.42, Fig 7.43, Fig. 7.44 and 7.45 for OPC, PPC, OPC+20FA and OPC+30FA concrete respectively at w/b ratio of 0.45 when exposed to 12% $MgSO_4$, 3% NaCl + 12% $MgSO_4$ and 5% NaCl + 12% $MgSO_4$ solutions with alternate wetting and drying cycles. These figures indicate more intense peaks of gypsum in blended cement concretes as compared to that in OPC concrete as indicated by its peak at 32.1° 2θ. Further, there was formation

of more amount ettringite (E) in PPC, OPC+20FA and OPC+30FA concrete as compared to that in OPC concrete as indicated by its peaks at 8.8° 2θ, 15.75° 2θ, 25.6° 2θ, and 27.5° 2θ in the XRD profiles shown in Fig. 7.42 to Fig 7.45.

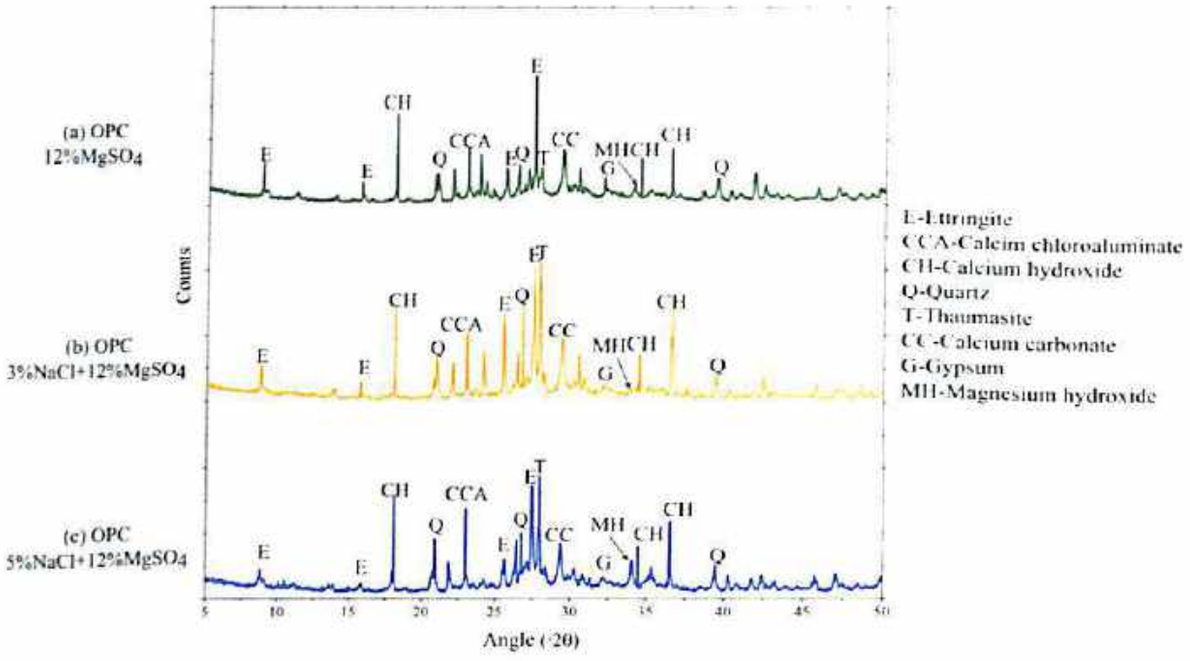

Fig. 7.42 XRD profile of OPC concrete at w/b ratio of 0.45 and exposed to $MgSO_4$ and $NaCl + MgSO_4$ solutions for a period of 360 days under full immersion with alternate wetting and drying cycles

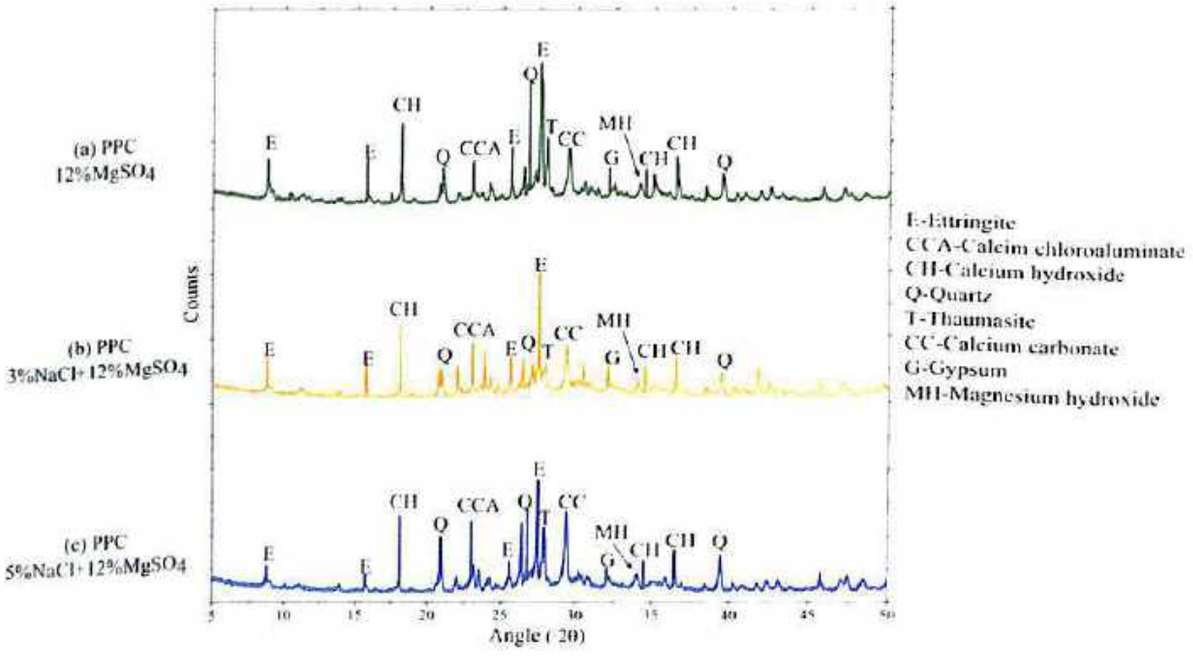

Fig. 7.43 XRD profile of PPC concrete at w/b ratio of 0.45 and exposed to $MgSO_4$ and $NaCl + MgSO_4$ solutions for a period of 360 days under full immersion with alternate wetting and drying cycles

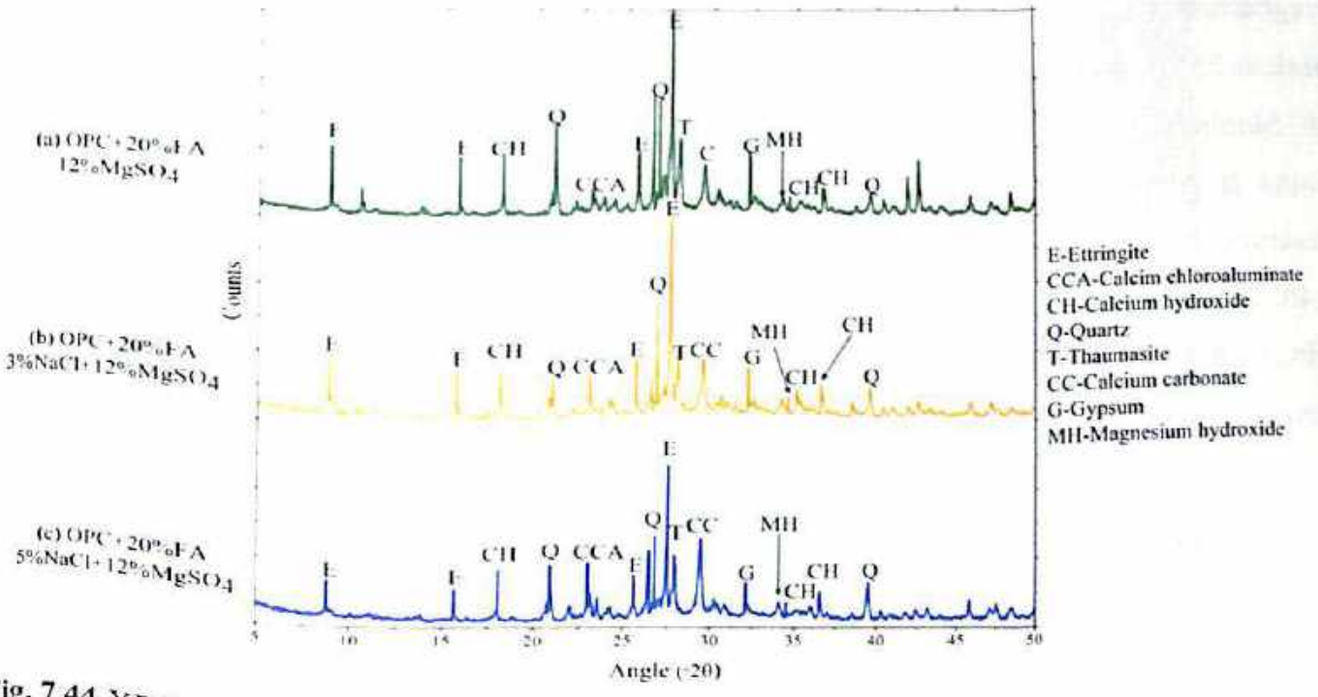

Fig. 7.44 XRD profile of OPC+20%FA concrete at w/b ratio of 0.45 and exposed to $MgSO_4$ and NaCl + $MgSO_4$ solutions for a period of 360 days under full immersion with alternate wetting and drying cycles

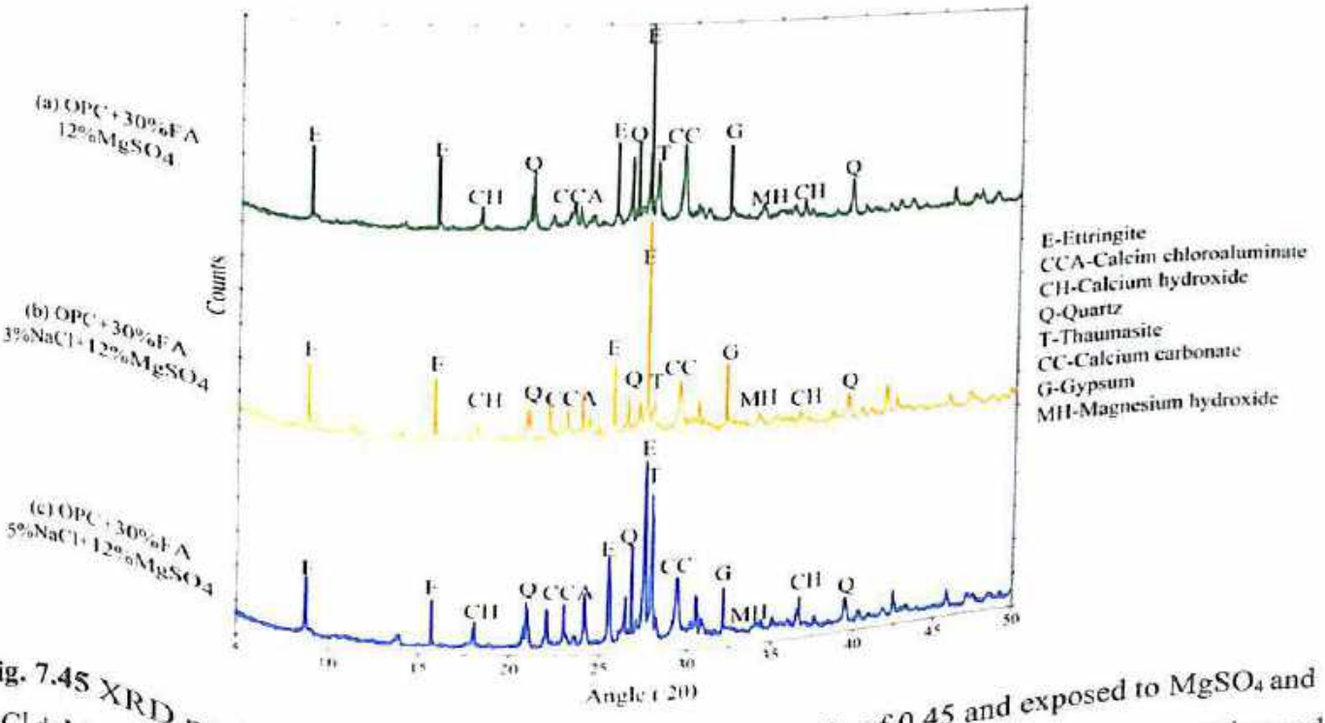

Fig. 7.45 XRD profile of OPC+30%FA concrete at w/b ratio of 0.45 and exposed to $MgSO_4$ and NaCl + $MgSO_4$ solutions for a period of 360 days under full immersion with alternate wetting and drying cycles

The XRD profiles shown in these figures (Fig. 7.42 to Fig 7.45) indicate the formation of magnesium hydroxide (MH) with peak at 33.9° 2θ, calcium chloroaluminate (CCA) with peak at 23° 2θ and calcium hydroxide (CH) with peaks at 18.08° 2θ, 34.2° 2θ, and 36.5° 2θ. Similarly, the peaks of quartz (Q), thaumasite (T) and calcium carbonate (CC) were found at 20.85° 2θ, 26.65° 2θ and 39.45° 2θ; 27.9° 2θ; and 29.4° 2θ respectively as observed from Fig. 7.42 to Fig. 7.45. The typical FESEM micrographs shown in Fig. 7.46, Fig. 7.47, Fig. 7.48 and Fig. 7.49 respectively for OPC, PPC, OPC+20FA and OPC+30FA also indicate the formation of calcium hydroxide, gypsum, ettringite and non-cementitious, fibrous M-S-H in these concrete mixes exposed to $MgSO_4$ solutions.

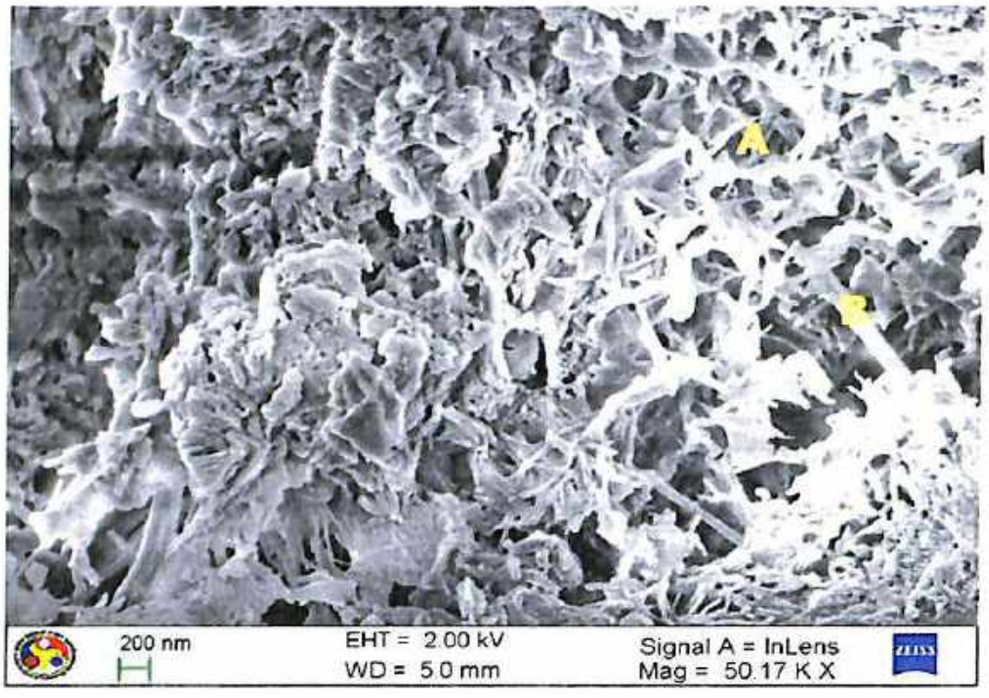

Fig. 7.46 FESEM micrograph of OPC concrete made at w/b ratio of 0.45 and exposed to 12% $MgSO_4$ solution under full immersion with alternate wetting and drying cycles for a period of 360 days: (A) Fibrous M-S-H and (B) Ettringite

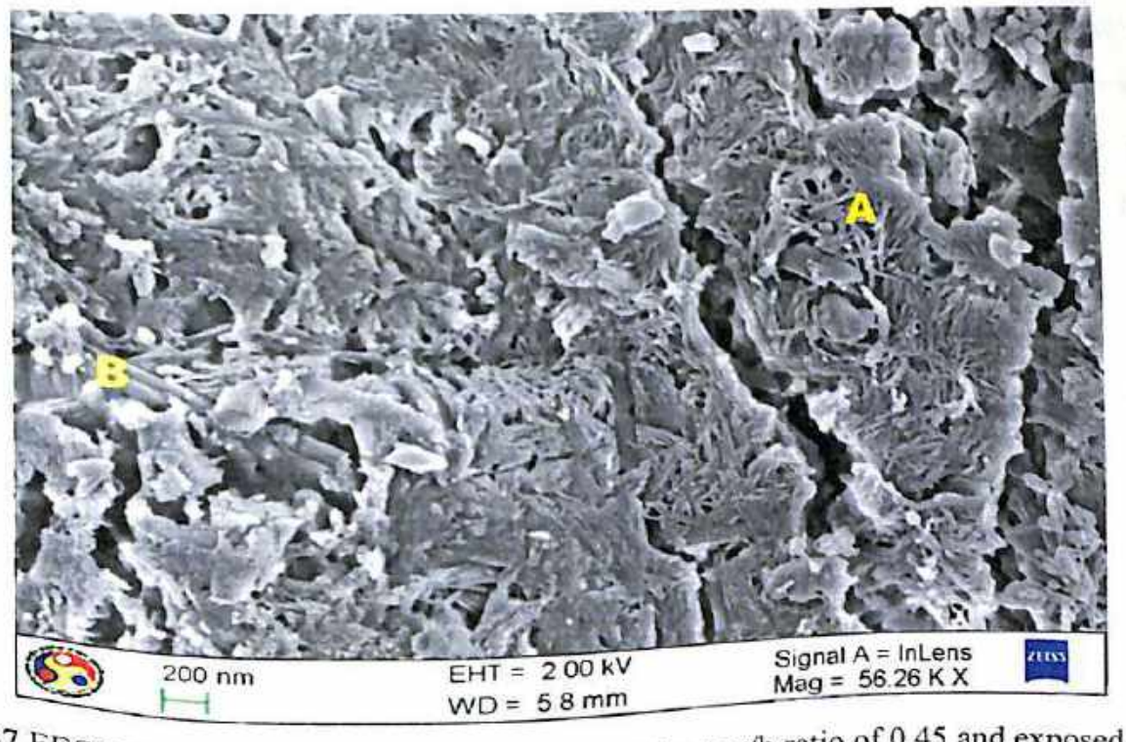

Fig. 7.47 FESEM micrograph of PPC concrete made at w/b ratio of 0.45 and exposed to 12% $MgSO_4$ solution under full immersion with alternate wetting and drying cycles for a period of 360 days (A) Fibrous M-S-H and (B) Gypsum

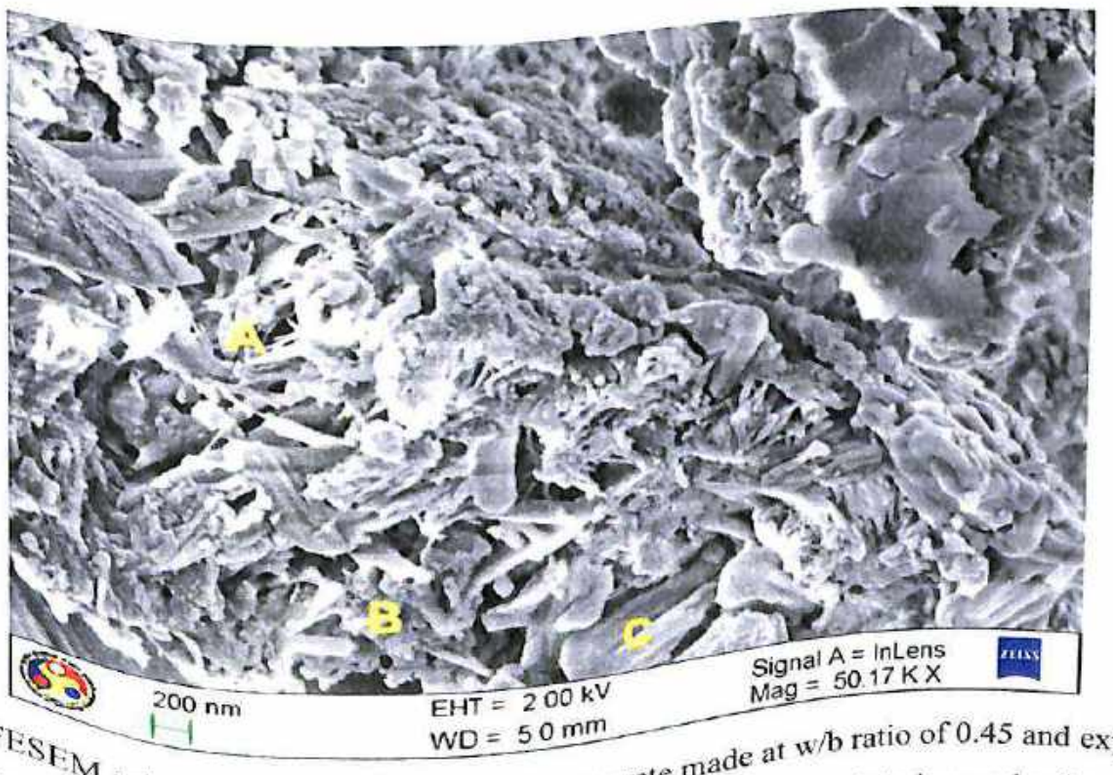

Fig 7.48 FESEM micrograph of OPC+20%FA concrete made at w/b ratio of 0.45 and exposed to 12% $MgSO_4$ solution under full immersion with alternate wetting and drying cycles for a period of 360 days (A) Fibrous M-S-H, (B) Ettringite and (C) Gypsum

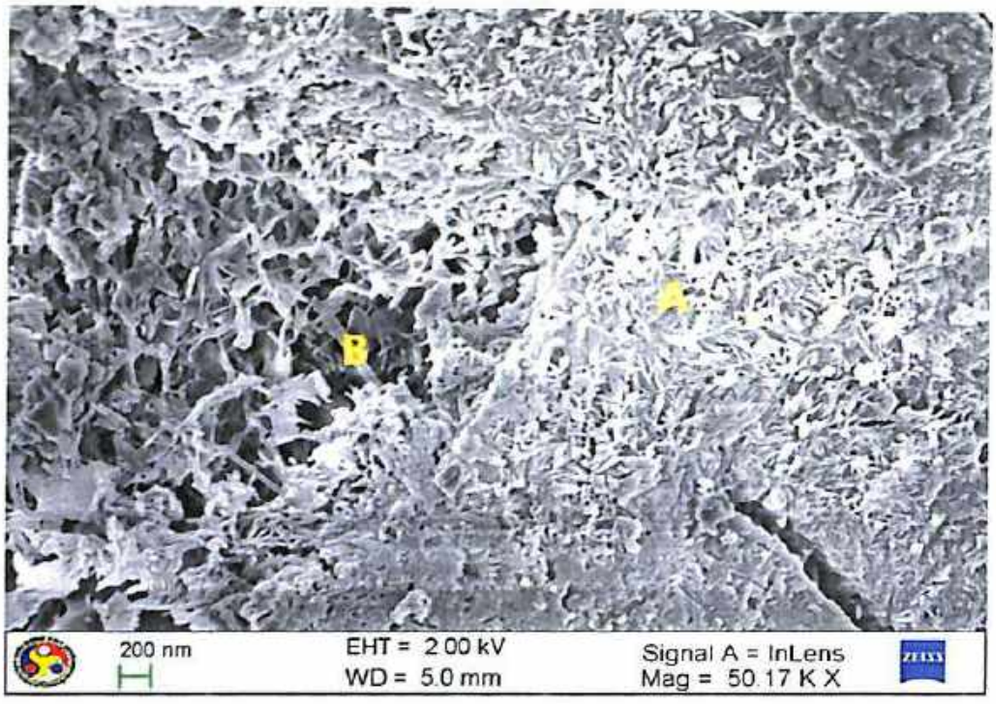

Fig. 7.49 FESEM micrograph of OPC+30%FA concrete made at w/b ratio of 0.45 and exposed to 12% $MgSO_4$ solution under full immersion with alternate wetting and drying cycles for a period of 360 days (A) Fibrous M-S-H and (B) Ettringite

7.4.2 Effect of w/b ratio on Compressive Strength of Concrete Subjected to Sulfate and Conjoint Chloride-Sulfate Environment

While analyzing the effect of w/b ratio on reduction in compressive strength of concrete, it is observed from Fig. 7.14 to Fig. 7.29 that, the average reduction in compressive strength of concrete made at w/b ratio of 0.45 vary from 43.6% to 54.6% and 13.1% to 29.9% respectively when exposed to Na_2SO_4 and NaCl + Na_2SO_4 solutions, whereas that at w/b ratio of 0.5 vary from 42.4% to 51.7% and 4.4% to 25% respectively when exposed to these solutions, irrespective of binder type, exposure condition and concentrations of NaCl and Na_2SO_4. Similarly, the average reduction in compressive strength of concrete at w/b ratio of 0.45 when exposed to $MgSO_4$ and NaCl + $MgSO_4$ solutions vary from 50.1% to 63.0% and 21.9% to 42.5% respectively and that at w/b ratio of 0.5 vary from 47.0% to 57.2% and 8.8% to 33.3% respectively when exposed to these solutions irrespective of binder type, exposure condition and concentrations of NaCl and $MgSO_4$. These results indicate that the concrete made at w/b ratio of 0.45 exhibited higher reduction in compressive strength as compared to that made at w/b ratio of 0.5. Thus, a decrease in w/b ratio enhanced the reduction in compressive strength of concrete when exposed to sulfate and conjoint chloride-sulfate solutions. The higher reduction in

compressive strength of concrete at lower w/b (0.45) ratio as compared to that at higher w/b (0.5) ratio is attributed to the salt crystallization in the pores of the concrete at lower w/b ratio. The finer pore structure (i.e. reduced pore space) of concrete at lower w/b ratio may not be sufficient to accommodate the expansive products formed as a result of reaction between cement hydrates; and sulfate and chloride salts as compared that at higher w/b ratio.

7.4.3 Effect of Exposure Condition on Compressive Strength of Concrete Subjected to Sulfate and Conjoint Chloride-Sulfate Environment

For evaluating the effect of exposure condition on compressive strength, the average reduction in compressive strength (%) of concrete has been compared between continuous full immersion condition and full immersion with alternate wetting and drying cycles. From the results presented in Fig. 7.14 to Fig. 7.29, it is observed that the average reduction in compressive strength of concrete varied from 42.4% to 51.7%, 47.0% to 57.2%, 11.7% to 26.5% and 16.5% to 39.9% respectively when exposed to Na_2SO_4, $MgSO_4$, $NaCl + Na_2SO_4$ and $NaCl + MgSO_4$ solutions under continuous full immersion condition, whereas that varied from 41.0% to 54.6%, 42.2% to 63.0%, 4.4% to 29.9% and 8.8% to 42.5% respectively when exposed to these solutions under full immersion with alternate wetting and drying cycles, irrespective of binder type, w/b ratio and concentration of chloride and sulfate salts.

From the above mentioned variations in compressive strength reduction, it is found that the maximum reduction in compressive strength of concrete under full immersion with alternate wetting and drying cycles is higher as compared to that under continuous full immersion condition. The higher reduction in compressive strength of concrete under full immersion with alternate wetting and drying cycles is attributed to the repetitive crystallization of salts in the pores of concrete due to alternate wetting and drying. As reported by Liu [136], under cyclic wetting and drying exposure condition, the soluble salts accumulate in high concentrations within the zone where the moisture front ends during the exposure of concrete to salt water and the salt crystals form and continue to grow as evaporation proceeds during drying. The crystallization pressure thus generated causes deterioration of the concrete. Therefore, in alternate wetting and drying exposure condition, the repetitive crystallization in the pores of concrete with the expansive products (formed as a result of reaction between cement hydrates; and sulfate and

chloride salts) might have exerted internal stresses thereby resulting in expansion and disruption of the concrete as compared to that in continuous full immersion condition.

7.4.4 Effect of Na_2SO_4, $MgSO_4$ and NaCl Concentration on Compressive Strength of Concrete

While evaluating the effect of Na_2SO_4 and $MgSO_4$ concentrations on reduction in compressive strength of concrete, it is observed from Fig. 7.14 to Fig. 7.29 that the average reduction in compressive strength (%) of concrete increased with an increase in concentration of Na_2SO_4 and $MgSO_4$ for sulfate and conjoint chloride-sulfate solutions in all the concrete mixes and for both exposure conditions i.e. continuous full immersion and full immersion with alternate wetting and drying cycles. The increase in reduction of compressive strength with increase in Na_2SO_4 concentration is attributed to the formation of higher amount of gypsum and ettringite and that with increase in $MgSO_4$ concentration is attributed to the formation of higher amount of gypsum and non-cementitious M-S-H in concrete. Further from Fig. 7.14 to Fig. 7.29, it is observed that the average percentage reduction in compressive strength of concrete decreased with an increase in NaCl concentration in the conjoint chloride-sulfate solutions in all the concrete mixes. This indicates that the deterioration of concrete due to sulfate attack is retarded with increase in NaCl concentration in the conjoint NaCl + Na_2SO_4 and NaCl + $MgSO_4$ solutions.

7.4.5 Comparison between the Effects of Sulfate ion and Conjoint Chloride-Sulfate ions on Compressive Strength of Concrete

While comparing the reduction in compressive strength of concrete in different exposure solutions, it is observed from Fig. 7.14 to Fig. 7.29 that the average reduction in compressive strength of concrete in Na_2SO_4, $MgSO_4$, NaCl + Na_2SO_4 and NaCl + $MgSO_4$ solutions varied from 41.0% to 54.6%, 42.2% to 63.0%, 4.4% to 29.9% and 8.8% to 42.5% respectively irrespective of binder type, w/b ratio, concentration of these salts and exposure condition. From the aforementioned values of average reduction in compressive strength (%), it is inferred that the reduction in compressive strength of concrete in $MgSO_4$ solution is higher as compared to that in Na_2SO_4 solution. The higher reduction in compressive strength of concrete in $MgSO_4$ environment is attributed to the conversion of C-S-H to non-cementitious fibrous M-S-H. This is also corroborated from FESEM micrographs shown in Fig. 7.46 to Fig. 7.49, which indicate the formation of non-

cementitious fibrous M-S-H in concrete exposed to $MgSO_4$ solution, whereas a relatively denser microstructure was observed in the concrete exposed to Na_2SO_4 solution as observed from FESEM micrographs shown in Fig. 7.34 to Fig. 7.37.

On comparison of the reduction in compressive strength of concrete between sulfate environment and conjoint chloride-sulfate environment, it is observed that in the presence of chloride ions, the sulfate attack on concrete is mitigated as indicated by lower reduction in compressive strength of concrete exposed to NaCl + Na_2SO_4 and NaCl + $MgSO_4$ solutions as compared to those exposed to Na_2SO_4 and $MgSO_4$ solutions. Thus, it implies that when chloride ions are present concomitantly with sulfate ions in the surrounding environment of concrete, it mitigates the sulfate attack.

The increased sulfate resistance of concrete in the concomitant presence of chloride and sulfate ions is attributed to differences in the diffusion rates of these two ions. The chloride ions diffuse into the concrete much faster than sulfate ions. The diffusion rate of chloride ions in concrete is generally 10 – 100 times faster than that of sulfate ions [137]. Thus, the higher rate of diffusion of chloride ions than sulfate ions into concrete allows the chloride ions to react preferentially with hydrated C_3A to form more amount of calcium chloroaluminate (Friedel's salt) in the concrete exposed to conjoint chloride-sulfate solutions as compared to that exposed to only sulfate solution. This is also confirmed from the higher peak intensity of calcium chloroaluminate observed in the XRD profiles (shown in Fig. 7.30 to Fig. 7.33 and Fig. 7.42 to Fig. 7.45) of the concrete exposed to NaCl + Na_2SO_4 and NaCl + $MgSO_4$ solutions as compared to that exposed to only Na_2SO_4 and $MgSO_4$ solutions. Thus, the availability of C_3A to react with sulfate ions is reduced thereby resulting in formation of lower amount of ettringite in the concomitant presence of NaCl plus Na_2SO_4 and NaCl plus $MgSO_4$ as compared to that in presence of only Na_2SO_4 and $MgSO_4$. Further, in the conjoint presence of chloride-sulfate ions, there may be increased solubility of the expansive products in the chloride solution, as reported by Harrison [90], the solubility of ettringite in chloride solution is three times greater than that in water. The formation of lower amount of ettringite in the concrete exposed to NaCl + Na_2SO_4 and NaCl + $MgSO_4$ solutions as compared to that in the concrete exposed to Na_2SO_4 and $MgSO_4$ solutions is also corroborated from the XRD profiles shown in Fig. 7.30 to Fig. 7.33 and Fig. 7.42 to Fig. 7.45, wherein the peak intensity of ettringite was lower in the concrete exposed to NaCl + Na_2SO_4 and NaCl + $MgSO_4$ solutions as compared to that in the concrete exposed to only Na_2SO_4 and $MgSO_4$ solutions.

While comparing the effect of cation type associated with sulfate ions in the conjoint chloride-sulfate environment, it is observed that the reduction in compressive strength of concrete in NaCl + $MgSO_4$ solution is higher as compared to that in NaCl + Na_2SO_4 solution. The higher reduction in compressive strength of concrete in NaCl + $MgSO_4$ solution is attributed to the more deleterious action of $MgSO_4$. In case of Na^+ cations associated with sulfate ions, the strength reduction is due to the expansion and cracking caused by formation of gypsum and ettringite, whereas in case of Mg^{++} cations associated with sulfate ions the strength reduction is due to the formation of insoluble magnesium hydroxide (brucite) and decalcification of C-S-H to non-cementitious M-S-H, along with the formation of ettringite and gypsum. Therefore, the effect of $MgSO_4$ is more deleterious than that of Na_2SO_4 leading to higher reduction in compressive strength of concrete. As stated earlier, the formation of magnesium hydroxide was confirmed through its peaks in the XRD profiles shown in Fig. 7.42 to Fig. 7.45 for the concrete exposed to $MgSO_4$ and NaCl + $MgSO_4$ solutions. Similarly, the formation of fibrous magnesium silicate hydrate (M-S-H) in the presence of Mg^{++} cations associated with sulfate ions is also corroborated from the FESEM micrographs shown in Fig. 7.46 to Fig. 7.49 for the concrete exposed to $MgSO_4$ environment.

7.5 SUMMARY

From the visual examination of concrete after exposure to Na_2SO_4 solutions, it is observed that the cube specimens showed deterioration at the edges, whereas exposure to $MgSO_4$ solutions showed deterioration in the form of peeling of the surface skin on all the faces of the cube specimens with the aggregates exposed. No significant deterioration was observed on surface of cube specimens exposed to NaCl + Na_2SO_4 and NaCl + $MgSO_4$ solutions.

The average change in weight (%) and average reduction in compressive strength (%) of concrete varied with binder type, w/b ratio, exposure solution and exposure condition. The variations in compressive strength of concrete attributed to the formation of compounds such as gypsum, ettringite, calcium chloroaluminate, magnesium hydroxide and M-S-H in the presence of sulfate and conjoint chloride-sulfate ions are corroborated from the results of XRD and FESEM analyses.

The blended cements (PPC, OPC+20FA and OPC+30FA) exhibited lower reduction in compressive strength as compared to OPC in sodium sulfate and sodium chloride plus

sodium sulfate environment whereas OPC showed lower reduction in compressive strength as compared to blended cements in magnesium sulfate and sodium chloride plus magnesium sulfate environment. Further the reduction in compressive strength was lower at w/b ratio of 0.5 as compared to that at 0.45. While comparing the exposure solutions, it is observed that the reduction in compressive strength of concrete decreased in the order: $MgSO_4$ > Na_2SO_4 > NaCl plus $MgSO_4$ > NaCl plus Na_2SO_4. Further, the reduction in compressive strength of concrete was higher under alternate wetting-drying exposure condition as compared to that under continuous full immersion condition.

CHAPTER 8

CONCLUSIONS AND SUGGESTIONS FOR FURTHER WORK

8.1 SUMMARY

In this chapter, the conclusions obtained from the comprehensive experimental investigation on the effect of chloride and conjoint chloride-sulfate contamination on 28-day compressive strength of concrete, microstructural changes occurred in concrete, and chemical composition of electrolytic concrete powder solution prepared from different concrete mixes are presented. In addition, the conclusions obtained from electrochemical behaviour of steel reinforcement in electrolytic concrete powder solutions contaminated with varying concentrations of sodium chloride, sodium chloride plus sodium sulfate and sodium chloride plus magnesium sulfate are also presented. Further, the conclusions drawn from corrosion behaviour of steel reinforcement embedded in concrete that is admixed with varying concentrations of chloride-sulfate ions and subsequently exposed to conjoint chloride-sulfate environment are presented. In addition, the conclusions obtained from performance of concrete in sulfate and conjoint chloride-sulfate environment under different exposure conditions are also enumerated.

8.2 CONCLUSIONS FROM COMPRESSIVE STRENGTH OF CONCRETE CONTAMINATED WITH CHLORIDE AND CHLORIDE-SULFATE IONS

- The concrete made from OPC exhibited lower compressive strength at the age of 28 days as compared to that made from PPC at all levels of chloride and conjoint chloride-sulfate contaminations for both w/c ratios (0.45 and 0.5).
- The specimens admixed with varying concentrations of sodium chloride showed higher compressive strength as compared to those admixed with varying concentrations of conjoint sodium chloride plus sodium sulfate and sodium chloride plus magnesium sulfate at w/c ratios of 0.45 and 0.5 for both OPC and PPC.
- While observing the effect of cation type associated with sulfate ions on 28-day compressive strength of concrete, it is found that concrete admixed with sodium

chloride plus magnesium sulfate exhibited lower compressive strength as compared to those admixed with sodium chloride plus sodium sulfate.

8.3 CONCLUSIONS FROM MICROSTRUCTURE OF CONCRETE AND ELECTROLYTIC CONCRETE POWDER SOLUTION (ECPS) CHEMISTRY

- The XRD profiles showed less peak intensity of ettringite (E) and more peak intensity of calcium chloroaluminate (CCA) in OPC concrete as compared to that in PPC concrete at all levels of admixed NaCl. This is attributed to the preferential reaction of chloride ions with C_3A to form more amounts of calcium chloroaluminate thereby, resulting in lesser availability of C_3A to react with gypsum to form lower amount of ettringite in OPC.
- In the conjoint presence of NaCl plus Na_2SO_4 and NaCl plus $MgSO_4$, the XRD profiles of concrete made from different types of cement (i.e. OPC and PPC) and w/c ratio (i.e. 0.45 and 0.5) showed variations in the formation of ettringite (E), gypsum (G), calcium chloroaluminate (CCA) and calcium hydroxide (CH) as indicated by their respective peak intensities.
- The Fourier transform infrared (FTIR) spectra of concrete contaminated with sodium chloride, sodium chloride plus sodium sulfate and sodium chloride plus magnesium sulfate for OPC and PPC indicated the functional groups associated with different products i.e. gypsum, calcium carbonate and ettringite formed in concrete through the transmittance bands of O-H, SO_4^{2-}, CO_3^{2-} and Al-O.
- The XRD profiles indicating the formation of different compounds in concrete in the presence of chloride and conjoint chloride-sulfate ions were consistent with the functional groups associated with those compounds as observed from FTIR spectrum analysis.
- The formation of C-S-H, calcium hydroxide, gypsum, ettringite, and calcium chloroaluminate in concrete contaminated with sodium chloride, sodium chloride plus sodium sulfate and sodium chloride plus magnesium sulfate were also substantiated by the FESEM micrographs of concrete made from OPC and PPC. In addition, the FESEM micrographs also indicated the formation of magnesium hydroxide (brucite) and non-cementitious M-S-H in the concrete admixed with sodium chloride plus magnesium sulfate.

- The chemical composition of electrolytic concrete powder solution (ECPS) prepared from various concrete mixes contaminated with sodium chloride, sodium chloride plus sodium sulfate and sodium chloride plus magnesium sulfate indicated that the concentrations of Cl^-, SO_4^{2-}, Na^+, Ca^{++} and K^+ ions vary significantly with varying concentrations of NaCl, NaCl plus Na_2SO_4 and NaCl plus $MgSO_4$.
- The electrolytic concrete powder solutions contaminated with varying dosages of NaCl, NaCl plus Na_2SO_4 and NaCl plus $MgSO_4$ showed higher concentrations of Cl^- ion and SO_4^{2-} ion at w/c ratio of 0.45 as compared to that at w/c ratio of 0.5 for both OPC and PPC.
- The concentration of Cl^- ions in electrolytic concrete powder solutions contaminated with varying dosages of NaCl, NaCl plus Na_2SO_4 and NaCl plus $MgSO_4$ decreased in the order: NaCl + $MgSO_4$ > NaCl > NaCl + Na_2SO_4.
- The concentration of SO_4^{2-} ions in electrolytic concrete powder solutions contaminated with varying concentrations of NaCl, NaCl plus Na_2SO_4 and NaCl plus $MgSO_4$ decreased in the order: NaCl + Na_2SO_4 > NaCl + $MgSO_4$ > NaCl.
- The electrolytic concrete powder solution contaminated with NaCl plus Na_2SO_4 showed higher pH as compared to that contaminated with NaCl plus $MgSO_4$ for both types of cement and w/c ratio.
- The conductivity of chloride contaminated electrolytic concrete powder solution prepared from PPC was higher than that prepared from OPC. This is attributed to higher concentration of Cl^- ion in PPC as compared that in OPC.
- The conductivity of electrolytic concrete powder solution was higher in the presence of NaCl plus $MgSO_4$ as compared to that in the presence of NaCl plus Na_2SO_4. This indicates that the presence of sulfate ions when associated with magnesium cation increases the conductivity of concrete in the presence of chloride ions.

8.4 CONCLUSIONS FROM PASSIVITY OF STEEL REINFORCEMENT IN ELECTROLYTIC CONCRETE POWDER SOLUTION

- Different zones of corrosion namely active zone, passive zone and pitting zone of steel reinforcement in electrolytic concrete powder solution (ECPS) in the presence of chloride and conjoint chloride-sulfate ions were obtained and the corresponding boundary potential values of these zones of corrosion were determined.
- In uncontaminated ECPS, the range of passive zone of steel reinforcement is more as compared to that in NaCl, NaCl plus Na_2SO_4 and NaCl plus $MgSO_4$ contaminated ECPS. This indicates that the presence of chloride and sulfate ions in concrete decreases the passivity of steel reinforcement.
- The range of passive zone decreased with increase in admixed NaCl concentration in all the concrete mixes, which indicates that the presence of chloride ions in concrete reduces the passivity of steel reinforcement.
- The range of passive zone is more in OPC as compared to PPC in chloride contaminated electrolytic concrete powder solutions for both types of steel and w/c ratio. This is attributed to more chloride binding in OPC as compared to that in PPC, which resulted in lower Cl^- ion concentration in ECPS prepared from OPC than that prepared from PPC. The higher chloride binding in OPC was also confirmed from the XRD profiles through more intense peaks of calcium chloroaluminate in OPC than that in PPC.
- In the conjoint presence of NaCl plus Na_2SO_4, PPC showed higher range of passivity as compared to OPC, whereas OPC showed higher range of passivity as compared to PPC in the conjoint presence of NaCl plus $MgSO_4$.
- Among steel type and w/c ratio, Tempcore TMT steel and w/c ratio of 0.5 exhibited higher range of passivity as compared to Thermex TMT steel and w/c ratio of 0.45 respectively in the ECPS contaminated with chloride ions and composite chloride-sulfate ions (for both cations).
- The presence of sulfate ions associated with Na^+ cation in chloride environment (i.e. NaCl plus Na_2SO_4) has mitigated the effect of chloride ions on reducing the passivity of both Tempcore TMT steel and Thermex TMT steel.

- For Tempcore TMT steel, the presence of sulfate ions associated with Mg^{++} cation in chloride environment (i.e. NaCl plus $MgSO_4$) has stimulated the effect of chloride ions on reducing the passivity of steel reinforcement, whereas for Thermex TMT steel the presence of sulfate ions associated with Mg^{++} cation in chloride environment has mitigated the effect of chloride ions on reducing the passivity of steel reinforcement.
- The range of passive zone of both types of steel reinforcement was more in the presence of NaCl plus Na_2SO_4 as compared to that in the presence of NaCl plus $MgSO_4$ for both types of cement and w/c ratio. This indicates that Mg-oriented sulfate attack is more aggressive in reducing the passivity of steel reinforcement as compared to Na-oriented sulfate attack in the presence of chloride ions.
- Overall, the passivity range of steel reinforcement in electrolytic concrete powder solutions contaminated with varying concentrations of NaCl, NaCl plus Na_2SO_4 and NaCl plus $MgSO_4$ decreased in the order: NaCl + Na_2SO_4 > NaCl > NaCl + $MgSO_4$.

8.5 CONCLUSIONS FROM CORROSION POTENTIAL AND CORROSION CURRENT DENSITY OF STEEL REINFORCEMENT IN ECPS

- The presence of chloride and conjoint chloride-sulfate ions increased the probability of occurrence of steel reinforcement corrosion in electrolytic concrete powder solution for both types of cement, steel and w/c ratio.
- The corrosion current density of steel reinforcement increased with increase concentration of NaCl in the ECPS contaminated with NaCl, NaCl plus Na_2SO_4 and NaCl plus $MgSO_4$.
- There was increase in corrosion current density of steel reinforcement with increase in $MgSO_4$ concentration in ECPS contaminated with NaCl plus $MgSO_4$, whereas there was no systematic variation in corrosion current density with concentration of Na_2SO_4 in ECPS contaminated with NaCl plus Na_2SO_4.
- Portland pozzolana cement (PPC) exhibited higher corrosion current density than ordinary Portland cement (OPC) in the presence of chloride ions. In the conjoint presence NaCl plus Na_2SO_4, OPC showed higher corrosion current density as compared to PPC, whereas PPC showed higher corrosion current density as

compared to OPC in the conjoint presence NaCl plus $MgSO_4$. This indicates that OPC is likely to exhibit longer corrosion propagation period in NaCl and NaCl plus $MgSO_4$ environment, whereas PPC is likely to exhibit longer corrosion propagation period in NaCl plus Na_2SO_4 environment.

- Among steel type and w/c ratio, Tempcore TMT steel and w/c ratio of 0.5 exhibited lower corrosion current density as compared to Thermex TMT steel and w/c ratio of 0.45 respectively in the presence of NaCl, NaCl plus Na_2SO_4 and NaCl plus $MgSO_4$.
- On comparison between NaCl and NaCl plus Na_2SO_4, the presence of sulfate ions associated with Na^+ cation has mitigated the effect of chloride ions on corrosion current density of both Tempcore TMT steel and Thermex TMT steel.
- On comparison between NaCl and NaCl plus $MgSO_4$, the presence of sulfate ions associated with Mg^{++} cation has stimulated the effect of chloride ions on corrosion current density of Tempcore TMT steel, whereas for Thermex TMT steel, the presence of sulfate ions associated with Mg^{++} cation has mitigated the effect of chloride ions on corrosion current density.
- In chloride-sulfate environment, the presence of sulfate ions associated with Mg^{++} cation has more deleterious effect than Na^+ cation in terms of higher corrosion current density of steel reinforcement.
- There exists a good correlation between passivity range and corrosion parameters (corrosion potential and corrosion current density) of steel reinforcement in sodium chloride, sodium chloride plus sodium sulfate and sodium chloride plus magnesium sulfate contaminated electrolytic concrete powder solutions.

8.6 CONCLUSIONS FROM CORROSION BEHAVIOUR OF STEEL REINFORCEMENT EMBEDDED IN CONCRETE

- The probability of occurrence of steel reinforcement corrosion in concrete increased in the presence of chloride and sulfate ions (associated with Na^+ and Mg^{++} cations) for all binders (OPC, PPC, OPC+20FA, OPC+30FA) and steel type (Tempcore TMT and Thermex TMT).

- The corrosion current density of steel reinforcement in concrete increased with an increase in NaCl, Na_2SO_4 and $MgSO_4$ dosage in all types of binder and for both types of steel reinforcement.
- The steel reinforcement in concrete showed higher corrosion current density in NaCl plus $MgSO_4$ environment as compared to that in NaCl plus Na_2SO_4 environment for all types of binder and steel reinforcement. Thus in the presence of chloride ions, the sulfate ions associated with Mg^{++} cation has more deleterious effect than that associated with Na^+ cation on corrosion performance of steel reinforcement.
- The corrosion current density of both types of steel in blended cement (PPC, OPC+20FA and OPC+30FA) concretes were lower than those in OPC concrete in the conjoint presence of sodium chloride plus sodium sulfate, whereas in the conjoint presence of sodium chloride plus magnesium sulfate, the steel reinforcement in OPC concrete showed lower corrosion current density as compared to that in blended cement concrete.
- Between steel type, Tempcore TMT steel exhibited lower corrosion density as compared to Thermex TMT steel in all the binders and in the conjoint presence of NaCl plus Na_2SO_4 and NaCl plus $MgSO_4$.
- Overall, OPC+30FA and Tempcore TMT steel showed best performance against the combined effect of sodium chloride plus sodium sulfate, whereas OPC and Tempcore TMT steel showed best performance against the combined effect of sodium chloride plus magnesium sulfate in terms of reduced corrosion current density as compared to other types of binder and steel reinforcement.

8.7 CONCLUSIONS FROM PERFORMANCE OF CONCRETE EXPOSED TO SULFATE AND CONJOINT CHLORIDE-SULFATE ENVIRONMENT

- The visual examination indicated that, concrete exposed to Na_2SO_4 solution showed deterioration at the edges of the cube specimens, whereas that exposed to $MgSO_4$ solution showed deterioration in the form of peeling of the surface skin on all the faces of the cube specimens with the aggregates exposed.
- The degree of surface deterioration was mitigated in the concrete exposed to NaCl + Na_2SO_4 and NaCl + $MgSO_4$ solutions as compared to that exposed to only

sulfate solutions (Na_2SO_4 and $MgSO_4$), as no significant deterioration was observed on the surface of cube specimens exposed to composite solutions.

- The effect of sulfate attack in terms of weight loss was more prominent in sulfate and composite chloride-sulfate solutions when the sulfate ion is associated with Mg^{++} cation as compared to that associated with Na^{+} cation.
- Blended cement (PPC, OPC+20FA and OPC+30FA) concretes exhibited better resistance to sodium sulfate attack (when exposed to Na_2SO_4 and $NaCl + Na_2SO_4$ solutions), whereas OPC concrete showed better resistance to magnesium sulfate attack (when exposed to $MgSO_4$ and $NaCl + MgSO_4$ solutions) in terms of lower reduction in compressive strength.
- Decrease in w/b ratio enhanced the reduction in compressive strength of concrete when exposed to sulfate and composite chloride-sulfate solutions.
- On comparison between the exposure conditions, the reduction in compressive strength of concrete was higher under full immersion with alternate wetting and drying cycles as compared to that under continuous full immersion condition.
- In sulfate and composite chloride-sulfate exposure solutions, the reduction in compressive strength of concrete increased with an increase in concentration of Na_2SO_4 and $MgSO_4$.
- The reduction in compressive strength of concrete decreased with an increase in NaCl concentration in the composite chloride-sulfate solutions in all the concrete mixes, which indicates that increase in NaCl concentration retards the deterioration of concrete due to sulfate attack when exposed to $NaCl + Na_2SO_4$ and $NaCl + MgSO_4$ environment.
- The variations in compressive strength of concrete attributed to the formation of compounds such as gypsum, ettringite, calcium chloroaluminate, magnesium hydroxide and M-S-H in the presence of sulfate and composite chloride-sulfate ions are corroborated from the results of XRD and FESEM analyses.
- While comparing the exposure solutions, the reduction in compressive strength of concrete decreased in the order: $MgSO_4$ > Na_2SO_4 > NaCl plus $MgSO_4$ > NaCl plus Na_2SO_4. Thus, when chloride ions are present concomitantly with sulfate ions in the surrounding environment of concrete, it mitigates the sulfate attack on concrete.

8.8 SUGGESTIONS FOR FURTHER WORK

Following are the suggestions for further study:

- The present study can be carried out by using ground granulated blast furnace slag (GGBS) and silica fume in the preparation of concrete at varying water-binder (w/b) ratios and evaluating their effect on properties of concrete against chloride and sulfate environment.
- The present investigation can also be extended to study the role of chloride and composite chloride-sulfate ions on performance of high strength concrete and self-compacting concrete.
- The present study can also be extended by incorporating different corrosion inhibitors in concrete and evaluating their performance against steel reinforcement corrosion against chloride and composite chloride-sulfate exposure conditions.

REFERENCES

[1] Soutsos, M. (2010). *Introduction*, In: Soutsos, M. *Concrete durability: A practical guide to the design of durable concrete structures*, Thomas Telford Ltd., 40 Marsh Wall, London, 1–13.

[2] Ramachandran, V.S. (2006). *Concrete science*, In: Ramachandran, V.S., and Beaudoin, J. J. *Handbook of analytical techniques in concrete science and technology: Principles, techniques and applications*, William Andrew/Noyes Publications, Norwich, NY 13815, 1–62.

[3] Khan, A. R. (2009). "Performance of different types of Pakistani cements exposed to aggressive environments." *SBEIDCO-1st International Conference on Sustainable Built Environment Infrastructures in Developing Countries*, ENSET Oran, Alegria, 153–158.

[4] Ukrainczyk, N., Ukrainczyk, M., Sipusic, J., Matusinovic, T. (2006). "Conference on Materials, Processes, Friction and Wear." *MATRIB. 06*, Vela Luka, 243–249.

[5] Rasheeduzzafar. (1992). "Influence of cement composition on concrete durability." *ACI Mater. J.*, 574–586.

[6] Neville, A.M., and Brooks, J.J. (2004). *Concrete Technology*, Pearson Education, Fourth Indian Reprint, Delhi.

[7] Mehta, P.K., and Monteiro, P.J.M. (2006). *Concrete: Microstructure, Properties, and Materials*, 3rd Ed., Tata McGraw-Hill publication, New Delhi.

[8] ASTM. (2010). "Examination of Hardened Concrete Using Scanning Electron Microscopy." *ASTM C1723*, West Conshohocken, PA.

[9] Gu, G.P., Beaudoin, J.J., Ramachandran, V.S. (2006). *Techniques for corrosion investigation in reinforced concrete*, In: Ramachandran, V.S., and Beaudoin, J.J. *Handbook of analytical techniques in concrete science and technology: Principles, techniques and applications*, William Andrew/Noyes Publications, Norwich, NY 13815, 441–501.

[10] Regourd, M. (1990). "Physico-chemical studies of cement pastes, mortars, and concretes exposed to sea water." *ACI SP*, 65, 63–82.

[11] Wee, T.H., Suryavanshi, A.K., Wong, S.F., and Rahman, A.K.M.A. (2000). "Sulfate resistance of concrete containing mineral admixtures." *ACI Mater. J.*, 97, 536–549.

[12] Lee, S.K. (2012). "Current State of Bridge deterioration in the U.S.–part 1." *NACE International*, 51, 62–67.

[13] Lee, S.K. (2012). "Current State of Bridge deterioration in the U.S.–part 2." *NACE International*, 51, 40–45.

[14] Broomfield, J. P., Davies, K., and Hladky, K. (2002). "The use of permanent corrosion monitoring in new and existing reinforced concrete structures." *Cem. Concr. Compos.*, 24, 27–34.

[15] Andrade, C. (1988). *Monitoring techniques*, In: Schiessl, P. *Corrosion of steel in concrete*, Report of the Technical Committee 60-CSC RILEM, London, New York, Chapman and Hall, 79–95.

[16] American Concrete Institute (ACI). (1985). "Corrosion of metals in concrete." *ACI Committee Report*, ACI 222R-85. Detroit.

[17] Broomfield, J. (2010). *Deterioration mechanisms – chemical*, In: Soutsos, M. *Concrete durability: A practical guide to the design of durable concrete structures*, Thomas Telford Ltd., 40 Marsh Wall, London, 48–107.

[18] Bertolini, L., Elsener, B., Pedeferri, P., Radaelli, E., and Polder, R. (2013). *Corrosion of steel in concrete: Prevention, diagnosis, repair*, 2nd Ed., WILEY-VCH Verlag GmbH & Co. KGaA, Weinheim.

[19] Al-Amoudi, O.S.B., and Maslehuddin, M. (1993). "The effect of chloride and sulfate ions on reinforcement corrosion." *Cem. Concr. Res.*, 23, 139–146.

[20] Revie, R.W., and Uhlig, H.H. (2008). *Corrosion and corrosion control: An introduction to corrosion science and engineering*, 4th Ed., John Wiley and Sons Publication, Hoboken New Jersey.

[21] Hansson, C.M., Poursaee, A., and Jaffer, S.J. (2007). "Corrosion of reinforcing bars in concrete." *R&D serial no. 3013, Portland cement association*, Skokie, Illinois, USA.

[22] Verbeck, G.J. (1975). "Mechanism of corrosion of steel in concrete." *ACI SP.*, 49, 21–38.

[23] Ahmad, S. (2003). "Reinforcement corrosion in concrete structures , its monitoring and service life prediction — a review." *Cem. Concr. Compos.*, 25, 459–471.

[24] Bungey, J.H., and Millard, S.G. (1996). *Testing of concrete in structures*, 3rd Ed., Chapman and Hall, Bishopbriggs, Glasgow G64 2NZ.

[25] Jones, D.A. (1996). *Principles and prevention of corrosion*, 2nd Ed., Prentice-Hall, USA.

[26] Page, C.L. (1988). *Basic principles of corrosion*, In: Schiessl P. *Corrosion of steel in concrete*, Report of the Technical Committee 60-CSC RILEM, London New York, Chapman and Hall, 3–21

[27] McCafferty, E. (2010). *Introduction to corrosion science*, Springer, New York, Dordrecht Heidelberg London.

[28] Gouda, V. K., and Halaka, W. Y. (1970). "Corrosion and corrosion inhibition of reinforced steel, I. Immersed in alkaline solutions." *Br. Corros. J.*, 5, 204–208.

[29] Kapat, C., Pradhan, B., and Bhattacharjee, B. (2006). "Potentiostatic study of reinforcing steel in chloride contaminated concrete powder solution extracts." *Corros. Sci.*, 48, 1757–1769.

[30] Somuah, S.K., Boah, J.K., Leblanc, P., Al-Tayyib, A.H.J., and Al-Mana, A.I. (1991). "Effect of sulfate and carbonate ions on reinforcing steel corrosion as evaluated using AC impedance spectroscopy." *ACI Mater. J.*, 88, 49–55.

[31] Saleem, M., Shameem, M., Hussain, S. E., and Maslehuddin, M. (1996). "Effect of moisture, chloride and sulphate contamination on the electrical resistivity Portland cement concrete." *Constr. Build. Mater.*, 10, 209–214.

[32] Pradhan, B., and Bhattacharjee, B. (2007). "Role of steel and cement type on chloride-induced corrosion in concrete." *ACI Mater. J.*, 104, 612–619.

[33] Pradhan, B., and Bhattacharjee, B. (2009). "Performance evaluation of rebar in chloride contaminated concrete by corrosion rate." *Constr. Build. Mater.*, 23, 2346–2356.

[34] Treadaway, K. (1988). *Corrosion period*, In: Schiessl P. *Corrosion of steel in concrete*, Report of the Technical Committee 60-CSC RILEM. London New York, Chapman and Hall, 56–69.

[35] Roberts, M. H. (1962). "Effect of calcium chloride on the durability of pre-tensioned wire in prestressed concrete." *Mag. Concr. Res.*, 14, 143–154.

[36] Mehta, P.K. (1977). *Effect of cement composition on corrosion of reinforcing steel in concrete*, In: Tonini D.E., and Dean S.W. *Chloride corrosion of steel in concrete*, ASTM STP 629,12–19.

[37] Diamond, S. (1986). "Chloride concentrations in concrete pore solutions resulting from calcium and sodium chloride admixtures." *Cem. Concr. Agg.*, 8, 97–102.

[38] Pavlik, V. (2000). "Water extraction of chloride, hydroxide and other ions from hardened cement pastes." *Cem. Concr. Res.*, 30, 895–906.

[39] Pradhan, B., and Bhattacharjee, B. (2009). "Half-cell potential as an indicator of chloride-induced rebar corrosion initiation in RC." *ASCE J. Mater. Civ. Eng.*, 21, 543–552.

[40] Bertolini, L. (2008). Steel corrosion and service life of reinforced concrete structures. *Struct. Infrastruct. Eng.*, 4, 123-137.

[41] Lothenbach, B., Bary, B., Bescop, P.L., Schmidt, T., and Letterrier, N. (2010). "Sulphate ingress in Portland cement." *Cem. Concr. Res.*, 1, 211–1225.

[42] Al-Amoudi, O. S. B., (1998). "Sulfate attack and reinforcement corrosion in plain and blended cements exposed to sulfate environments." *Constr. Build. Mater.*, 33, 53–61.

[43] Al-amoudi, O. S. B. (2002). "Attack on plain and blended cements exposed to aggressive sulfate environments." *Cem. Concr. Compos.*, 24, 305–316.

[44] Hossain, K.M.A. (2009). "Resistance of scoria-based blended cement concrete against deterioration and corrosion in mixed sulfate environment." *ASCE J. Mater. Civ. Eng.*, 21, 299–308.

[45] Cohen, M. D., and Bentur, A. (1988). "Durability of Portland cement-silica fume pastes in magnesium sulfate and sodium sulfate solutions." *ACI Mater. J.*, 85, 148–157.

[46] Rasheeduzzafar, Al-Amoudi, O.S.B., Abduljauwad, S. N., and Maslehuddin, M. (1994). "Magnesium-sodium sulfate attack in plain and blended cements." *ASCE J. Mater. Civ. Eng.*, 6, 201–222.

[47] De Weerdt, K., Justnes, H., and Geiker, M. R. (2014). "Changes in the phase assemblage of concrete exposed to sea water". *Cem. Concr. Compos.*, 47, 53–63.

[48] Hooton, R. D., Thomas, M. D., and Ramlochan, T. (2010). "Use of pore solution analysis in design for concrete durability." *Adv. Cem. Res.*, 22, 203–210.

[49] Vollpracht, A., Lothenbach, B., Snellings, R., and Haufe, J. (2016). "The pore solution of blended cements: a review." *Mater. Struct.* 49, 3341–3367.

[50] Gjorv, O. E., and Vennesland, O. (1976). "Sea Salts and Alkalinity of Concrete." *ACI J.*, 73, 512–516.

[51] Yonezawa, T., Ashworth, V., and Procter, R. P. M. (1988). "Pore Solution Composition and Chloride Effects on the Corrosion of Steel in Concrete." *Corrosion.*, 44, 489–499.

[52] Andersson, K., Allard, B., Bengtsson, M., and Magnusson, B. (1989). "Chemical composition of cement pore solutions". *Cem. Concr. Res.*, 19, 327–332.

[53] Goni, S., and Andrade, C. (1990). "Synthetic concrete pore solution chemistry and rebar corrosion rate in the presence of chlorides." *Cem. Concr. Res.*, 20, 525–539.

[54] Dehwah, H. A. F., Maslehuddin, M., and Austin, S. A. (2003). "Effect of cement alkalinity on pore solution chemistry and chloride-induced reinforcement corrosion." *ACI Mater. J.*, 99, 227–233.

[55] Dehwah, H. A. F. (2003). "Effect of sulfate ions and associated cation type on the pore solution chemistry in chloride-contaminated plain and blended cements." *Cem. Concr. Compos.*, 25, 513–525.

[56] Henriksen, J.F. (2007). "The corrosion and protection of steel in saturated $Ca(OH)_2$ contaminated with NaCl." *Corros. Sci.*, 20, 1241–1249.

[57] Al-Tayyib, A.J., Somuah, S.K., Boah, J.K., Leblanc, P., and Al-Manna, A.I. (1988). "Laboratory study on the effect of sulfate ions on rebar corrosion." *Cem. Concr. Res.*, 18, 774–782.

[58] Pistorius, P.C., and Burstein, G.T. (1992). "Growth of corrosion pits on stainless steel in chloride solution containing dilute sulphate." *Corros. Sci.*, 33, 1885–1897.

[59] Pistorius, P.C., and Burstein, G.T. (1994). "Aspects of the effects of electrolyte composition on the occurance of metastable pitting on stainless steel." *Corros. Sci.*, 36, 525–538.

[60] Bertolini, L., Bolzoni, F., Pastore, T., and Pedeferri, P. (1996). "Behaviour of stainless steel in simulated concrete pore solution." *Br. Corros. J.*, 31, 218–222.

[61] Saremi, M., and Mahallati, E. (2002). "A study on chloride-induced depassivation of mild steel in simulated concrete pore solution." *Cem. Concr. Res.*, 32, 1915–1921.

[62] Moreno, M., Morris, W., Alvarez, M.G., and Duffo, G.S. (2004). "Corrosion of reinforcing steel in simulated concrete pore solutions: Effect of carbonation and chloride content." *Corros. Sci.*, 46, 2681–2699.

[63] Mammoliti, L., and Hansson, C.M. (2005). "Influence of cation on corrosion behaviour of reinforcing steel in high-pH sulfate solutions." *ACI Mater. J.*, 102, 279–285.

[64] Pradhan, B., and Bhattacharjee, B. (2007). "Corrosion zones of rebar in chloride contaminated concrete through potentiostatic study in concrete powder solution extracts." *Corros. Sci.*, 49, 3935–3952.

[65] Aal, E. E. A. El, Wanees, S. A. El, Diab, A., and Haleem, S. M. A. El. (2009). "Environmental factors affecting the corrosion behavior of reinforcing steel III. Measurement of pitting corrosion currents of steel in Ca $(OH)_2$ solutions under natural corrosion conditions." *Corros. Sci.*, 51, 1611–1618.

[66] Zhang, F., Pan, J., and Lin, C. (2009). "Localized corrosion behaviour of reinforcement steel in simulated concrete pore solution." *Corros. Sci.*, 51, 2130–2138.

[67] Ghods, P., Isgor, O. B., McRae, G., and Miller, T. (2009). "The effect of concrete pore solution composition on the quality of passive oxide films on black steel reinforcement." *Cem. Concr. Compos.*, 31, 2–11.

[68] Chen, W., Du, R. G., Ye, C. Q., Zhu, Y. F., and Lin, C. J. (2010). "Study on the corrosion behavior of reinforcing steel in simulated concrete pore solutions using in situ Raman spectroscopy assisted by electrochemical techniques." *Electrochim. Acta.*, 55, 5677–5682.

[69] Haleem, S. M. A. El., Abd El Wanees, S., Abd El Aal, E. E., and Diab, A. (2010). "Environmental factors affecting the corrosion behavior of reinforcing steel II. Role of some anions in the initiation and inhibition of pitting corrosion of steel in Ca(OH)2 solutions." *Corros. Sci.*, 52, 292–302.

[70] Moser, R. D., Singh, P. M., Kahn, L. F., and Kurtis, K. E. (2012). "Chloride-induced corrosion resistance of high-strength stainless steels in simulated alkaline and carbonated concrete pore solutions." *Corros. Sci.*, 57, 241–253.

[71] Alhozaimy, A., Hussain, R. R., Al-Negheimish, A., Al-Zaid, R., and Singh, D. D. N. (2014). "Effect of simulated concrete pore solution chemistry, chloride ions, and temperature on passive layer formed on steel reinforcement." *ACI Mater. J.*, 111, 411–422.

[72] Tang, Y., Zuo, Y., Wang, J., Zhao, X., Niu, B., and Lin, B. (2014). "The metastable pitting potential and its relation to the pitting potential for four materials in chloride solutions." *Corros. Sci.*, 80, 111–119.

[73] Padilla, V., and Alfantazi, A. (2014). "Corrosion film breakdown of galvanized steel in sulphate-chloride solutions." *Constr. Build. Mater.*, 66, 447–457.

[74] Zhang, Y., and Poursaee, A. (2015). "Passivation and corrosion behavior of carbon steel in simulated concrete pore solution under tensile and compressive stresses." *ASCE J. Mater. Civ. Eng.*, 27, 1–9.

[75] Liu, R., Jiang, L., Xu, J., Xiong, C., and Song, Z. (2014). "Influence of carbonation on chloride-induced reinforcement corrosion in simulated concrete pore solutions." *Constr. Build. Mater.*, 56, 16–20.

[76] Liu, G., Zhang, Y., Ni, Z., and Huang, R. (2016). "Corrosion behavior of steel submitted to chloride and sulphate ions in simulated concrete pore solution." *Constr. Build. Mater.*, 115, 1–5.

[77] Scott, A., and Alexander, M. G. (2016). "Effect of supplementary cementitious materials (binder type) on the pore solution chemistry and the corrosion of steel in alkaline environments." *Cem. Concr. Res.*, 89, 45–55.

[78] Cheng, T.P., Lee, J.T., Tsai, W.T. (1990). "Corrosion of reinforcements in artificial sea water and concentrated sulfate solution." *Cem. Concr. Res.*, 20, 243–252.

[79] Al-Tayyib, A.J., and Khan, M. S. (1991). 'Effect of sulfate ions on the corrosion of rebars embedded in concrete'. *Cem. Concr. Compos.*, 13, 123–127.

[80] Al-Amoudi, O. S. B., Rasheeduzzafar, Maslehuddin, M., and Al-Mana, A. I. (1993). "Prediction of long-term corrosion resistance of plain and blended cement concretes." *ACI Mater. J.*, 90, 564–570.

[81] Al-Amoudi, O. S. B. (1995). "Performance of 15 reinforced concrete mixtures in magnesium-sodium sulphate environments." *Constr. Build. Mater.*, 9, 149–158.

[82] Asrar, N., Malik, A. U., Ahmad, S., and Mujahid, F. S. (1999). "Corrosion protection performance of microsilica added concretes in NaCl and seawater environments." *Constr. Build. Mater.*, 13, 213–219.

[83] Alonso, C., Andrade, C., Castellote, M., and Castro, P. (2000). "Chloride threshold values to depassivate reinforcing bars embedded in a standardized OPC mortar." *Cem. Concr. Res.*, 30, 1047–1055.

[84] Dehwah, H. A. F. (2002). "Long-term effect of sulfate ions and associated cation type on chloride-induced reinforcement corrosion in Portland cement concretes." *Cem. Concr. Compos.*, 24, 17–25.

[85] Turkmen, I., and Gavgali, M. (2003). "Influence of mineral admixtures on the some properties and corrosion of steel embedded in sodium sulfate solution of concrete." *Mater. Lett.*, 57, 3222–3233.

[86] Sakr, K. (2005). "Effect of cement type on the corrosion of reinforcing steel bars exposed to acidic media using electrochemical techniques." *Cem. Concr. Res.*, 35, 1820–1826.

[87] Maslehuddin, M., Al-Zahrani, M. M., Ibrahim, M., Al-Mehthel, M. H., and Al-Idi, S. H. (2007). "Effect of chloride concentration in soil on reinforcement corrosion." *Constr. Build. Mater.*, 21, 1825–1832.

[88] Pradhan, B. (2014). "Corrosion behavior of steel reinforcement in concrete exposed to composite chloride-sulfate environment." *Constr. Build. Mater.*, 72, 398–410.

[89] Kwon, S., Lee, H., Karthick, S., Saraswathy, V., and Yang, H. (2017). "Long-term corrosion performance of blended cement concrete in the marine environment – A real-time study." *Constr. Build. Mater.*, 154, 349–360.

[90] Harrison. W. H. (1990). "Effect of chloride in mix ingredients on sulphate resistance of concrete." *Mag. Concr. Res.*, 42, 113–126.

[91] Bonen. D. (1993). "A microstructural study of the effect produced by magnesium sulfate on plain and silica fume-bearing Portland cement mortars". *Cem. Concr. Res.*, 23, 541–553.

[92] Akoz. F., Turker, F., Koral, S., and Yuzer, N. (1995). "Effects of Sodium Sulfate Concentration on the Sulfate." *Cem. Concr. Res.*, 25, 1360–1368.

[93] Lee. S. T., Moon, H.Y., and Swamy, R.N. (2005). "Sulfate attack and role of silica fume in resisting strength loss." *Cem. Concr. Compos.*, 27, 65–76.

[94] Zuquan, J., Wei, S., Yunsheng, Z., Jinyang, J., and Jianzhong, L. (2007). "Interaction between sulfate and chloride solution attack of concretes with and without fly ash." *Cem. Concr. Res.*, 37, 1223–1232.

[95] Lee, S.T., Park, D. W., and Ann, K. Y. (2008). "Mitigating effect of chloride ions on sulfate attack of cement mortars with or without silica fume." *Can. J. Civ. Eng.*, 35, 1210–1220.

[96] Aye, T., and Oguchi, C. T. (2011). "Resistance of plain and blended cement mortars exposed to severe sulfate attacks." *Constr. Build. Mater.*, 25, 2988–2996.

[97] Sotiriadis, K., Nikolopoulou, E., and Tsivilis, S. (2012). "Sulfate resistance of limestone cement concrete exposed to combined chloride and sulfate environment at low temperature." *Cem. Concr. Compos.*, 34, 903–910.

[98] Maes, M., and Belie, N. De. (2014). "Resistance of concrete and mortar against combined attack of chloride and sodium sulphate". *Cem. Concr. Compos.*, 53, 59–72.

[99] Chen, Y., Gao, J., Tang, L., and Li, X. (2016). "Resistance of concrete against combined attack of chloride and sulfate under drying – wetting cycles." *Constr. Build. Mater.*, 106, 650–658.

[100] Wang, D., Zhou, X., Meng, Y., and Chen, Z. (2017). "Durability of concrete containing fly ash and silica fume against combined freezing-thawing and sulfate attack." *Constr. Build. Mater.*, 147, 398–406.

[101] BIS (Bureau of Indian Standards). (2004). "Specifications for 53 grade ordinary Portland cement" *IS 12269–1987*, New Delhi, India.

[102] ASTM. (2012). "Standard Specification for Portland Cement." *ASTM C150/C150M-12*, West Conshohocken, PA.

[103] BIS (Bureau of Indian Standards). (2005). "Specifications for Portland pozzolana cement. Part 1: Fly ash based" *IS 1489–1991*, New Delhi, India.

[104] ASTM. (2012). "Standard Specification for Blended Hydraulic Cements." *ASTM C595/C595M-12*, West Conshohocken, PA.

[105] ASTM. (2012). "Standard Specification for Coal Fly Ash and Raw or Calcined Natural Pozzolan for Use in Concrete." *ASTM C618-12*, West Conshohocken, PA.

[106] BIS (Bureau of Indian Standards). (2002). "Methods of test for aggregates for concrete. Part III: Specific gravity, density, voids, absorption and bulking." *IS 2386–1963*, New Delhi, India.

[107] BIS (Bureau of Indian Standards). (2002). "Methods of test for aggregates for concrete. Part I: particle size and shape." *IS 2386–1963*, New Delhi, India.

[108] BIS (Bureau of Indian Standards). (2002). "Specification for coarse and fine aggregates from natural sources for concrete." *IS 383–1970*, New Delhi, India.

[109] ASTM. (2013). "Standard Specification for Concrete Aggregates." *ASTM C33/C33M–13*, West Conshohocken, PA.

[110] BIS (Bureau of Indian Standards). (2004). "Methods of tests for strength of concrete." *IS 516–1959*, New Delhi, India.

[111] APHA (American Public Health Association). (2005). "Standard methods for the examination of water and wastewater." 21st edition, Washington.

[112] Poursaee, A. (2010). "Potentiostatic transient technique, a simple approach to estimate the corrosion current density and Stern-Geary constant of reinforcing steel in concrete." *Cem. Concr. Res.*, 40, 1451–1458.

[113] Otieno, M., Beushausen, H., and Alexander, M. (2016). "Chloride-induced corrosion of steel in cracked concrete - Part I: Experimental studies under accelerated and natural marine environments." *Cem. Concr. Res.*, 79, 373–385.

[114] Rivera-Corral, J. O., Fajardo, G., Arliguie, G., Orozco-Cruz, R., Deby, F., and Valdez, P. (2017). "Corrosion behavior of steel reinforcement bars embedded in concrete exposed to chlorides: Effect of surface finish." *Constr. Build. Mater.*, 147, 815–826.

[115] Shi, J., Ming, J., Sun, W., and Zhang, Y. (2017). "Corrosion performance of reinforcing steel in concrete under simultaneous flexural load and chlorides attack." *Constr. Build. Mater.*, 149, 315–326.

[116] Ben-Yair, M. (1974). "The effect of chlorides on concrete in hot and arid regions." *Cem. Concr. Res.*, 4, 405–416.

[117] Suryavanshi, A. K., Scantleburyb, J. D., and Lyod, S. B. (1998). "Corrosion of reinforcement steel embedded in high water-cement ratio concrete contaminated with chloride." *Cem. Concr. Compos.*, 20, 263–281.

[118] De Weerdt, K., Justnes, H., and Geiker, M. R. (2014). "Changes in the phase assemblage of concrete exposed to sea water". *Cem. Concr. Compos.*, 47, 53–63.

[119] Al-Amoudi O.S.B., Maslehuddin, M., and Saadi, M.M. (1995). "Effect of magnesium sulfate and sodium sulfate on the durability performance of plain and blended cements." *ACI Mater. J.*, 92, 15–23.

[120] Rasheeduzzafar, Hussain, S.E., and Al-Saadoun, S.S. (1992). "Effect of tricalcium aluminate content of cement on chloride binding and corrosion of reinforcing steel in concrete." *ACI Mater. J.*, 89, 3–12.

[121] Loser, R., Lothenbach, B., Leemann, A., and Tuchschmid, M. (2010). "Chloride resistance of concrete and its binding capacity - comparison between experimental results and thermodynamic modeling." *Cem. Concr. Compos.*, 32, 34–42.

[122] Xu, J., Zhang, C., Jiang, L., Tang, L., Gao, G., and Xu, Y. (2013). "Releases of bound chlorides from chloride-admixed plain and blended cement pastes subjected to sulfate attacks." *Constr. Build. Mater.*, 45, 53–59.

[123] Zhu, Q., Jiang, L., Chen, Y., Xu, J., and Mo, L. (2012). "Effect of chloride salt type on chloride binding behavior of concrete." *Constr. Build. Mater.*, 37, 512–517.

[124] Ramezanianpour, A. M., and Hooton, R. D. (2013). "Thaumasite sulfate attack in Portland and Portland-limestone cement mortars exposed to sulfate solution." *Constr. Build. Mater.*, 40, 162–173.

[125] Abdalkader, A. H. M., Lynsdale, C. J., and Cripps, J. C. (2015). "The effect of chloride on cement mortar subjected to sulfate exposure at low temperature." *Constr. Build. Mater.*, 78, 102–111.

[126] Hughes, T.L., Methven, C.M., Jones, T.G.J., Pelham, S.E., Fletcher, P., and Hall, C. (1995). "Determining cement composition by Fourier transform infrared." *Adv. Cement Base Mater.*, 2, 91–104.

[127] Ylmen, R., Jaglid, U., Steenari, B., and Panas, I. (2009). "Early hydration and setting of Portland cement monitored by IR, SEM, and vicat technique." *Cem. Concr. Res.*, 39, 433–439.

[128] Wang, S., Peng, X., Tang, L., Zeng, L., and Lan, C. (2014). "Influence of inorganic admixtures on the 11 Å-tobermorite formation prepared from steel slags: XRD and FTIR analysis." *Constr. Build. Mater.*, 60, 42–47.

[129] Mollah, M.Y.A., Yu, W., Schennach, R., and Cocke, D.L. (2000). "A Fourier transform infrared spectroscopic investigation of the early hydration of Portland cement and the influence of sodium lignosulfonate." *Cem. Concr. Res.*, 30, 267–273.

[130] Silva, D.A., Roman, H.R., and Gleize, P.J.P. (2002). "Evidences of chemical interaction between EVA and hydrating Portland cement." *Cem. Concr. Res.*, 32, 1383–1390.

[131] Al-amoudi, O.S.B. (1995). "Role of chloride ions on expansion and strength reduction in plain and blended cements in sulfate environments." *Constr. Build. Mater.*, 9, 25–33.

[132] Jarrah, N.R., Al-amoudi, O.S.B., Ashiru, O.A., and Al-mana, A. (1995). "Electrochemical behaviour of steel in plain and blended cement concretes in sulphate and/or chloride environments." *Constr. Build. Mater.*, 9, 97–103.

[133] ASTM. (2013). "Standard Test Method for Corrosion Potentials of Uncoated Reinforcing Steel in Concrete." *ASTM C876*, West Conshohocken, PA.

[134] Jiang, L., and Niu, D. (2016). "Study of deterioration of concrete exposed to different types of sulfate solutions under drying-wetting cycles". *Constr. Build. Mater.*, 117, 88–98.

[135] Al-amoudi, O. S. B. (1998). "Sulfate attack and reinforcement corrosion in plain and blended cements exposed to sulfate environments". *Build. Environ.*, 33, 53–61.

[136] Liu, R., Jiang, L., Huang, G., Zhu, Y., Liu, X., Chu, H., and Xiong, C. (2016). "The effect of carbonate and sulfate ions on chloride threshold level of reinforcement corrosion in mortar with/without fly ash." *Constr. Build. Mater.*, 113, 90–95.

[137] Liu, P. C. (1991). "Damage to concrete structures in a marine environment." *Mater. Struct.*, 24, 302–307.

APPENDIX-A

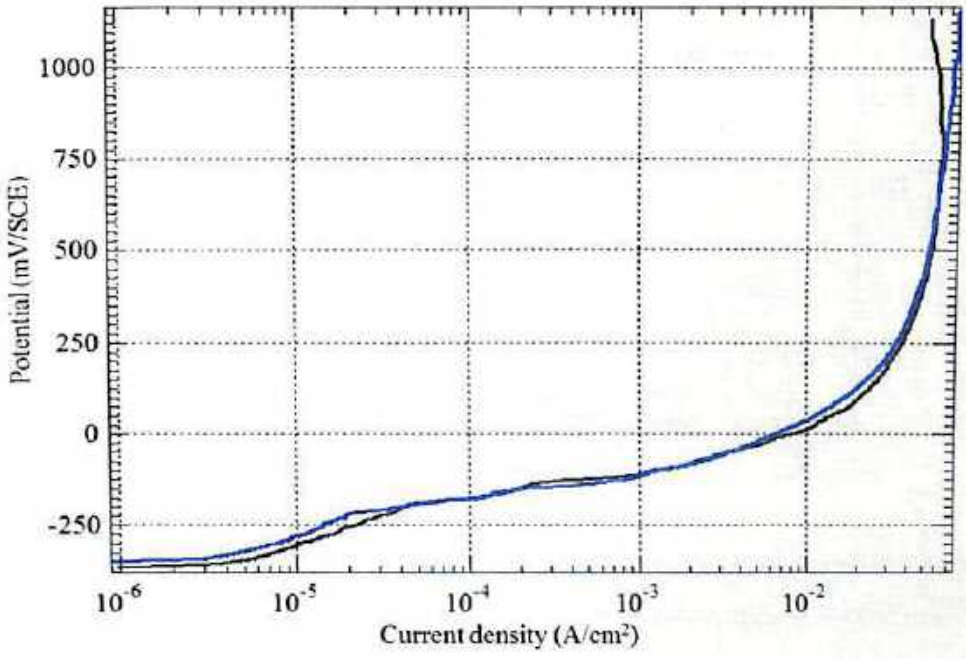

Fig. A1 Anodic polarization curves of Tempcore TMT steel obtained for two replicate steel specimens in ECPS prepared from OPC concrete at w/c ratio of 0.45 and admixed with 3% NaCl by mass of cement

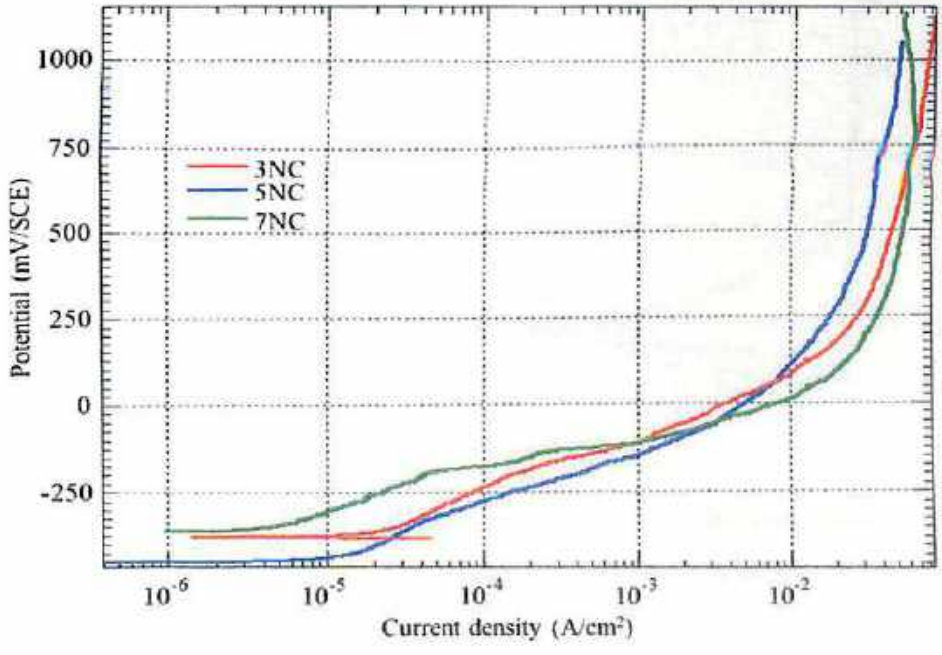

Fig. A2 Anodic polarization curves of Tempcore TMT steel in ECPS prepared from OPC and w/c ratio of 0.45 at varying concentrations of NaCl (NC) admixed by mass of cement

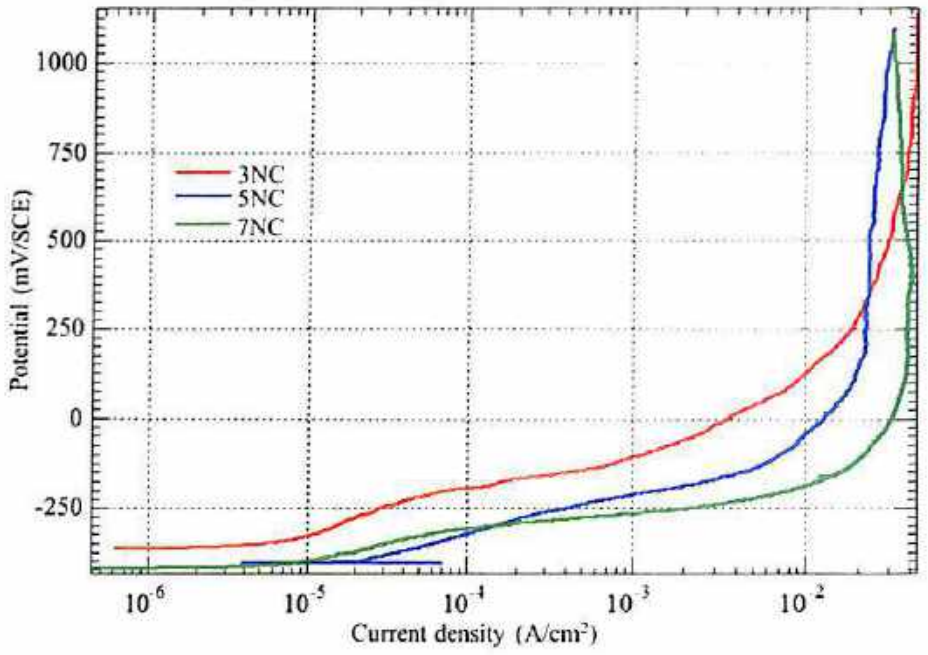

Fig. A3 Anodic polarization curves of Tempcore TMT steel in ECPS prepared from PPC and w/c ratio of 0.45 at varying concentrations of NaCl (NC) admixed by mass of cement

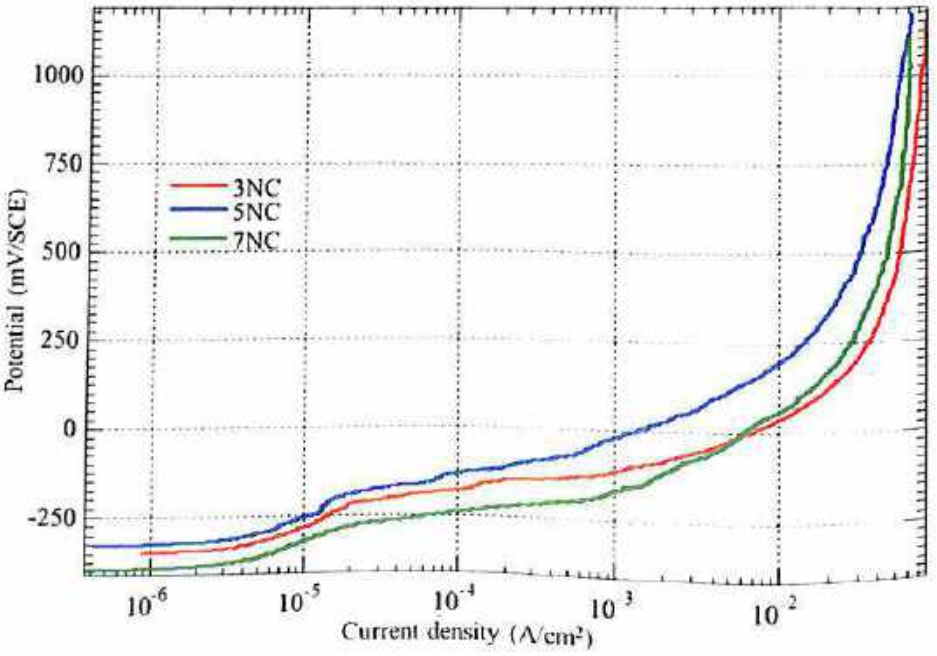

Fig. A4 Anodic polarization curves of Tempcore TMT steel in ECPS prepared from OPC and w/c ratio of 0.5 at varying concentrations of NaCl (NC) admixed by mass of cement

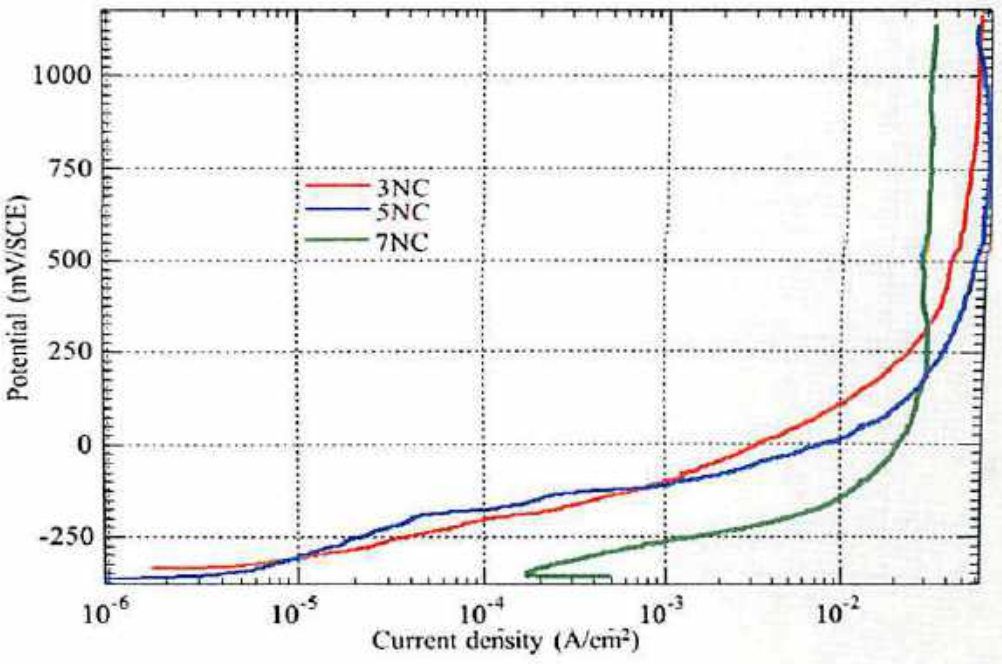

Fig. A5 Anodic polarization curves of Tempcore TMT steel in ECPS prepared from PPC and w/c ratio of 0.5 at varying concentrations of NaCl (NC) admixed by mass of cement

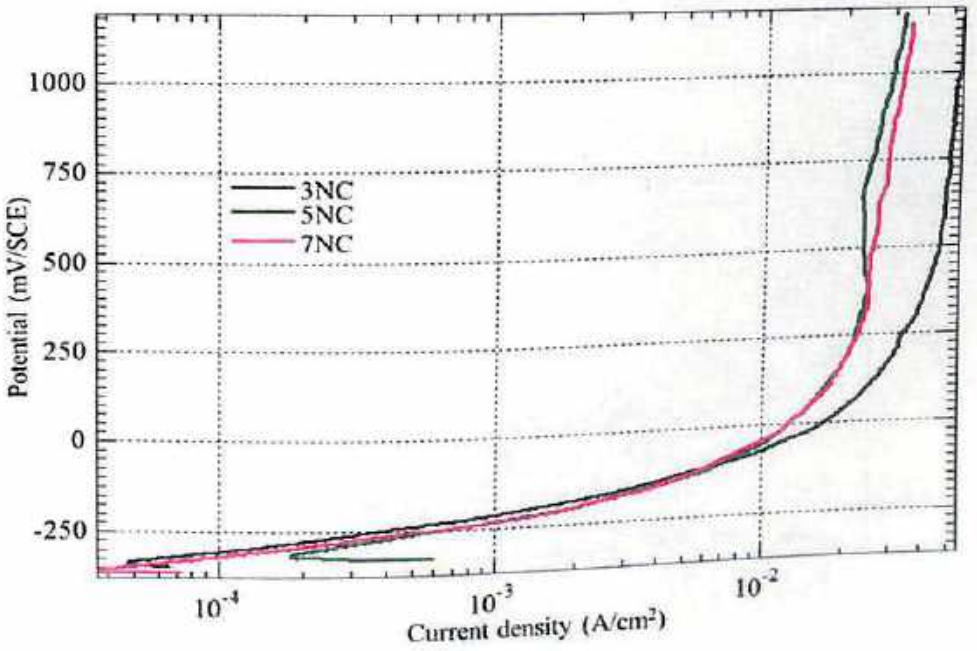

Fig. A6 Anodic polarization curves of Thermex TMT steel in ECPS prepared from OPC and w/c ratio of 0.45 at varying concentrations of NaCl (NC) admixed by mass of cement

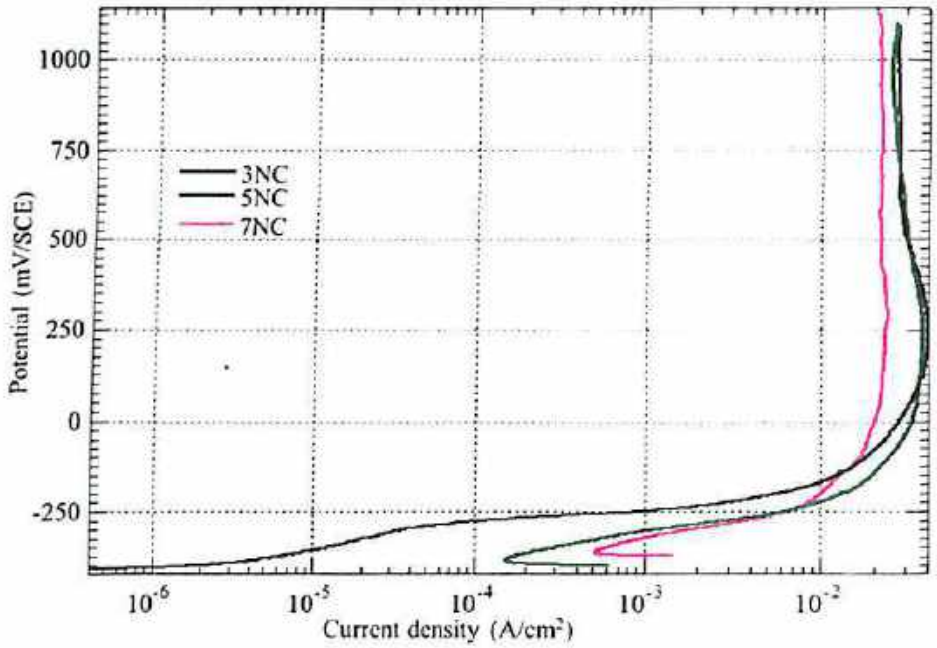

Fig. A7 Anodic polarization curves of Thermex TMT steel in ECPS prepared from PPC and w/c ratio of 0.at varying concentrations of NaCl (NC) admixed by mass of cement

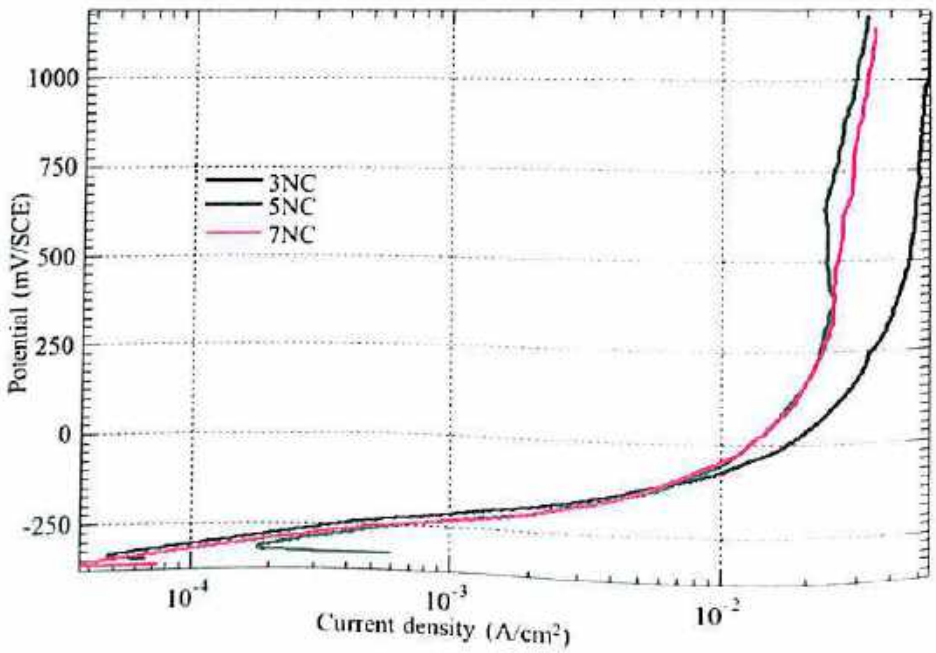

Fig. A8 Anodic polarization curves of Thermex TMT steel in ECPS prepared from OPC and w/c ratio of 0.5 at varying concentrations of NaCl (NC) admixed by mass of cement

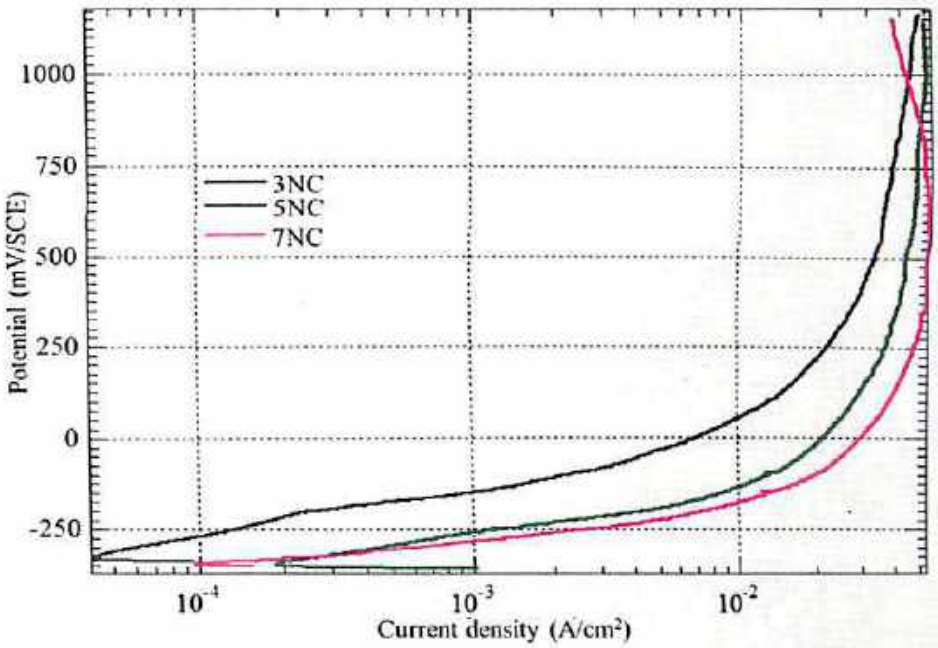

Fig. A9 Anodic polarization curves of Thermex TMT steel in ECPS prepared from PPC and w/c ratio of 0.5 at varying concentrations of NaCl (NC) admixed by mass of cement

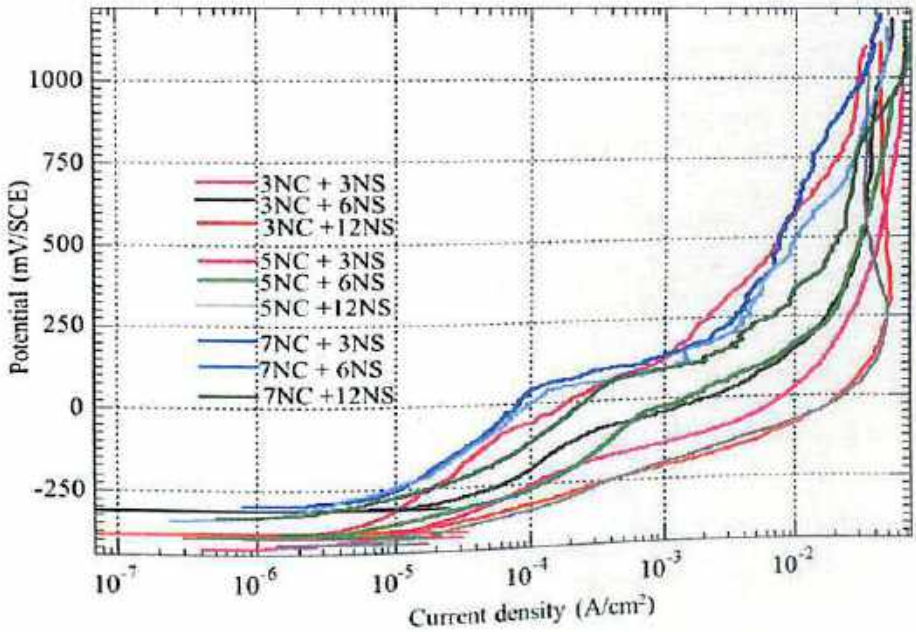

Fig. A10 Anodic polarization curves of Tempcore TMT steel in ECPS prepared from OPC and w/c ratio of 0.45 at varying concentrations of NaCl (NC) and Na_2SO_4 (NS) admixed by mass of cement

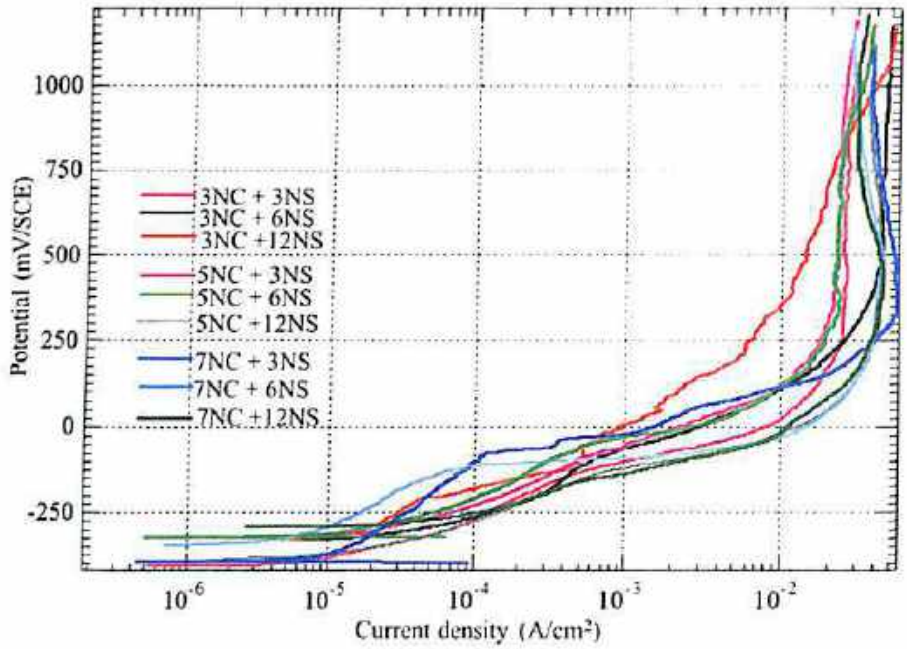

Fig. A11 Anodic polarization curves of Tempcore TMT steel in ECPS prepared from PPC and w/c ratio of 0.45 at varying concentrations of NaCl (NC) and Na_2SO_4 (NS) admixed by mass of cement

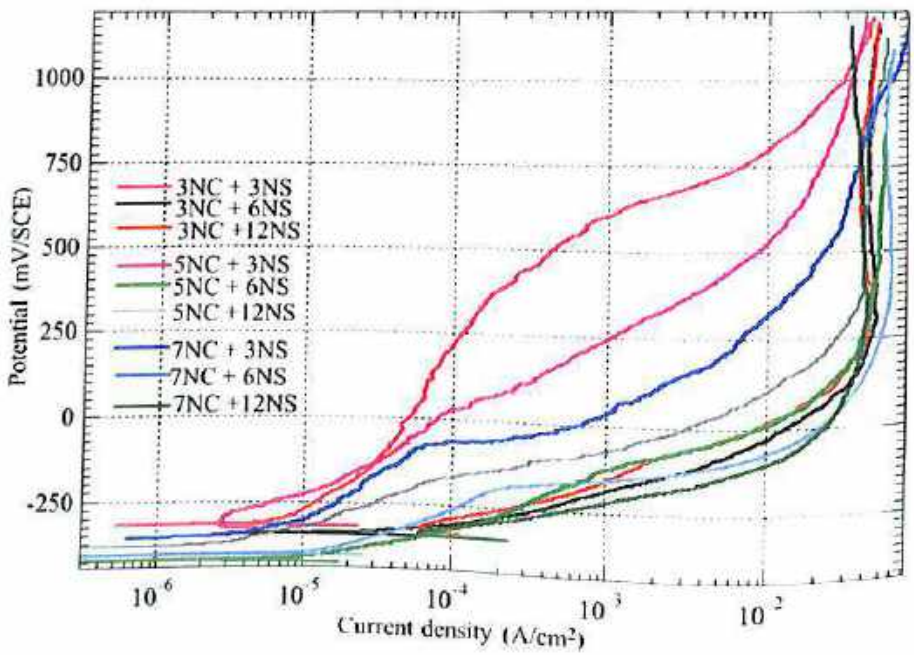

Fig. A12 Anodic polarization curves of Tempcore TMT steel in ECPS prepared OPC and w/c ratio of 0.5 at varying concentrations of NaCl (NC) and Na_2SO_4 (NS) admixed by mass of cement

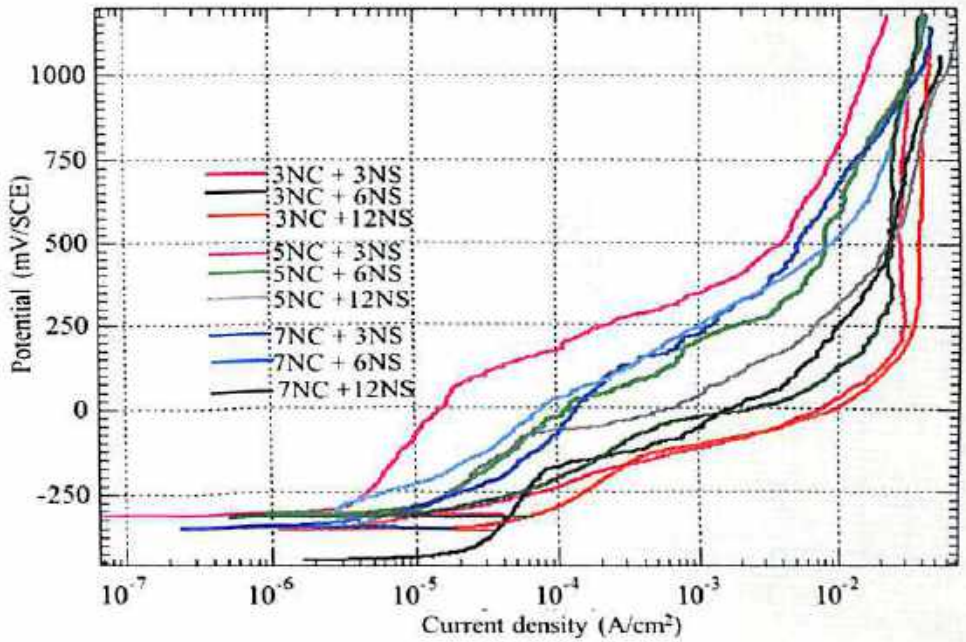

Fig. A13 Anodic polarization curves of Tempcore TMT steel in ECPS prepared from PPC and w/c ratio of 0.5 at varying concentrations of NaCl (NC) and Na_2SO_4 (NS) admixed by mass of cement

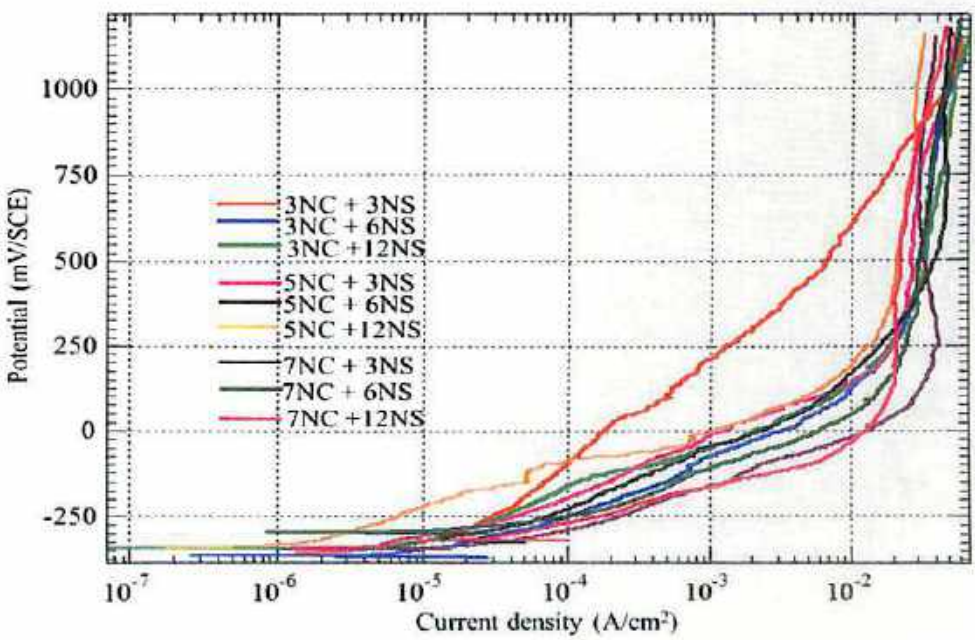

Fig. A14 Anodic polarization curves of Thermex TMT steel in ECPS prepared from OPC and w/c ratio of 0.45 at varying concentrations of NaCl (NC) and Na_2SO_4 (NS) admixed by mass of cement

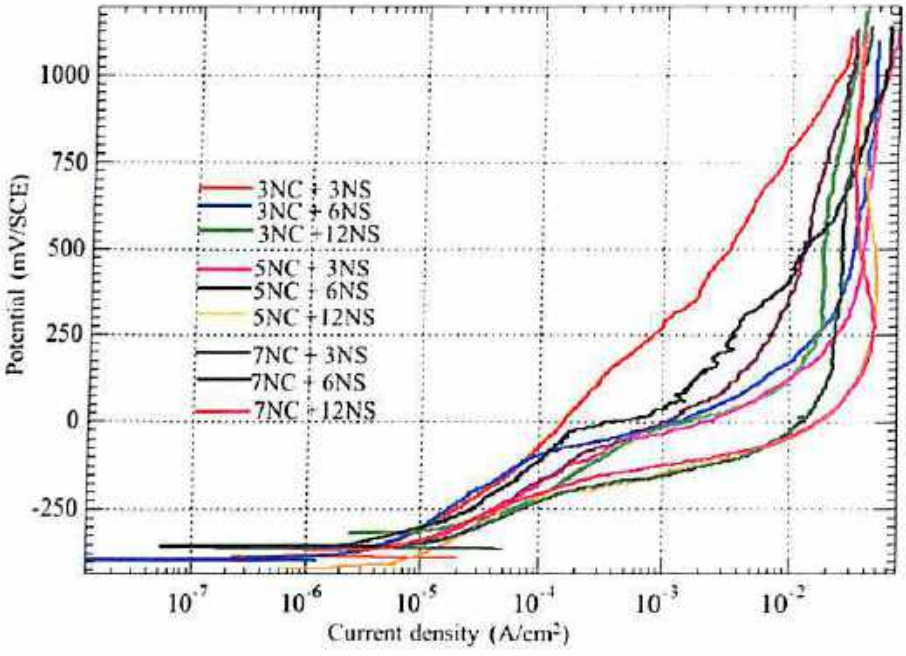

Fig. A15 Anodic polarization curves of Thermex TMT steel in ECPS prepared from PPC and w/c ratio of 0.45 at varying concentrations of NaCl (NC) and Na_2SO_4 (NS) admixed by mass of cement

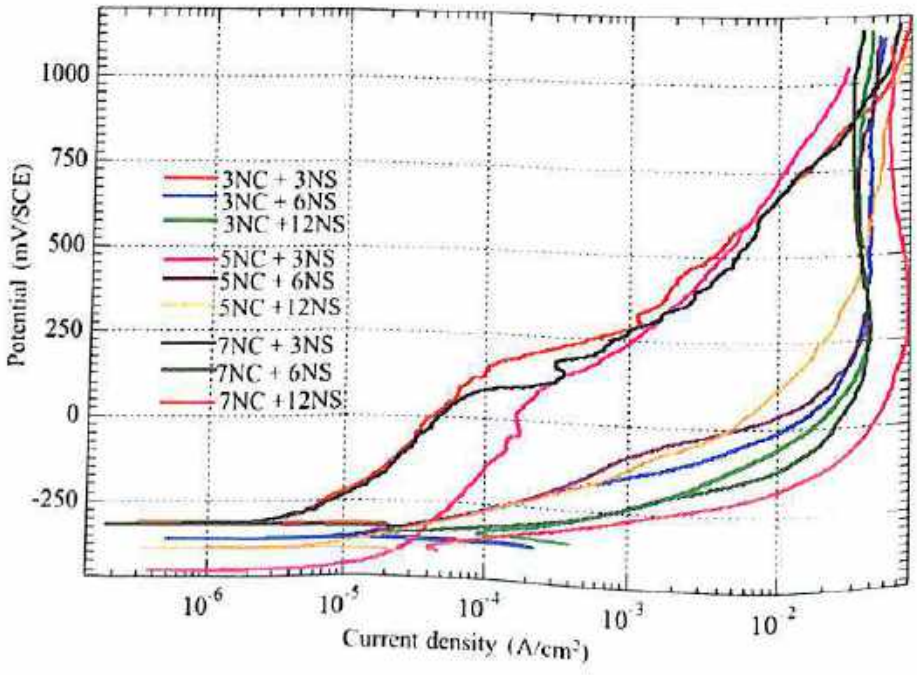

Fig. A16 Anodic polarization curves of Thermex TMT steel in ECPS prepared from OPC and w/c ratio of 0.5 at varying concentrations of NaCl (NC) and Na_2SO_4 (NS) admixed by mass of cement

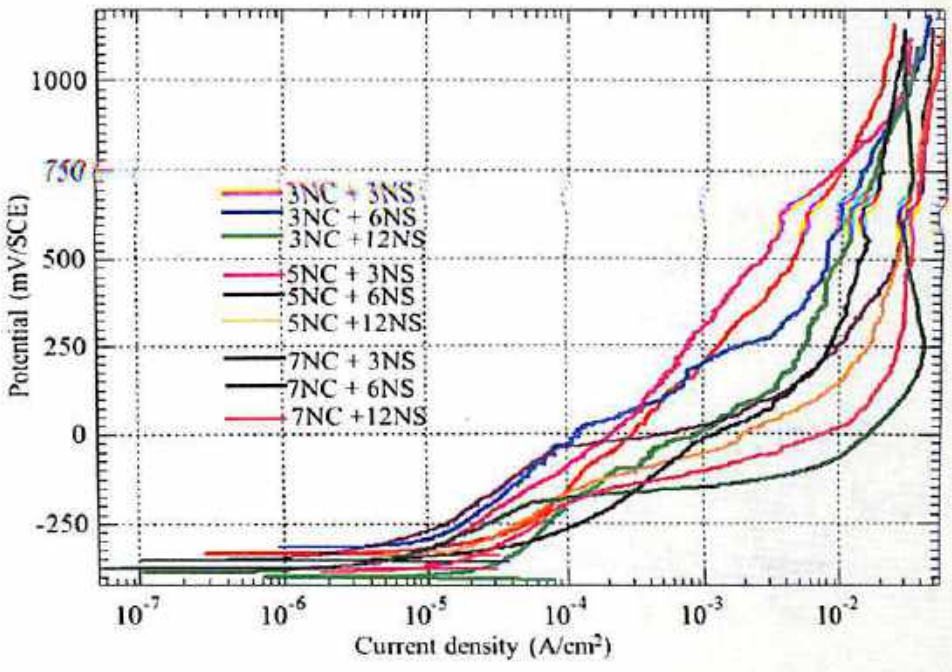

Fig. A17 Anodic polarization curves of Thermex TMT steel in ECPS prepared from PPC and w/c ratio of 0.5 at varying concentrations of NaCl (NC) and Na_2SO_4 (NS) admixed by mass of cement

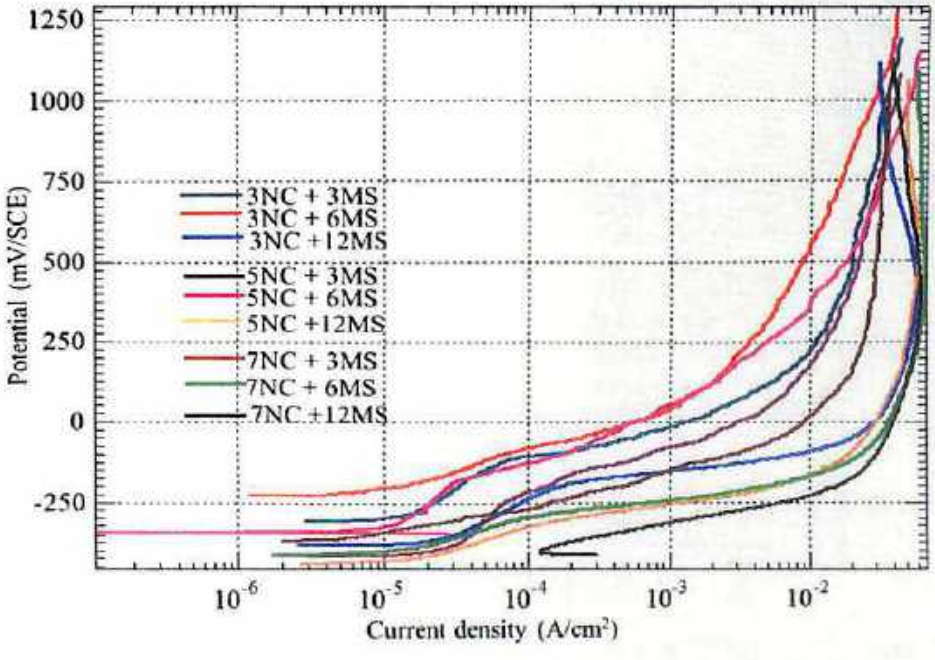

Fig. A18 Anodic polarization curves of Tempcore TMT steel in ECPS prepared from OPC and w/c ratio of 0.45 at varying concentrations of NaCl (NC) and $MgSO_4$ (MS) admixed by mass of cement

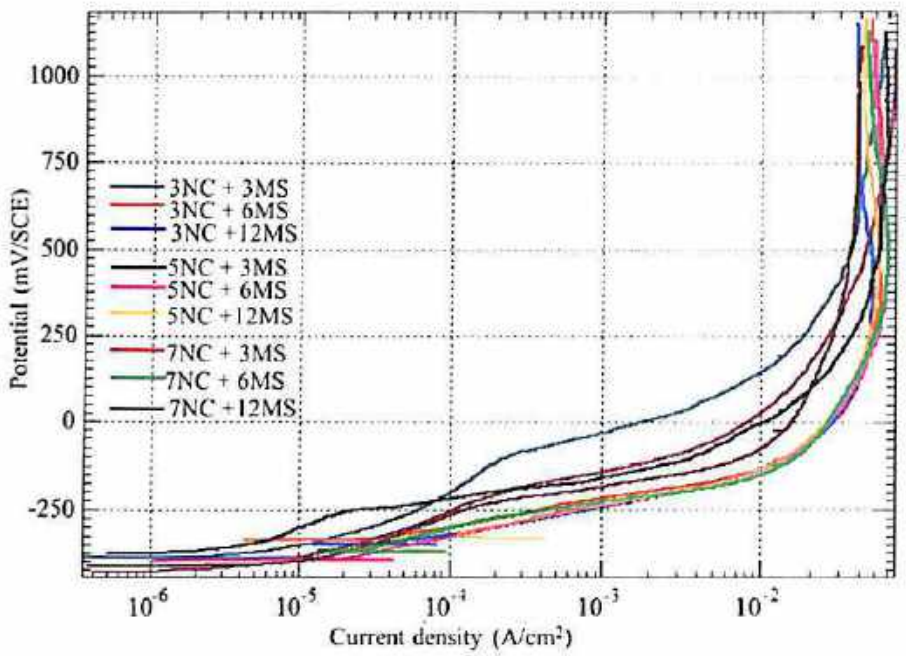

Fig. A19 Anodic polarization curves of Tempcore TMT steel in ECPS prepared from PPC and w/c ratio of 0.45 at varying concentrations of NaCl (NC) and $MgSO_4$ (MS) admixed by mass of cement

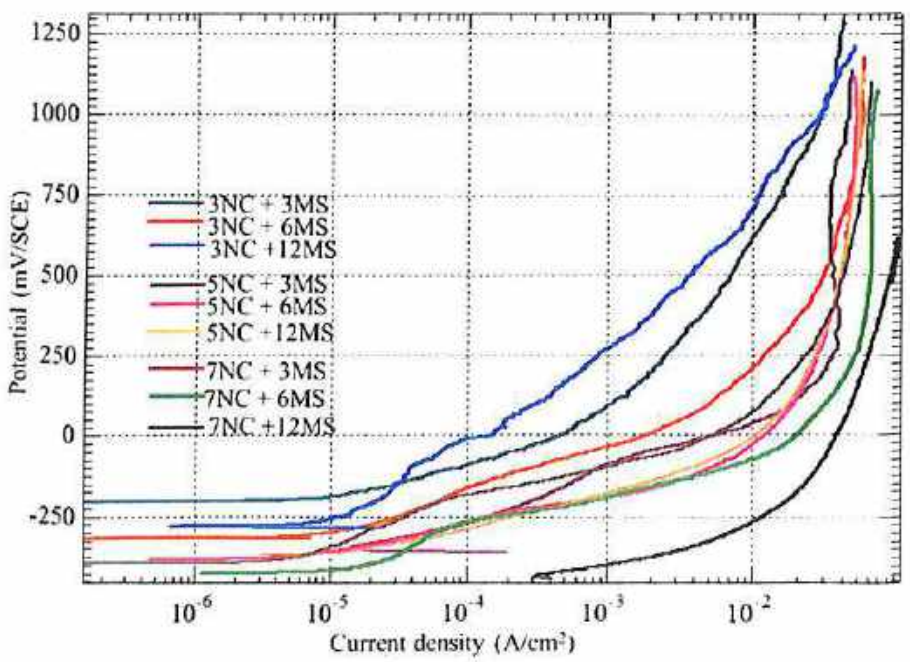

Fig. A20 Anodic polarization curves of Tempcore TMT steel in ECPS prepared from OPC and w/c ratio of 0.5 at varying concentrations of NaCl (NC) and $MgSO_4$ (MS) admixed by mass of cement

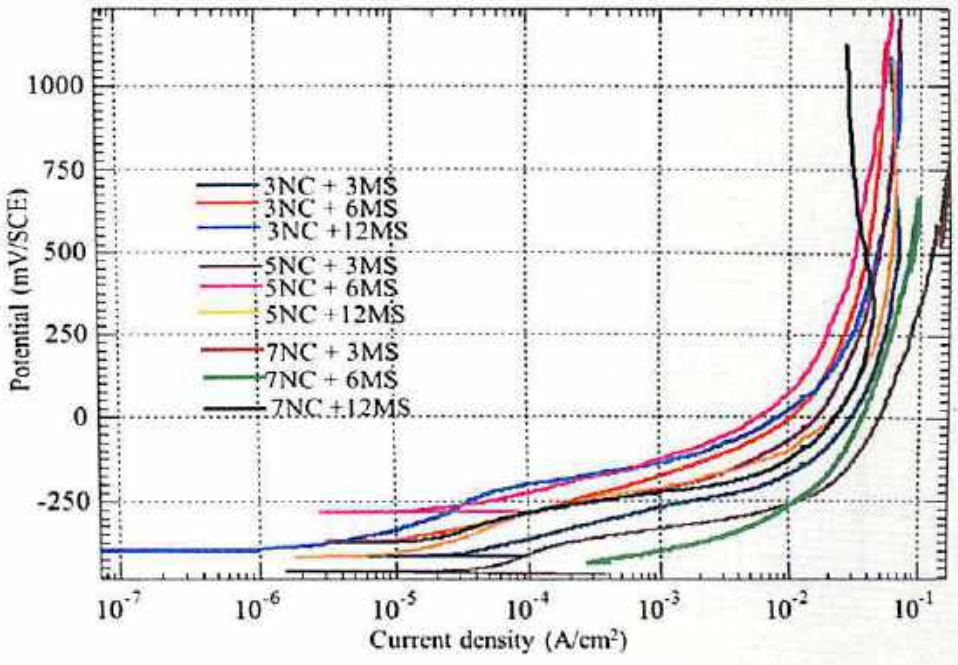

Fig. A21 Anodic polarization curves of Tempcore TMT steel ECPS prepared from PPC and w/c ratio of 0.5 at varying concentrations of NaCl (NC) and $MgSO_4$ (MS) admixed by mass of cement

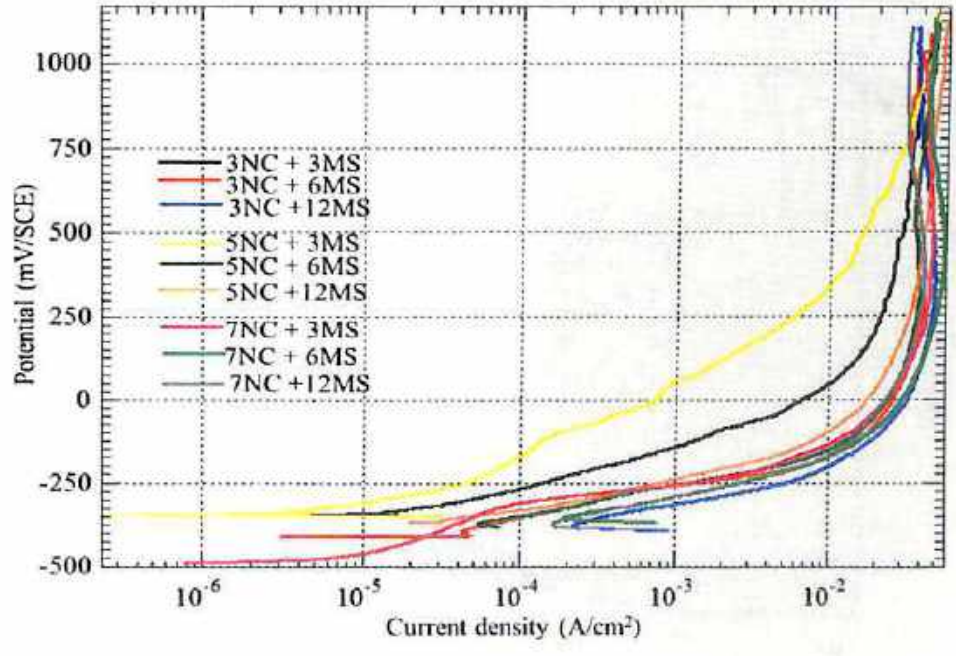

Fig. A22 Anodic polarization curves of Thermex TMT steel in ECPS prepared from OPC and w/c ratio of 0.45 at varying concentrations of NaCl (NC) and $MgSO_4$ (MS) admixed by mass of cement

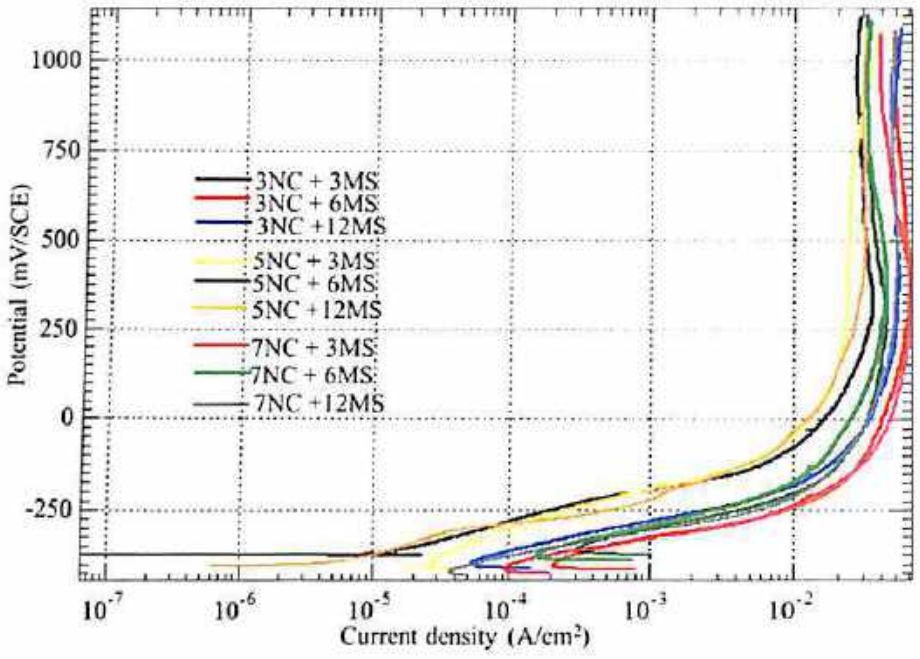

Fig. A23 Anodic polarization curves of Thermex TMT steel in ECPS prepared from PPC and w/c ratio of 0.45 at varying concentrations of NaCl (NC) and $MgSO_4$ (MS) admixed by mass of cement

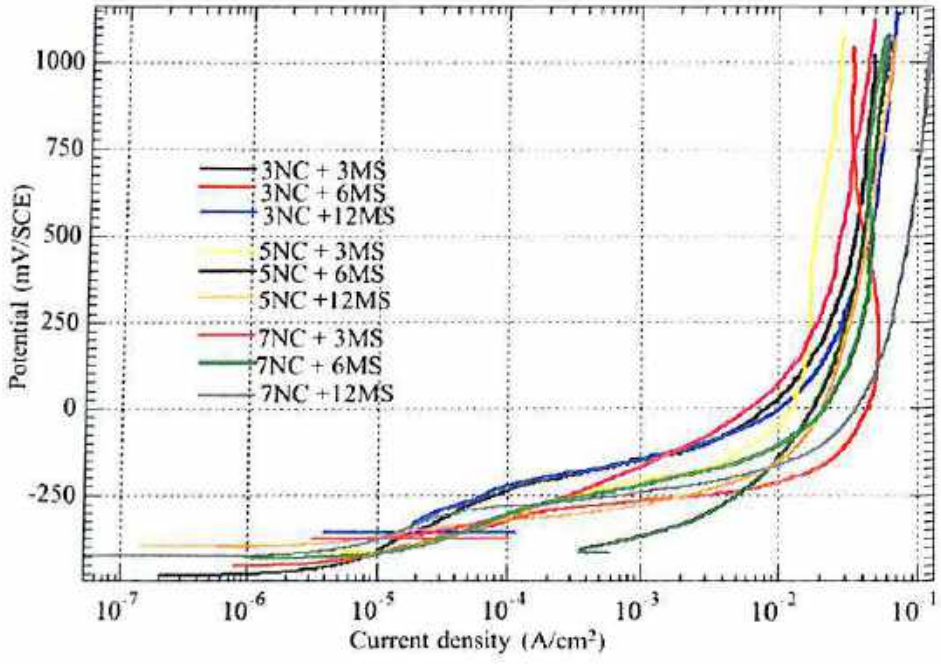

Fig. A24 Anodic polarization curves of Thermex TMT steel in ECPS prepared from OPC and w/c ratio of 0.5 at varying concentrations of NaCl (NC) and $MgSO_4$ (MS) admixed by mass of cement

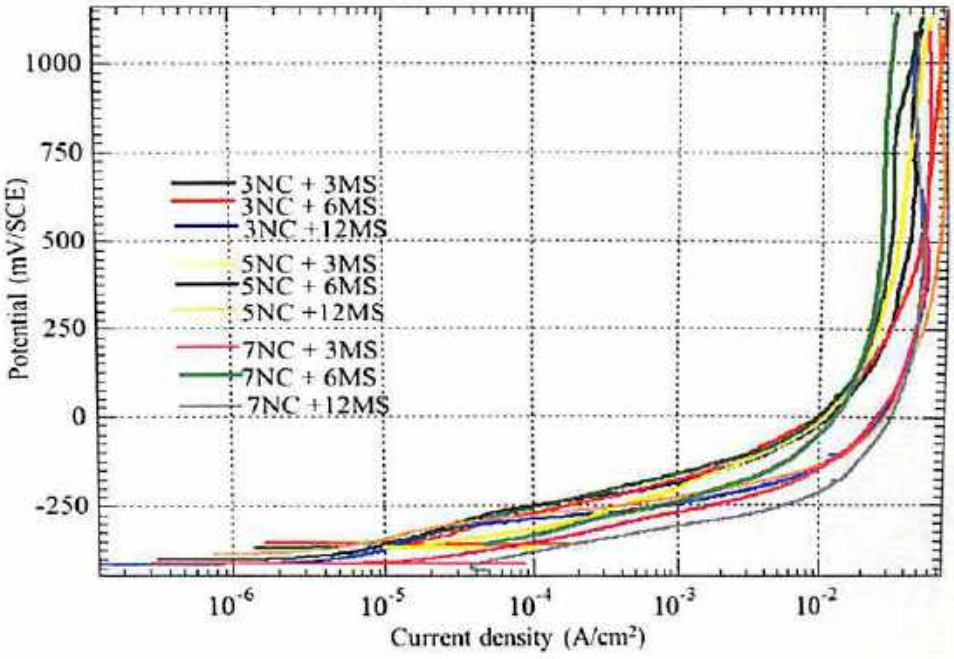

Fig. A25 Anodic polarization curves of Thermex TMT steel in ECPS prepared from PPC and w/c ratio of 0.5 at varying concentrations of NaCl (NC) and $MgSO_4$ (MS) admixed by mass of cement

LIST OF PUBLICATIONS

INTERNATIONAL JOURNALS

1. Fouzia Shaheen and Bulu Pradhan (2015), "Effect of chloride and conjoint chloride-sulfate ions on corrosion of reinforcing steel in electrolytic concrete powder solution (ECPS)", *Construction and Building Material*, Vol. 101, 99-112.

2. Fouzia Shaheen and Bulu Pradhan (2017), "Influence of sulfate ion and associated cation type on steel reinforcement corrosion in concrete powder aqueous solution in the presence of chloride ions" *Cement and Concrete Research*, Vol. 91, 73-86.

CONFERENCES

1. Fouzia Shaheen and Bulu Pradhan (2013), "Potentiodynamic polarization study on bare steel in concrete powder solution extracts contaminated with chloride and sulphate ions", International Conference on Structural Engineering and Mechanics (ICSEM 2013), NIT Rourkela, December 20-22.

2. Fouzia Shaheen and Bulu Pradhan (2014), "Electrochemical behaviour of steel in contaminated concrete powder solution extracts", Structural Engineering Convention (SEC 2014), Vol. 3, 1895-1905, IIT Delhi, December 22-24.

3. Fouzia Shaheen and Bulu Pradhan (2015), "Performance of steel in Portland cement and fly ash added concrete admixed with chloride and sulfate ions", UKIERI Concrete Congress, 119-127, NIT Jalandhar, November 2-5.

4. Fouzia Shaheen and Bulu Pradhan (2015), "Behaviour of steel reinforcement in chloride and combined chloride-sulfate contaminated concrete powder solution extracts", 2nd R. N. Raikar Memorial International Conference and Banthia-Basheer International Symposium on Advances in Science & Technology of Concrete, Vol. II, 547-552, Mumbai, December 18-19.

5. Fouzia Shaheen and Bulu Pradhan (2015), "Effect of sulfate on chloride-induced corrosion behaviour of reinforcing steel in concrete powder solution", Eighteenth National Congress on Corrosion Control, Chennai, February 24-26.